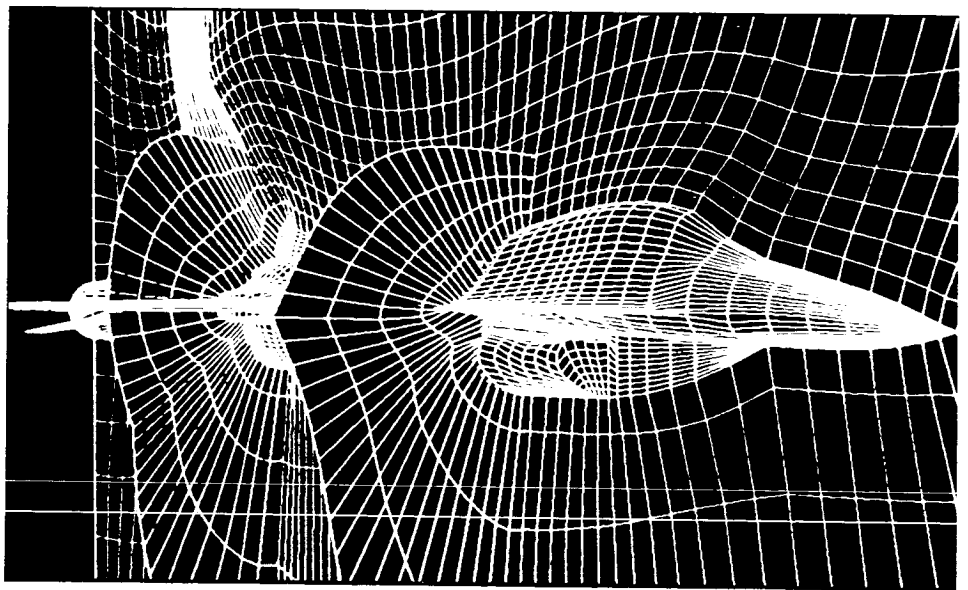


NASA Technical Memorandum 4175

NASA Aerodynamics Program Annual Report 1989

Bruce Holmes, Edward Schairer, Gary Hicks,
Stephen Wander, Isiaiah Blankson, Raymond Rose,
Lawrence Olson, and George Unger

FEBRUARY 1990



NASA

NASA Technical Memorandum 4175

NASA Aerodynamics Program Annual Report 1989

**Bruce Holmes, Edward Schairer, Gary Hicks,
Stephen Wander, Isiaiah Blankson, Raymond Rose,
Lawrence Olson, and George Unger**
*NASA Office of Aeronautics and Space Technology
Aerodynamics Division
Washington, D.C.*



National Aeronautics and
Space Administration
Office of Management
Scientific and Technical
Information Division

1990

INTRODUCTION

The Aerodynamics Division is one of five technical divisions that comprise NASA's Office of Aeronautics and Space Technology (OAST). This division sponsors research in the areas of fluid and thermal physics and applied aerodynamics. This annual report documents the most significant accomplishments during the past year. The report has been prepared to serve as the primary mechanism for coordinating NASA activities with industry. This document also is intended to communicate significant technical accomplishments within the NASA community, to project engineers, to other government agencies and to universities.

The Aerodynamics Program consists of the following major elements: (1) computational methods and applications, (2) CFD validation, (3) transition and turbulence physics, (4) numerical aerodynamic simulation, (5) drag reduction, (6) test techniques and instrumentation, (7) configuration aerodynamics, (8) aeroacoustics, (9) aerothermodynamics, (10) hypersonics, (11) subsonic transport/commuter aviation, (12) fighter/attack aircraft and (13) rotorcraft. The principal objectives in FY 1989 for each area are described in the following paragraphs.

Computational Methods and Applications - develops and applies analysis and computational methods for solving complex fluid dynamics problems.

CFD Validation - produces detailed, archival experimental databases that can be used to validate computational fluid dynamics codes.

Transition and Turbulence Physics - develops a fundamental understanding of flow structures relating to turbulence and transition and incorporates these flow structures into flow models for use with computational methods.

Numerical Aerodynamic Simulation - develops a fundamental understanding of flow structures relating to turbulence and transition and incorporates these flow structures into flow models for use with computational methods.

Drag Reduction - develops technology for aerodynamic drag reduction and flow control for aircraft across the speed range. Research areas include hybrid laminar flow control, turbulence control (including turbulent skin friction drag reduction), flow separation control, wave drag reduction and induced drag reduction.

Test Techniques and Instrumentation - provides the technology for critical research capability required to improve the measurement of the fundamental flow properties of fluids and the overall aerodynamic performance of aircraft components and configurations. Emphasis is placed on instrumentation for real-time flow diagnosis with focus on nonintrusive sensing.

Configuration Aerodynamics - provides the fundamental aerodynamic databases and analytical methods necessary for the efficient and accurate analysis and prediction of aerodynamic flows about advanced aircraft components and configurations.

Aeroacoustics - develops a fundamental understanding, predictive capability and control techniques for aeroacoustic phenomena, including aeroacoustic loads, acoustic interaction with boundary layer flows and sound propagation through the atmosphere.

Aerothermodynamics - develops, validates and applies predictive capabilities and tools to enable the aerodynamic and aeroheating design and optimization of aerospace vehicles required to enter and maneuver in Earth and/or planetary atmospheres.

Hypersonics - develops a fundamental understanding of the physics and chemistry of gas dynamic behavior as it pertains to slender, air-breathing, hypersonic vehicles that use highly integrated airframe/propulsion systems.

Subsonic Transport/Commuter Aviation - provides advanced technology base, design data and analytical codes for future subsonic airplanes having improved efficiency and safety. Technology applications will result in advanced low-drag airplane configurations with increased fuel economy, flight safety and improved ride and handling qualities.

Fighter/Attack Aircraft - develops both experimentally and analytically the enabling aerodynamic technology base required for the design of future fighter/attack aircraft. Current areas of emphasis include enhanced agility at subsonic speeds, high angle of attack aerodynamics and aircraft control, as well as ground effects, subsonic and supersonic aerodynamics and handling qualities of powered lift aircraft.

Rotorcraft - provides the enabling technologies for helicopters and other rotor-borne aircraft to achieve quiet, low vibration operation with increased performance, agility, maneuverability and stability with acceptable handling qualities.

To aid in the communication of program efforts, the names and phone numbers of headquarters and center managers and technologists involved with this report are included in their respective sections.

Acting Deputy Director: Dr. Bruce J. Holmes
(OAST/RF)
(804)864-6398

TABLE OF CONTENTS

INTRODUCTION.....	i
CHAPTER ONE COMPUTATIONAL METHODS AND APPLICATIONS.....	1-1
1.1 INTRODUCTION.....	1-1
1.2 INCOMPRESSIBLE FLOW SOLVER.....	1-3
1.3 NAVIER-STOKES SOLUTIONS ON MASSIVELY PARALLEL COMPUTERS	1-5
1.4 SURFACE AND GRID GENERATION SOFTWARE	1-7
1.5 FLOW VISUALIZATION SOFTWARE	1-9
1.6 COMPUTATION OF MULTI-STAGE COMPRESSOR FLOWS....	1-11
1.7 HYPERSONIC NAVIER-STOKES COMPUTATIONS.....	1-13
1.8 UNSTEADY MULTIPLE BODY AERODYNAMICS	1-15
1.9 PARABOLIZED NAVIER-STOKES ALGORITHM FOR CHEMICALLY REACTING FLOWS.....	1-17
1.10 MULTIGRID ACCELERATION TECHNIQUE FOR NAVIER-STOKES EQUATIONS	1-19
1.11 A PRECONDITIONED CONJUGATE GRADIENT METHOD FOR THE COMPRESSIBLE NAVIER-STOKES EQUATIONS.....	1-21
1.12 NON-REFLECTING OUTFLOW BOUNDARY TREATMENT FOR TRANSITION SIMULATIONS	1-23
1.13 AN EMBEDDED- AND MULTIPLE -GRID ALGORITHM APPLIED TO DELTA WINGS.....	1-25
1.14 MULTIBLOCK MULTIGRID CALCULATIONS OF NOZZLE EXHAUST FLOWS	1-27
1.15 GRAPHICAL DISPLAY OF FLUID FLOW RESULTS ON UNSTRUCTURED GRIDS	1-29
1.16 MULTIGRID SOLUTION OF THE NAVIER-STOKES EQUATIONS ON UNSTRUCTURED MESHES	1-31
1.17 UNSTRUCTURED GRID AND FLOW SOLUTION FOR F-18 AIRPLANE.....	1-33
1.18 UNSTRUCTURED GRID AND FLOW SOLUTION FOR A TYPICAL INLET CONFIGURATION	1-35
1.19 ANALYSIS OF LOW FREQUENCY FLUCTUATIONS IN A CYLINDER WAKE	1-37
1.20 SHOCK-SHOCK INTERACTION ON BLUNT BODIES IN HYPERSONIC FLOWS.....	1-39
1.21 NAVIER-STOKES COMPUTER.....	1-41
1.22 DISTRIBUTED PROCESSING WITH NETWORKED COMPUTERS	1-43

TABLE OF CONTENTS (CONT.)

CHAPTER TWO	CFD VALIDATION	2-1
2.1	INTRODUCTION.....	2-1
2.2	CODE-VALIDATION STUDY FOR HYPERSONIC COMPRESSION-CORNER FLOWS.....	2-3
2.3	TRANSONIC WIND TUNNEL TEST DATA ACQUIRED ON A HEMISPHERE MODEL WITH A CYLINDRICAL AFTERBODY FOR LASER VELOCIMETER SEEDING INVESTIGATION	2-5
2.4	DETECTION OF SHOCK-INDUCED SEPARATION USING MEDS ³ TECHNIQUE	2-7
2.5	CROSSFLOW-VORTEX INSTABILITY ON A 45 DEGREE SWEEP WING	2-9
2.6	COMPUTATIONAL VALIDATION OF A PARABOLIZED NAVIER-STOKES SOLVER ON A SHARP-NOSE CONE AT HYPERSONIC SPEEDS.....	2-11
2.7	CODE VALIDATION EXPERIMENTS FOR TURBULENT FLOW.....	2-13
2.8	SPACE SHUTTLE MAIN ENGINE CODE VALIDATION	2-15
2.9.	ALL-BODY HYPERSONIC WIND TUNNEL TESTS AND CFD VALIDATION	2-17
CHAPTER THREE	TRANSITION AND TURBULENCE PHYSICS	3-1
3.1	INTRODUCTION.....	3-1
3.2	TURBULENCE MODELING USING DIRECT SIMULATION DATA	3-3
3.3	IMPROVED TURBULENCE MODEL FOR TRANSONIC FLOW..	3-5
3.4	STRUCTURE OF PLANE MIXING LAYERS.....	3-7
3.5	PHYSICS OF NUMERICALLY SIMULATED TURBULENCE	3-9
3.6	LOW REYNOLDS NUMBER TURBULENT FLOW EXPERIMENTS.....	3-11
3.7	FINITE DIFFERENCE METHOD FOR TURBULENT FLOW.....	3-13
3.8	TEMPORALLY-EVOLVING MIXING LAYERS.....	3-15
3.9	LINEAR STABILITY OF BOUNDED FREE SHEAR FLOWS.....	3-17
3.10	DEVELOPMENT AND IMPLEMENTATION OF THE PARABOLIC STABILITY EQUATION.....	3-19
3.11	NONLINEAR WAVE INTERACTIONS IN THREE DIMENSIONAL BOUNDARY LAYERS.....	3-21
3.12	EVOLUTION OF A 2-D SECOND MODE WAVE IN A MACH 4.5 BOUNDARY LAYER	3-23
3.13	COMPUTATION OF SPATIALLY UNSTABLE THREE-DIMENSIONAL WAVES IN A SUPERSONIC BOUNDARY LAYER	3-25
3.14	LARGE-EDDY SIMULATION (LES) TRANSITION MODELING.	3-27

TABLE OF CONTENTS (CONT.)

3.15	STUDIES IN DIRECT SIMULATION OF HIGH SPEED MIXING LAYERS.....	3-29
3.16	THREE-DIMENSIONAL BOUNDARY-LAYER.....	3-31
3.17	SUPERSONIC TRANSITION ON CONES AND FLAT PLATES ..	3-33
3.18	EFFECT OF LEADING EDGE BLUNTNESS ON FLAT PLATE TRANSITION	3-35
3.19	INFLUENCE OF COMBINING DISTURBANCE FIELDS ON TRANSITION-ROUGHNESS AND ACOUSTICS.....	3-37
3.20	SUPERSONIC FREE-SHEAR LAYER TRANSITION	3-39
3.21	ADVANCES IN QUIET NOZZLE DEVELOPMENT.....	3-41
3.22	LAMINAR FLOW CONTROL ON A FLAT PLATE USING LOCALIZED HEATING	3-43
3.23	NUMERICAL SIMULATION OF CHAOTIC STATES IN FINITE-LENGTH TAYLOR-COUETTE FLOW.....	3-45
3.24	DIRECT SIMULATION OF COMPRESSIBLE TURBULENCE....	3-47
3.25	JOHNSON-KING TURBULENCE MODEL FOR 3-D FLOWS.....	3-49
3.26	A DEFECT STREAM FUNCTION, LAW OF THE WALL/WAKE METHOD FOR COMPRESSIBLE TURBULENT BOUNDARY LAYER.....	3-51

CHAPTER FOUR NUMERICAL AERODYNAMIC SIMULATION (NAS)..... 4-1

4.1	INTRODUCTION.....	4-1
4.2	CRAY Y-MP INSTALLATION	4-3
4.3	INSTALLATION OF EARLY RELEASE UNICOS 5.0 ON THE CRAY Y-MP	4-4
4.4	INSTALLATION OF ALPHA TEST UNICOS 5.0 ON THE CRAY-2.....	4-5
4.5	MASS STORAGE SYSTEM (MSS-I) RELEASE 7.0.....	4-7
4.6	AUTOMATED TAPE LIBRARIES	4-8
4.7	MSS-II DEVELOPMENT	4-9
4.8	RESEARCH INTERNET GATEWAY (RIG).....	4-11
4.9	THE PANEL LIBRARY.....	4-12
4.10	PERFORMANCE OF AN EULER CODE ON HYPERCUBES.....	4-13
4.11	COMPUTATIONAL FLUID DYNAMICS ON A MASSIVELY PARALLEL COMPUTER.....	4-15

CHAPTER FIVE DRAG REDUCTION 5-1

5.1	INTRODUCTION.....	5-1
5.2	RIBLETS FOR TURBULENT DRAG REDUCTION IN SUPERSONIC FLIGHT	5-3
5.3	INDUCED DRAG REDUCTION	5-5

TABLE OF CONTENTS (CONT.)

5.4	COMPOSITE STRUCTURE AND TYPES OF VORTEX BREAKDOWN	5-7
5.5	HYDRODYNAMIC STABILITY OF THREE-DIMENSIONAL VORTICES	5-9
5.6	SUBMERGED VORTEX GENERATORS	5-11
5.7	CONTROL OF TURBULENCE AND TRANSITION	5-13
5.8	HYBRID LAMINAR-FLOW CONTROL FLIGHT EXPERIMENT ..	5-15
5.9	APPLICATION OF LAMINAR-FLOW CONTROL TO SUPERSONIC TRANSPORT CONFIGURATIONS	5-17
CHAPTER SIX TEST TECHNIQUES AND INSTRUMENTATION.....		6-1
6.1	INTRODUCTION	6-1
6.2	VISUALIZATION OF VORTICAL FLOW USING THE LASER VAPOR SCREEN TECHNIQUE	6-3
6.3	LARGE SEMI-SPAN MODEL TEST TECHNIQUES	6-5
6.4	NONINTRUSIVE INSTRUMENTATION FOR HYPERSONIC FLOW	6-7
6.5	PRESSURE SENSITIVE FLUORESCENT PAINT	6-9
6.6	PRESSURE PROBE DESIGN	6-11
6.7	IMPROVEMENTS TO A SLOTTED-WALL, WIND TUNNEL INTERFERENCE ASSESSMENT CODE (PANCOR)	6-13
6.8	STUDY OF SIDE WALL BOUNDARY LAYER REMOVAL EFFECTS ON AIRFOIL TESTS IN THE LANGLEY 0.3-M TCT ADAPTIVE WALL TEST SECTION	6-15
6.9	TEST TECHNIQUE FOR THIN FIGHTER WING AT HIGH REYNOLDS NUMBER	6-17
6.10	SUBSONIC STING INTERFERENCE ON THE DRAG OF SLANTED-BASE OGIVE CYLINDERS	6-19
6.11	TRANSITION DETECTION AT SUPERSONIC SPEEDS USING A MICRO-THIN, HOT-FILM SYSTEM	6-21
6.12	HIGH TEMPERATURE SKIN FRICTION BALANCE DEVELOPMENT	6-23
6.13	A PRECISION ELECTRO-OPTICAL DISPLACEMENT MEASURING SYSTEM	6-25
6.14	ELECTRONICALLY SCANNED CYROGENIC PRESSURE MODULE	6-27
6.15	BOUNDARY LAYER PROFILE MEASUREMENTS ON A 5-DEGREE HALF-ANGLE CONE USING A LASER TRANSIT ANEMOMETER IN THE UNITARY PLAN WIND TUNNEL	6-29
6.16	FREQUENCY DOMAIN LASER VELOCIMETER SIGNAL PROCESSOR	6-31

TABLE OF CONTENTS (CONT.)

CHAPTER SEVEN	CONFIGURATION AERODYNAMICS	7-1
7.1	INTRODUCTION.....	7-1
7.2	COMPRESSIBILITY EFFECTS ON DYNAMIC STALL.....	7-3
7.3	APPLICATION OF A TRANSONIC/SUPERSONIC DESIGN METHOD TO COMPLEX GEOMETRIES AND ISOLATED AIRCRAFT COMPONENTS.....	7-5
7.4	NAVIER-STOKES SOLUTIONS FOR VORTICAL FLOWS OVER A FOREBODY.....	7-7
7.5	EFFECT OF WING PLANFORM AND THE MODIFICATION AND WAKE ROLLUP ON INDUCED DRAG	7-9
7.6	EULER CODE VALIDATION/THEORY-EXPERIMENT INTEGRATION	7-11
7.7	ASYMMETRICAL VISCOUS FLOW CALCULATIONS USING LANS3D.....	7-13
7.8	LOW REYNOLDS NUMBER TRANSONIC WING TEST (F-8/VHASA).....	7-15
7.9	TRANAIR DEVELOPMENT AND VALIDATION.....	7-17
7.10	RADAR CROSS SECTION CALCULATIONS WITH EMTRANAIR.....	7-19
7.11	STOVL FIGHTER AIRCRAFT CONFIGURATION AERODYNAMICS.....	7-21
7.12	TRANAIR AND EULER COMPUTATIONS OF A GENERIC FIGHTER	7-23
7.13	EULER AND POTENTIAL CODE EVALUATION.....	7-25
CHAPTER EIGHT	AEROACOUSTICS.....	8-1
8.1	INTRODUCTION.....	8-1
8.2	ENROUTE AIRCRAFT NOISE.....	8-3
8.3	NON-AXISYMMETRIC SUPERSONIC JET FLOWFIELD	8-5
8.4	SUPERSONIC JET NOISE RESEARCH	8-7
8.5	NUMERICAL PREDICTION OF SHOCK/VORTEX INTERACTION NOISE	8-9
8.6	ASSESSMENT OF SHAPED SONIC BOOMS.....	8-11
8.7	B1-B TWIN ENGINE NOISE REDUCTION.....	8-13
8.8	AEROACOUSTIC LOADS OF ADVANCED CONFIGURATIONS.....	8-15
8.9	ADVANCED STOVL ACOUSTIC LOADS IN LEWIS RC's 9-FOOT BY 15-FOOT LOW SPEED WIND TUNNEL.....	8-17
8.10	ASTOVL SONIC FATIGUE LOADS	8-19
8.11	FLUCTUATING PRESSURE LOADS IN HYPERSONIC BOUNDARY LAYERS.....	8-21

TABLE OF CONTENTS (CONT.)

8.12	FLUCTUATING PRESSURE LOADS IN A SCRAMJET ENGINE MODEL	8-23
8.13	NUMERICAL SIMULATION OF AERODYNAMIC NOISE	8-25
CHAPTER NINE AEROTHERMODYNAMICS		9-1
9.1	INTRODUCTION.....	9-1
9.2	ADVANCES IN COMPUTATIONAL CAPABILITY.....	9-3
9.3	ADVANCES IN DIRECT SIMULATION MONTE CARLO COMPUTATIONAL CAPABILITIES USING PARALLEL PROCESSING.....	9-5
9.4	AEROASSIST FLIGHT EXPERIMENT (AFE) FLOWFIELD SIMULATIONS	9-7
9.5	CODE CALIBRATION IN SUPPORT OF THE AEROASSIST FLIGHT EXPERIMENT.....	9-9
9.6	RAREFIED FLOWS OVER THE AFE VEHICLE.....	9-11
9.7	EXPERIMENTAL HYPERSONIC AERODYNAMIC AND AEROTHERMODYNAMIC CHARACTERISTICS FOR AFE.....	9-13
9.8	EXPERIMENTAL HYPERSONIC-HYPERVELOCITY AERODYNAMIC/AEROTHERMODYNAMIC CHARACTERISTICS FOR PROPOSED HIGH ENERGY AEROBRAKING CONCEPTS.....	9-15
9.9	HIGH ENERGY AEROBRAKING STUDIES	9-17
9.10	RANDOM ATMOSPHERE SIMULATION FOR MONTE CARLO TRAJECTORY ANALYSIS	9-19
9.11	SHUTTLE INFRARED LEESIDE TEMPERATURE SENSING (SILTS).....	9-21
9.12	ATMOSPHERE DENSITY MEASUREMENTS BETWEEN 60 AND 160 KM.....	9-23
9.13	REACTION CONTROL SYSTEM PLUME/FLOWFIELD INTERACTION STUDY.....	9-25
9.14	BOUNDARY LAYER STABILITY ANALYSIS ON CONES IN FREE FLIGHT AT HYPERSONIC SPEEDS.....	9-27
9.15	LIFTING-BODY CONFIGURATION ANALYSIS.....	9-29
9.16	LIFTING-BODY ENTRY CROSS RANGE ANALYSIS	9-31
9.17	LIFTING-BODY ENTRY FLIGHT DYNAMICS ANALYSIS.....	9-33
9.18	LIFTING-BODY LANDING-SPEED ANALYSIS.....	9-35
9.19	LIFTING-BODY CROSSWIND LANDING ANALYSIS.....	9-37
9.20	EXPERIMENTAL AERODYNAMIC AND AEROTHERMODYNAMIC CHARACTERISTICS FOR PROPOSED PERSONNEL LAUNCH SYSTEM LIFTING BODY CONCEPT.....	9-39
9.21	ASSURED CREW RETURN VEHICLE FLOWFIELD ANALYSIS.....	9-41

TABLE OF CONTENTS (CONT.)

9.22	NASA/ONERA COOPERATIVE AGREEMENT: WIND-TUNNEL TEST COLLABORATION IN HYPERSONIC AEROTHERMODYNAMICS.....	9-43
9.23	GRID GENERATION FOR COMPLEX GEOMETRIC SHAPES ...	9-45
9.24	SOLID MODELLING AEROSPACE RESEARCH TOOLS (SMART).....	9-47
9.25	THERMAL MAPPING/HEAT TRANSFER MEASUREMENTS IN HYPERSONIC WIND TUNNELS.....	9-49
9.26	COMPRESSIBLE-EULER-NAVIER-STOKES TWO-DIMENSIONAL HYPERSONIC (CENS2H) CODE FOR NONEQUILIBRIUM AIR	9-51
9.27	TWO DIMENSIONAL AND AXISYMMETRIC MULTI-TEMPERATURE NAVIER-STOKES HYPERSONIC FLOW SIMULATION.....	9-53
9.28	THREE DIMENSIONAL NONEQUILIBRIUM FLOW SIMULATION OF THE AEROASSIST FLIGHT EXPERIMENT VEHICLE.....	9-55
9.29	CONTINUUM EXTENSION-NONLINEAR TRANSPORT	9-57
9.30	DIRECT PARTICLE SIMULATION OF HYPERSONIC FLOWS ..	9-59
9.31	HIGH-ENERGY AEROBRAKING CONCEPTUAL VEHICLE DESIGN	9-61
9.32	TITAN ATMOSPHERIC COMPOSITION FROM HIGH VELOCITY SHOCK LAYER RADIATION.....	9-63
9.33	TWO DIMENSIONAL, SELF-ADAPTIVE GRID CODE, SAGE....	9-65
9.34	THREE DIMENSIONAL, SELF-ADAPTIVE GRID CODE, SAGE 3-D	9-67
9.35	REAL-GAS DATA FROM BALLISTIC RANGES AND CFD CALIBRATION	9-69
9.36	RATES FOR COUPLED ROTATION-VIBRATION-DISSOCIATION PHENOMENON IN DIATOMIC MOLECULES ..	9-71
9.37	RADIATIVE PROPERTIES OF THE OH MOLECULE.....	9-73
9.38	RADIATIVE INTENSITY FACTORS FOR AIR SPECIES.....	9-75
9.39	TRANSPORT PROPERTIES FOR AIR SPECIES.....	9-77
9.40	REACTION RATE CONSTANTS.....	9-79
CHAPTER TEN HYPERSONIC AERODYNAMICS.....		10-1
10.1	INTRODUCTION.....	10-1
10.2	INVERSE WAVERIDER DESIGN.....	10-5
10.3	EVALUATION OF OPTIMIZED WAVERIDERS.....	10-7
10.4	CONCEPTUAL DESIGN AND OPTIMIZATION OF WAVERIDER CONFIGURATIONS.....	10-9
10.5	TRANSONIC NAVIER-STOKES SOLUTIONS ABOUT A COMPLEX, HIGH-SPEED CONFIGURATION	10-11

TABLE OF CONTENTS (CONT.)

10.6	LOW SPEED PROPULSION/AIRFRAME INTEGRATION	10-13
10.7	SCRAMJET EXHAUST SIMULATION STUDIES AT MACH 6 ...	10-15
10.8	NASP HIGH-SPEED DYNAMIC STABILITY TESTS	10-17
10.9	HYPERSONIC FOREBODY DESIGN STUDY	10-19
10.10	TTD FOREBODY REDESIGN	10-21
10.11	EFFECT OF REAL-GAS ON FIRST AND SECOND MODE INSTABILITY IN HYPERSONIC BOUNDARY LAYERS	10-23
10.12	MODELING FUEL-AIR MIXING AND REACTION IN A SCRAMJET COMBUSTOR	10-25
10.13	A ZONAL METHODOLOGY FOR HIGH SPEED FOREBODY/INLET CONFIGURATIONS	10-27
10.14	ALGEBRAIC HYPERSONIC TRANSITION MODELING	10-29
10.15	PEGASUS AEROTHERMAL FLIGHT MEASURES	10-31
CHAPTER ELEVEN SUBSONIC TRANSPORT/COMMUTER AVIATION.....		11-1
11.1	INTRODUCTION	11-1
11.2	NATURAL LAMINAR FLOW CERTIFICATION PROGRAM.....	11-3
11.3	TRANSITION PHYSICS FLIGHT EXPERIMENT	11-5
11.4	AERODYNAMIC CHARACTERISTICS OF CRESCENT WING PLANFORMS	11-7
CHAPTER TWELVE FIGHTER/ATTACK AIRCRAFT.....		12-1
12.1	INTRODUCTION	12-1
12.2	EVALUATION OF LEADING- AND TRAILING-EDGE FLAPS ON A FLAT AND CAMBERED DELTA WING AT SUPERSONIC SPEEDS	12-3
12.3	A PARAMETRIC CFD STUDY OF INCIPIENT LEADING -EDGE SEPARATION	12-5
12.4	STOL/STOVL CONCEPTS FOR HIGH PERFORMANCE AIRCRAFT.....	12-7
12.5	DYNAMIC STALL RESEARCH	12-9
12.6	SIMULATION STUDIES OF ENHANCED COMBAT MANEUVERING FOR USING ADVANCED CONTROLS	12-11
12.7	VORTEX INTERACTION RESEARCH.....	12-13
12.8	SUPERSONIC STOVL TECHNOLOGY.....	12-15
12.9	STOL TRANSPORT TECHNOLOGY	12-17
12.10	STOVL FLYING QUALITIES EVALUATION.....	12-19
12.11	STOVL E-7A TESTS IN THE 40-FOOT BY 80-FOOT WIND TUNNEL	12-21
12.12	F-111 CREW ESCAPE MODULE 40-FOOT BY 80-FOOT WIND TUNNEL TEST	12-23

TABLE OF CONTENTS (CONT.)

12.13	NUMERICAL SIMULATION OF STOVL AIRCRAFT AERODYNAMICS.....	12-25
CHAPTER THIRTEEN ROTORCRAFT		13-1
13.1	INTRODUCTION.....	13-1
13.2	NUMERICAL SIMULATION OF ROTORCRAFT AERODYNAMICS.....	13-3
13.3	THREE DIMENSIONAL DRAG PREDICTION FOR ROTOR BLADES.....	13-5
13.4	PRESSURE-INSTRUMENTED MODEL ROTOR NOISE TEST....	13-7
13.5	UH-60 LOADS AND PERFORMANCE FLIGHT INVESTIGATIONS.....	13-9
13.6	UH-60 ROTOR AIRLOADS PROGRAM.....	13-11
13.7	COMPLEMENTARY ROTOR AIRLOADS AND ACOUSTIC PROGRAMS.....	13-13
13.8	ROTOR/FUSELAGE AERODYNAMIC INTERACTIONS.....	13-15
13.9	ROTOR INFLOW/WAKE RESEARCH (USING THE LASER VELOCIMETER).....	13-17
13.10	ROTOR WAKE GEOMETRY IN FORWARD FLIGHT USING WIDE-FIELD SHADOWGRAPHY.....	13-19
13.11	LONG-RANGE LASER VELOCIMETER PERFORMANCE TEST.....	13-21
13.12	ROTONET DEVELOPMENT	13-23
13.13	ACOUSTIC RESULTS OF THE SIKORSKY S-76 VARIABLE ROTOR-SPEED TESTS.....	13-25
13.14	HELICOPTER BLADE-VORTEX NOISE INTERACTION REDUCTION.....	13-27
13.15	ROTOR BLADE-VORTEX INTERACTION NOISE DIRECTIVITY.....	13-29
13.16	SIMULATION OF REALISTIC BLADE-VORTEX INTERACTIONS.....	13-31
13.17	AEROACOUSTIC MODIFICATION OF THE 40-FOOT BY 80-FOOT WIND TUNNEL.....	13-33
13.18	ACTIVE CONTROL OF PANEL RADIATED NOISE.....	13-35
13.19	REDUCTION OF ROTOR BLADE-VORTEX INTERACTION NOISE USING HIGHER HARMONIC PITCH CONTROL	13-37
13.20	USE OF BLADE NON-STRUCTURAL MASS REDUCES ROTORCRAFT VIBRATIONS	13-39
13.21	TDT TESTS EVALUATE PERFORMANCE CHARACTERISTICS OF ADVANCED DESIGN HELICOPTER ROTOR BLADES.....	13-41

TABLE OF CONTENTS (CONT.)

13.22	GROUND VIBRATION TEST OF HELICOPTER AIRFRAME IDENTIFIES IMPORTANT CONTRIBUTIONS TO VIBRATION RESPONSES	13-43
13.23	OPTIMIZATION APPROACH FOR HELICOPTER VIBRATION REDUCTION DEMONSTRATED	13-45
13.24	INTEGRATED AERODYNAMIC LOAD/DYNAMIC OPTIMIZATION OF HELICOPTER ROTOR BLADES.....	13-47
13.25	CH-47 FLIGHT RESEARCH--1989	13-49
13.26	ROTORCRAFT FLIGHT DYNAMICS MATH MODEL DEVELOPMENT.....	13-51
13.27	HELICOPTER MANEUVER ENVELOPE ENHANCEMENT (HelMEE).....	13-53
13.28	TILTROTOR TECHNOLOGY	13-55
13.29	V-22 ROTOR/WING PERFORMANCE TEST	13-57
13.30	XV-15/ATB FLIGHT INVESTIGATIONS.....	13-59
13.31	XV-15 TILTROTOR NOISE TEST.....	13-61
13.32	MV-22 TILTROTOR SIMULATION.....	13-63
13.33	CIVIL TILTROTOR AIRWORTHINESS CRITERIA	13-65

LIST OF FIGURES

Chapter One Computational Methods and Applications

Figure 1.1.	SSME Turbopump Inducer	1-2
Figure 1.2.	Ames Interactive Surface Editing Tool	1-6
Figure 1.3.	Flow Analysis Software Tools.....	1-8
Figure 1.4.	Instantaneous Entropy Contours in a 2.5 Stage Compressor.....	1-10
Figure 1.5.	Lower Surface Heat Transfer Distribution.....	1-12
Figure 1.6.	Time-Accurate Simulation of the Space Shuttle	1-14
Figure 1.7.	Parabolized Navier-Stokes Algorithm for Chemically Reacting Flows.....	1-16
Figure 1.8.	Effect of Grid Density on Convergence.....	1-18
Figure 1.9.	Transonic Turbulent Flow Over an RAE7822 Airfoil	1-20
Figure 1.10.	Non-Reflecting Outflow Boundary Treatment	1-22
Figure 1.11.	Streamwise Velocity Contours.....	1-24
Figure 1.12.	3 Degree Ramp Nozzle and Plume.....	1-26
Figure 1.13.	Graphical Display of Fluid Flow Results on Unstructured Grids.....	1-28
Figure 1.14.	Navier-Stokes Solutions on Unstructured Meshes	1-30
Figure 1.15.	Pressure Contours on F-18 Airplane	1-32
Figure 1.16.	Unstructured Grid and Flow Solution for a Typical Inlet Configuration.....	1-34
Figure 1.17.	Analysis of Low Frequency Fluctuations in a Cylinder Wake	1-36
Figure 1.18.	Mach Number Contours for Cowl Forebody.....	1-38
Figure 1.19.	16-Node Navier-Stokes Computer	1-40
Figure 1.20.	Implementation Overview.....	1-42

Chapter Two CFD Validation

Figure 2.1.	Code Validation Study	2-2
Figure 2.2.	Basic Aerodynamic Research Facility	2-4
Figure 2.3.	Phase Shifts at Separation and Reattachment.....	2-6
Figure 2.4.	Experimental and Theoretical Spectra	2-8
Figure 2.5.	PNS Code Validation Study.....	2-10
Figure 2.6.	An Experiment to Guide Turbulence Modeling for 3-D Boundary Layers	2-12
Figure 2.7.	SSME Turn-Around Duct Experiment	2-14
Figure 2.8.	All-Body Hypersonic Wind Tunnel Tests and CFD Validation	2-16

Chapter Three Transition and Turbulence Physics

Figure 3.1.	Turbulent Kinetic Energy in a Channel.....	3-2
Figure 3.2.	RANS Transonic Airfoil Predictions.....	3-4
Figure 3.3.	Undisturbed Mixing Layer.....	3-6

LIST OF FIGURES (CONT.)

Figure 3.4.	Crossed Hotwire.....	3-10
Figure 3.5.	Root-Mean-Square Velocity Fluctuation Normalized by the Wall Shear Velocity.....	3-12
Figure 3.6.	Surface of Constant Vorticity Magnitude	3-14
Figure 3.7.	High Oscillatory Structure of Modes	3-16
Figure 3.8.	Spatial Marching Method for Boundary Layer Transition	3-18
Figure 3.9.	Nonlinear Wave Interaction in Three Dimensional Boundary Layers ..	3-20
Figure 3.10.	Nonlinearities in Critical Layer/Generalized Inflection Point Region...	3-22
Figure 3.11.	Numerical Results	3-24
Figure 3.12.	Filtered, Direct and Large-Eddy Simulations	3-26
Figure 3.13.	High-Speed Mixing Layer.....	3-28
Figure 3.14.	Skin Friction Coefficient Comparisons	3-30
Figure 3.15.	Comparison of Transition-Onset Reynolds Numbers	3-32
Figure 3.16.	Effect of Leading Edge Bluntness on Flat Plate Transition	3-34
Figure 3.17.	Crossflow Instability	3-36
Figure 3.18.	Transition Physics Indication from Present Experiment	3-38
Figure 3.19.	Rapid Expansion Nozzle.....	3-40
Figure 3.20.	Wall Law-Transition Delay	3-42
Figure 3.21.	Three-Dimensional Unsteady Wavy Taylor-Couette Flow	3-44
Figure 3.22.	Divergence of Velocity	3-46
Figure 3.23.	Effect of Turbulence Model on Pressure Distribution for ONERA M6 Wing.....	3-48
Figure 3.24.a	Effect of Me and β	3-50
Figure 3.24.b	Comparison of a Velocity Profile with Experiment.....	3-50
 Chapter Four Numerical Aerodynamic Simulation (NAS)		
Figure 4.1.	Mass Storage System Transfer Rate Increases	4-6
Figure 4.2.	RIB/RIG Testbed Diagram	4-10
Figure 4.3.	Comparison of ARC2D on One Processor XMP	4-14
 Chapter Five Drag Reduction		
Figure 5.1.	Supersonic Riblet Drag Reduction.....	5-2
Figure 5.2.	Induced Drag Reduction	5-4
Figure 5.3.	Contour Plots of Total Vorticity.....	5-6
Figure 5.4.	Three Dimensional Vortex Stability.....	5-8
Figure 5.5.	Wheeler Vortex Generators.....	5-10
Figure 5.6.	Control of Turbulence Stream.....	5-12
Figure 5.7.	HLFC Flight Experiment	5-14
Figure 5.8.	Results of BCA Study.....	5-16
Figure 5.9.	Optimization of the U.S. National Transonic Facility Control System	5-18

LIST OF FIGURES (CONT.)

Chapter Six Test Techniques and Instrumentation

Figure 6.1.	Visualization of Vortical Flow.....	6-2
Figure 6.2.	Effect of Wall Boundary Condition on Outer Flowfield	6-4
Figure 6.3.	Nonintrusive Instrumentation for Hypersonic Flow.....	6-6
Figure 6.4.	Pressure Sensitive Fluorescent Paint	6-8
Figure 6.5.	Cone Probe Surface Pressure Distribution.....	6-10
Figure 6.6.	NTF Interference Corrections at Model	6-12
Figure 6.7.	Effect of Side Wall Boundary Layer Removal on Wall Streamlining...	6-14
Figure 6.8.	Test Technique for Thin Fighter Wing at High Reynolds Number	6-16
Figure 6.9.	Subsonic Sting Interference on the Drag of Slanted-Base Ogive Cylinders.....	6-18
Figure 6.10.	Transition Detection at Supersonic Speeds	6-20
Figure 6.11.	High Temperature Skin Friction Balance	6-22
Figure 6.12.	Electro-Optical Displacement Measurement System	6-24
Figure 6.13.	Model Pressure Instrumentation	6-26
Figure 6.14.	Typical Turbulent Boundary Layer Profile Measurement.....	6-28
Figure 6.15.	Signal Processor Performance	6-30

Chapter Seven Configuration Aerodynamics

Figure 7.1.	Computed Density Gradient Superimposed	7-2
Figure 7.2.	Wing Root Design to Eliminate Shock	7-4
Figure 7.3.	Helicity Density Contours	7-6
Figure 7.4.	Wing-Tip Blowing Model in Water Tunnel.....	7-8
Figure 7.5.	Euler Code Validation/Theory-Experiment Integration.....	7-10
Figure 7.6.	LANS 3DNS Asymmetrical Flow Solution for a Generic, Hypersonic All-Body Configuration	7-12
Figure 7.7.	Effect of Reynolds Number on Wing/Body Drag Polar.....	7-14
Figure 7.8.	F-16A W/TIP Missiles, Fuel Tanks.....	7-16
Figure 7.9.	F-16A Configuration at 300 MHz	7-18
Figure 7.10.	PANAIR and LINAIR Input Geometries	7-20
Figure 7.11.	Generic Fighter with Chine.....	7-22
Figure 7.12.	Potential Wing/Body Computation with B.L. Correction.....	7-24

Chapter Eight Aeroacoustics

Figure 8.1.	Enroute Aircraft Noise	8-2
Figure 8.2.	Non-Axisymmetric Supersonic Jet Flowfield	8-4
Figure 8.3.	Supersonic Jet Noise Research.....	8-6
Figure 8.4.	Numerical Prediction of Shock/Vortex Interaction Noise.....	8-8
Figure 8.5.	Assessment of Shaped Sonic Booms.....	8-10
Figure 8.6.	B1-B Twin Engine Noise Reduction.....	8-12

LIST OF FIGURES (CONT.)

Figure 8.7.	Aeroacoustic Loads of Advanced Configurations.....	8-14
Figure 8.8.	Advanced STOVL Model in Lewis RC's 9-Foot by 15-Foot	8-16
	Low Speed Wind Tunnel	
Figure 8.9.	ASTOVL Sonic Fatigue Loads.....	8-18
Figure 8.10.	Fluctuating Pressure Loads in Hypersonic Boundary Layers	8-20
Figure 8.11.	Fluctuating Pressure Loads in a Scramjet Engine Model.....	8-22
Figure 8.12.	Acoustic Power Versus Mach Number.....	8-24
 Chapter Nine Aerothermodynamics		
Figure 9.1.	Program LAURA Chemical Kinetic Models.....	9-2
Figure 9.2.	Direct Simulation Monte Carlo Analysis on Parallel Processors	9-4
Figure 9.3.	Log Electron Number Density.....	9-6
Figure 9.4.	Rarefied Flows over the Aeroassist Flight Vehicle (AFE)	
	Experiment.....	9-8
Figure 9.5.	Predicted Lift-to-Drag (L/D) Variation as a Function of Altitude.....	9-10
Figure 9.6.	Comparison of Measured and Predicted Heat Transfer Distributions ..	9-12
Figure 9.7.	Measured Heating Distribution and Shock Shape for 130°/70°	9-14
Figure 9.8.	Flight Domain and Stagnation Point Heating.....	9-16
Figure 9.9.	Random Atmosphere Simulation for Monte Carlo.....	9-18
Figure 9.10.	SILTS Qualitative Results Fuselage	9-20
Figure 9.11.	Shuttle Accelerometry (HiRAP/IMU) Density Measurements.....	9-22
Figure 9.12.	Orbiter RCS/Flowfield Interactions.....	9-24
Figure 9.13.	Calculated Transition Location	9-26
Figure 9.14.	ACRC Phase B Study Matrix	9-28
Figure 9.15.	Day Landings From Space Station.....	9-30
Figure 9.16.	Complete 6 DoF Entry	9-32
Figure 9.17.	Comparison of ACRC, X-24 and HL-10 Landing Speed Estimates ...	9-34
Figure 9.18.	Crosswind Capability	9-36
Figure 9.19.	Summary Aerodynamic Characteristics	9-38
Figure 9.20.	Mach Number Contour Plots.....	9-40
Figure 9.21.	NASA/ONERA Cooperative Agreement.....	9-42
Figure 9.22.	Symmetry and Outflow Plane Volume Grids.....	9-44
Figure 9.23.	Solid Modeling Aerospace Research Tools (SMART).....	9-46
Figure 9.24.	Windward Surface Temperature Mapping on a Transatmospheric.....	9-48
Figure 9.25.	Comparison Between Experimental and Computed Interferograms ...	9-50
Figure 9.26.	2-D and Axisymmetric Multi-Temperature Navier-Stokes.....	9-52
Figure 9.27.	Translational Temperature Contours.....	9-54
Figure 9.28.	Shock Reciprocal Thickness for Two Rotational Models.....	9-56
Figure 9.29.	Normalized Temperature.....	9-58
Figure 9.30.	High-Energy Aerobraking Conceptual Vehicle Analysis.....	9-60
Figure 9.31.	Titan Atmospheric Composition from High Velocity.....	9-62
Figure 9.32.	2-D Self-Adaptive Grid Code SAGE -- Example Result.....	9-64

LIST OF FIGURES (CONT.)

Figure 9.33.	3-D Self-Adaptive Grid Code SAGE 3-D.....	9-66
Figure 9.34.	Real-Gas Data from Ballistic Range and CFD Validation.....	9-68
Figure 9.35.	Rates for a Coupled Rotation-Vibration-Dissociation	9-70
Figure 9.36.	OH A2 Σ^+ Life Time.....	9-72
Figure 9.37.	Electronic Transition Moments.....	9-74
Figure 9.38.	Transport Properties for Air Species	9-76
Figure 9.39.	Reaction Rate Constants	9-78

Chapter Ten Hypersonic Aerodynamics

Figure 10.1.	Inverse Waverider Design	10-4
Figure 10.2.	Mach 4 Turbulent Waverider	10-6
Figure 10.3.	Conceptual Design and Optimization of Waverider Configurations	10-8
Figure 10.4.	Navier-Stokes Mach Contours	10-10
Figure 10.5.	Powered Ground Effects for Generic NASP-Like Configurations	10-12
Figure 10.6.	Scramjet Exhaust Simulation Model.....	10-14
Figure 10.7.	Roll Damping at M 4.6.....	10-16
Figure 10.8.	Load Heat Transfer Rates (q).....	10-18
Figure 10.9.	Computational Design of the TTD Forebody.....	10-20
Figure 10.10.	Effect of Gas Chemistry on Spatial Growth Rates.....	10-22
Figure 10.11.	Generic Scramjet Combustor.....	10-24
Figure 10.12.	Forebody/Inlet Configurations	10-26
Figure 10.13.	Transition Model vs. Mach 6 Cone.....	10-28
Figure 10.14.	Pegasus	10-30

Chapter Eleven Subsonic Transport/Commuter Aviation

Figure 11.1.	Cessna T210.....	11-2
Figure 11.2.	Transition Physics Flight Experiments.....	11-4
Figure 11.3.	Aerodynamic Characteristics of Crescent Wings.....	11-6

Chapter Twelve Fighter/Attack Aircraft

Figure 12.1.	Flat and Cambered Delta Wing.....	12-2
Figure 12.2.	Incipient Separation Computational Study.....	12-4
Figure 12.3.	Comparison of Static and Dynamic Ground Effects.....	12-6
Figure 12.4.	Dynamic Stall Research	12-8
Figure 12.5.	Simulation Studies of Enhanced Combat Maneuvering	12-10
Figure 12.6.	F/A-18 Fin Root Bending Moment	12-12
Figure 12.7.	Supersonic STOVL Technology	12-14
Figure 12.8.	STOL Transport Technology.....	12-16
Figure 12.9.	STOVL Flying Qualities Evaluation.....	12-18

LIST OF FIGURES (CONT.)

Figure 12.10. STOVL E-7A Tests in the 40-foot by 80-foot Wind Tunnel.....	12-20
Figure 12.11. F-111 Crew Escape Module.....	12-22
Figure 12.12. Experimental Versus Numerical Flow Visualization.....	12-24

Chapter Thirteen Rotorcraft

Figure 13.1. BERP Rotor	13-2
Figure 13.2. Comparison of Predicted and Measured Torque for a Non-Lifting, Hovering Aircraft	13-4
Figure 13.3. UTRC Model Rotor System.....	13-6
Figure 13.4. UH-60 with Instrumented Blade Set	13-8
Figure 13.5. The UH-60	13-10
Figure 13.6. The AH-1G Rotor	13-12
Figure 13.7. Bell 412 Rotor/Model 576 Test Stand in a 40-Foot by 80-Foot Wind Tunnel.....	13-14
Figure 13.8. Rotor Inflow Measurements.....	13-16
Figure 13.9. Long-Range Laser Velocimeter Test.....	13-20
Figure 13.10. ROTONET Development	13-22
Figure 13.11. Acoustic Results of the Sikorsky S-76 Variable Rotor-Speed Tests....	13-24
Figure 13.12. Helicopter Blade-Vortex Interaction Noise Reduction.....	13-26
Figure 13.13. Variation of BVI Noise Directivity with Flight Angle Discovered	13-28
Figure 13.14. Predicted and Measured Surface Differential	13-30
Figure 13.15. New Aeroacoustic Lining Concept for 40-Foot by 80-Foot Test Section	13-32
Figure 13.16. Active Control of Panel Radiated Noise.....	13-34
Figure 13.17. BVI Noise Reduction by Higher Harmonic Pitch.....	13-36
Figure 13.18. Use of Blade Non-Structural Mass Reduces Rotorcraft Vibrations....	13-38
Figure 13.19. TDT Tests.....	13-40
Figure 13.20. Ground Vibration Test of Helicopter Airframe.....	13-42
Figure 13.21. Optimization Approach for Helicopter Vibration.....	13-44
Figure 13.22. Integrated Aerodynamic Load/Dynamic Optimization	13-46
Figure 13.23. CH-47 Flight Research--1989.....	13-48
Figure 13.24. Rotorcraft Flight Dynamics Math Model Development.....	13-50
Figure 13.25. Typical Helicopter Limits	13-52
Figure 13.26. Tiltrotor Technology.....	13-54
Figure 13.27. V-22 Rotor/Wing Performance Test.....	13-56
Figure 13.28. XV-15 Tiltrotor Research Aircraft	13-58
Figure 13.29. X-15 Tiltrotor Noise Test.....	13-60
Figure 13.30. Civil Tiltrotor Airworthiness Criteria.....	13-64

CHAPTER ONE

COMPUTATIONAL METHODS AND APPLICATIONS

1.1 INTRODUCTION

The objective of the Computational Methods and Applications Program is to develop and apply advanced analysis and computational methods for solving complex, fluid dynamics problems. Problems of interest include simulating turbulence and transition and computing complex flows (steady and unsteady, inviscid and viscous) over two- and three-dimensional geometries ranging in speed from zero to hypersonic and including such effects as mass injection and withdrawal. Additional objectives are to (1) demonstrate proof-of-concept computations for pioneering applications, (2) disseminate validated computer codes to the aerospace community and provide maintenance and consultation on their use and (3) develop innovative techniques for scientific visualization of flowfield solutions.

Currently, linearized and nonlinear isentropic, inviscid flow codes are very mature and are widely used throughout the aerospace community. Nonlinear, inviscid codes, i.e., Euler codes, coupled to interacting boundary-layer calculations are routinely used by the aircraft industry in the design process. Solutions to the Reynolds-averaged, Navier-Stokes equations for aircraft geometries and realistic aerospace vehicle components currently are being obtained.

The Computational Methods and Applications Program is focused on the technology needs of the aerospace community. These needs include (1) developing faster and more efficient numerical algorithms to facilitate solutions of the full Navier-Stokes equations by large-eddy, simulation/small-scale turbulence modeling and by direct simulation of all turbulence scales; (2) developing advanced geometric modeling and grid generation techniques for complex, three-dimensional configurations; (3) improving understanding of the effects of grid characteristics on solution accuracy, convergence and stability; (4) enhancing computational capabilities through development and use of advanced computer architectures and expert systems concepts and (4) developing improved methods for numerical simulation of aerothermodynamic flow phenomena associated with hypersonic cruise and maneuver vehicles including real-gas chemistry.

Program Manager: Mr. Edward T. Schairer
OAST/RF
Washington, DC 20546
(202)453-2819

ORIGINAL PAGE
BLACK AND WHITE PHOTOGRAPH

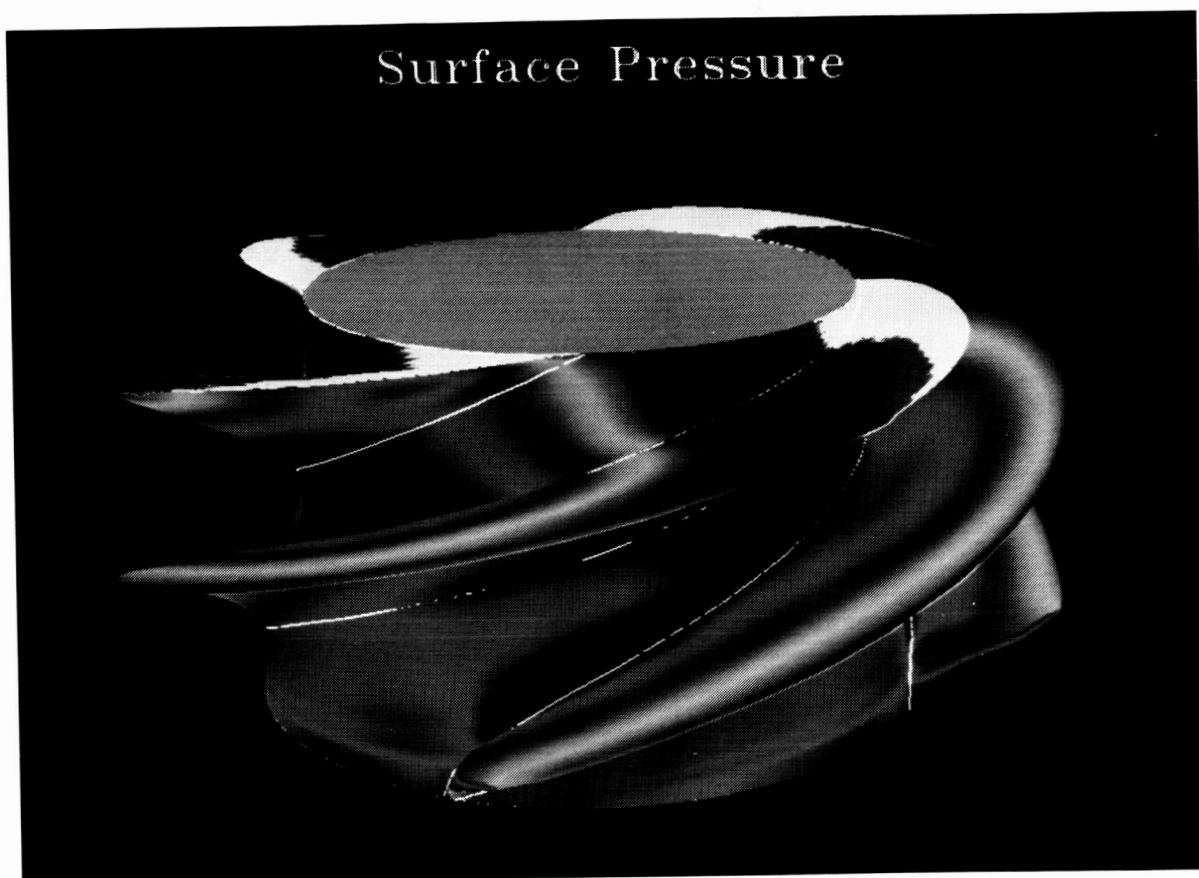


Figure 1.1. SSME Turbopump Inducer

This page is intentionally left blank.

1.1 INCOMPRESSIBLE FLOW SOLVER

1.2.1 Objective

To develop an efficient, accurate solver for three-dimensional, viscous, incompressible flow.

1.2.2 Accomplishments

An efficient code for solving the full, Navier-Stokes equations based on a new, implicit algorithm was developed. Preliminary solution of the space shuttle main engine turbopump inducer was obtained (See Figure 1.1).

1.2.3 Significance

A major impact on the design of rocket propulsion systems is expected. Computation with 250,000 grid points requires just 25 minutes on Cray Y-MP.

1.2.4 Status/Plans

Further validation of the code and complete impeller simulation is in progress.

S. Yoon and D. Kwak
Applied Computational Fluids Branch
Ames Research Center
(415)604-4482

1.3 NAVIER-STOKES SOLUTIONS ON MASSIVELY PARALLEL COMPUTERS

1.3.1 Objective

To demonstrate the utility of a massively parallel computer for solving large, three-dimensional Navier-Stokes problems.

1.3.2 Approach

The approach involved implementing three-dimensional Navier-Stokes flow code on the Connection Machine with 32,768 processors.

1.3.3 Accomplishments

NASA achieved computation rates comparable to supercomputer performance.

1.3.4 Significance

Dramatic speedups in computation rates can be achieved with massively parallel computers.

1.3.5 Status/Plans

NASA is continuing development and improvement of a three-dimensional Navier-Stokes flow solver.

D. C. Jespersen and C. Levit
Computational Fluid Dynamics Branch
Ames Research Center
(415)604-6742

ORIGINAL PAGE
BLACK AND WHITE PHOTOGRAPH

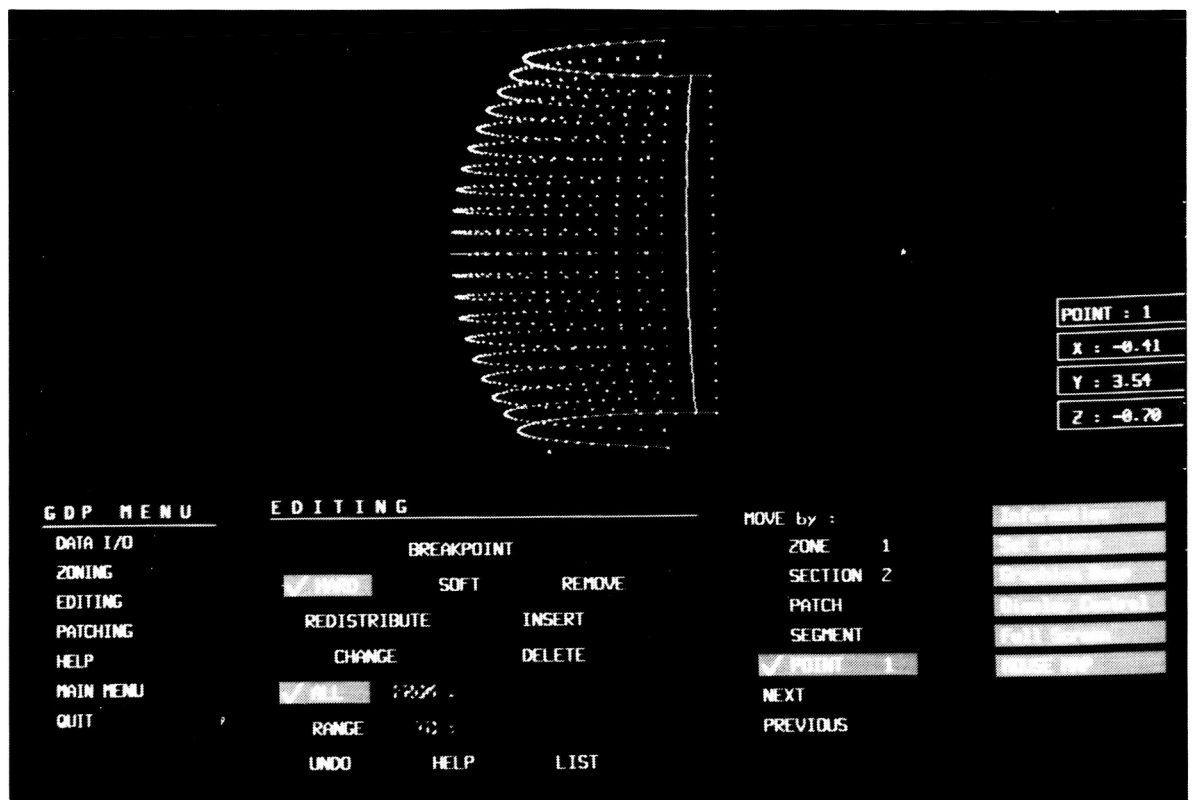


Figure 1.2. Ames Interactive Surface Editing Tool

1.4 SURFACE AND GRID GENERATION SOFTWARE

1.4.1 Objective

To develop software for accelerating surface definition and grid generation in Computational Fluid Dynamics (CFD).

1.4.2 Accomplishments

NASA completed an interactive, geometry-editing and surface-grid-generation software tool for three-dimensional flow (See Figure 1.2).

1.4.3 Significance

This software is the first step in the development of a powerful, integrated aerospace design tool which quickly can apply CFD to aerodynamic design issues.

1.4.4 Status/Plans

NASA is continuing development of interactive surface definition and grid generation software and incorporating the latest grid generation, evaluation and adaption research. In addition, a knowledge base for future automation using artificial intelligence is being constructed.

W. R. Van Dalsem and A. A. Vogel
Applied Computational Fluids Branch
Ames Research Center
(415)604-4469

ORIGINAL PAGE
BLACK AND WHITE PHOTOGRAPH

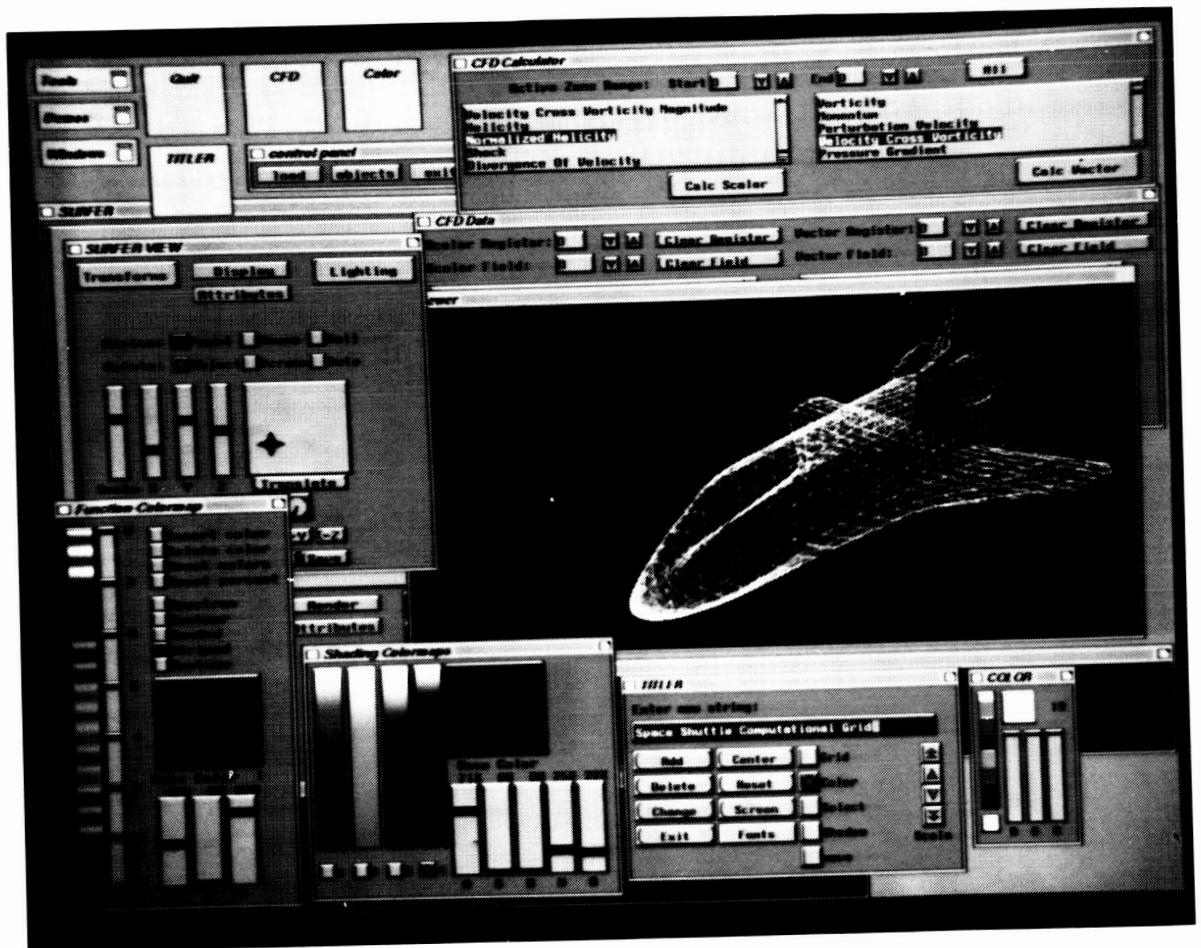


Figure 1.3. Flow Analysis Software Tools

1.5 FLOW VISUALIZATION SOFTWARE

1.5.1 Objective

To develop software for more effective analysis of results from fluid dynamics experiments and computations.

1.5.2 Accomplishments

NASA created a new program, Flow Analysis Software Tools (FAST), that contains more functionality than the existing programs (PLOT3D, GAS, SURF and RIP), unifies the user interface for the functions, exploits the features of the new graphics workstations and utilizes distributed processing (See Figure 1.3).

1.5.3 Significance

This program provides a major improvement in performance and ease of use of software for visualization of fluid dynamic results.

1.5.4 Status/Plans

The software is ninety percent complete with alpha testing underway.

V. R. Watson
Workstation Application Office
Ames Research Center
(415)604-6421

ORIGINAL PAGE
BLACK AND WHITE PHOTOGRAPH

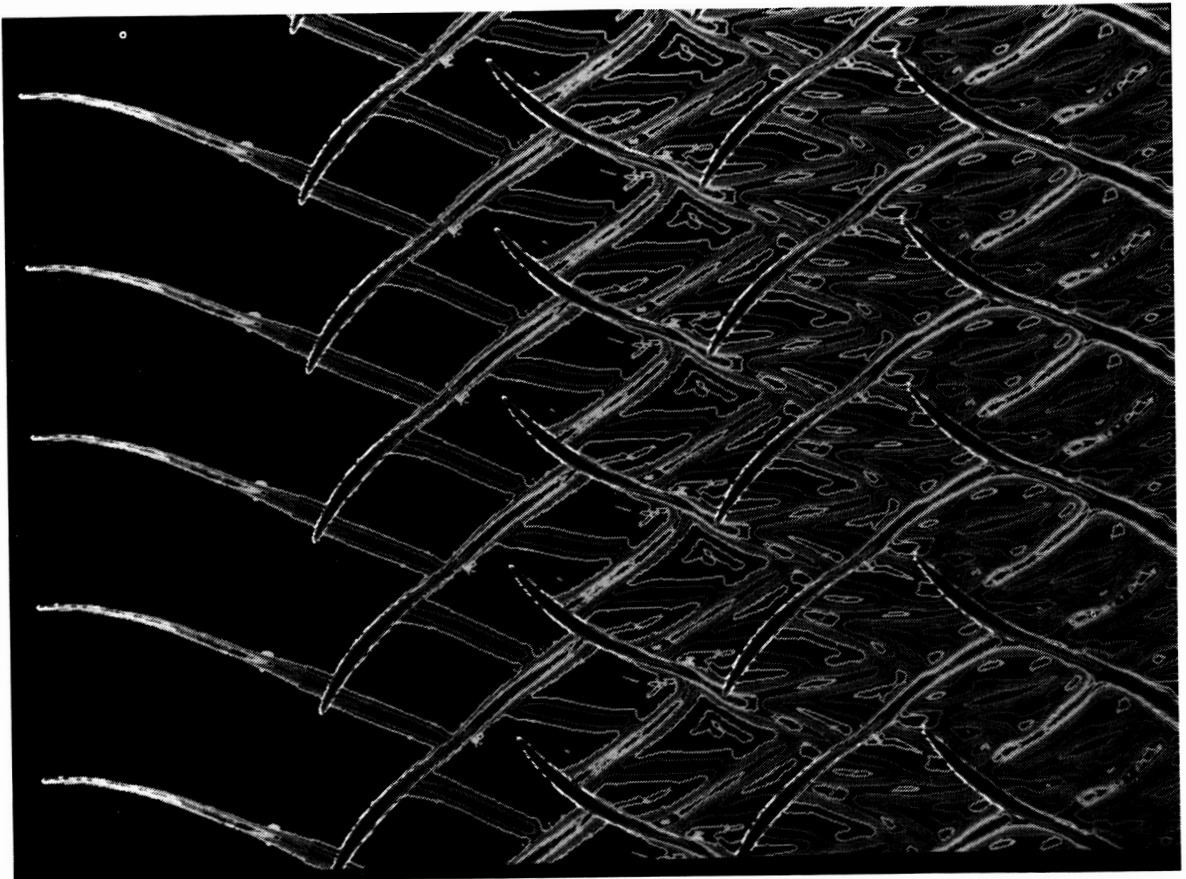


Figure 1.4. Instantaneous Entropy Contours in a 2.5 Stage Compressor

1.6 COMPUTATION OF MULTI-STAGE COMPRESSOR FLOWS

1.6.1 Objective

To develop capability for calculating unsteady viscous flows within multi-stage turbomachinery.

1.6.2 Accomplishments

NASA calculated two-dimensional flow in a 2.5 stage compressor with good agreement between computed time-averaged pressures and experimental data. NASA implemented a Baldwin-Lomax turbulence model in each airfoil's frame of reference (See Figure 1.4).

1.6.3 Significance

A better understanding of unsteady flow in turbomachinery will lead to reliable designs that are more efficient, lighter and more compact.

1.6.4 Status/Plans

NASA plans to extend current capability for multi-stage turbomachinery calculations to three-dimensional flow.

K. L. Gundy-Burlet
Applied Computational Fluids Branch
Ames Research Center
(415)604-4475

ORIGINAL PAGE
BLACK AND WHITE PHOTOGRAPH

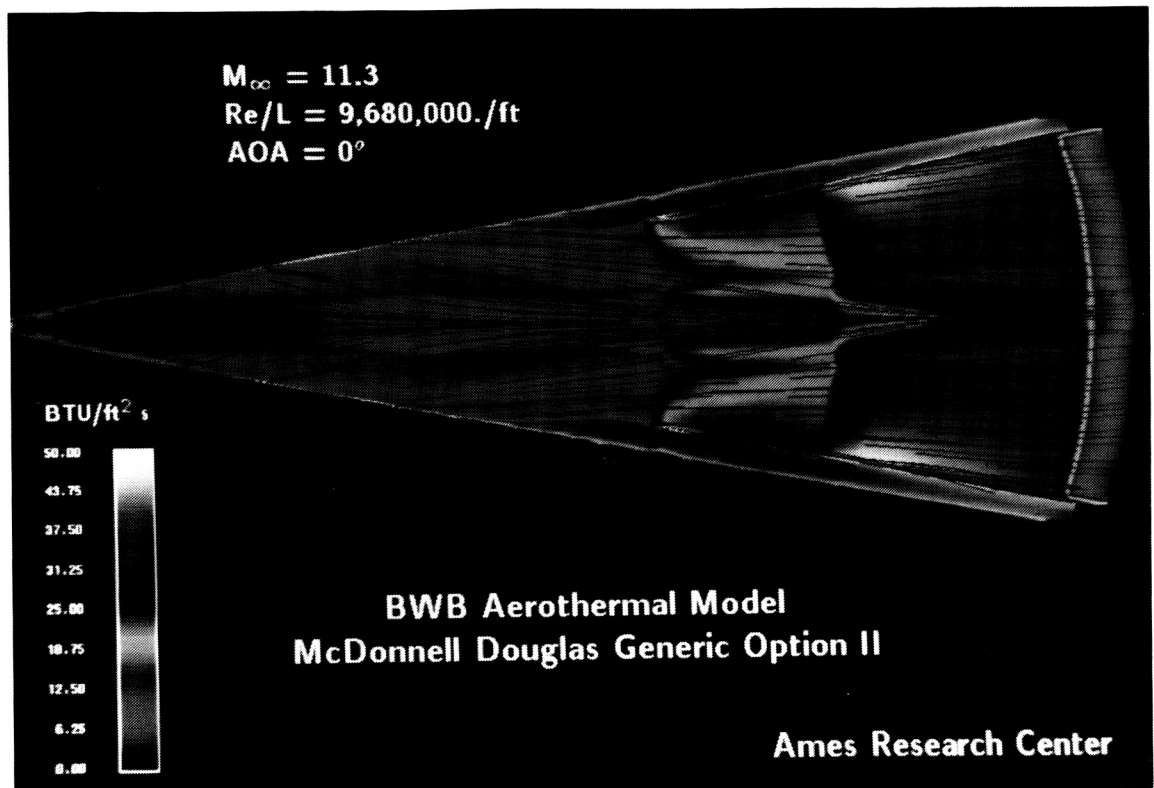


Figure 1.5. Lower Surface Heat Transfer Distribution

1.7 HYPERSONIC NAVIER-STOKES COMPUTATIONS

1.7.1 Objective

To develop codes for calculating viscous hypersonic flow about complicated geometries using equilibrium real-gas and non-equilibrium, finite-rate chemistry gas properties.

1.7.2 Accomplishments

NASA developed space-marching code for equilibrium and non-equilibrium flow and a time-marching code for equilibrium flow. NASA completed solutions for complicated geometries with both codes, which can be coupled. (See Figure 1.5).

1.7.3 Significance

Utilization of coupled codes allows cost-efficient solutions for complicated geometries and will play a key role in the national aerospace plane project.

1.7.4 Status/Plans

NASA will continue validation of codes and investigate nose to tail calculations. NASA also will include grid adaption in the space-marching code and non-equilibrium chemistry and nozzle/combustion capability in the time-marching code.

S. L. Lawrence, J. Flores and T. A. Edwards
Applied Computational Fluids Branch
Ames Research Center
(415)604-4050

ORIGINAL PAGE
BLACK AND WHITE PHOTOGRAPH

PRESSURE CONTOURS

$$M_{\infty} = 4.5$$

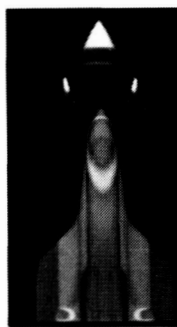
$$\alpha = +2^{\circ}$$

$$R_e = 6.95 \times 10^6$$

ASSUMPTIONS:

- SIMPLIFIED GEOMETRY
- NO PLUMES
- PRESCRIBED SRB TRAJECTORY

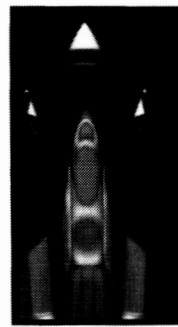
(MEAKIN, SUHS)



t = 0.00 sec



t = 0.34 sec



t = 0.68 sec

DISCRETIZATION

GRIDS:

ET 73X39X45

SRB 53X37X21

ORB 74X77X33

TIME-STEP =

1.36×10^{-3} sec

500 STEPS THROUGH BSM

BURN

BOOSTER

SEPARATION

MOTOR

(BSM)

BURN-TIME = 0.68 sec

Figure 1.6. Time-Accurate Simulation of the Space Shuttle
SRB Separation Sequence

1.8 UNSTEADY MULTIPLE BODY AERODYNAMICS

1.8.1 Objective

To develop a capability for time-accurate calculation of viscous flow over general three-dimensional multiple bodies in relative motion.

1.8.2 Approach

The approach involved developing a computer code to solve the flowfield around a space shuttle in launch configuration, including orbiter, external tank and Solid Rocket Boosters (SRB).

1.8.3 Accomplishments

NASA obtained a time-accurate simulation of aerodynamics during SRB separation (See Figure 1.6).

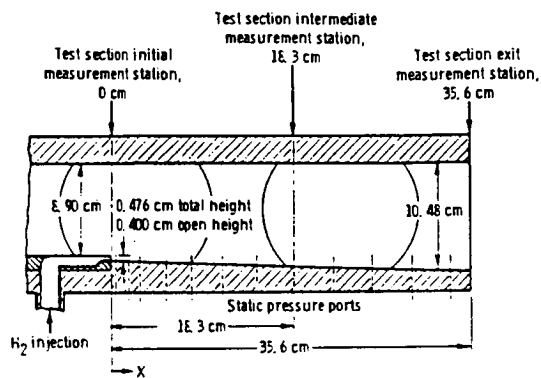
1.8.4 Significance

This program analyzes the aerodynamics problems during launch from lift-off to final vehicle separation. These problems may occur with booster failure, emergency escape procedures or abnormal flight trajectories.

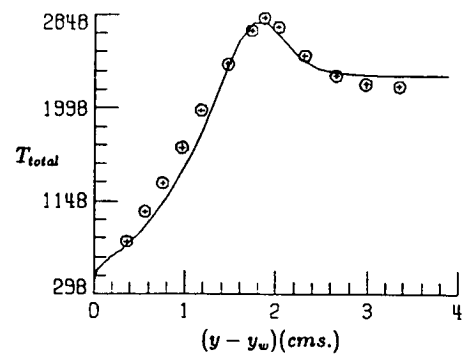
1.8.5 Status/Plans

NASA plans to improve efficiency and accuracy of basic algorithms and to validate codes. NASA also will develop trajectory prediction routines.

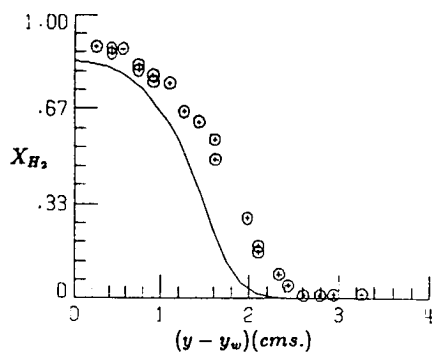
P. G. Buning
Applied Computational Fluids Branch
Ames Research Center
(415)604-5194



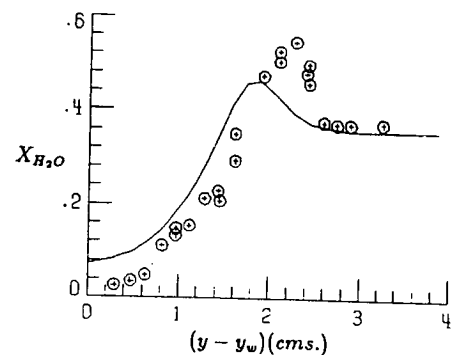
Schematic diagram of test section.



Total temperature comparison.



H_2 mole fraction comparison.



H_2O mole fraction comparison.

Figure 1.7. Parabolized Navier-Stokes Algorithm for Chemically Reacting Flows

1.9 PARABOLIZED NAVIER-STOKES ALGORITHM FOR CHEMICALLY REACTING FLOWS

1.9.1 Objective

To develop computational techniques for the efficient modeling of high-speed, chemically reacting flows typical of those found in scramjets.

1.9.2 Approach

A generalized algorithm was used to solve the parabolized form of the governing equations for three-dimensional, chemically reacting flows with finite-rate chemistry.

1.9.3 Accomplishments

A computer code was developed to solve the parabolized governing equations for chemically reacting flows. The second-order algorithm is based on the MacCormack explicit scheme. It has the capability to treat the chemical source term implicitly as well as accounting for the multicomponent diffusion and convection of chemical species. The complex interactions that occur in a chemically reacting flow can be efficiently computed by the parabolized solver. A test case was considered in order to demonstrate the capabilities of the algorithm. It involved streamwise hydrogen injection at sonic velocity into a Mach 2.44 vitiated air stream and the subsequent turbulent mixing leading to chemical reaction. The hydrogen-air combustion was modeled with detailed chemical kinetics involving nine species and a 18-step reaction. Comparisons were made with available experimental data, plotted as functions of the distance from the lower wall at $x = 0.356$ m location. It may be observed that the computed flow quantities possess the essential trends exhibited by the experimental data. The quantitative agreement between the computed and experimental profiles for the total temperature and hydrogen mole fraction is reasonable; however, the computed profile for the water mole fraction underpredicts the peak when compared with the experimental data (See Figure 1.7).

1.9.4 Significance

The use of parabolized governing equations instead of the full unsteady governing equations results in a significant reduction in computer memory requirements and execution times. The parabolized solver can be used in conjunction with the existing elliptic version of the code for accurate and efficient computation of scramjet flow fields, leading to improvements in combustor design.

1.9.5 Status/Plans

A characteristic-based upwind scheme using Roe's flux-difference splitting algorithm will be incorporated to enhance the capabilities of the parabolized code.

H. Kamath and J.P. Drummond
Computational Methods Branch
Langley Research Center
(804)864-2321

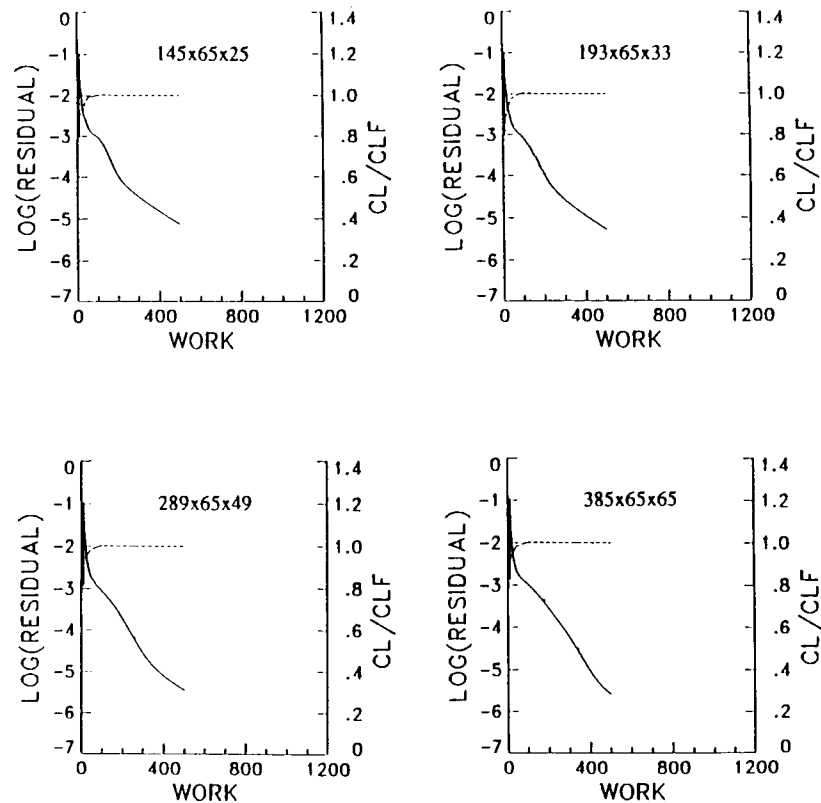


Figure 1.8. Effect of Grid Density on Convergence

1.10 MULTIGRID ACCELERATION TECHNIQUE FOR NAVIER-STOKES EQUATIONS

1.10.1 Objective

To develop an efficient numerical technique for predicting high Reynolds number, transonic flows over aircraft components.

1.10.2 Approach

A multi-stage, Runge-Kutta time-stepping scheme with multigrid acceleration technique was employed for computing steady-state solutions of the thin-layer, Navier-Stokes equations. A Baldwin-Lomax turbulence model was used for turbulence closure.

1.10.3 Accomplishments

A numerical scheme was developed for computing high Reynolds number viscous flows over aircraft components. The efficiency of the scheme was enhanced significantly through a multigrid acceleration technique. The multigrid technique resulted in reducing the computational time by almost an order of magnitude. The scheme was applied to solve the flow over a finite lifting wing, namely the ONERA M6 wing. Because of the improved efficiency of the code, essentially grid converged solutions were obtained for the attached flow case. Figure 1.8 shows the convergence history for four mesh densities. Based on the results shown here, it is clear that the multigrid technique is performing quite. It results in relatively small differences in the number of iterations required to obtain converged results over such a large variation in total number of mesh points.

1.10.4 Significance

A numerical procedure of the type described here can be used to conduct parametric studies in an efficient manner.

1.10.5 Status/Plans

The method will be generalized to accommodate block-structured grids so that flow over complex configurations can be computed.

V. N. Vatsa and Bruce W. Wedan
Theoretical Aerodynamics Branch
Langley Research Center
(804)864-2236

($M_\infty = 0.73$, $\alpha = 2.79^\circ$, $Re = 6.5 \times 10^6$)

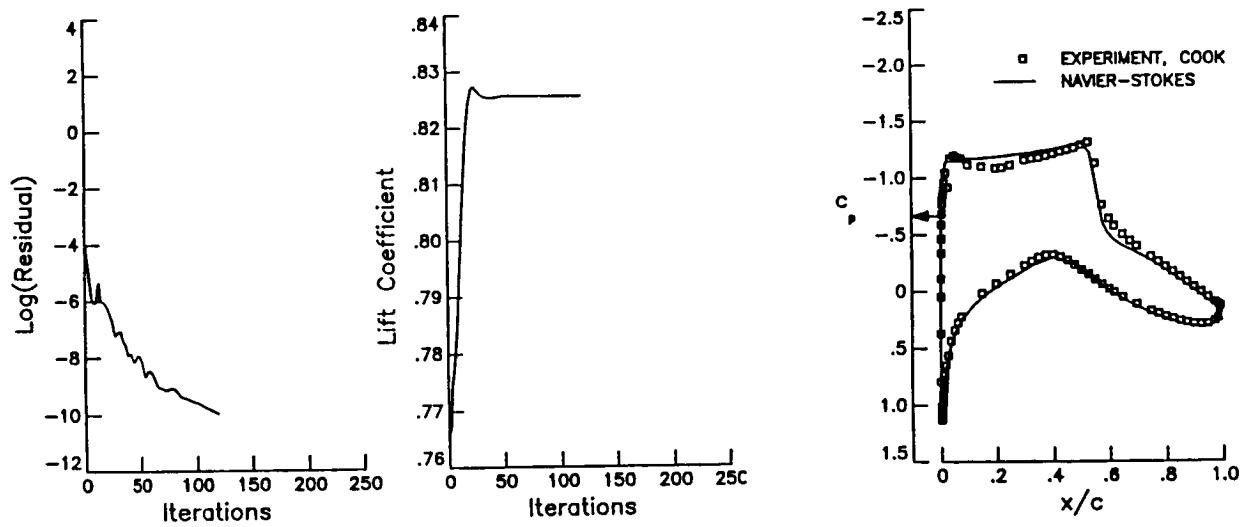


Figure 1.9. Transonic Turbulent Flow Over an RAE7822 Airfoil

1.11 A PRECONDITIONED CONJUGATE GRADIENT METHOD FOR THE COMPRESSIBLE NAVIER-STOKES EQUATIONS

1.11.1 Objective

To develop an implicit algorithm for solving the compressible Navier-Stokes equations for structured and unstructured applications.

1.11.2 Approach

The spatial discretization was performed using an upwind scheme. The system of linear equations was solved at each time step by a preconditioned iterative procedure. An incomplete LU factorization served as the preconditioner followed by the well known procedure of Generalized Minimum Residual algorithm (GMRES).

1.11.3 Accomplishments

Results were obtained for inviscid and viscous transonic test cases in two-dimensions (See Figure 1.9). Although solving the linear system exactly at each time step can lead to quadratic convergence (Newton's method), it was found to be far more efficient to solve the linear system inexactly and then to proceed to the next time step. A restart GMRES procedure with three cycles and four search directions was found to be optimal over a wide range of problems. An algebraic turbulence model also was incorporated. A domain decomposition method in which the domains are made up of rings around the airfoil, was implemented on a parallel machine. The preconditioning and the forward and back solution stages are all done in parallel.

1.11.4 Significance

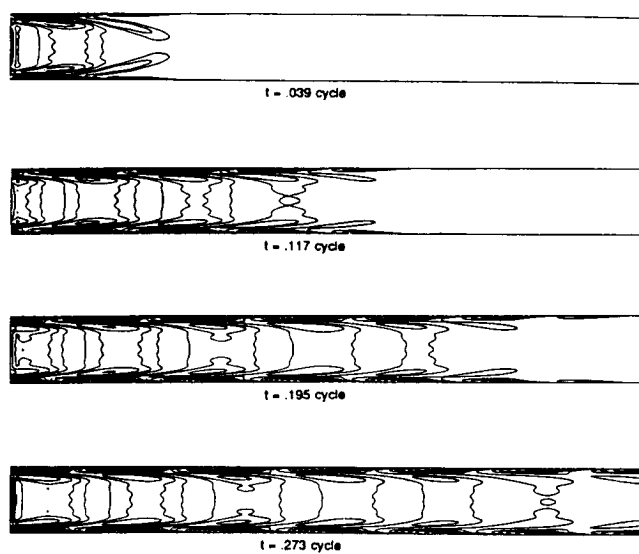
The method requires much less memory than a direct solver. The algorithm is competitive with the best current schemes, but has wide applications in parallel computing and unstructured grids.

1.11.5 Status/Plans

Research is being pursued on extending the ideas to unstructured meshes and three dimensional applications. Implementation on a distributed memory parallel machine also is planned.

V. Venkatakrishnan
Theoretical Aerodynamics Branch
Langley Research Center
(804)864-2224

CHANNEL FLOW STARTUP



WALL VORTICITY

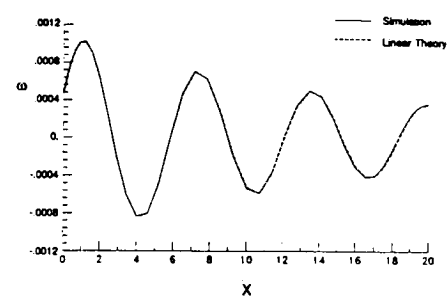


Figure 1.10. Non-Reflecting Outflow Boundary Treatment

1.12 NON-REFLECTING OUTFLOW BOUNDARY TREATMENT FOR TRANSITION SIMULATIONS

1.12.1 Objective

To develop a computational technique which allows the accurate simulation of spatially-developing transition physics, eliminating the numerically-motivated assumptions of previous transition simulations.

1.12.2 Approach

For accuracy and efficiency considerations, the discretization method of choice for such simulations is spectral collocation. This method is pathologically sensitive to incorporation of mathematically well-posed boundary conditions; thus, the development of a boundary condition at the outflow end of a computational domain, which is capable of passing an arbitrary unsteady disturbance without reflection back into the domain, was problematic. Outflow boundary conditions suggested from CFD applications of low-order, finite-difference methods were shown to be incapable of performing in this context.

1.12.3 Accomplishments

A viable outflow treatment, based on earlier spectral multi-domain technology developed earlier, was developed for the incompressible Navier-Stokes equations. The method currently is being verified against linear stability theory for the problem of plane Poiseuille flow in a channel and against linear and weakly-nonlinear theory for boundary-layer flow. Contours of disturbance vorticity were used to show how the leading wave of a periodic disturbance imposed at the inflow boundary passes out of the domain of interest without reflection back into the domain. The imposed upstream disturbance is the most unstable eigenmode of the corresponding linear stability problem; quantitative verification with linear theory also shows good performance of the method. An additional test problem, possessing a global instability character as opposed to the convective instability of channel and boundary-layer flow, also was studied (See Figure 1.10).

1.12.4 Significance

Previous transition simulations used the ansatz of a linear transformation between time and downstream distance and the assumption of a parallel mean flow to allow periodic streamwise discretizations to be used. This neglects all effects of streamwise change of the mean flow including normal velocity effects and creates a difficulty in relating quantitatively the development of simulated transition features to experimental data. The present method allows transition simulations to be carried out in the proper, spatially developing setting.

1.12.5 Status/Plans

After detailed verification with linear theory for channel and boundary-layer flow is complete, the technique will be incorporated into a simulation code which will allow the study of the effects of pressure gradient, roughness, external environment, etc., on

transition in boundary layers. Transition in free shear layers, for which nonparallel effects are important, also will be studied.

Craig L. Streett
Theoretical Aerodynamics Branch
Langley Research Center
(804)864-2230

$$x/L = 0.7 ; \alpha = 20.5^\circ$$

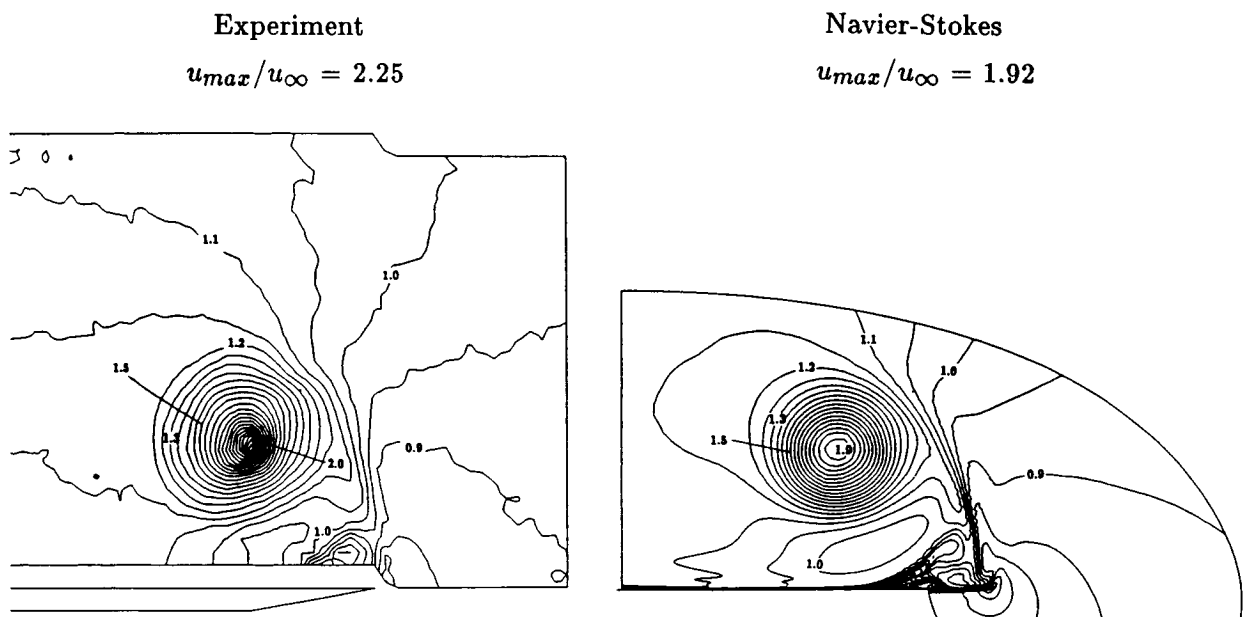


Figure 1.11. Streamwise Velocity Contours

1.13 AN EMBEDDED- AND MULTIPLE- GRID ALGORITHM APPLIED TO DELTA WINGS

1.13.1 Objective

To develop a capability to increase the local resolution of Navier-Stokes calculations efficiently and to compare them with detailed experimental measurements in the core of the leading-edge vortex of a delta wing at large incidence.

1.13.2 Accomplishments

An embedded-grid scheme coupled with multigrid convergence acceleration was incorporated into the Navier-Stokes code CFL3D. Applications were made to a 75 degree swept delta wing at 20.5 degree angle of attack. Streamwise velocity contours from experiment and computation are at 70 percent of the distance from the wing apex (See Figure 1.11). The maximum streamwise velocity from the computation is slightly lower than the experimental value in the vortex core but is substantially higher than the computation reported previously using the single-grid scheme.

1.13.3 Significance

For the first time, greater resolution was demonstrated from 3-D Navier-Stokes calculations without large increases in computer resource requirements by using embedded grids. This technology is an essential building block for a 3-D, self-adaptive grid, Navier-Stokes code.

1.13.4 Status/Plans

Work is underway to improve further the numerical results by embedding finer grids and to improve/automate the process of identifying regions where increased resolution is necessary.

J. L. Thomas and S. L. Krist
Analytical Methods Branch
Langley Research Center
(804)864-2146

ORIGINAL PAGE
BLACK AND WHITE PHOTOGRAPH

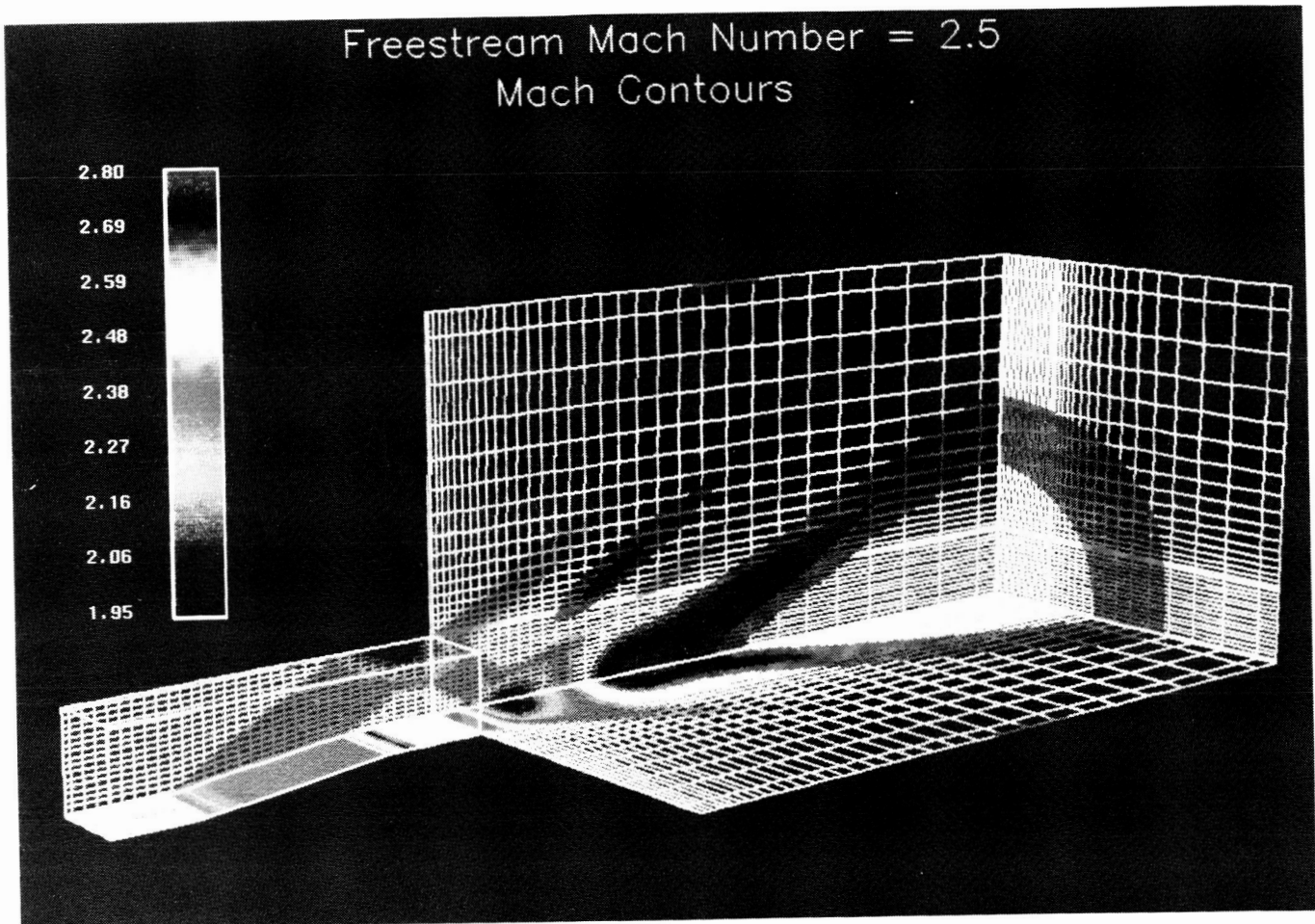


Figure 1.12. 3 Degree Ramp Nozzle and Plume

1.14 MULTIBLOCK MULTIGRID CALCULATIONS OF NOZZLE EXHAUST FLOWS

1.14.1 Objective

The object was to develop a flexible, efficient computational tool for the study of three-dimensional nozzle plume flow.

1.14.2 Approach

An existing three-dimensional isentropic Euler code was modified to add the capability of multiple block grids. The multiblock strategy provided greater geometric flexibility than the usual single block method. Odd shaped flows and combinations of internal and external flows were easily handled. To maintain good rates of convergence, multigrid acceleration was used to accelerate either an explicit modified Warming-Beam algorithm or an implicit approximate factorization algorithm. Spatial discretization was carried out using van Leer's flux vector splitting with MUSCL type differencing.

1.14.3 Accomplishments

A flexible, efficient Euler equation solver was developed using a multiblock structure and multigrid acceleration. Several plume flows were calculated (See Figure 1.12). Mach 2.5 flow entered the nozzle from the left. The flow was first compressed by a three degree ramp and then turned back three degrees to realign with the freestream direction. This flow then was exited to a freestream of Mach 2.5. The ensuing shocks, expansions and reflections are apparent with no distortions caused by the block interfaces.

1.14.4 Significance

Inviscid calculations of nozzle exhaust flows can be performed easily and quickly. This type of calculation is very important for configurations with highly integrated exhaust nozzles such as the NASP.

1.14.5 Status/Plans

Additional flexibility will be incorporated in the multiblock structure and the isentropic Euler equations will be replaced with the full Euler equations. Viscous terms then will be added.

Frank E. Cannizzaro, N. Duane Melson and Ernst von Lavante
Theoretical Aerodynamics Branch
Langley Research Center
(804)864-2227

ORIGINAL PAGE
BLACK AND WHITE PHOTOGRAPH

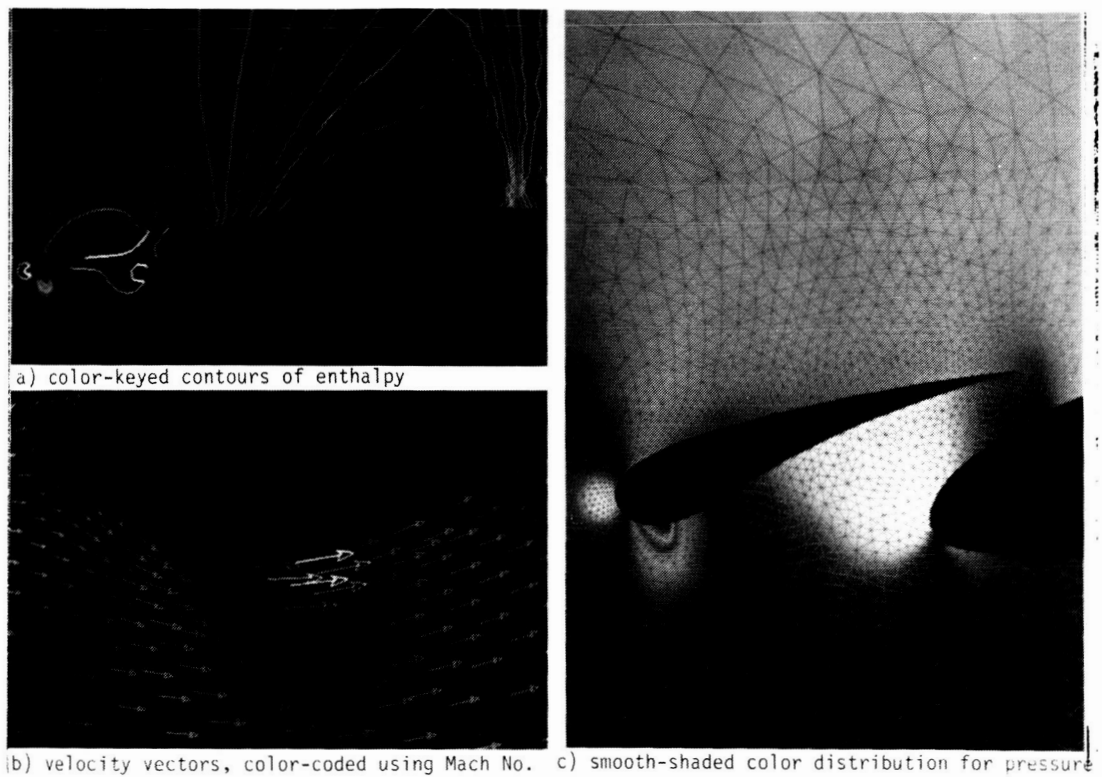


Figure 1.13. Graphical Display of Fluid Flow Results
on Unstructured Grids

1.15 GRAPHICAL DISPLAY OF FLUID FLOW RESULTS ON UNSTRUCTURED GRIDS

1.15.1 Objective

To develop software using the X-windows graphics protocol on inexpensive color workstations for the display of CFD results on unstructured as well as structured flowfield grids to provide a researcher with an easily-learned, interactive ability to rapidly examine the details of computational flowfield results.

1.15.2 Approach

Workstation software was written that employs a convenient, mouse-driven user interface with pull-down menus for feature selection and other mouse-button/motion combinations for rapid manipulation of the image. Since typical low-end color workstations have graphics hardware for drawing only constant-color 2-D lines, curves and polygons (filled and unfilled), software is used to emulate smooth-shading and 3-D drawing. This emulation also is necessary with current X-windows functionality.

1.15.3 Accomplishments

The graphics software initially was implemented on VAX workstations with 256-color capability. The user can select some typical window displays for viewing a set of 2-D unstructured results. A gray-scale rendition of the color image can be generated for output to a Post Script laser printer (See Figure 1.13).

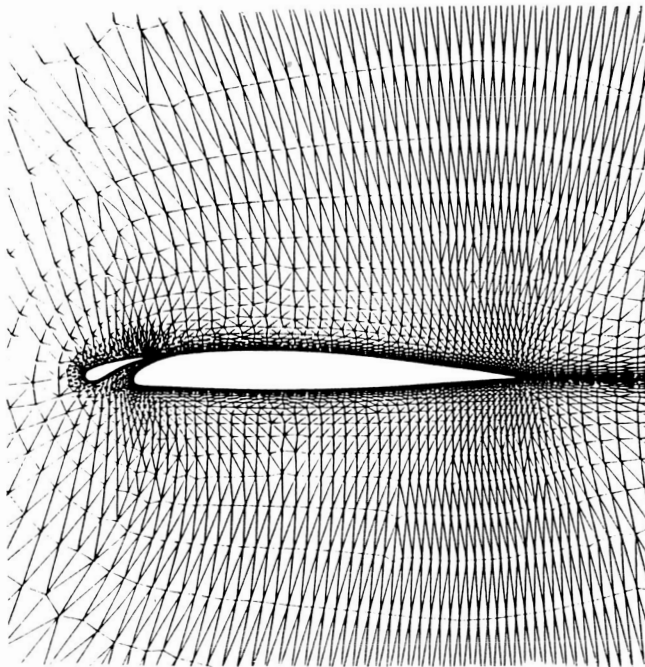
1.15.4 Significance

Researcher productivity is enhanced by the ability to use the inexpensive workstation on one's desk for the routine display of computational grids and flowfield solutions and as an alternative to competing for time on the scarce and expensive resources of a central, sophisticated 3-D graphics workstation.

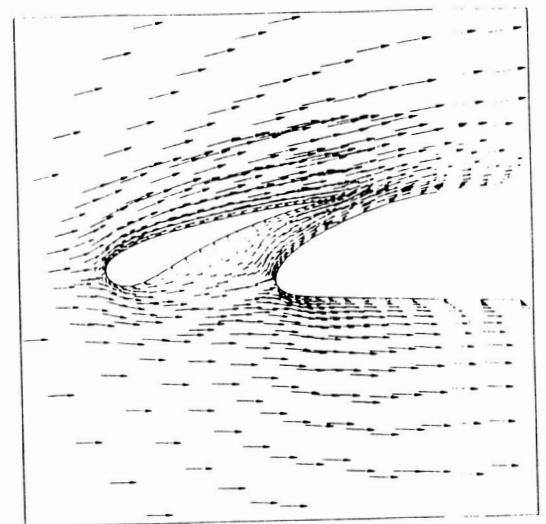
1.15.5 Status/Plans

Work is underway to provide 3-D hidden-surface removal in the workstation software. Additional features will be added for improved display control, color manipulation, labeling and extended functionality.

Robert P. Weston
Analytical Methods Branch
Langley Research Center
(804)864-2149



Unstructured Mesh



Computed Velocity Vectors

Mach = 0.5 Re = 5000 Incidence = 3°

Figure 1.14. Navier-Stokes Solutions on Unstructured Meshes

1.16 MULTIGRID SOLUTION OF THE NAVIER-STOKES EQUATIONS ON UNSTRUCTURED MESHES

1.16.1 Objective

To develop an accurate and efficient method for computing viscous compressible flow about complex configurations.

1.16.2 Approach

The steady-state, two-dimensional Navier-Stokes equations were solved on an unstructured, triangular mesh by a Galerkin, finite-element approach. Mesh adaptivity is employed to enhance solution accuracy and an unstructured, multigrid technique is used to accelerate the convergence to steady-state.

1.16.3 Accomplishments

A method for generating two-dimensional, unstructured meshes with highly stretched triangular elements in the boundary-layer wake regions, suitable for viscous flow calculations, was developed. The method is based on the application of local stretching functions to a triangulation technique previously employed for inviscid flow calculations. An accurate and efficient procedure for the laminar Navier-Stokes equations on highly stretched unstructured meshes in two dimensions was developed. The equations are discretized in space using a Galerkin, finite-element formulation and the steady-state solution was obtained by integrating the equations in time using a five-stage, Runge-Kutta, time-stepping scheme. Convergence was accelerated by use of a multigrid also developed for unstructured meshes and improved solution accuracy was obtained through the use of adaptive mesh enrichment. Navier-Stokes solutions were obtained for low Reynolds number flows over multi-element airfoil configurations (See Figure 1.14).

1.16.4 Significance

The ability to predict viscous flows about complex geometries, such as high-lift multi-element airfoil configurations in 2-D and aircraft configurations in 3-D, are of particular importance to the aircraft industry.

1.16.5 Status/Plans

Future work will center on the inclusion of a suitable turbulence model for high Reynolds number calculations on unstructured mesh about arbitrary two-dimensional configurations. The extension of the solver to three dimensions also is planned.

Dimitri J. Mavriplis
Theoretical Aerodynamics Branch
Langley Research Center
(804)864-2213

ORIGINAL PAGE
BLACK AND WHITE PHOTOGRAPH

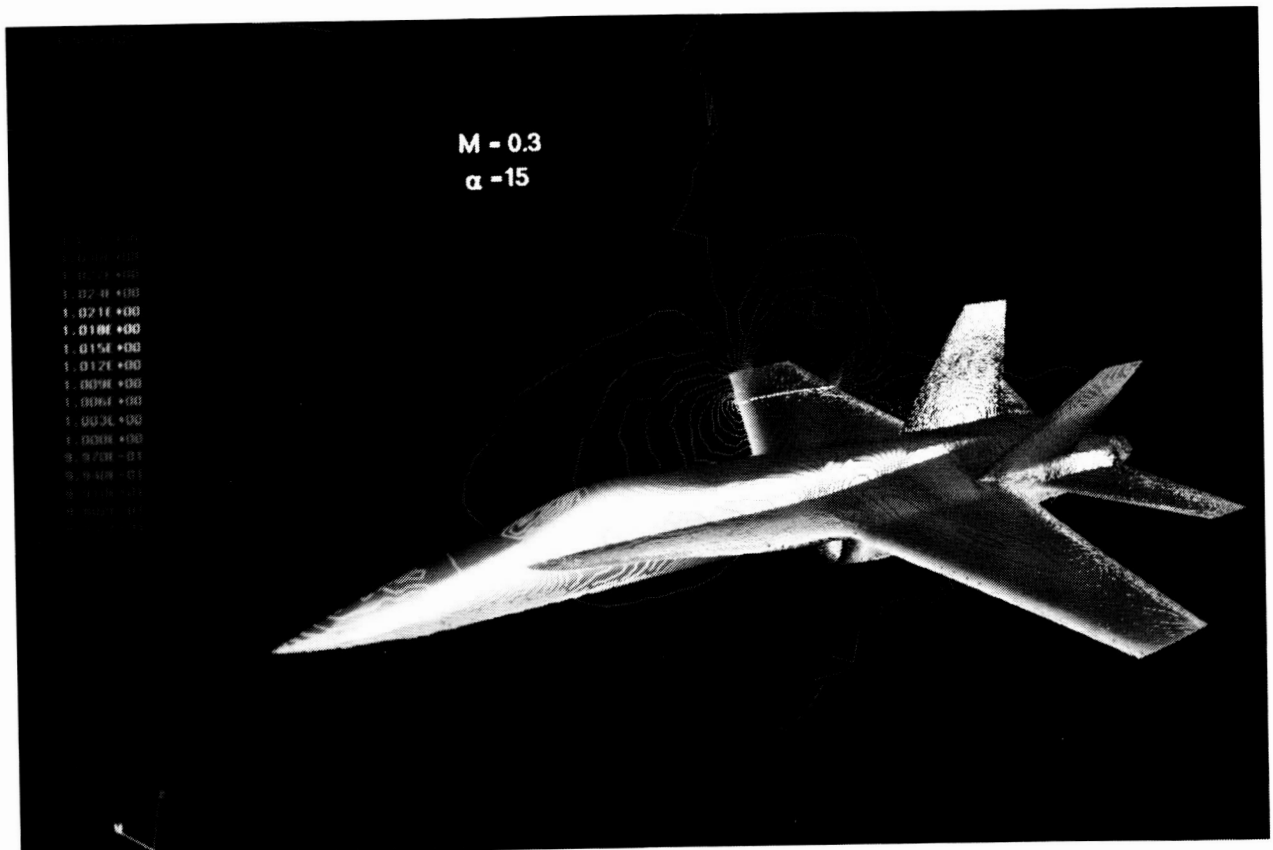


Figure 1.15. Pressure Contours on F-18 Airplane

1.17 UNSTRUCTURED GRID AND FLOW SOLUTION FOR F-18 AIRPLANE

1.17.1 Objective

To compute the inviscid flow over the F-18 configuration.

1.17.2 Approach

Unstructured grids are well-suited for complex configurations such as the F-18 aircraft. An unstructured grid generator is being developed which uses the advancing front technique to propagate a set of fine segments over a surface to generate triangles and then to propagate that set of triangles through space to fill the computational volume with tetrahedrons. A finite element flow code is being developed to solve the steady state Euler equations on such meshes and a postprocessing code is being developed for displaying the properties of the resulting flowfield.

1.17.3 Accomplishments

A grid was generated for the F-18 which consists of 642,000 tetrahedrons which connect 114,700 points, 13,400 of which define the aircraft surface. Figure 1.15 shows pressure contours on the aircraft surface and a vertical plane which intersect the wing. These contours represent the flow solution for a freestream Mach number of 0.30 and an angle of attack of 15 degrees. The solution was obtained after 159 minutes on the NAS Cray-2 supercomputer.

1.17.4 Significance

Using unstructured grids and accompanying flow solvers, flowfield solutions can be generated for complete complex aircraft configurations.

1.17.5 Status/Plans

The grid generator and flow solver codes will be made more robust and efficient in order to decrease the time required to develop the mesh and obtain the flow solution.

Shahyar Pirzadeh and Clyde Gumbert
Theoretical Aerodynamics Branch
Langley Research Center
(804)864-2221

ORIGINAL PAGE
BLACK AND WHITE PHOTOGRAPH

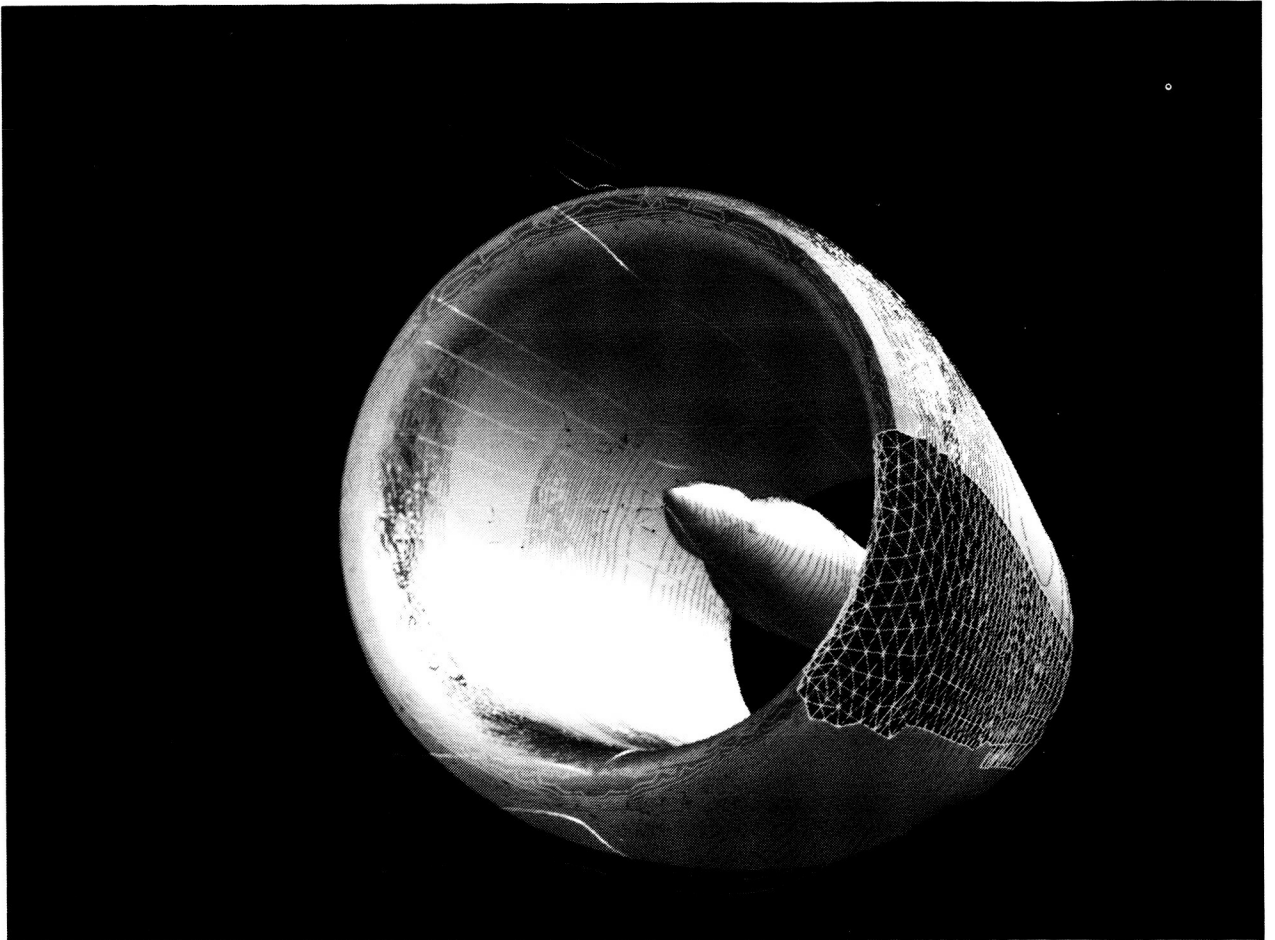


Figure 1.16. Unstructured Grid and Flow Solution for a Typical Inlet Configuration

1.18 UNSTRUCTURED GRID AND FLOW SOLUTION FOR A TYPICAL INLET CONFIGURATION

1.18.1 Objective

To compute the inviscid flow around a typical inlet configuration.

1.18.2 Approach

An unstructured grid generator and finite element flow solver package developed for complex configurations was applied to this nearly axisymmetric engine configuration.

1.18.3 Accomplishments

The grid developed for the configuration (See Figure 1.16) consists of 26,800 points defining 144,000 tetrahedrons. Contours of the surface pressure are displayed as well as particle traces at the symmetry plane. These contours and particle traces represent the flow solution for a freestream Mach number of 0.82 and an angle of attack of four degrees. The solution was obtained after 3000 time steps which required about three hours on the NAS Cray-2 supercomputer.

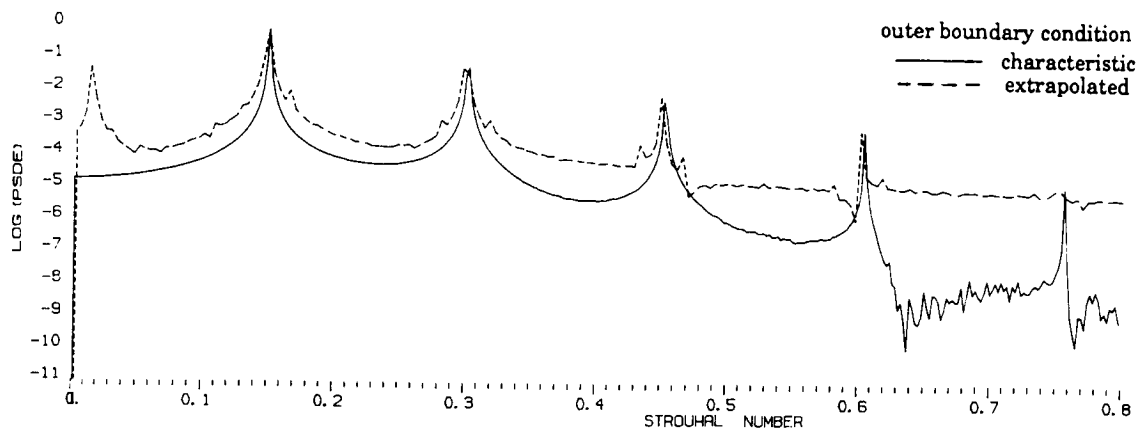
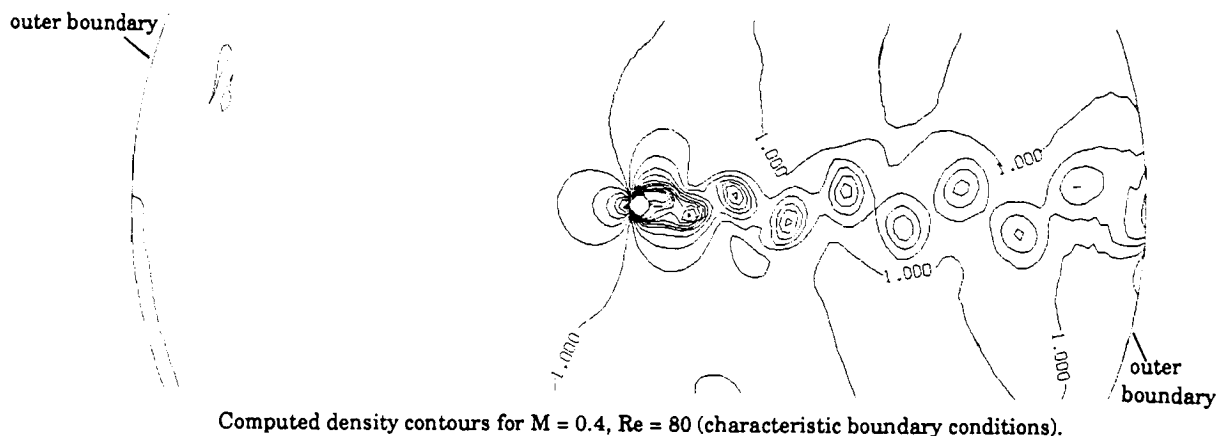
1.18.4 Significance

Using the unstructured grid and flow solver techniques, flow solutions can be obtained for complex configurations of which engine nacelles and pylons are often integral parts.

1.18.5 Status/Plans

The grid generation and flow solver codes need to be made more robust and more efficient so that the flowfield over configurations with over half a million tetrahedrons can be obtained with less computation time and effort.

Paresh Parikh and Clyde Gumbert
Theoretical Aerodynamics Branch
Langley Research Center
(804)864-2221



Frequency spectra for old (extrapolated) and new (characteristic) outer boundary conditions ($M = 0.4$, $Re = 80$).

Figure 1.17. Analysis of Low Frequency Fluctuations in a Cylinder Wake

1.19 ANALYSIS OF LOW FREQUENCY FLUCTUATIONS IN A CYLINDER WAKE

1.19.1 Objective

To determine the origin of low-frequency fluctuations which were found in the computed wake behind a circular cylinder (von Karman vortex street), were not harmonically related to the shedding frequency and were similar to those found in an experimental study, by repeating the computations using the same, time-accurate, two-dimensional, compressible, Navier-Stokes finite-difference code and polar grid, but vary the Reynolds number and computational outer boundary conditions as needed to eliminate the low-frequency fluctuations.

1.19.2 Approach

In the previous study (at Reynolds number 80), special boundary conditions were used where the vortices pass through the outer computational boundary, but the flow through the rest of the boundary was expected to be close enough to the uniform free stream to extrapolate from the interior without adding disturbances. As part of the present study, these extrapolated boundary conditions were used for computations at a Reynolds number of 20, where no shedding occurs. The low frequency occurred as before, proving that it was not produced from the shed vortex wake. Location, Mach-number and domain-size dependencies for the low frequency suggested waves were being reflected in the computational domain.

1.19.3 Accomplishments

New nonreflecting boundary conditions were developed for the inflow and outflow computational boundaries, using incoming and outgoing Euler-equation characteristics. These boundary conditions eliminated the secondary frequency at both Reynolds number 20 and 80 (See Figure 1.17). Peaks corresponding to the secondary frequency and its harmonics were eliminated by the new boundary condition, while the shedding-frequency peaks are relatively unchanged.

1.19.4 Significance

The new nonreflecting boundary conditions remove an important source of spurious fluctuations in unsteady compressible flow computations while improving efficiency by allowing the computational domain to be limited. Also, in this particular case, the computations led to a re-examination of the experimental results which has indicated that there too the secondary frequency may be associated with reflections from boundary surfaces.

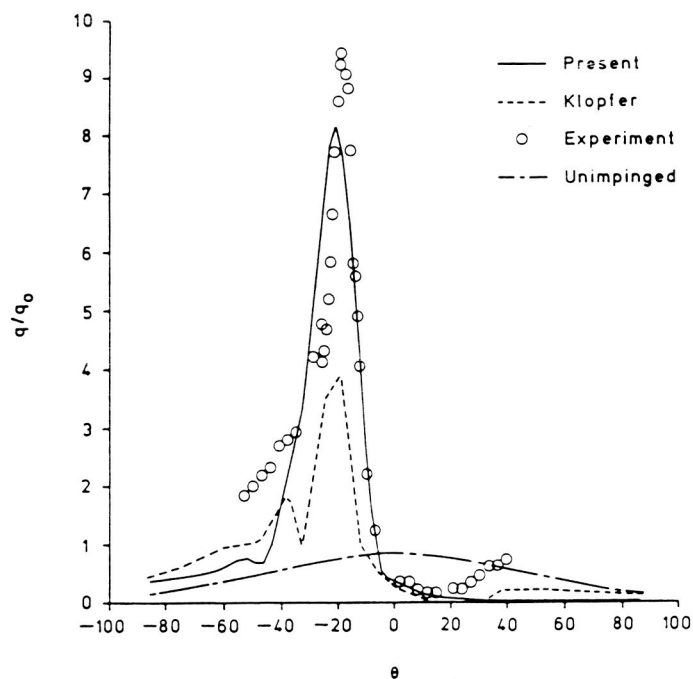
1.19.5 Status/Plans

Computations now are being made at higher Reynolds numbers, looking for indications of the beginning of transition.

ORIGINAL PAGE
BLACK AND WHITE PHOTOGRAPH



Mach number contours for the cowl forebody.



Variation of wall heat transfer for the cowl forebody.

Figure 1.18. Mach Number Contours for Cowl Forebody

1.20 SHOCK-SHOCK INTERACTION ON BLUNT BODIES IN HYPERSONIC FLOWS

1.20.1 Objective

To develop accurate solution procedures to determine the shock interference pattern and to accurately predict the surface pressure and the wall heat transfer for a shock impinging on the cowl lip at high Mach numbers.

1.20.2 Approach

The interaction of the bow shock with an extraneous impinging shock was studied by two dimensional Navier-Stokes computations. The governing equations were solved using a finite volume flux splitting algorithm ascribed to van Leer. The impinging shock was treated as a sharp discontinuity across which exact shock jump conditions were applied. The adaptive grid techniques were utilized to properly resolve the flowfield and accurately predict the heat transfer. The cowl plate of the scramjet inlet was modeled by a cylindrically blunted wedge and the forebody shock by the extraneous impinging shock.

1.20.3 Accomplishments

The blunt body solution was obtained in the presence of an impinging shock. The bow shock, shear layers and the boundary-layer were very well captured by the solution algorithm. The flow around the body was significantly altered due to shock-shock interaction. The pressure was amplified nine times and the heat transfer eight times the stagnation point values for the undisturbed blunt body flow. Laminar flow of air at 8.03 was considered. The surface was assumed to have a constant prescribed wall temperature. The results were compared with the available numerical and experimental data (See Figure 1.18).

1.20.4 Significance

When the forebody shock interacts with the inlet shock produced by the cowl leading edge, a very complex flowfield is produced with localized zone of high pressure and intense heating. The large temperature gradients cause thermal stresses which could result in structural failure. In order to relieve the influence of thermal stresses, some form of active cooling is needed. To determine the cooling requirements, pressure and heating rates on the body need to be predicted accurately.

1.20.5 Status/Plans

Efforts currently are underway to investigate the interaction of the forebody shock with the leading edge shock of the swept compression sidewall of a scramjet inlet. Due to orientation of the line of interaction, the flow is fully three dimensional for this configuration. Some preliminary results were obtained for this case and are being analyzed.

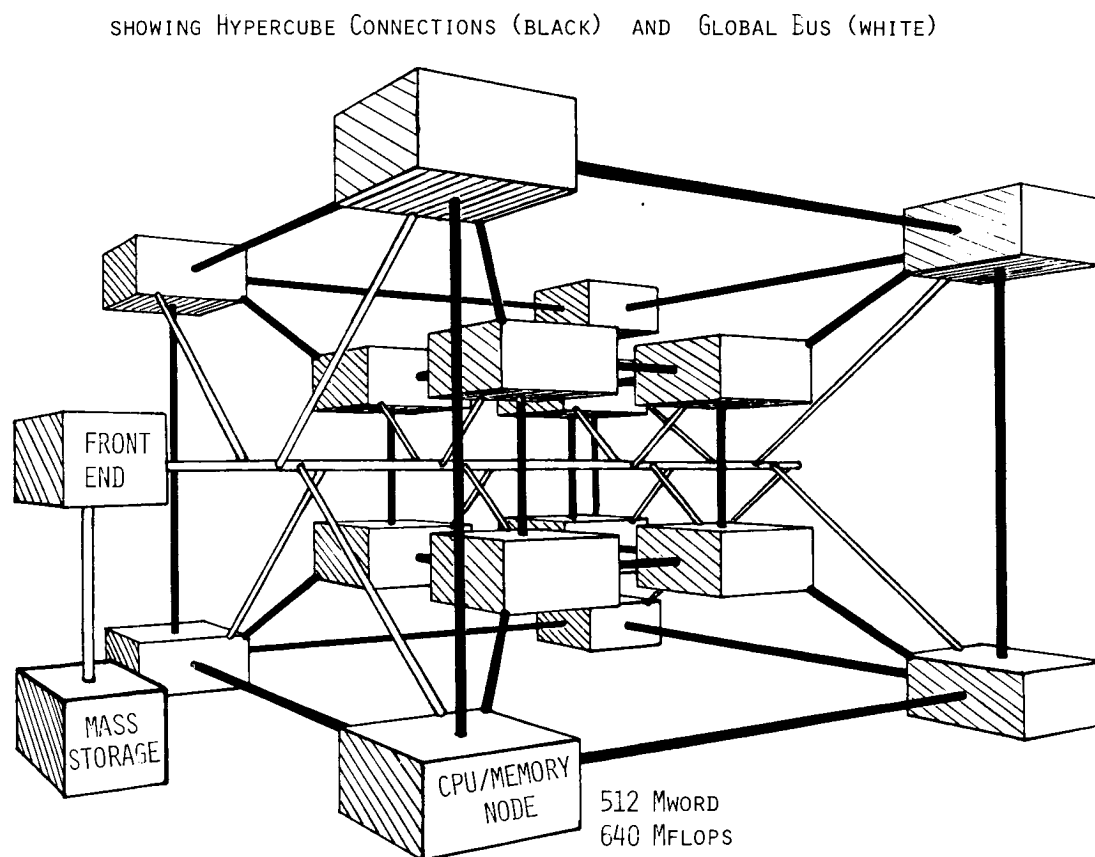


Figure 1.19. 16-Node Navier-Stokes Computer

1.21 NAVIER-STOKES COMPUTER

1.21.1 Objective

To design, construct and demonstrate a special-purpose, parallel computer for CFD applications.

1.21.2 Approach

The design utilizes a moderate number of powerful, individual, local memory processors with each processor itself a complex parallel computer.

1.21.3 Accomplishments

NASA constructed and debugged two complete Navier-Stokes Computer (NSC) Mininodes, which are the prototype local memory processors. NASA designed, constructed and installed two printed circuit boards to replace the remaining wire-wrapped boards in NSC Mininode. NASA constructed and installed inter-node communication hardware and developed a NSC Mininode Assembler to facilitate coding of NSC applications. NASA wrote a NSC Mininode Simulator to interface with both the NSC Mininode and the NSC Mininode Assembler (See Figure 1.19).

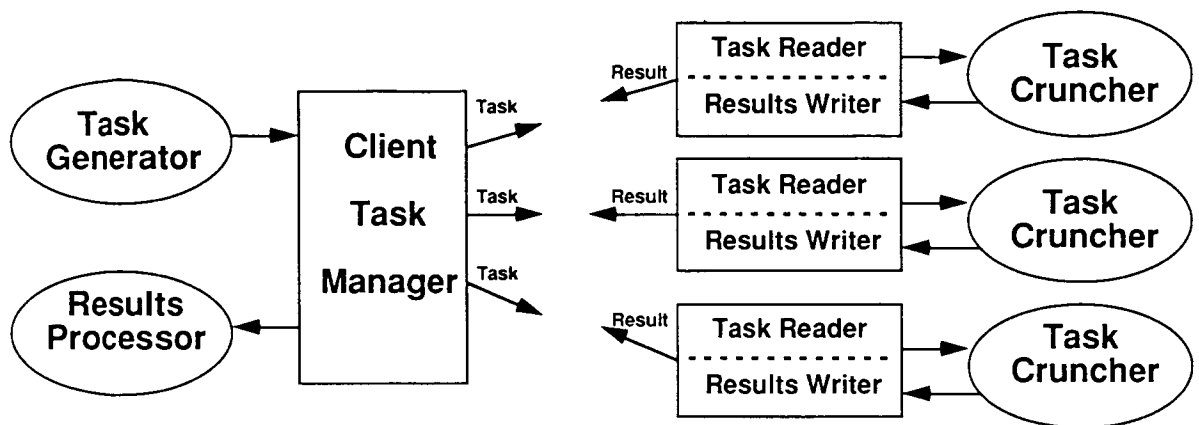
1.21.4 Significance

The completion of these NSC Mininodes establishes confidence in the basic design philosophy of individual processors. The installation of the printed circuit boards greatly increases the reliability of the hardware. The inter-node communication hardware is a key element in producing a workable multi-processor NSC. The Mininode Assembler improves the programmability of the machine, making it far easier to develop application programs.

1.21.5 Status/Plans

NASA plans to complete assembly of a four Mininode system (finish two additional Mininodes, additional internode communication hardware and integration of the complete system). NASA also will develop application codes for single and multiple Mininodes and will participate in the DARPA DST Project (support porting of CRT and Langley codes to NSC Mininode).

D. Nosenchuck and T. A. Zang
Computational Methods Branch
Langley Research Center
(804)864-2307



- Boxes represent task management routines
- Ellipses represent task execution routines (supplied by user)
- Any box or ellipse can theoretically run on a separate processor

Figure 1.20. Implementation Overview

1.22 DISTRIBUTED PROCESSING WITH NETWORKED COMPUTERS

1.22.1 Objective

To develop software which allows use of multiple networked computers to process a single job, while dynamically load-balancing the job tasks to optimally use the available resources of each computer.

1.22.2 Approach

A pilot code was developed which distributes job tasks across multiple networked computers. Code features include (1) fully dynamic load-balancing, to allow processors with different performance levels and job mixes to contribute any available resources to the distributed job; (2) fault tolerance, to allow individual processors to fail without killing the distributed job and (3) ease of use, to enable a researcher to use the distributed technique without addressing the details of task scheduling (See Figure 1.20).

1.22.3 Accomplishments

As an initial test, the code was used to compute elements of the Mandelbrot set, which typically takes about 30 minutes to compute on a single VAX 750. The same job takes only about one minute to compute when distributed across the VAX 750 and 14 VAX workstations of varying CPU capabilities. The aggregate CPU capability of the 15 VAXs is approximately 30.5 times that of the single VAX 750, thus yielding typical efficiencies of 90-100 percent CPU utilization for this problem.

1.22.4 Significance

The pilot code demonstrates that, at least for compute-bound jobs with low data interdependencies, large speedups can be obtained by efficient use of heterogeneous networked computer resources. Such resources can range from available workstation CPU cycles to networked supercomputers. This technique is particularly important for computer graphics/flow visualization tasks and may have an impact on interdisciplinary computing in the future.

1.22.5 Status/Plans

Work is underway to extend this distributed processing approach to other problems of interest and to other network architectures. The use of multiple, networked supercomputers also is being investigated.

James P. Chamberlain
Analytical Methods Branch
Langley Research Center
(804)864-2147

This page is intentionally left blank.

CHAPTER TWO

CFD VALIDATION

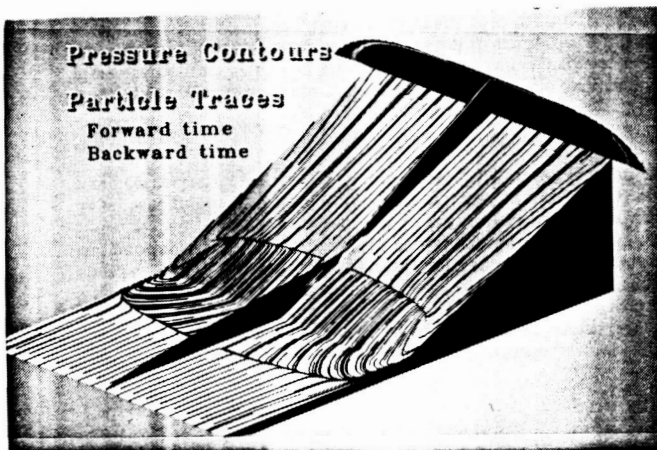
2.1 INTRODUCTION

The objective of the CFD Validation Program is to perform detailed, benchmark experiments using redundant facilities and instrumentation to produce high-quality, archival data sets to which CFD solutions can be compared. Experiments designed to validate CFD codes must provide data that is taken in the form and detail consistent with CFD modeling requirements. In addition, the accuracy and limitations of the experimental data must be thoroughly understood and documented. Likewise, the accuracy and limitations of the numerical algorithm, grid-density effects and physical basis of the CFD code being validated must be equally known and understood over a range of specified parameters.

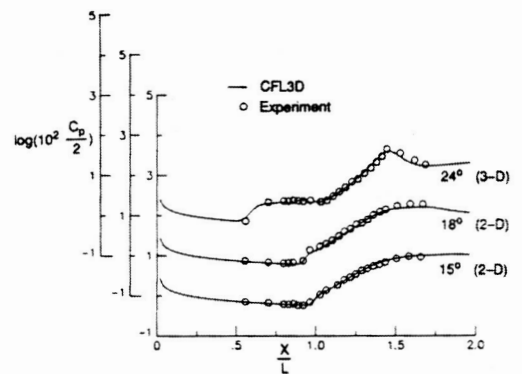
Experiments are designed for comparison with numerical CFD results in order to (1) understand flow physics, (2) develop physical models for CFD codes, (3) calibrate CFD codes and (4) validate CFD codes. Approximately 100 experiments that fall into one or more of these categories were performed at the three OAST Centers. The experiments range in speed from subsonic to hypersonic and include a variety of configurations including generic, fighter/attack, subsonic transport, rotorcraft, ASTOVL and propulsion systems. Future work will include developing high-quality databases for several classes of flows, including (1) high- and low-aspect ratio wings in subsonic and transonic flows; (2) simple 3-D turbulent flows, including time histories; (3) flow fields about aircraft components; (4) propulsive lift flow interactions in ground effect and (5) unsteady flow interaction in rotor flow fields.

Program Manager: Mr. Edward T. Schairer
OAST/RF
Washington, DC 20546
(202)453-2819

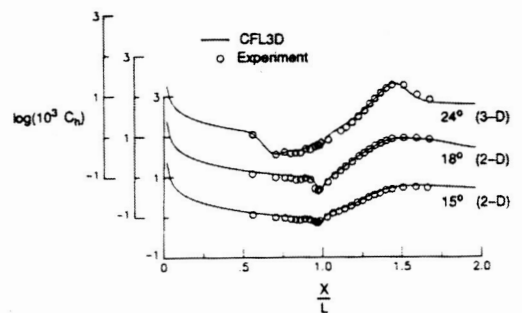
ORIGINAL PAGE
BLACK AND WHITE PHOTOGRAPH



3-D computation for 24° wedge.



Surface pressure for 15°, 18°, and 24° wedges.



Surface heat transfer for 15°, 18°, and 24° wedges.

Figure 2.1. Code Validation Study

2.2 CODE-VALIDATION STUDY FOR HYPERSONIC COMPRESSION-CORNER FLOWS

2.2.1 Objective

To conduct a code validation study, comparing with experimental data a hypersonic flow with laminar viscous-inviscid interaction typical of those found in scramjet inlets using four different Navier-Stokes codes.

2.2.2 Approach

The flow over a nominally two-dimensional compression corner was completed using four different Navier-Stokes codes and compared with data obtained in the CALSPAN 48-inch shock tunnel.

2.2.3 Accomplishments

For a 15 degree wedge with fully-attached flow, 2-D calculations with the four codes gave virtually identical results for a sufficiently refined grid. For the most highly separated flow (24 degree wedge), 2-D calculations overpredicted the size of the separated flow region. Three-dimensional calculations, which included the finite-span effect of the experiment, were required in order to obtain agreement with the data. These effects were important in determining the extent of separation as well as the time required to establish steady state flow. NASA arrived at summary comparison plots of the CFL3D solutions of surface pressure and heat transfer with experimental data for three compression corners (See Figure 2.1).

2.2.4 Significance

The study demonstrated that the four codes are capable of accurately representing, both qualitatively and quantitatively, the types of complex hypersonic flows with strong viscous-inviscid interactions considered; therefore, these codes can be used in the design and analysis of the NASP for high-speed flow conditions for which experimental data cannot be obtained in ground-based facilities.

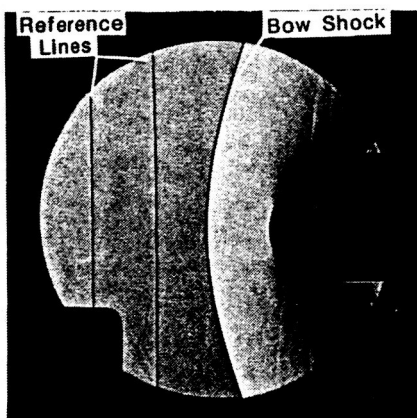
2.2.5 Status/Plans

Code comparisons will be made for other types of laminar and turbulent hypersonic flows.

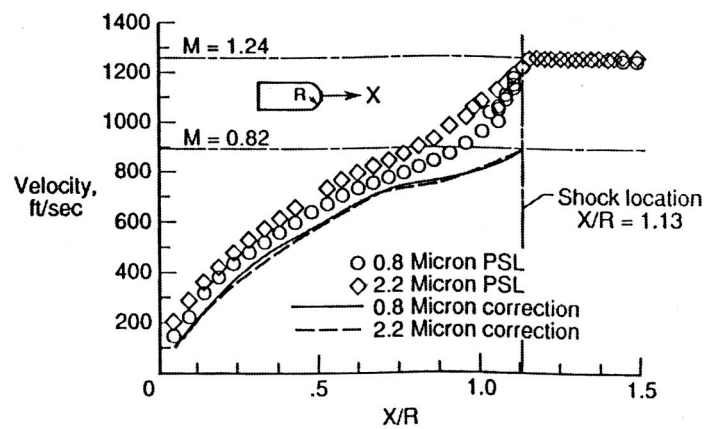
David H. Rudy, James L. Thomas, Ajay Kumar,
Peter A. Gnoffo and Sukumar R. Chakravarthy
Computational Methods Branch
Langley Research Center
(804)864-2297

Hemisphere at AOA = 0, $R = 0.825$ in., $M = 1.24$, $Re = 530,000$

SCHLIEREN



STAGNATION STREAMLINE VELOCITY



ORIGINAL PAGE
BLACK AND WHITE PHOTOGRAPH

Figure 2.2. Basic Aerodynamic Research Facility

2.3 TRANSONIC WIND TUNNEL TEST DATA ACQUIRED ON A HEMISPHERE MODEL WITH A CYLINDRICAL AFTERBODY FOR LASER VELOCIMETER SEEDING INVESTIGATION

2.3.1 Objective

To evaluate the errors in Laser Velocimeter (LV) flow field measurements at transonic speeds which are due to seeding particle lag.

2.3.2 Approach

Detailed flow field data were obtained on a simple hemisphere geometry. LV velocity profiles, model and wall pressures, six-component force, liquid-crystal visualization and schlieren measurements were acquired for comparison to an inviscid potential computational code and a thin-layer Navier-Stokes code.

2.3.3 Accomplishments

A significant result was that surface pressure distributions did not compare as well as expected to the predictions at transonic speeds. Comparisons of LV velocity measurements to computational results along the stagnation streamline of the hemisphere model were used to determine the particle dynamics involved in LV seeding (See Figure 2.2). Results in the outer flow field showed good agreement in trend between experimental and computational data. LV particle lag existed at all test Mach numbers, but was particularly significant across the bow shock. These errors were corrected with a 1-D method developed under this program.

2.3.4 Significance

The experimental database will help to evaluate the accuracy of LV for non-intrusive wind tunnel velocity measurements. With the particle size and velocity gradients measured, velocities can be corrected for particle lag. In addition, the database will assist in computational fluid dynamics code validation efforts by providing details in the flow field. This experiment also highlighted the need for investigation of improved dispersion or injection techniques for solid particulates, i.e., polystyrene latex micro-spheres currently being used at Langley, Lewis and Ames Research Centers.

2.3.5 Status/Plans

Detailed laser velocimeter flow field measurements are continuing on the hemisphere model for Mach numbers covering the range from 0.2 to 1.2.

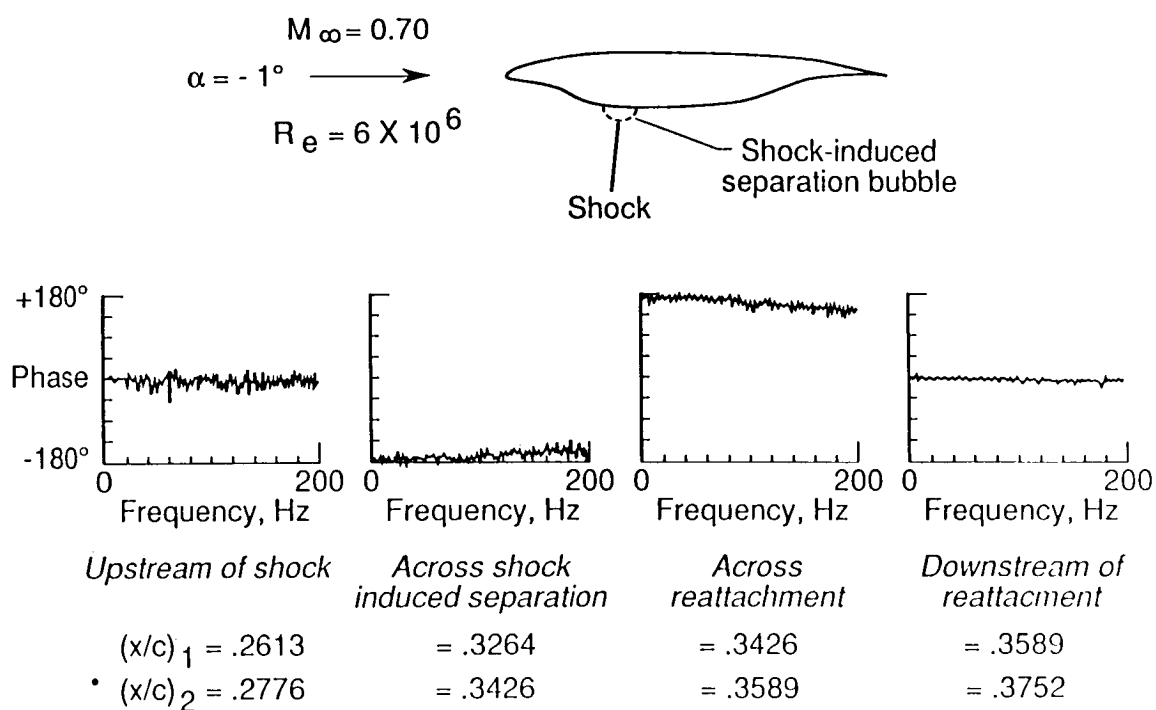


Figure 2.3. Phase Shifts at Separation and Reattachment

2.4 DETECTION OF SHOCK-INDUCED SEPARATION USING MEDS³ TECHNIQUE

2.4.1 Objective

To develop a reliable flow diagnostic tool to accurately detect shock-induced separation on airfoils at transonic speeds.

2.4.2 Approach

The Multielement Dynamic Shear Stress Sensor (MEDS³) technique is used to detect shock-induced separation on a supercritical airfoil model at transonic speeds in the Langley 0.3-Meter Transonic Cryogenic Tunnel.

2.4.3 Accomplishments

Shock-induced separation is clearly detected by phase-reversal in low-frequency dynamic shear stress signals using the MEDS³ technique. When shear stress fluctuation from adjacent surface hot-film sensors are compared, a -180 degree phase shift is observed across the shock-induced separation, a +180 degree phase shift is observed across the reattachment and zero phase shifts are obtained upstream and downstream of the separation bubble (See Figure 2.3).

2.4.4 Significance

It was established that the MEDS³ technique can be used not only at low speeds but also at transonic speeds to accurately locate flow separation. Since the phase-reversal phenomenon appears to be independent of the speed regime, there is reason to believe that the technique also may be applicable to supersonic and hypersonic flows.

2.4.5 Status/Plans

Future plans include efforts to apply the MEDS³ technique in flight tests and conduct more detailed fundamental experiments to understanding the physical significance of the phase reversal phenomenon.

S. M. Mangalam, J. P. Stack, V. Kalburgi, W. G. Sewall and E. J. Ray
Fluid Dynamics Branch
Langley Research Center
(804)864-1050

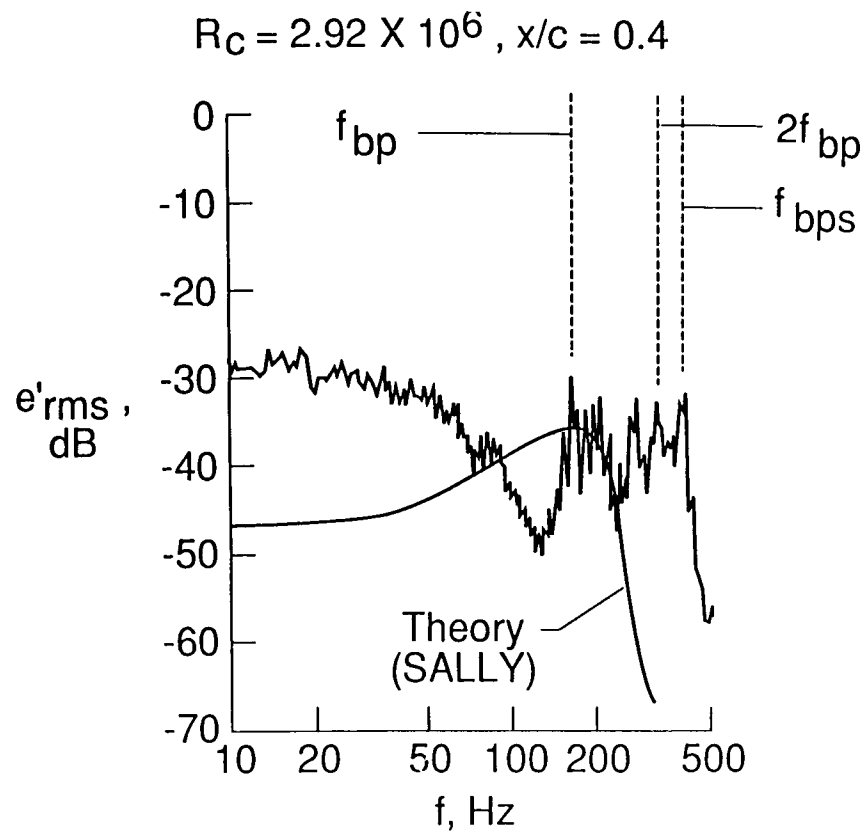


Figure 2.4. Experimental and Theoretical Spectra

2.5 CROSSFLOW-VORTEX INSTABILITY ON A 45 DEGREE SWEPT WING

2.5.1 Objective

To determine the crossflow vortex wavelengths, growth rates and evolution pattern on a 45-degree swept wing for comparison with computational models of the instability.

2.5.2 Approach

Crossflow-dominated transition is obtained by simulating infinite swept wing flow on a 1.83 m wing using contoured end liners.

2.5.3 Accomplishments

Stationary fixed-wavelength crossflow vortices with wavelengths 25 percent less than predicted were observed. Traveling waves in the frequency range predicted by linear stability theory are present. In addition, higher-frequency traveling waves which may be harmonics of the primary crossflow waves generated by a parametric resonance phenomena are also observed (See Figure 2.4).

2.5.4 Significance

The normal-mode assumption of linear stability theory requires appropriate constraint relations to connect the local solutions to form the global solution. The experiment shows that the fixed-wavelength constraint appears to be most appropriate for linear crossflow instability on an infinite swept wing. The observed high-frequency waves which are not predicted by linear theory must be further investigated.

2.5.5 Status/Plans

Three-dimensional surveys of the flow field using both hot wires and laser doppler velocimetry are planned to firmly establish the vortex evolution pattern and to determine the growth rates.

J. Ray Dagenhart, William S. Saric,
Marc C. Mousseux and J. Peter Stack
Fluid Dynamics Branch
Langley Research Center
(804)864-1006

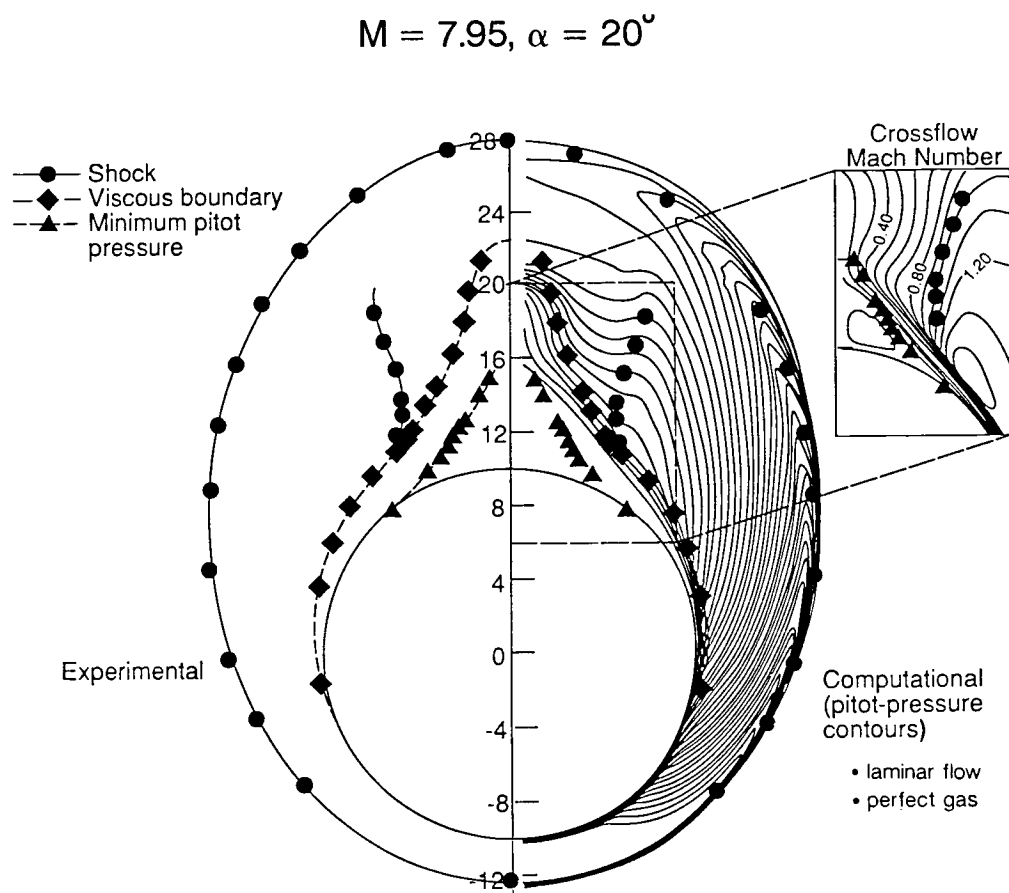


Figure 2.5. PNS Code Validation Study

2.6 COMPUTATIONAL VALIDATION OF A PARABOLIZED NAVIER-STOKES SOLVER ON A SHARP-NOSE CONE AT HYPERSONIC SPEEDS

2.6.1 Objective

To conduct validation studies for a recently developed, parabolized Navier-Stokes (PNS) solver, CFL3DE, in support of the National Aero-Space Plane (NASP) program.

2.6.2 Approach

The approach involved: (1) selecting a carefully defined, thorough experimental data set for the hypersonic laminar flow of a perfect gas over a simple shape; (2) computing the flowfield with the PNS solver comparing computed results with experimental surface and flowfield data and (3) assessing the effect of grid density, grid clustering and convergence criteria for adequately resolving the flowfield, especially the boundary layer, through a comparison with surface pressure, heat transfer and flowfield pitot pressure surveys.

2.6.3 Accomplishments

Solutions have been obtained for a 10 degree, half-angle, sharp-nose circular cone at Mach 7.95, a unit Reynolds number of 4.2-feet by 105-feet and four angles of attack. The study of grid density and convergence criteria showed that the surface pressure and flowfield characteristics were well resolved for a grid of 41 uniformly spaced circumferential points in the half plane, 75 body normal points clustered near the body and 21 marching planes, provided that the residual of the initial conical solution was reduced four orders of magnitude. Only a two order-of-magnitude reduction was necessary for downstream solution planes; however, these criteria were insufficient to provide good heat-transfer estimates. It was found that the additional restriction of cell Reynolds number, Rec , of about two or less was required to provide accurate heat-transfer estimates; therefore, the solution of viscous phenomena such as heat transfer (and by inference, skin friction) requires a better resolution of the boundary layer than those quantities which are primarily inviscid, i.e., pressure. A comparison of flowfield data with computational total pressure contours and isoMachs indicates that the locations of the bow shock, the embedded shock and the edge of the boundary layer are well predicted by the PNS code (See Figure 2.5).

2.6.4 Significance

The validation of the code for the hypersonic, laminar flow of a perfect gas over a simple geometry that is similar to the forebody of some NASP concepts gives confidence for its use in forebody evolution and analysis studies under similar flow conditions.

2.6.5 Status/Plans

The validated PNS solver was used to study the hypersonic flow on the forebody of the Langley Test Technique Demonstrator model.

Lawrence D. Huebner (Vigyan) and James L. Pittman
Supersonic/Hypersonic Aerodynamics Branch
Langley Research Center
(804)864-5583

ORIGINAL PAGE
BLACK AND WHITE PHOTOGRAPH

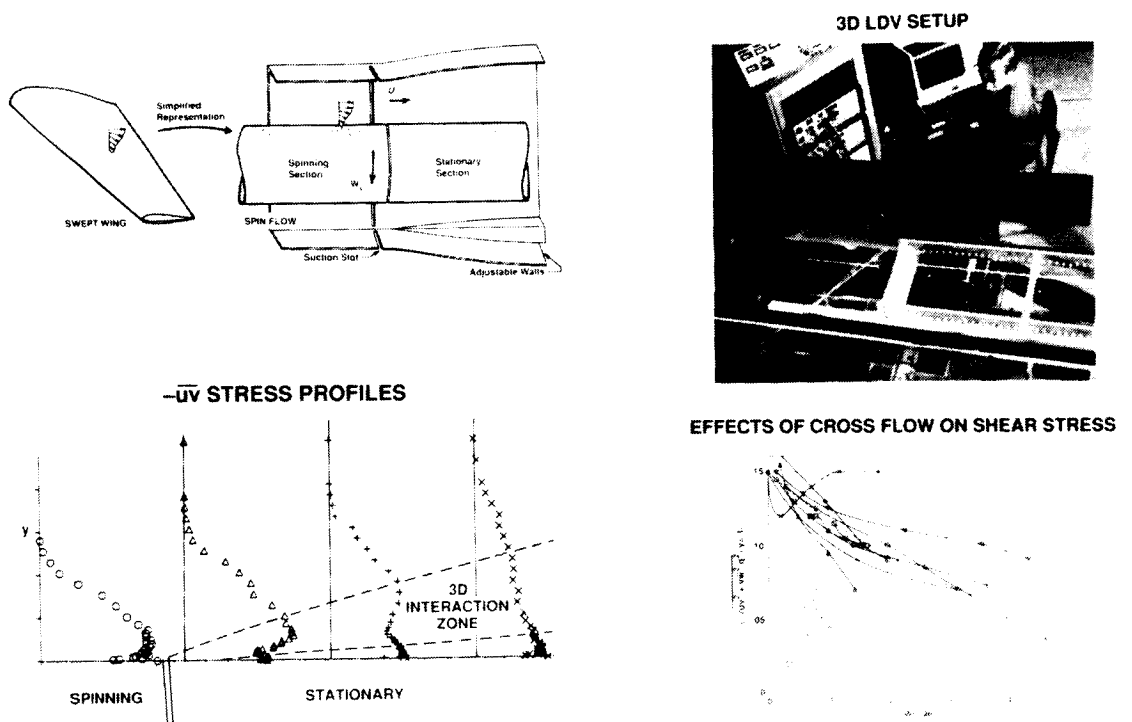


Figure 2.6. An Experiment to Guide Turbulence Modeling for 3-D Boundary Layers

2.7 CODE VALIDATION EXPERIMENTS FOR TURBULENT FLOW

2.7.1 Objective

To determine the effects of adverse pressure gradient on three dimensional turbulent boundary layers and to examine the validity of current turbulence models.

2.7.2 Accomplishments

NASA discovered the correlation between level of shear stress decay seen in experiments and magnitude of cross-flow velocity (See Figure 2.6). Effects of pressure gradient and three-dimensionality combine linearly.

2.7.3 Status/Plans

Experiments were completed. New modeling ideas will be incorporated in a three-dimensional flow solver. NASA will make improvements to turbulence models and computer codes for three-dimensional turbulent flow.

D. M. Driver
Experimental Fluid Dynamics Branch
Ames Research Center
(415)604-6156

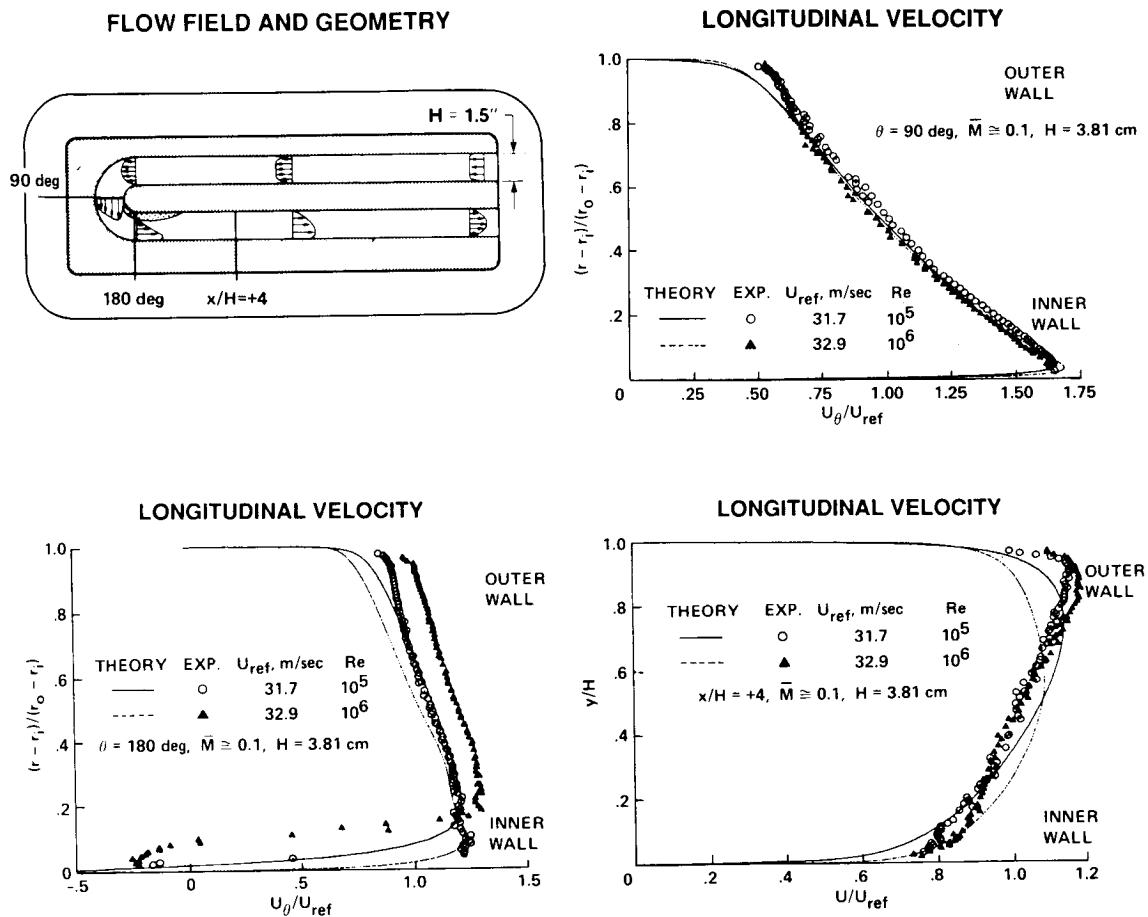


Figure 2.7. SSME Turn-Around Duct Experiment

2.8 SPACE SHUTTLE MAIN ENGINE CODE VALIDATION

2.8.1 Objective

To simulate and document flow in the Turn-Around Duct (TAD) of the Space Shuttle Main Engine (SSME) in support of turbulence model and Navier-Stokes code development for internal flows with extreme curvature.

2.8.2 Approach

A large, experimental database for flow in TAD at low and high Reynolds numbers was obtained, including profiles of mean and turbulence velocities, static pressure and skin friction. NASA compared experimental results with Navier-Stokes calculations using several widely used algebraic turbulence models (See Figure 2.7).

2.8.3 Significance

Unmodified algebraic turbulence models are inadequate for calculating important features of flow and cannot be relied upon to predict flow in TAD of actual SSME.

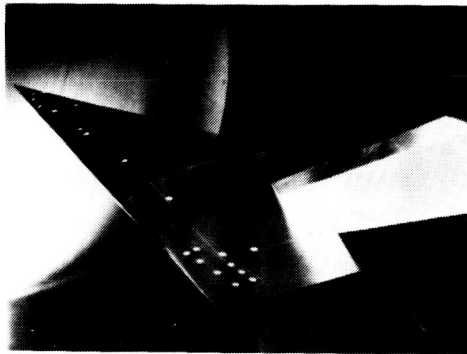
2.8.4 Status/Plans

Experimental results will be used to modify turbulence models to account for strong curvature and pressure gradient effects. Improved code will be used to design variable-area TAD with no separation, which will be tested to verify code prediction.

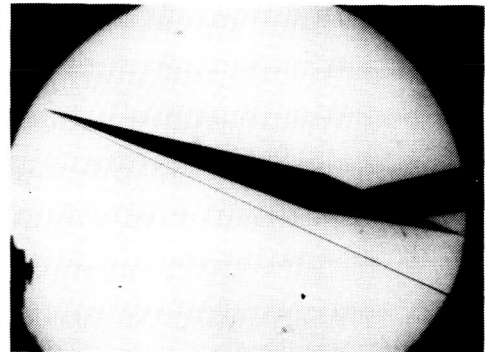
D. J. Monson
Experimental Fluid Dynamics Branch
Ames Research Center
(415)604-6255

ORIGINAL PAGE
BLACK AND WHITE PHOTOGRAPH

MODEL IN AMES 3.5-FOOT HWT



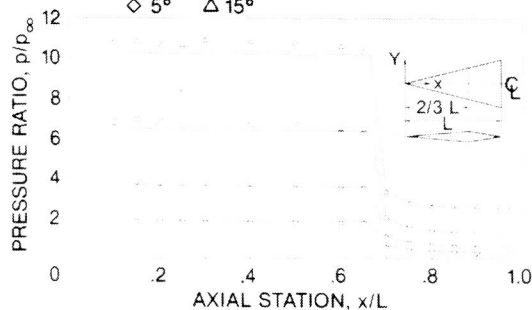
SHADOWGRAPH



WINDWARD SURFACE PRESSURES

Centerline; $M_\infty = 7.4$; $Re_{\infty,L} = 15 \times 10^6$

EXPERIMENT; α UPS CODE
 \circ 0° \square 10° — TURBULENT
 \diamond 5° \triangle 15°



PITOT-PRESSURE DISTRIBUTIONS

Centerline; $x/L = 0.8$; $M_\infty = 7.4$; $Re_{\infty,L} = 15 \times 10^6$

EXPERIMENT; α UPS CODE
 ∇ -15° \triangle 15° — TURBULENT
 \boxplus -10° \square 10°
 \diamond -5° \diamond 5°
 \circ 0°

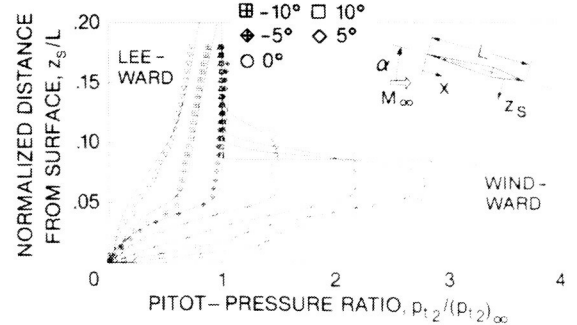


Figure 2.8. All-Body Hypersonic Wind Tunnel Tests and CFD Validation

2.9. ALL-BODY HYPERSONIC WIND TUNNEL TESTS AND CFD VALIDATION

2.9.1 Objective

To establish a benchmark experimental database for a generic hypersonic vehicle shape for validation and/or calibration of advanced Computational Fluid Dynamics (CFD) computer codes.

2.9.2 Approach

NASA implemented a comprehensive test program for a generic all-body hypersonic aircraft model in the Ames 3.5-foot wind tunnel over a broad range of test conditions to obtain pertinent surface and flow-field data which are a measure of the flow physics. Test conditions included free-stream Mach numbers of 5, 7 and 10; free-stream Reynolds numbers (based on a model length of three feet) ranged from 1.5 million to 25 million (laminar to turbulent flows) and model angles of attack from 0 degrees to 15 degrees (attached and separated flows). Measurements provided flow-visualization data (shadowgraphs and surface oil-flow patterns), surface pressures, surface heat transfer and flow-field surveys of pitot pressure (probes) and mean velocities (laser velocimetry). The experimental data were compared to results from various CFD codes to assess whether the codes capture the flow physics. The primary comparisons were made with the Upwind Parabolized Navier-Stokes Solver (UPS) code at Ames (See Figure 2.8).

2.9.3 Accomplishments

Experimental data on flow visualization, surface pressures and pitot-pressure surveys were obtained and compared to results from the UPS code.

2.9.4 Significance

These data and code results show the significant flow changes with varying angle of attack and demonstrate the generally good agreement between the experiment and UPS code computations (some differences at higher angles of attack), thus indicating the validity of the code for the given range of test conditions.

2.9.5 Status/Plans

NASA will (1) complete data analysis and code comparisons for surface heat-transfer data recently obtained, (2) complete ongoing test for pitot-pressure surveys and make code comparisons for additional test conditions, (3) perform flow-field surveys using Laser Doppler Velocimetry (LDV) upon completion of LDV system under development and (4) if desired, perform additional tests with instrumented control surfaces on the model.

William K. Lockman
Aerothermodynamics Branch
Ames Research Center
(415)604-5235

Scott L. Lawrence
Applied Computational Fluids Branch
Ames Research Center
(415)604-4050

Joseph W. Cleary
Eloret Institute
Sunnyvale, CA

CHAPTER THREE

TRANSITION AND TURBULENCE PHYSICS

3.1 INTRODUCTION

The objective of the Transition and Turbulence Physics Program is to develop a fundamental understanding of flow structures relating to turbulence and transition and to incorporate these flow structures into sophisticated flow models for use with computational methods. Turbulence models are needed for compressible, chemically-reacting, time-dependent flows. The program includes the development of test techniques and advanced instrumentation for time-dependent measurements of unsteady flow about both simple and complex configurations. The program also includes the development of numerical codes for simulating transitional and turbulent flows. The program supports the Center for Turbulence Research which assembles world renown experts to generate new concepts regarding turbulence.

Program Manager: Mr. Edward T. Schairer
OAST/RF
Washington, DC 20546
(202)453-2819

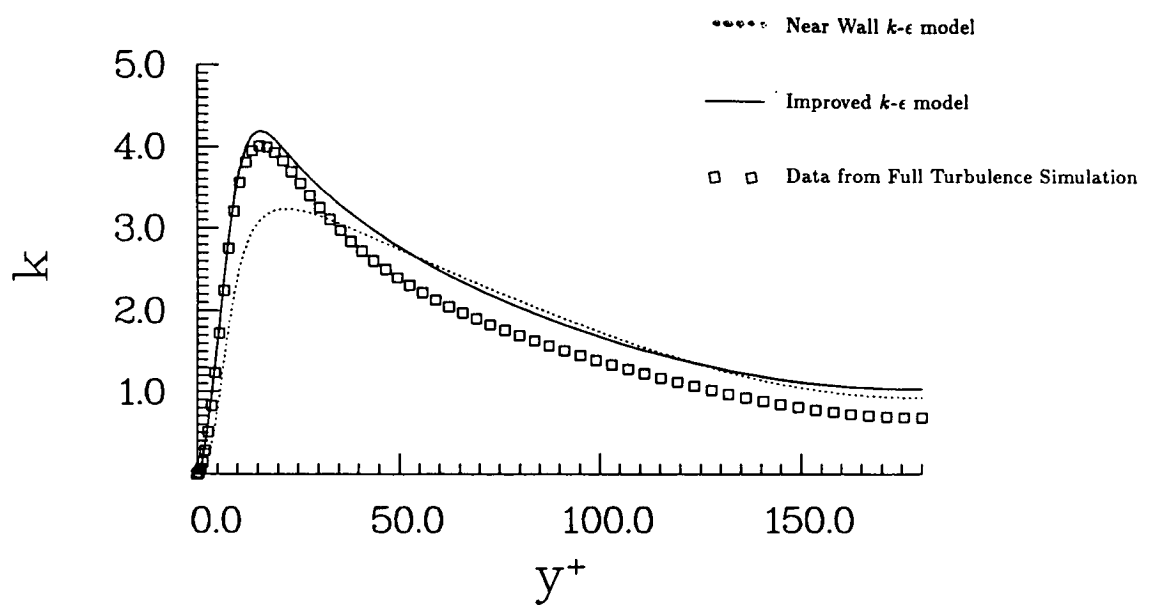


Figure 3.1. Turbulent Kinetic Energy in a Channel

3.2 TURBULENCE MODELING USING DIRECT SIMULATION DATA

3.2.1 Objective

To develop phenomenological turbulence models for Reynolds-averaged, Navier-Stokes codes using data from direct numerical simulation of turbulence.

3.2.2 Accomplishments

The program resulted in new, near-wall corrections for eddy viscosity and dissipation rate equations (See Figure 3.1).

3.2.3 Significance

The turbulence model can be used in three-dimensional, Reynolds-averaged, Navier-Stokes code to account for near-wall effects.

3.2.4 Status/Plans

Work is in progress to develop the Reynolds stress model.

N. N. Mansour
Computational Fluid Dynamics Branch
Ames Research Center
(415)604-6420

TURBULENCE MODELING IMPROVEMENTS RAE 2822 AIRFOIL

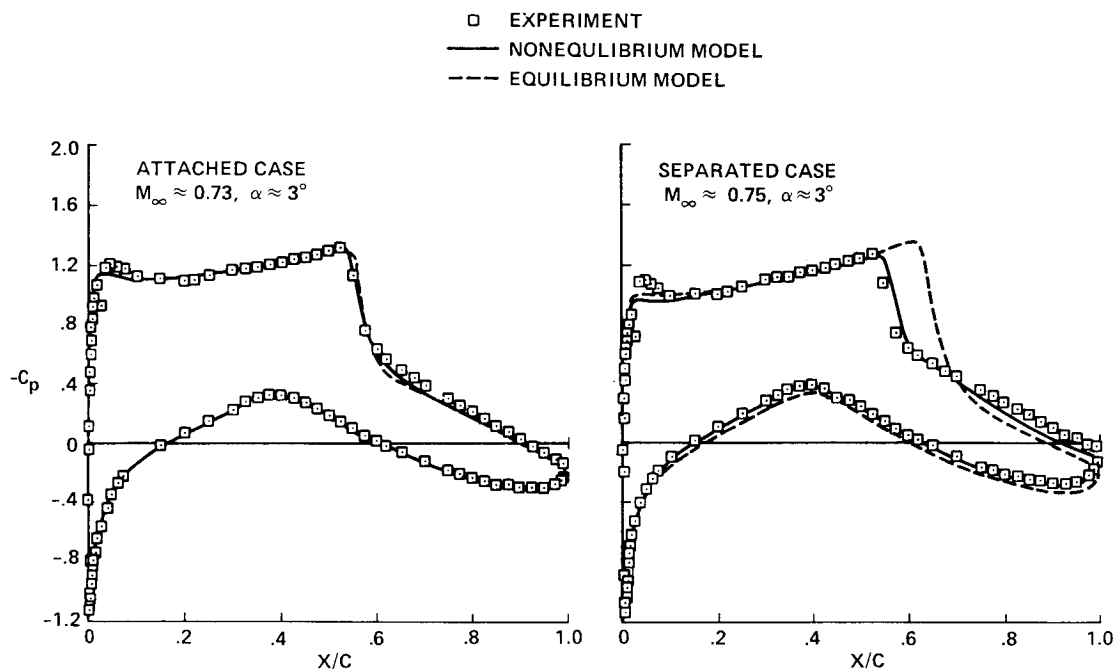


Figure 3.2. RANS Transonic Airfoil Predictions

3.3 IMPROVED TURBULENCE MODEL FOR TRANSONIC FLOW

3.3.1 Objective

To develop for transonic flow over airfoils and wings, a turbulence model capable of predicting performance accurately up to maximum lift coefficient.

3.3.2 Approach

The approach involved conducting computer experiments to develop an improved turbulence model (See Figure 3.2).

3.3.3 Accomplishments

NASA developed a computationally efficient, nonequilibrium model to accurately describe behavior of turbulence for weak and strong interaction, using differential equation for maximum Reynolds shear stress.

3.3.4 Significance

The use of Reynolds-averaged, Navier-Stokes methods for transonic airfoil and wing design is enhanced by the improved turbulence model.

3.3.5 Status/Plans

Further demonstrations are planned for the performance of wings.

D.A. Johnson
Experimental Fluids Branch
Ames Research Center
(415)604-5399

ORIGINAL PAGE
BLACK AND WHITE PHOTOGRAPH

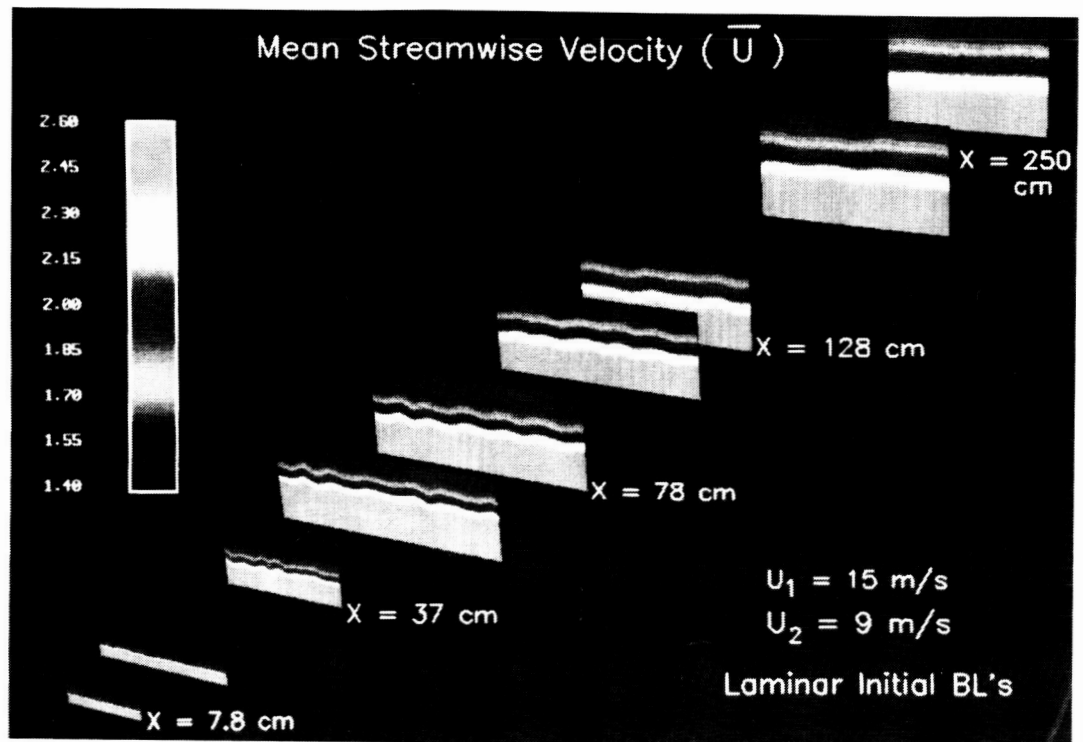


Figure 3.3. Undisturbed Mixing Layer

3.4 STRUCTURE OF PLANE MIXING LAYERS

3.4.1 Objective

To (1) improve the basic understanding of turbulent mixing layers through detailed experiments, with the aim of overall control of structure and mixing; (2) document inflow boundary conditions and (3) create a database for comparison with Navier-Stokes numerical simulations.

3.4.2 Approach

The approach involved (1) measuring directly for the first time, secondary (streamwise) vortex structure in plane mixing layers and (2) conducting a survey of mechanisms for triggering these structures (See Figure 3.3).

3.4.3 Accomplishments

Experimental data have revealed important details regarding origin, reorganization and decay of secondary structure.

3.4.4 Significance

Data also suggest ways in which secondary structure may be controlled to enhance turbulent mixing.

3.4.5 Status/Plans

Experiments are in progress with tripped boundary layers to simulate higher (more practical) Reynolds numbers. Future plans include multi-probe correlation and phase-averaged measurements in mixing layer with spanwise and normal forcing.

R.D. Mehta
Fluid Dynamics Research Branch
Ames Research Center
(415)604-4141

This page is intentionally left blank.

3.5 PHYSICS OF NUMERICALLY SIMULATED TURBULENCE

3.5.1 Objective

To identify spatial character and temporal evolution of turbulent boundary layer motions responsible for turbulence production and dissipation, wall pressure and skin friction fluctuations and entrainment of outer, non-turbulent fluid.

3.5.2 Approach

The approach involved investigating kinematics of all major turbulence structure elements, including embedded vortices, in a numerically simulated boundary layer.

3.5.3 Accomplishments

The program enabled identification of major sources of turbulence production, wall pressure fluctuations and internal vortex structures.

3.5.4 Significance

This was the deepest physical understanding yet of turbulent boundary layers with first integration of all structural features into consistent kinematic framework.

3.5.5 Status/Plans

NASA is developing an advanced conceptual model of turbulence dynamics for application to modeling and control methodologies.

S. K. Robinson
Experimental Fluid Dynamics Branch
Ames Research Center
(415)604-6220

ORIGINAL PAGE
BLACK AND WHITE PHOTOGRAPH

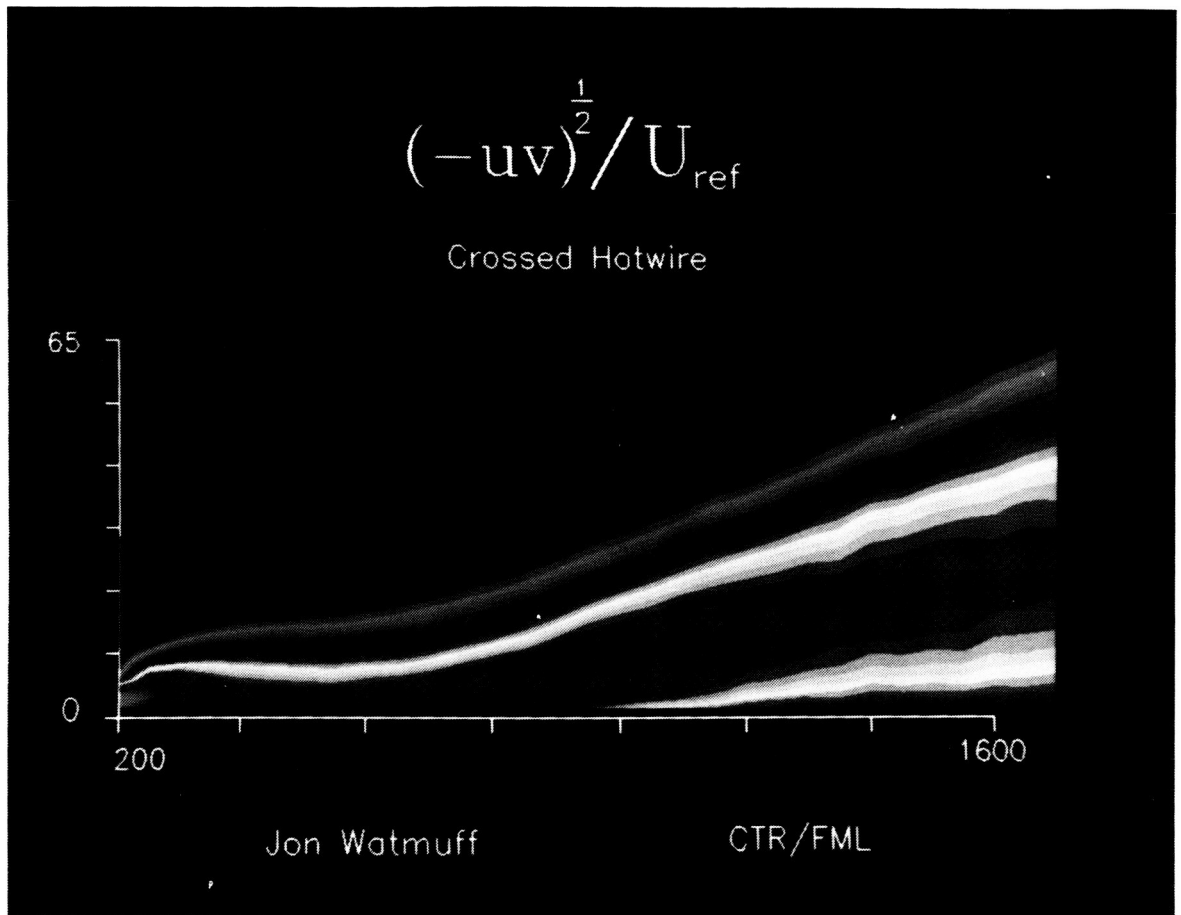


Figure 3.4. Crossed Hotwire

3.6 LOW REYNOLDS NUMBER TURBULENT FLOW EXPERIMENTS

3.6.1 Objective

To acquire massive quantities of turbulent flow data for use in code validation by totally automated, computer controlled experiments.

3.6.2 Accomplishments

NASA completed the longest continuous, single experimental run to date with no manual intervention of 59 hours. NASA consumed 46 hours of Micro-Vax CPU time and processed and wrote to disk, at one million samples per minute (See Figure 3.4).

3.6.3 Significance

This program fills the void of low Reynolds number data for turbulent boundary layer with adverse pressure gradient.

3.6.4 Status/Plans

NASA plans to measure all Reynolds stresses with a crossed hot wire probe at spatially dense locations. The probe will be traversed through regions of high turbulence intensity at high speed where data from stationary probes are inaccurate.

J. H. Watmuff
Fluid Dynamics Research Branch
Ames Research Center
(415)604-4150

WALL COORDINATES, SCHEME C; FINE-GRID

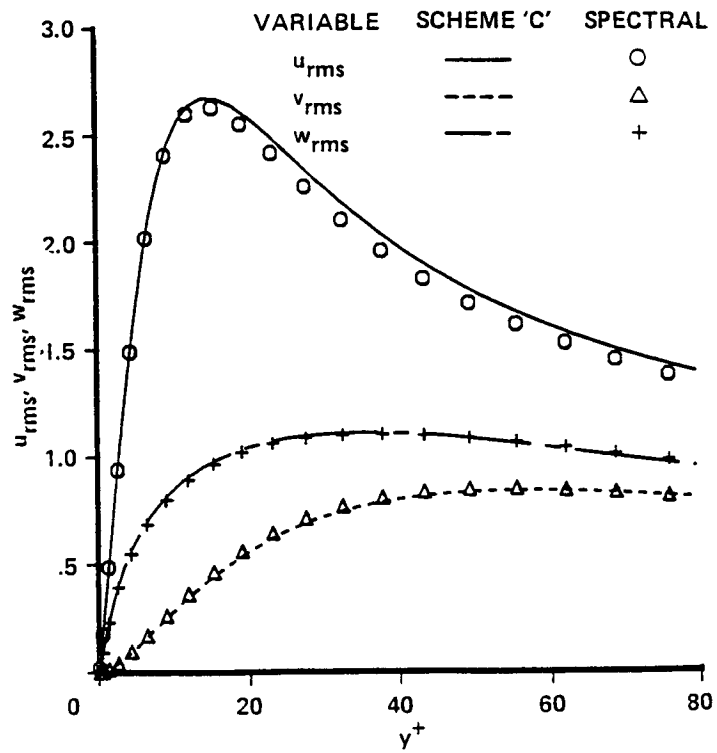


Figure 3.5. Root-Mean-Square Velocity Fluctuation Normalized by the Wall Shear Velocity

3.7 FINITE DIFFERENCE METHOD FOR TURBULENT FLOW

3.7.1 Objective

To develop a high-order-accurate finite-difference method for direct and large-eddy simulations of turbulent flow.

3.7.2 Approach

The approach involved developing a fifth-order accurate, upwind method to simulate incompressible, low Reynolds number, fully developed turbulent flow in a channel (See Figure 3.5).

3.7.3 Accomplishments

Results compare well with experimental data and results from earlier simulations using the spectral method.

3.7.4 Significance

Unlike spectral methods, the finite-difference method can be modified in a straight-forward manner for complex geometries.

3.7.5 Status/Plans

A method is being extended to compressible flow with application to a boundary layer transition on flat plate.

M.M. Rai
Applied Computational Fluids Branch
Ames Research Center
(415)604-4499

Surface of constant vorticity magnitude (2x initial peak level) illustrating streamwise rib-like vortices and cup-like structures of spanwise vorticity.

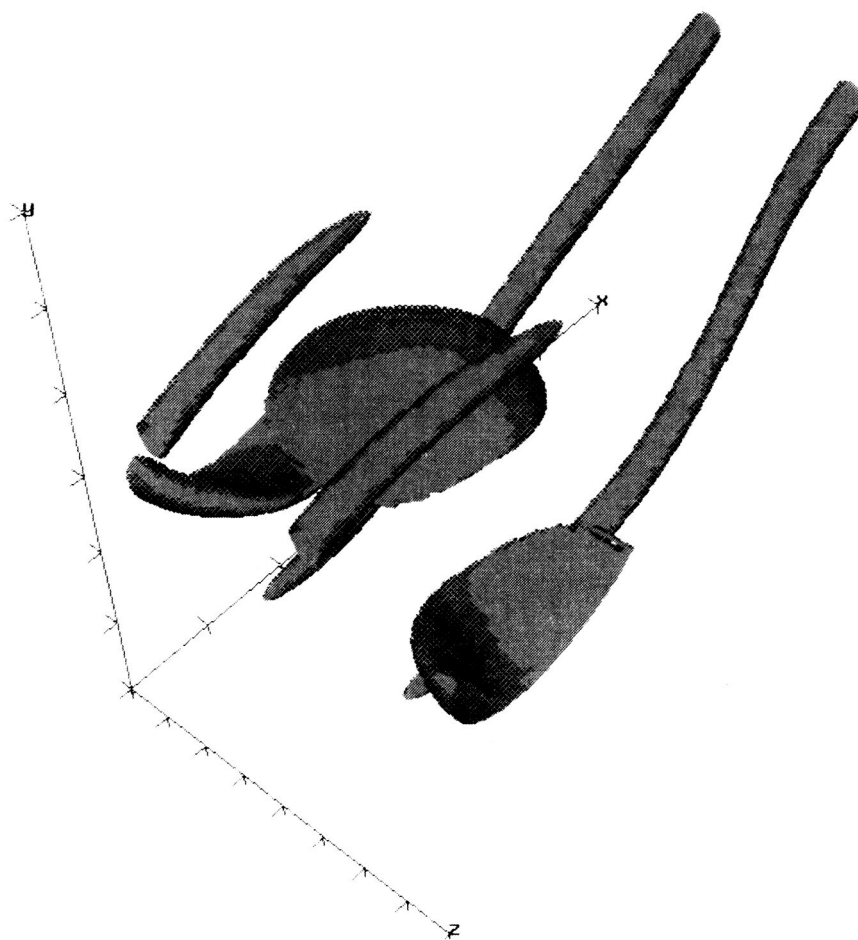


Figure 3.6. Surface of Constant Vorticity Magnitude

3.8 TEMPORALLY-EVOLVING MIXING LAYERS

3.8.1 Objective

To understand development of three-dimensional mixing layers from a broad range of initial disturbances.

3.8.2 Approach

The approach involved generating a large database of numerical simulations.

3.8.3 Accomplishments

NASA completed simulations illustrating evolution of typical mixing layer vortex structures through roll-up and pairing (See Figure 3.6).

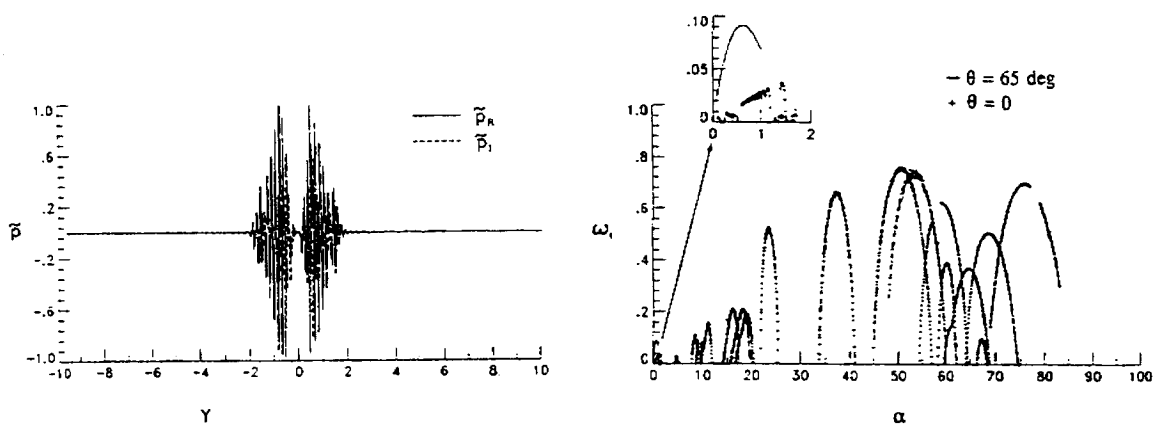
3.8.4 Significance

Simulation results provide insight into development of mixing layers, particularly, poorly understood onset of three-dimensionality.

3.8.5 Status/Plans

NASA will continue generating three-dimensional simulations, including second pairing, turbulence and chemical reactions.

M. M. Rogers and R. D. Moser
Computational Fluid Dynamics Branch
Ames Research Center
(415)604-4732



Pressure disturbance versus normal coordinate of highly-amplified disturbance of mixing-layer. $M_\infty = 3.5$.

Growth rate versus streamwise wavenumber indicating most amplified disturbances at low α , $\theta = 65$ degrees, and most amplified disturbances at high α , $\theta = 0$ degrees. $M_\infty = 3.5$.

Figure 3.7. High Oscillatory Structure of Modes

3.9 LINEAR STABILITY OF BOUNDED FREE SHEAR FLOWS

3.9.1 Objective

To understand the evolution of bounded mixing layers so that this knowledge may eventually be used to enhance mixing between a fuel and air stream emitted from a scramjet combustor. Since mixing is greatly enhanced by turbulent flow, understanding the instabilities which lead to turbulence of high-speed mixing layers was the initial focus.

3.9.2 Approach

The initial stages of instability of a bounded mixing layer were studied by solving the linearized, compressible, Navier-Stokes equations discretized by a highly accurate, spectral collocation, pressure-staggered solution technique.

3.9.3 Accomplishments

Using a Spectral Compressible Linear Stability (SPECLS) code, it was found that the experimentally observed drop in mixing efficiency at high Mach number may be due to low frequency, 3-D disturbances which are naturally present in the beginning stages of mixing layer instability. These disturbances have much lower growth rates than the predominant disturbances at low Mach number; however, the study also shows that there exist highly amplified 2-D (disturbance wave angle, $\theta=0$ degrees), supersonic disturbances at very high frequency, i.e., high streamwise wave number, α . The highly oscillatory structure of these modes is displayed in Figure 3.7, which is a plot of the pressure disturbance, \tilde{p} , versus normal coordinate, y . The growth rates, w_i , of these disturbances, are an order of magnitude greater than the most amplified disturbances at low frequency, which are 3-D ($\theta=65$ degrees). Figure 3.7 displays these growth rates versus α for a mixing layer comprised of a quiescent gas and a $M_\infty=3.5$ gas.

3.9.4 Significance

Forcing these high frequencies in high Mach number mixing layers at the beginning of the mixing-layer evolution may excite the highly-amplified modes and thereby induce transition to turbulence and enhanced mixing. If this occurs (as is hoped), the construction of a scramjet combustor, which requires efficient mixing of fuel and air streams within a practical streamwise distance, will become practical.

3.9.5 Status/Plans

These highly-amplified disturbances will be further studied in a nonlinear simulation of a mixing layer's instability and transition. The exact impact these disturbances have on early transition and mixing enhancement will be gained from these studies.

(2-D TS Wave With 0.25% Initial Amplitude)

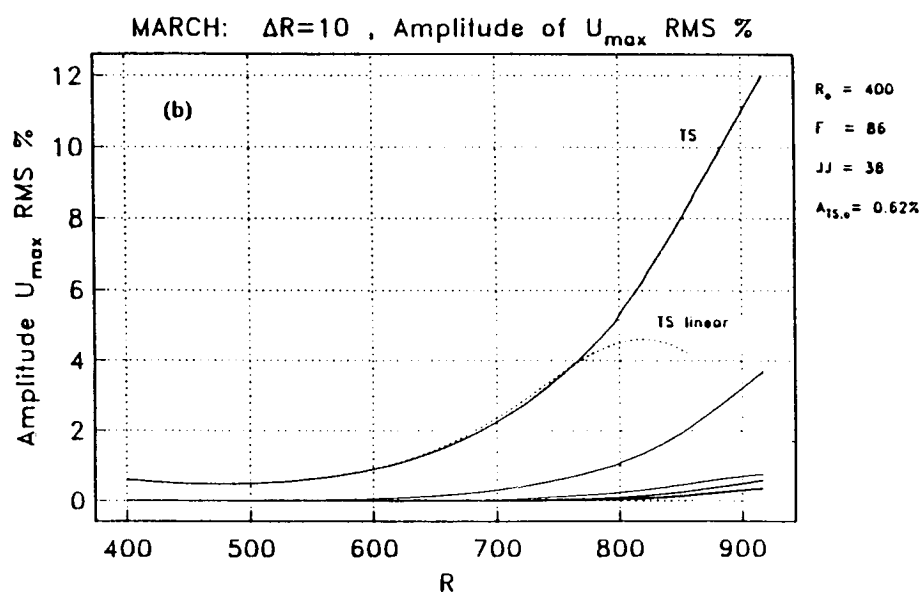


Figure 3.8. Spatial Marching Method for Boundary Layer Transition

3.10 DEVELOPMENT AND IMPLEMENTATION OF THE PARABOLIC STABILITY EQUATION

3.10.1 Objective

To study linear and nonlinear stages of transition using the Parabolic Stability Equation (PSE).

3.10.2 Approach

The equation is based on the split of a disturbance's stream function into the product of a profile function and a wavelike function. Under proper adjustment of the wave function, one may apply the boundary layer approximation to the shape profiles and obtain a parabolic governing equation.

3.10.3 Accomplishments

A family of codes based on the PSE for the analysis of two dimensional waves in a Blasius boundary layer was developed and fully tested. The marching code was run with up to eight harmonics of the TS wave, at amplitudes of up to eight percent ($U_{\max rms}$) (See Figure 3.8). A complete analysis of the linear growth of the TS wave in a nonparallel boundary layer was completed. The results of previous investigators were accurately duplicated and some issues were clarified. The nonlinear calculations are in agreement with the full Navier- Stokes simulations of Spalart, at Ames.

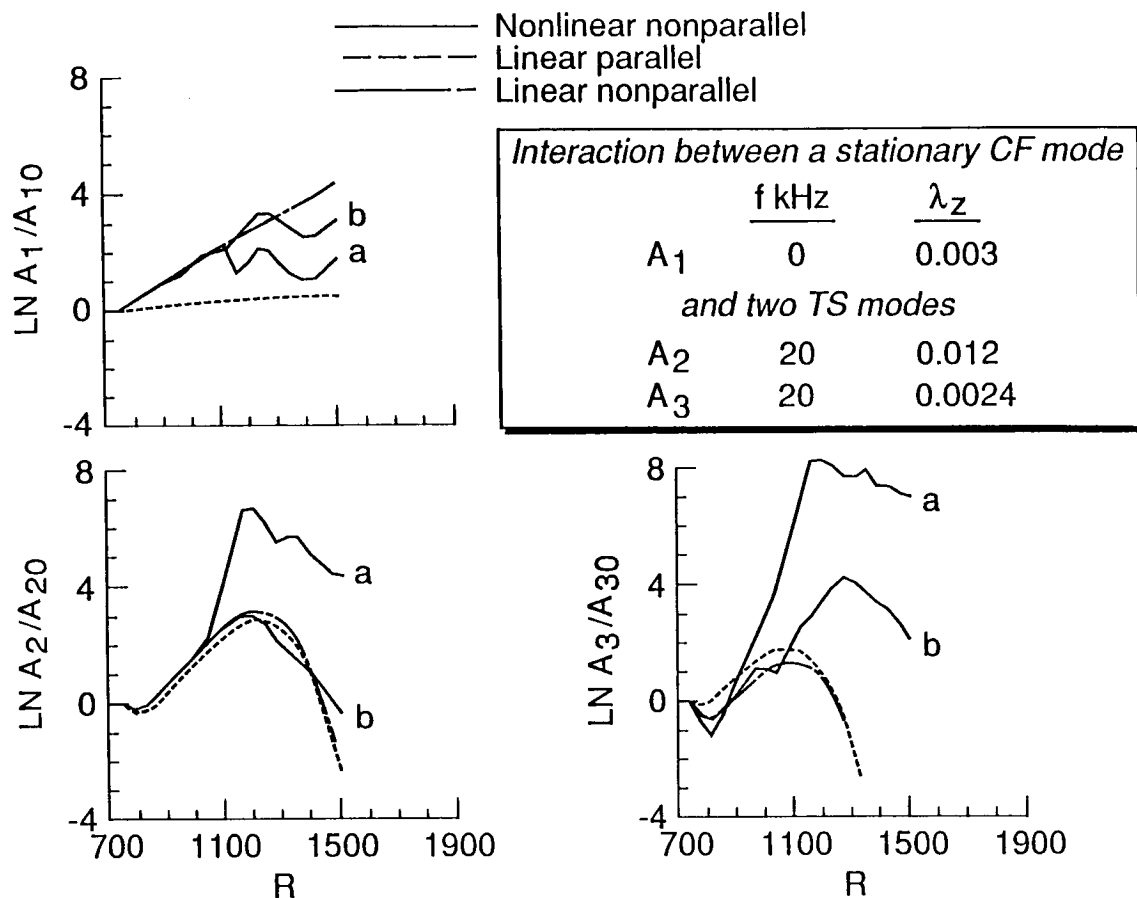
3.10.4 Significance

The PSE is an alternative tool for the accurate analysis of transition in the linear and nonlinear regions up to, but not including, the first spike stage and rapid spectrum widening. The computational expense of solving the PSE is orders of magnitude lower than the full Navier-Stokes equation.

3.10.5 Status/Plans

The incompressible studies will be completed by performing a detailed analysis of three dimensional disturbances in the Blasius boundary layer, with a particular focus on the nonlinear stages following the onset of secondary instability. An extension of the theory and investigations to compressible flows will be done as a feasibility study.

F.P. Bertolotti, Th. Herbert and G. Erlebacher
Computational Methods Branch
Langley Research Center
(804)864-2308



The nonlinear nonparallel amplitude modulation of a stationary CF mode A_1 and two TS modes A_2 and A_3 for various initial amplitudes of the interacting modes. (a) $A_{10} = 0.05$, $A_{20} = A_{30} = 0.0001$; (b) $A_{10} = 0.01$, $A_{20} = A_{30} = 0.005$.

Figure 3.9. Nonlinear Wave Interactions in Three Dimensional Boundary Layers

3.11 NONLINEAR WAVE INTERACTIONS IN THREE DIMENSIONAL BOUNDARY LAYERS

3.11.1 Objective

Three dimensional (3-D) boundary layers are usually rich in different instability modes, i.e., Stationary Crossflow (CF), Traveling CF, Vertical Vorticity (VV) and Tollmien-Schlichting (TS) modes. One expects the possible evolution of many resonant triads whose components can take part in several resonant interactions. The mechanism of resonance of three waves plays an important role in determining the nonlinear characteristics of the development of disturbances leading to transition. To study the spatial evolution of these triads to promote the understanding of the transition process in 3-D flows.

3.11.2 Approach

A nonlinear nonparallel stability analysis code was developed to examine the modulation of the amplitudes and phases of three instability modes satisfying triad resonant conditions in time and space in 3-D flows. The meanflow was the boundary layer on a 23 degree swept infinite span wing with $M_\infty=0.82$ and $R_c=20 \times 10^6$. Different examples of interaction were found. A triad interaction of three traveling CF modes exhibited strong resonance and resulted in the amplification of a superharmonic or a subharmonic depending on the spectrum of the initial amplitude and phases of the interacting waves. A damped VV mode resonated with two traveling CF modes and became strongly unstable. A stationary CF vortex resonated with two traveling CF modes resulting in rapid growth of these modes. Figure 3.9 shows an example of the rapid growth of two TS waves due to interaction with stationary CF vortex.

3.11.3 Accomplishments

An important role in the nonlinear process is played by the initial spectrum of amplitudes and phases of the triad components. Strong interaction continues to exist between the triad components even if the resonant conditions are not perfectly tuned. In 3-D flows, transition prediction methods may not treat the modes independently because these modes do interact nonlinearly, even if they are weakly amplified. Nonparallel flow effects are important only during the initial development of the triad components, as the amplitudes increase, nonlinear effects control their subsequent spatial development.

3.11.4 Status/Plans

The theory developed here will be extended to high Mach numbers and the interaction model will be compared with experimental findings.

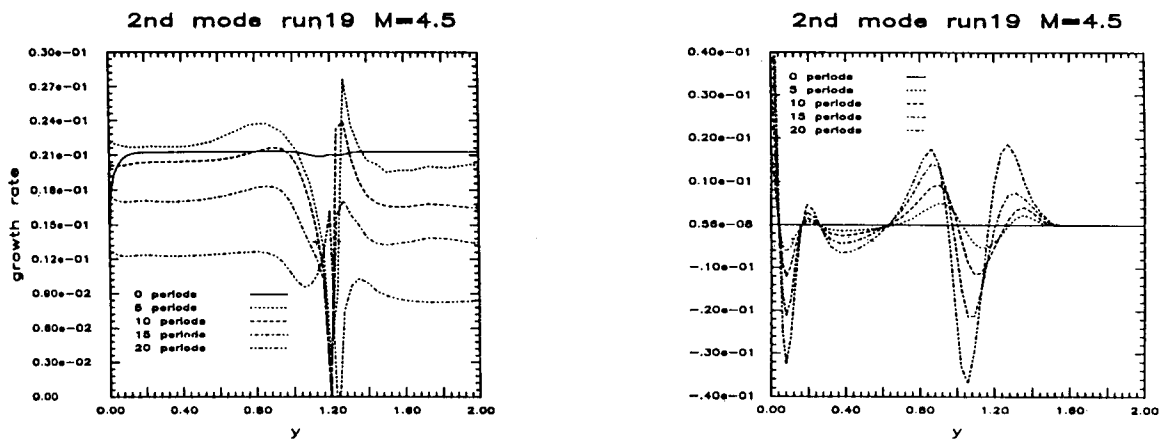


Figure 3.10. Nonlinearities in Critical Layer/Generalized Inflection Point Region

3.12 EVOLUTION OF A 2-D SECOND MODE WAVE IN A MACH 4.5 BOUNDARY LAYER

3.12.1 Objective

To demonstrate the existence of a saturated state of the two-dimensional second mode. This saturated state will then become the primary flow for a secondary instability analysis. To this end, the time-dependent Navier-Stokes equations are solved using a fully spectral algorithm (for reasons of accuracy).

3.12.2 Approach

An existing three-dimensional spectral compressible code that solves the Navier-Stokes equations applied to a flat plate geometry was used to track a 2-D second mode over multiple wave periods. Flow conditions are $M_\infty=4.5$, Re and the streamwise wave length $\alpha=2.25$. The simulation was conducted on a grid of $16 \times 64 \times 4$ and the wave length was tracked for 20 time periods. As a point of reference, the linear wave amplification is approximately seven percent per period.

3.12.3 Accomplishments

Results after 20 periods indicate that non-linearities are developing in the critical layer/generalized inflection point region. These nonlinearities were proven to be the result of the cubic interactions in the momentum equations, which is not surprising in light of the large density fluctuations (ten percent). These non-linearities are demonstrated in Figure 3.10 a, which shows a plot of the primary wave growth rate as a function of the normal coordinate y at 0, 5, 10, 15 and 20 periods. For reference, the curve is a horizontal line in the linear regime. Figure 3.10b shows that the perturbation vorticity starts forming in the wall region and near the critical layer. After 20 periods, there was loss of resolution which ended the simulation; however, numerical experiments suggest that a weakly non-linear, asymptotic theory might lead to the saturated state. This then will permit a practical parameter study of the existence of the saturated state as a function of Reynolds number, Mach number and wave number.

3.12.4 Significance

The stability characteristics of the saturated, two dimensional state are expected to provide an important clue towards understanding the mechanisms that underlie transition at hypersonic speeds. This is of fundamental importance for the design of hypersonic aircraft.

3.12.5 Status/Plans

NASA plans to conduct an asymptotic analysis to determine the saturated state and compare it with the direct simulation results. NASA will perform a detailed energy budget analysis to determine why the second mode is unstable.

$$M_\infty = 4.5, Re/c = 2.4 \times 10^6$$

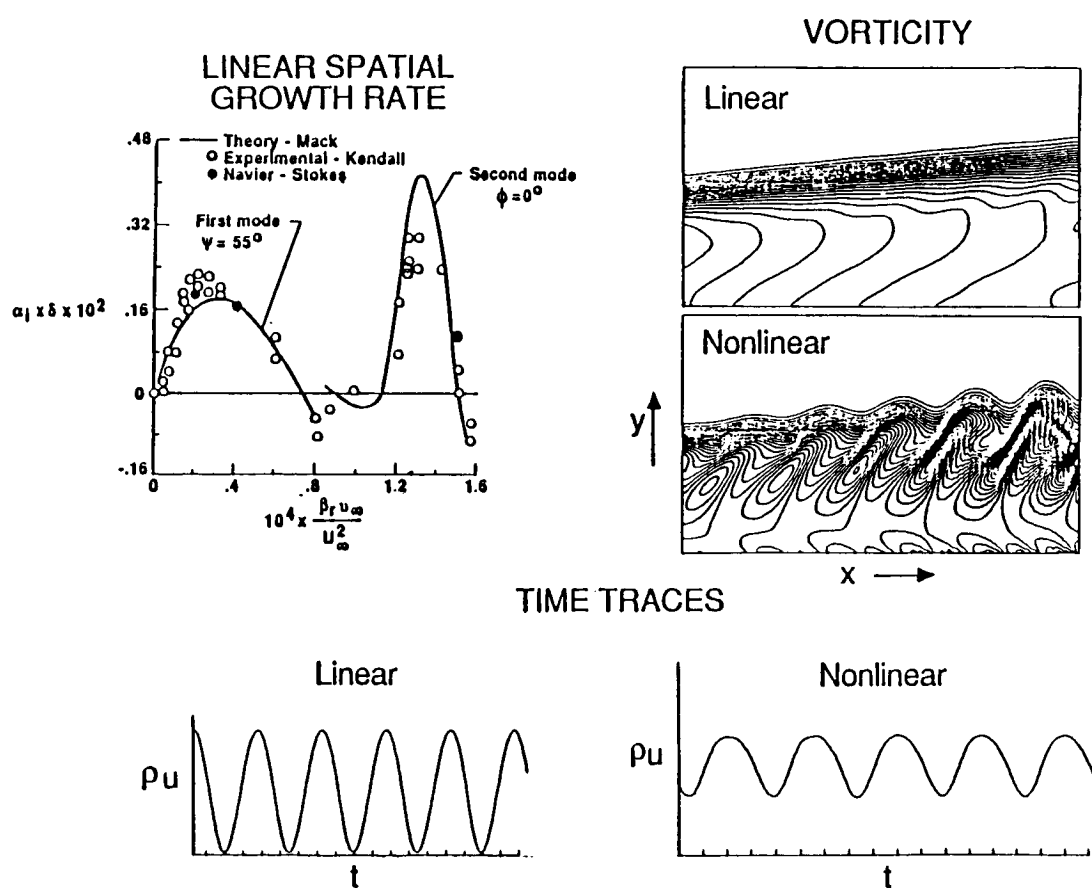


Figure 3.11. Numerical Results

3.13 COMPUTATION OF SPATIALLY UNSTABLE THREE-DIMENSIONAL WAVES IN A SUPERSONIC BOUNDARY LAYER

3.13.1 Objective

To numerically evaluate the nonlinear behavior of spatially-unstable, three-dimensional waves in a supersonic boundary layer .

3.13.2 Approach

A supersonic boundary layer flow was perturbed by imposing a disturbance represented by a harmonic, linear stability eigenfunction at the inflow boundary. The spatial evolution of the disturbance was computed by numerically solving the unsteady, three dimensional, Navier-Stokes equations using a fourth order, accurate, finite-difference scheme.

3.13.3 Accomplishments

In the linear range, good agreement was found among this spatial method, linear stability calculations and the experiment. By increasing the disturbance amplitude, nonlinear distortion was computed. This nonlinear distortion takes the form of relaxation-type oscillations of the time signal and a progressive clustering of vorticity contours as the downstream distance increases (See Figure 3.11).

3.13.4 Significance

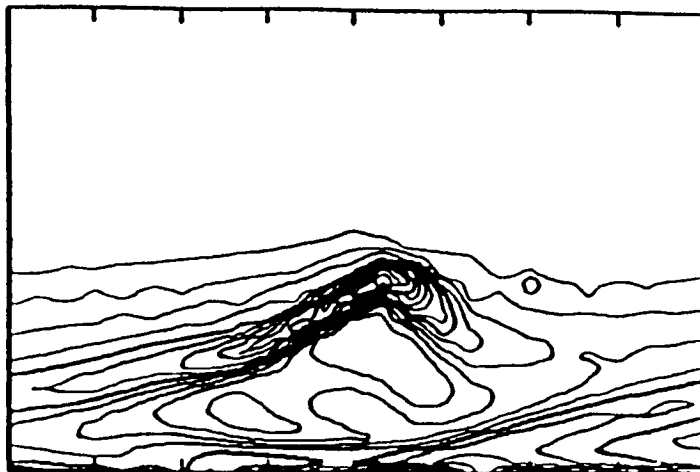
The results of this research enable, for the first time, the study of nonparallel effects in the nonlinear growth and transition in supersonic boundary layers.

3.13.5 Status/Plans

Further nonlinear disturbances will be investigated using higher resolution. The effect of in-plane surface curvature also will be studied.

L. Maestrello, R. Krishnan and A. Bayliss
Fluid Dynamics Branch
Langley Research Center
(804)864-1067

FILTERED DIRECT SIMULATION



LARGE-EDDY SIMULATION

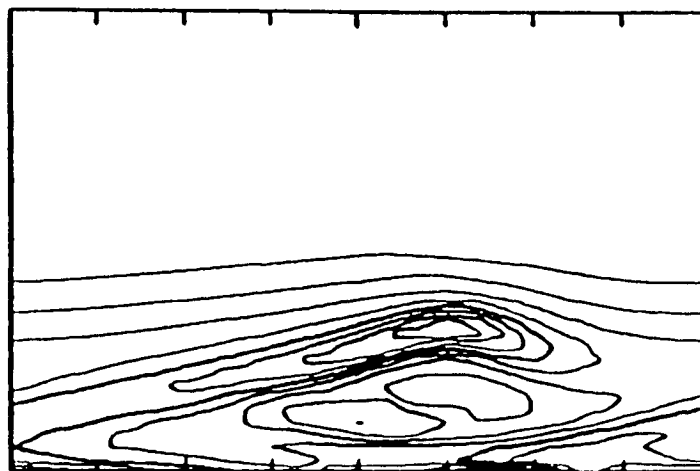


Figure 3.12. Filtered, Direct and Large-Eddy Simulations

3.14 LARGE-EDDY SIMULATION (LES) TRANSITION MODELING

3.14.1 Objective

To develop and calibrate Large-Eddy Simulation (LES) models for transitional flows. The models required a subgrid-scale viscosity that is tuned for transitional rather than turbulent flows. The models were calibrated against direct numerical simulations of transitional channel and boundary layer flows.

3.14.2 Approach

A priori tests of LES models were performed on high resolution databases for both channel and flat plate boundary layer transition. The results suggest that the conventional turbulent LES model needs modification for transitional flows. Both ad hoc and Renormalization Group (RNG) modifications were proposed and tested (See Figure 3.12).

3.14.3 Accomplishments

Actual large-eddy simulations of transitional, boundary layer flow were performed. The RNG model works exceptionally well in comparison with the direct simulation data.

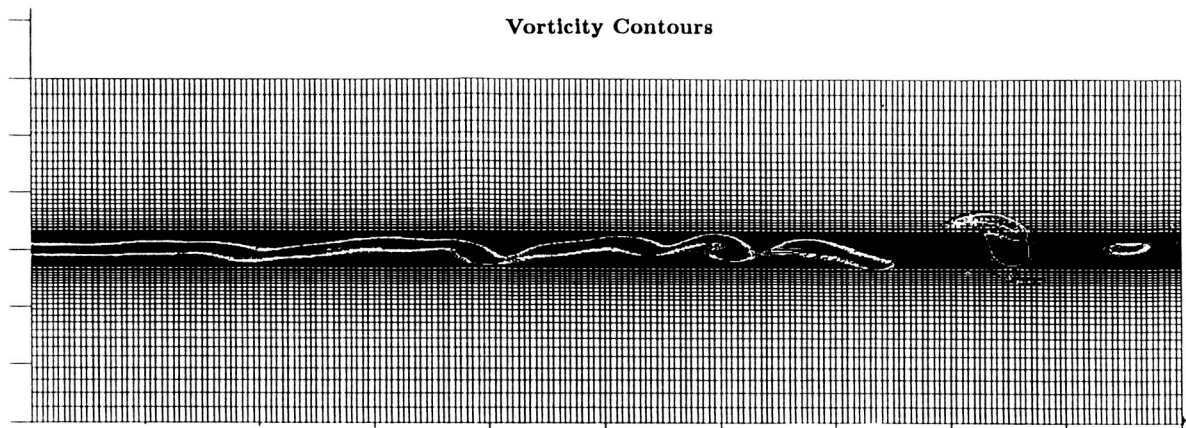
3.14.4 Significance

This is the first LES transition modeling work that has focused on the key issue of predicting the length and detailed properties of the transition region. Earlier attempts were content to produce a valid final turbulent state from a laminar initial state, but made wildly inaccurate predictions for the transition zone itself. This new capability opens the door to many numerous types of transition simulations that are not feasible with direct simulation techniques.

3.14.5 Status/Plans

Exhaustive tests of the LES transition model predictions will be made against existing high-quality transition databases for incompressible flow. The model will be extended to compressible flow and to more complex geometries.

U. Piomelli, C. Speziale, M. Hussaini and T. A. Zang
Computational Methods Branch
Langley Research Center
(804)864-2307



MIXING LAYER VORTICITY AS A FUNCTION OF
DISTURBANCE LEVEL

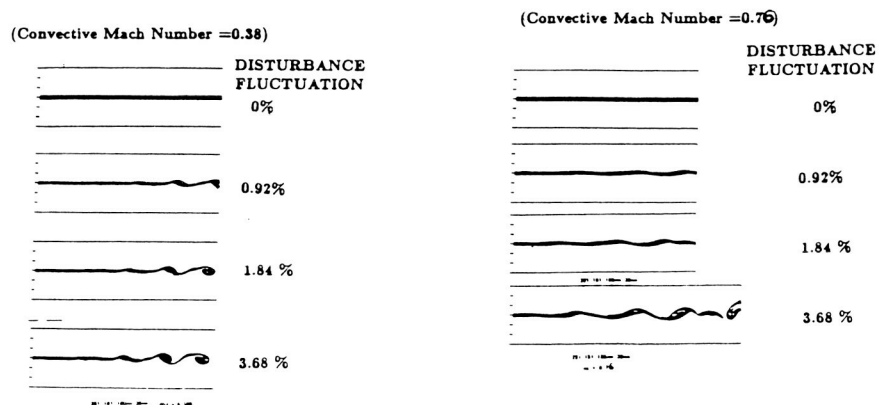


Figure 3.13. High-Speed Mixing Layer

3.15 STUDIES IN DIRECT SIMULATION OF HIGH SPEED MIXING LAYERS

3.15.1 Objective

To examine the effects of convective Mach number, disturbance level, nature of initial profiles and Reynolds number on the structure of a high speed mixing layer.

3.15.2 Approach

The SPARK code, based on a fourth-order accurate scheme in the cross stream direction and a third-order upwind scheme in the streamwise direction, was used with a second-order time accurate scheme to compute high-speed, mixing-layer flowfields

3.15.3 Accomplishments

High-speed mixing-layer calculations were made at convective Mach numbers of 0.38 and 0.76 for a number of initial disturbance levels, for two initial profiles and for a range of Reynolds numbers using the SPARK 2-D code with high-order algorithms and fine grid resolution (See Figure 3.13). From the calculations, NASA concluded that (1) the assumed hyperbolic tangent profiles need large disturbance levels to make the flow transitional; (2) boundary layer profiles lead to predictions of a transitional Reynolds number comparable with the experimental results of Demetriades and King, etc. Excitation of the shear layer in the Strouhal number range of 0.007 causes early rollup and mixing; (3) the concept of a convective Mach number needs review at high convective Mach numbers because the structures dilate significantly, leading to a large variation in the speeds of the structure and (4) the growth rates obtained from the time averaged data compare reasonably well with existing experimental data, illustrating the compressibility effects.

3.15.4 Significance

Direct numerical simulation of high-speed mixing layers improved the understanding of fuel-air mixing in scramjet combustors. This knowledge is critical to the design of an efficient propulsion system for the National Aero-Space Plane. Current studies enable determination of several important techniques for producing high levels of mixing and combustion efficiency in a scramjet combustor and suggest how these techniques could be incorporated into an actual engine design.

3.15.5 Status/Plans

The effect of reaction on the mixing-layer growth will be studied with single-step and with multiple-step finite-rate chemistries. Also, a set of three-dimensional calculations will be carried out to determine whether three dimensionality introduces any change in the

structure of the layer. These calculations will be very useful in evaluating the mixing process in an actual combustor.

S. Mukunda, B. Sekar, M. Carpenter and J. P. Drummond
Computational Methods Branch
Langley Research Center
(804)864-2311

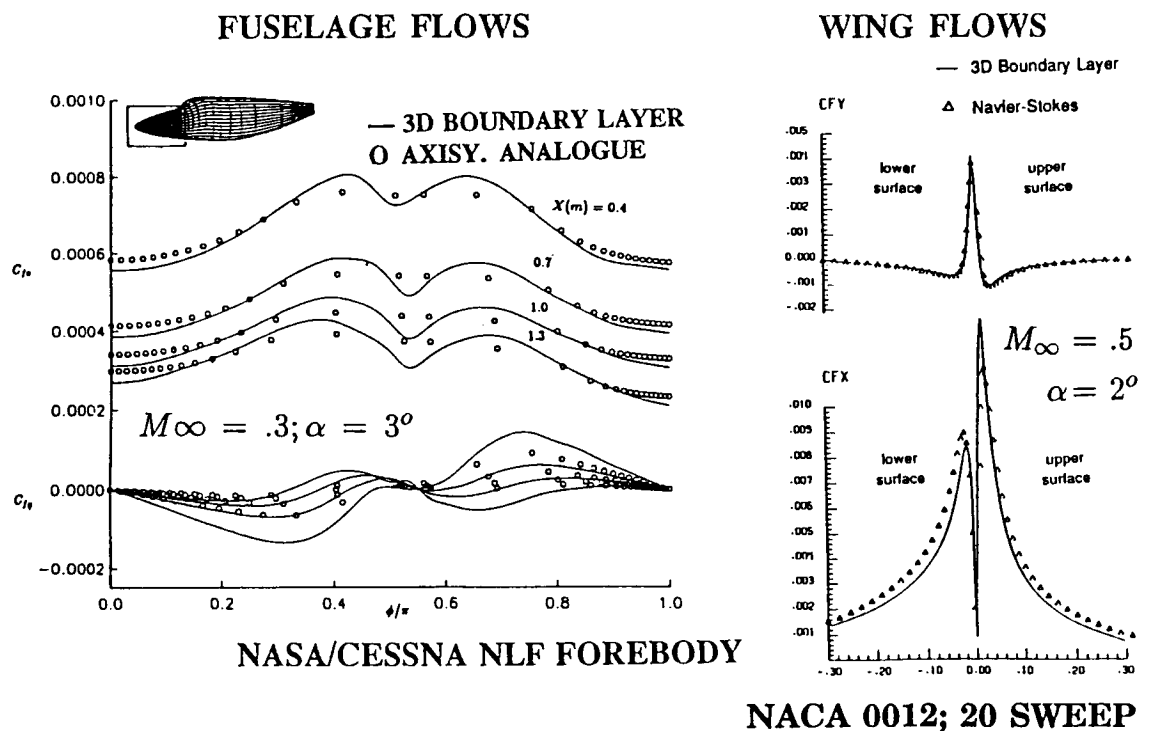


Figure 3.14. Skin Friction Coefficient Comparisons

3.16 THREE-DIMENSIONAL BOUNDARY LAYER

3.16.1 Objective

To develop 3-D boundary layer software for aerospace configurations with emphasis on accuracy required for transition prediction.

3.16.2 Approach

The approach involved developing (1) numerical procedures and software for 3-D, compressible boundary layer equations and (2) theory and software for interface procedures between an inviscid flowfield and the boundary layer including coordinate system generators and graphics.

3.16.3 Accomplishments

A general interface program was developed that couples most existing inviscid solvers with two efficient and accurate boundary layer algorithms. Procedures were verified by comparisons of numerical results with existing solutions and experimental data. Results for a general aviation fuselage and a swept wing at angle of attack were presented (See Figure 3.14). Axisymmetric analogue theory was compared with the solution and failed to predict the correct trends for $\phi/\pi \sim 0.5$. Comparisons with thin-layer Navier-Stokes for a swept wing were presented.

3.16.4 Significance

Software will be used at a fraction of the cost associated with Navier-Stokes solutions. Output will provide accurate initial values for transition prediction.

3.16.5 Status/Plan

Release software to all research/development centers (U.S. Government and contractors) working on laminar flow control, drag reduction and transition.

J. Harris, V. Iyer and Y. Wie
Computational Methods Branch
Langley Research Center
(804)864-2285

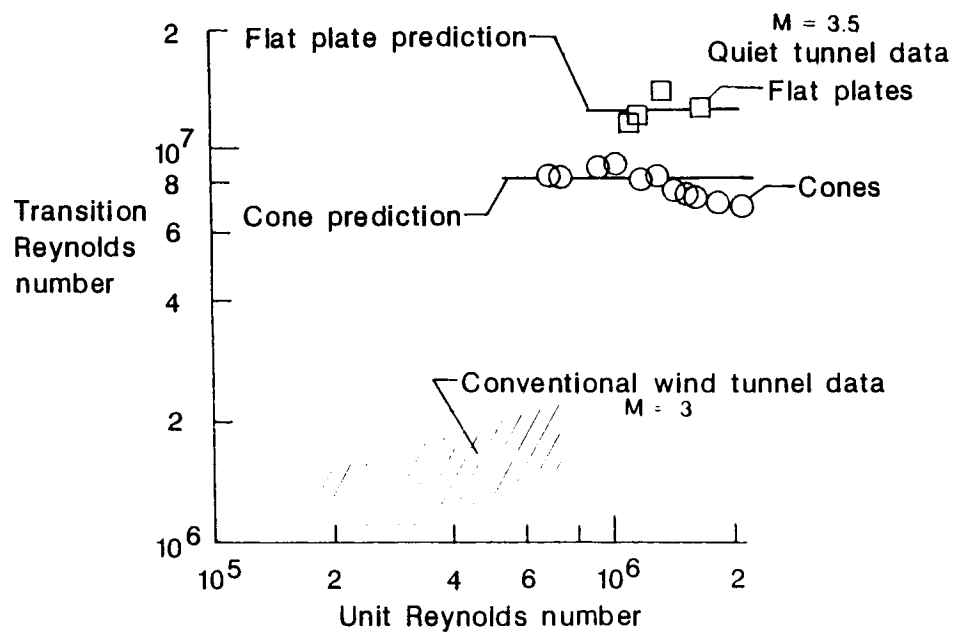


Figure 3.15. Comparison of Transition-Onset Reynolds Numbers

3.17 SUPERSONIC TRANSITION ON CONES AND FLAT PLATES

3.17.1 Objective

To determine if wind-tunnel disturbances can account for the observed, 30-year old disagreement between theory and measurement for supersonic boundary layer transition on cones and flat plates. The low-disturbance, free-stream conditions assumed by the theory can now be simulated by the Langley Mach 3.5 Low-Disturbance Tunnel. A re-examination of the cone/flat-plate discrepancy in transition Reynolds number is desirable.

3.17.2 Approach

Flat-plate and cone transition data were obtained in the Mach 3.5 Pilot Low-Disturbance Tunnel. The ratios of cone-to-flat-plate transition Reynolds numbers are about 0.6 compared with about 2 to 2.5 at this Mach number in conventional tunnels. Transition predictions based on the e^N method with $N=10$ are in excellent agreement with the measured locations of transition onset for both the cone and flat-plate data (See Figure 3.15).

3.17.3 Accomplishments

These results account for the long-standing disagreement between theory and measurements of transition on flat plates and cones. In the Low-Disturbance Pilot Tunnel, the acoustic energy radiated to the upstream sensitive regions of the cone and flat-plate boundary layers is extremely small at all frequencies and under these conditions stability theory accurately predicts transition.

3.17.4 Significance

These results reinforce dramatically two issues, (1) the importance of using quiet tunnels for high-speed transition studies and (2) the apparent usefulness of the e^N method for transition "prediction."

3.17.5 Status/Plans

Experimental investigations of the apparent different receptivities of the cone and flat-plate boundary layers will be conducted. Further development of the theory to address the receptivity problem is also planned.

Ivan E. Beckwith
Viscous Flow Branch
Langley Research Center
(804)864-5544

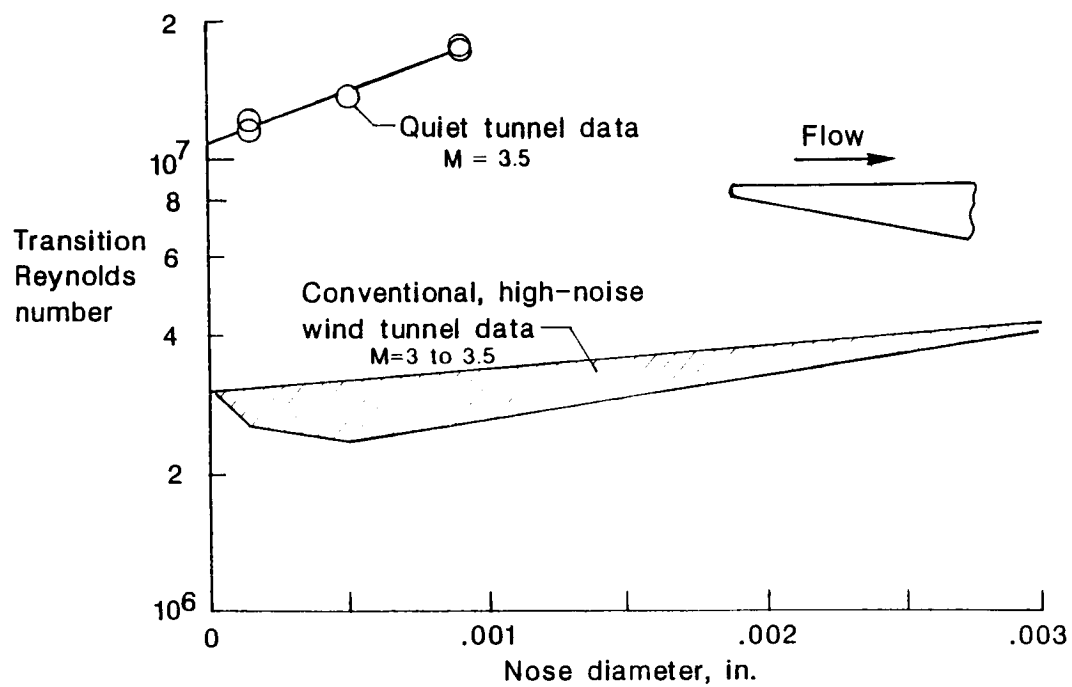


Figure 3.16. Effect of Leading Edge Bluntness on Flat Plate Transition

3.18 EFFECT OF LEADING EDGE BLUNTNES ON FLAT PLATE TRANSITION

3.18.1 Objective

To determine if wind-tunnel noise, which is present in all conventional, high-speed wind tunnels, has any influence on the previously observed effects of bluntness on transition. The effect of bluntness on flat plate transition has been the object of many experimental investigations in wind tunnels since the 1950s.

3.18.2 Approach

The Mach 3.5 Quiet Tunnel was used for this investigation in both a high-noise and low-noise mode. A flat-plate model with various nose radii was tested in this facility to study the effects of noise on blunt-nose transition. The onset of transition was determined by hot-wire probes.

3.18.3 Accomplishments

Figure 3.16 shows the variation of typical data for transition Reynolds numbers with leading-edge thickness. Transition for low-noise levels in the Quiet Tunnel are compared with previous high-noise data from AEDC Tunnel A. The values of transition Reynolds number for low noise in the Quiet Tunnel are much larger than the conventional tunnel data and also show increased sensitivity to bluntness.

3.18.4 Significance

These results illustrate another situation where wind-tunnel noise dominates a transition related phenomenon. It is clear that the wind tunnel noise drastically reduces both the transition Reynolds numbers and the dependence of transition on bluntness. These results are of critical importance to NASP-type vehicles where blunt-leading edge flows may be dramatically destabilized by external noise.

3.18.5 Status/Plans

Further tests with larger bluntness values and an increased range of unit Reynolds numbers will be made. Evaluation/calibration of the e^N method as a viable transition prediction tool will be made.

F.J. Chen and I. E. Beckwith
Viscous Flow Branch
Langley Research Center
(804)864-5732

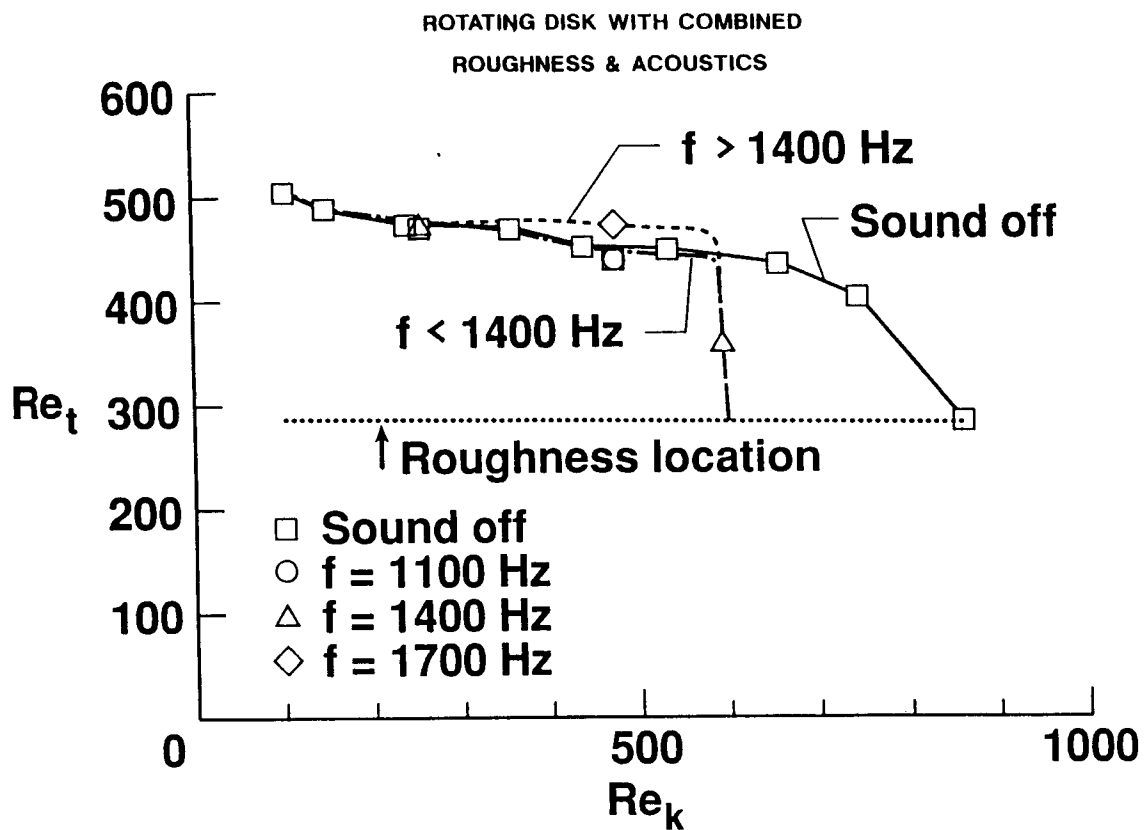


Figure 3.17. Crossflow Instability

3.19 INFLUENCE OF COMBINING DISTURBANCE FIELDS ON TRANSITION--ROUGHNESS AND ACOUSTICS

3.19.1 Objective

To explore and quantify the effects of roughness and acoustic forcing, both alone and in combination, on a boundary layer flow exhibiting the crossflow instability. Efforts to study the stability and transition of three-dimensional flows have often focused on the effects of discrete disturbance modes. It is necessary, however, to investigate combinations of disturbances as well.

3.19.2 Approach

Isolated hemispherical roughness elements of various sizes were fixed to a flat disk rotating in quiescent fluid. The roughness-perturbed flow was subjected to intense, acoustic irradiation at forcing frequencies, f , in the range $800\text{Hz} < f < 2,800\text{Hz}$. A hot wire was used to record flow structure and the location of the first turbulent burst.

3.19.3 Accomplishments

Figure 3.17 shows the general effect of forcing frequency and roughness height on transition downstream of isolated hemispherical roughness elements in terms of the roughness height Reynolds number Re_k and the transition Reynolds number, Re_t . Without roughness and for small hemispheres ($Re_k < 275$), no response to intense forcing was noted. For medium-sized roughness elements ($275 < Re_k < 590$), intense acoustic forcing at frequencies above 1400 Hz suppressed the amplitudes of the primary instabilities in the wave packet downstream of the roughness element. For large roughness elements ($Re_k > 590$), the flow was highly receptive to intense forcing at all frequencies.

3.19.4 Significance

This information is critical for the design of laminar flow control systems on swept wings where the presence of engine noise and manufacturing inhomogeneities may adversely influence transition. These results show that maximum allowable roughness heights may be dramatically reduced when high intensity sound is present.

3.19.5 Status/Plans

Future work will focus on the effects of distributed roughness in an effort to simulate the suction surface on a laminar flow control wing.

Ian A. Waitz
Viscous Flow Branch
Langley Research Center
(804)864-5540

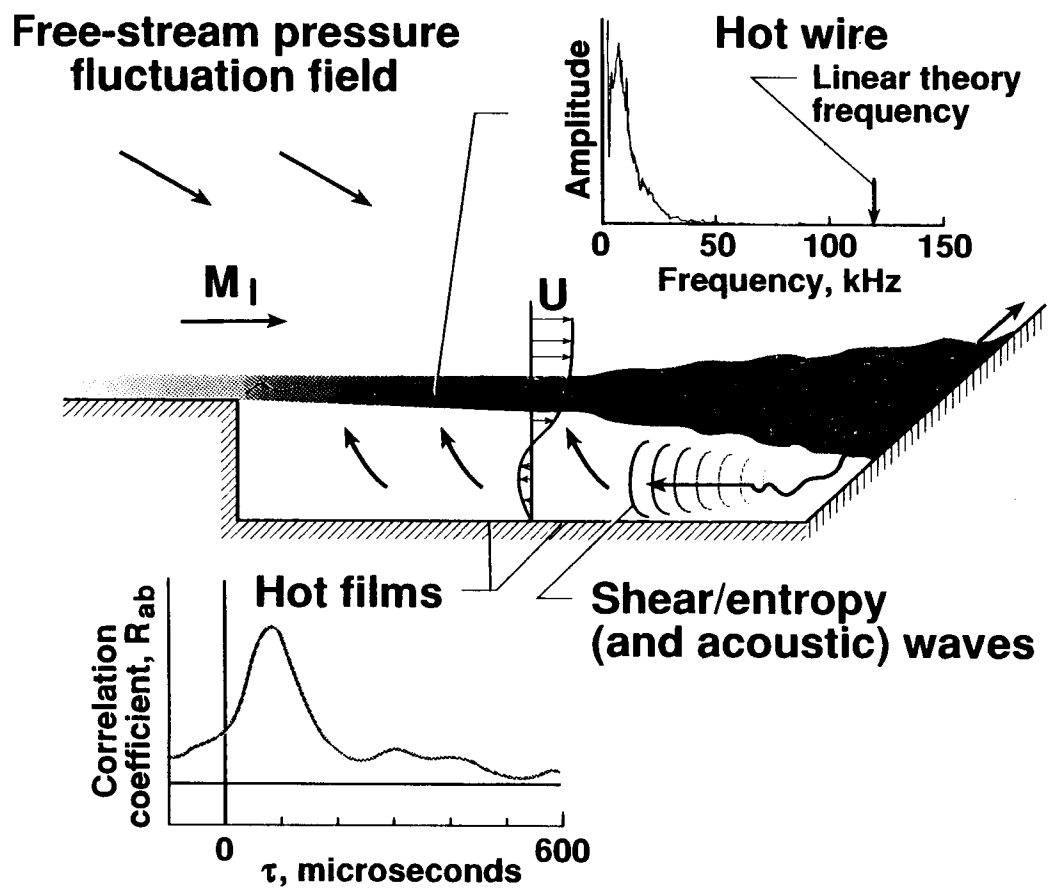


Figure 3.18. Transition Physics Indication from Present Experiment

3.20 SUPERSONIC FREE SHEAR LAYER TRANSITION

3.20.1 Objective

To determine the influence of free-stream disturbances on the location of transition in free-shear layers. Free shear layer transition at supersonic speeds is critical to scramjet-combustor design and performance due to its strong influence on the fuel/air mixing process.

3.20.2 Approach

The Langley Mach 3.5 Low Disturbance Tunnel was used to provide both low and high levels of incident noise on a free-shear layer generated by an aft-facing, step-wedge combination. The adjacent surface downstream of the step simulated a geometry common in combustor design and the downstream wedge was used to balance the pressure across the shear layer. Measurements were made with hot wires and thin film gages (See Figure 3.18).

3.20.3 Accomplishments

Free-stream noise was found to have little or no influence on the location of transition in the present free-shear layer. The figure illustrates that surface hot-film correlations showed the transition process was dominated by slow-moving, upstream-feeding disturbances through the subsonic cavity region. Hot-wire data in the shear layer indicated that the most amplified frequencies were much lower than those expected from linear stability theory.

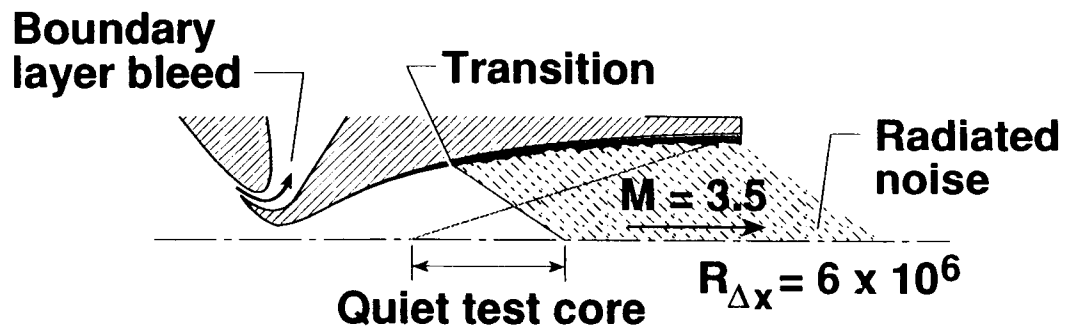
3.20.4 Significance

The free-shear layer transition process is dominated by upstream feeding disturbances (transition "bypass") for cavity-type flows with turbulent reattachment and adjacent surfaces. This process is not predicted by linear theory.

3.20.5 Status/Plans

Intersecting shocks will be used to generate isolated free-shear layers. These layers will be examined to determine the influence of free-stream noise on transition without adjacent surfaces/recirculating regions/ transitional/turbulent reattachment.

Rudolph A. King
Viscous Flow Branch
Langley Research Center
(804)864-5727



SLOW EXPANSION NOZZLE

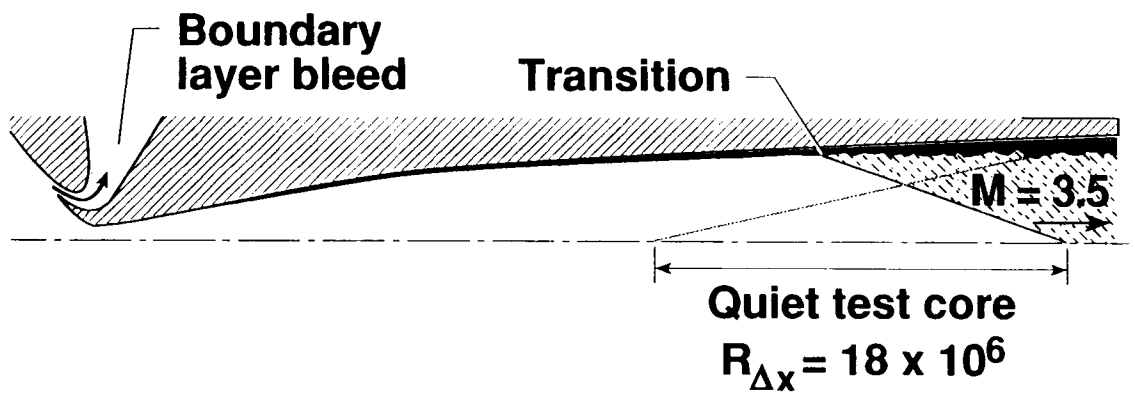


Figure 3.19. Rapid Expansion Nozzle

3.21 ADVANCES IN QUIET NOZZLE DEVELOPMENT

3.21.1 Objective

To acquire new nozzle designs that maximize the length of the quiet test core for tests with large models. Laminar nozzle wall boundary layers are required for low-disturbance wind tunnels to avoid the adverse effects of radiated noise on supersonic transition studies. The "quiet" test core size is a direct function of the length of laminar flow on the nozzle walls.

3.21.2 Approach

Current laminar flow nozzles use the rapid expansion concept to maintain laminar flow through the effect of strong, favorable pressure gradients. Such nozzles are strongly inflected and generate Gortler vortices which eventually cause transition. A new concept based on linear stability theory was used to design slower expansion nozzles that minimized Gortler vortex growth while retaining the required level of favorable pressure gradient effect (See Figure 3.19).

3.21.3 Accomplishments

A new, slow-expansion, nozzle design technique was verified that produces a quiet test core three times larger than previous rapid-expansion designs. The figure shows the increased test core size obtained with a Mach 3.5 nozzle fabricated to this design.

3.21.4 Significance

These results provide full confirmation of the theory and provide confidence in the technique for new nozzle designs. Significantly larger, more complex models can now be tested under "quiet" conditions, allowing more detailed studies of the factors affecting supersonic boundary layer transition.

3.21.5 Status/Plans

New, slow-expansion designs are underway for a Mach 6 and a Mach 8 nozzle to allow quiet testing at hypersonic Mach numbers.

Ivan E. Beckwith
Viscous Flow Branch
Langley Research Center
(804)864-5544

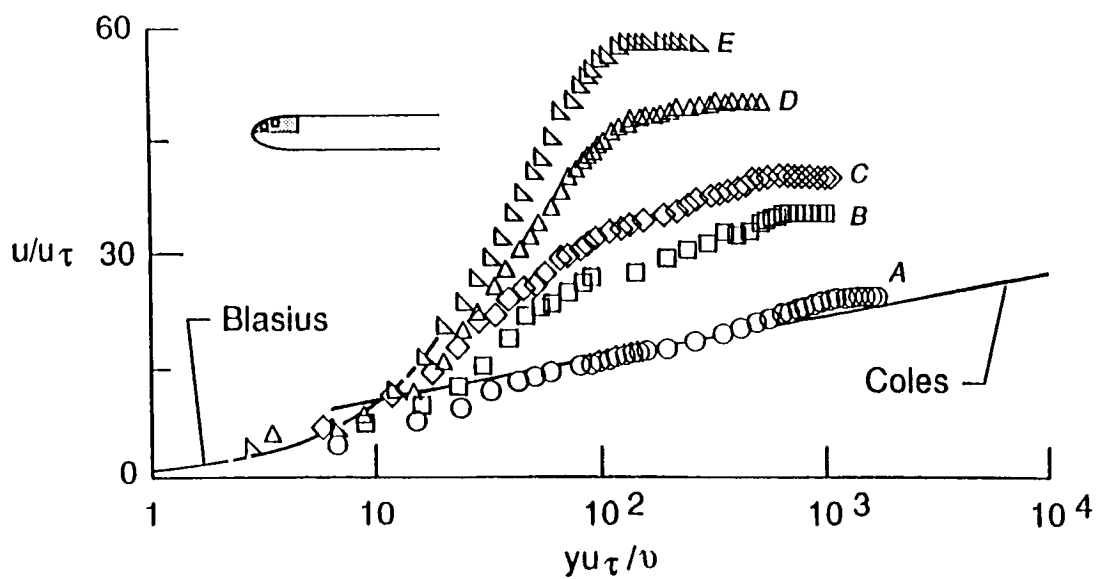


Figure 3.20. Wall Law-Transition Delay

3.22 LAMINAR FLOW CONTROL ON A FLAT PLATE USING LOCALIZED HEATING

3.22.1 Objective

To demonstrate that drag reduction can be achieved by delaying the onset of transition on a flat plate due to localized active/passive heating at the leading edge of the model.

3.22.2 Approach

Localized heating was placed on the leading edge of the model in the region of favorable pressure gradient. The accelerating flow in this region was coupled with the cooling downstream of the heat source to delay transition. As the temperature of the leading edge heat source was increased, the flow which is initially turbulent at the measurement location, went through several stages from randomly intermittent into a fully laminar stage.

3.22.3 Accomplishments

Figure 3.20 shows these changes in a law-of-the-wall plot, i.e., turbulent stage (A) to fully laminar stage (E). During this process, the Reynolds number based on momentum thickness is reduced from 3,141 to 983 with a corresponding reduction in boundary layer thickness and skin friction.

3.22.4 Significance

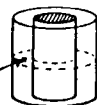
Localized leading edge heating with attended downstream cooling is shown to be effective in delaying boundary layer transition and reducing skin friction at low speeds and low Reynolds number.

3.22.5 Status/Plans

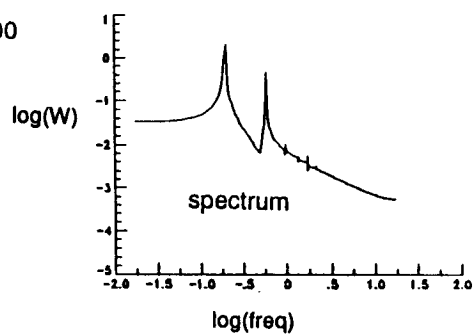
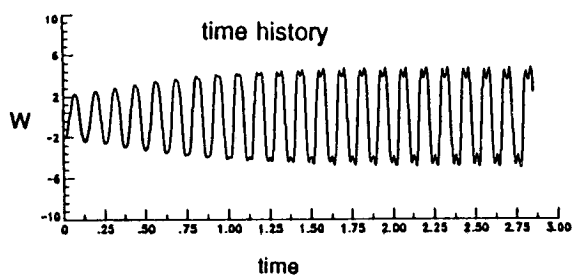
Transition delay using surface heating is being investigated on more complex configurations including concave-convex curvatures and a fuselage with three-dimensional flow.

L. Maestrello and K. A. Nagabushana
Fluid Dynamics Branch
Langley Research Center
(804)864-1067

axial velocity data
taken @ .98 gap
on mid-height plane



Quasi-Periodic Mode, $R=2000$



Chaotic Mode, $R=2500$

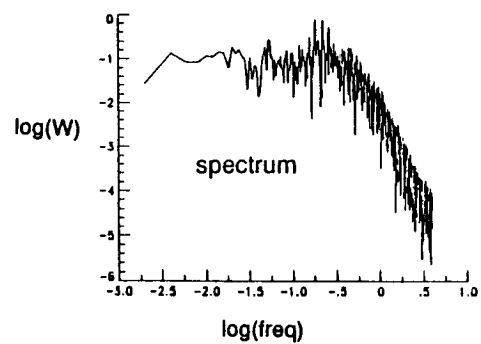
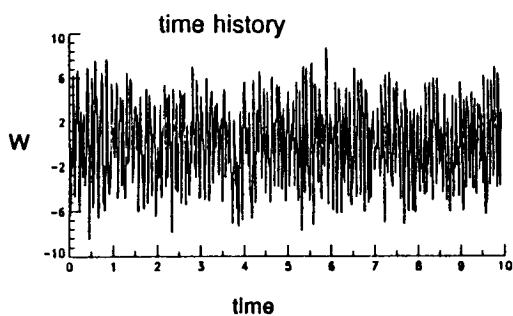


Figure 3.21. Three-Dimensional Unsteady Wavy Taylor-Couette Flow

3.23 NUMERICAL SIMULATION OF CHAOTIC STATES IN FINITE-LENGTH TAYLOR-COUETTE FLOW

3.23.1 Objective

To study the progression of a model flow with increasing Reynolds number through periodic and quasi-periodic oscillatory instabilities to a chaotic flow state and to eventual transition to turbulence.

3.23.2 Approach

The approach involved obtaining a numerical simulation of the flow via highly-accurate solutions to the incompressible time-dependent Navier-Stokes equations using a spectral collocation method. The model flow chosen was that of Taylor-Couette flow, the shear-driven flow between concentric, counter-rotating cylinders. This flow is well-known to be subject to a sequence of instabilities. The first produces a series of toroidal vortices which fill the gap between the cylinders. A number of researchers have performed extensive experimental investigations of these flow states.

3.23.3 Accomplishments

Full three-dimensional, time-accurate simulations were carried out for a particular length/gap geometry to examine the progression of the wavy vortex states through transition to turbulence as the rotation rate increases (See Figure 3.21). The upper left figure shows the time history of the axial velocity measured at a specific location in the flow for a particular scaled rotation rate (Reynolds number, R); the regular oscillatory nature of the signal indicates a smooth unsteady wavy vortex flow. The frequency spectrum of this oscillatory time history (upper right figure) indicates that the flow has just two dominant frequencies of oscillation at this rotation rate. At a higher rotation rate, the flow transitions to a weakly-turbulent or "chaotic state," as seen in the lower figures. The time history is irregular and disordered and the frequency spectrum is broadband, showing no dominant components.

3.23.4 Significance

Simulations and analysis of a chaotic flow will (1) help establish whether or not there is a connection between the mathematical theory of strange attractors in nonlinear dynamical systems and the appearance of turbulence; (2) possibly explain certain physical mechanisms in restrained transition processes (such as occurring in shear layers); and (3) further the understanding of nonlinear dynamical systems in general.

3.23.5 Status/Plans

Continued simulations will pursue the chaotic flow state to higher levels of "disorder." Techniques for analyzing simple chaotic systems (phase portraits, Poincare sections, Lyapunov exponents, etc.) will be extended for application to data produced by the simulations. One Navier-Stokes algorithm developed in the course of this work will be applied to the simulation of spatially developing boundary layer transition.

Craig L. Streett
Theoretical Aerodynamics Branch
Langley Research Center
(804)864-2230

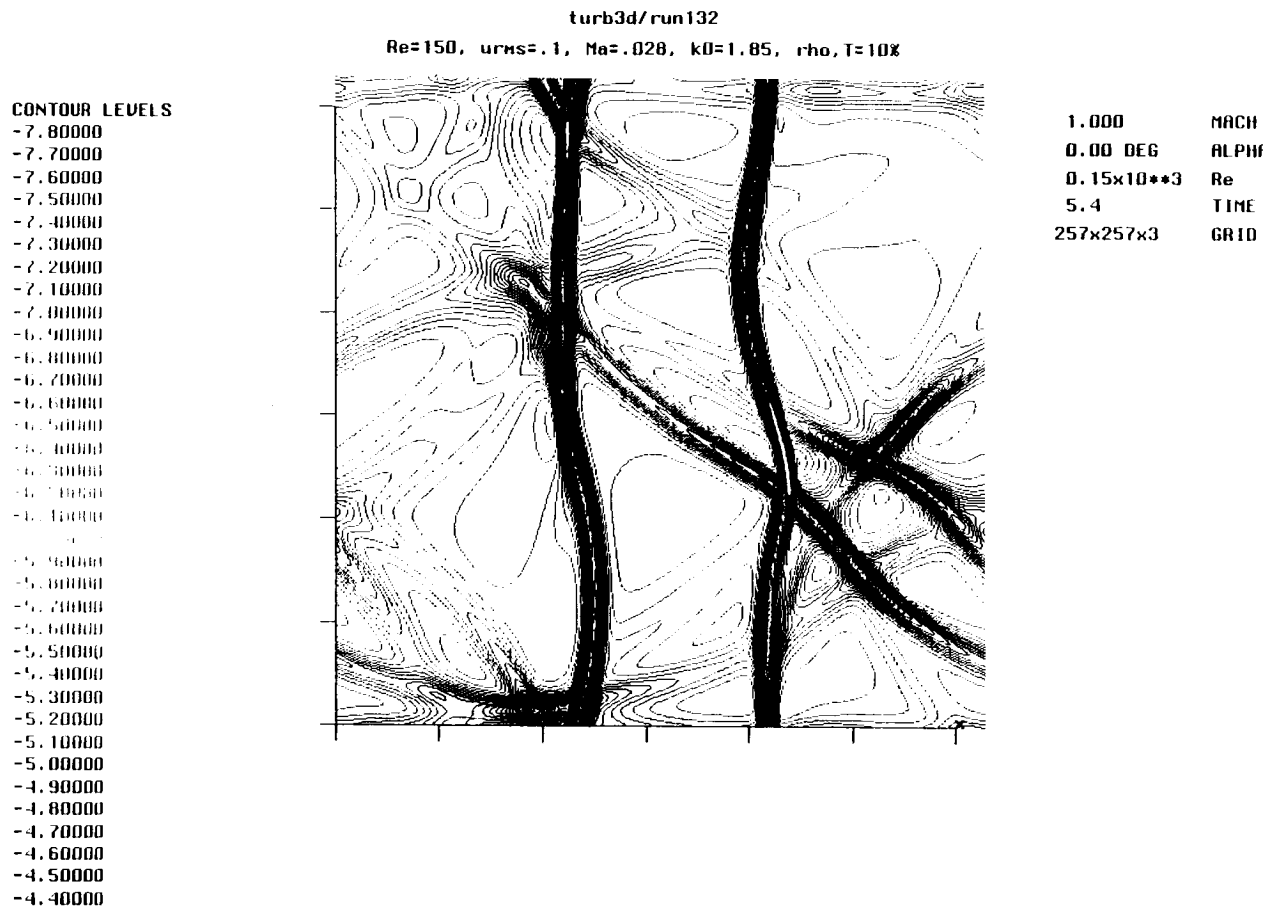


Figure 3.22. Divergence of Velocity

3.24 DIRECT SIMULATION OF COMPRESSIBLE TURBULENCE

3.24.1 Objective

To study the physics of compressible homogeneous turbulence and to generate accurate databases against which turbulence models can be evaluated.

3.24.2 Approach

The approach involved (1) numerically solving the time-dependent Navier-Stokes equations in a periodic, three-dimensional box using a fully spectral algorithm and (2) devising diagnostics to distinguish the compressible from the incompressible flow characteristics.

3.24.3 Accomplishments

A new implicit algorithm was developed to treat the acoustic terms. This results in a factor of 10 speedup on the Cray 2 when the fluctuating Mach number is less than 0.05. Initial conditions were chosen to generate weak shocks/shocklets. Under these circumstances, the kinetic energy contained in the compressible modes is greater than 70 percent of the total kinetic energy. Long time simulations of two-dimensional turbulence indicate that weak shocks form after an initial transient period and propagate at the speed of sound. Random spot checks have confirmed that local regions of vorticity are enhanced by the passage of the shock and that a pressure pulse is emitted when the shock wave hits the center of a vortex region. Figure 3.22 shows the divergence of velocity at a frozen time level. The shocks are characterized by local regions of strongly negative velocity divergence.

3.24.4 Significance

Two- and three-dimensional direct simulations improve our understanding of turbulence and can provide a good foundation upon which to build turbulence models. Ultimately, the knowledge gained from this work will lead to airplanes with reduced drag characteristics and to scramjets with improved mixing properties.

3.24.5 Status/Plans

NASA will perform two- and three-dimensional simulations of turbulent shear flows to assess whether the presence of weak curved shocks enhance mixing when the convective Mach number is supersonic.

G. Erlebacher and T.A. Zang
Computational Methods Branch
Langley Research Center
(804)864-2308

($M_\infty = 0.84$, $\alpha = 6.06^\circ$)

289x65x49 grid computations

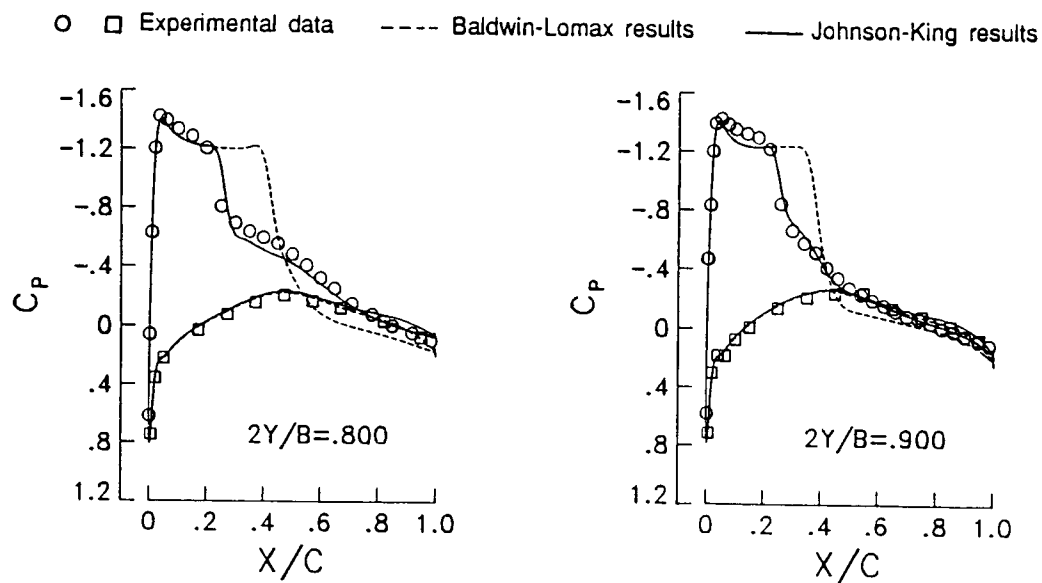


Figure 3.23. Effect of Turbulence Model on Pressure Distribution for ONERA M6 Wing

3.25 JOHNSON-KING TURBULENCE MODEL FOR 3-D FLOWS

3.25.1 Objective

To develop a non-equilibrium turbulence model for predicting separated flows over aircraft components.

3.25.2 Approach

A numerical scheme developed for thin Navier-Stokes equations was applied to solve the flow over a finite lifting wing. During the course of this study, it was established that the present method produces accurate solutions for attached flows with the Baldwin-Lomax turbulence model; however, the Baldwin-Lomax turbulence model, which is an equilibrium type model, is found to be inadequate for separated flows. A non-equilibrium turbulence model, namely the Johnson-King model developed originally for 2-D flows, was extended to 3-D flows (See Figure 3.23).

3.25.3 Accomplishments

Based on comparison of computed pressures with experimental data, it is clear that the Johnson-King model predictions for the shock location and the overall pressure distribution are in much better agreement with the data than the Baldwin-Lomax model predictions for separated flows over the ONERA M6 wing. The Johnson-King model results in a much larger reverse flow region compared to that predicted by the Baldwin-Lomax model. This improves the pressure predictions in the post shock region significantly. A mushroom type of streamline pattern observed experimentally for transonic lifting wings is produced by using the Johnson-King model.

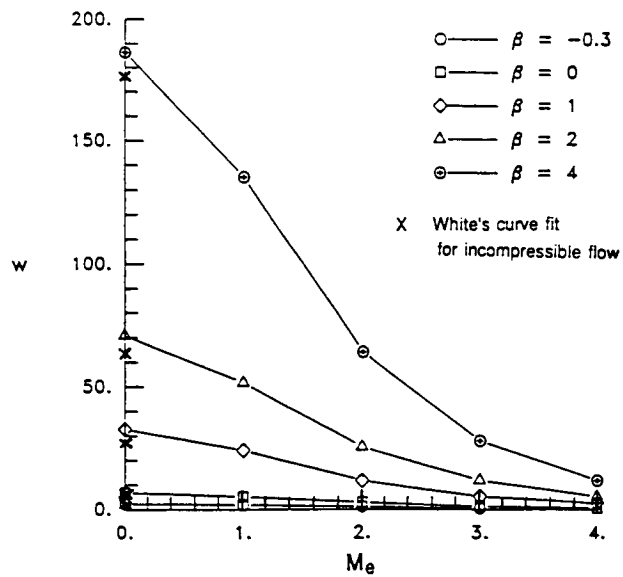
3.25.4 Significance

Non-equilibrium type of turbulence models that include history effects are required for accurate prediction of separated flows.

3.25.5 Status/Plans

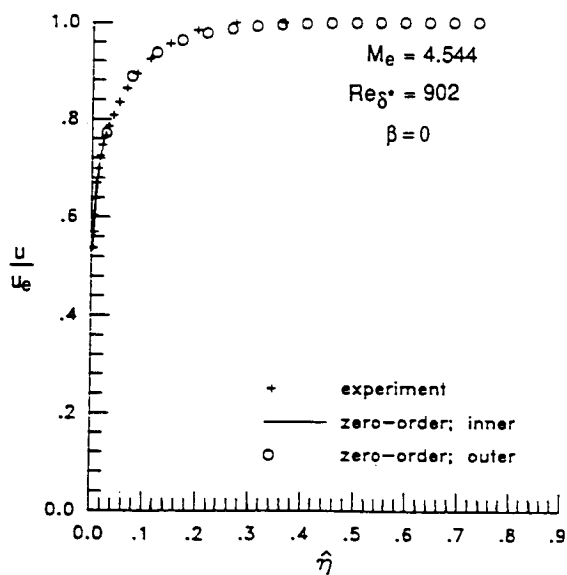
The present model is being extended for juncture flows.

V. N. Vatsa, Ridha Abid and Bruce W. Wedan
Theoretical Aerodynamics Branch
Langley Research Center
(804)864-2236



The effect of M_e and β
on the wake function coefficient.

Figure 3.24.a. Effect of M_e and β



Comparison of a velocity profile with experiment.

Figure 3.24.b. Comparison of a Velocity Profile
with Experiment

3.26 A DEFECT STREAM FUNCTION, LAW OF THE WALL/WAKE METHOD FOR COMPRESSIBLE TURBULENT BOUNDARY LAYERS

3.26.1 Objective

To simplify and improve the physical model for compressible turbulent boundary layers while reducing the computational grid requirements near walls for aircraft fluid dynamics computations.

3.26.2 Approach

Compressible laws of the wall and wake were used to model the inner region rather than an eddy viscosity model. The defect stream function formulation was exploited in the outer region. The numerically computed outer region solution was patched to the empirical inner region solution at a point determined as part of the computation.

3.26.3 Accomplishments

A defect stream function of the governing equations was formulated assuming an arbitrary turbulence model had been derived for nonequilibrium, compressible turbulent boundary layers. The formulation is advantageous because it has a highly accurate zero-order approximation with respect to the wall shear stress for which the tangential momentum equation has a first integral. Previous problems with this type of formulation near the wall were eliminated by using the empirically based, compressible law of the wall and the associated compressible law of the wake to define the flow near the wall. A method for determining the compressible law of the wake valid near the wall was developed and evaluated with the present computations of equilibrium boundary layers. The resulting wake function coefficient W is a function of the edge Mach number, M_e and the pressure gradient parameter, β (See Figure 3.24). The method was successfully tested against previous computations and experimental data for incompressible and compressible equilibrium boundary layers with adiabatic walls. The velocity defect comparison of the present method with a compressible, flat plate experiment is $Re_{\zeta}^* = 902$.

3.26.4 Significance

The computational effort required to resolve turbulent boundary layers is significantly reduced by modeling the inner region empirically, thus eliminating the fine grid requirements near the wall. The determination and use of the compressible law of the wake extends the range of the empirical description beyond the logarithmic region of the boundary layer and completely eliminates the need for an inner region eddy viscosity model. The defect stream function formulation yields a simple and yet accurate, approximation of the governing equations. The method can be incorporated into existing Navier-Stokes codes for aircraft fluid dynamics computations and enable significant computational savings for these existing codes.

3.26.5 Status/Plans

The present techniques are being incorporated and tested in an existing Navier-Stokes code assuming local equilibrium flow. The full nonequilibrium method will then be incorporated. It is planned to extend the method to three-dimensional flows. The effect of various turbulence models and nonadiabatic wall effects will also be studied.

Richard A. Wahls
Computational Methods Branch
Langley Research Center
(804)864-2303

CHAPTER FOUR

NUMERICAL AERODYNAMIC SIMULATION (NAS)

4.1 INTRODUCTION

Numerical Aerodynamic Simulation (NAS) provides a large-scale simulation capability that is recognized as a key element of NASA's aeronautics program. It provides readily accessible supercomputing capability to the United States' top aeronautical researchers in Government, industry and academia. The NAS program also includes research and technology development to ensure the application of emerging technologies to computational fluid dynamics and other computational sciences.

The objectives of NAS are to (1) maintain a pathfinding role in providing leading-edge supercomputing capabilities to NASA, DoD and other Government agencies, industry and universities as a critical element for continued leadership in computational aeronautics and related fields; (2) stimulate the development of state-of-the-art, large-scale, computer systems and advanced computational tools for pioneering research and development and (3) provide a strong research tool for OAST.

To maintain the lead in large-scale, computing capability, NAS is implementing a strategy of installing, at the earliest possible opportunity, the most powerful, high-speed processor (HSP) available. NAS maintains at least two high-speed processors, one which is fully operational and represents more mature technology and the other which is a higher performance prototype or early production model. This strategy began in September 1986 with the installation of the first, full-scale Cray-2, as HSP-1. A second Cray-2 was added in January 1988 and was replaced by HSP-2, a Cray Y-MP, in November 1988. NAS was the first customer for the Cray Y-MP, which is the first computer to sustain a computation rate of a billion calculations per second. Current plans are to replace the Cray-2 with a new processor (HSP-3) in 1991.

NAS was the first supercomputing facility to install a standard operating system and communication software on all processors. All NAS computers run under a form of the UNIX operating system, which offers the flexibility of both batch and interactive computing and provides a common user interface on all user-visible subsystems. NAS is linked to 26 remote locations nationwide by NASnet, a unique, high-performance communication network. With communication speed reaching 1,544 Kbits/sec., NASnet allows researchers at remote locations to have virtually the same interactive capability as users at the NAS facility.

The vision for the NAS program is to provide by the year 2000 an operational computing system capable of simulating an entire aerospace vehicle system within a computing time range from one to several hours. It is estimated that a computing time rate of one trillion operations per second (TFLOPS) is required to accomplish this. This represents a 1000-fold increase in speed over today's most powerful computers.

Program Manager: Mr. Edward T. Schairer
OAST/RF
Washington, DC 20546
(202)453-2819

4.2 CRAY Y-MP INSTALLATION

4.2.1 Objective

To place the first Cray Y-MP into production as rapidly as possible.

4.2.2 Approach

The Cray Y-MP was delivered to NAS in late 1988 followed by extensive acceptance testing and the correction of hardware and software problems. Standard procedures and utilities used on the NAS Cray-2 were installed on the Y-MP. Documentation of the differences between the systems was developed to help users make use of the new system. Software was developed to control the use of the batch queues which provided the best overall job throughput. Temporary fixes were developed for features and functions which did not yet exist and feedback was provided to Cray research regarding the needs for a fully functioning production system.

4.2.3 Accomplishments

The Y-MP was placed into production with over 1,000 NAS users on February 15, 1989. During acceptance testing, the system met or exceeded all contractual requirements, including a 1.0 GFLOPS performance rate on both a scientific application FORTRAN workload and on individual multi-tasked FORTRAN codes.

4.2.4 Significance

The supercomputer system was the first Cray Y-MP delivered to a customer site and early software and hardware problems were resolved in a realistic production environment. Users obtained early access to today's most powerful computer system that accounts for 80 percent of the computing capacity of the NAS System.

4.2.5 Status/Plans

NASA plans to continue upgrading the service of the Y-MP by adding function and performance improvements.

John T. Barton
NAS Systems Development
Ames Research Center
(415)604-4409

William T. C. Kramer
NAS Computational Services Branch
Ames Research Center
(415)604-4600

4.3 INSTALLATION OF EARLY RELEASE UNICOS 5.0 ON THE CRAY Y-MP

4.3.1 Objective

To provide an improved operating system for the Cray Y-MP supercomputer, which will correct many of the deficiencies of the first release of the operating system (UNICOS 4.0).

4.3.2 Approach

The new operating system was installed by local Cray Research personnel working with the NAS support staff. During early testing, major problems were discovered with local modifications. These were due to Cray redesigning the kernel to be multi-threaded (to run concurrently on multiple CPUs) which created timing problems. It took several sessions of dedicated time to resolve these issues. While testing was underway, procedures to improve the effectiveness of the Solid State Disk (SSD) were developed and documented. Since this entailed changing the way NAS users accessed the SSD, documentation was provided to them in advance.

4.3.3 Accomplishments

UNICOS 5.0 provided important features lacking in the first release of the Cray Y-MP UNICOS operating system, such as the networking implementation of Berkeley 4.3 UNIX, efficient methods to manage the SSD and the support of new hardware.

4.3.4 Significance

UNICOS 5.0 provided benefits for the NAS users through increased functionality and improved performance. It provided complete support for much of the early and beta test software and hardware installed on the Y-MP and allowed improved use of the SSD. It also allowed the implementation of improved networking throughout the entire NAS System.

4.3.5 Status/Plans

NASA plans to continue investigating UNICOS 5.0 features which will improve the service of the Cray Y-MP at NAS.

William T. C. Kramer
NAS Computational Services Branch
Ames Research Center
(415)604-4600

4.4 INSTALLATION OF ALPHA TEST UNICOS 5.0 ON THE CRAY-2

4.4.1 Objective

To provide a very rapid installation and test of an untried version of the operating system for the Cray-2 supercomputer.

4.4.2 Approach

The new operating system was installed by Cray Research personnel working with local support staff. This was the first installation and many problems and bugs were found. After the installation, significant local modifications were added and then the entire system was tested in several nights of intensive effort.

4.4.3 Accomplishments

Within three weeks of arrival, the new operating system was in production with over 1,000 NAS users. NAS was the first site (including internal Cray systems) to run a complete version of 5.0.

4.4.4 Significance

UNICOS 5.0 provided benefits for the NAS user community through increased functionality and improved performance. It provided complete support for much of the software and hardware previously installed on the Cray-2 as early and beta test versions. In addition to the improved software, the feedback to Cray Research concerning problems and issues led to an improved release for the general customer base.

4.4.5 Status/Plans

UNICOS 5.0 was a prerequisite to using the Cray autotasking software which was installed in May. It provides the first ability to automatically multitask a program on the Cray-2.

William T. C. Kramer
NAS Computational Services Branch
Ames Research Center
(415)604-4600

(in Megabits per sec., aggregate file rate)

<u>Version</u>	<u>Streams</u>	<u>HSP to MSS</u>		<u>MSS to HSP</u>		<u>Rate</u>
		<u>10 Mbyte File</u>	<u>100 Mbyte File</u>	<u>10 Mbyte File</u>	<u>100 Mbyte File</u>	
6.0	1	4.16	4.50	4.76	5.13	Production
7.0	1	9.25	9.37	5.76	6.44	Production
7.0	2	14.00	14.10	12.00	12.10	Tested
7.0	3	22.00	22.14	18.09	18.20	Tested
7.0	4	30.00	30.15	27.00	27.15	Tested

Figure 4.1. Mass Storage System Transfer Rate Increases

4.5 MASS STORAGE SYSTEM (MSS-I) RELEASE 7.0

4.5.1 Objective

To improve the transfer performance between the supercomputers and the Mass Storage System (MSS).

4.5.2 Approach

An analysis of the bottlenecks in the MSS 6.0 software was completed to identify major areas of possible improvement; then, the MSS software architecture was redesigned and new software was implemented. The file access method was redesigned so that data are written on multiple disks (striped) to improve performance. To further increase performance, the flow of control information is separated from the flow of data. Control information flows through the UTS (UNIX-based) part of the MSS to set up the transfer, but the data actually flows directly from the supercomputer to the MSS disks under the control of the MVS operating system. Finally, Storage Technology Tape Robots were integrated into the system.

4.5.3 Accomplishments

Release 7.0 of the MSS was implemented in February 1989. The MSS 7.0 software shows significant performance improvements for both single file and multiple file transfers. The average sustained speed currently is six to nine Mbits/sec., as opposed to the several hundred Kbits/second seen in the first production release, MSS 5.0. Average tape mount times are reduced from six minutes to 15 seconds (See Figure 4.1).

4.5.4 Significance

Improved MSS performance already increases the effectiveness of the NAS supercomputers by providing more rapid access to a much greater data storage capacity than available on the supercomputers themselves and at less cost.

4.5.5 Status/Plans

The system is in production and plans are to increase further performance by network striping.

Julian Richards
NAS Computational Services Branch
Ames Research Center
(415)604-4611

4.6 AUTOMATED TAPE LIBRARIES

4.6.1 Objective

To identify alternative storage devices to use in conjunction with the existing rotating storage. The devices had to (1) be compatible with the current Mass Storage Subsystems as well as the goals of the Mass Storage Subsystem II currently under development and (2) provide increased storage density and better price performance over rotating storage while providing acceptable data access rates.

4.6.2 Approach

The approach involved (1) analyzing the storage and interface requirements for the current MSS and (2) determining the follow-on requirements for MSS-II. These requirements included functionality, performance, capacity, media compatibility and expendability. Both existing and emerging technologies were surveyed to determine candidate devices.

4.6.3 Accomplishments

This effort resulted in the acquisition of two STK 4,400 Automated Tape Libraries. The systems are interconnected with each holding approximately 6,000 IBM 3,480 tape cartridges. Each cartridge has a capacity of 200 Mb and each library has a capacity of 1.2TB. Each library has eight tape drives and provides tape mounts in an average of 15 seconds when a tape drive is available, without operator intervention. The tapes are read at three Mb/second.

4.6.4 Significance

Access to far greater amounts of user data has dramatically increased while decreasing operator workload. The introduction of this system is the first application of online levels of hierarchical storage in the MSS. This concept will be greatly expanded in MSS II.

4.6.5 Status/Plans

The acquisition has the option to expand the number of libraries to eight over the next three years. The rate of expansion will depend on the data growth rate as well as the incorporation of media density improvements that are likely to occur. The libraries will be incorporated in the MSS II.

Mark Tangney
NAS Development Branch
Ames Research Center
(415)604-4415

4.7 MSS-II DEVELOPMENT

4.7.1 Objective

To develop high performance, highly reliable and user transparent mass storage system for integration into the Unix and TCP/IP open systems architecture environment.

4.7.2 Approach

MSS-II was designed to appear on the NAS network as another Unix system with a very large complement of very fast, very reliable disks. It was accomplished by incorporating three separate changes to Amdahl's UTS implementation of Unix. The first was the High Performance File System, a fault-tolerant, parallel-access disk file system, which achieves very fast file access to large files and which eliminates the need for system interruptions for backups. The second was Rapid Access Storage Hierarchy, which makes files appear to be on disk when the infrequently used files are really on less expensive tape. The third was the Volume Manager, with removable media, capable of controlling automated and manual volume mounts and dismounts. To make this system's file transfer capabilities available to the supercomputers on the network, a high performance parallel network access method was included.

4.7.3 Accomplishments

The hardware is largely in place and the software design is complete. The major software components of the system are implemented. Unix System V.3 File System Switch port to UTS 1.2 is complete. The parallel-access disk file system is in the final stages of integration with File System Switch.

4.7.4 Significance

MSS-II will offer NAS users the highest file transfer performance (10 Mb/sec.) of any MSS of which NASA are aware and also the most suited for use in the Unix and TCP/IP environment. It will be able to survive any single hardware or media failure without data loss, permitting it to be run without interruptions for backups. Its automatic restoration of archived files upon demand will permit users to remain unaware of whether their data are on disk or tape. MSS-II will provide these benefits while appearing to the user to be just another Unix system on the network.

4.7.5 Status/Plans

The major software components of the system work separately and will be integrated one-at-a-time after the parallel-access disk file system. The parallel-access network connection software and hardware also are underway. Initial production use is scheduled for Winter 1989.

David Tweten
NAS System Development Branch
Ames Research Center
(415)604-4416

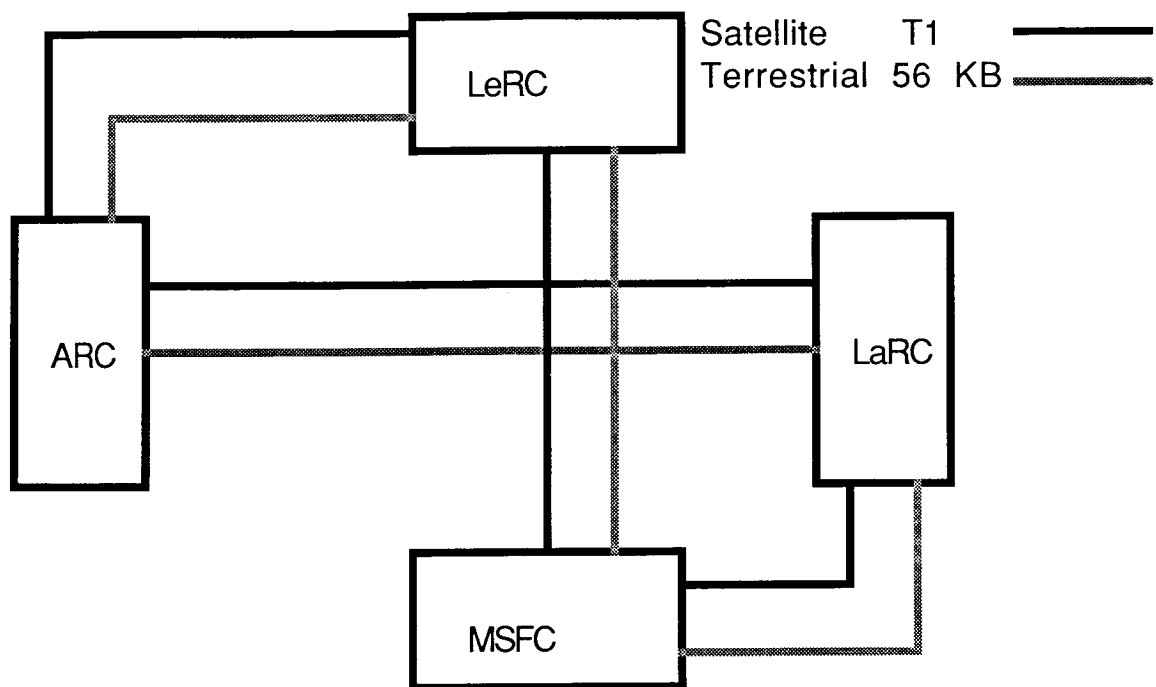


Figure 4.2. RIB/RIG Testbed Diagram

4.8 RESEARCH INTERNET GATEWAY (RIG)

4.8.1 Objective

To (1) provide a research testbed for wide area network development, (2) increase the throughput and provide network management capabilities and (3) follow up with procurement for operational systems.

4.8.2 Approach

A cooperative agreement among NASA, DARPA and DOE was established to build a series of testbeds for a next generation, wide area network. Advanced network gateways for the testbeds were developed to handle increased network throughput over wide areas. The testbeds drove multiple T1 (1.544 Mbits/sec.) lines and lead to T3 capability (45 Mbits/second). The ability to handle and manage more complex topology, through the use of new software controls in routing and network monitoring, is being developed (See Figure 4.2).

4.8.3 Accomplishments

Engineering is in progress on this effort. Vendor contracts for hardware and software development were awarded to GTE/Proteon, SRI/Cisco Systems and BBN. NASA PSCN circuits for this testbed and DARPA National Network Testbed (NNT) circuits are in the process of being installed.

4.8.4 Significance

Cooperation among NASA, DARPA and DOE to solve a common problem is being demonstrated. The capability to control and manage large, high performance data networks will be developed, which did not exist before. Higher performance data networking will be provided to OAST users at lower cost when applied to an operational data network such as NASnet and CNS.

John Lekashman
NAS Development Branch
Ames Research Center
(415)604-4359

4.9 THE PANEL LIBRARY

4.9.1 Objective

To provide a uniform set of man-machine interface tools for users of the NAS graphics workstations (currently the Silicon Graphics IRIS 2500T and 3000 Series).

4.9.2 Approach

A library of C language functions and procedures was developed which permits the easy construction of user interfaces to application codes on the NAS graphics workstations (the Silicon Graphics 4-D Series is also supported). Tools were provided to control sliders, buttons, pop-down menus, strip charts, dialog boxes, file I/O, command scripting, etc. A thorough manual documenting the Panel Library was completed. Numerous demonstration programs and a lecture/tutorial are available. The Panel Library was described to both university and industry audiences. Its distribution and upgrade are provided over the Internet, where this work was very well received.

4.9.3 Significance

The Panel Library will greatly shorten the time it takes both developers and researchers to program new applications. Minimal time will be required on the user interface; thus, greater time can be spent on the core aspects of the application.

4.9.4 Status/Plans

NASA will complete documentation and are planning future enhancements.

David Tristram
NAS Applied Research Office
Ames Research Center
(415)604-4404

4.10 PERFORMANCE OF AN EULER CODE ON HYPERCUBES

4.10.1 Objective

To evaluate CFD performance on a multiple-instruction, multiple data (MIMD) stream, hypercube architecture.

4.10.2 Approach

The approach involved parallelizing Jameson's FLO52 (a 2-D Euler code) for a 16-node Intel Personal Supercomputer (iPSC/2) at Stanford and a 512-node NCUBE/10 at Caltech.

4.10.3 Accomplishments

Considerable effort was invested optimizing the code for both machines. Overall efficiency (time on one processor/ $N \times$ time on N processors) increased from 57 percent to 88 percent. Although it was a challenge to produce efficient parallel code on these MIMD architectures, the overall computing performance is promising. The iPSC/2 ran within one tenth of the performance of a single processor Cray X-MP and the 512-node NCUBE, within one third of the performance.

4.10.4 Significance

This work demonstrates that CFD can be done on MIMD architectures. The machines considered had node-based, personal computer components. These architectures should be scalable with RISC components to Cray performance at a fraction of the cost.

E. Barszcz, T. Chan, Dennis Jespersion and R. Tuminaro
NAS Applied Research Office
Ames Research Center
(415)604-6014

Comparison of ARC2D on 1 processor XMP
with similar code on 16K processor CM2 with floating point

	MFLOP			SEC/STEP		
	CM2	XMP	Ratio	XMP	CM2	Ratio
(implicit)						
128 X 128	58	63	0.92	0.34	0.43	0.79
256 X 128	86	63	1.36	0.69	0.60	1.15
512 X 512	106	63	1.68	5.50	4.20	1.31
(explicit)						
128 X 128	63	51	1.24	0.69	0.43	1.60
256 X 128	123	51	2.41	1.40	0.44	3.18
512 X 512	241	51	4.72	11.0	1.80	6.11

Figure 4.3. Comparison of ARC2D on One Processor XMP

4.11 COMPUTATIONAL FLUID DYNAMICS ON A MASSIVELY PARALLEL COMPUTER

4.11.1 Objective

To study the feasibility of performing CFD calculations on a massively parallel, Single Instruction, Multiple Data (SIMD) stream architecture.

4.11.2 Approach

The approach involved mapping the functionality of ARC2-D and ARC3-D (2-D and 3-D Navier-Stokes codes) to a Thinking Machines 32,000 node Connection Machine 2 (CM2) (See Figure 4.3).

4.11.3 Accomplishments

Both the 2-D and 3-D versions of this code were successfully mapped to the CM2. Performance was comparable to that of a single processor Cray-2 for implicit methods and several times faster for explicit methods.

4.11.4 Significance

It is generally accepted that significant advances in supercomputing performance will come only through the use of parallel computers having many processors. This work demonstrates that CFD can be done on a massively parallel SIMD architecture.

Creon Levit and Dennis Jespersen
NAS Applied Research Office
Ames Research Center
(415)604-4403

This page is intentionally left blank.

DRAG REDUCTION.

Research is being conducted in drag reduction and separated flow control for aircraft across the speed range. Emphasis is being placed on control of boundary layer flows by both passive and active approaches to reduce friction and induced drag and to improve aircraft stability and performance. Detailed flow experiments are being used to better understand the physics of boundary layer flows in order to facilitate developing effective concepts for boundary layer flow control.

Drag reduction efforts include wind tunnel, flight and computational research to explore the control of boundary layer transition, turbulence, vortical flows and shock-induced flowfield development. Also, transonic and supersonic laminar flow control, vorticity control for reducing induced drag and separation and supersonic wave drag reduction research projects are underway.

Design methodologies and technologies are being developed for practical, reliable and maintainable viscous drag reduction systems for military and civil subsonic transport aircraft. Flight and computational research is being conducted to minimize the risks associated with both the near-term and far-term applications of laminar flow and hybrid laminar flow control to transport aircraft. Flight experiments validate methodology and provide operational performance and reliability data in representative environments at practical unit and length Reynolds numbers.

Computer codes are under development for the analysis and design of new Laval nozzles for the design of a laminar, supersonic, boundary layer wind tunnel.

Flow transition research includes (1) methods for calculating the amplitude and phase of the unstable wave motion in growing incompressible and compressible 2-D and 3-D boundary-layers and in free shear flows, (2) identifying receptivity mechanisms by which freestream turbulence and other environmental disturbances interact with a boundary layer to produce instability waves and other disturbances relevant to transition and (3) use of receptivity and wave-growth investigations to develop rational methods for the prediction and control of transition.

5-1

ORIGINAL PAGE
BLACK AND WHITE PHOTOGRAPH

NASA Dryden flight tests - 42,000 ft, F-106
Net reduction is 4-8% over treated area

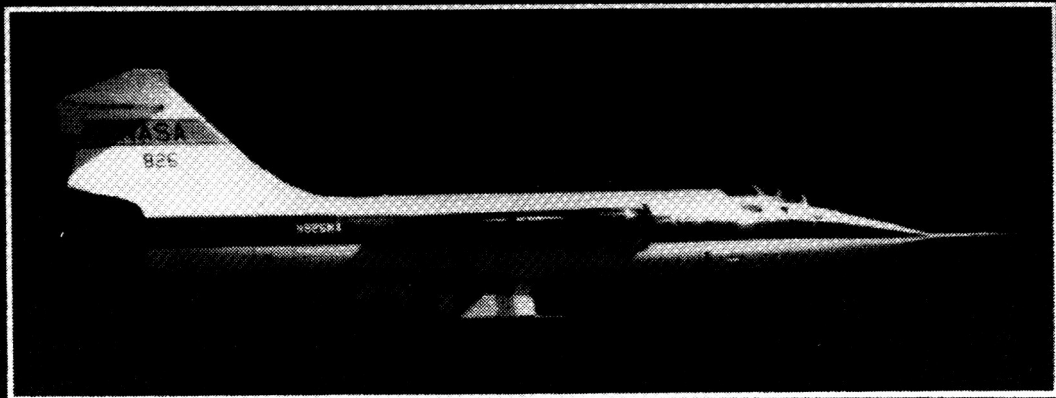
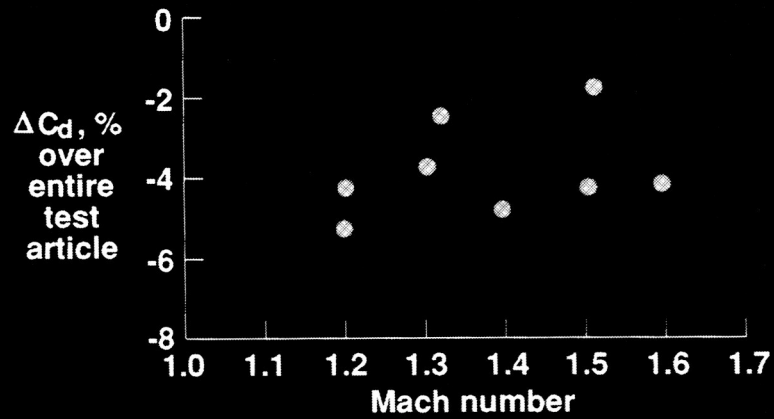


Figure 5.1. Supersonic Riblet Drag Reduction

5.2 RIBLETS FOR TURBULENT DRAG REDUCTION IN SUPERSONIC FLIGHT

5.2.1 Objective

To extend the database to supersonic flow. Riblets have been shown to reduce skin-friction drag six to ten percent in low-speed wind-tunnel tests and on transonic aircraft.

5.2.2 Approach

The Flight Test Fixture (FTF) on a F-104 aircraft at Ames/Dryden was used to evaluate the skin-friction reduction performance of riblets at supersonic speeds in the flight environment. Online data allowed the pilot to maintain zero Crossflow on the FTF for Mach 0.8 to 1.7 at a variety of altitudes. Surface pressures, local skin friction and boundary layer surveys were obtained with and without riblet film installed on a portion of the FTF. Riblets reduced the overall drag of the FTF by two to five percent. This is equivalent to a skin-friction reduction of six to eight percent over the riblet test area. Furthermore, these tests show that, up to Mach 1.7, the drag reduction is essentially independent of Mach number (See Figure 5.1).

5.2.3 Accomplishments

The study demonstrated that riblets are a viable concept for aerodynamic vehicles with extensive turbulent flow in the Mach number regime up to M 1.7.

5.2.4 Significance

As a result of the apparent insensitivity of riblet performance to Mach number, drag reduction at somewhat higher Mach numbers can be expected, i.e., for the currently considered supersonic transport.

5.2.5 Status/Plans

Because the current results are dependent upon computed initial conditions, additional measurements are planned in a second phase of the experiment. A boundary layer rake will be mounted at the upstream location and data will be gathered for the same flight conditions used in Phase I. This will allow a more accurate determination of the net drag reduction obtainable and the geometrical scaling laws.

Arild Bertelrud
Viscous Flow Branch
Langley Research Center
(804)864-5559

**Constant lift and wing-root bending moment
Optimum (variable) span loading**

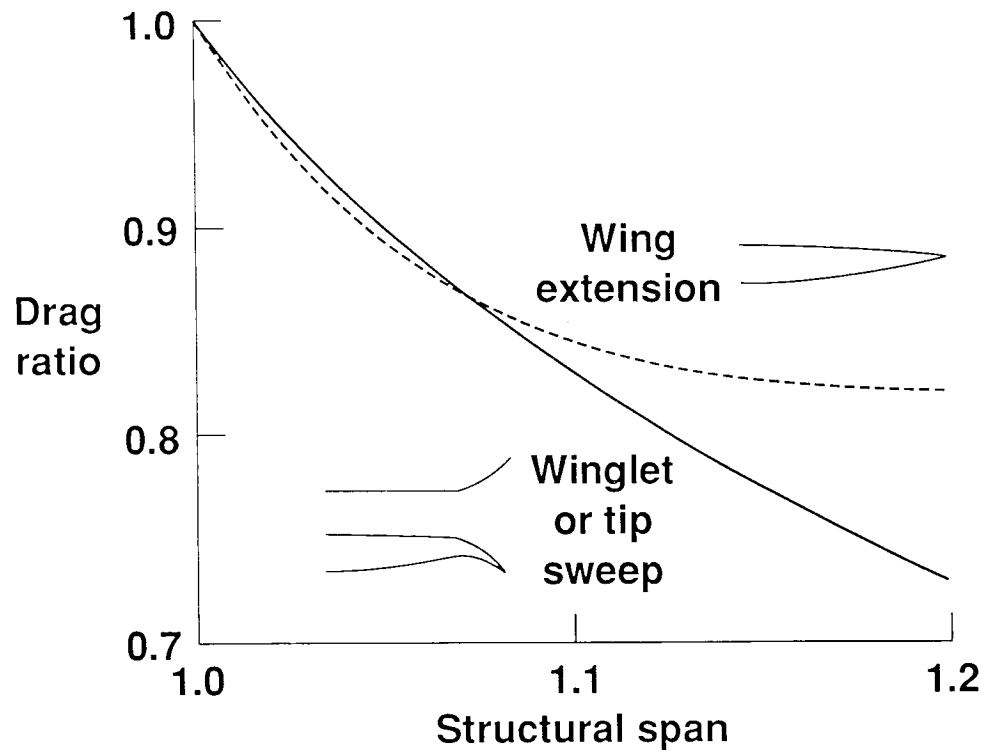


Figure 5.2. Induced Drag Reduction

5.3 INDUCED DRAG REDUCTION

5.3.1 Objective

To develop a rational method for evaluating and optimizing wings for induced drag reduction.

5.3.2 Approach

A recently developed theory was used to predict the relative drag characteristics of wings with winglets, tip sweep and simple span extension. The theory was a "viscous lifting line" approach in which the drag is based on the entropy generated by spanwise gradients in circulation. The induced drag reduction was predicted for wings with constant area, lift and wing-root bending moment as a function of their structural span. The structural span was defined as the length of the "lifting line" normalized by a reference span.

5.3.3 Accomplishments

The results were for a straight span increase (labeled wing extension) and a curved span increase using winglets or tip sweep (which are equivalent in the current theory). Winglets and tip sweep are less efficient initially than a straight span increase but are not limited by the bending moment constraint (See Figure 5.2).

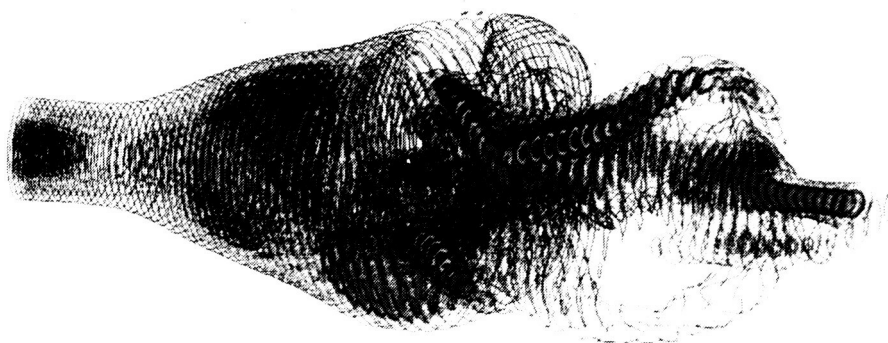
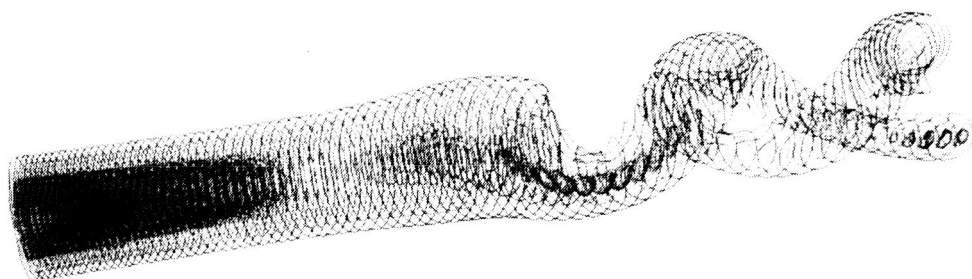
5.3.4 Significance

Theory predicts that the induced drag of an optimum wing can be reduced further by increasing the structural span, either by wing extension, winglets or tip sweep. In the absence of structural constraints, wing extension is predicted to be the most efficient. With structural constraints, the optimum aerodynamic configuration is determined by the imposed constraints; therefore, early interaction of aerodynamic and structural disciplines is imperative in the research/design process.

5.3.5 Status/Plans

A cooperative Langley Aero/Structures research effort is anticipated to develop a wing-weight constraint model for incorporation in the induced drag theory.

George C. Greene
Viscous Flow Branch
Langley Research Center
(804)864-5545



Contour plots of total vorticity for double helix and bubble type vortex breakdown flows.

Figure 5.3. Contour Plots of Total Vorticity

5.4 COMPOSITE STRUCTURE AND TYPES OF VORTEX BREAKDOWN

5.4.1 Objective

To identify and analyze five distinct types of vortex breakdown (or states of disruption) in order to understand the mechanisms responsible for such flows.

5.4.2 Approach

A numerical simulation, using the full incompressible, unsteady Navier-Stokes equations, was performed. The results were compared with previous experimental flow visualization studies to validate the numerical results. The computed flow variables, such as vorticity, velocity and pressure, were then analyzed in order to identify key breakdown mechanisms. Currently, the helix, double helix, spiral and bubble types of breakdown have been uniquely identified (See Figure 5.3). These images are in qualitative agreement with the dye injection results of previous experimental studies.

5.4.3 Accomplishments

To date, the only information available regarding the asymmetric forms of vortex breakdown has been derived from experiments. Studies utilizing dye injection are necessarily restricted to the qualitative aspects of vortex breakdown. The few LDV studies that have been done are limited in scope, treating only the bubble-type breakdown. By contrast, the present numerical simulations are providing details of the unsteady velocity and vorticity distributions within four distinct types of vortex breakdown flows.

5.4.4 Significance

These computations will aid in identifying the as yet unknown mechanisms responsible for such diverse types of vortical flow behavior.

5.4.5 Status/Plans

The fifth type of breakdown, the flattened bubble, needs to be isolated. Upon completion of this task, the data will be analyzed in an attempt to quantify the triggering mechanisms in each of the breakdown modes. The applicability of existing theories to these highly nonlinear vortical flows will be investigated.

Robert E. Spall and Thomas B. Gatski
Viscous Flow Branch
Langley Research Center
(804)864-5561

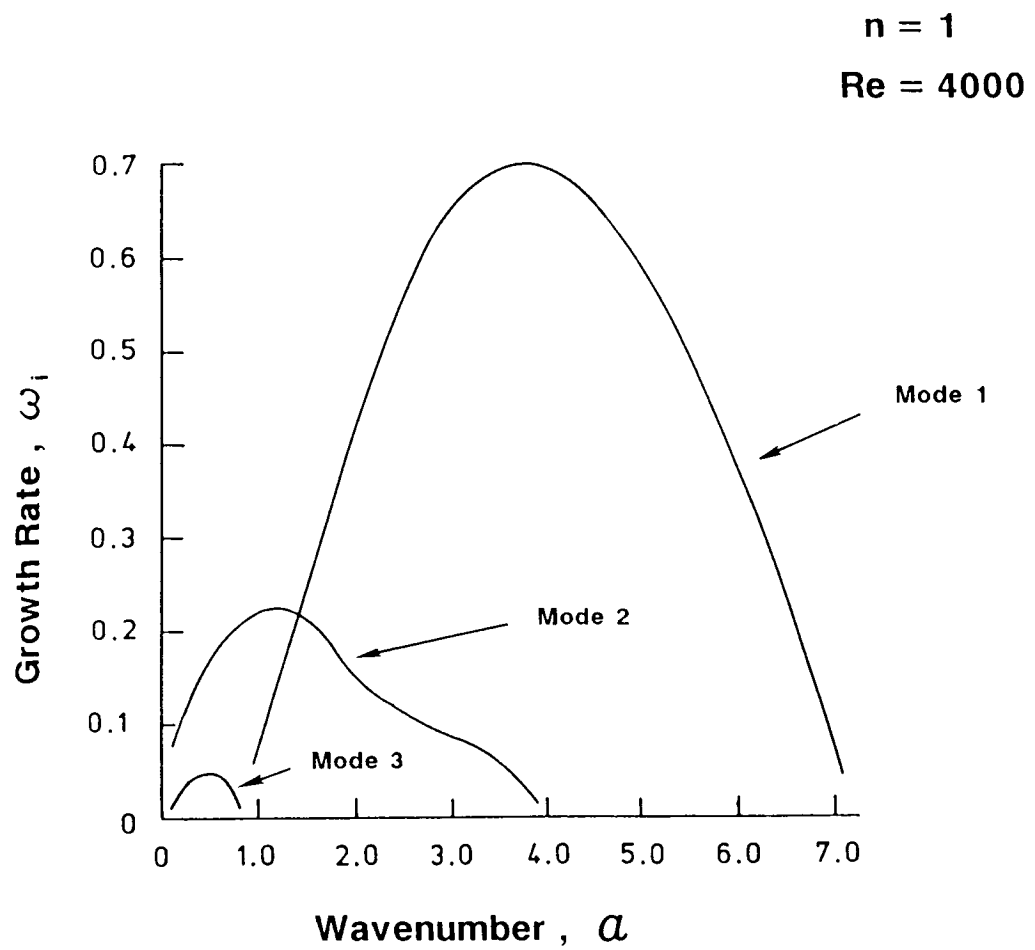


Figure 5.4. Three Dimensional Vortex Stability

5.5 HYDRODYNAMIC STABILITY OF THREE-DIMENSIONAL VORTICES

5.5.1 Objective

Control of organized longitudinal vortical motions is of interest for several applications such as high-lift systems and reduced, induced drag. The objective concerned vortex control via alteration of the vortex stability characteristics through modification of the initial three-dimensional vortex mean-velocity field.

5.5.2 Approach

Linear-stability calculations were carried out for a general class of three-dimensional vortices perturbed by three-dimensional disturbances (See Figure 5.4). The effect of the disturbances on the stability of the vortex was then obtained. There is a variation of temporal growth rate, as measured by its complex frequency component, with axial wave number. The particular vortex considered for the results shown was a two-cell system with $Re=4000$ based on core radius subjected to an azimuthal perturbation with a single period per cycle ($n=1$). The two-cell system is that commonly found as the trailing vortex behind aircraft.

5.5.3 Accomplishments

For the two-cell vortex, the present calculations indicate that the maximum growth rate for mode one shows a two-fold increase compared to the maximum growth rate of a single-cell vortex; furthermore, there is a significantly expanded dependency of growth rate upon axial wave number. This is an important feature to identify since there would be a larger spectrum of axial wave numbers at one's disposal to destabilize the vortex.

5.5.4 Significance

These results indicate that the two-cell vortex has a significant sensitivity to three-dimensional disturbances, offering the possibility of early demise of the vortex if this instability can be excited.

5.5.5 Status/Plans

Future research will investigate various types of instability modes and their growth rates as a function of the initial, three-dimensional, vortex velocity field. This will allow vortex control (for early demise or increased persistence) via tailoring of the vortex inception region.

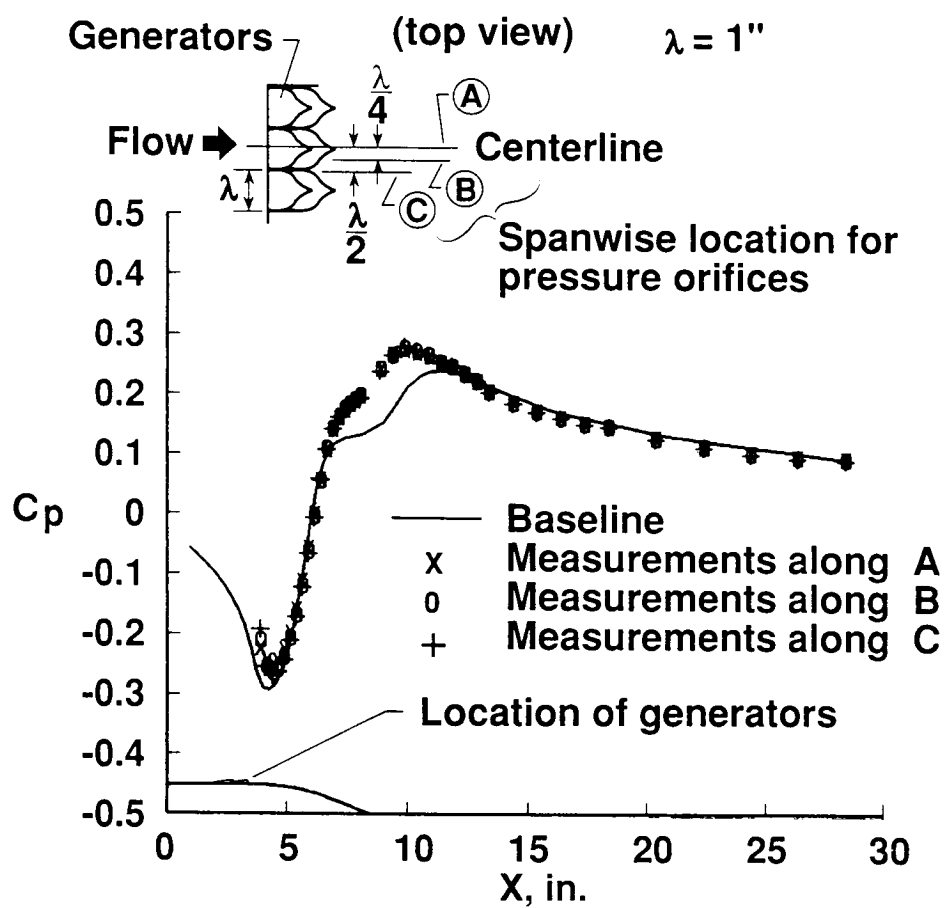


Figure 5.5. Wheeler Vortex Generators

5.6 SUBMERGED VORTEX GENERATORS

5.6.1 Objective

To develop effective low-drag vortex generator designs. Vortex generators have long been the method of choice for controlling boundary layer separation on aircraft. Conventional generators are typically vanes set at an angle to the flow and are approximately equal to the boundary layer thickness in height. This configuration, though effective, imposes a significant device-drag penalty.

5.6.2 Approach

The Langley 20-inch by 28-inch Shear Flow Control Tunnel was used to evaluate various passive and active methods of controlling turbulent, boundary layer separation over a two-dimensional, downstream-facing ramp. Surface oil-flow visualizations and pressure distributions were used to document the effectiveness of the control techniques.

5.6.3 Accomplishments

Wheeler-type vortex generators with heights of only 10 percent of the boundary layer thickness have been shown to be effective separation control devices (See Figure 5.5). Reattachment length (distance from base of ramp to reattachment) was reduced by 66 percent over the baseline case.

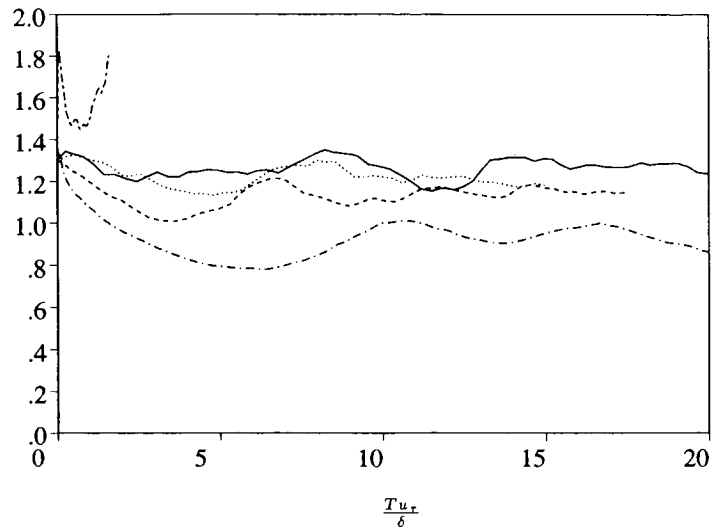
5.6.4 Significance

Submerged, Wheeler-type, vortex generators perform almost as well as conventional, vane-type generators for reducing the extent of mildly separated flows and impose a device-drag penalty of only 10 percent of that for vane-type generators. This is important for application where device drag is critical, i.e., standby separation control system.

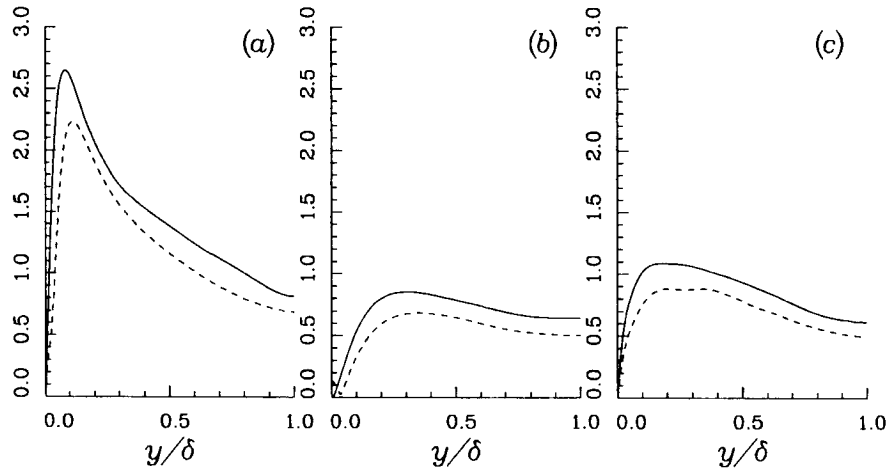
5.6.5 Status/Plans

A number of new, active separation control techniques will be investigated including fluid-driven, periodic unsteadiness and steady and pulsed injection jets.

John C. Lin
Viscous Flow Branch
Langley Research Center
(804)864-5556



Time history of the required pressure gradient to drive the same mass flow rate: —, unperturbed channel; ·····, perturbed channel with sensor at $y_r^+ \approx 2$; ----, $y_r^+ \approx 5$; - · - ·, $y_r^+ \approx 10$; — · —, $y_r^+ \approx 25$.



Profiles of *r.m.s.* fluctuations of turbulence intensities: —, unperturbed channel; ·····, perturbed channel. (a) $\langle u^2 \rangle^{1/2}$, (b) $\langle v^2 \rangle^{1/2}$, and (c) $\langle w^2 \rangle^{1/2}$. All intensities are normalized with the wall-shear velocity of the unperturbed channel.

Figure 5.6. Control of Turbulence Stream

5.7 CONTROL OF TURBULENCE AND TRANSITION

5.7.1 Objective

To control turbulence structure for the purpose of reducing drag and delaying transition.

5.7.2 Approach

The approach involved using numerical simulations to develop and to implement a control strategy (See Figure 5.6).

5.7.3 Accomplishments

The program achieved 20 percent drag reduction and suppression of small disturbances at super critical Reynolds numbers.

5.7.4 Significance

Significant reduction of drag is possible by manipulation of turbulence structures.

5.7.5 Status/Plans

An algorithm that requires information only at the surface is being sought for use in turbulence simulations.

J.J. Kim
Computational Fluid Dynamics Branch
Ames Research Center
(415)604-5867



Figure 5.7. HLFC Flight Experiment

5.8 HYBRID LAMINAR-FLOW CONTROL FLIGHT EXPERIMENT

5.8.1 Objective

To evaluate the effectiveness of Hybrid Laminar Flow Control (HLFC) for high-speed subsonic transports.

5.8.2 Approach

The approach involved replacing a 17-real-gas span of the leading-edge box on the Boeing 757 test aircraft with a suction panel having a microperforated titanium skin and conducting flight tests (See Figure 5.7).

5.8.3 Accomplishments

The Critical Design Review was conducted and all engineering drawings were completed. All tooling was fabricated, the suction skin was formed and fabrication is underway on the flight hardware components.

5.8.4 Significance

HLFC offers potential reductions in drag or fuel usage of 15 to 20 percent when applied to new aircraft.

5.8.5 Status/Plans

The Boeing 757 test aircraft will be modified to the HLFC configuration in Fall 1989 and flight tests will start in February 1990.

Richard D. Wagner
Laminar Flow Control Project Office
Langley Research Center
(804)864-1906

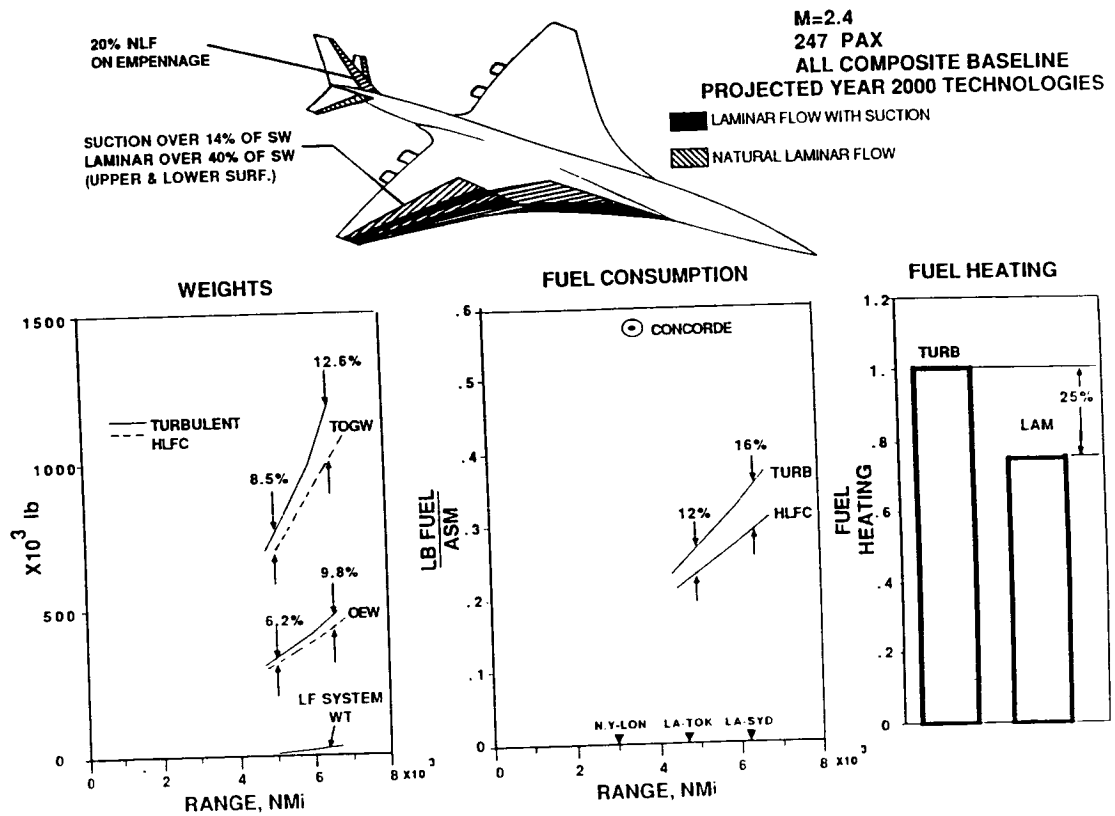


Figure 5.8. Results of BCA Study

5.9 APPLICATION OF LAMINAR-FLOW CONTROL TO SUPERSONIC TRANSPORT CONFIGURATIONS

5.9.1 Objective

To evaluate the application of laminar-flow control to supersonic transport configurations.

5.9.2 Approach

In separate studies conducted at Douglas and Boeing, the feasibility and impact of implementing a laminar-flow control system on supersonic transport configurations were studied.

5.9.3 Accomplishments

Both studies showed extremely attractive performance gains might be achieved with either full chord suction laminar flow control (DAC approach), or with a hybrid of suction control and natural laminar flow (BCA approach). Figure 5.8 shows some results of the BCA study. The studies also identified critical technology areas for research needed before implementation of this technology can be considered.

5.9.4 Significance

The studies demonstrated the aerodynamic feasibility of achieving significant laminarization on the wing surface of a supersonic transport configuration. Preliminary assessment of systems and structural requirements to achieve this laminarization showed that the aerodynamic benefits of drag reduction outweigh the system weight, volume and power requirement penalties. The net benefits in terms of reductions in MTOW, OEW and fuel consumption are impressive and improve with increasing mission range.

5.9.5 Status/Plans

Studies are complete and final reports are being published. Work will continue under the High-Speed Civil Transport New Initiative.

Richard D. Wagner
Laminar Flow Control Project Office
Langley Research Center
(804)864-1906

This page is intentionally left blank.

CHAPTER SIX

TEST TECHNIQUES AND INSTRUMENTATION

6.1 INTRODUCTION

Technology is being provided for critical experimental research capability required to improve the measurement of the fundamental flow properties of fluids and the overall aerodynamic performance of aircraft components and configurations. The primary testing errors due to wind tunnel wall and support interference for both static and dynamic testing are being analyzed and the development of instrumentation and measurement techniques for real-time, flow diagnosis is being performed with emphasis on non-intrusive methods. These developments occur across the range of conditions from cryogenic to high temperature and from low subsonic to hypersonic speeds. The research areas being addressed are (1) real-time, interferometry techniques for unsteady flows; (2) miniature Laser Doppler Velocimeter (LDV) systems for internal applications in ground and flight tests; (3) advanced methods for accurately sensing and handling aerodynamic flight test data, both boundary layer and off-surface flows; (4) measurement techniques for time-varying, turbulent velocity fields; (5) advanced methods for simultaneous measurement of velocity, density and temperature; (6) laser based air data system for high angle-of-attack flight test; (7) flight testing of prototype flight information systems; (8) improvements in the optical, signal processing and structural performance of the 40-foot by 80-foot by 120-foot wind tunnel laser velocimeter and (9) test Raman Doppler velocimeter survey of supersonic flowfield about a delta wing leading edge vortex.

Program Manager: Mr. Gary Hicks
OAST/RF
Washington, DC 20546
(202)453-2830

ORIGINAL PAGE
BLACK AND WHITE PHOTOGRAPH

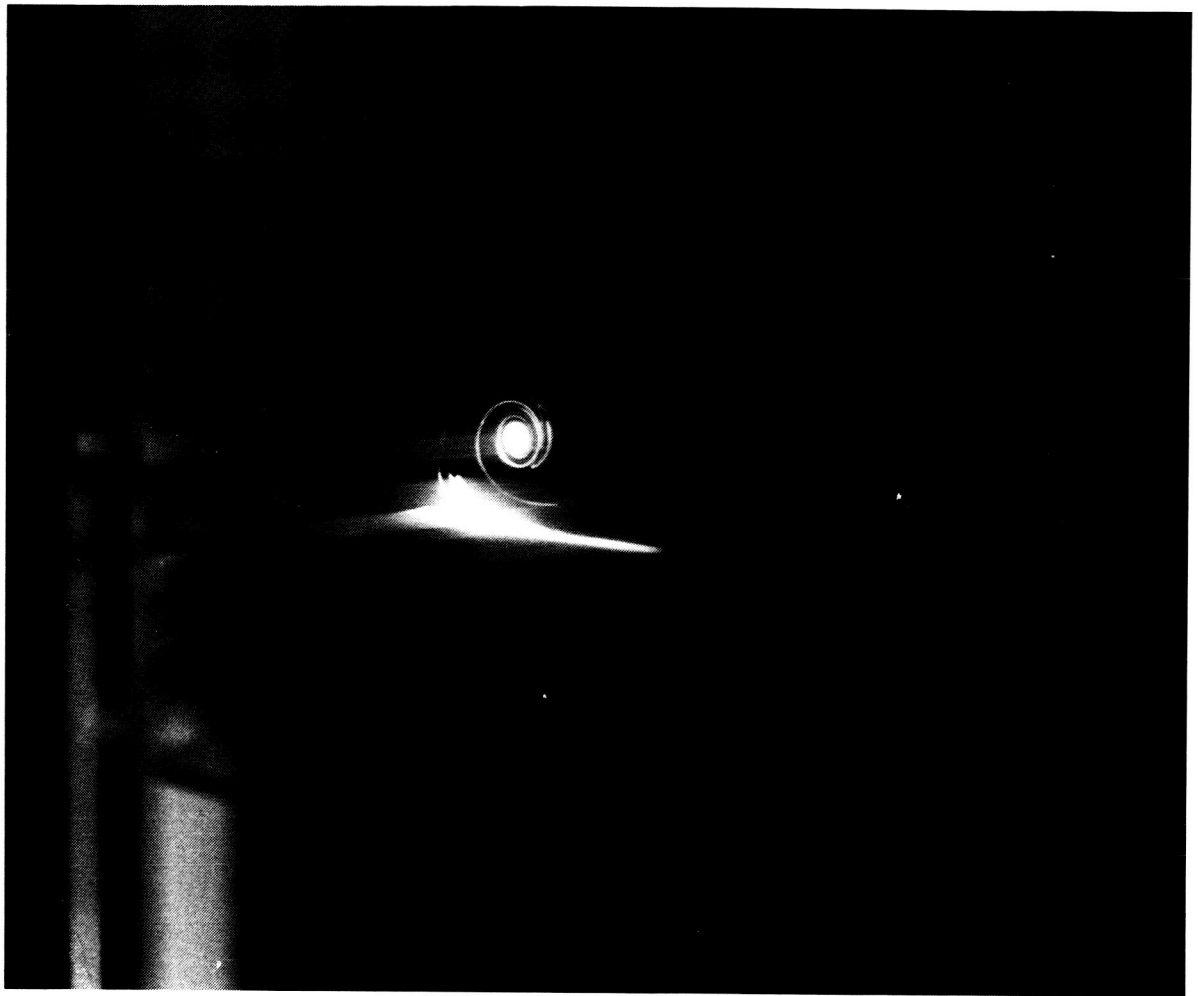


Figure 6.1. Visualization of Vortical Flow

6.2 VISUALIZATION OF VORTICAL FLOW USING THE LASER VAPOR SCREEN TECHNIQUE

6.2.1 Objective

To (1) visualize complex, interacting, vortex and vortex-shock dominated flowfields for improved understanding of flowfield structure, dynamics and control methods and (2) develop prediction methods and image enhancement techniques for improved test planning and data analysis.

6.2.2 Approach

The approach involved conducting tests in subsonic, transonic and supersonic wind tunnels with advanced fighter configurations to develop expertise in visualizing critical elements of flow structure (See Figure 6.1). NASA also conducted research in thermodynamic prediction of the condensation process, flow structure formation, image acquisition and post processing on workstations using custom software.

6.2.3 Accomplishments

NASA completed three highly successful laser vapor screen flow visualization experiments. These tests resulted in two published reports. NASA also awarded directors discretionary funding for research on prediction methodology and image enhancement and processing.

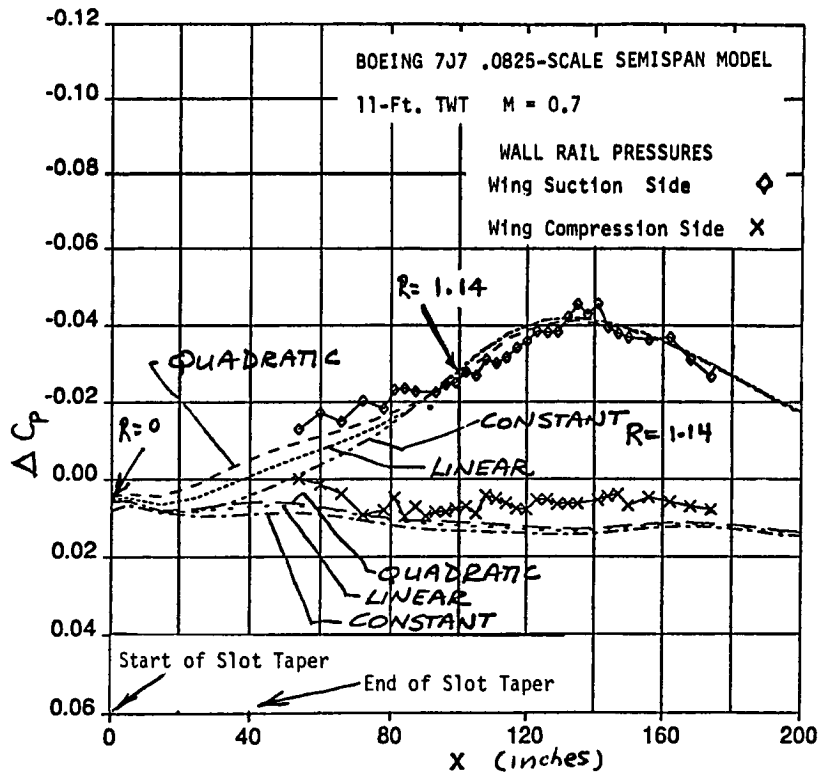
6.2.4 Significance

Testing resulted in the publication of two papers discussing several unexpected flowfield behaviors, including the coexistence of a vortex and shock wave and the interaction of forebody vortices with LEX vortices for yaw and roll control on a F-18-like configuration.

6.2.5 Status/Plans

A DDF effort is planned through 1991 and flow visualization evaluation testing is planned for FY 1990.

John A. Schreiner and Bruce L. Gilbaugh
Advanced Aerodynamic Concepts Branch
Ames Research Center
(415)604-5860



EQUIVALENT HOMOGENEOUS
WALL BOUNDARY CONDITION

$$R \phi_n + \phi_n = 0$$

QUADRATIC vs LINEAR R
is EQUIVALENT TO $\Delta C_p = .0003$

Figure 6.2. Effect of Wall Boundary Condition on Outer Flowfield

6.3 LARGE SEMI-SPAN MODEL TEST TECHNIQUES

6.3.1 Objective

To develop the techniques required for achieving maximum Reynolds number for the validation of wing designs through testing of the largest possible size of semi-span models. The focus of this work was on reflection plane simulation and wall-interference corrections.

6.3.2 Approach

The approach involved conducting a cooperative program with Boeing to (1) obtain experimental data to allow quantification of the effects of the reflection plane and simulation of the flow distortions caused by the wind tunnel walls; (2) develop and validate a math model for the simulation of the flow at the outer computational boundary which includes the effects of the tunnel walls and (3) use the validated math model for the tunnel walls to establish a procedure for correcting the experimental results for tunnel-induced spatial variations in stream non-uniformity including flow angle, flow curvature and velocity gradient.

6.3.3 Accomplishments

Data were obtained with two different designs for reflection plane simulation. Analysis is in progress and additional tests are anticipated. An initial math model for walls in comparison with experimental results shows the need for accounting for the effects of wall boundary layer and/or crossflow velocity on a wall math model (See Figure 6.2).

6.3.4 Significance

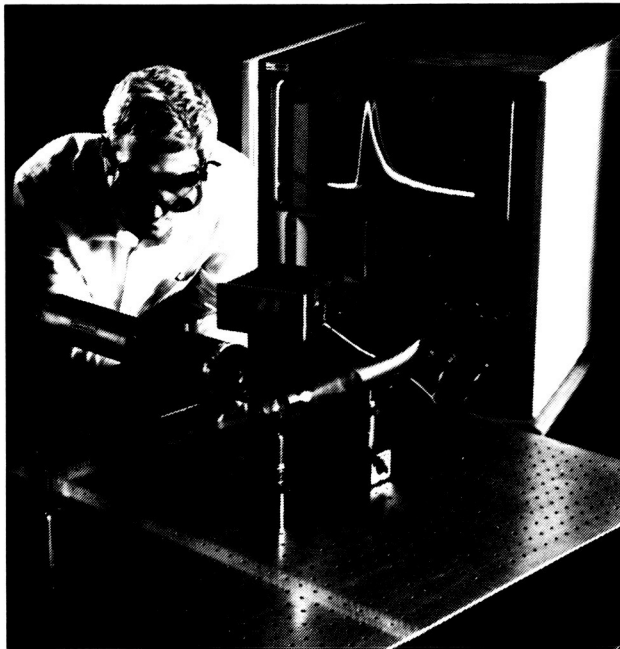
Accounting for the effects of reflection plane simulation and tunnel walls are design-significant in the areas of cruise-drag, drag rise and buffet-onset.

6.3.5 Status/Plans

The next series of tests were scheduled for July and August 1989. They included new reflection-plane simulation and additional measurements of the outer flowfield near the tunnel walls.

Frank W. Steinle, Jr.
Aerodynamic Facilities Branch
Ames Research Center
(415)604-5848

ORIGINAL PAGE
BLACK AND WHITE PHOTOGRAPH



Temperature Measurements in Low Speed Air Flow
Using Laser-Induced Fluorescence

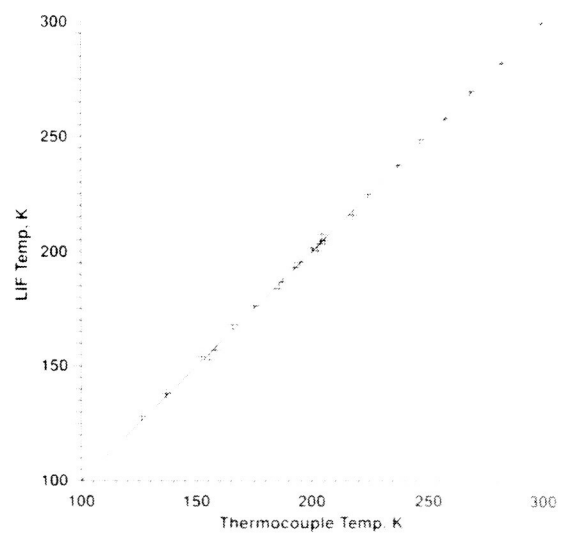


Figure 6.3. Nonintrusive Instrumentation for Hypersonic Flow

6.4 NONINTRUSIVE INSTRUMENTATION FOR HYPERSONIC FLOW

6.4.1 Objective

To develop instrumentation for the nonintrusive measurement of flow properties in hypersonic wind tunnels.

6.4.2 Significance

New instrumentation makes possible the previously unavailable capability for nonintrusive measurements of temperature, density and their fluctuations, which are necessary for code validation and turbulence model development (See Figure 6.3).

6.4.3 Status/Plans

Development of instrumentation is in progress to allow demonstration in a small, supersonic wind tunnel and in a low speed flow which duplicates the thermodynamic conditions in a hypersonic wind tunnel at Mach 10. Engineering for installation in Ames' 3.5-foot Hypersonic Wind Tunnel will begin in 12 to 18 months.

R. L. McKenzie
Experimental Fluid Dynamics Branch
Ames Research Center
(415)604-6158

ORIGINAL PAGE
BLACK AND WHITE PHOTOGRAPH

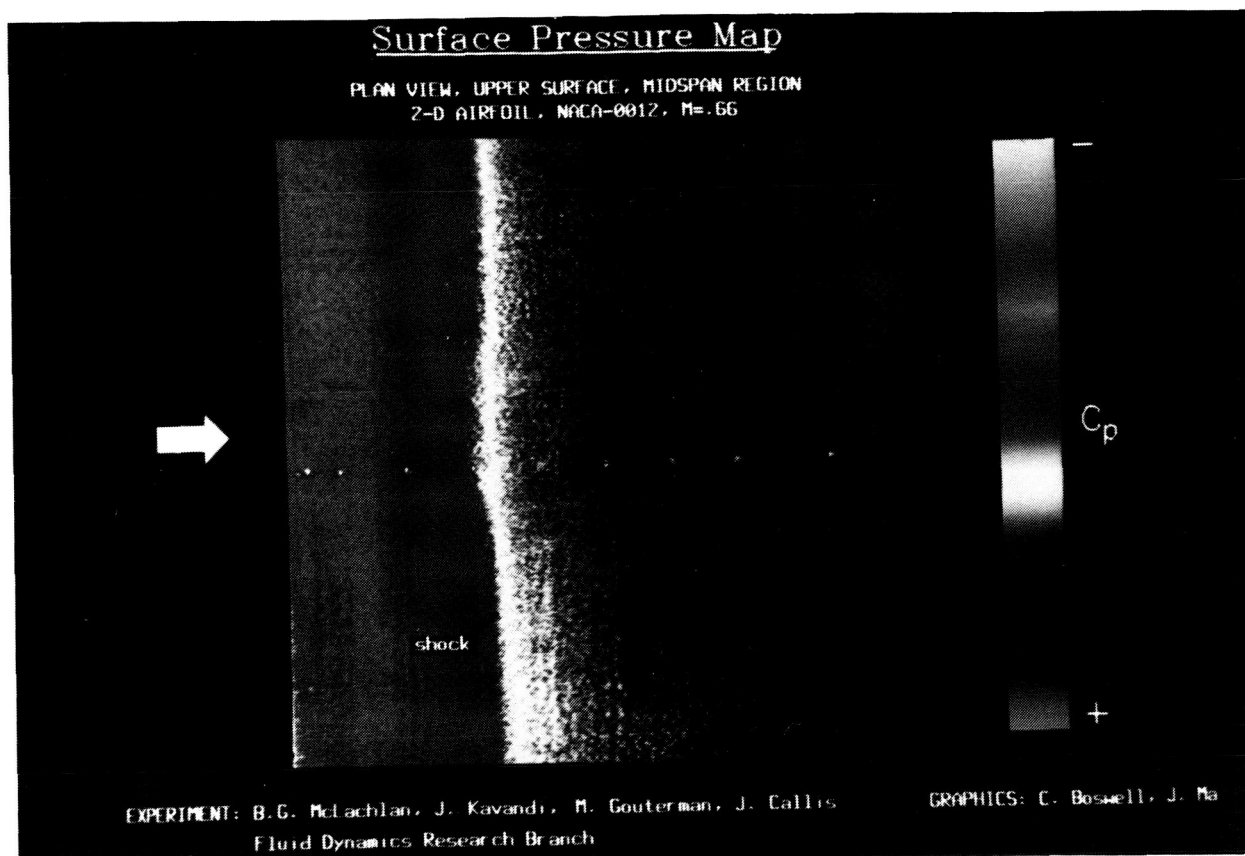


Figure 6.4. Pressure Sensitive Fluorescent Paint

6.5 PRESSURE SENSITIVE FLUORESCENT PAINT

6.5.1 Objective

To develop pressure sensitive paint based on the fluorescence phenomenon of oxygen quenching for use in aerodynamic tests.

6.5.2 Approach

The approach involved studying paint chemistry and experimental methodology with wind tunnel tests (See Figure 6.4).

6.5.3 Accomplishments

NASA demonstrated the feasibility with wind tunnel tests of a two-dimensional airfoil coated with trial paint developed by M. Gouterman and J. Callis of the University of Washington. Surface pressure maps obtained from computer processed video images were compared with conventional pressure tap readings.

6.5.4 Significance

Continuous surface pressure distributions are obtained rather than at discrete points with a potential for measuring fluctuations.

6.5.5 Status/Plans

Further developmental work is required. Use of trial paint for unsteady pressure measurement and in flight test environment will be assessed.

B. G. Mc Lachlan
Fluid Dynamics Research Branch
Ames Research Center
(415)604-4142

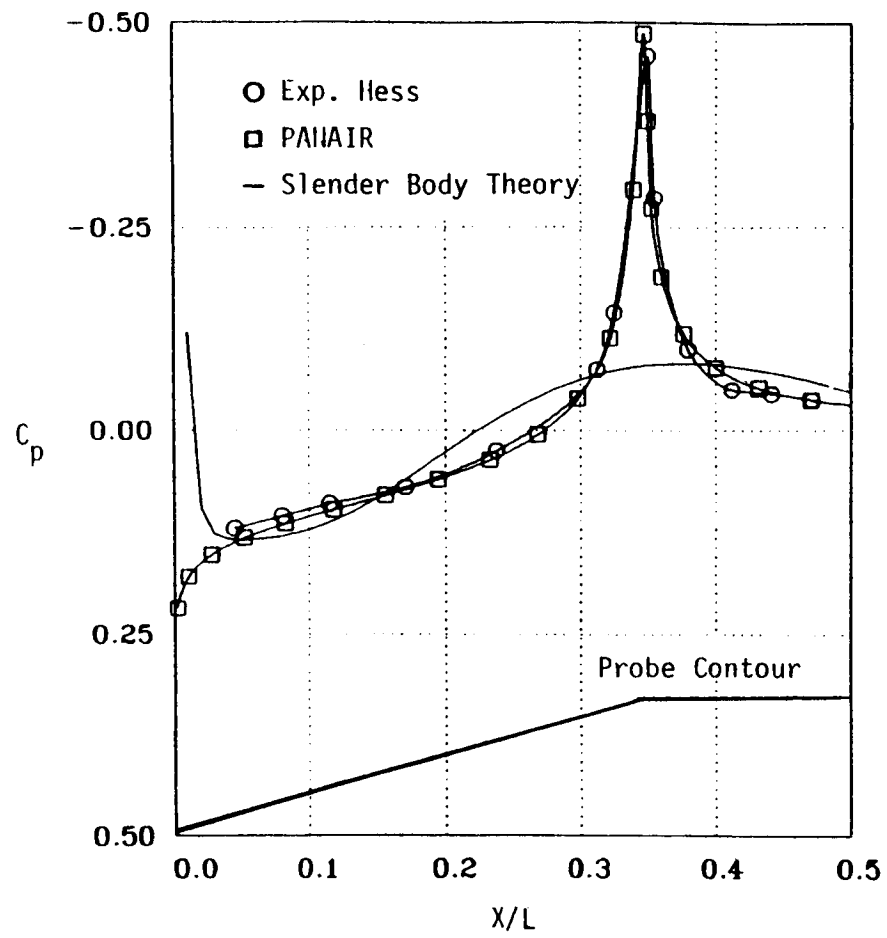


Figure 6.5. Cone Probe Surface Pressure Distribution

6.6 PRESSURE PROBE DESIGN

6.6.1 Objective

To predict multi-hole pressure probe performance.

6.6.2 Approach

The approach involved developing a general model of pressure probe behavior.

6.6.3 Accomplishments

NASA completed the general model and validated it with a panel method (PANAIR) computer code (See Figure 6.5).

6.6.4 Significance

Application specific pressure probes may be designed with confidence using rational non-empirical procedures.

6.6.5 Status/Plans

Specialized probes are being designed for a wing tip vortex study.

G. Zilliac
Fluid Dynamics Research Branch
Ames Research Center
(415)604-3904

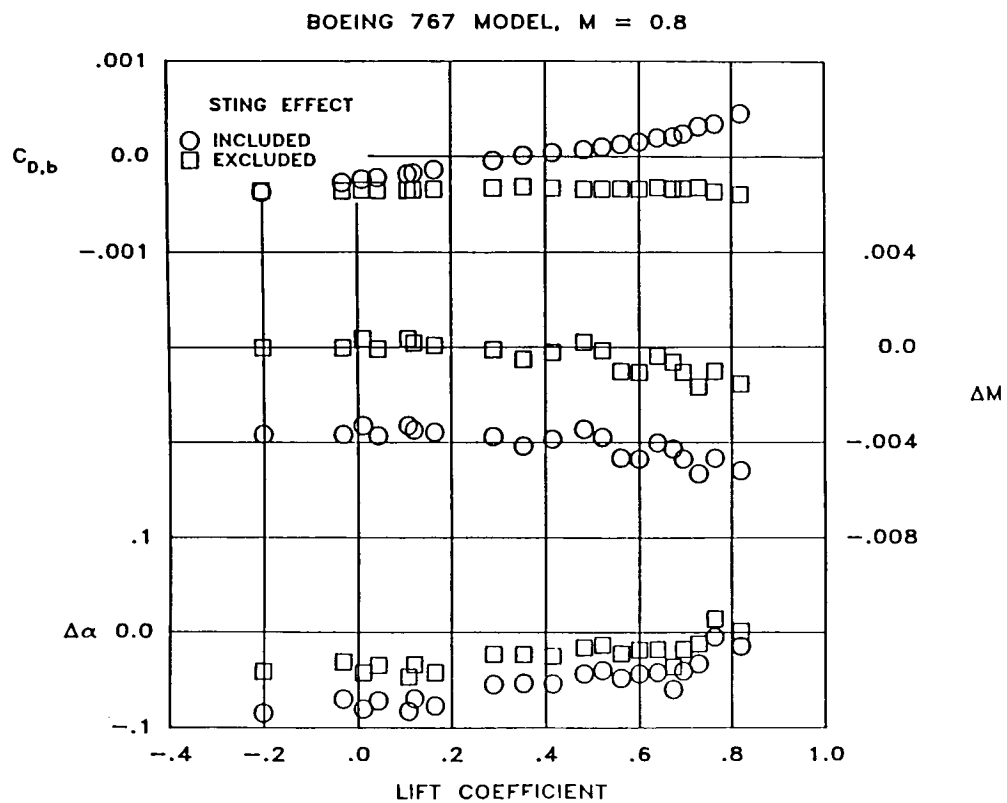


Figure 6.6. NTF Interference Corrections at Model

6.7 IMPROVEMENTS to A SLOTTED-WALL, WIND TUNNEL INTERFERENCE ASSESSMENT CODE (PANCOR)

6.7.1 Objective

To provide output in the format of interference corrections at the model, with sting interference accounted for separately from the remaining tunnel interference. The PANCOR wind tunnel interference assessment code is a computer program based on high-order panel method technology for assessing interference due to the wind-tunnel environment including walls with discrete, finite-length slots, the slot flow reentry region and the model support system. Mixed boundary conditions include both geometry specifications and measured pressures on slotted walls. Basic results describe the interference flow perturbation field.

6.7.2 Approach

The tunnel flow satisfies the boundary conditions in the presence of disturbances from the model with its measured forces and moments and from the sting at its actual orientation. The total interference is evaluated at a set of points on the model by summing the flow perturbations from all singularities except those representing the model. By omitting the sting singularities, the interference from only the tunnel walls is obtained. Mach number and angle of attack corrections are averaged over the wing planform and the buoyancy drag correction is the summed effect of longitudinal interference pressure gradient at each element of model volume.

6.7.3 Accomplishments

The PANCOR code as implemented for the NTF has been modified as described and applied to tests of a Boeing 767 transport configuration. Figure 6.6 shows the interference corrections, both with and without sting effects, in a single pitch run. The model support sting for this test was unconventional, with a shape like a thick vertical tail mounted at its tip to a more conventional sting. The figure shows that this sting configuration produced a buoyancy drag correction that varied as much as eight drag counts over the pitch range and reductions in both Mach number and angle of attack. Without the sting effect, the tunnel interference called for an essentially constant buoyancy drag correction of about minus four drag counts, with very small Mach number corrections.

6.7.4 Significance

The newly achieved separation of the sting and tunnel interference assessment provides both an alternative to the usual tedious methods of evaluating sting tares and tunnel interference results which are more amenable to interpretation because they are uncontaminated by sting effects. The method provides heretofore unavailable insight into slotted, tunnel flow phenomena.

6.7.5 Status/Plans

The method is not yet sufficiently reliable for routine correction of test data because of its high sensitivity to minor variations in measured wall pressures due to imperfections in orifice installation and wall shape. Studies are underway for various possible improvements.

William B. Kemp, Jr.
High Reynolds Number Aerodynamics Branch
Langley Research Center
(804)864-5138

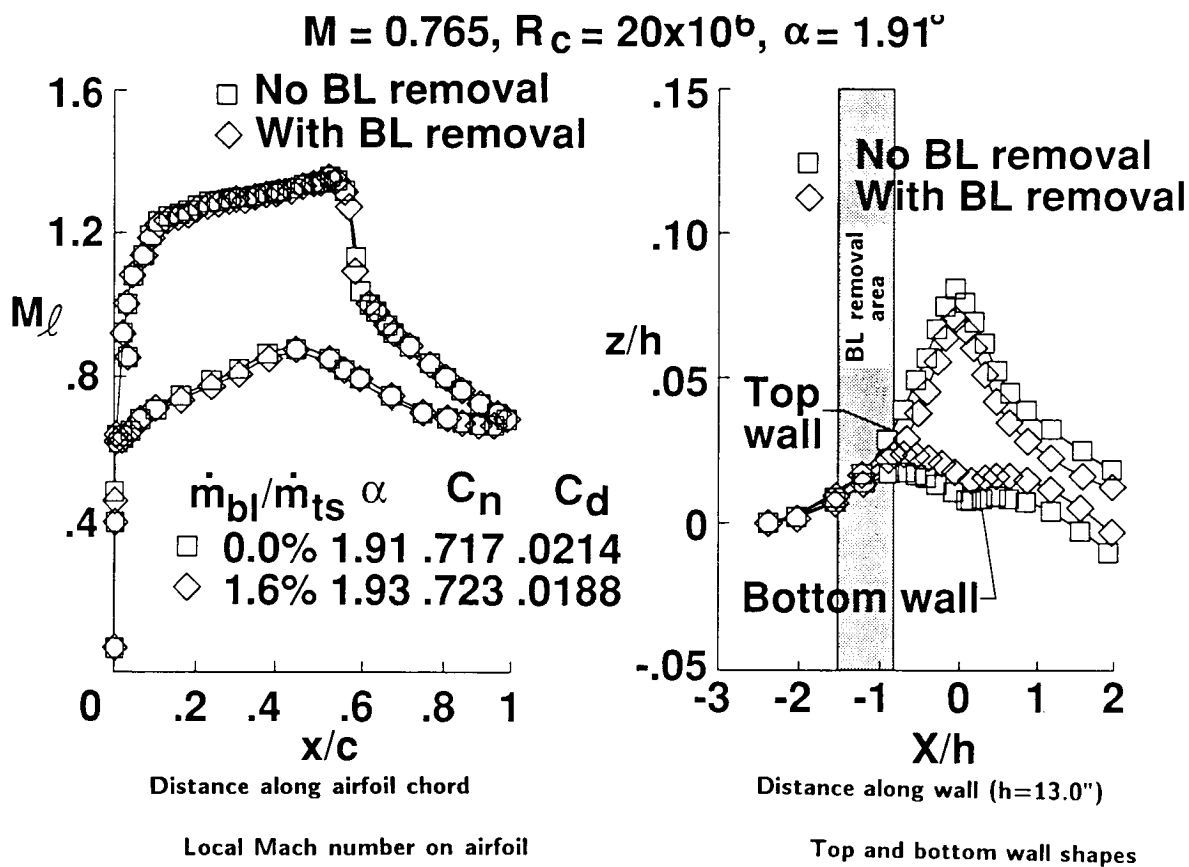


Figure 6.7. Effect of Side Wall Boundary Layer Removal on Wall Streamlining

6.8 STUDY OF SIDE WALL BOUNDARY LAYER REMOVAL EFFECTS ON AIRFOIL TESTS IN THE LANGLEY 0.3-M TCT ADAPTIVE WALL TEST SECTION

6.8.1 Objective

To validate the combined wall adaptation and side wall boundary layer removal operation for airfoil tests in the Langley 0.3-m Transonic Cryogenic Tunnel (0.3-m TCT).

6.8.2 Approach

The boundary layer development on the test section side walls forms a source of interference in airfoil testing. To keep this influence small, the 0.3-m TCT has provisions for removing the boundary layer flow on the side walls ahead of the model. The removal of flow from the side walls reduces the boundary layer thickness but also introduces a change in the test Mach number. The adaptive capability of the top and bottom walls permit the walls to move to correct for the change in test Mach number. With this approach, it was possible to evaluate the side wall boundary layer removal influence while maintaining the test Mach number constant.

6.8.3 Accomplishments

Tests were made with and without boundary layer removal in the empty test section as well as with a model installed. The decrease in boundary layer thickness with upstream removal was measured in the empty test section using a fixed, boundary layer rake. The measurements showed the side wall boundary layer displacement thickness decreases from about 1.0 to 0.6 percent of the test section width under maximum removal conditions. The airfoil tests consisted of pressure measurements on a long chord (9.0 inches), super-critical airfoil model. The top and bottom wall positions were moved iteratively to nearly free air streamline shapes for conditions with and without boundary layer removal. The test Mach number was 0.765 and the Reynolds number was 20 million.

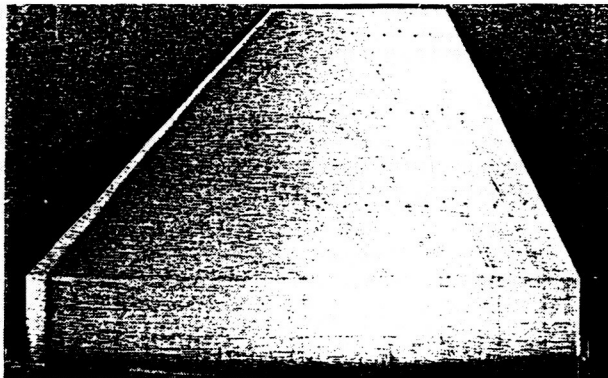
6.8.4 Significance

For the conditions tested, the influence of boundary layer removal on pressure measurements at airfoil mid-span was small (See Figure 6.7); however, the effect on wall shapes was significant enough to account for the change in massflow due to boundary layer removal. The integrated wall adaptation and side wall boundary layer removal under cryogenic conditions makes 0.3-m TCT a unique facility for testing airfoils at flight equivalent conditions with the ability to produce side wall as well as top and bottom wall interference effects. The airfoil pressure measurements indicate that the side wall influence in the 0.3-m TCT is probably small, compared to other similar tunnels due to relatively thin boundary-layers.

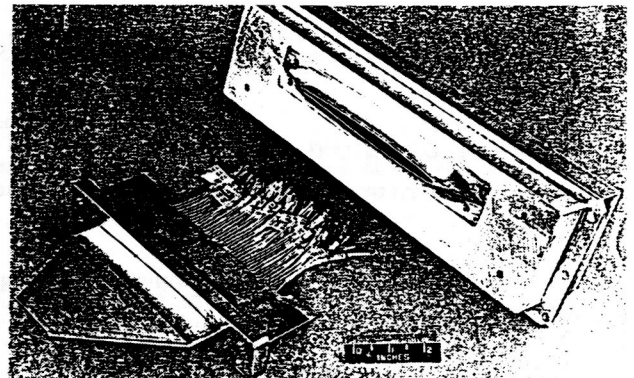
6.8.5 Status/Plans

The side wall boundary layer removal will be used in airfoil tests on a selective basis to check data points suspected of significant side wall interference. Further testing with side wall boundary layer removal at other locations such as around the model or at a downstream station are under consideration.

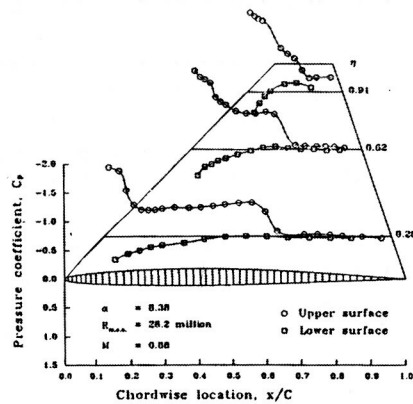
A. V. Murthy and E. J. Ray
High Reynolds Number Aerodynamics Branch
Langley Research Center
(804)864-6359



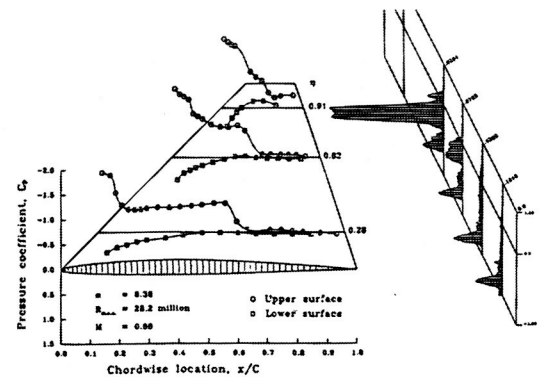
Upper surface of canard model showing bond planes and orifice rows.



Canard model and mounting block to fit sidewall turntable.



Sample of pressure data on canard model for the three spanwise rows.



Pressure and drag data. Drag profiles from the 0.3-m TCT survey rake.

Figure 6.8. Test Technique for Thin Fighter Wing at High Reynolds Number

6.9 TEST TECHNIQUE FOR THIN FIGHTER WING AT HIGH REYNOLDS NUMBER

6.9.1 Objective

To determine the performance of a fighter wing at transonic speeds and flight Reynolds number.

6.9.2 Approach

The first step was testing the X29 canard in Langley's 0.3-m Transonic Cryogenic Tunnel (0.3-m TCT) to provide a database of pressure distributions and drag profiles. The experimental data were enriched by a Navier-Stokes code to allow integration of the lift and drag. These results provided baseline performance values with details of the flow for a thin wing. The X29 canard has a maximum thickness of five percent of chord and it is highly tapered from root to tip, making pressure instrumentation modeling very challenging. A Langley-developed technique that uses chemically etched pressure channels in the bond planes between multiple sheets of metal was used to construct the model. There are 53 orifices on the upper surface and 37 on the lower surface (See Figure 6.8).

6.9.3 Accomplishments

The model was mounted on the sidewall turntable in the Adaptive Wall Test Section of the 0.3-m TCT and was tested in May 1988. Testing was over the full range of conditions available.

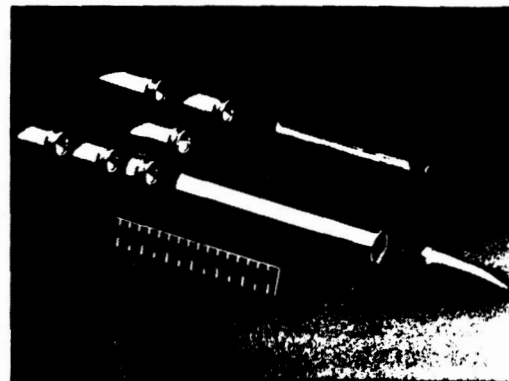
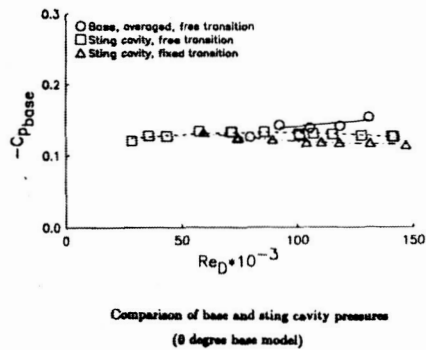
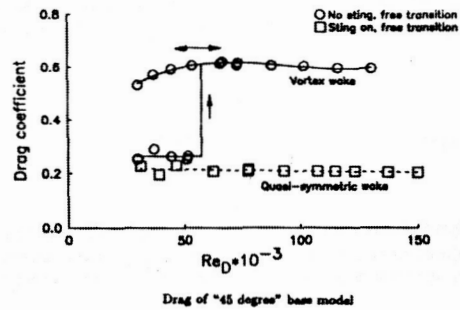
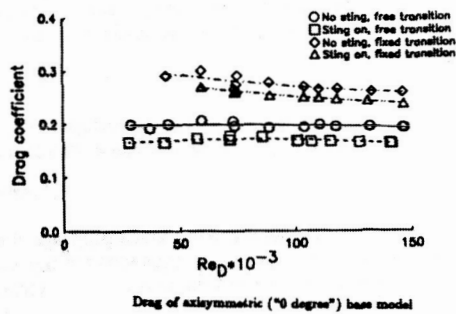
6.9.4 Significance

For the first time, a low cost testing technique is demonstrated that, in concert with computational techniques, will provide thin wing lift and drag performance as well as details of the wing flow and wake structure.

6.9.5 Status/Plans

A NASA TM is being prepared to serve as a database catalog for code development. Early work is underway for grid definition. First efforts will be to model an unusual Reynolds number dependent, leading edge separation. Later efforts will model the experimental drag profiles. The wake/juncture region also will be computed. Success in these efforts will lead to more sophisticated wall juncture fillets and an improved wing to test. The cycle then will be renewed in the 0.3-m TCT.

Pierce L. Lawing
High Reynolds Number Aerodynamics Branch
Langley Research Center
(804)864-5137



Model, showing magnetic core and interchangeable bases

ORIGINAL PAGE
BLACK AND WHITE PHOTOGRAPH

ORIGINAL PAGE IS
OF POOR QUALITY

Figure 6.9. Subsonic Sting Interference on the Drag of Slanted-Base Ogive Cylinders

6.10 SUBSONIC STING INTERFERENCE ON THE DRAG OF SLANTED-BASE OGIVE CYLINDERS

6.10.1 Objective

To study the effects of a sting support on the aerodynamic characteristics of simple base geometries. Slanted-base ogive models were chosen due to the availability of relevant experimental results from several sources. Comparisons between interference-free and sting-supported data provided guidance for future tests in conventional wind tunnels and a database for sting interference correction.

6.10.2 Approach

An aluminum ogive cylinder model, 1.212 inches in diameter, was fitted with interchangeable bases and an iron magnetic core. Support interference-free measurements were made with the model magnetic ally suspended in the Langley 13-inch Magnetic Suspension and Balance System. Tests were repeated with a dummy sting support protruding into a cavity into the base of the model. A second model was used for measurements of interference-free base pressures, using onboard pressure instrumentation and remote data telemetry (See Figure 6.9).

6.10.3 Accomplishments

The current test program commenced in October 1988. Drag measurements were made for six different base slants, with and without boundary layer transition fixed and with and without a dummy support present (24 configurations). Measurement of base pressure is 50 percent complete.

6.10.4 Significance

An experimental method of evaluating sting interference was demonstrated. The magnitude of sting interference on drag was shown to be extremely large under certain circumstances (up to factor of three discrepancy between sting-supported and true drag). A database is now available for sting interference correction or validation of interference correction methods.

6.10.5 Status/Plans

Drag measurements are complete. Base pressure measurements will be completed and correlated with drag results. Data for lift and pitching moment will be reduced. A comprehensive data catalog will be prepared.

Dr. Colin P. Britcher
High Reynolds Number Aerodynamics Branch
Langley Research Center
(804)864-5029

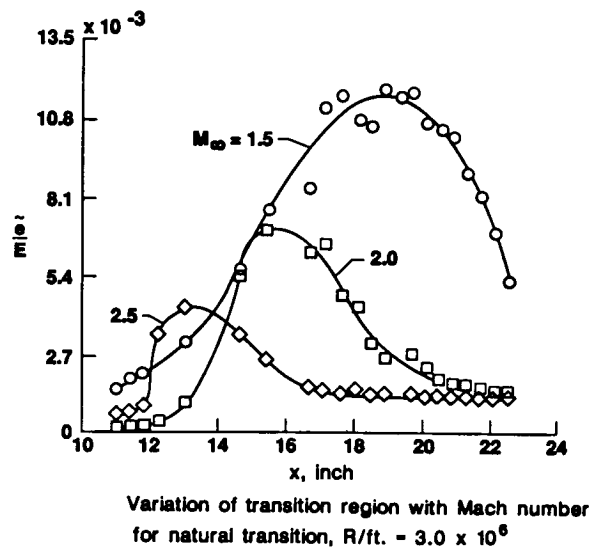
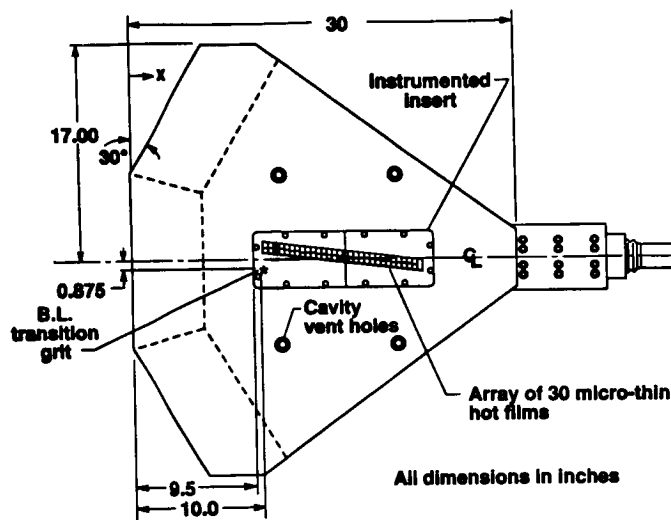


Figure 6.10. Transition Detection at Supersonic Speeds Using a Micro-Thin, Hot-Film System

6.11 TRANSITION DETECTION AT SUPERSONIC SPEEDS USING A MICRO-THIN, HOT-FILM SYSTEM

6.11.1 Objective

To obtain online, boundary layer transition characteristics at supersonic Mach numbers over a range of Reynolds numbers for both natural transition and for a grit-induced turbulence wedge.

6.11.2 Approach

A test program was initiated to compare four techniques for obtaining boundary layer transition on a flat plate at supersonic speeds. The transition detection technique used as a standard to compare the other three methods was a micro-thin hot-film system, since this system had demonstrated the capability to detect on-line, boundary layer transition at low speeds and transonic conditions. An array of 30 micro-thin, hot-films was vapor deposited on the surface of a two-piece stainless steel insert and mounted in the flat plate (See Figure 6.10). The films were located from 11.5-inches to 24.5-inches from the leading edge of the plate in a region where boundary layer transition could be detected for most of the test conditions. A desktop computer was used to control the multi-channel, hot-film instrumentation, acquire the data, reduce the data and display the results in graphic form online.

6.11.3 Accomplishments

A transition detection study was made in the Unitary Plan Wind Tunnel with 30 micro-thin, hot films on a flat plate at Mach numbers of 1.5, 2.0 and 2.5 and over a range of Reynolds numbers from 1.0 to 4.5 million per foot. The first phase of the test was conducted with natural transition for all test conditions. In the second phase of the test, characteristics of a grit-induced turbulence wedge were studied. Figure 6.10 shows typical examples of online data from the array of films for three Mach numbers. The RMS values of the fluctuating voltages were normalized by the mean voltage of the anemometer output. The test showed the effect of Mach number and Reynolds number on both natural transition and the grit-induced turbulence wedge.

6.11.4 Significance

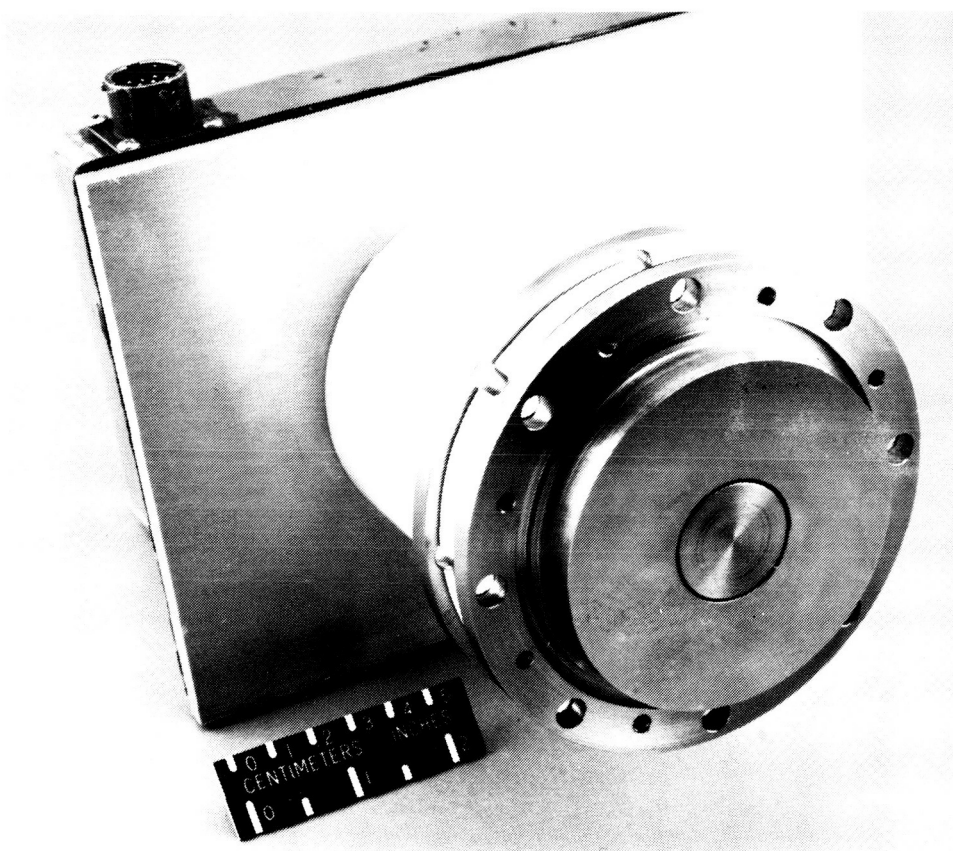
The micro-thin hot-film system was able to display the real-time progression of boundary layer transition through the use of on-line plots at Mach numbers from 1.5 to 2.5 over a wide range of Reynolds numbers. In addition, it is believed this is the first supersonic boundary layer transition study where a closely spaced array of vapor-deposited, hot-film sensors were able to repeatedly detect, with on-line data acquisition, transition locations over a wide range of test conditions for both natural transition and for a grit-induced, turbulence wedge intersecting the array of sensors.

6.11.5 Status/Plans

Follow on experiments with the micro-thin, hot-film system are planned for the 0.3-meter Transonic Cryogenic Tunnel to evaluate a "NTF- type" hot-film installation. In addition, when the two Langley, large-scale, vapor deposition chambers become operational, a 51-inch span Pathfinder wing will be instrumented with micro-thin, hot-films and tested in the NTF.

Charles B. Johnson,
Fluid Dynamics Branch
Langley Research Center
(814)864-5025

Debra L. Carraway
Electro-Mechanical Instrumentation Branch
Langley Research Center
(814)864-5025



ORIGINAL PAGE
BLACK AND WHITE PHOTOGRAPH

Figure 6.11. High Temperature Skin Friction Balance

6.12 HIGH TEMPERATURE SKIN FRICTION BALANCE DEVELOPMENT

6.12.1 Objective

To initiate the development of a mechanical balance capable of making direct skin friction or aerodynamic drag measurements in high temperature environments.

6.12.2 Approach

The approach involved modifying existing balances developed at Langley and testing them in a hypersonic wind tunnel (See Figure 6.11).

6.12.3 Accomplishments

A balance developed for flight usage was modified and tested in the hypersonic propulsion laboratory at Langley. Test data indicated that the balance functioned satisfactorily with the surface temperature exceeding 1,000 degrees. A number of minor mechanical problems were identified.

6.12.4 Significance

Aerodynamic drag measurements are critical to the design of aerodynamic and propulsion systems encountered in the hypersonic flight regime. A mechanical device is needed as a basis or standard for developing alternate types of aerodynamic drag measuring techniques. Technical data acquired from these devices are needed for computer simulation validation as well as verification of theories.

6.12.5 Status/Plans

Development work is being continued. Additional modifications to correct identified deficiencies and further tests will be made.

Ping Tcheng
Electro-Mechanical Instrumentation Branch
Langley Research Center
(804)864-4717

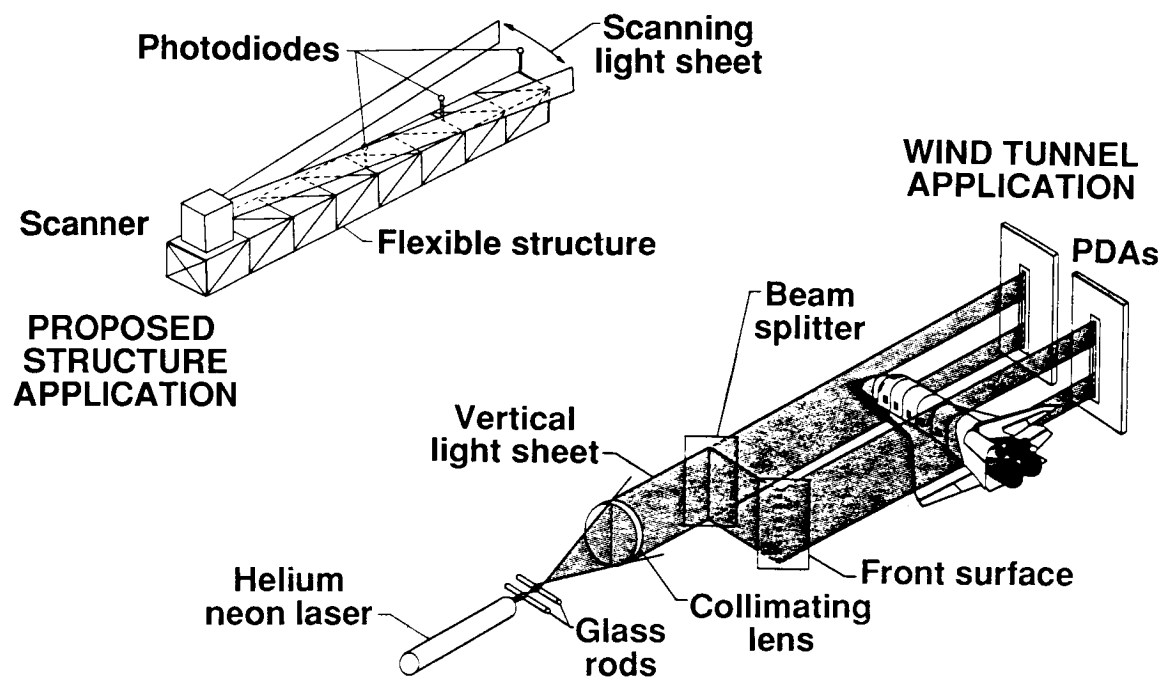


Figure 6.12. Electro-Optical Displacement Measurement System

6.13 A PRECISION ELECTRO-OPTICAL DISPLACEMENT MEASURING SYSTEM

6.13.1 Objective

A non-contact method of measuring wind tunnel model position or Angle of Attack (AOA) is desirable when the physical size of the model limits the use of internal AOA instrumentation. An electro-optical position measurement system was developed several years ago and is presently in the 13-inch Magnetic Suspension and Balance System (MSBS) at Langley. The system enhances the performance of the 13-inch MSBS but has a limited AOA range of ± 8 degrees. To at least double the AOA range of the 13-inch MSBS position sensing system. Successful development of such a system would not only improve the capabilities of the 13-inch MSBS, but might offer many facilities a solution to their unique measurement requirements.

6.13.2 Approach

A new, extended range two channel electro-optical system was developed using high resolution linear Photodiode Arrays (PDAs) (See Figure 6.12). The PDAs, which function similar to CCD cameras used in household Cam-corders, were illuminated by a sheet of laser light. The shadow formed on the PDAs when a wind tunnel model obstructed the laser light. The shadow was used to sense the model's position. Each PDA had its own electronics to detect where the light obstruction had taken place. The AOA of a wind tunnel model could then be computed from these data. The position data were refreshed at a rate of 256 times per second.

6.13.3 Accomplishments

A complete system was fabricated and bench tested in the laboratory. The system was able to measure linear displacement of the model to an accuracy of ± 0.0005 inches (12.7 microns), and angular position to an accuracy of less than ± 0.015 degrees. The angular range of the system is ± 17 degrees.

6.13.4 Significance

The extended range position sensing system is particularly useful in magnetic suspension applications where physical contact with the wind tunnel model cannot be tolerated. Other applications include AOA measurements of wind tunnel models which may be too small for convenient installation of conventional internal AOA instrumentation. This method is directly applicable in making both displacement and velocity measurements of large, flexible structure to be used in space.

6.13.5 Status/Plans

The system in its present form is being prepared for installation in the 13-inch MSBS. Optical refinements in the system, such as custom built optics, are slated as well as improvements in the electronics. These improvements will make the system a viable means of non-contact wind tunnel measurements. Development work also has been initiated in using a variation of this electro-optical measurement technique to make deflection measurements of a large space structure.

Ping Tcheng
Electro-Mechanical Instrumentation Branch
Langley Research Center
(804)864-4717

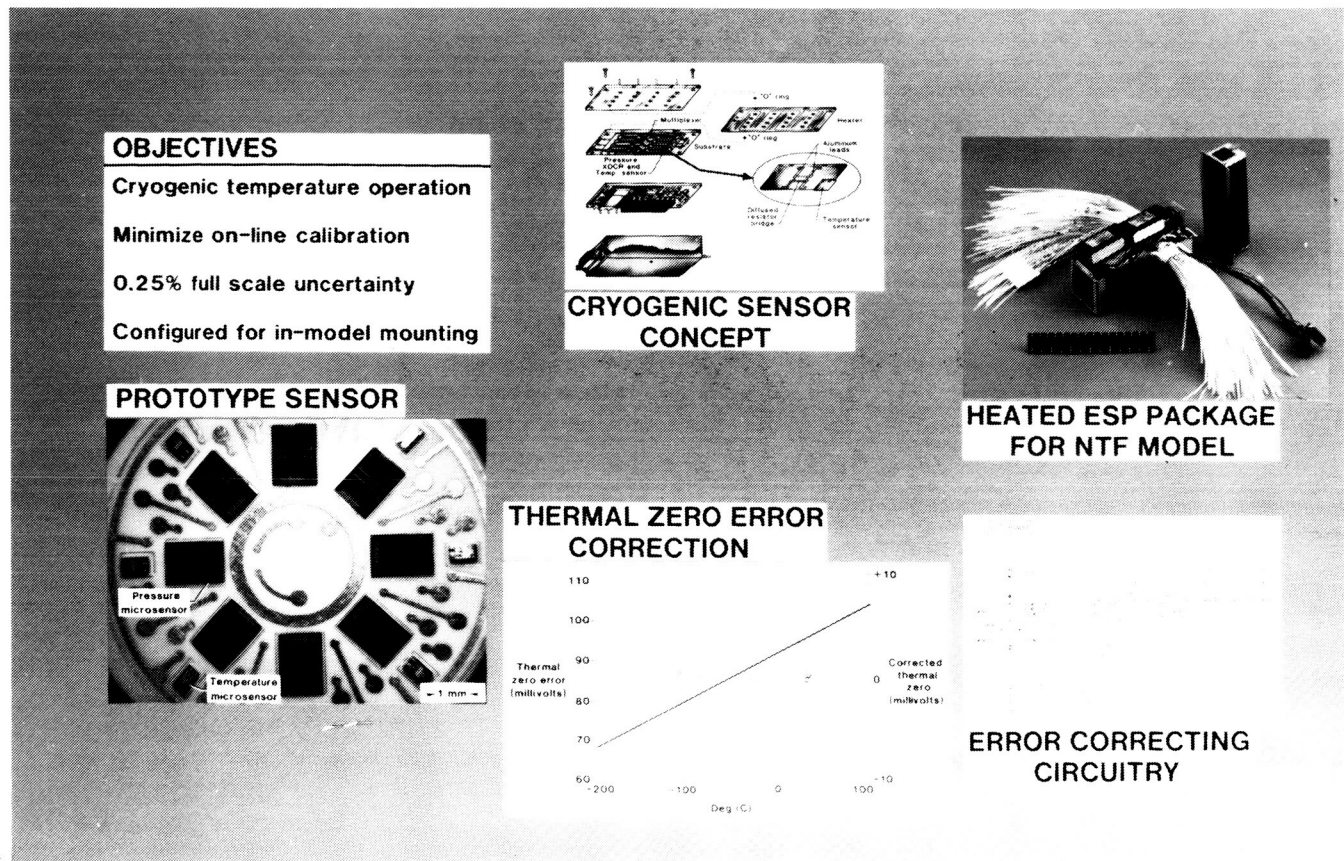


Figure 6.13. Model Pressure Instrumentation

6.14 ELECTRONICALLY SCANNED CYROGENIC PRESSURE MODULE

6.14.1 Objective

To develop a cryogenically functional, multi-channel, error correcting pressure module capable of operating over a temperature range of 100 to 350 K for applications to the National Transonic Facility and 0.3-meter Transonic Cryogenic Tunnel. An experimental system was developed to evaluate and determine the operating characteristics of silicon pressure sensors over a temperature range of 100 to 350 K. A modified, 286-based pc was transformed to (1) perform data acquisition, (2) analyze data, (3) perform thermal error corrections and (4) plot the results.

6.14.2 Approach

The approach involved cryogenically testing commercially available silicon micropressure sensors to determine characteristics at cryotemperatures. NASA applied qualified micropressure sensors to develop a multi-channel design. Development efforts included (1) qualification of electronic components required to control and scan sensor outputs at cryogenic temperatures, (2) design of an automated test system for pressure and temperature environments for the testing and (3) development of pc based software for the control of the module and acquisition, analysis and error correction of the pressure module signals (See Figure 6.13).

6.14.3 Accomplishments

The pc-based data acquisition system has been used to conduct research of solid state pressure sensors at extremely low temperatures. The data acquisition, analysis and plotting of sensor offset and sensitivity characteristics with temperature was accomplished. The system has been used to compute correction codes for a digital error correction loop to compensate single channel sensors for thermally induced errors. Two technical papers have been presented to the ISA 35th International Instrumentation Symposium, (1) "A Temperature and Pressure Controlled Calibration System for Pressure Sensors," and (2) "Piezoresistive Silicon Sensors in Cryogenic Environment." A prototype cryogenic, eight channel, plus or minus five psid pressure module has been assembled and tested from 77°K to 350°K.

6.14.4 Significance

A cryogenically functional experimental multi-channel sensor module has been built. The ability to compensate thermally induced sensor errors to within 0.1 percent error F. S. has been demonstrated. The results of cryogenically tested, commercially produced silicon microsensors are very encouraging. This development will simplify installation of model pressure instrumentation in cryogenic models.

6.14.5 Status/Plans

The development of software based digital error correction techniques will allow accurate multi-channel pressure measurements to be made in cryogenic environments. Module design will be completed along with laboratory testing leading to experimental application in the NTF environment.

John J. Chapman and Dr. Seun K. Kahng
Instrument Application Branch
Langley Research Center
(804)864-4834

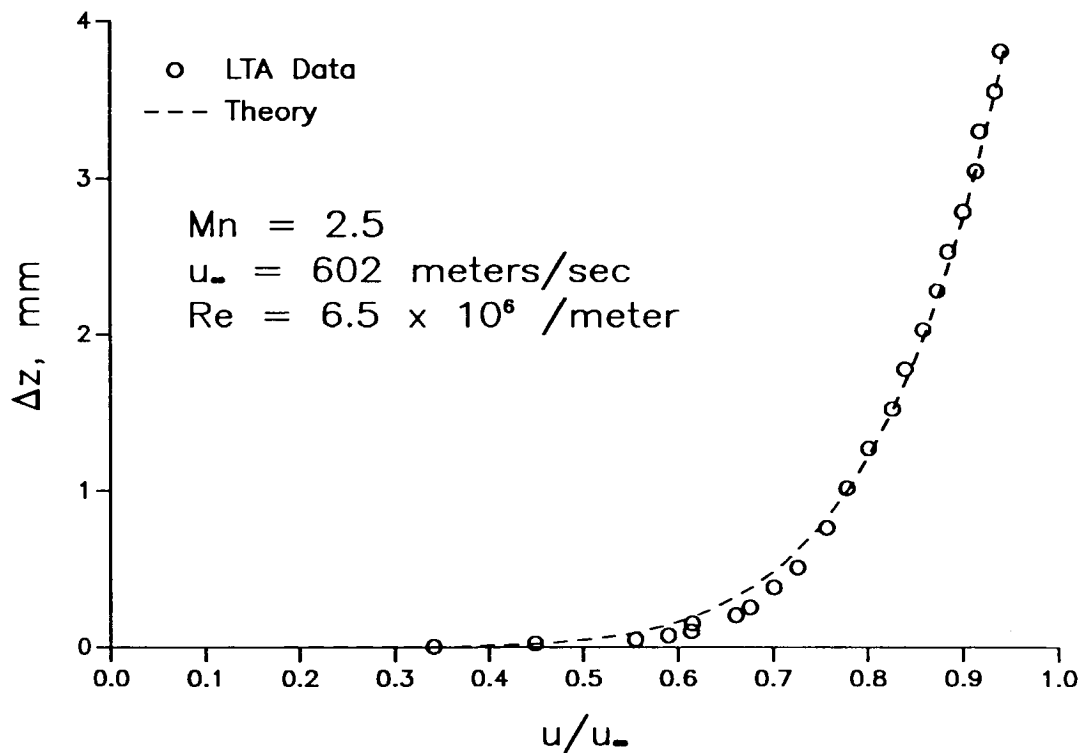


Figure 6.14. Typical Turbulent Boundary Layer Profile Measurement

6.15 BOUNDARY LAYER PROFILE MEASUREMENTS ON A 5-DEGREE HALF-ANGLE CONE USING A LASER TRANSIT ANEMOMETER IN THE UNITARY PLAN WIND TUNNEL

6.15.1 Objective

To provide nonintrusive measurements of mean velocity, flow angle and turbulence intensity at supersonic speed regimes in the boundary layer of a slender (5-degree half angle) cone.

6.15.2 Approach

Research programs such as the National Aero-Space Plane (NASP) are becoming increasingly dependent on having accurate flow diagnostic information in supersonic flows. Mie scattering-based laser anemometry, utilizing only a laser beam to probe the test medium, offers a nonintrusive method of measuring the flow velocity, flow angle, turbulence intensity and shear stress around a test model under various flow conditions. To demonstrate the usefulness of Mie scattering-based systems in supersonic facilities, an experiment was conducted in the Langley Unitary Plan Wind Tunnel using a laser transit anemometry (LTA) system to probe the boundary layer on a slender (five degree half angle) cone model at Mach numbers of 2.50 and 4.50. The anemometry system utilized a pair of laser beams with a diameter of 40 mm spaced 1,230 mm apart to measure the transit times of ensembles of seeding particles using a cross correlation technique. The tunnel seeding system consisted of a small vibrated, fluidized bed containing dry kaolin dust with a nominal particle size of 0.9 mm. The kaolin was injected directly into the boundary layer via nine 1.32-mm orifices (three rows of three each) in the model nose. The choice of using dry kaolin dust as the seeding material was made to eliminate the problems of condensation present among seeding systems using liquid carriers such as ethanol. These problems are particularly severe in facilities such as the Unitary Plan Wind Tunnel.

6.15.3 Accomplishments

The measured boundary layer profiles, representing the boundary layer velocity normalized to the freestream as a function of height above the model surface were corrected for a zero angle of attack, Mach numbers of 2.5 and 4.5 and Reynolds numbers of 3.281×10^6 -meter and 6.562×10^6 -meter and were corrected in a vertical plane that bisected the model's longitudinal centerline at a location 635-mm from the tip of the forebody cone (See Figure 6.14). The results indicated an excellent ability of the LTA system to make boundary layer velocity measurements to within tens of microns of the model surface; however, because of disturbances in the flowfield caused by the onboard seeding system, premature transition to a turbulent boundary layer occurred, implying that upstream seeding is mandatory if model flowfield integrity is to be maintained. These results indicate that with upstream seeding (in the settling chamber), good measurement accuracy is possible with excellent spatial resolution.

The results from these initial tests indicate an excellent ability of the LTA system to measure boundary layer profiles at supersonic speeds and represent the first nonintrusive, off-model boundary layer measurements performed in the Unitary Plan Wind Tunnel.

6.15.4 Significance

The results from these initial tests indicate an excellent ability of the LTA system to measure boundary layer profiles at supersonic speeds and represent the first, nonintrusive, off-model boundary layer measurements performed in the Unitary Plan Wind Tunnel.

6.15.5 Status/Plans

Follow-on experiments are planned in the Unitary Plan Wind Tunnel using upstream seeding in the setting chamber to improve the results presented here. In addition, an LTA entry into the 20-inch Mach 6 tunnel is planned in support of the NASP program.

William M. Humphreys, Jr. and William W. Hunter, Jr.
Measurement Physics Branch
Langley Research Center
(804)864-4601

Monte Carlo Simulation

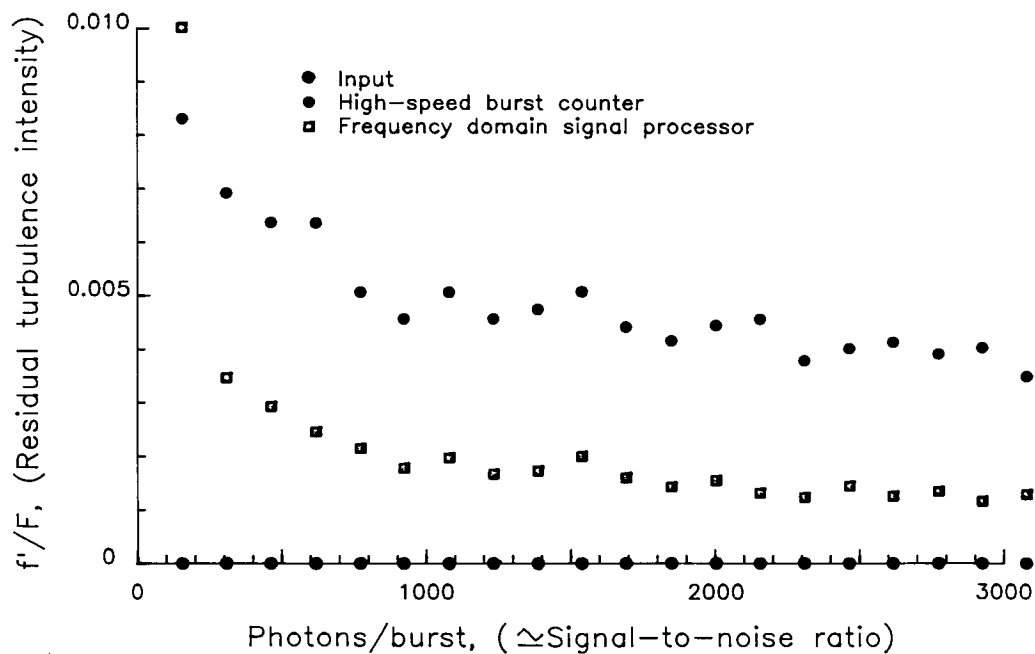


Figure 6.15. Signal Processor Performance

6.16 FREQUENCY DOMAIN LASER VELOCIMETER SIGNAL PROCESSOR

6.16.1 Objective

To convert the theoretical model of a frequency domain laser velocimeter signal processor into a cost effective hardware system.

6.16.2 Approach

The advent of high-speed digital signal processing integrated circuits allowed frequency domain signal processing techniques to be applied to randomly occurring chirp frequency bursts of the type obtained from a laser velocimeter. A software simulation of a frequency domain based signal processor was developed and tested using simulated and transient recordings of laser velocimeter signal bursts. These tests indicated theoretical increases in accuracy of a factor of five over standard high-speed burst counters with a factor of five lower residual turbulence intensity. The control and feedback algorithms remained stable from near photon resolved signals to signals reaching photomultiplier saturation levels without operator intervention (See Figure 6.15).

6.16.3 Accomplishments

Following its presentation at the Third International Symposium on Applications of Laser Anemometry to Fluid Mechanics, 1986, Macrodyne, Inc. of Schenectady, New York, expressed interest in developing the technology for commercial application. Macrodyne was awarded a Phase I SBIR contract to develop a low frequency prototype to test the basic algorithms. The success of the prototype resulted in a Phase II SBIR contract to develop the high frequency system. During the course of the Phase II contract, Macrodyne also developed a mid-frequency (20 MHz maximum input frequency) unit. The first mid-frequency unit was constructed and delivered to Ames where testing indicated a far greater dynamic range in signal level and signal-To-noise ratio than present high-speed burst counters.

6.16.4 Significance

The frequency domain laser velocimeter signal processor provides a greater dynamic range of measurable signal levels and signal-To-noise ratios with higher accuracy than present technology. It requires minimal operator intervention, making the laser velocimeter easier to use while minimizing measurement errors due to improper instrument settings.

6.16.5 Status/Plans

The present high-speed burst counters at Langley will be phased out and replaced with frequency domain laser velocimeter signal processors.

James F. Meyers
Measurement Physics Branch
Langley Research Center
(804)864-4598

CHAPTER SEVEN

CONFIGURATION AERODYNAMICS

7.1 INTRODUCTION

Fundamental aerodynamic databases and analytical methods are generated for the efficient and accurate prediction of aerodynamic flows about advanced aircraft components and configurations. Experimental investigations are performed across the speed range in wind tunnels and in flight to provide improved understanding of complex aerodynamic flows and to identify and refine innovative concepts and configurations. Work is underway on advanced laminar-flow and high-lift airfoils, boundary layer transition prediction and control, the prediction and innovative applications of separation-induced vortex flow technology and high Reynolds number research in the NTF.

Computational methods are being developed for full potential and Navier-Stokes equations, which embed complicated vehicle configurations in adaptive meshes. The development and application of conventional methods for three dimensional viscous and inviscid flows for aircraft components and the conduct of wind tunnel, water tunnel and flight experiments is in progress.

Test-validated sophisticated techniques are being developed for predicting 3-D wing flow separation and for providing an improved understanding of wing/body vortical flows and vortex production/breakdown phenomena. TRANAIR development now includes solution-adaptive grid refinement, vortex shedding from sharp edges and supersonic free-stream considerations. Wing/airfoil optimization is performed to support agency/industry aerodynamic design for subsonic, transonic, and supersonic flows.

Program Manager: Mr. Gary Hicks
OAST/RF
Washington, DC 20546
(202)453-2830

ORIGINAL PAGE
BLACK AND WHITE PHOTOGRAPH

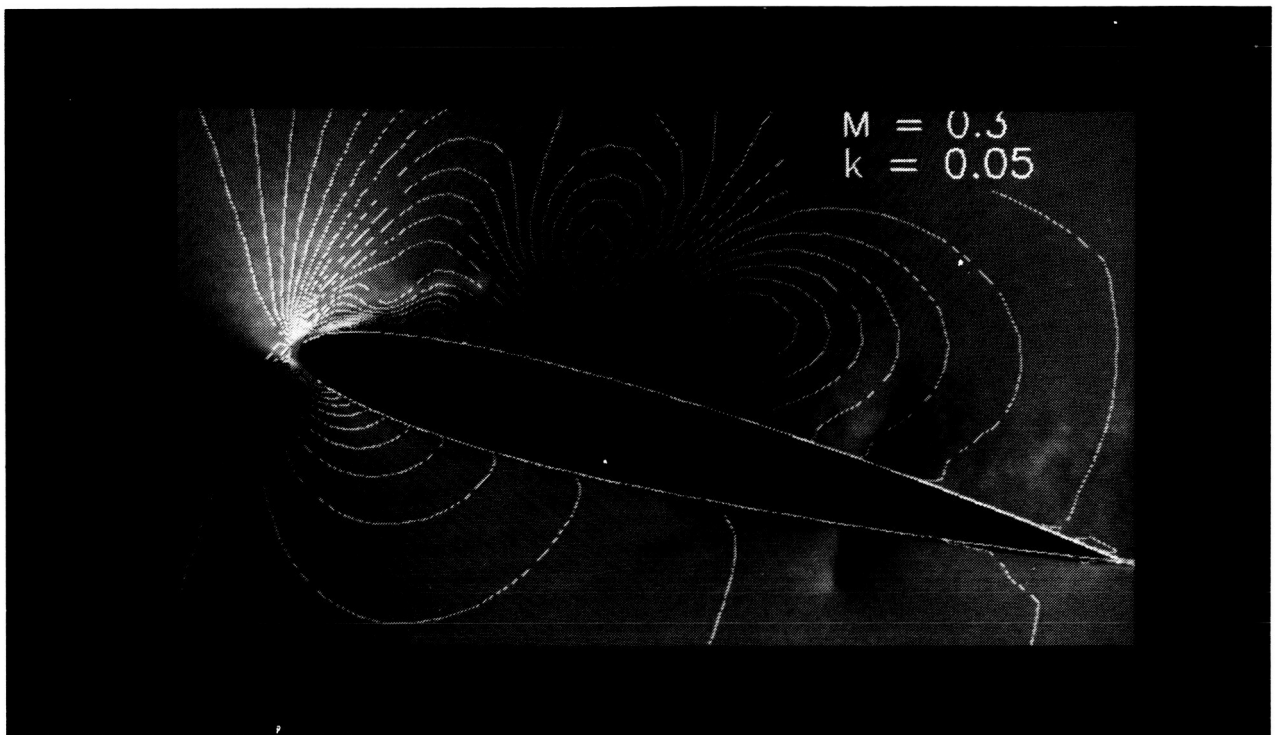


Figure 7.1. Computed Density Gradient Superimposed on the Stroboscopic Schlieren Picture

7.2 COMPRESSIBILITY EFFECTS ON DYNAMIC STALL

7.2.1 Objective

To experimentally quantify dynamic stall behavior of airfoils with increasing Mach number and to document unsteady flow field for code development and validation.

7.2.2 Approach

The approach involved designing and commissioning a compressible dynamic stall facility (CDSF) to oscillate an airfoil supported between two optical quality glass windows that provide a complete view of the airfoil and flow field. NASA completed a series of stroboscopic Schlieren studies to highlight dynamic stall vortex behavior (See Figure 7.1).

7.2.3 Significance

NASA obtained new insight in the compressibility effects stall process with partial quantification of behavior.

7.2.4 Status/Plans

Detailed studies of unsteady flow field are in progress, using laser Doppler velocimetry and holography to generate data for code development and flow field analysis.

M. S. Chandrasekhara and L. W. Carr
Fluid Dynamics Research Branch
Ames Research Center
(415)604-4269

$M = 0.74$

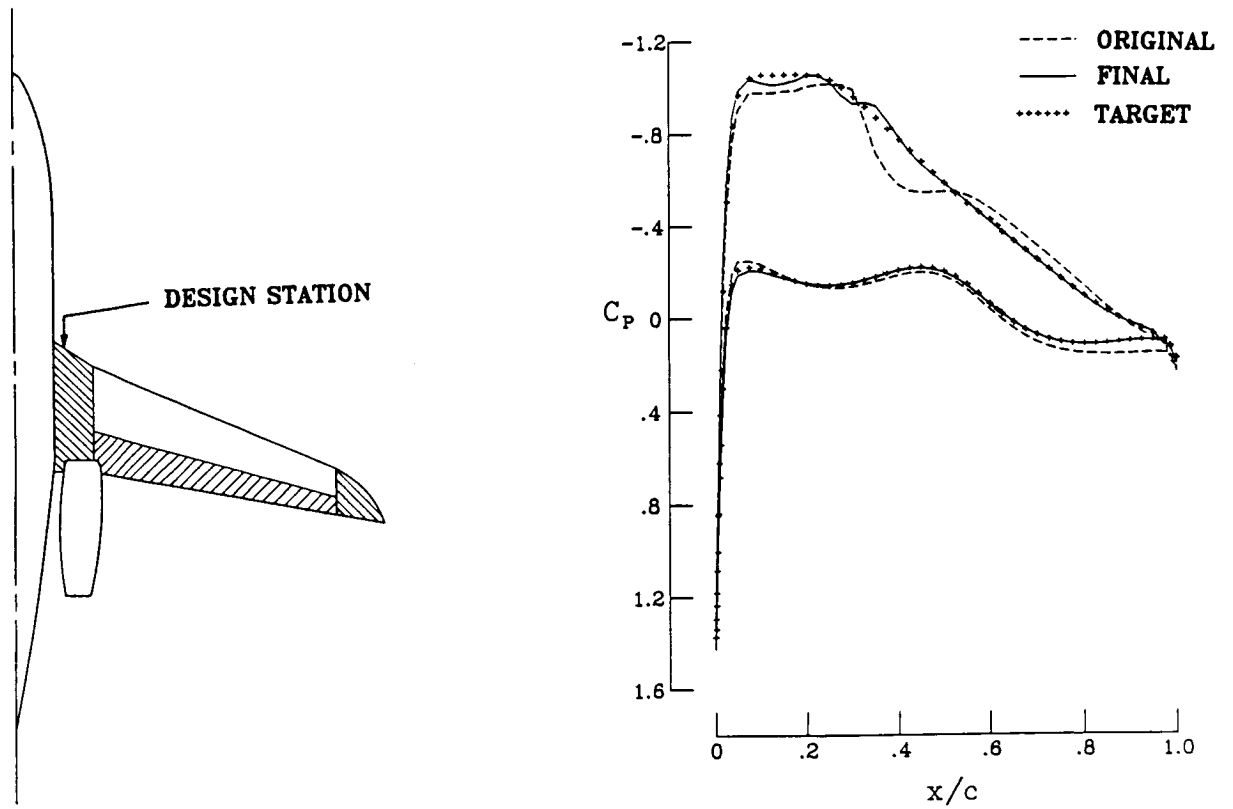


Figure 7.2. Wing Root Design to Eliminate Shock

7.3 APPLICATION OF A TRANSONIC/SUPERSONIC DESIGN METHOD TO COMPLEX GEOMETRIES AND ISOLATED AIRCRAFT COMPONENTS

7.3.1 Objective

To apply a transonic/supersonic wing design method to realistic aircraft configurations and to extend the method to include the design of other aircraft components such as winglets, fuselages and nacelles.

7.3.2 Approach

During the last five years, Langley was involved in several research programs that required designing or modifying a wing to achieve a given pressure distribution at transonic speeds. A method was developed that modifies the surface curvatures and slopes of an initial geometry so that a target pressure distribution is matched. This approach was extended to include effects of viscosity and static aeroelastic deflections. The method proved to be fast, robust and accurate for relatively simple configurations. Efforts were initiated to apply these design codes to flows about more complex geometries, to explore their application to the design of bodies and to evaluate the design approach in predominantly supersonic flows.

7.3.3 Accomplishments

Several design exercises involving more complex geometries were made. These configurations included wing winglet designs, wings with fuselage-mounted nacelles and wings with pylons and nacelles underneath. Results were gained for an executive transport with fuselage-mounted nacelles (See Figure 7.2). A wing root plug was to be added to the existing wing. The original wing plug has a fairly strong shock near $x/c=0.4$. The design method was used to achieve a target pressure distribution which eliminates this shock and to give a more uniform isobar pattern in this region. The final pressure distribution from the design code is in good agreement with the target. Two new design codes also were developed based on this design approach. The first of these uses an axisymmetric Euler code to design isolated, powered or flow-through nacelles. The other pilot code is a supersonic full-potential method, which will be used in the design of wings using laminar flow control at supersonic speeds.

7.3.4 Significance

These methods provide a means of rapidly designing or modifying an aircraft component to achieve a given pressure distribution and thus reduce or eliminate undesirable flow characteristics or adverse interference effects between different components.

7.3.5 Status/Plans

The existing codes will continue to be applied to various configurations to build an experience base for future applications. The design of certain aircraft configurations will make it necessary to couple the design method to Euler and Navier-Stokes codes. Particular attention will be given to defining efficient design interaction procedures.

Richard L. Campbell and Leigh A. Smith
Transonic Aerodynamics Branch
Langley Research Center
(804)864-2872

ORIGINAL PAGE BLACK AND WHITE PHOTOGRAPH

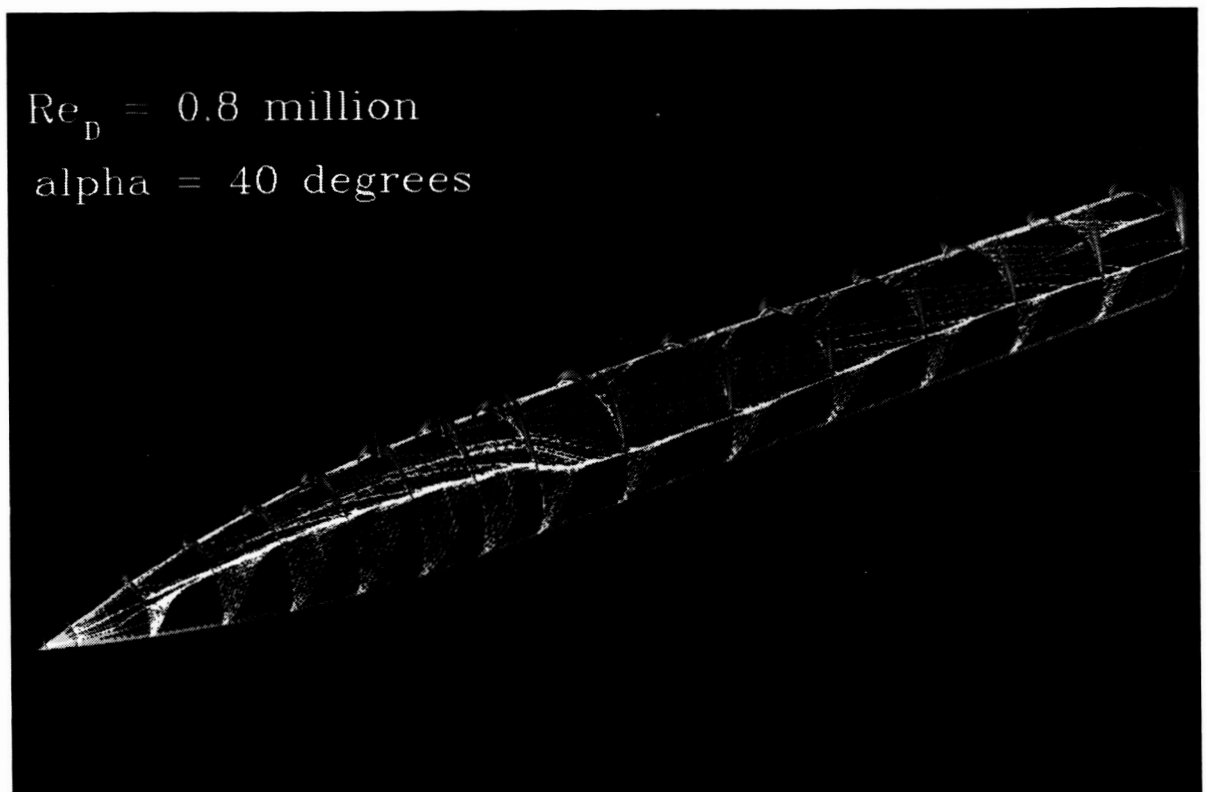


Figure 7.3. Helicity Density Contours

7.4 NAVIER-STOKES SOLUTIONS FOR VORTICAL FLOWS OVER A FOREBODY

7.4.1 Objective

The objective was the computational assessment of the effects of Reynolds number and angle of attack on vortical flows over a pointed slender body.

7.4.2 Approach

Steady-state solutions for vortical flows with $0.2 \text{ million} < \text{Re}_D \leq 3.0 \text{ million}$ and $20^\circ < \alpha < 40^\circ$ over a 3.5 caliber tangent-ogive cylinder will be obtained using FMC1, a time-implicit upwind method for the three-dimensional, incompressible Navier-Stokes equations. This solver comprises flux-difference splitting, a TVD-like discretization of the inviscid fluxes, and several extensions to the algebraic turbulence model by Baldwin and Lomax to handle flows with massive crossflow separation.

7.4.3 Accomplishments

A rational extension to the Baldwin-Lomax turbulence model has been devised. That extension allows, for the first time, computational modeling of transitional crossflow separation (i.e., flows with three-dimensional laminar, equatorial separation bubbles and subsequent transition in the separating shear layers which roll up into two primary vortices). In addition, it proves to be less sensitive toward the choice of adjustable parameters in simulations of fully turbulent crossflow separations than an established modification to the Baldwin-Lomax turbulence model. For $\alpha \geq 30^\circ$ and $\text{Re}_D = 0.8 \text{ million}$, a perturbation of the geometry into a slightly elliptic cross section just at the nose tip eliminates multiple steady-state solutions with asymmetric vortex patterns along the forebody (See Figure 7.3). A typical solution when the major axis of an "elliptic" nose tip is rolled by 45° in counterclockwise direction (pilot's view) out of its horizontal position. Four shedding events are shown by means of helicity density contours (helicity density is defined as the scalar product of local velocity and vorticity vectors). An almost perfect mirror image is produced when the nose tip is rolled for another 90° . This supports earlier conjectures that slight imperfections in the vicinity of the apex of slender bodies with sharp noses control the asymmetric pattern along the entire body. Reynolds number effects for $\alpha = 30^\circ$ are found to diminish for $\text{Re}_D \geq 1.0 \text{ million}$. All computational results compare well with experimental surface pressures and flow visualizations.

7.4.4 Significance

Knowledge about transition and other driving mechanisms controlling vortex asymmetries could enhance the flight envelope of fighter aircraft and missiles.

7.4.5 Status/Plans

A Navier-Stokes analysis of a F/A-18 or a F-16 forebody with a modified nose tip will exploit the methodology and the insights into the physics of vortical forebody flows.

Peter M. Hartwich, Robert M. Hall and Michael J. Hemsch
Transonic Aerodynamics Branch
Langley Research Center
(804)864-2881

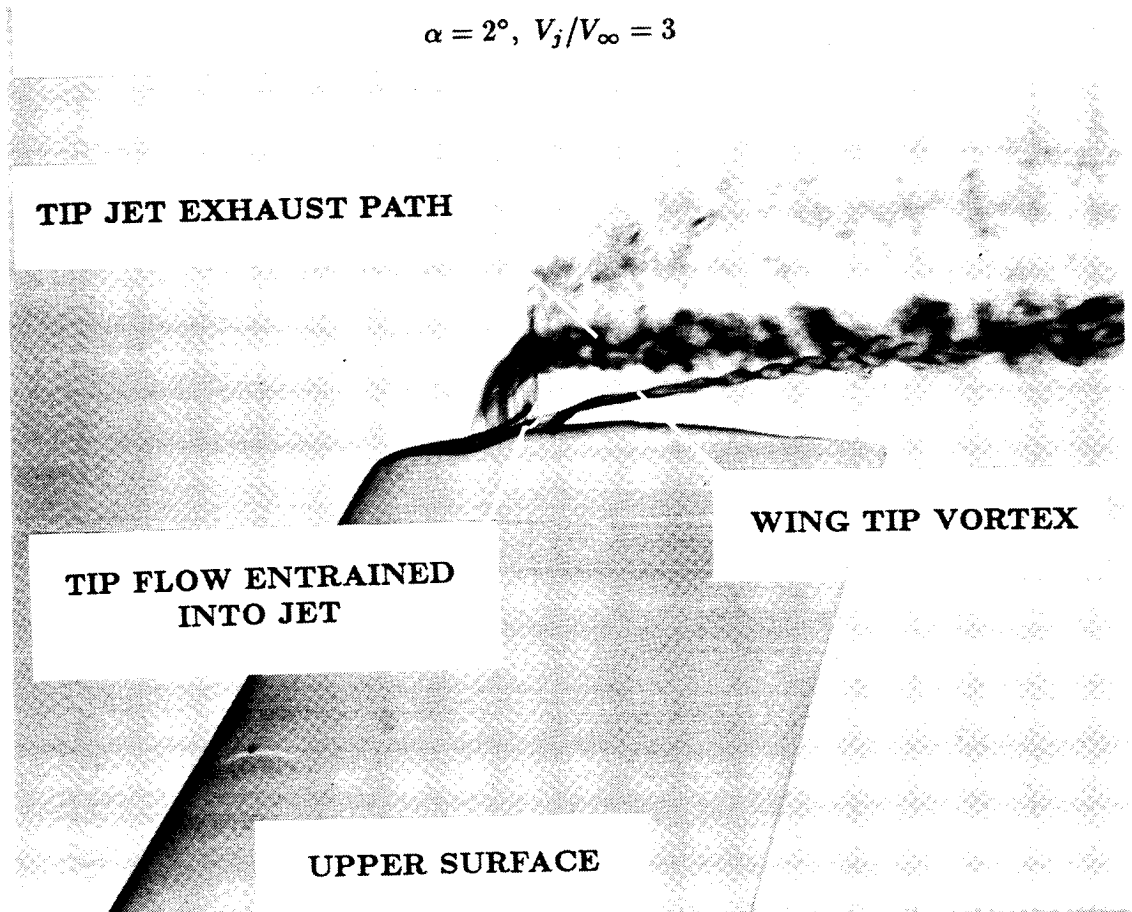


Figure 7.4. Wing-Tip Blowing Model in Water Tunnel

7.5 EFFECT OF WING PLANFORM AND THE MODIFICATION AND WAKE ROLLUP ON INDUCED DRAG

7.5.1 Objective

To reduce the induced drag of both high and low aspect ratio wings.

7.5.2 Approach

Studies to determine the fundamental causes of induced drag, the role of wing wake rollup in induced drag and the relative benefits of particular induced drag reduction concepts are planned. Analytically designed winglets for low speed ratio wings will be experimentally investigated. The effects of in-plane and out-of-plane modifications to the wing planform, the effects of spanwise blowing from the wing-tip and the effects of changes to the tip planform and edge shape will be studied.

7.5.3 Accomplishments

The wings for the studies of the effect of wing planform and wake rollup are being built. Analytical studies of the effect of winglets on low aspect ratio wings have been completed. Studies of spanwise blowing from the wing tip have been completed in the Langley 16-inch by 24-inch water tunnel. Figure 7.4 shows the interaction of the spanwise exhausting jet and the wing-tip vortex. A wind tunnel model with 11 interchangeable wing-tips has been built. These tips will be used to study the effect of raking the edge of the tip towards and away from the fuselage, the effect of sharpening the edge of the tip to generate vortex lift, the effect of the jet exit position on the tip, of the jet exhaust direction, of the jet exit length and of the jet momentum on the span load distribution and the drag.

7.5.4 Significance

The analytical studies of adding winglets to low aspect ratio wings indicated significant improvements in the lift to drag ratio at moderate lift coefficients and transonic speeds. The tip blowing studies suggest that the addition of blowing increases the lift over the outer portion of the wing and the tip vortex is diffused and displaced outboard. The wing lift will be increased and the induced drag decreased.

7.5.5 Status/Plans

Experiments to determine the effects of wing planform on induced drag and on the near and far field wakes are planned for the 8-foot Transonic Pressure Tunnel. Experiments to verify the benefits of winglets on low aspect ratio wings are planned for the 7-foot by 10-foot High Speed Tunnel. Follow-on tests of the spanwise blowing from the tip are planned for the Low Turbulence Pressure Tunnel in Spring 1990 to study the effect of the blowing on the vorticity in the wake.

ORIGINAL PAGE
BLACK AND WHITE PHOTOGRAPH

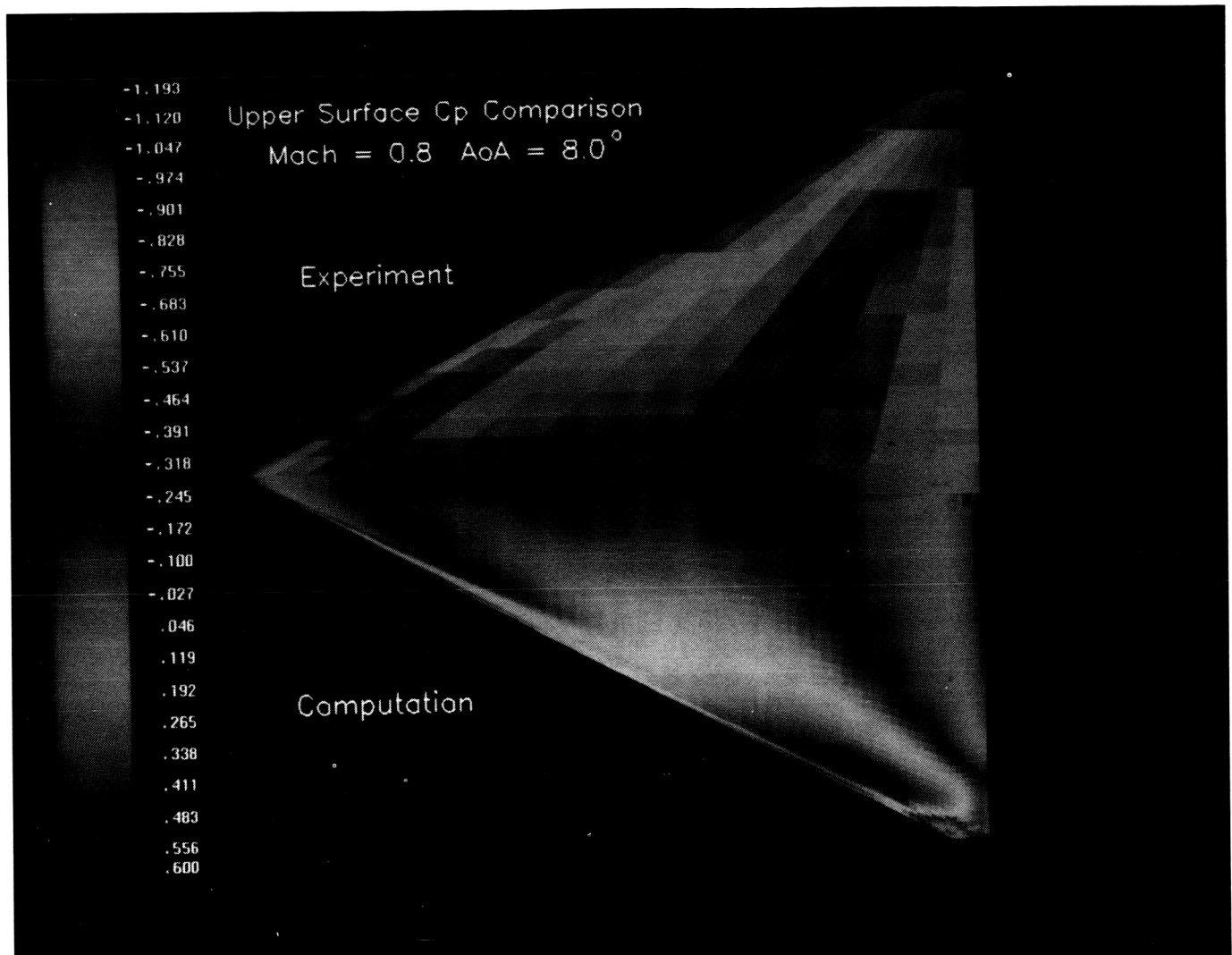


Figure 7.5. Euler Code Validation/Theory-Experiment Integration

7.6 EULER CODE VALIDATION/THEORY-EXPERIMENT INTEGRATION

7.6.1 Objective

To (1) validate the FLO57, a widely used Euler Code, for use on delta wing configurations over the transonic and low supersonic Mach numbers and angle of attack and yaw of 20 degrees and (2) integrate computational and experimental data to enhance techniques of integrating experimental surface pressures to yield accurate forces and moments.

7.6.2 Approach

The FLO57 was modified to handle O-H grid topologies. Detailed comparisons were made with the data from a highly instrumented (force and pressure) delta wing wind tunnel model. Computational results were used to correct the integration of the pressure data (See Figure 7.5).

7.6.3 Accomplishments

For vortex dominated flows, the computational and experimental results were in excellent agreement. This demonstrated that computational results can be used to define a discretization drag increment associated with sparse experimental data.

7.6.4 Significance

NASA validated the FLO57 for delta wing configurations; increased accuracy of force and moment predictions from experimental pressure distribution integrations inward and reduced instrumentation requirements for complex wind tunnel models reduced.

7.6.5 Status/Plans

NASA will analyze lateral-directional forces, moments and pressure distributions and incorporate an integral boundary layer correction for fully attached flows.

John E. Melton, David D. Robertson and Seth Moyer
Applied Aerodynamics Branch
Ames Research Center
(415)604-6208

ORIGINAL PAGE
BLACK AND WHITE PHOTOGRAPH

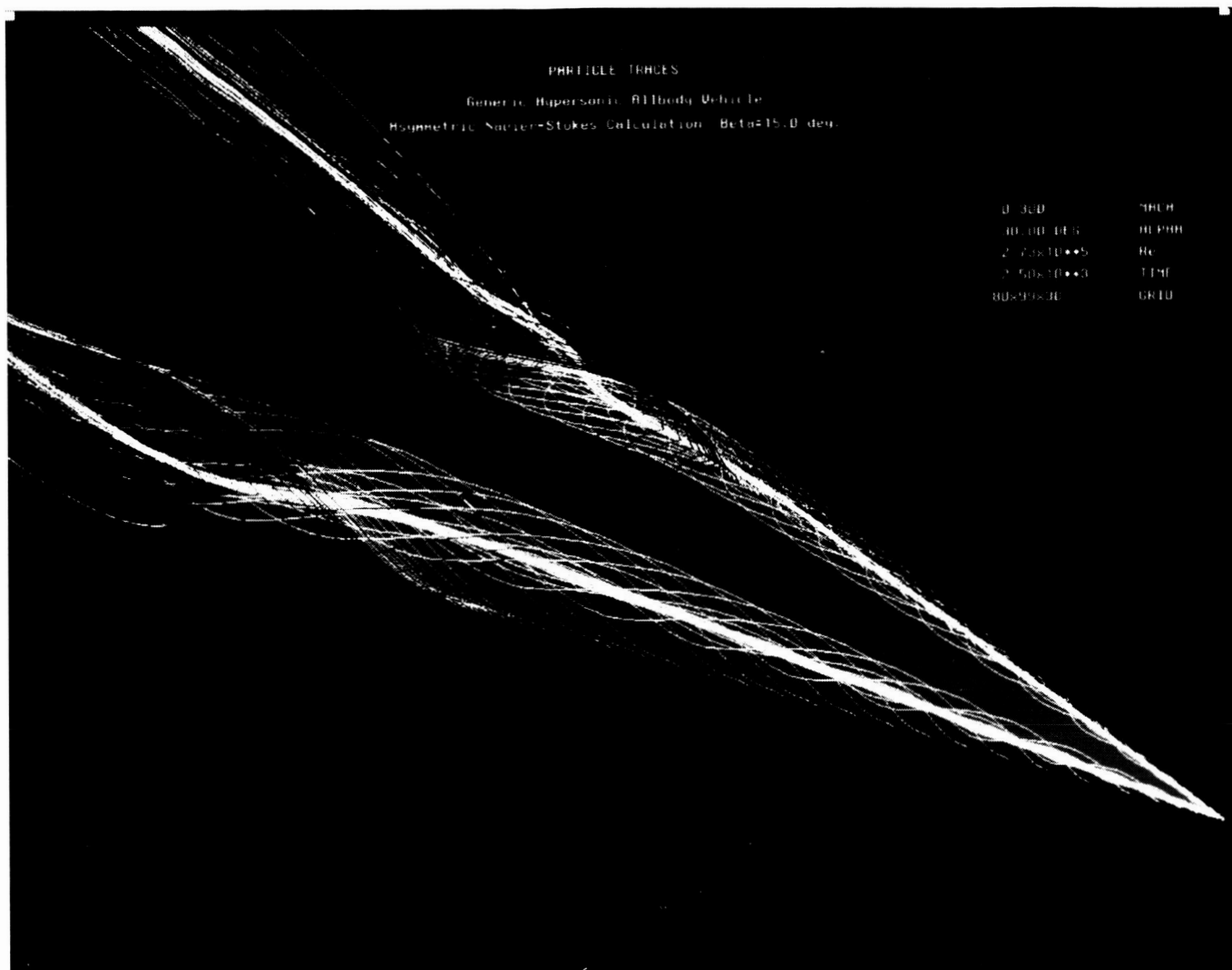


Figure 7.6. LANS3D NS Asymmetrical Flow Solution for a Generic,
Hypersonic All-Body Configuration

7.7 ASYMMETRICAL VISCOUS FLOW CALCULATIONS USING LANS3D

7.7.1 Objective

To modify an existing and validated three-dimensional, Navier-Stokes analysis program to perform asymmetric calculations of aircraft configurations at sideslip.

7.7.2 Approach

NASA used a dual approach, depending on available computer memory.

Small Memory: NASA obtained the required boundary condition information for each half of the full configuration from the opposing side of model. This method lends itself to smaller-memory, large, secondary storage, computer architectures such as the Cray Y-MP. It also retains and computes on only one half of the model in main memory, the opposing side being placed on secondary storage.

Large Memory: This is an extension of the small memory approach permitting calculation on both sides of the configuration using a single grid block with required boundary overlap. This method can be applied on large memory computers, such as the Cray-2. Both methods yielded identical results (See Figure 7.6).

7.7.3 Accomplishments

The LANS3D program was modified in a few weeks to handle both approaches. Test calculations were performed on the Ames Cray X-MP and the NAS Cray Y-MP and Cray-2 to verify both methods on different computer architectures. LANS3D is ready for production running on all systems.

7.7.4 Significance

This approach of performing asymmetric calculations using either multiple grid blocks or a single block, both with overlapping grid point, was implemented in a fraction of the time that would have been necessary to convert the entire LANS3D program to the more standard approach of employing a periodic boundary condition. In addition, the capability for doing more general, multiple grid block calculations for complex geometries was provided.

7.7.5 Status/Plans

LANS3D will continue to be validated against experimental data available for configurations at sideslip.

Gary B. Cosentino
Applied Aerodynamics Branch
Ames Research Center
(415)604-6133

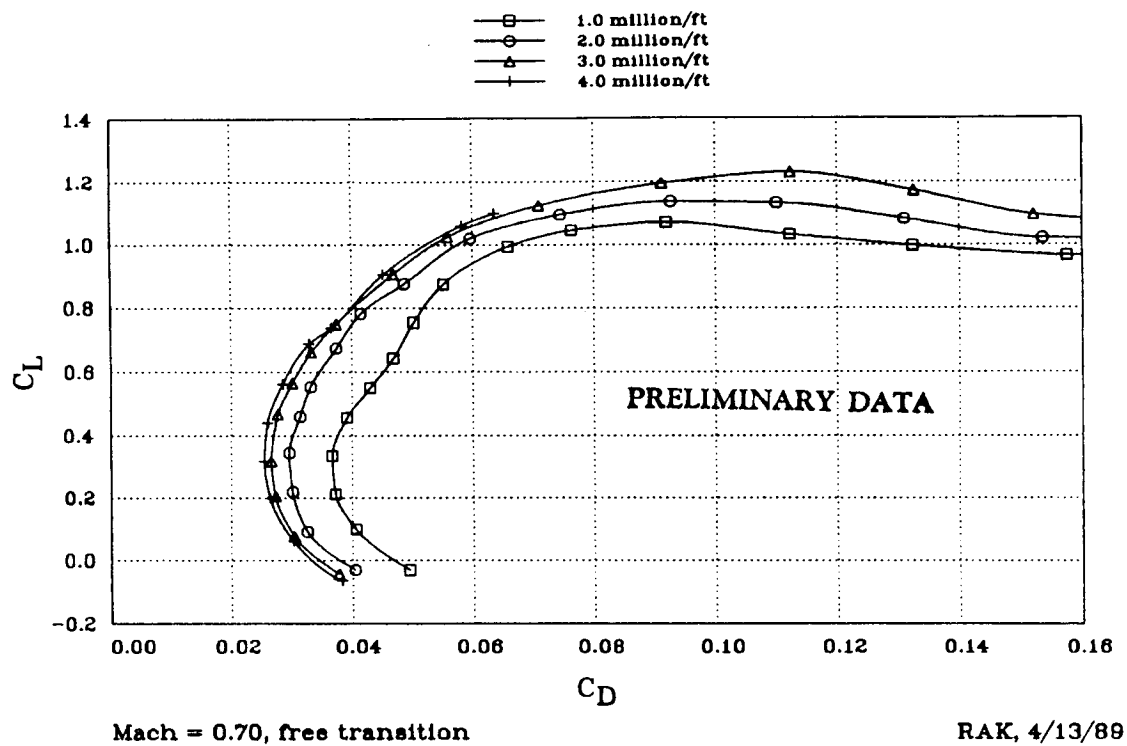


Figure 7.7. Effect of Reynolds Number on Wing/Body Drag Polar

7.8 LOW REYNOLDS NUMBER TRANSONIC WING TEST (F-8/VHASA)

7.8.1 Objective

In support of a proposed Very High Altitude Sampling Aircraft (VHASA) capable of flight at up to 100,000 feet, a brief wind tunnel test of a thick, high aspect ratio wing was conducted at flight Reynolds number.

7.8.2 Accomplishments

An existing wing/body model designed for high lift at transonic speeds was modified slightly and tested at unusually low Reynolds numbers in the Ames 11-foot Transonic Wind Tunnel in April 1989 (See Figure 7.7).

7.8.3 Significance

There is very little existing data on transonic flight at low Reynolds numbers, so the results of even this quick look should be helpful in the conceptual design of the vehicle. The preliminary data indicate that the wing will not be a critical item for the high altitude airplane, although there is room for further development.

7.8.4 Status/Plans

A data report is in preparation. In the event that the program is funded, further work on low Reynolds number transonic airfoil design and testing is being planned. One phase of such follow-on work might be to instrument the existing wing for surface pressure measurements and retest.

Robert A. Kennelly, Jr., James M. Strong, Steven C. Smith and Raymond M. Hicks
Advanced Aerodynamic Concepts Branch
Ames Research Center
(415)604-5944

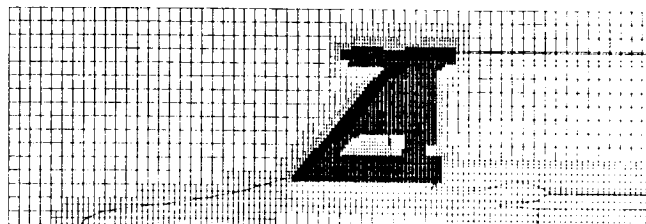
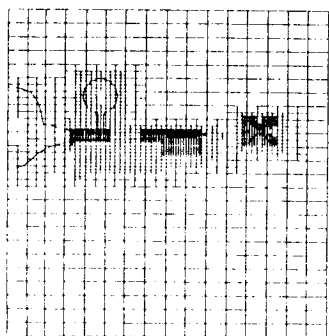
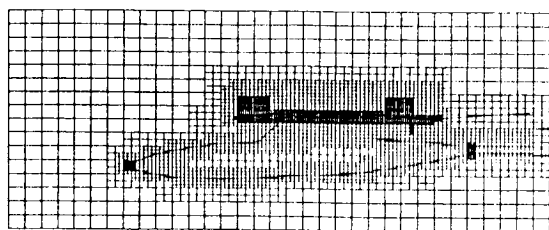
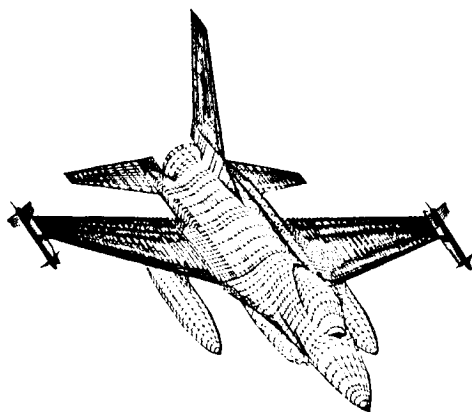


Figure 7.8. F-16A W/TIP Missiles, Fuel Tanks

Michael D. Madson
Advanced Aerodynamic Concepts Branch
Ames Research Center
(415)604-3621

ORIGINAL PAGE
BLACK AND WHITE PHOTOGRAPH

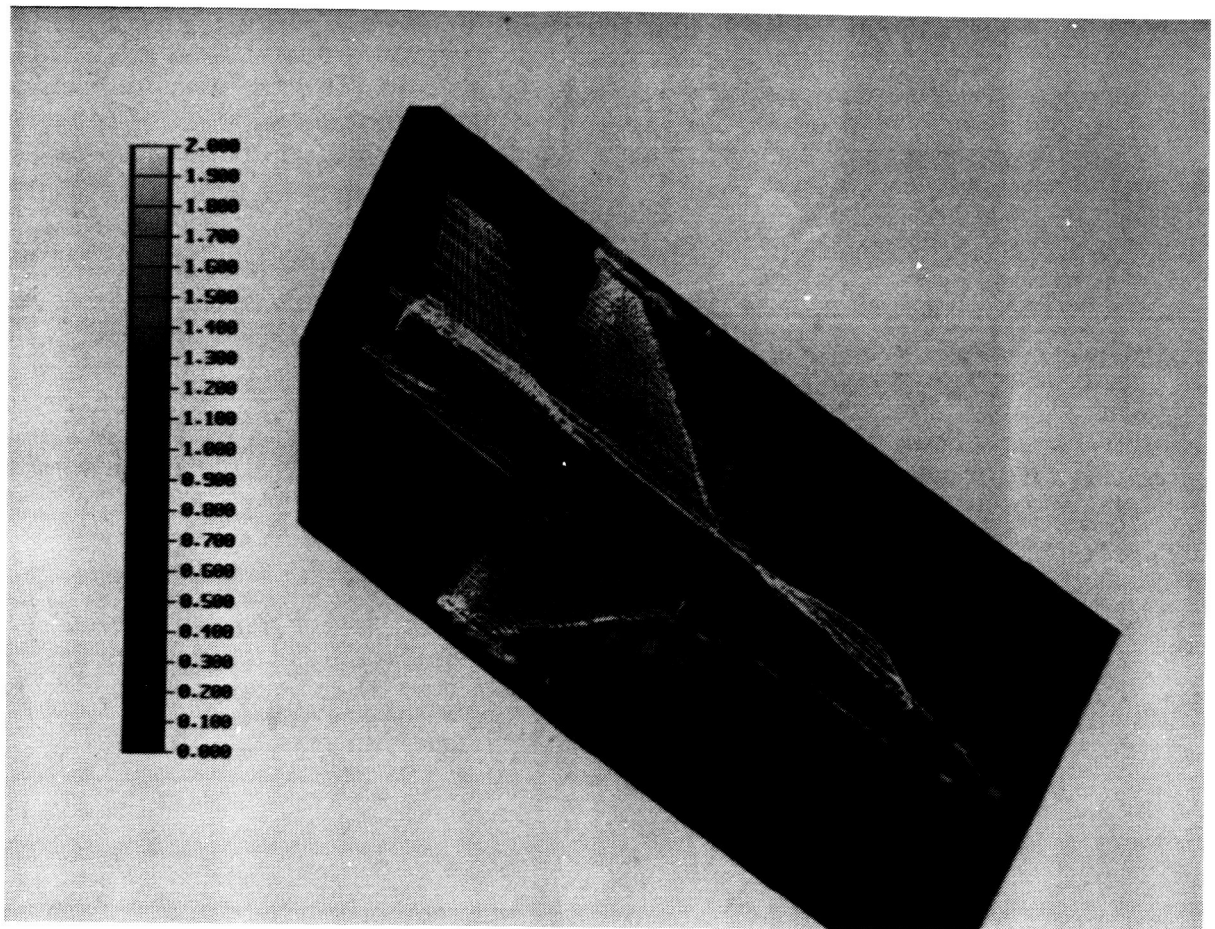


Figure 7.9. F-16A Configuration at 300 MHz

7.9 TRANAIR DEVELOPMENT AND VALIDATION

7.9.1 Objective

To develop and validate a computational method which utilizes an unstructured rectangular grid in the analysis of complex aircraft configurations in the transonic flow regime.

7.9.2 Approach

The TRANAIR full-potential code being developed by Boeing under NASA contract, embeds accurately defined surface panel models of very general and complex configurations in a rectangular array of flow field grid points. This grid was locally refined in order to more accurately resolve shocks and regions where large flow gradients exist. The grid was discretized with finite elements and the resulting set of nonlinear algebraic equations were iteratively solved.

7.9.3 Accomplishments

The implementation of a solution adaptive, grid refinement capability already has improved the efficiency and generally of the TRANAIR code. Several other efficiency modifications were implemented which made the code extremely economical in terms of both CPU and storage requirements. Both NASA and Boeing applied the code to several diverse geometries ranging from a plain wing, to a flow-through nacelle, to complete configurations such as the Boeing 747 and the General Dynamics F-16A with wing-tip missiles and under-wing fuel tanks. Results from these geometries compared very well with experimental data and results from other CFD codes (See Figure 7.8).

7.9.4 Significance

TRANAIR models may be generated with relative ease, and the ability of the code to routinely solve the transonic flow problem about very general geometries represents a major advancement in the field of CFD. Also, several breakthroughs in the solution of finite element problems were developed during the course of this work.

7.9.5 Status/Plans

The current contract expires in November 1989. It is expected that the code in its current form will become a CFD workhorse within both the Aerodynamics Division at Ames and Boeing's applications group. Several areas for possible further development were identified, including the coupling of a boundary layer method with the current code and the solution of the Euler equations using the same unstructured grid format. Both of these developments are considered necessary to the future success of the code.

7.10 RADAR CROSS SECTION CALCULATIONS WITH EMTRANAIR

7.10.1 Objective

To develop the capability to calculate the Radar Cross Section (RCS) of aircraft components and complete configurations for radar frequencies with 5-20 wavelengths across a target.

7.10.2 Approach

Time-Harmonic Maxwell's Equations were solved on a rectangular grid which penetrates the target by what is now called the CG-FFT method, an iterative preconditioned GMRES Conjugate Gradient method and a FFT-based far field preconditioner. In addition, a sparse matrix method also provided a near field preconditioner. The boundary conditions were imposed by local volume finite elements which surround perfect conductors and model dielectric and magnetic materials.

7.10.3 Accomplishments

A three-dimensional demonstration code was developed under contract with the Boeing Company and validated against test measurements provided by Wright-Patterson Research Labs. A full F-16A configuration was modeled at 300 MHz with approximately 20 wavelengths from tip to tail (See Figure 7.9).

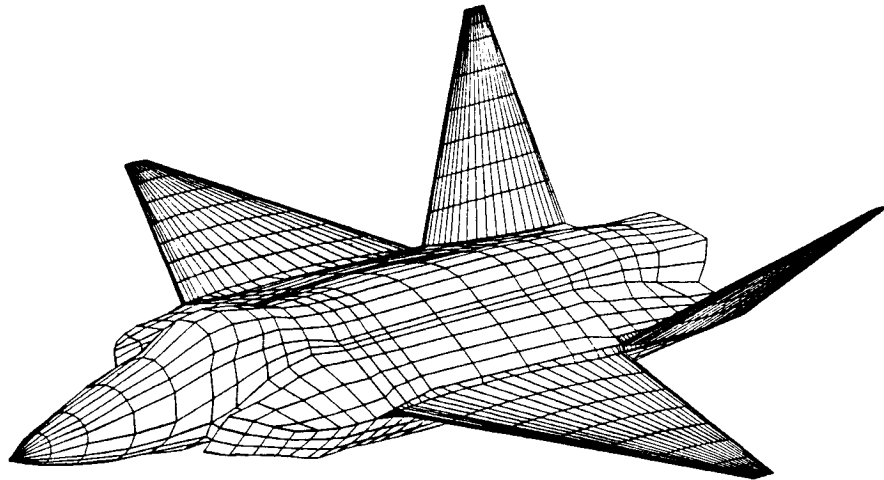
7.10.4 Significance

EMTRANAIR can compute RCS at higher frequencies than current "Method of Moment" codes. It was a leader in applying iterative conjugate gradient solution methods to complex, nonselfadjoint, indefinite problems and in using local finite elements to model curved geometry within a rectangular grid.

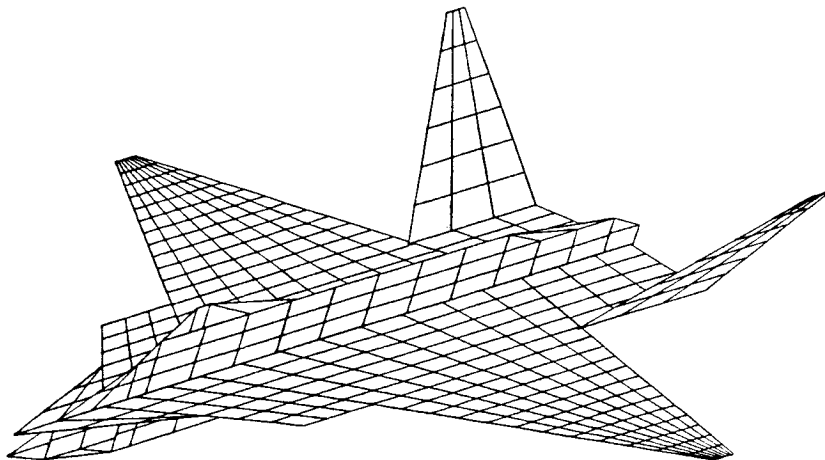
7.10.5 Status/Plans

No follow-on work or contract is planned for EMTRANAIR.

Alex C. Woo
Advanced Aerodynamic Concepts Branch
Ames Research Center
(415)604-6010



PANAIR Geometry — Full Configuration Modeling



LINAIR Geometry — Mean Surface Modeling

Figure 7.10. PANAIR and LINAIR Input Geometries

7.11 STOVL FIGHTER AIRCRAFT CONFIGURATION AERODYNAMICS

7.11.1 Objective

To (1) analyze configuration aerodynamics of the McDonnell Douglas Mixed Flow Vectored Thrust (MFVT), Advanced Short Take Off Vertical Landing (ASTOVL) concept and (2) provide data for flight simulation studies.

7.11.2 Approach

Various aerodynamic prediction codes were run and results were evaluated along with contractor predictions. The codes used were (1) PANAIR, a linear potential panel method; (2) LINAIR, a vortex lattice method and (3) DATCOM, an empirical method. Figure 7.10 shows input geometries for PANAIR and LINAIR.

7.11.3 Accomplishments

A full set of longitudinal and lateral directional power-off aerodynamic estimates (including steady-state rotary derivatives) were generated for the MFVT configuration at approach and transition speeds (Mach 0.2 and 0.4). Figure 7.10 shows comparisons of the directional (C_{ng}) and lateral (C_{lg}) stability derivatives from each of the above methods. The spread among the data provides a range of stability which can be evaluated in the simulator and later checked against wind tunnel data should it become available.

7.11.4 Significance

Such aerodynamic analyses and piloted evaluations are an essential part of the technology development for future supersonic STOVL fighter aircraft.

7.11.5 Status/Plans

Preparations are being made to run the MFVT geometry through the PMARC code (Panel Method Ames Research Center, an update of VSAERO) because this code has provision for modeling time-stepping wakes and is expected to yield better results for the steady-state rotary derivatives.

Donald A. Durston
Advanced Aerodynamic Concepts Branch
Ames Research Center
(415)604-6216

ORIGINAL PAGE
BLACK AND WHITE PHOTOGRAPH

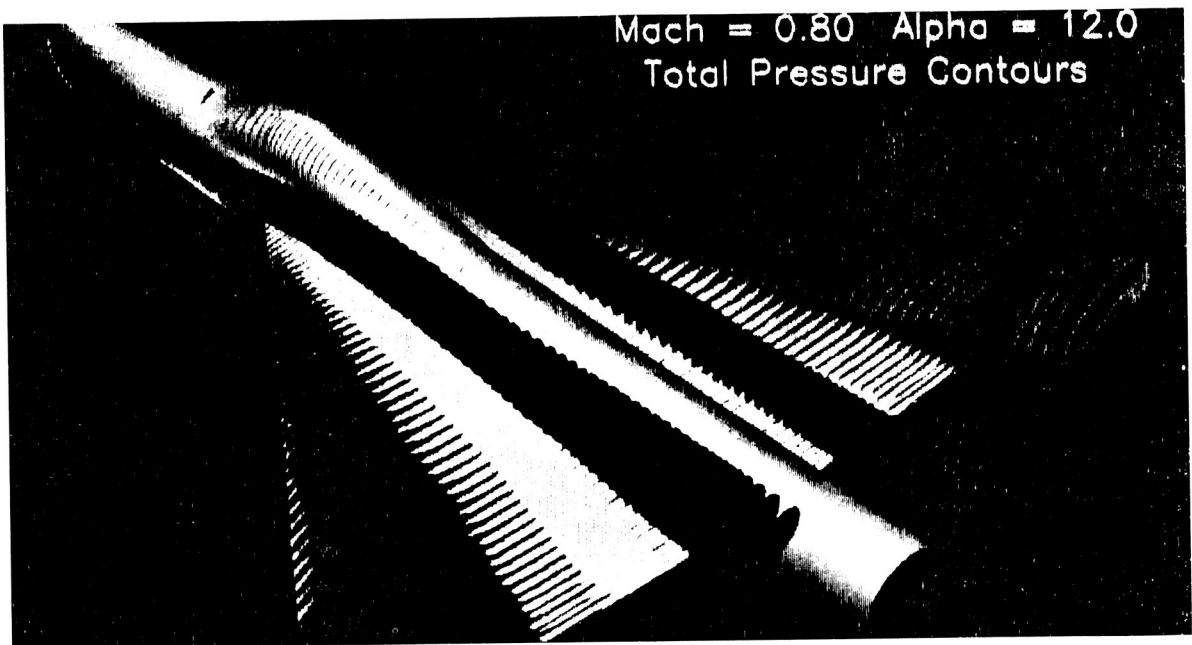


Figure 7.11. Generic Fighter with China

7.12 TRANAIR AND EULER COMPUTATIONS OF A GENERIC FIGHTER

7.12.1 Objective

To evaluate the solutions of transonic flow fields about a generic fighter obtained from both Euler and transonic potential codes in order to determine their validity over a wide range of angles of attack.

7.12.2 Approach

The Euler computations were performed using a modified version of FLO57, originally written by A. Jameson and modified by several users in order to accommodate an O-H grid topology. The TRANAIR full-potential code being developed by Boeing under NASA contract, embeds accurately defined surface panel models of complex configurations in a rectangular array of flow field grid points. Computed surface pressure distributions, forces and moments were compared to experimental data.

7.12.3 Accomplishments

TRANAIR and FLO57 solutions were obtained at Mach 0.60 and 0.80. Two configurations were examined, wing/body and wing/body/chine (See Figure 7.11). Below $\alpha=8$ degrees, both TRANAIR and FLO57 solutions compare well with experimental results. Both codes show poor correlation with experimental results at $\alpha=8$ degrees; however, the Euler results improve at higher angles of attack before vortex breakdown becomes significant over the main wing. The overall comparisons between computational and experimental results improved with the addition of the chine. All Euler solutions were obtained on the Cray-2 with a minimum of 1,200 iterations requiring 10,300 seconds per 1,000 iterations. 3-D solutions were obtained on the Cray X-MP/48 requiring 60-180 iterations and 0.35 to 1.2 CPU hours. A publication and videotape were prepared describing the work.

7.12.4 Significance

The validity of transonic flow solutions about complex configurations is critical to the successful computational analysis of current and future aircraft geometrics. The only method of determining the validity is to compute and analyze numerous solutions over a broad range of conditions and to compare them to experimental results.

7.12.5 Status/Plans

Solutions at Mach 1.2 will be computed and analyzed in order to extend the range of the flow regime to supersonic speeds. Also, Navier-Stokes computations will be started on the wing/body configuration.

$M = 0.80$, $RE = 8,000,000$, $C_L = .55$

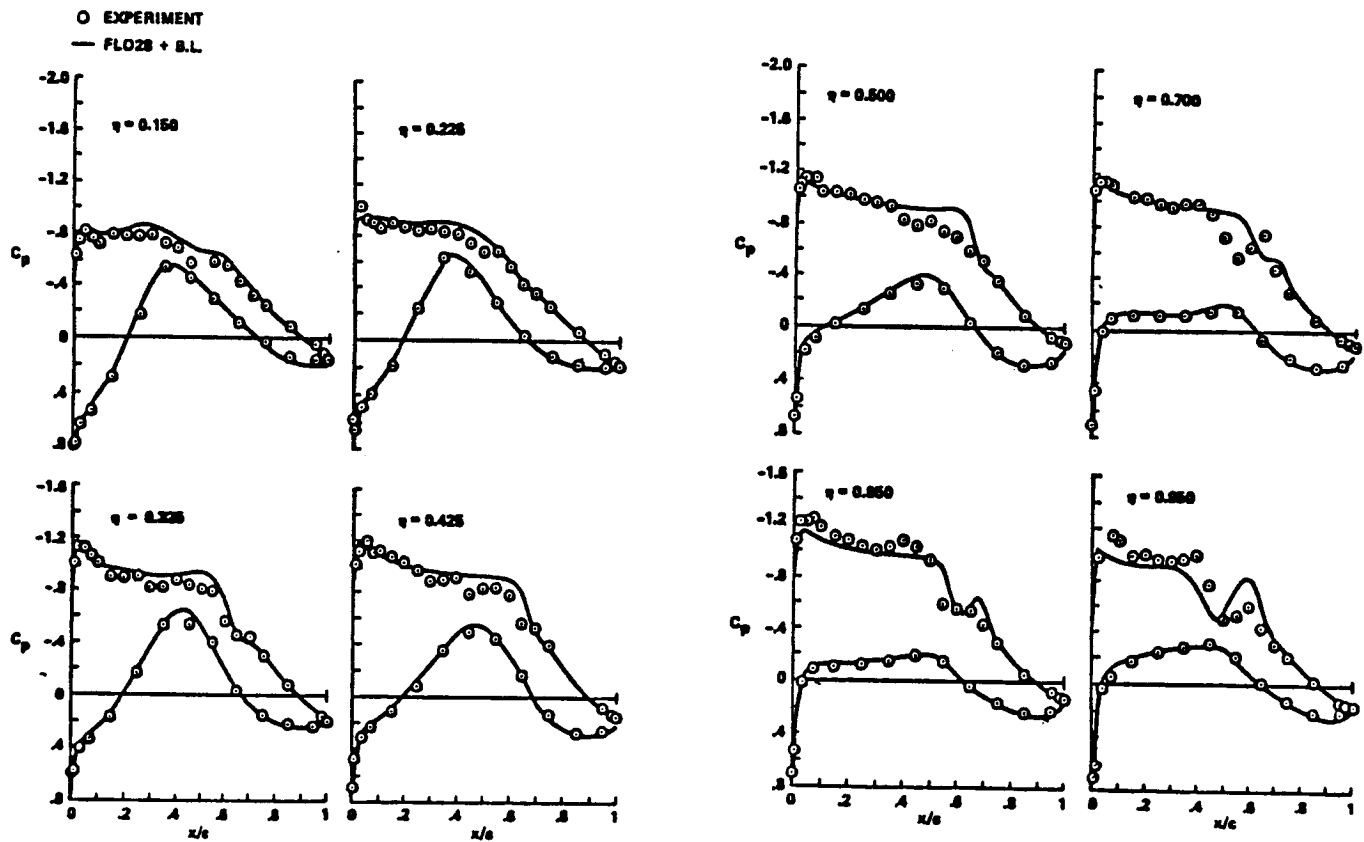


Figure 7.12. Potential Wing/Body Computation with B.L. Correction

7.13 EULER AND POTENTIAL CODE EVALUATION

7.13.1 Objective

To evaluate advanced CFD codes for application to commercial transport wing design and analysis.

7.13.2 Accomplishments

NASA compared CFD codes with wind tunnel data for four closely related commercial transport wings. Wing/body computations with Euler equations gave poor correlation with the experiment for moderate to strong shocks. Isolated-wing potential computations with B.L. correction gave acceptable correlation with the experiment for moderate shocks. Wing/body potential computations with B.L. correction gave acceptable correlation with experiment for moderate shocks (See Figure 7.12).

7.13.3 Significance

CFD code accuracy is configuration-dependent. Extensive experiment-CFD correlations are needed to assess code applicability to aerodynamic design.

7.13.4 Status/Plans

NASA plans to investigate new grid topologies and algorithms for the Euler equations and Navier-Stokes computations for transport wings.

Raymond M. Hicks and Susan E. Cliff-Hovey
Advanced Aerodynamic Concepts Branch
Ames Research Center
(415)604-5656

This page is intentionally left blank.

CHAPTER EIGHT

AEROACOUSTICS

8.1 INTRODUCTION

Aeroacoustics is concerned with the physics of noise produced by the motion of fluids and bodies moving through the atmosphere and the response of people and structures to that noise. The current program focus is on the noise produced by supersonic jet flowfields and its effects both in the nearfield where high levels of acoustic loads may lead to structural failure of aircraft components and in the farfield where community response is a major concern. The approach is to develop theoretical and computational methods for the understanding and control of fundamental noise mechanisms and to investigate jet flow and jet/surface interactions with scale model experiments. Recent accomplishments include application of CFD techniques for the prediction of shock/vortex interaction noise, an analytical exploratory study of noise reduction through the use of active flow control, fundamental aeroacoustic studies of non-axisymmetric jet nozzles and determination of aeroacoustic loads on wind tunnel models of the B-1B, F-15 and ASTOVL concepts. Emphasis in aeroacoustics research is not limited to improving facility capability and computational techniques; it also includes effecting technology transfer to full scale operation.

Program Manager: Mr. Stephen Wander
OAST/RF
Washington, DC 20546
(202)453-2820

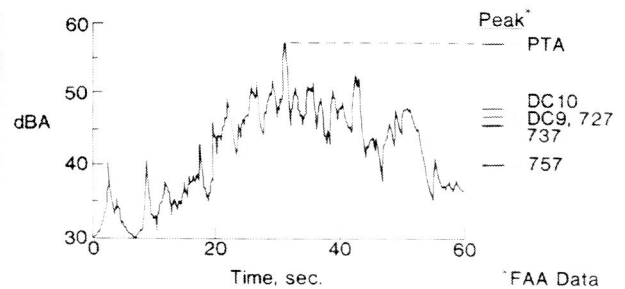
ORIGINAL PAGE
BLACK AND WHITE PHOTOGRAPH

CRUISE CONDITIONS: 33-39KFT ALT, 0.7-0.8 MACH NO.

NASA PTA AIRCRAFT



FLYOVER NOISE



- PTA AIRCRAFT GROUND LEVEL HIGHER THAN JET TRANSPORT
- PROPAGATION VARIABILITY NOT WELL UNDERSTOOD

Figure 8.1. Enroute Aircraft Noise

8.2 ENROUTE AIRCRAFT NOISE

8.2.1 Objective

Development of advanced turboprops has led to concerns of enroute noise. Advanced turboprops generate low-frequency, periodic noise signatures which when operating at cruise altitudes, can be audible from the ground. The assessment of the enroute noise issue is difficult because of the variability of the received noise levels due to atmospheric propagation and the uncertainty in predicting community response to the relatively low noise levels, compared to airport operations.

8.2.2 Approach

In conjunction with the FAA, a flight test was conducted in Alabama to evaluate the noise levels received on the ground of an advanced turboprop operating at cruise conditions. The test aircraft, shown in Figure 8.1, was Langley's PTA aircraft which has an advanced turboprop mounted on its left wing. Shown in the figure is a typical, single microphone, A-weighted, PTA sound pressure level time history from Mach 0.7, 33,000 feet, level flyby. Included in the figure are typical, peak A-weighted sound pressure levels for today's commercial airline turbofan fleet.

8.2.3 Accomplishments

Noise levels from advanced turboprops operating at cruise conditions will exceed those of turbofans and will be clearly audible on the ground. The large variability in the PTA noise level time history is due to propagation. This propagation induced variability is not well understood and is not predictable.

8.2.4 Significance

In response to the enroute noise issue, NASA and the FAA developed an Aircraft Enroute Noise Technology Program which will help to focus and leverage the enroute noise research efforts of NASA and the FAA.

8.2.5 Status/Plans

A three year memorandum of understanding between NASA and the FAA was negotiated. Basic acoustic propagation and subjective response studies are planned. A propagation test was recently conducted using the PTA aimed at investigating the propagation induced variability.

William L. Willshire, Jr.
Applied Acoustics Branch
Langley Research Center
(804)864-5270

ORIGINAL PAGE
BLACK AND WHITE PHOTOGRAPH

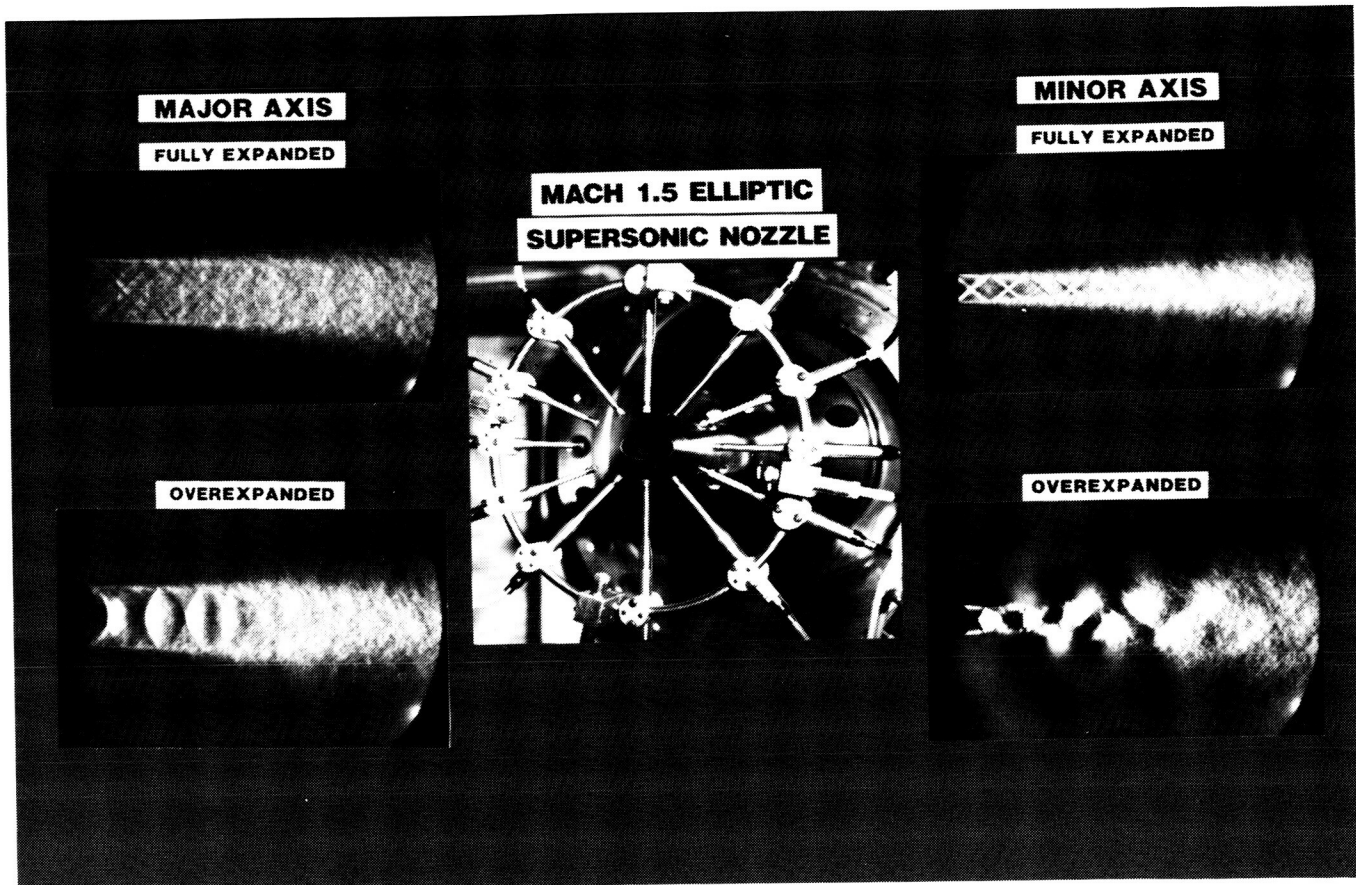


Figure 8.2. Non-Axisymmetric Supersonic Jet Flowfield

8.3 NON-AXISYMMETRIC SUPERSONIC JET FLOWFIELD

8.3.1 Objective

To (1) analyze jet exit geometries that enhance rapid mixing of the exhaust plume with the surrounding medium (resulting in noise reduction) and (2) provide an accurate database for predicting the three-dimensional flow field associated with non-axisymmetric nozzle exit geometries.

8.3.2 Approach

The exit plane internal boundary layer of round nozzles is uniform, whereas for elliptic and rectangular nozzles it is non-uniform. Previous research with subsonic elliptic nozzles show that this non-uniformity leads to enhanced growth along the minor axis, i.e., rapid mixing with the surrounding medium. A supersonic elliptic nozzle was designed at an exit Mach number of 1.5 with an aspect ratio of two, i.e., ratio of major to minor diameters, in order to study the mixing process for supersonic flows.

8.3.3 Accomplishments

Phase averaged schlieren optical records, mean flow velocity profiles and near field microphone array measurements were acquired. Figure 8.2 shows schlieren records indicating that operation at the nozzle design point (fully expanded) produces shock free flow. In contrast, the schlieren records for off-design operation (over-expanded) indicate strong shocks. No rapid mixing is observed for the fully expanded case; however, the minor axis, overexpanded photo suggests a more sudden mixing does occur.

8.3.4 Significance

Understanding the fluid mechanics of rapid mixing nozzles of different geometry is essential to the design of low noise supersonic nozzles.

8.3.5 Status/Plans

Future work will focus on high temperature, rectangular supersonic nozzles with application to low noise designs for high speed civil transports.

John M. Seiner
Aeroacoustics Branch
Langley Research Center
(804)864-6276

ORIGINAL PAGE
BLACK AND WHITE PHOTOGRAPH

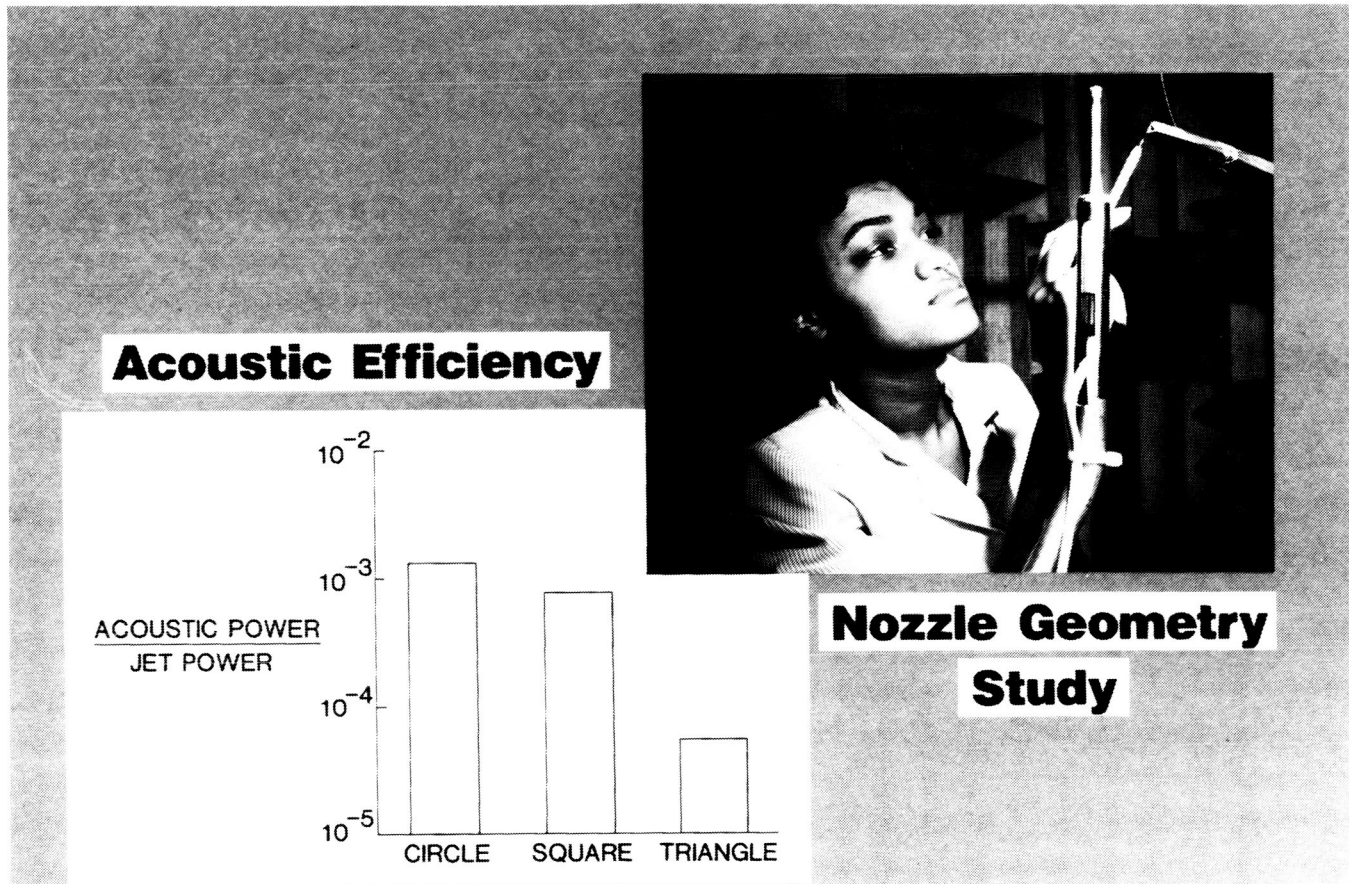


Figure 8.3. Supersonic Jet Noise Research

8.4 SUPERSONIC JET NOISE RESEARCH

8.4.1 Objective

To investigate the acoustic performance of square, equilateral triangle and circular nozzles at constant ideal thrust. For many years, intense research was done on suppressing noise from axisymmetric nozzles. Very little research was conducted to investigate the acoustic behavior of non-circular nozzles.

8.4.2 Approach

The experiment was performed in a small, anechoic chamber at the Langley Research Center. High pressure unheated air was pumped through the nozzles to create a low supersonic flowfield. A traverse moved a .25-inch Bruel and Kjaer microphone throughout the chamber. Sound power was obtained by integrating the microphone output. Ideal thrust was kept constant in order to make direct comparisons among the nozzles (See Figure 8.3).

8.4.3 Accomplishments

The results for the three nozzles are presented in terms of an acoustic efficiency. Acoustic efficiency is a ratio of acoustic power to jet power. A nozzle with a high sound output for a given thrust will have a high acoustic efficiency. The results show that at constant ideal thrust the equilateral triangle nozzle exhibits a lower acoustic efficiency than the square or circular nozzle.

8.4.4 Significance

The results from this basic research show that nozzle geometry has a measurable and significant effect on supersonic jet noise. Supersonic jet noise reduction can be achieved through simple nozzle geometry change with no apparent thrust penalty.

8.4.5 Status/Plans

More tests will be performed using additional nozzle shapes and larger nozzles to further develop scaling relationships.

Martha C. Brown
Aeroacoustics Branch
Langley Research Center
(804)864-6277

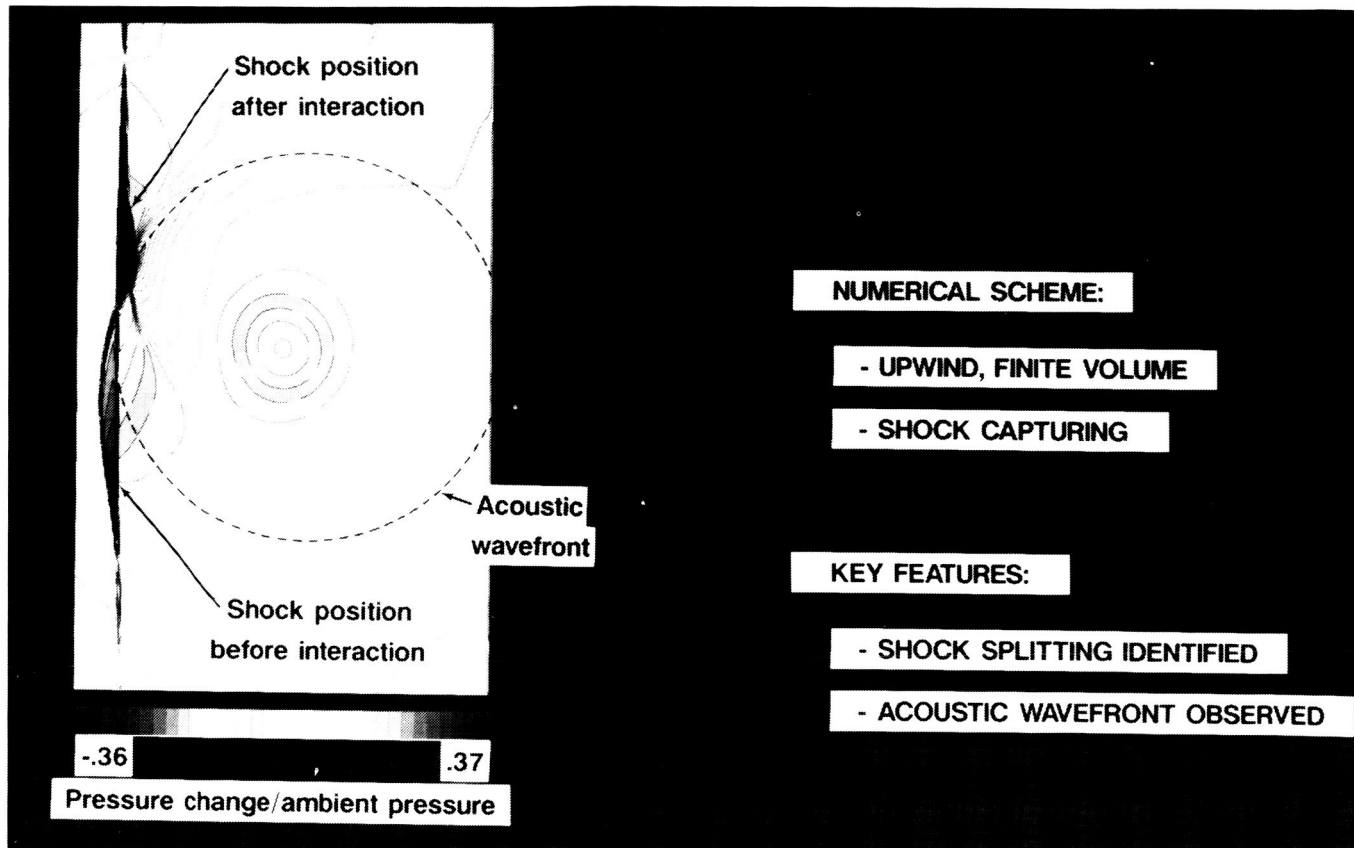


Figure 8.4. Numerical Prediction of Shock/Vortex Interaction Noise

8.5 NUMERICAL PREDICTION OF SHOCK/VORTEX INTERACTION NOISE

8.5.1 Objective

To develop a numerical method for predicting sound generated in supersonic flows. This investigation was part of an overall program to develop computational aeroacoustics methodology for the understanding and prediction of aeroacoustic phenomena of interest to aeronautical applications.

8.5.2 Approach

The passage of turbulence through shock waves is known to generate shock associated noise, one of several mechanisms for supersonic jet noise. This particular mechanism was modeled by the passage of a vortex through a normal shock. A vortex which models turbulence was superimposed on a Mach 1.1 flow upstream of a stable normal shock and allowed to convect with the flow through the shock. The Euler equations in conservative form were solved on a grid of 132 points in the axial direction and 122 points in the normal direction with a second order accurate upwind finite volume technique. In this numerical method, the shock is captured rather than fitted so that situations where shock vortex interaction may cause secondary shocks also can be investigated.

8.5.3 Accomplishments

The results show the change in pressure downstream of the shock after interaction with a strong vortex (See Figure 8.4). The heavy lines represent the location of the shocks before and after the interaction. The deflection and splitting of the shock are seen in this figure as well as the formation of two distinct pressure regions at the points of maximum shock excursion. The pressure region indicated by the solid lines represents an increase in pressure from the pre-interaction state; the region indicated by dashed lines represents a decrease in pressure. Analysis of the observed wavefront shows that it travels at the local speed of sound in the fluid and is, therefore, a sound wave. The acoustic wavefront is shown for illustrative purposes by a dotted circular arc passing through the compression and expansion regions.

8.5.4 Significance

The method shows promise of predicting shock/vortex interaction noise even in cases of severe shock deflection where classical linear acoustic theory is not applicable.

8.5.5 Status/Plans

Enhancements to the current computer code will be investigated to provide a quantitative prediction of the acoustic wavefront.

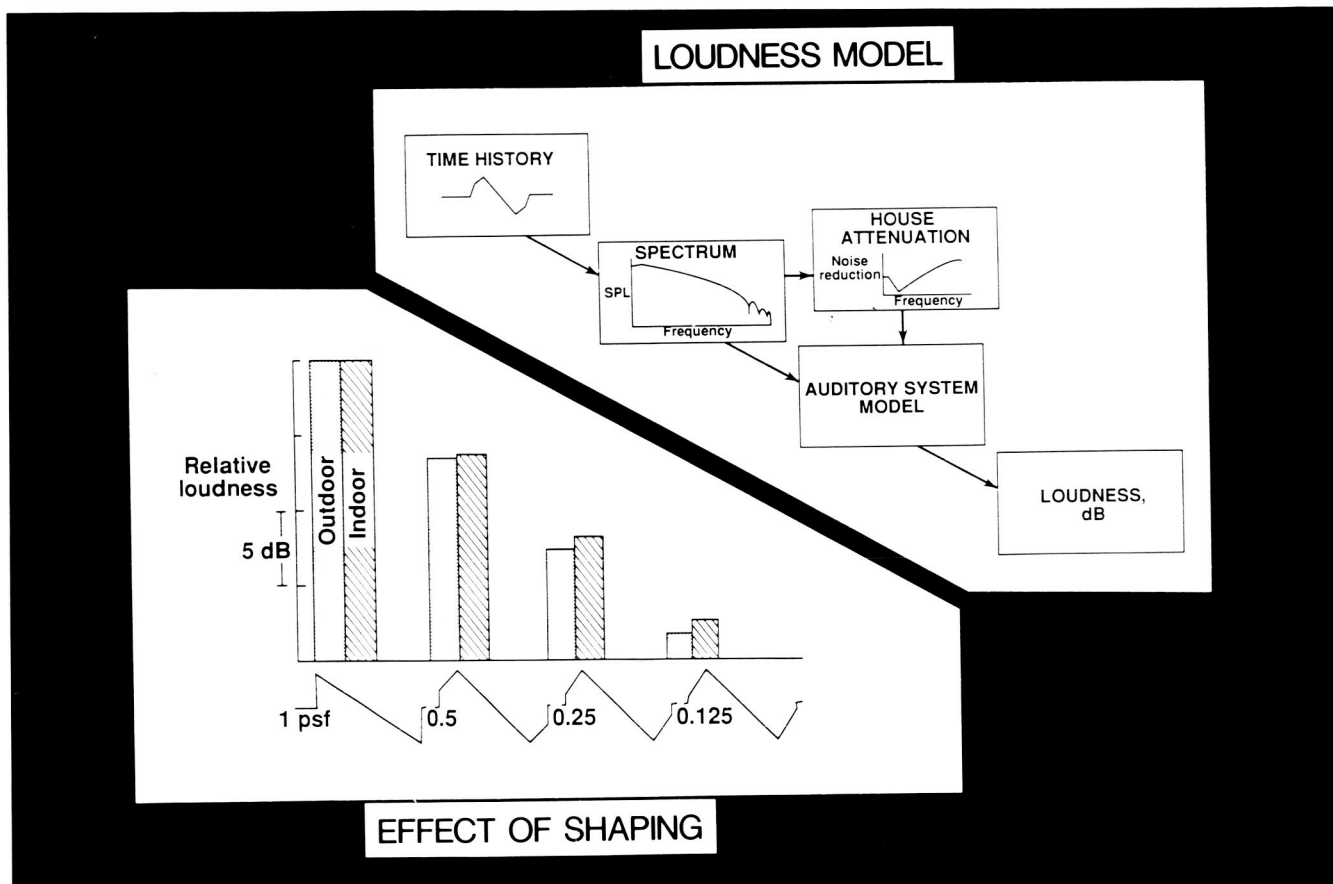


Figure 8.5. Assessment of Shaped Sonic Booms

8.6 ASSESSMENT OF SHAPED SONIC BOOMS

8.6.1 Objective

To (1) develop a model to assess human response to sonic booms and (2) quantify the potential benefits of sonic boom shaping.

8.6.2 Approach

Based on known characteristics of the human auditory system, a loudness model was formulated to assess human response to impulsive sounds such as sonic booms. The pressure-time signature of the boom was transformed to the frequency domain and adjustments were made to reflect the characteristics of the auditory system, thus yielding a value of loudness. People exposed to sonic booms from a supersonic transport would be located both indoors and outdoors and, therefore, it was necessary that an assessment of the benefits of sonic boom shaping include the sound transmission characteristics of typical buildings.

8.6.3 Accomplishments

Figure 8.5 shows loudness values calculated for a range of sonic booms heard indoors and outdoors. The first column in the figure contains data for a conventional N-wave, which is characterized by a rapid rise in pressure to the peak, followed by a relatively slow decrease in pressure and an abrupt return to ambient pressure. The other columns in the figure contain data for a range of shaped booms, which are characterized by a rapid rise to the initial shock amplitude and a more gradual rise to the peak pressure. For the shaped booms, the initial shock amplitudes range from 0.125 to 0.5 psf. For illustrative purposes, the rise time of the initial shock and the peak pressure were held constant for all boom signatures. The calculated values of loudness for the shaped booms are shown relative to the loudness of an N-wave heard under the same conditions, indoors or outdoors. The results indicate that substantial reductions in loudness can be achieved through shaping, even for signatures having the same peak pressure. Furthermore, these reductions are found to be of similar magnitude for observers located either indoors or outdoors.

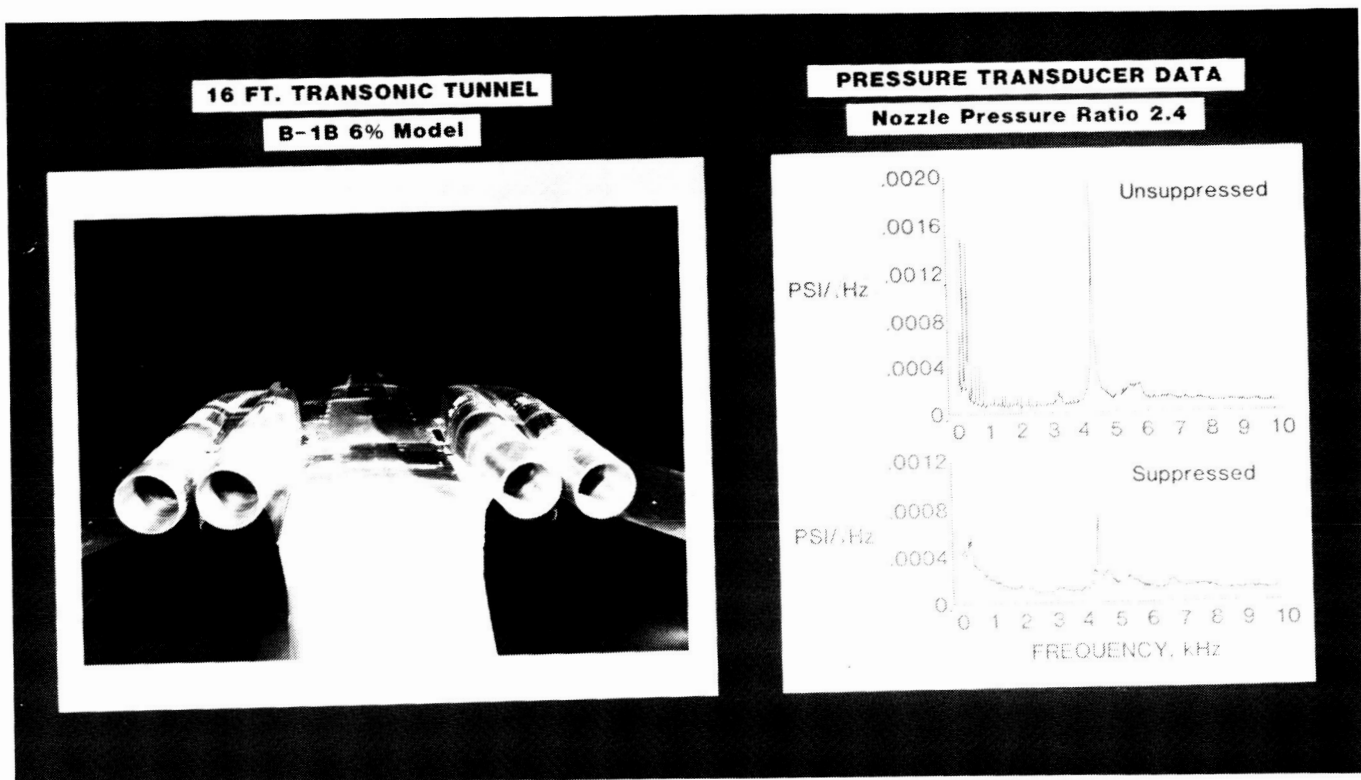
8.6.4 Significance

The shaping of sonic booms offers the potential of substantial reductions in loudness and hence in community impact; thus, overland supersonic flight may be possible.

8.6.5 Status/Plans

Laboratory studies using a sonic boom simulator will be performed in order to validate these loudness predictions.

Kevin P. Shepherd
Structural Acoustics Branch
Langley Research Center
(804)864-3583



ORIGINAL PAGE
BLACK AND WHITE PHOTOGRAPH

Figure 8.6. B1-B Twin Engine Noise Reduction

8.7 B1-B TWIN ENGINE NOISE REDUCTION

8.7.1 Objective

To (1) determine the importance of twin jet resonance relative to failure of engine nozzle outer flaps on the G. E. F101 engines installed on B1-B aircraft and (2) examine the effectiveness of suppression devices for reducing dynamic flap loads.

8.7.2 Approach

Previous research involving twin supersonic jet plumes showed that coupling of turbulent large scale structures between each jet plume leads to significant amplification of inter-nozzle dynamic pressures. To determine the relative importance of this mechanism on flap loads, a six percent full span model of the B1-B aircraft (See Figure 8.6) was instrumented with dynamic pressure transducers on nozzle exterior surfaces and tested in the Langley 16-foot Transonic Wind Tunnel. The model was tested over an extensive nozzle pressure ratio and flight Mach number range, including supersonic. A small tube jet ($d/D=0.035$, where d is the tube diameter and D is the jet diameter) was installed at the nozzle exit.

8.7.3 Accomplishments

Dynamic flap loads were found to be dominated by the twin jet resonance mechanism from static conditions up to Mach 0.5. The tube jet suppressor was found to be effective in reducing twin jet coupling and dynamic loads associated with this mechanism. Above a flight Mach number of 0.5, turbulent separation from the upstream wing/body produces dominant flap loads.

8.7.4 Significance

The origin of dynamic pressure loads on the external engine nozzle flaps of B1-B aircraft were identified for complete mission profile. An effective method for reducing twin jet resonance was identified.

8.7.5 Status/Plans

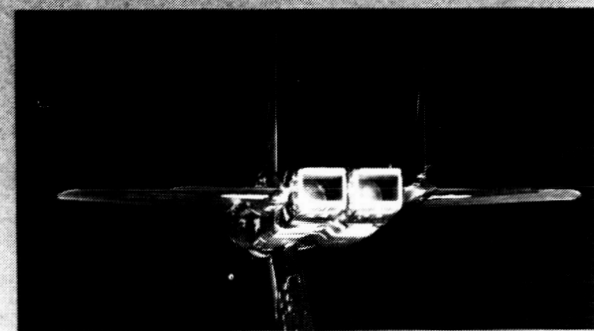
Flight tests currently are being conducted to verify model scale results.

John M. Seiner
Aeroacoustics Branch
Langley Research Center
(804)864-6276

ORIGINAL PAGE
BLACK AND WHITE PHOTOGRAPH



Flight Test



8% Model in Wind Tunnel

Figure 8.7. Aeroacoustic Loads of Advanced Configurations

8.8 AEROACOUSTIC LOADS OF ADVANCED CONFIGURATIONS

8.8.1 Objective

To determine the origin and magnitude of dynamic loads associated with the use of twin rectangular nozzle ducts associated with F-15 STOL demonstrator.

8.8.2 Approach

Previous model research showed that twin plume resonance associated with supersonic rectangular exhaust nozzles is significantly higher in amplitude (dynamic pressure fluctuations) than the resonance associated with axisymmetric nozzles. To study this mechanism, for the F-15 STOL demonstrator, an 8.33 percent full span model of the F-15 was instrumented with dynamic pressure transducers on the forebody, vertical tails and exhaust nozzles. Both axisymmetric and rectangular exhaust geometries were studied over an extensive range of operating conditions (See Figure 8.7).

8.8.3 Accomplishments

A high quality data set was obtained for this model that will enable determination of the origin for engine nozzle flap loads.

8.8.4 Significance

The test will directly aid McAir's assessment of aeroacoustic loads associated with F-15 STOL flight demo tests.

8.8.5 Status/Plans

NASA will make a complete analysis of the wind tunnel database. NASA also will make recommendations for flight test program.

John M. Seiner
Aeroacoustics Branch
Langley Research Center
(804)864-6276

ORIGINAL PAGE
BLACK AND WHITE PHOTOGRAPH

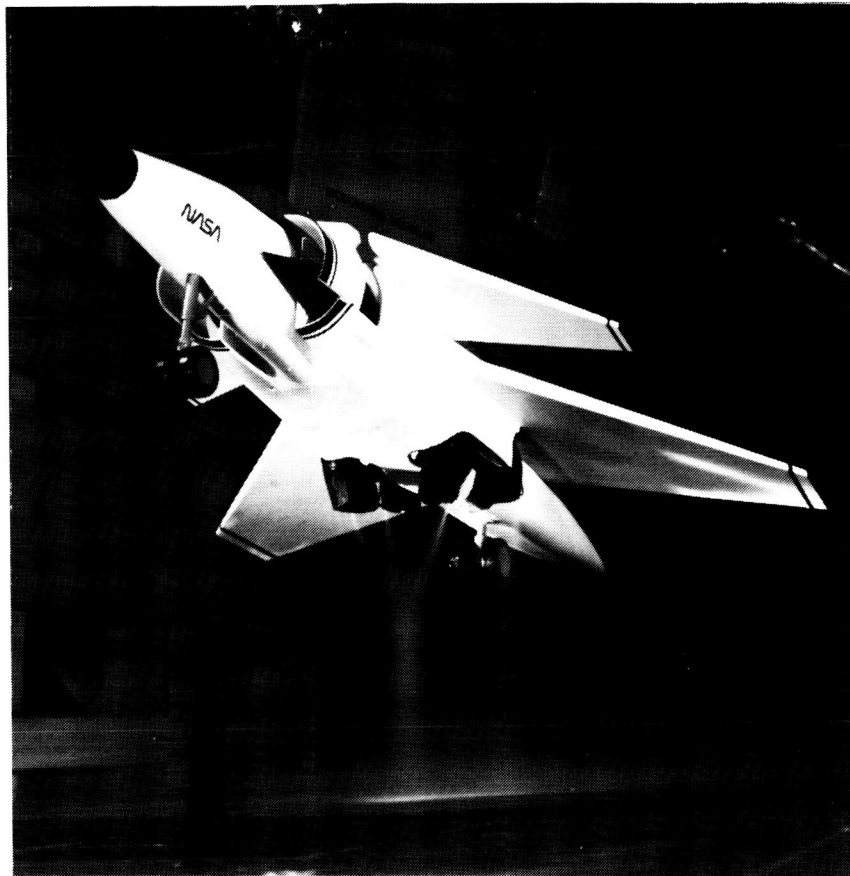


Figure 8.8. Advanced STOVL Model in LeRC's 9-Foot by 15-Foot Low Speed Wind Tunnel

8.9 ADVANCED STOVL ACOUSTIC LOADS IN LEWIS RC's 9-FOOT BY 15-FOOT LOW SPEED WIND TUNNEL

8.9.1 Objective

Fluctuating pressure loads caused by jet impingement noise and deflected exhaust flowfields may lead to excessive fatigue loads on the structure of advanced short takeoff and vertical landing (ASTOVL) aircraft. The current series of tests were designed to quantify these loads on an ASTOVL model in hover over a wide range of operating conditions.

8.9.2 Approach

A McAir ASTOVL Hot Gas Ingestion (HGI) model was tested in Lewis' 9-foot by 15-foot Low Speed Wind Tunnel (See Figure 8.8). The model was instrumented with a series of dynamic pressure transducers on the underside of both the fuselage and wing. Fluctuating pressures were measured for a range of nozzle pressure ratios, heights above ground plane, wind tunnel speeds and exhaust temperatures to 500 degrees Fahrenheit.

8.9.3 Accomplishments

Large changes in the measured dynamic loads were obtained as either the nozzle pressure ratio or aircraft-to-ground distance was changed, with smaller effects due to changes in jet temperature and wind tunnel speed. Fluctuating pressure levels of 180 dB (almost three psi) were measured when the deflected exhaust jet fountain impinged on the fuselage.

8.9.4 Significance

The higher nozzle pressure ratios utilized by an ASTOVL aircraft over its lower speed counterpart, i.e., Harrier, lead to higher levels of fluctuating pressure on the aircraft. The higher loading may require stronger and heavier material (and hence, a weight penalty) in the design of the aircraft structure.

8.9.5 Status/Plans

The Phase II HGI testing of the ASTOVL model is scheduled for late 1989. Better height adjustment and jet temperatures to 1,000°F will be obtained. Water cooled dynamic pressure transducers are being designed to enable measurement of fluctuating loads at these higher temperatures.

Thomas D. Norum
Aeroacoustics Branch
Langley Research Center
(804)864-3620

ORIGINAL PAGE
BLACK AND WHITE PHOTOGRAPH

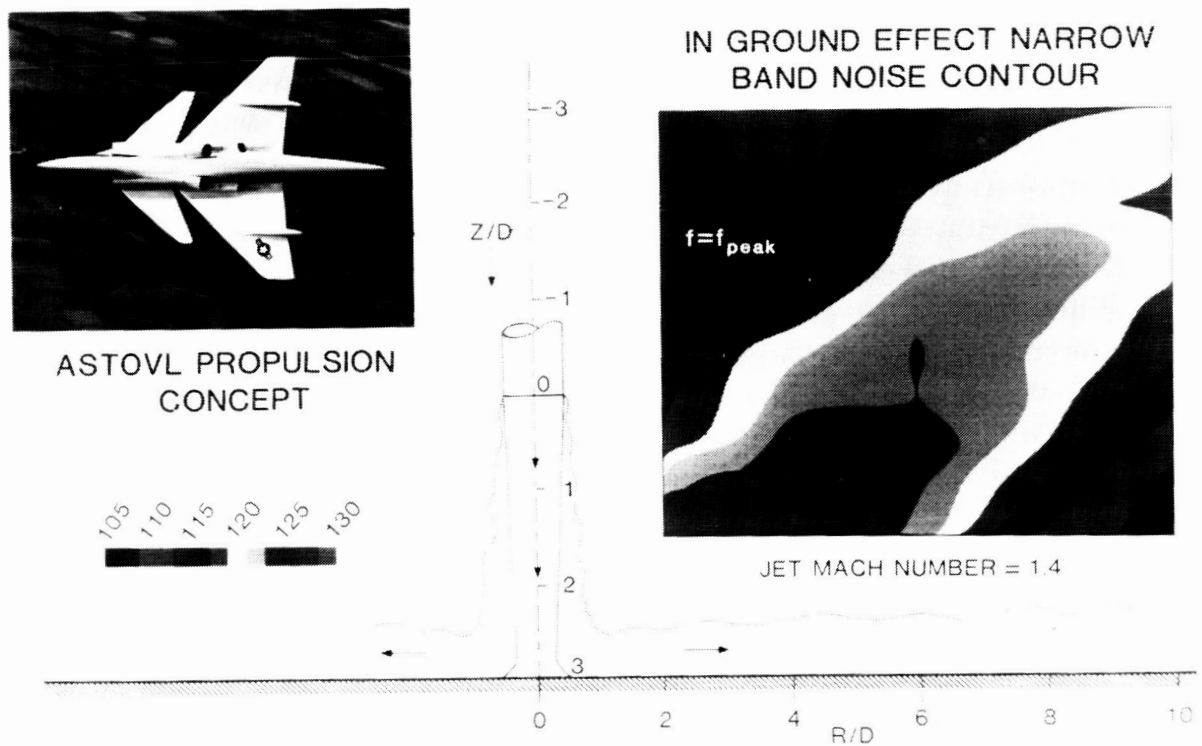


Figure 8.9. ASTOVL Sonic Fatigue Loads

8.10 ASTOVL SONIC FATIGUE LOADS

8.10.1 Objective

To characterize the thermal/acoustic fatigue loads produced by supersonic jet plumes of typical, Advanced, Short Take-Off and Vertical Landing (ASTOVL) aircraft.

8.10.2 Approach

The conceptual ASTOVL aircraft showed that the lift and propulsive nozzles may cluster near the center of gravity of the aircraft (See Figure 8.9). At takeoff and landing, jet impingement on the ground surface altered the turbulent mixing and the feedback processes resulting in a unique nearfield acoustic environment. A large portion of the airframe was exposed to high intensity thermal/acoustic fatigue loads. Existing data of thermal/acoustic loads for supersonic jets in these conditions were insufficient for airframe design purposes. The approach taken here was to conduct accurate measurements of nearfield fatigue loads using model scale nozzle configurations in order to establish scaling laws for loads prediction.

8.10.3 Accomplishments

Figure 8.9 shows an example to illustrate key features of the nearfield sonic fatigue environment during vertical landing. A single 0.4-inch circular jet operated at Mach 1.4 is placed at three jet diameters above the ground. Detailed acoustic spectra obtained in the nearfield indicate the existence of dominant mixing noise. A contour plot of the narrow band acoustic intensity near the peak frequency of mixing noise is shown in this figure. The distribution of acoustic loads indicates high intensity and shows that a significant portion of the outboard wing structure can be exposed to fatigue loads.

8.10.4 Significance

Experimental data obtained in the current research program indicate that acoustic loads can increase by as much as 20 dB with ground impingement resulting in levels that can cause structural fatigue.

8.10.5 Status/Plans

Plans for further research include the measurement of thermal/acoustic fatigue loads for selected ASTOVL aircraft configurations, such as the McAir Hot Gas Ingestion Model and the validation of scaling laws for design applications.

John S. Preisser
Aeroacoustics Branch
Langley Research Center
(804)864-3618

ORIGINAL PAGE
BLACK AND WHITE PHOTOGRAPH



Figure 8.10. Fluctuating Pressure Loads in Hypersonic Boundary Layers

8.11 FLUCTUATING PRESSURE LOADS IN HYPERSONIC BOUNDARY LAYERS

8.11.1 Objective

To develop methods for measuring high-frequency pressure fluctuations in supersonic and hypersonic boundary layers.

8.11.2 Approach

A 107-inch by 51-inch test model was fabricated from a high-temperature alloy and installed in the Langley eight-foot High Temperature Tunnel (See Figure 8.10). Fluctuating pressures were measured with ten flush-mounted sensors (.093-inch in diameter). Water cooling was used to protect the sensors from aerodynamic heating at the Mach 5 flow speed during a four second test run.

Dynamic calibrations of the sensor array over the entire operating frequency range were conducted with a specially-designed waveguide calibrator. This calibration procedure provided a means to detect and correct for any spurious installation effects or sensor resonances. Time history data were digitized at a sampling rate of 125 kHz and stored on hard disk to permit analysis up to 62.5 kHz.

8.11.3 Accomplishments

Fluctuating pressures were successfully measured in a fully-developed turbulent boundary layer on the flat plate test model immersed at a 13 degree angle of attack in a high temperature, Mach 5 flow. Tests were conducted for two different Reynolds numbers of 18 and 24 million. Generally, the power spectra exhibited exponential rolloff with increasing frequency out to 38 kHz. Beyond about 38 kHz, no significant contribution to the total power was evident. The total RMS pressures were found to be 0.46 percent and 0.17 percent of the dynamic pressure at the boundary layer edge for the low and high Reynolds number runs, respectively. Total RMS pressures were found to exhibit little dependence on the Reynolds number for the stated test conditions.

8.11.4 Significance

The results presented here demonstrate the ability to measure high-frequency loads in a high-temperature, high-speed flow environment. Particular elements of concern were sensor installation, data acquisition and calibration. This measurement capability is essential in defining fluctuating pressure loads on high-speed vehicles.

8.11.5 Status/Plans

Fluctuating pressures and shock loads will be measured in scramjet engines in the Langley Scramjet Engine Test Facility. Further calibration procedures will be developed for these measurements.

ORIGINAL PAGE
BLACK AND WHITE PHOTOGRAPH

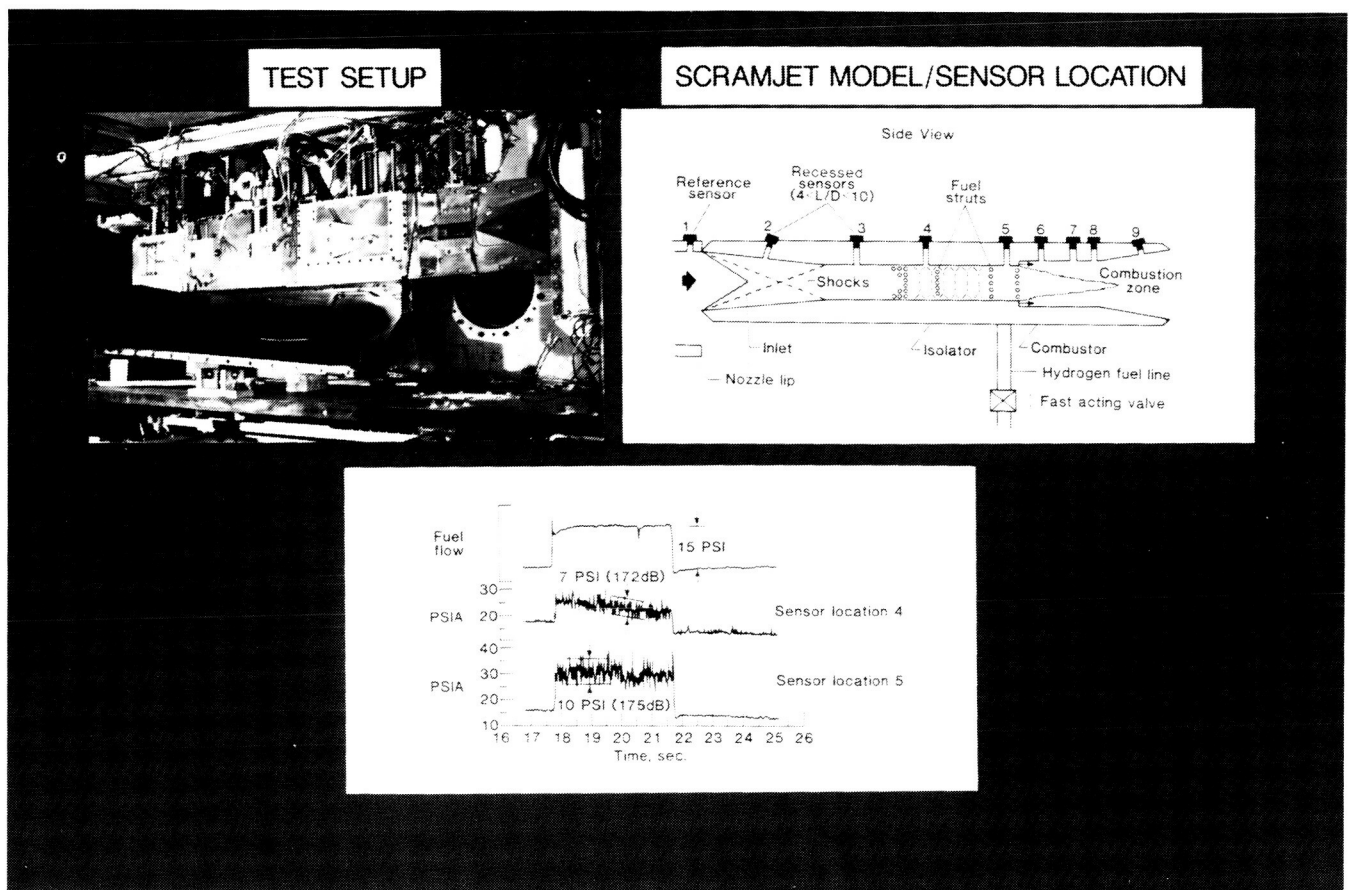


Figure 8.11. Fluctuating Pressure Loads in a Scramjet Engine Model

8.12 FLUCTUATING PRESSURE LOADS IN A SCRAMJET ENGINE MODEL

8.12.1 Objective

To develop measurement technology for fluctuating pressure loads in the high-speed, hostile environments of scramjet engines. Fluctuating pressure measurements in the boundary layers of scramjet engines are of interest from the standpoints of combustion instability onset and structural design of engine components. The fluctuating loads are generated by combustion processes, boundary layer turbulence and shock/boundary layer interactions.

8.12.2 Approach

A scramjet engine model designed by the Johns Hopkins Applied Physics Laboratories was installed in the Combustion Heated Scramjet Test Facility at Langley (See Figure 8.11). Pressure transducers were installed at eight locations on the top wall of the scramjet model, including the inlet and combustor sections. During the 25-second test run, step changes in heat release rate were induced by a fast acting valve in the hydrogen fuel supply line.

8.12.3 Accomplishments

At the bottom of the figure, time histories for sensor locations four and five, upstream of the combustor, show the dramatic effect of these changes in heat release rate on the fluctuating pressures in the boundary layer. Peak-to-peak pressures range from seven psi (sensor four) to ten psi (sensor five) at the high heat release rate as compared to less than two psi peak-to-peak for the low heat release rate. Assuming a Gaussian type probability density distribution for these pressures, the corresponding sound pressure levels at the high heat release rates would be 172 dB and 175 dB, respectively. These levels are at least 11 to 14 dB above corresponding levels at the low heat release rates.

8.12.4 Significance

Changes in levels of fluctuating boundary layer pressures upstream of the combustor have been correlated with changes in heat release in a scramjet engine model. A knowledge of the characteristics and propagation of boundary layer pressure fluctuations is crucial to the design of scramjet engine components.

8.12.5 Status/Plans

Further measurements are underway to refine the interpretation of fluctuating pressures and transient disturbances (shocks) measured with recessed pressure sensors.

Tony L. Parrott
Applied Acoustics Branch
Langley Research Center
(804)864-5273

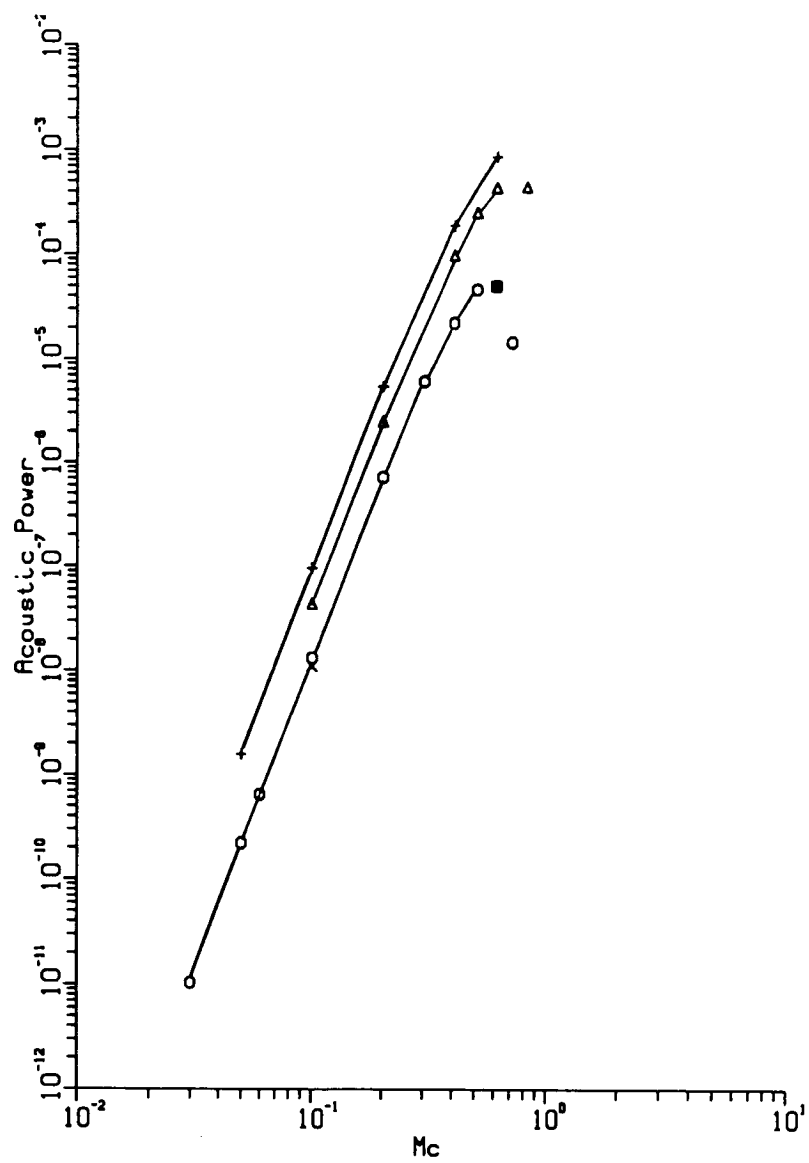


Figure 8.12. Acoustic Power Versus Mach Number

This page is intentionally left blank.

CHAPTER NINE

AEROTHERMODYNAMICS

9.1 INTRODUCTION

Future aerospace vehicles, such as Aeroassist Space Transfer Vehicles (ASTV), the aerospace plane and hypersonic cruise and maneuver vehicles, must be capable of sustained hypersonic, hypervelocity flight in both rarefied and continuum flow flight regimes. The design of these vehicles presents some formidable performance prediction challenges. To meet these challenges, the aerothermodynamics program is pursuing the following objectives: (1) development and application of advanced computational methods and numerical techniques covering the entire spectrum of continuum, transitional and rarefied flows; (2) development of accurate and detailed real-gas chemistry and high speed turbulent flow models and the efficient integration of these models with standard computational flow codes; (3) establishment of a high quality ground and flight experimental database for code validation/verification; (4) direct correlation and comparison of numerical computations with available ground and flight data; (5) establishment of a detailed aerothermal loads database and development of a fully integrated analysis technique and (6) enhancement of engineering design codes and advanced configuration analysis capability to support future vehicle/mission requirements.

Program Manager: Mr. Stephen Wander
OAST/RF
Washington, DC 20546
(202)453-2820

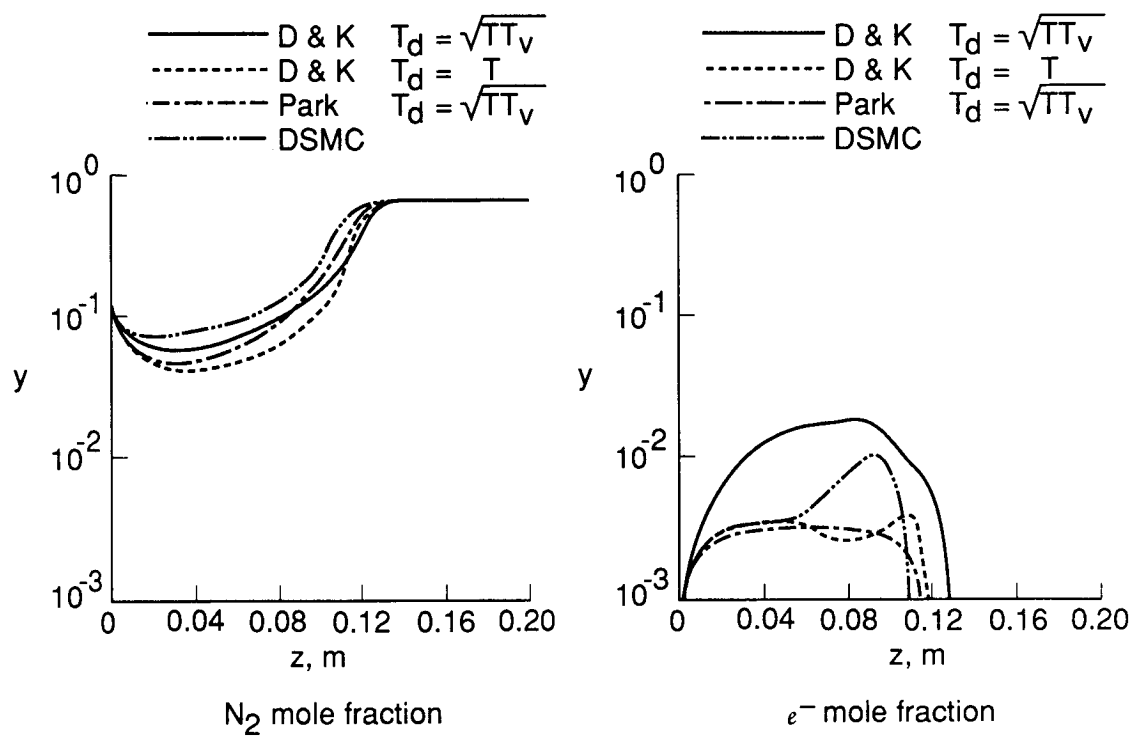


Figure 9.1. Program LAURA Chemical Kinetic Models

9.2 ADVANCES IN COMPUTATIONAL CAPABILITY: PROGRAM LAURA

9.2.1 Objective

One of the challenges of hypersonic flowfield simulation is the proper modeling of nonequilibrium processes within a Computational Fluid Dynamics (CFD) code. A second challenge of hypersonic flowfield simulation, which is shared by simulations over all speed ranges, is the development of an algorithm which can effectively utilize supercomputer resources to decrease the computational time required for a solution. The objective was the development and application of a computational fluid dynamic code, the Langley Aerothermodynamic Upwind Relaxation Algorithm (LAURA), to address these challenges. The detailed development of LAURA focused on the design needs of the Aeroassist Flight Experiment (AFE), a project designed to obtain the aerobraking flight data required for code validation.

9.2.2 Approach

An upwind-biased, point-implicit relaxation algorithm for obtaining the numerical solution to the governing equations for three-dimensional, viscous, hypersonic flows in thermochemical nonequilibrium was implemented. Multiple domains were used to define the complete Flowfield. Further details of the algorithm were documented in AIAA 89-1972-CP. The chemical kinetic model included 11 species and used either the 26-reaction-pair model of Dunn and Kang or the 21-reaction-pair model of Park. Thermal nonequilibrium was modeled using a two-temperature approximation. The total model, in its most general form, involved the simultaneous solution of 16 partial differential equations. Further details of the thermochemical nonequilibrium gas model are documented in NASA TP 2867.

9.2.3 Accomplishments

Program LAURA is now an operational research code. It was implemented on a CRAY 2 but can also effectively utilize both synchronous parallel and asynchronous parallel supercomputer architectures. The influence of grid-induced errors and the effects of uncertainties in various aspects of thermochemical models were studied and documented. Figure 9.1 shows results that illustrate the differences noted in the species predictions across the stagnation streamline for the AFE vehicle between the Dunn and Kang (D&K) and the Park kinetics models. These results also are compared with those from a noncontinuum, Direct Simulation Monte Carlo (DSMC) method. The code was checked against both ground and flight test data and was used for AFE flowfield simulations.

9.2.4 Significance

The present capability is the most comprehensive and general available for the study of thermochemical nonequilibrium effects in three-dimensional, continuum, hypersonic flows around aeroassisted space transfer vehicles.

9.2.5 Status/Plans

A turbulence model is now being tested in a perfect-gas version of the code. Inclusion of radiative energy transfer and a closer coordination with noncontinuum analysis techniques are planned for the future. Research and development of asynchronous relaxation strategies on parallel computers are continuing.

Peter A. Gnoffo
Space Systems Division
Langley Research Center
(806)864-4380

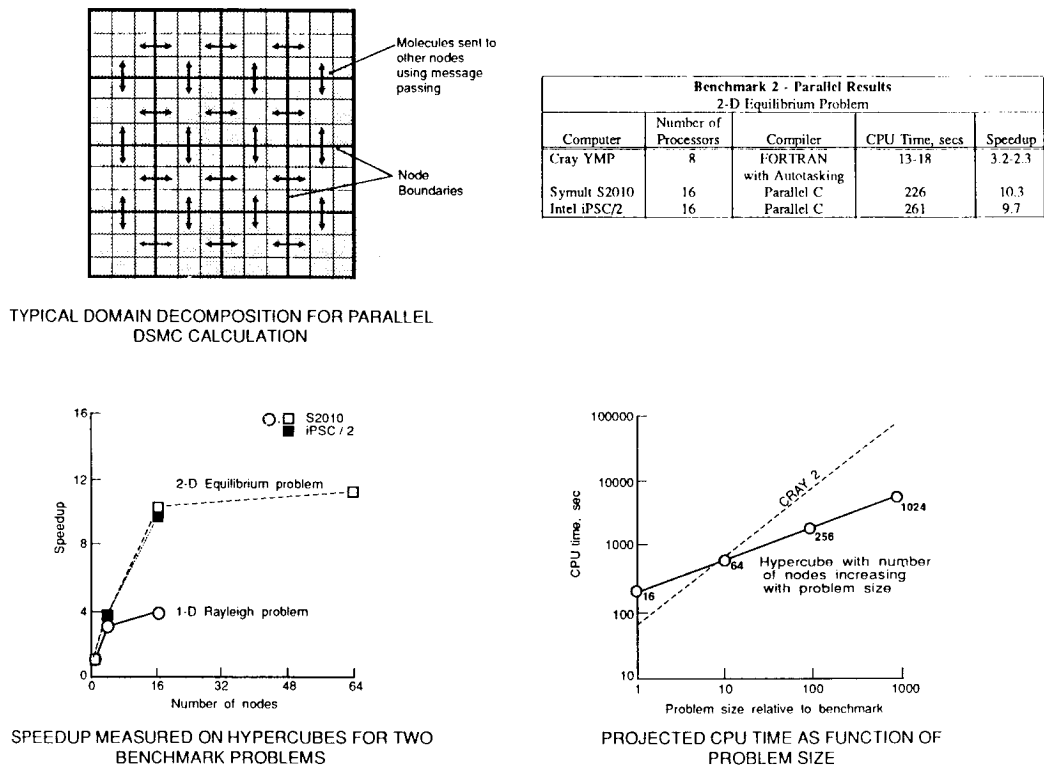


Figure 9.2. Direct Simulation Monte Carlo Analysis on Parallel Processors

9.3 ADVANCES IN DIRECT SIMULATION MONTE CARLO COMPUTATIONAL CAPABILITIES USING PARALLEL PROCESSING

9.3.1 Objective

To reduce the computational time required for Direct Simulation Monte Carlo (DSMC) analysis, thereby allowing the method to be extended to lower altitudes and to more complex problems.

9.3.2 Approach

A number of different parallel algorithms were investigated to determine the optimal strategy for parallel DSMC analysis. These included both coarse-grain and fine-grain algorithms suitable for distributed memory multicomputers and algorithms that combined vectorization with parallel processing on shared memory.

9.3.3 Accomplishments

Benchmark tests were performed on hypercubes using domain decomposition to distribute the physical domain among multiple processors and using message passing to communicate molecules that cross domain boundaries. Speedups of ten or more were obtained on a Symult System S2010 and an Intel iPSC/2, each having 16 processor nodes. Speedups of two to three also were obtained on the Cray YMP using the autotasking compiler (See Figure 9.2).

9.3.4 Significance

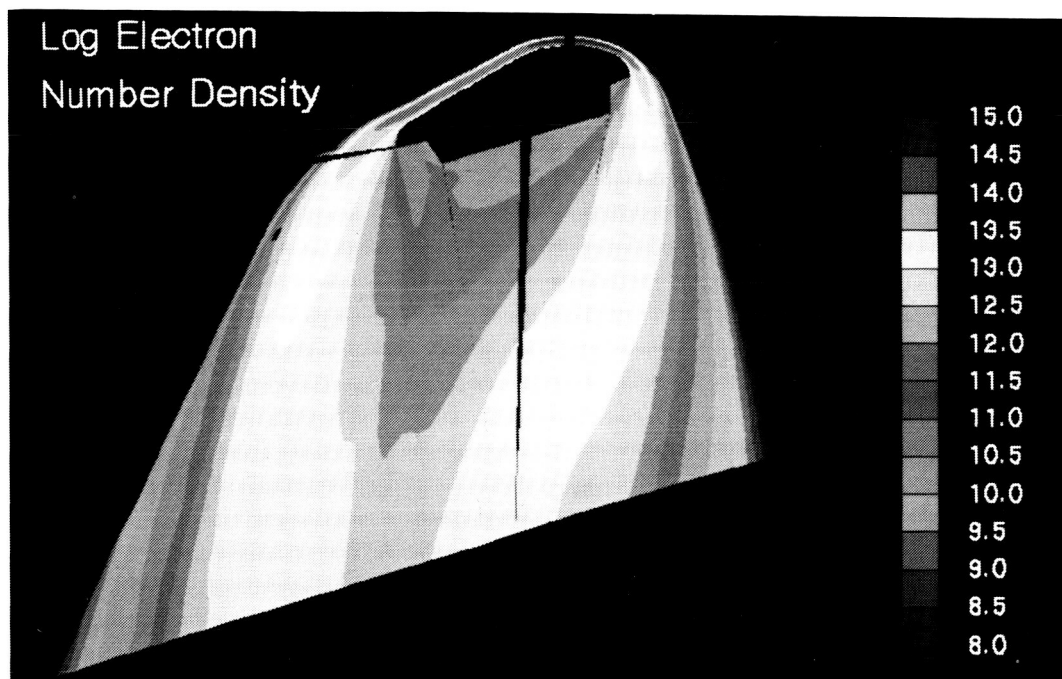
This research demonstrated that significant reductions in DSMC computational times are possible using parallel processing. Although results to date have been obtained with a relatively small number of processors, projections based on these results show that with proper sizing of the problem to the number of available processors, performance exceeding that of current supercomputers is possible.

9.3.5 Status/Plans

Work currently is underway to develop domain decomposition methods coupled with adaptive gridding to provide improved load balancing on massively parallel systems. Research also has been initiated on modifications to the DSMC algorithm that will allow vectorization to be used more effectively.

Richard G. Wilmoth
Space Systems Division
Langley Research Center
(804)864-4368

ORIGINAL PAGE
BLACK AND WHITE PHOTOGRAPH



Electron number densities in the plane of symmetry of the AFE for a velocity of 9.326 km/sec, altitude of 75.15 km, and angle of attack of -5° are presented. The angle of attack is measured relative to the vertical axis of the elliptic nose and is directed towards the "short" side of the aerobrake. Gaps in the contours are an artifact of the method used to supply data to the plotting routine and are indicative of the distance between cell centers in adjacent domains.

Figure 9.3. Log Electron Number Density

9.4 AEROASSIST FLIGHT EXPERIMENT (AFE) FLOWFIELD SIMULATIONS

9.4.1 Objective

To assemble the models developed for the various nonequilibrium processes into a single, computational, fluid dynamic code for the purpose of model-to-model comparison and for simulation of three-dimensional, nonequilibrium flow around aeroassisted space transfer vehicles.

9.4.2 Approach

Aeroassisted space transfer vehicles will use the upper regions of the Earth's atmosphere to generate the lift and drag forces required for deceleration into low-Earth orbit on return from geosynchronous Earth orbit, the Moon or Mars. The aeropass will carry the vehicle through flight regimes in which thermochemical nonequilibrium processes within the surrounding shock layer significantly influence the forces and heating acting on its surface (See Figure 9.3). Nonequilibrium processes, such as molecular dissociation, occur when the accommodation time for the process is of the same order as the transit time required for the gas to cross the shock layer.

9.4.3 Accomplishments

Forebody and near wake flow fields over the Aeroassist Flight Experiment (AFE) were computed for three different trajectory points and two angles of attack. Results were provided to the AFE project office for vehicle and experiment design applications. The entire collection of models and options is documented in NASA TP 2867. Model-to-model comparisons, comparisons with noncontinuum calculations and grid refinement studies are described therein. The computer code, the Langley Aerothermodynamic Upwind Relaxation Algorithm (LAURA), has been documented in a series of AIAA reports, the most recent being AIAA 89-1972.

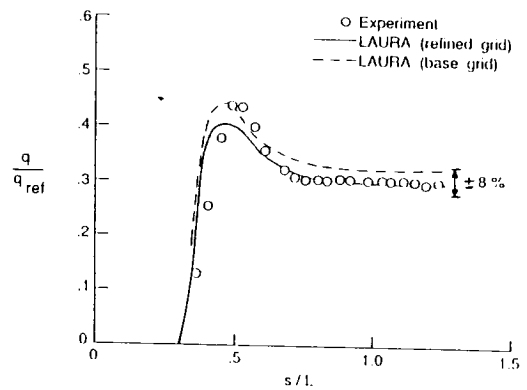
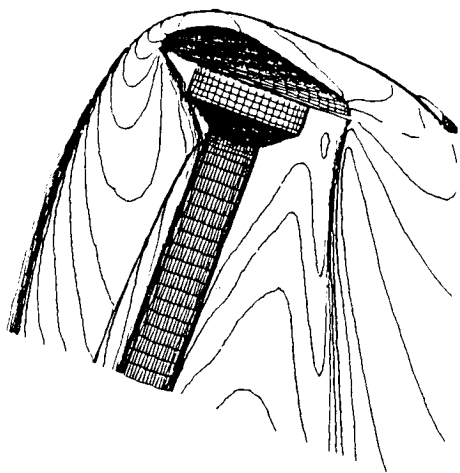
9.4.4 Significance

The flowfield simulation capability for AFE conditions is established, although further validation of some aspects of the thermochemical models is needed.

9.4.5 Status/Plans

Turbulence and radiation models will be included. Grid reformulations will be investigated to remove problems associated with a coordinate singularity in the stagnation region. The code is being distributed to several other users for other applications.

Peter A. Gnoffo
Space Systems Division
Langley Research Center
(804)864-4380



Mach number contours over the AFE in a wind-tunnel test at Mach 10 as predicted by Program LAURA show sharply captured shock waves over the aerobrake and sting as well as the free shear layers flowing off the aft corner of the brake. The corresponding heating on the windside of the sting, behind the shock, as obtained by experiment and calculation using a nominal and a refined grid are presented on the right.

Figure 9.4. Rarefied Flows over the Aeroassist Flight Experiment (AFE) Vehicle

9.5 CODE CALIBRATION IN SUPPORT OF THE AEROASSIST FLIGHT EXPERIMENT

9.5.1 Objective

To conduct calibration runs of the Langley Aerothermodynamic Upwind Relaxation Algorithm (LAURA) to assess its strengths and weaknesses with regard to eventual Aeroassist Flight Experiment (AFE) and Aeroassisted Space Transfer Vehicles (ASTV) applications.

9.5.2 Approach

The AFE is a project designed to obtain critical flight data which will be used in the validation of Computation Fluid Dynamic (CFD) approximation methods. These CFD codes require flight data for validation because of the complexity of the important physical processes which must be modeled in order to accurately predict aerodynamic forces and convective and radiative heating for planned ASTV. Until validation quality flight data become available, the codes must be calibrated with available experimental data sets which include some elements of the intended application.

9.5.3 Accomplishments

Calibration runs were made using perfect-gas, wind-tunnel tests over a scale model of the AFE and on both flight and ground tests which challenge some aspect of the thermochemical nonequilibrium model. In the first case, the gas model is simple, but the grid-related problems of defining the real vehicle are present. In the second case, the vehicle geometries are simple, but nonequilibrium processes must be modeled correctly in order to compare with the experimental data. These tests of the thermochemical nonequilibrium model include ballistic range data for shock shape, shock tunnel data for shock shape and interferograms, project FIRE data for surface heating and project RAM C data for electron number density. Comparisons are generally good, except for some anomalies in the predicted electron number density profiles which are still under investigation. Results are documented in AIAA Paper 89-1673.

9.5.4 Significance

The calibration data sets provide necessary, but not sufficient, check points in the code validation process for AFE and ASTV application. The sting heating results, shown in Figure 9.4, demonstrate the capability of resolving shear layer impingement heating on ASTV payloads.

9.5.5 Status/Plans

Additional calibration tests are ongoing. More comprehensive grid refinement studies are planned.

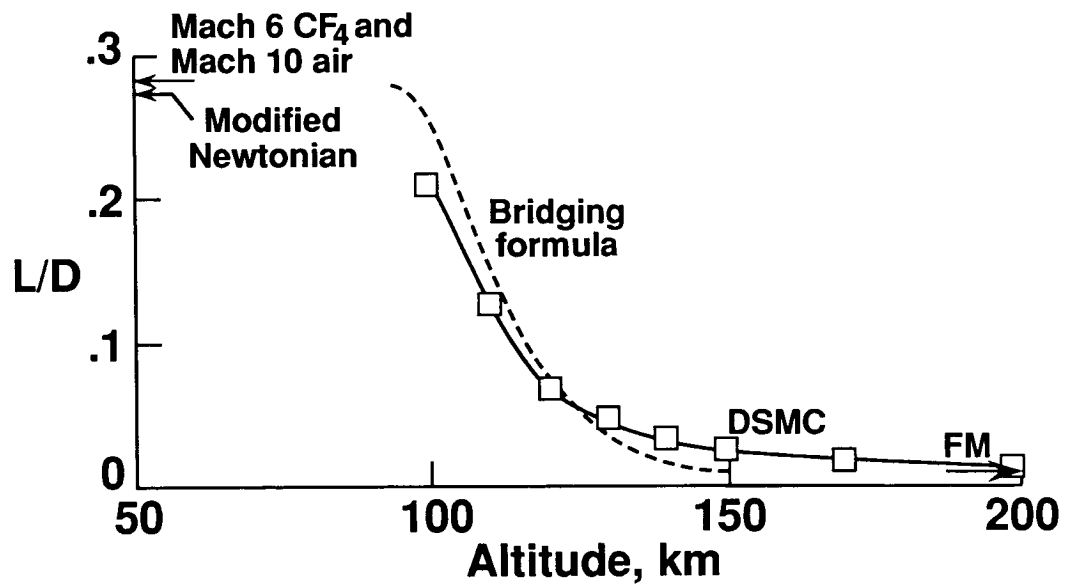


Figure 9.5. Predicted Lift to Drag (L/D) Variation
as a Prediction of Altitude

9.6 RAREFIED FLOWS OVER THE AFE VEHICLE

9.6.1 Objective

To provide an understanding of the potential effects of nonequilibrium phenomena (translational, thermal, chemical and radiative) on the flow structure, aerodynamic forces and heating which will be experienced by the Aeroassist Flight Experiment (AFE).

9.6.2 Approach

The Direct Simulation Monte Carlo (DSMC) method is used to calculate the flow environment about the AFE configuration. For the more rarefied portion of the entry trajectory (200 to 100 km), a 3-D code was used to calculate the flow about the actual configuration. For less rarefied conditions, axisymmetric and stagnation streamline codes were used where ionization and thermal radiation effects have been included in the simulation.

9.6.3 Accomplishments

Stagnation convective heating was calculated for the atmospheric encounter of the AFE along with the radiative heating at a few selected conditions. The three-dimensional calculations provide the first results for the aerodynamic coefficients over most of the transitional flow regime. Figure 9.5 shows the predicted Lift Drag ratio (L/D) as a function of altitude.

9.6.4 Significance

The calculations show that the flow approaches the Free Molecule (FM) limit very gradually with increasing altitude and even at 200 km, the flow is not completely collisionless. Prior to these calculations, it was assumed that free-molecule flow existed for the AFE vehicle near 150 km. Consequently, these results have important implications for the interpretation of aerodynamic coefficients extracted from flight measurements under rarefied conditions. Dissociation is shown to be important at altitudes of 110 km and below. The maximum level of ionization was about two percent.

9.6.5 Status/Plans

NASA plans to examine and implement ways of increasing the computational speed while retaining the ability to adapt to the physical requirements of the problem. NASA also will compare calculations with ground-based measurements for both blunt and lifting-body configurations using 2-D and 3-D codes.

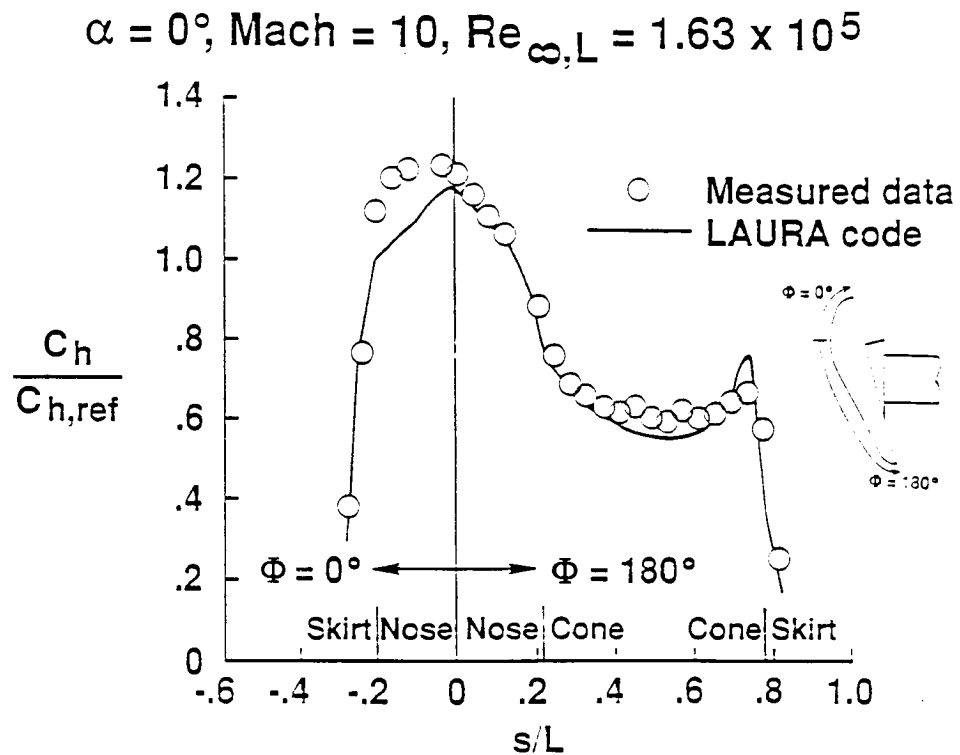


Figure 9.6. Comparison of Measured and Predicted Heat Transfer Distributions

9.7 EXPERIMENTAL HYPERSONIC AERODYNAMIC AND AEROTHERMODYNAMIC CHARACTERISTICS FOR AFE

9.7.1 Objective

To generate a comprehensive, benchmark hypersonic aerodynamic and aerothermodynamic database for the Aeroassist Flight Experiment (AFE) baseline configuration for extrapolation to flight in the continuum and near-continuum regime and for calibration of Computational Fluid Dynamics (CFD) codes.

9.7.2 Approach

The approach involved designing and fabricating force and moment models, including the instrument carrier and rocket motor pressure models and heat transfer models using thin-film gages or the thin-skin transient calorimeter technique for quantitative measurements and the phase change paint technique for qualitative measurements. NASA are testing models over the wide range of flow conditions provided by the Langley Hypersonic Facilities Complex (HFC). NASA also is extending the database to the hypervelocity real-gas regime through tests in an expansion tube and a piston-driven shock tunnel (See Figure 9.6).

9.7.3 Accomplishments

A comprehensive database of experimental characteristics, shock shapes, pressure distributions, surface streamlines, thermal mapping and distributions of heating has been developed over a range of hypersonic Mach numbers and Reynolds numbers. Detailed quantitative heat transfer distributions obtained in Mach 10 tests with thin-film gages revealed the highest heating on the nose region and a spike in the distribution at the skirt. Comparison with predictions from one of the most advanced CFD codes (LAURA) illustrates the difficulty in predicting heat transfer over highly three-dimensional surfaces such as the AFE nose region. Surface streamlines and detailed heating measurements on the cylinder in the near wake show the location and magnitude of the heating associated with impingement of the free shear layer originating at the forebody shoulder. These results provide additional confidence in the Navier-Stokes CFD codes such as LAURA for predicting flow phenomena around the entire body.

9.7.4 Significance

The heat transfer data represent the first such measurements for the AFE and the first ever with a solid MACOR thin-film model. These data are expected to be of interest to designers of the thermal protection system, to principal investigators of onboard experiments and to the CFD community.

9.7.5 Status/Plans

NASA will (1) determine flow impingement/heating on afterbody protuberances, i.e., control motors, booms, antennas, grapple fixture, etc.; (2) measure forebody and wake heat transfer distributions in CF₄ to determine the effects of density ratio; (3) perform pitot pressure surveys in the wake region at Mach 6 in air and compare predictions; (4) determine aerodynamic characteristics at the new low Reynolds number conditions of the CF₄ tunnel and (5) explore feasibility of extending the aerodynamic database to Mach ≥ 14 and much lower test gas densities in facilities at USAF-WRDC and Calspan Corporation.

William L. Wells and John R. Micol
Space Systems Division
Langley Research Center
(804)864-5221

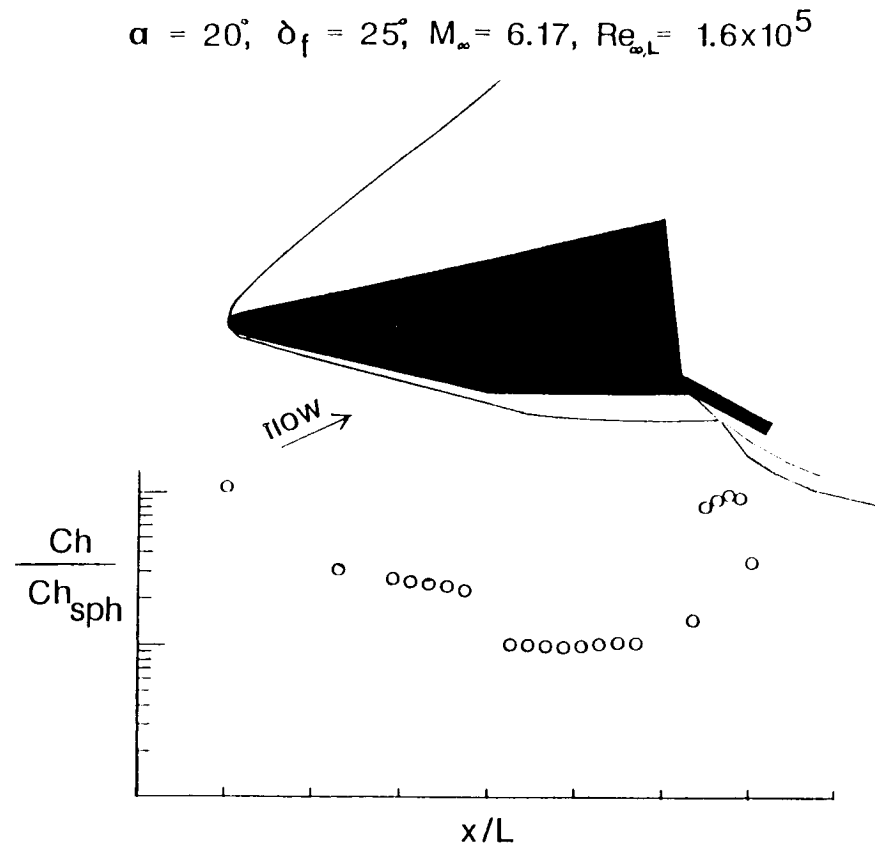


Figure 9.7. Measured Heating Distribution and Shock Shape for 130/70 Biconic with Flap in CF₄

9.8 EXPERIMENTAL HYPERSONIC-HYPERVELOCITY AERODYNAMIC/AEROTHERMODYNAMIC CHARACTERISTICS FOR PROPOSED HIGH ENERGY AEROBRAKING CONCEPTS

9.8.1 Objective

To develop hypersonic-hypervelocity experimental database for candidate High Energy Aerobraking (HEAB) concepts having a range of lift-to-drag ratio (L/D) to determine aerodynamic and aerothermodynamic characteristics and to calibrate Computational Fluid Dynamic (CFD) codes.

9.8.2 Approach

The approach involved performing aerodynamic and aerothermodynamic thermal mapping and heating tests over a wide range of flow conditions with emphasis on tests in CF_4 to simulate real-gas effects and heating studies at velocities in excess of 15,000 fps by tests in an expansion tube and in a piston-driven shock tunnel. The concepts provide a range of L/D from near zero to about two.

9.8.3 Accomplishments

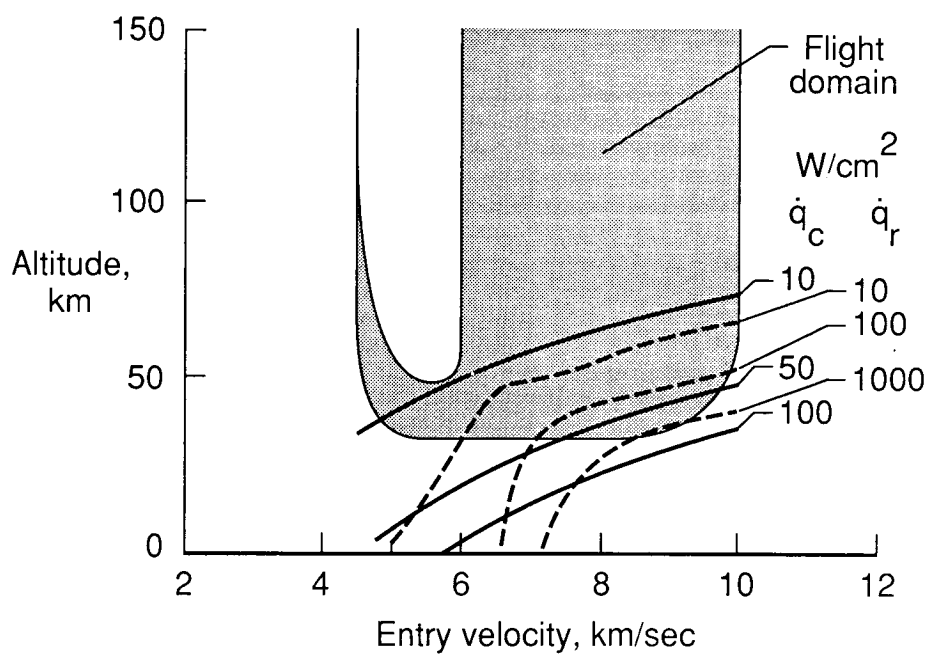
Detailed heat-transfer distributions were measured on a family of large-angle spherically blunted cones at Mach 6 and 10 in air and used to calibrate CFD codes. Pressure and thin-film heat-transfer models of a high-fidelity, drag brake with a payload were designed, fabricated, instrumented and scheduled for tests. Modifications to existing biconic force and moment models were initiated; heat-transfer measurements on thirteen degree/seven degree biconics, including control surfaces, were performed at Mach 6 in air and CF_4 and data are being analyzed (See Figure 9.7). Heat-transfer measurements obtained on a biconic model in the Australian National Laboratory T3 Shock Tunnel in air and nitrogen at velocities up to 20,000 fps also are being analyzed.

9.8.4 Significance

This evolving, experimental database for three categories of configurations based on L/D (low, $L/D < 0.5$; moderate, $L/D = 0.75$ to 1.25 and high, $L/D > 1.5$) provides a broad foundation upon which to evaluate aerodynamic and aerothermodynamic characteristics for proposed HEAB flight vehicles and for CFD code calibration. This database involves detailed heat-transfer measurements on payloads attached to the base and on control surfaces; the database also includes simulation and duplication of real-gas effects by testing the same models in conventional and impulse facilities.

9.8.5 Status/Plans

NASA plans to (1) document heat-transfer results for a family of blunt cones and for slender biconic with control surfaces; (2) test drag brake with payload in the near future and (3) continue the design/fabrication/testing of conical frustum models in both conventional wind tunnels and high-enthalpy impulse facilities.



Convective heating (\dot{q}_c) based on Sutton-Graves Equation
Radiative heating (\dot{q}_r) based on Sutton's inviscid equilibrium method

Figure 9.8. Flight Domain and Stagnation Point Heating Rate During Mars Atmospheric Passage

9.9 HIGH ENERGY AEROBRAKING STUDIES

9.9.1 Objective

To determine the stagnation region convective and radiative aerothermal environment during Mars aerocapture over a modified Aeroassist Flight Experiment (AFE) shape (lift-drag ratio of 0.28) as part of Langley's High Energy Aerobraking (HEAB) studies, .

9.9.2 Approach

The convective heating rate results (present in the boundary layer) were based upon the Sutton-Graves equation, whereas the radiative results (which are shock induced) were obtained by utilizing Sutton's inviscid equilibrium solution. Both stagnation point heating rate solutions were integrated into the Program to Optimize Simulated Trajectories (POST); hence, solutions were obtained throughout the atmospheric passage. In accordance with interplanetary trajectory results, the Mars atmospheric entry velocities ranged from six to ten km/second.

9.9.3 Accomplishments

Figure 9.8 shows the radiative contribution to the total stagnation point heating rate is largely dependent upon atmospheric entry velocity. For a low speed entry (velocity below 6.2 km/second), the effects of radiation are minimal; however, for an entry of approximately 7.0 km/second, the relative contributions of the radiative and convective effects are of the same order of magnitude. As the entry velocity increases (above 8.5 km/second), radiative effects dominate the aerothermal environment.

9.9.4 Significance

Over a majority of the Mars entry speeds associated with a high energy aerobraking mission, radiative effects will be significant for blunt configurations (like the AFE shape).

9.9.5 Status/Plans

Current research focuses on improving our understanding of the relationship between the interplanetary and atmospheric trajectories and performing a detailed design analysis of several candidate aerobrake shapes.

R.W. Powell
Space Systems Division
Langley Research Center
(804)864-4506

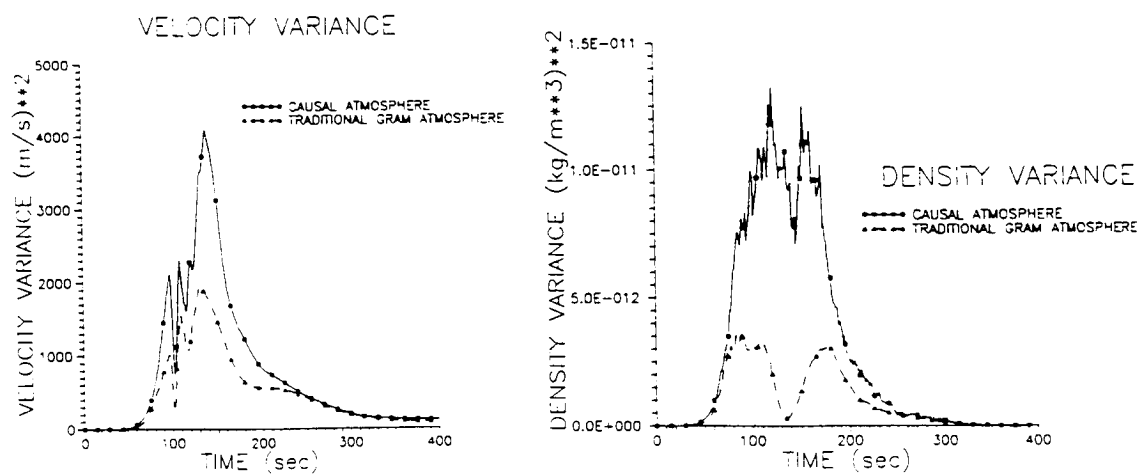


Figure 9.9. Random Atmosphere Simulation for Monte Carlo Trajectory Analysis

9.10 RANDOM ATMOSPHERE SIMULATION FOR MONTE CARLO TRAJECTORY ANALYSIS

9.10.1 Objective

To develop a random atmosphere simulation approach for use in Monte Carlo trajectory simulations.

9.10.2 Approach

The approach developed is applicable to both Earth and Mars atmospheres. The random atmosphere along a trajectory is represented as a mean, along with spatially correlated random variations. The statistics of the mean and variations are functions of altitude, latitude and longitude and are propagated in space in parallel with the trajectory simulation's time-domain propagation. A number of modifications of the Global Random Atmosphere Model (GRAM) were made in order to render the atmosphere simulation consistent with the time-domain simulation, including an analytical measure for controlling the spatial bandwidth of the perturbations while preserving statistical stationarity and the appropriate pointwise perturbation covariances.

9.10.3 Accomplishments

An adaptation of the GRAM was implemented and used in aerospace guidance simulations. Figure 9.9 shows the results of 160 Monte Carlo runs using an Aeroassist Flight Experiment (AFE) model and the Johnson Space Center (JSC) guidance law of Cerimele and Gamble. Eighty of the runs were made with the atmosphere simulated in the "usual" manner, representing the random atmosphere samples as tabular functions of altitude. The other eighty were calculated using the new approach. Significant differences were seen in key trajectory statistics.

9.10.4 Significance

This allows realistic simulations of trajectories with proper representation of the statistics of the atmospheric parameters. It is a necessary tool for proper simulation of stochastic feedforward/feedback guidance laws.

9.10.5 Status/Plans

The earth model was completed. The code will directly accept the expected Georgia Tech Martian atmosphere model. This software will be used extensively as a validation tool for high energy aerobraking guidance.

ORIGINAL PAGE
BLACK AND WHITE PHOTOGRAPH

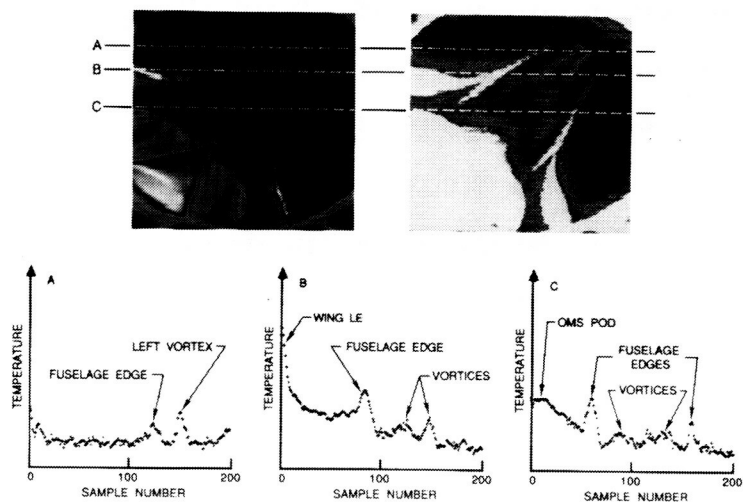


Figure 9.10. SILTS Qualitative Results Fuselage

9.11 SHUTTLE INFRARED LEESIDE TEMPERATURE SENSING (SILTS)

9.11.1 Objective

To obtain high-spatial resolution temperature measurements of the Orbiter leeside surface during entry. The data will help characterize the aerothermal environment in a complex, three-dimensional, vortical, separated flowfield not adequately simulated in ground-test facilities and will provide a database for maturing computational fluid dynamic codes.

9.11.2 Approach

An infrared camera was mounted in the tip of the vertical tail and alternately senses infrared radiation emanating from the Orbiter fuselage and left wing surfaces. The electronic signals were recorded onboard the Shuttle and post-flight processing procedures provided detailed surface temperature profiles from which aeroheating distributions can be computed.

9.11.3 Accomplishments

The Columbia vehicle made only one flight, STS-61 C, since installation of the SILTS experiment. Several anomalies in the SILTS hardware performance degraded the expected flight results; however, modifications were made to the automated data reduction program to account, where possible, for the data deficiencies. A total of 61 images on the wing and 10 on the fuselage were processed into a color graphic format for analyses.

9.11.4 Significance

Although anomalies in the SILTS system compromised the precision of data measured during the first flight on STS-61 C, intensive efforts with the data reduction techniques produced qualitative results on the leeside aerothermal environment. Higher temperatures on the leading edge (LE) and shock interaction region on the wing were highlighted. Figure 9.10 shows the peak fuselage temperatures on the wing and fuselage edges, on the orbital maneuvering systems (OMS) pod and near the centerline from vortical scrubbing. The test demonstrated the feasibility and advantages of the concept.

9.11.5 Status/Plans

Modifications to the hardware should assure high-quality data on future flights and connection of leeside thermocouples should provide valuable comparisons.

E. V. Zoby
Space Systems Division
Langley Research Center
(804)864-4386

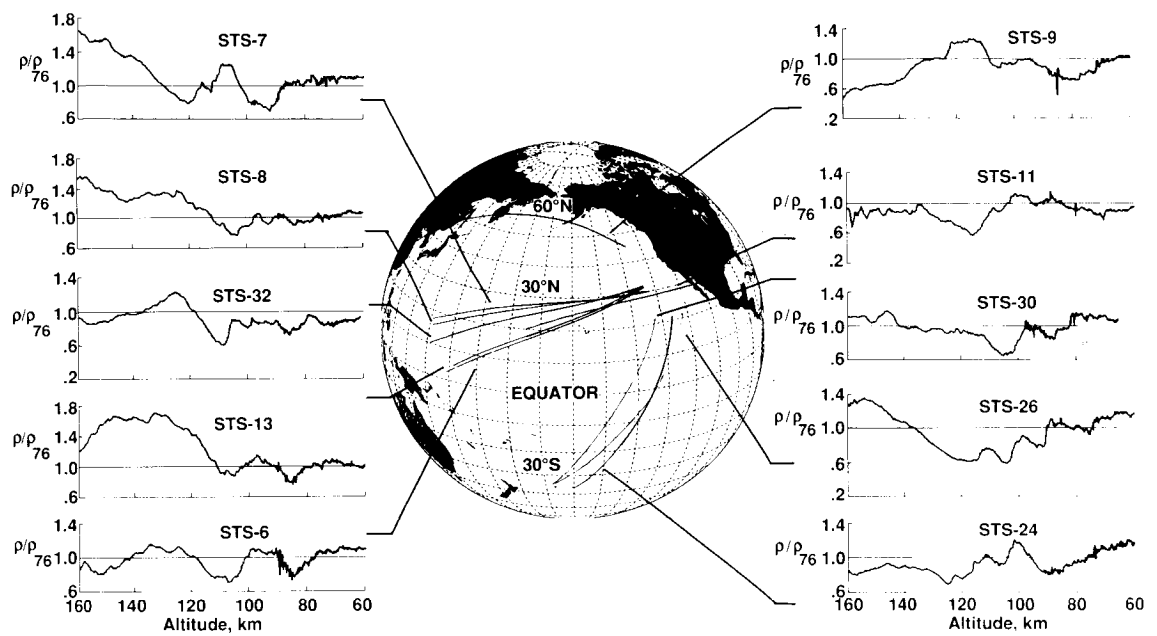


Figure 9.11. Shuttle Accelerometry (HiRAP/IMU) Density Measurements

9.12 ATMOSPHERE DENSITY MEASUREMENTS BETWEEN 60 AND 160 KM

9.12.1 Objective

To provide a database of atmosphere density profiles in a region of the atmosphere inaccessible to orbiting spacecraft and beyond typical sounding rocket sampling altitudes.

9.12.2 Approach

Research acceleration instrumentation on the Shuttle Orbiter (the High Resolution Accelerometer Package, HiRAP) and the navigation equipment (the Inertial Measurement Units, IMU) provide a means to sample density in the altitude region of interest upon each reentry. Solving for the rarefield flow aerodynamics of a winged reentry vehicle (which includes control surface effects) over multiple flights allows the determination of in situ density using a technique developed a decade ago for planetary entry science investigations and used for both Mars and Venus missions.

9.12.3 Accomplishments

Ten samples, covering a period of three years, were analyzed to provide a significant database gain with respect to the body of data collected by other techniques. The data along the flight path of the Orbiter are unique in that they cover a very wide horizontal range during each flight (See Figure 9.11) and thus provide a component not available to the near vertical profiles collected by sounding rockets and ground lidars. Further, the data also exhibit a wave feature when compared with various atmosphere models. The characteristics of the density waves are (1) the amplitude appears to have a dependence on solar activity and time of year and (2) the wavelength is approximately constant (37 km), but the phase is independent of altitude.

9.12.4 Significance

Variations of measured density from current atmosphere models are large (in excess of 50 percent). These measured variations will provide important design applications insights for NASA/DoD aerobrake missions and new insights for improvements of atmosphere models.

9.12.5 Status/Plans

One HiRAP will continue to collect data on the OV-102 (Columbia). Results will be combined with mass spectrometer data (Shuttle Upper Atmosphere Mass Spectrometer, SUMS) also scheduled to fly on the Columbia.

Robert C. Blanchard
Space Systems Division
Langley Research Center
(804)864-4391

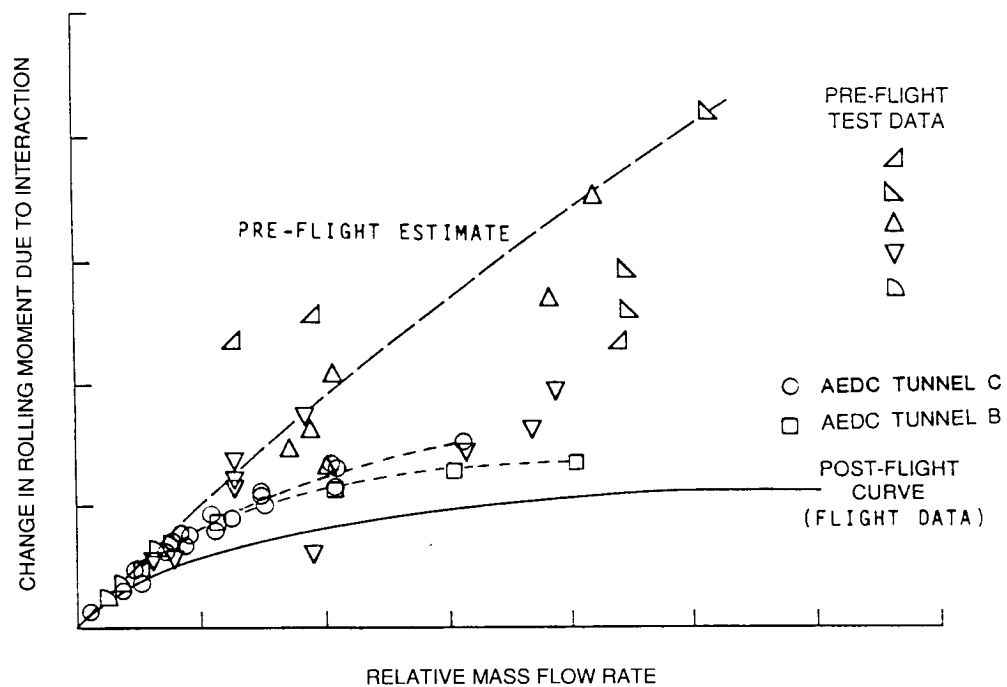


Figure 9.12. Orbiter RCS/Flowfield Interactions

9.13 REACTION CONTROL SYSTEM PLUME/FLOWFIELD INTERACTION STUDY

9.13.1 Objective

To establish improved ground-to-flight extrapolation techniques for reaction control system (RCS) plume/flowfield interactions on advanced space transportation system vehicles during atmospheric reentry.

9.13.2 Approach

The approach involved comparing pressure distributions and corresponding moments measured on the wing upper surface, fuselage and vertical tail of the Space Shuttle Orbiter (OV-102) during reentry with measurements made on a 0.0125-scale Orbiter model tested at Mach 2.5 to 10. Comparisons of pressure distributions from flight and ground tests with and without RCS yaw thrusters firing will be correlated with calculated leeside flow fields to derive applicable ground-to-flight extrapolation methods. (See Figure 9.12).

9.13.3 Accomplishments

Tests on the 0.125-scale pressure model were performed in the Langley Unitary Plan Wind Tunnel (UPWT) at Mach 2.5, 3.5 and 4.5 and in the AEDC Tunnel C at Mach 10. Force and moment tests were conducted in the AEDC Tunnel B at Mach 6. The tests provided a much more consistent and accurate data set than those on which preflight predictions were based. They represent a significant improvement in agreement with flight data, thereby providing credibility to the carefully developed test techniques employed in this study. These data agree reasonably well with flight data obtained from onboard inertial measurements.

9.13.4 Significance

Subject data are the first wind-tunnel measurements illustrating the response of the wing upper surface pressures to plumes from RCS thrusters. RCS/flowfield interactions were found to be relatively insensitive to plume shape or number of thrusters firing for a given momentum ratio. Whereas large differences between pre-flight wind-tunnel and first Shuttle flight data occurred, the new Mach 6 and 10 data (classified) compared more favorably with flight data than with preflight data. The original data were judged to be qualitatively and quantitatively insufficient to predict RCS/flowfield interactions.

9.13.5 Status/Plans

This completes the Langley studies of the RCS/flowfield interactions for the Shuttle Orbiter during entry. A generic transatmospheric vehicle model is being built to study the ascent and entry RCS/flowfield interactions on slender-bodied configurations.

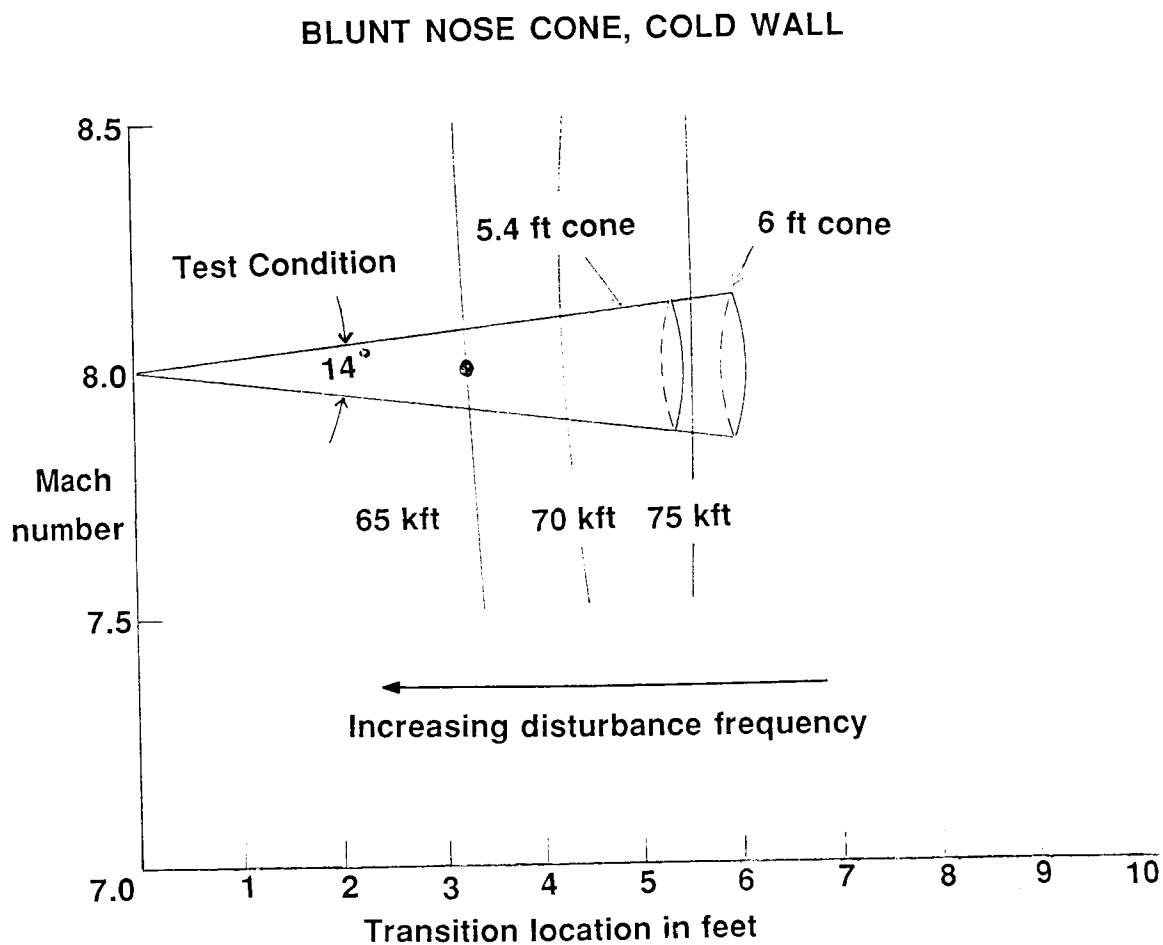


Figure 9.13. Calculated Transition Location

9.14 BOUNDARY LAYER STABILITY ANALYSIS ON CONES IN FREE FLIGHT AT HYPERSONIC SPEEDS

9.14.1 Objective

To determine the feasibility of using sounding rockets to study transition physics in free flight and to study the sensitivity of transition location on sharp and blunt cones with variations in Mach number and altitude.

9.14.2 Approach

The approach involved hypersonic stability analysis on sharp and blunt cone with a seven degree half angle at various altitudes and hypersonic Mach numbers. Onset of transition was predicted by the e^n method with $n=10$ (See Figure 9.13).

9.14.3 Accomplishments

Dominant frequencies and instability modes leading to transition were identified. Onset of transition was more sensitive to altitude than Mach number changes. Onset of transition location can shift one foot with a 5,000 foot change in altitude on a cone with a total length of 5.4 feet.

9.14.4 Significance

Results will enable payload/sensor integration design and definition of ballistic/controlled launch vehicle and mission requirements.

9.14.5 Status/Plans

Results of the stability analysis will be used by Wallops Flight Facility to define a launch vehicle, conduct trajectory dispersion analyses and define the launch vehicle control requirements. Definition of a specific flight experiment, mission requirements and preliminary payload design are contingent upon FY 1990 funding.

Simha S. Dodbele and J.W. Usry
Flight Research Branch
Langley Research Center
(804)864-3863

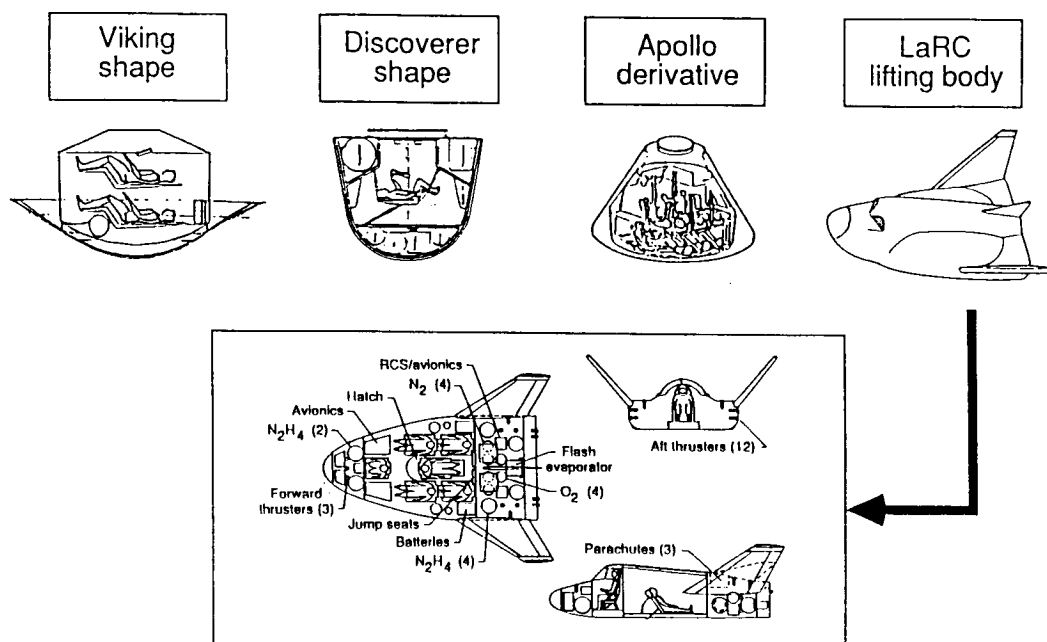


Figure 9.14. ACRC Phase B Study Matrix

9.15 LIFTING-BODY CONFIGURATION ANALYSIS

9.15.1 Objective

To make a preliminary assessment of the ability of the lifting-body concept to perform the ACRC mission. A lifting-body concept derived from NASA and Air Force studies in the late sixties is being developed for possible application to the Assured Crew Return Capability (ACRC) mission for the Space Station Freedom and Personnel Launch System (PLS) assured manned access to space missions. The concept is being extensively tested in wind tunnels and is being analyzed using computational fluid dynamics (CFD) techniques. Also, subsystem designs for the various missions and ascent and entry trajectories are being developed.

9.15.2 Approach

Configuration analyses were conducted to assess entry aerodynamics, stability, control and performance; aerodynamic heating; landing stability and control and cross range benefits for application of the lifting-body concept to perform the ACRC mission (See Figure 9.14).

9.15.3 Accomplishments

The results of the systems analyses and configuration assessment resulted in inclusion of the lifting body in the phase A/B studies to be initiated by Johnson Space Center later this year.

9.15.4 Significance

This program opened up the options being studied for the ACRC to include more than the low-lift-to-drag-ratio blunt bodies being initially studied.

9.15.5 Status/Plans

NASA will continue analyses to further mature the vehicle database to support the phase A/B studies.

D. C. Freeman
Space Systems Division
Langley Research Center
(804)864-4502

From 220 nmi orbit; December 1 + Day = 1 hr before sunrise to 2 hr before sunset

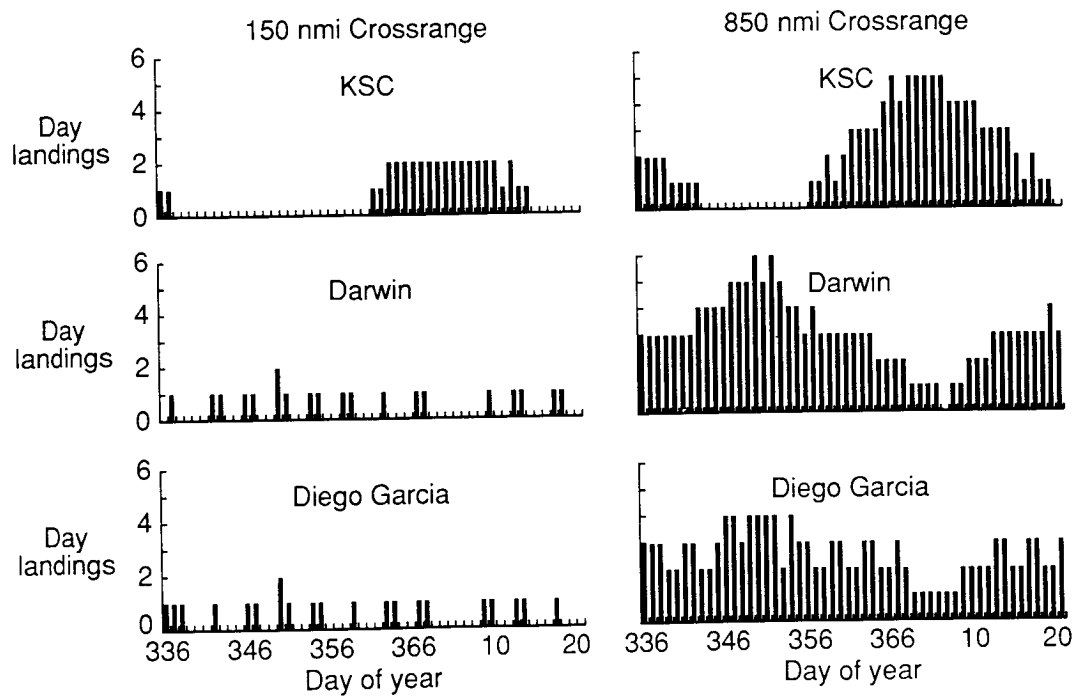


Figure 9.15. Day Landings From Space Station

9.16 LIFTING-BODY ENTRY CROSS RANGE ANALYSIS

9.16.1 Objective

To assess the impact of cross range on landing opportunities (See Figure 9.15). A lifting-body concept derived from NASA and Air Force studies in the late sixties is being developed for possible application to the Assured Crew Return Capability (ACRC) mission for the Space Station Freedom and Personnel Launch System (PLS) assured manned access to space missions. The concept is being extensively tested in wind tunnels and is being analyzed using computational fluid dynamics (CFD) techniques. Also, subsystem designs for the various missions and ascent and entry trajectories are being developed.

9.16.2 Approach

The approach involved conducting three-degree-of-freedom entry studies to identify entry/landing opportunities from the Space Station Freedom. For the analysis, 850 nautical miles of the 1,150-nautical-mile cross range available were used.

9.16.3 Accomplishments

The lifting-body vehicle with an entry cross range of 1,150 nautical miles provides a minimum of three landing opportunities a day. In comparison, ballistic-type/low-lift-drag-ratio concepts with typical cross ranges of 150 nautical miles have periods of five days with no landing opportunities.

9.16.4 Significance

The additional landing opportunities for the lifting-body concept provide increased return options and will require fewer recovery sites.

9.16.5 Status/Plans

These analyses are completed.

D. C. Freeman
Space Systems Division
Langley Research Center
(804)864-4502

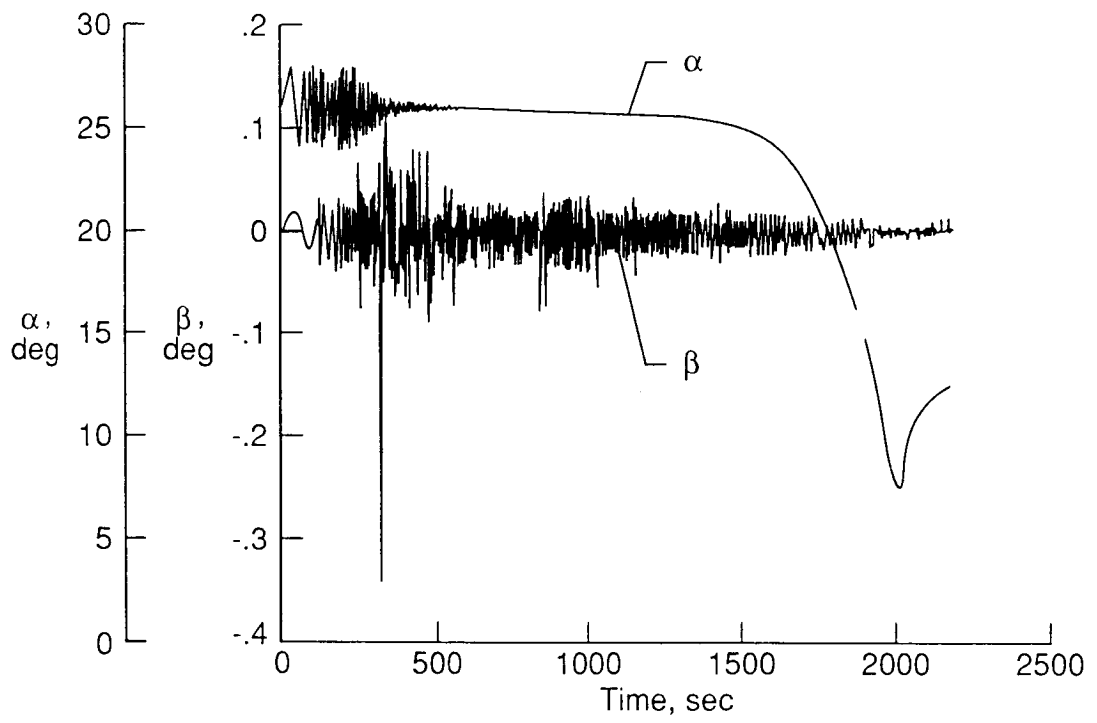


Figure 9.16. Complete 6 DoF Entry

9.17 LIFTING-BODY ENTRY FLIGHT DYNAMICS ANALYSIS

9.17.1 Objective

To study the ability to control the vehicle motions along the entry trajectory. A lifting-body concept derived from NASA and Air Force studies in the late sixties is being developed for possible application to the Assured Crew Return Capability (ACRC) mission for the Space Station Freedom and Personnel Launch System (PLS) assured manned access to space missions. The concept is being extensively tested in wind tunnels and is being analyzed using Computational Fluid Dynamics (CFD) techniques. Also, subsystem designs for the various missions and ascent and entry trajectories are being developed.

9.17.2 Approach

A six-degree-of-freedom (6 DOF) simulation of the entry trajectory and a simple flight control system were developed and maneuvers were introduced at several points along the trajectory to analyze the vehicle controllability.

9.17.3 Accomplishments

The vehicle was found to be easily controllable throughout the speed range that was studied (hypersonic speeds to Mach 2) using small reaction control system (RCS) thrusters. Figure 9.16 shows time histories of the angle of attack, α , and the sideslip angle, β , from entry into the atmosphere to about Mach 2.

9.17.4 Significance

The highly refined concept is stable and easily controllable at high speeds and therefore is a good candidate for a relatively inexpensive manned entry vehicle for a possibly deconditioned crew.

9.17.5 Status/Plans

Entry stability and control analyses are continuing.

D.C. Freeman
Space Systems Division
Langley Research Center
(804)864-4502

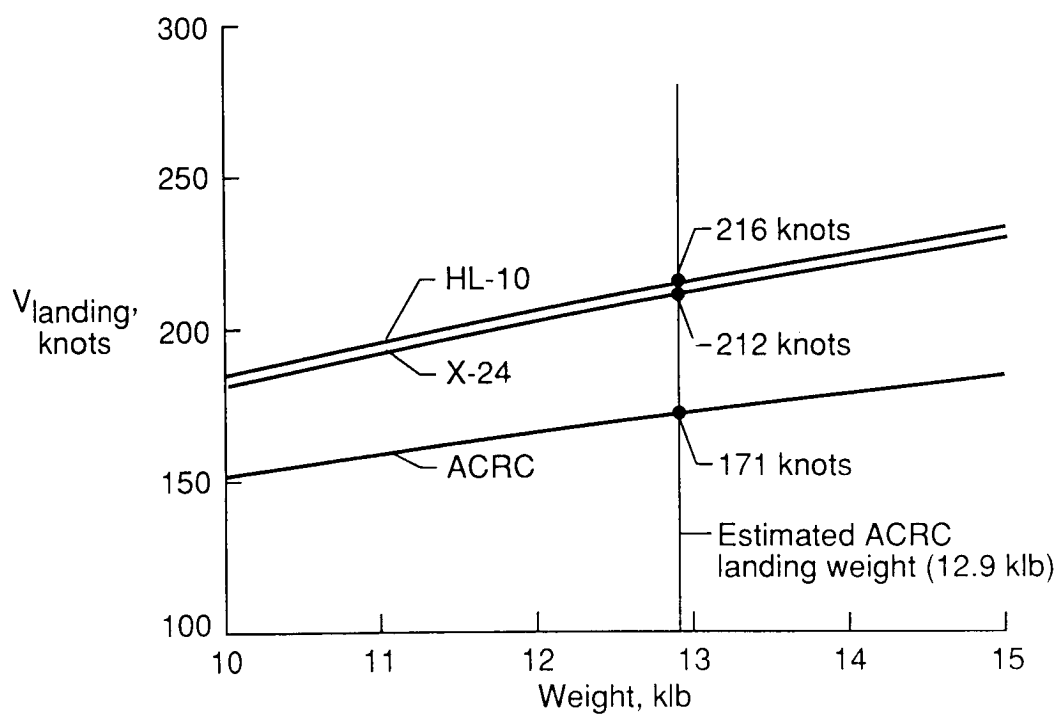


Figure 9.17. Comparison of ACRC, X-24 and HL-10 Landing Speed Estimates

9.18 LIFTING-BODY LANDING-SPEED ANALYSIS

9.18.1 Objective

To determine the low-speed stability and control and landing characteristics of this vehicle. A lifting-body concept derived from NASA and Air Force studies in the late sixties is being developed for possible application to the Assured Crew Return Capability (ACRC) mission for the Space Station Freedom and Personnel Launch System (PLS) assured manned access to space missions. The concept is being extensively tested in wind tunnels and is being analyzed using Computational Fluid Dynamics (CFD) techniques. Also, subsystem designs for the various missions and ascent and entry trajectories are being developed.

9.18.2 Approach

The approach involved conducting static-force, forced-oscillation and free-flight wind-tunnel tests in the Langley Full-Scale Wind Tunnel to determine the low-speed stability and control of the lifting-body concept.

9.18.3 Accomplishments

The static low-speed stability and control characteristics of the vehicle were measured by the Flight Dynamics Branch of the Flight Applications Division. The results of these tests show that the low-speed stability of the vehicle is so favorable that landing attitudes as high as 18 degrees are feasible and provide lift coefficients as high as 0.6. At the estimated vehicle landing weight of 12,900 pounds with a lift coefficient of 0.6, a landing speed as low as 171 knots can be achieved (See Figure 9.17).

9.18.4 Significance

The landing speed of 171 knots is at least 30 knots slower than that of the Shuttle Orbiter and significantly lower than that of previous lifting bodies.

9.18.5 Status/Plans

Additional tests are planned to better define the vehicle controllability, dynamic stability and free-flight characteristics.

D.C. Freeman
Space Systems Division
Langley Research Center
(804)864-4502

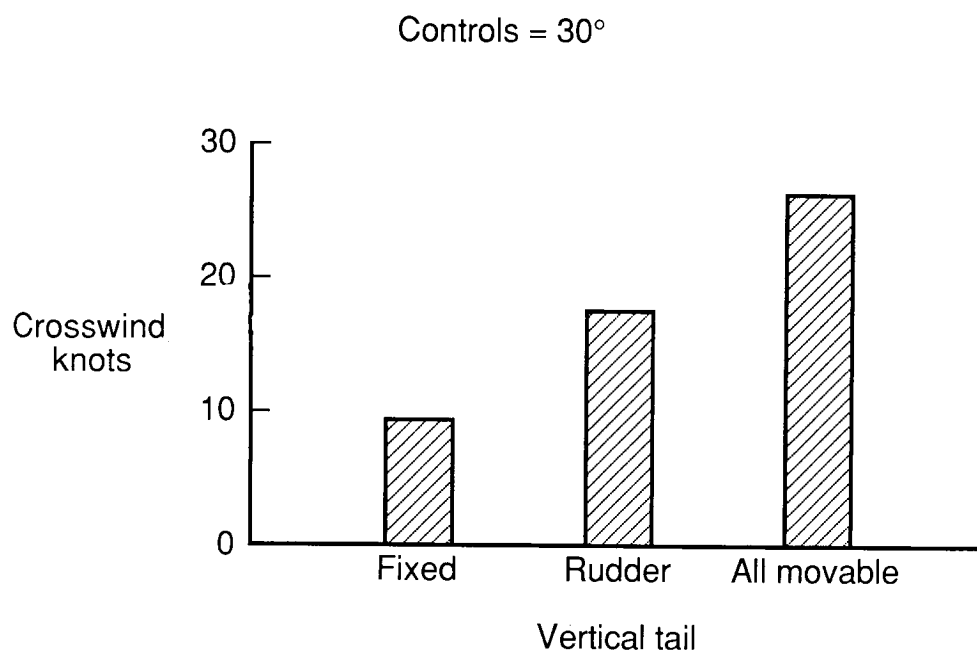


Figure 9.18. Crosswind Capability

9.19 LIFTING-BODY CROSSWIND LANDING ANALYSIS

9.19.1 Objective

To assess the limitations imposed on the vehicle by crosswinds during landing. A lifting-body concept derived from NASA and Air Force studies in the late sixties is being developed for possible application to the Assured Crew Return Capability (ACRC) mission for the Space Station Freedom and Personnel Launch System (PLS) assured manned access to space missions. The concept is being extensively tested in wind tunnels and is being analyzed using Computational Fluid Dynamics (CFD) techniques. Also, subsystem designs for the various missions and ascent and entry trajectories are being developed.

9.19.2 Approach

Static wind-tunnel test results were analyzed by the Flight Dynamics Branch of the Flight Applications Division to determine the crosswind landing capability of the lifting-body vehicle (See Figure 9.18).

9.19.3 Accomplishments

With the control deflections limited to 30 degrees, the vehicle was capable of landing in a 10-knot crosswind without the rudder on the centerline vertical tail. Using the rudder extended this capability to about 18 knots and making the centerline vertical tail all movable further extended the capability to 25-knots. The results of these preliminary analyses show the potential for providing a capability to handle a 20-knot crosswind when the control effectiveness and control coordination are better defined.

9.19.4 Significance

With the emphasis in the ACRC program on returning deconditioned crewmen from Space Station Freedom, automatic landing and entry must be considered. Coupling the capability to handle significant crosswinds with the decreased landing speed provides vehicle characteristics which make automatic landing feasible.

9.19.5 Status/Plans

More in depth analyses are being made to better define the control system requirements and to incorporate vehicle dynamics.

D.C. Freeman
Space Systems Division
Langley Research Center
(804)864-4502

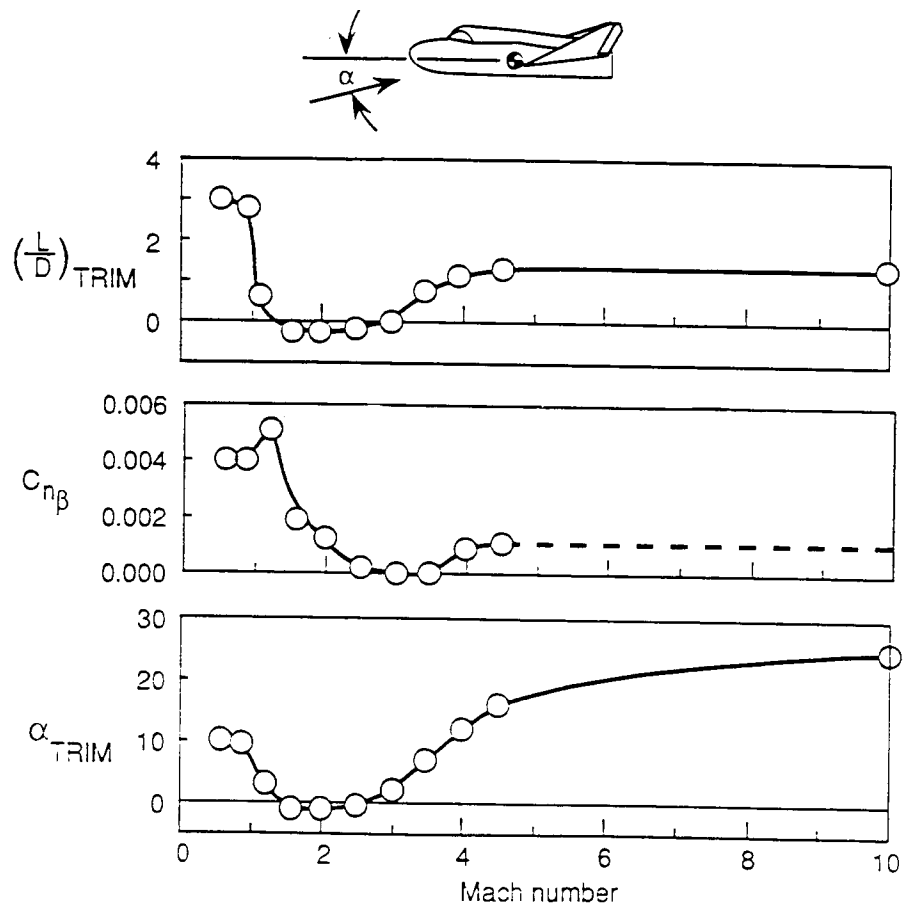


Figure 9.19. Summary Aerodynamic Characteristics of PLS Lifting Body Configuration

9.20 EXPERIMENTAL AERODYNAMIC AND AEROTHERMODYNAMIC CHARACTERISTICS FOR PROPOSED PERSONNEL LAUNCH SYSTEM LIFTING-BODY CONCEPT

9.20.1 Objective

To (1) determine transonic/supersonic/hypersonic aerodynamic and hypersonic aerothermodynamic characteristics of a proposed Personnel Launch System (PLS) lifting body, (2) assess the performance of this vehicle and compare it with other similar lifting configurations and (3) establish a benchmark hypersonic experimental database for this class of configuration for Computational Fluid Dynamics (CFD) code calibration.

9.20.2 Approach

The approach involved augmenting the experimental aerodynamic database for the lifting-body concept by conducting wind-tunnel tests in the Calspan 8-foot Transonic Tunnel from Mach 0.6 to 1.2, in the Langley Unitary Plan Wind Tunnel from Mach 1.6 to 4.5 and in the Langley Hypersonic Facilities Complex (HFC) from Mach 6 to 22. NASA performed qualitative aerothermodynamic (thermal mapping) tests over a wide range of hypersonic flow conditions. NASA simulated real-gas effects on aerodynamic and aerothermodynamic characteristics by testing in the Langley Hypersonic CF₄ Tunnel. NASA built and tested high-fidelity force, pressure and heat transfer models to calibrate CFD codes in conventional and high-enthalpy impulse tunnels (See Figure 9.19).

9.20.3 Accomplishments

These tests have shown that the configuration is longitudinally stable over the Mach range. It is naturally trimmed (controls undeflected) at maximum L/D at hypersonic and subsonic speeds with values of 1.4 and 3.0, respectively. In the Mach range from about 1.5 to 3.0, pitch control input will be necessary to trim to positive lift conditions. Transonic results have been published in NASA TM 4117 and supersonic results are in publication. Preliminary thermal mapping tests have shown high heating regions on the nose, fin leading edges, canopy and regions of flow reattachment on the upper surface.

9.20.4 Significance

The proposed lifting-body concept has aerodynamic characteristics that make it an attractive candidate for a PLS. It is longitudinally and laterally stable and naturally trimmed, i.e., zero control deflection over most of the speed regime. Hypersonic L/D values give it sufficient cross range capability and the subsonic L/D offers the possibility of a conventional aircraft-like landing. The aerodynamic/aerothermodynamic data generated from this study are an essential portion of the information needed to define, evaluate and select a PLS vehicle.

9.20.5 Status/Plans

NASA plans to complete testing in the Langley HFC and analyze aerodynamic heating data and document the findings. NASA also will initiate design, fabrication and testing of highly instrumented, high-fidelity models for CFD code calibration.

George M. Ware, John R. Micol and Thomas J. Horvath
Space Systems Division
Langley Research Center
(804)864-5221

ORIGINAL PAGE
BLACK AND WHITE PHOTOGRAPH

$$M_{\infty} = 10 \quad \alpha = 25^{\circ} \quad \gamma = 1.4$$



Figure 9.20. Mach Number Contour Plots

9.21 ASSURED CREW RETURN VEHICLE FLOWFIELD ANALYSIS

9.21.1 Objective

Currently within NASA, there is an ongoing activity to define candidate approaches for crew rescue from the Space Station Freedom. While a number of Assured Crew Return Capability (ACRC) vehicle concepts have been identified for study over the next two years, interest at Langley has focused on a lifting-body shape derived from work initiated by NASA and the Air Force in the late sixties in studying the Dynasoar, HL-10, X24 and M2F2 vehicles.

Extensive system studies were conducted to determine gross operational characteristics of this proposed vehicle. Refinement of the operational envelope requires a more detailed analysis of the aerodynamic and aerothermodynamic characteristics of the vehicle through the use of Computational Fluid Dynamics (CFD) techniques. The CFD analysis of this complex aerodynamic shape required not only robust CFD software, but also state-of-the-art surface definition, grid generation and data presentation techniques.

9.21.2 Approach

The vehicle surface was defined by spline interpolation of a database constructed from measured cross-sectional shapes of a wind-tunnel model. The surface and volume grids were constructed through a combination of algebraic techniques and transfinite interpolation. An inviscid version of the Langley Aerothermodynamic Upwind Relaxation Algorithm (LAURA) code was used for the CFD analysis.

9.21.3 Accomplishments

Figure 9.20 indicates the type of detailed flowfield information available through a CFD analysis. These contour plots at three axial locations reveal the extent of the bow shock and details of the flow in the shock layer.

9.21.4 Significance

Surface pressures derived from CFD computations are used directly in determination of vehicle aerodynamic characteristics and in vehicle structural analysis and the computed velocity fields can be combined with approximate boundary layer techniques to determine surface heating.

9.21.5 Status/Plans

The LAURA code is being upgraded to include the effects of equilibrium air chemistry. The code will then be used to compute inviscid and viscous (Navier-Stokes) solutions at flight conditions.

ORIGINAL PAGE
BLACK AND WHITE PHOTOGRAPH

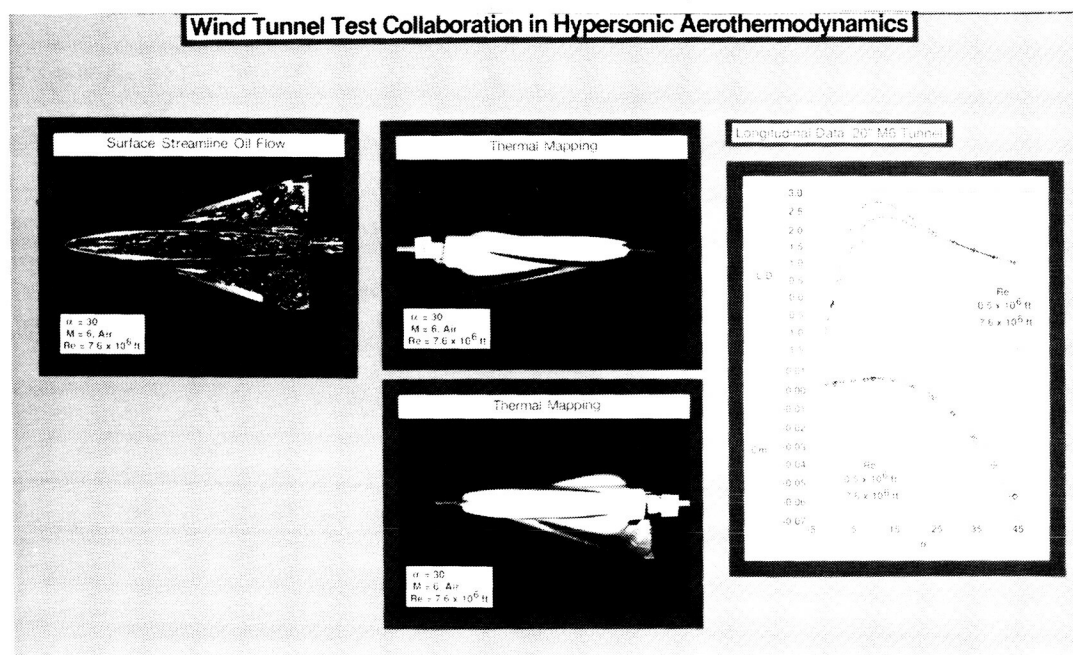


Figure 9.21. NASA/ONERA Cooperative Agreement

9.22 NASA/ONERA COOPERATIVE AGREEMENT: WIND-TUNNEL TEST COLLABORATION IN HYPERSONIC AEROTHERMODYNAMICS

9.22.1 Objective

To (1) develop an aerodynamic/aerothermodynamic database for a generic winged reentry vehicle under a cooperative agreement between NASA and the French agency ONERA (See Figure 9.21) and (2) evaluate test techniques and wind tunnel performance by comparing data from tests in two Langley and two ONERA wind tunnels at Mach 6 and 10 in air.

9.22.2 Approach

Each agency will (1) determine aerodynamic characteristics for a high-fidelity model constructed at Langley by measurement of forces and moments over a range of angle of attack and Reynolds number at Mach 6 and 10 in air and (2) generate a corresponding qualitative aerothermodynamic database by measurement of thermal mappings on models fabricated by the respective agency. The data will be compared at a workshop to evaluate test/measurement techniques.

9.22.3 Accomplishments

A high-fidelity force and moment model was designed, fabricated and tested in the Langley 20-inch Mach 6 and 31-inch Mach 10 tunnels over a range of angle of attack (α) from -2° to 45° and a range of Reynolds numbers. Preliminary analysis reveals that a maximum lift-to-drag ratio (L/D) of about 2.7 at an angle of attack of 11 degrees was obtained at Mach 6 with a stable trim point near 21 degrees. Similarly, a maximum L/D of 2.2 at $\alpha=15^\circ$ was observed for Mach 10 with a trim point at 24 degrees. Immediately upon completion of these tests, the model was sent to ONERA. Models for the phase change paint technique were fabricated and thermal mappings were measured at Mach 6 over a range of angle of attack (α) and Reynolds number. Force and moment and thermal mapping data at Mach 6 were augmented with the measurement of surface streamline patterns by the oil flow technique and with schlieren photographs.

9.22.4 Significance

The aerodynamic model fabrication and testing portion of the Langley commitment to the cooperative agreement is complete and the model is being prepared by ONERA for their tests at Mach 6 and Mach 10.

9.22.5 Status/Plans

Thermal mapping tests will be performed in the 31-inch Mach 10 tunnel to complete the aerothermodynamic portion of the Langley commitment to the agreement. A workshop will be scheduled to compare results obtained in Langley and ONERA wind tunnels and to exchange details of test measurement and data analysis techniques.

Gregory J. Brauckmann
Space Systems Division
Langley Research Center
(804)864-5221

ORIGINAL PAGE
BLACK AND WHITE PHOTOGRAPH



Figure 9.22. Symmetry and Outflow Plane Volume Grids

9.23 GRID GENERATION FOR COMPLEX GEOMETRIC SHAPES

9.23.1 Objective

The Computational Fluid Dynamics (CFD) analysis of complex aerodynamic shapes depends not only on robust CFD software, but also on the ability to construct surface grids on and volume grids about complex geometric shapes. In the past, the construction of such grids has been a laborious and time-consuming task which was limited to relatively simple shapes. The increased reliance on CFD analysis in the design process for such national programs as National Aero-Space Plane (NASP) and Assured Crew Return Capability (ACRC) has focused attention on the need to, in a timely fashion, generate and alter CFD grids.

Currently, an effort is being made to determine appropriate gridding techniques for the ACRC vehicle. Several approaches such as the integration of Computer Aided Design (CAD) techniques into the grid generation process are being evaluated.

9.23.2 Approach

The vehicle surface was defined by spline interpolation of a database constructed from measured cross-sectional shapes of a wind-tunnel model. Surface-smoothing techniques were used to enhance the surface quality before any attempt was made to grid the vehicle. The surface and volume grids were constructed through a combination of algebraic techniques and transfinite interpolation.

9.23.3 Accomplishments

Figure 9.22 shows the grid generated for the ACRC vehicle. The grid in the upper and lower symmetry planes is shown along with the grid at the outflow boundary. The grid was constructed from two grid blocks which allowed greater grid resolution in the vicinity of the vehicle wings. The grid has been used along with the Langley Aerothermodynamics Upwind Relaxation Algorithm (LAURA) code to generate flowfield solutions about the ACRC vehicle at hypersonic speeds and high angles of attack.

9.23.4 Significance

Mathematical techniques and software are available to generate a quality computational grid about a complex configuration like the ACRC vehicle; however, these tools are not mature enough for general use.

9.23.5 Status/Plans

Grid generation is still a time-consuming process which is ill-suited for quickly responding to vehicle design changes. In an attempt to overcome this lack of response time, an effort will be made to integrate CAD software such as Solid Modelling Aerospace Research Tool (SMART) and mature grid generation software such as the Eglin Arbitrary Geometry Implicit Euler (EAGLE) code.

K. J. Weilmuenster
Space Systems Division
Langley Research Center
(804)864-4363

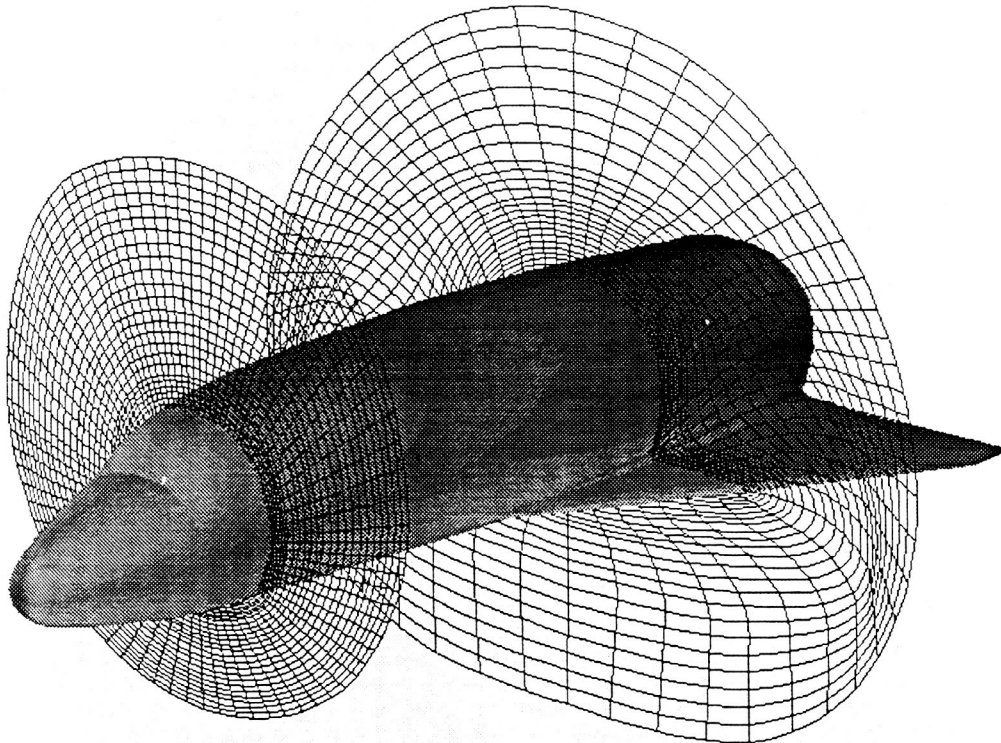


Figure 9.23. Solid Modeling Aerospace Research Tools (SMART)

9.24 SOLID MODELING AEROSPACE RESEARCH TOOLS (SMART)

9.24.1 Objective

To develop a geometry system for the conceptual and preliminary analysis of advanced aerospace vehicles in order to integrate engineering disciplines such as aerodynamics, aerothermodynamics, structures, weights and mass properties

9.24.2 Approach

The approach involved integrating state-of-the-art computer graphics hardware with mathematical surface definitions to develop an easy to use geometry system that can be utilized by all design and analysis codes that require geometric coordinates, derivatives and/or properties (See Figure 9.23).

9.24.3 Accomplishments

Version Two of SMART was completed for generating geometry, creating photo realistic images, computing geometric properties and generating finite elements for wings. Interfaces exist for the Aerodynamic Preliminary Analysis System (APAS), the PATRAN finite element system, the Langley Wireframe Geometry Standard (LAWGS) and the Integrated Geometry Exchange Standard (IGES), which is a standard for the computer-aided design/computer-aided manufacturing industry. External and internal geometry was developed for the Advanced Manned Launch System configurations, the Assured Crew Return Capability (ACRC) vehicle, government and industry National Aero-Space Plane configurations and the Space Shuttle. For the ACRC vehicle, a computational grid was generated and Euler solutions were obtained.

9.24.4 Significance

Productivity and quality of analysis were dramatically improved through reduced modeling time, increased surface fidelity and integrated design and analysis functions.

9.24.5 Status/Plans

Currently, the program is being distributed to industry and a short course is being developed. Surface smoothing and grid generation capabilities for computational fluid dynamics and internal vehicle structure for finite element analysis are under development.

Mark L. McMillin
Space Systems Division
Langley Research Center
(804)864-4521

ORIGINAL PAGE
BLACK AND WHITE PHOTOGRAPH

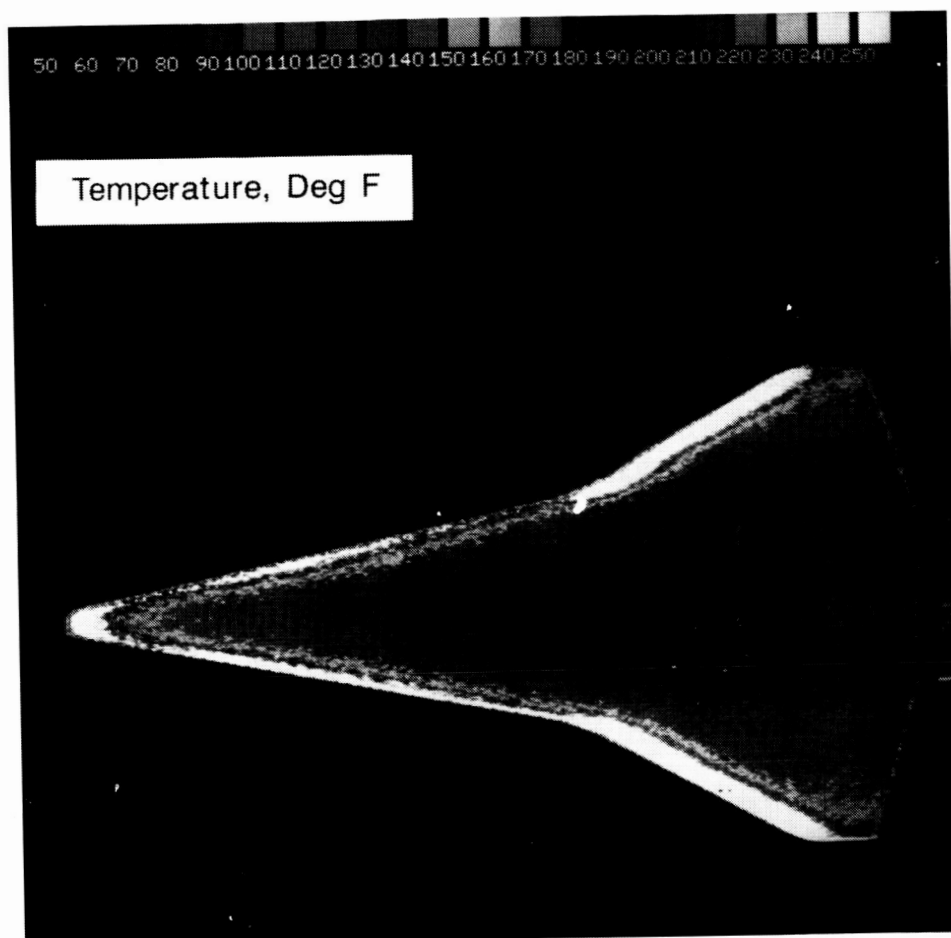


Figure 9.24. Windward Surface Temperature Mapping on a
Transatmospheric Model in 31-Inch Mach 10 Tunnel

9.25 THERMAL MAPPING/HEAT TRANSFER MEASUREMENTS IN HYPERSONIC WIND TUNNELS

9.25.1 Objective

To (1) develop optical (nonintrusive) technique(s) for measurement of quantitative thermal mapping time histories having high spatial resolution in hypersonic wind tunnels and (2) obtain system hardware/software capable of providing detailed heat transfer distributions on models shortly following completion of tunnel run.

9.25.2 Approach

The approach involved developing a thermal imaging technique based on the ratio of blue to green emission from a UV-excited phosphor coating which was applied to the surface of cast ceramic or stycast models (See Figure 9.24). A two-color thermographic system records separately filtered images with a three-tube color camera; data were recorded on analog video tape and images were digitized and processed. NASA developed software to rapidly reduce data to quantitative surface temperature time histories from which heat transfer rates may be inferred. NASA examined the feasibility of using Infrared (IR) thermography to accomplish the same objectives but without the need for coating.

9.25.3 Accomplishments

Highly successful demonstrations of the Langley-developed, two-color thermographic phosphor system were performed in the Langley 20-inch Mach 6 and 31-inch Mach 10 Tunnels on a National Aero-Space Plane (NASP)-like configuration [Langley Test Technique Demonstrator (TTD), data secret]. These demonstrations utilized an advanced image data acquisition and processing computer system. Hardware operation was flawless and minor refinements to the software were performed to optimize performance. Concurrently, an IR thermography system under development at Langley was tested in these same two facilities and preliminary comparisons with other thermal mapping techniques were initiated.

9.25.4 Significance

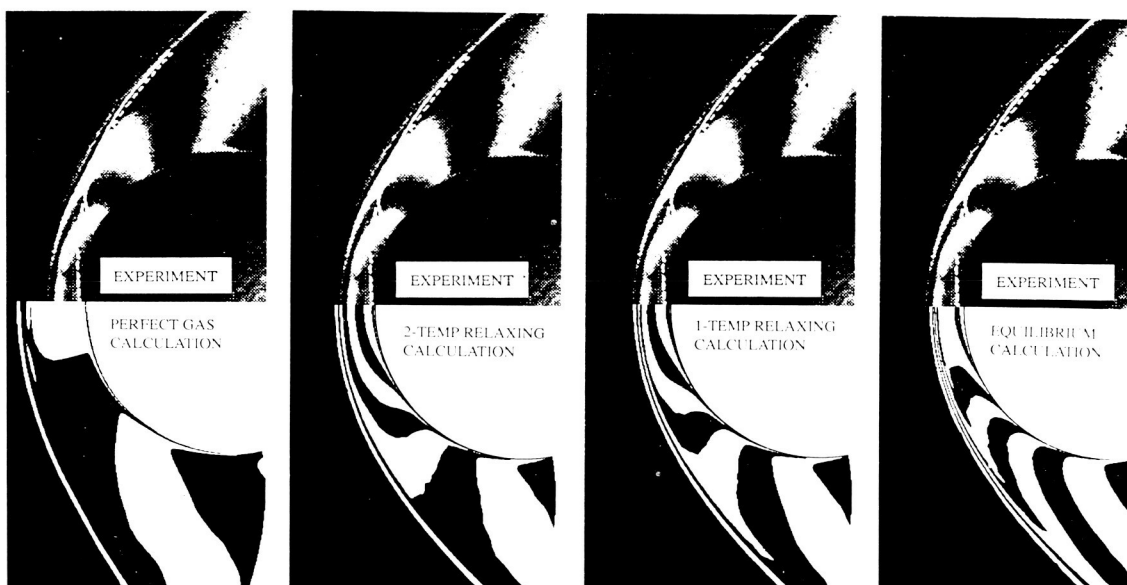
The two-color Thermographic Phosphor System (TPS) provides a unique capability for chromatic image data acquisition, processing and analysis for aerothermodynamic measurements in hypersonic wind tunnels. This technique provides detailed, global, quantitative surface temperature time histories quickly and economically; the TPS is expected to replace the widely used Phase Change Paint Technique (PCPT) because the phosphor system provides a measurement of surface temperature everywhere on the model in view of the camera at a specific time, whereas the PCPT provides only an isotherm and the model does not require recoating after a run. The TPS and IR techniques should essentially eliminate the lag that occurred in the past between the generation of aerodynamic and aerothermodynamic databases.

9.25.5 Status/Plans

Langley personnel are being instructed on the operation of the TPS. System capabilities will be enhanced by additional mass storage and software refinements. Development of the IR technique will continue with emphasis on correcting for emittance variation with temperature and angular direction. Knowledge developed for the Orbiter experiment Shuttle Infrared Leaside Temperature Sensing (SILTS) will be incorporated to provide global heat transfer rates.

Gregory M. Buck
Space Systems Division
Langley Research Center
(804)864-5221

CYLINDER FLOW: GAS = NITROGEN, $M = 6.1$, $T_\infty = 1800$ K, $\rho_\infty = 10^{-3}$ kg/m³, DIA = 5 cm
EXPERIMENT BY HORNUNG (1972), CALCULATION BY PARK AND YOON(CENS2H)



ORIGINAL PAGE
BLACK AND WHITE PHOTOGRAPH

Figure 9.25. Comparison Between Experimental and Computed Interferograms

9.26 COMPRESSIBLE-EULER-NAVIER-STOKES TWO-DIMENSIONAL HYPERSONIC (CENS2H) CODE FOR NONEQUILIBRIUM AIR

9.26.1 Objective

To develop an efficient computer code, Compressible Euler-Navier-Stokes Two-dimensional-Hypersonic (CENS2H), to compute the aerodynamic characteristics of two-dimensional bodies flying in the sub-orbital hypersonic flight speed range in air including the thermo-chemical nonequilibrium effects.

9.26.2 Approach

The compressible Navier-Stokes equations are solved implicitly in two dimensions including the thermo-chemical nonequilibrium effects using the lower-upper symmetric Gauss-Seidel algorithm. The vibrational and electronic excitation and molecular dissociation and the interaction among these processes, are accounted for assuming air to consist of N, O, NO, N₂ and O₂. The steady-state solution is obtained only through the Newton's iteration technique.

9.26.3 Accomplishments

The code was run for an Apollo-like two-dimensional blunt body, a circular cylinder and an airfoil at hypersonic Mach numbers. The solutions are found to converge monotonically to a very small error margin. The computing time is 88 micro-seconds per node-point per iteration. Solutions with an error smaller than 0.00001 are obtained within about 700 iterations, corresponding to a computing time typically of 1.5 minutes for a small grid and of five minutes for a large grid in a Cray X-MP computer. Reasonably accurate aerodynamic coefficients (lift, drag and pitching moment coefficients) can be obtained at fewer than 700 iterations. The density field computed by this code is compared with an experimental data. Agreement was excellent, as shown in Figure 9.25. It is shown also that the aerodynamic coefficients vary by 10 to 20 percent due to the thermo-chemical nonequilibrium phenomena.

9.26.4 Status/Plans

The aerodynamic coefficients will be calculated for a typical hypersonic wing over a wide range of conditions in order to determine the changes in the coefficients due to the thermo-chemical nonequilibrium phenomena. A three-dimensional and time-accurate versions of the code will be developed.

Chul Park
Aerothermodynamics Branch
Ames Research Center
(415)604-5394

Seokkwan Yoon
MCAT Institute
Sunnyvale, CA

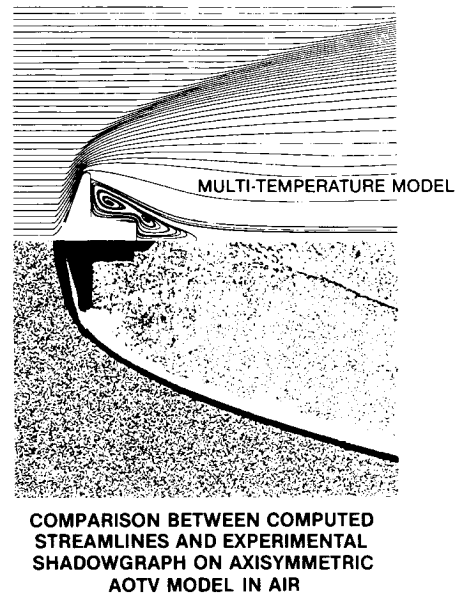
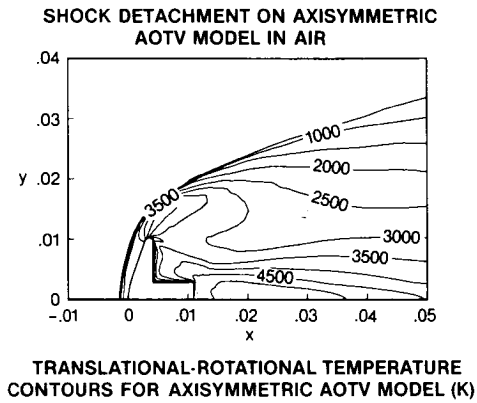
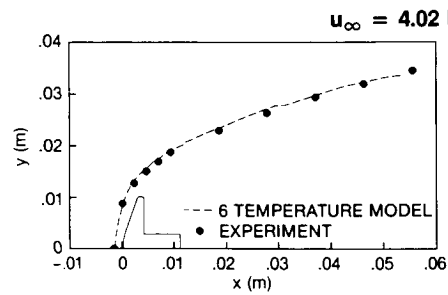


Figure 9.26. 2-D and Axisymmetric Multi-Temperature Navier-Stokes Hypersonic Flow Simulation

9.27 TWO DIMENSIONAL AND AXISYMMETRIC MULTI-TEMPERATURE NAVIER-STOKES HYPERSONIC FLOW SIMULATION

9.27.1 Objective

To develop a numerical method to simulate the flow about hypersonic vehicles in the regime where the flowfield is hot enough that chemical reactions and thermal excitation occur in the gas. Particular emphasis was placed on the part of the vehicle's trajectory where thermo-chemical nonequilibrium is important.

9.27.2 Approach

The motion and thermo-chemical dynamics of the gas in the flowfield were computed by solving the appropriate mass, momentum and energy conservation equations. A separate mass conservation equation had to be solved for each chemical species that was considered. Each dimension of the flowfield required a momentum equation and each temperature that was allowed needed an energy equation. Currently a seven species model for air is employed (chemical species are N_2 , O_2 , NO , NO^+ , N , O and e^-), in two dimensions and with six temperatures (a translational-rotational temperature, a vibrational temperature for each diatomic species and an electron-electronic temperature) for a total of fifteen equations. These equations were solved in a fully coupled manner using an implicit Gauss-Seidel line-relaxation algorithm (See Figure 9.26).

9.27.3 Accomplishments

Results were obtained about a number of vehicle configurations. Numerous calculations were made to compare the computation to experiment with excellent results. An example is the flow about an axisymmetric model of an ASTV flying in a ballistic range at 4.02 km/second. Other calculations include the comparison with a flight experiment of electron number density on a sphere-cone, comparisons of shock shapes and interferograms with experiments and the prediction of the radiation from an ASTV-like vehicle.

9.27.4 Status/Plans

Work is under way to improve the efficiency of the numerical method and the program so that solutions about more complicated vehicles may be obtained. Also studies are being performed to improve the thermo-chemical model and the accuracy of the results. More chemical species will be included and boundary conditions for treating a variety of conditions at the body surface will be implemented.

Graham Candler
Aerothermodynamics Branch
Ames Research Center
(415)604-4227

ORIGINAL PAGE
BLACK AND WHITE PHOTOGRAPH

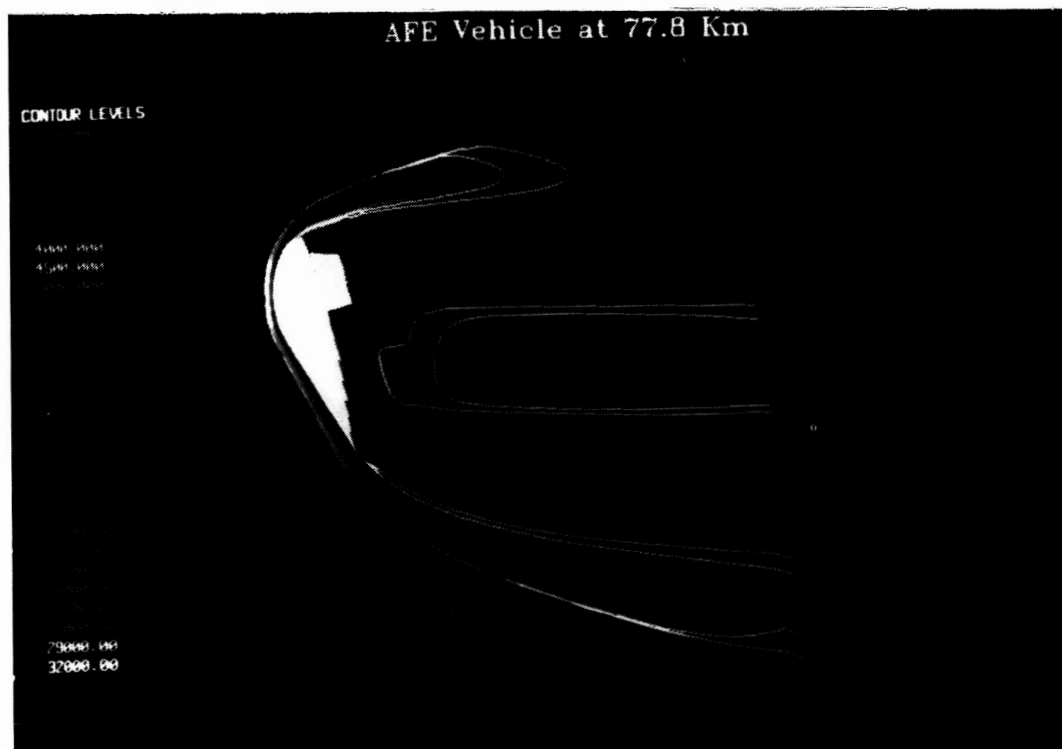


Figure 9.27. Translational Temperature Contours

9.28 THREE DIMENSIONAL NONEQUILIBRIUM FLOW SIMULATION OF THE AEROASSIST FLIGHT EXPERIMENT VEHICLE

9.28.1 Objective

To compute the full, three dimensional flow over the Aeroassist Flight Experiment (AFE) vehicle at one of its trajectory points including the base region. Proper design of both the AFE itself and the experiments to be carried aboard required a detailed knowledge of the flow around the spacecraft.

9.28.2 Approach

The three-dimensional, thin-layer Navier-Stokes equations were solved about the AFE configuration using an explicit, upwind differenced, fully-coupled, thermochemical nonequilibrium code. The two-temperature model of Park accounted for thermal nonequilibrium effects. Seven chemical species were considered.

9.28.3 Accomplishments

A technique of controlling the changes in species mass fractions allows a significantly larger time step than would otherwise be possible with an explicit code. The algorithm has been validated by comparison to a variety of experimental and computational data. Flow was computed over the AFE at an altitude of 77.8 km with a freestream velocity of 8914 m/second. Significant three-dimensional and nonequilibrium effects were seen in the base region. Figure 9.27 shows translational temperature contours over the AFE.

9.28.4 Status/Plans

Additional ionic species will be added to the chemical model. Additional comparisons will be made with results from other continuum codes, direct particle simulations and high Mach number ballistic range results as they become available.

Grant Palmer
Aerothermodynamics Branch
Ames Research Center
(415)604-4226

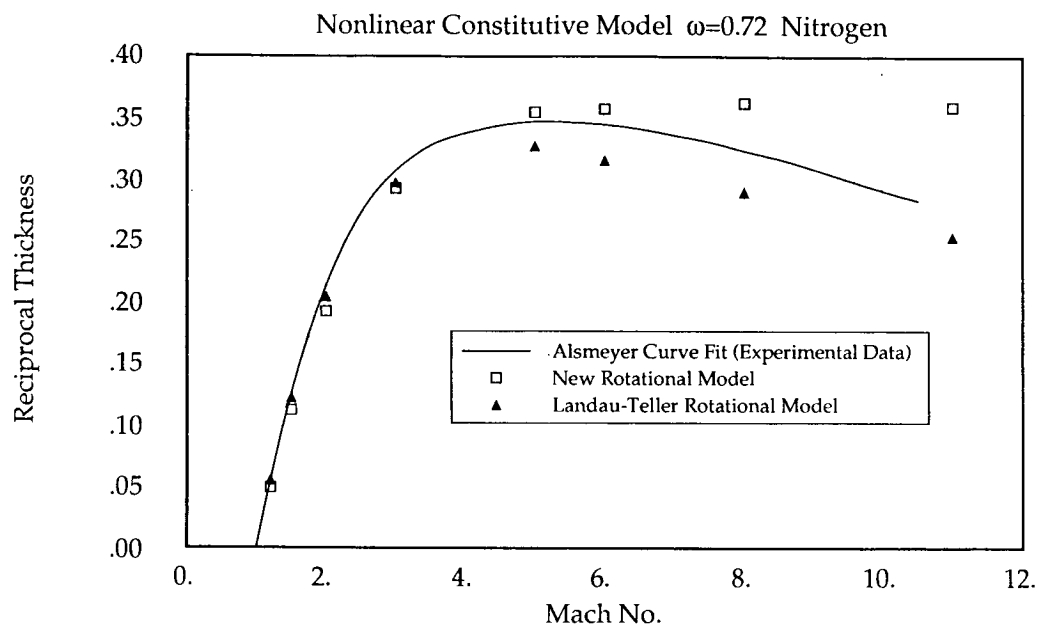


Figure 9.28. Shock Reciprocal Thickness for Two Rotational Models

9.29 CONTINUUM EXTENSION-NONLINEAR TRANSPORT

9.29.1 Objective

To extend the continuum description of fluid mechanics to low density by considering higher order constitutive relations.

9.29.2 Approach

The Chapman-Enskog expansion of the Boltzmann equation was proposed as a method deriving improved constitutive relations. The Navier-Stokes equations are themselves the first order Chapman-Enskog expansion. The Burnett equations, the second order expansion, were proposed as one modification to the constitutive relations. Due to the complexity of the Burnett equations, a simplified nonlinear set of constitutive relations also was proposed. This simplified constitutive model attempted to capture the most significant features of the Burnett constitutive relations with only a slight increase in complexity over the Navier-Stokes equations. Two methods of modeling rotational nonequilibrium were proposed. The first, the widely used Landau-Teller model, is based on assumptions which are violated in hypersonic flow. To determine if the Landau-Teller model is accurate beyond the limits of these assumptions.

9.29.3 Accomplishments

The Burnett constitutive relations (for hard spheres) as well as the simplified constitutive model were applied to shocks in nitrogen. Both the Landau-Teller model and the new rotational model were incorporated into these simulations. Figure 9.28 shows comparison of the shock reciprocal thickness obtained using the simplified constitutive model and those measured experimentally. This constitutive model was used to evaluate (on the basis of shock reciprocal thickness) the accuracy of the two rotational models since it was adjusted to give the experimental reciprocal thickness in argon.

9.29.4 Status/Plans

The new rotational model proposed herein is based on transition rates which are accurate to only 2,000K; therefore, improved transition rates, as they become available, will be incorporated into the new model. Details of the shock structure from both rotational models will be compared to experimental data, if any exists, to determine which model more accurately captures the detailed physics. The Burnett derivation will be generalized to account for more realistic molecular potentials.

Forrest E. Lumpkin and Dean R. Chapman
Stanford University

ORIGINAL PAGE
BLACK AND WHITE PHOTOGRAPH



Figure 9.29. Normalized Temperature

9.30 DIRECT PARTICLE SIMULATION OF HYPERSONIC FLOWS

9.30.1 Objective

To extend the capabilities of a new discrete particle simulation method for rarified hypersonic flows to realistic, three dimensional geometries with non-equilibrium chemistry.

9.30.2 Approach

Direct particle simulation methods model the flow as a large collection of discrete particles that interact with each other through mutual collisions. Simplified physical models may be used to represent these interactions. To restrict the possible results of a collision to a small, predefined subset of all possible outcomes and to choose among these on a quasi-random basis with a minimum of calculation.

9.30.3 Accomplishments

Substantial work was done on the structure of the algorithm to take advantage of the vector and parallel computer architectures now available. Figure 9.29 shows the normalized temperature field of the three-dimensional flow about the Aeroassisted Flight Experiment at 100 km and Mach 35.4. The number of particles used to represent the flow was 9.52 million. This calculation required 4.5 hours of Cray-2 CPU-time and one gigabyte of memory.

9.30.4 Significance

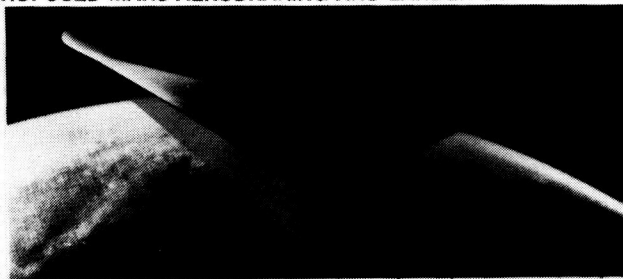
The national interest in hypersonic flight requires a computational predictive capability for the aerodynamic and thermal environment to be found around vehicles such as the proposed aerospace plane or ASTV. Due to difficulties in applying the continuum equations to the very low density hypersonic flight regimes that they will encounter, it is appropriate to consider the application of direct particle simulation methods. The numerical efficiency of the current approach enables direct particle simulations on a much larger scale than previously possible, providing a more viable means for the solution of practical hypersonic rarified flow problems.

9.30.5 Status/Plans

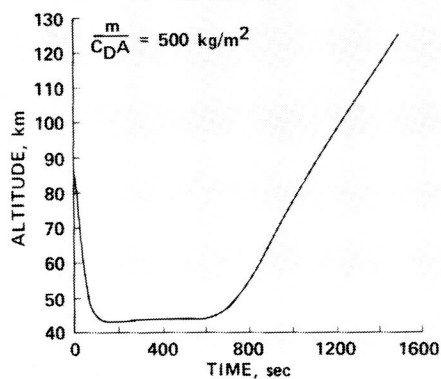
Molecular interaction models now under investigation allow the partition of energy among translational, rotational and vibrational molecular states as well as the representation of multiple chemical species. As additional physical complexity is modeled, computational efficiency will prevail as a prime consideration for algorithm design.

ORIGINAL PAGE
BLACK AND WHITE PHOTOGRAPH

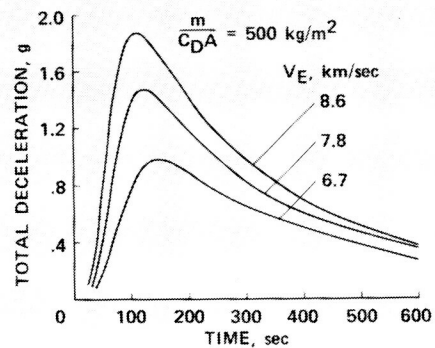
PROPOSED MARS AEROBRAKING AND LANDER CONFIGURATION



ATMOSPHERIC BRAKING
TRAJECTORY ON ARRIVAL AT
MARS AT INERTIAL VELOCITY OF
7.8 km/sec



VARIATION OF TOTAL
DECELERATION IN EARTH G's
DURING ATMOSPHERIC BRAKING



TAUBER

Figure 9.30. High-Energy Aerobraking Conceptual Vehicle Analysis

9.31 HIGH-ENERGY AEROBRAKING CONCEPTUAL VEHICLE DESIGN

9.31.1 Objective

To "tailor" the flight conditions during entry for manned Mars missions which use aerobraking at Mars and at Earth. By limiting deceleration loads during Mars aerobraking and landing, it was possible to avoid the large weight penalty and mechanical complexity required to provide artificial gravity during the voyage.

9.31.2 Approach

The approach involved (1) using a high-lift and high L/D vehicle for aerobraking and landing at Mars, (2) calculating "optimum" entry trajectories and vehicle heating for representative entry speeds of 6.7 to 8.6 km/sec. (for Earth return, entry velocities may range up to 16 km/sec) and (3) studying the heat-shielding requirements.

9.31.3 Accomplishments

Figure 9.30 shows the manned vehicle configuration proposed for Mars aerobraking and landing. Also presented is an aerobraking trajectory at Mars; after atmospheric capture the vehicle enters into a low planetary orbit before landing. The peak deceleration loads are shown to range from one to 1.9 Earth g. Radiative cooling of the vehicle is possible. Earth entries at up to 16 km/sec are being studied; ablative heat shields must be used. Five pertinent AIAA papers have been presented since June 1988, three by Tauber, one by Menees and one by Park.

9.31.4 Status/Plans

The heating calculations will be upgraded by adding recently developed equilibrium shock-layer radiation data for Mars and Earth to the existing codes. The potential effect of Martian atmospheric dust on vehicle design is being studied. The severe deceleration and heating intensities encountered during Earth return will be studied in much more detail, including the effect of using different heat shielding materials.

Michael Tauber, Gene Menees and Chul Park
Aerothermodynamics Branch
Ames Research Center
(415)604-6086

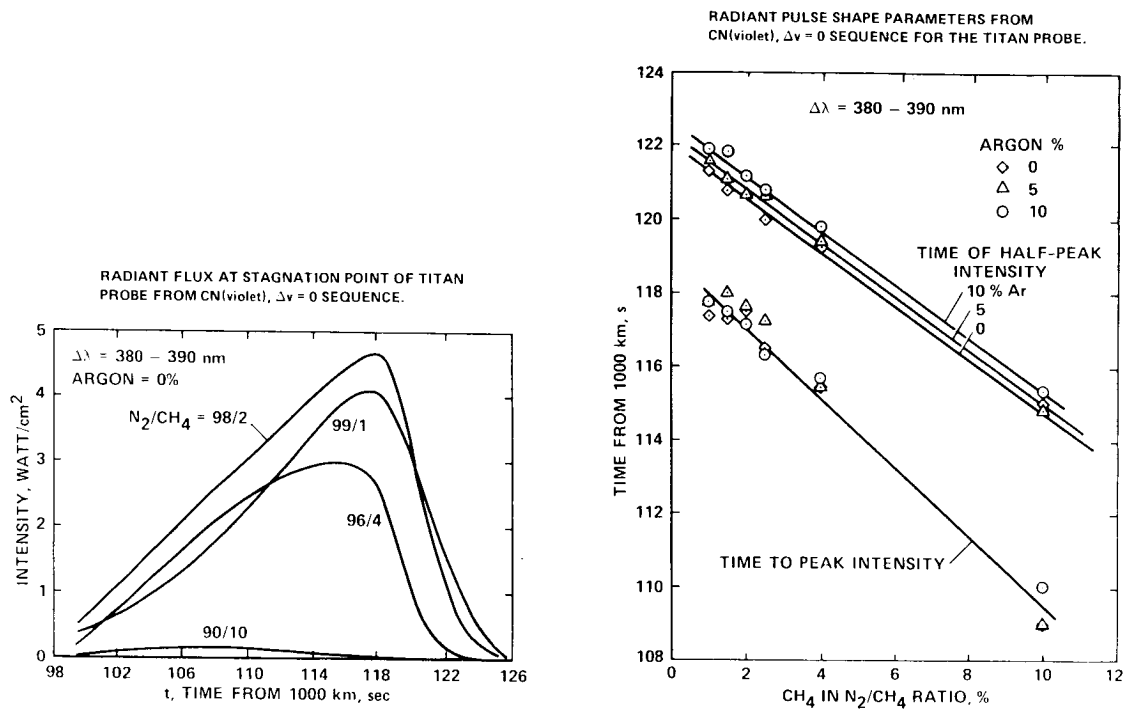


Figure 9.31. Titan Atmospheric Composition from High Velocity Shock Layer Radiation

9.32 TITAN ATMOSPHERIC COMPOSITION FROM HIGH VELOCITY SHOCK LAYER RADIATION

9.32.1 Objective

To develop an in-situ shock layer radiometer experiment to reliably measure shock layer emission during Titan entry and determine the high altitude (200 to 400 km) composition of the Titan's atmosphere. Current knowledge from indirect inference is that its composition is primarily N₂, argon and Methane, but that their uncertainties are large; the mole fraction of N₂ lies between 0.65 and 0.98, argon between 0.0 and 0.25 and CH₄ between 0.02 and 0.10.

9.32.2 Approach

The shock layer will be in thermal and chemical nonequilibrium during most of the Titan atmospheric entry. Calculations were made over a range of possible atmosphere compositions using a version of the Stagnation Point Radiation Air Program that includes important carbonaceous species which will be present in the shock layer. The atmospheric composition is determined from the maximum value of the shock layer radiation within specific wavelength intervals that occur during the entry and the time it takes the maximum radiation to fall to one-half its peak value (See Figure 9.31).

9.32.3 Accomplishments

The results showed that reliable values for the mole fraction of N₂ in the Titan atmosphere can be determined within 0.015, argon within 0.01 and CH₄ within 0.003 using as few as two radiometer channels; one is on the CN (violet) D v=0 sequence, near 380 nm and one is measuring the background radiation. In addition, the nonequilibrium stagnation point heating due to radiation is shown to be important at a velocity of 4.5 km/sec and an altitude of 200 km.

9.32.4 Status/Plans

NASA plans to add more radiating species to the program including the C₂ (Swan), NH(3300), CH(3900), and CH(4300) molecular bands and the N, C and H atomic lines. More accurate spectral information will enable optimum spectral locations for additional radiometer channels to be selected and will increase the accuracy of the radiative heating calculations.

Chul Park
Aerothermodynamics Branch
Ames Research Center
(415)604-5235

H. F. Nelson
University of Missouri-Rolla

E. Whiting
Eloret
Sunnyvale, CA

COWL BLUNT BODY, MACH STEM AND REFLECTED SHOCKS

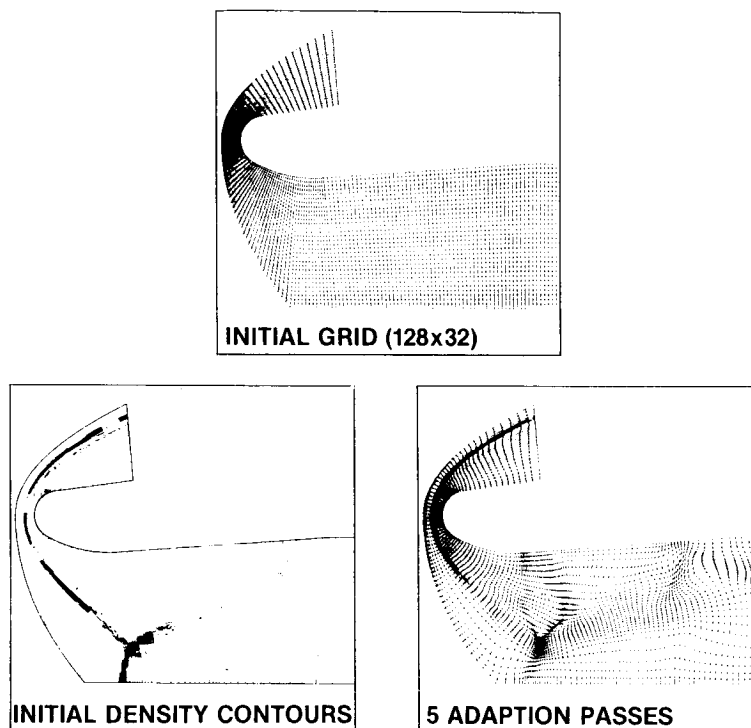


Figure 9.32. 2-D Self-Adaptive Grid Code SAGE -- Example Result

9.33 TWO DIMENSIONAL, SELF-ADAPTIVE GRID CODE, SAGE

9.33.1 Objective

To develop an efficient, robust, user-friendly discretization scheme to optimally distribute grid points for two-dimensional CFD flow codes.

9.33.2 Approach

A code was developed to distribute grid points based on the Nakahashi and Deiwert variational scheme. This method was posed in an algebraic manner and is analogous to redistributing the grid points by minimizing the energy of a system of tension and torsion springs whose strengths are proportional to flowfield gradients at each grid point. Orthogonality and smoothness constraints were imposed to maintain these qualities and user specified maximum and minimum grid spacings determined control constants. Efficiency was assured by using directional splitting concepts and by one-sided constraints that permit marching procedures.

9.33.3 Accomplishments

The SAGE code was applied to a wide variety of flow problems, including the shock impingement on cowl lip problem (See Figure 9.32). Documentation, including a user's manual and sample cases, was prepared and the code was distributed to a large number of users throughout the U. S. Computational efficiency and accuracy of CFD flow codes is greatly enhanced by minimizing the number and optimal placement of grid points required for accurate solutions. Maximum and minimum allowable grid spacings are specified by the user and are used to specify the grid distribution control parameters.

9.33.4 Status/Plans

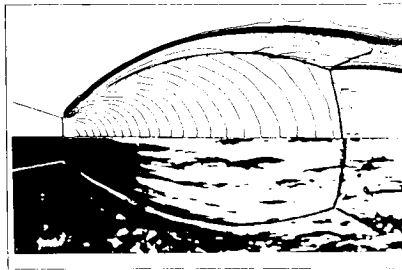
The SAGE code will continue to be upgraded based on information received from the user community. Particular emphasis will be placed on enhanced flexibility and treatment near computational boundaries and in initial grid distribution procedures.

Carol Davies
Sterling Software
Palo Alto, CA
(415)604-6204

Ethiraj Venkatapathy
Eloret Institute
Sunnyvale, CA

George S. Deiwert
Ames Research Center
(415)604-6198

SUPERSONIC AXISYMMETRIC PLUME FLOW
 $M_\infty = 7.3$, $M_j = 2.5$, $P_j/P_\infty = 30.0$
SHADOWGRAPH AND ADAPTED GRID SOLUTION COMPARISON



THREE-DIMENSIONAL TWO-NOZZLE PLUME FLOW PROBLEM
 $M_\infty = 4.22$, $M_j = 2.5$, $P_j/P_\infty = 715.0$

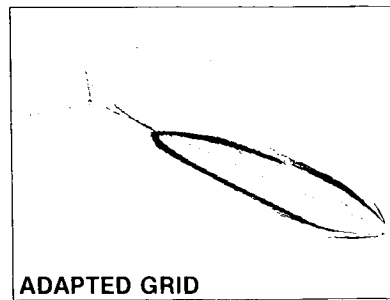
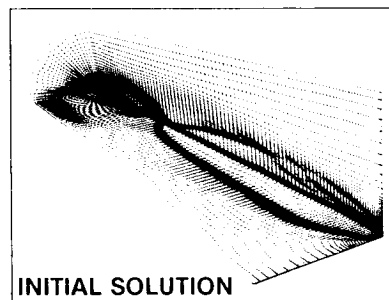


Figure 9.33. 3-D Self-Adaptive Grid Code SAGE 3-D

9.34 THREE DIMENSIONAL, SELF-ADAPTIVE GRID CODE, SAGE 3-D

9.34.1 Objective

To extend the two dimensional Self-Adaptive Grid Code (SAGE) to an efficient grid distribution method for three-dimensional CFD flow codes.

9.34.2 Approach

The approach involved extending the 2-D SAGE self adaptive grid distribution code, which is based on the Nakahashi and Deiwert scheme to three dimensions. This method was based on variational principles and is posed in an algebraic manner. The procedure was analogous to redistributing the grid points by minimizing the energy of a system of tension and torsion springs whose strengths are proportional to flowfield gradients at each grid point. Orthogonality and smoothness constraints were imposed to maintain these qualities and user specified maximum and minimum grid spacings determine control constants. Efficiency was assured by using directional splitting concepts and by one-sided constraints that permit marching procedures (See Figure 9.33)

9.34.4 Accomplishments

The first version of the SAGE 3-D code was developed and results for a variety of applications demonstrated the feasibility of the underlying concept of the approach. The code was successfully applied to complex flowfield problems in high speed regimes associated with generic geometries of bodies such as two nozzle plume flows, the orbital transfer vehicle and the single sided scramjet nozzle configurations.

9.34.5 Significance

The SAGE 3-D code will be further enhanced and made even more user-friendly. The sensitivity of the method to certain critical control parameters such as torsion coefficients which are used to maintain smoothness and orthogonality of the grid will be assessed. A user manual and sample test cases will be prepared for distribution to users requesting this three-dimensional grid distribution code.

M. Jahed Djomehri
NRC Associate
Ames Research Center
(415)604-6198

George S. Deiwert
Ames Research Center
(415)604-6198

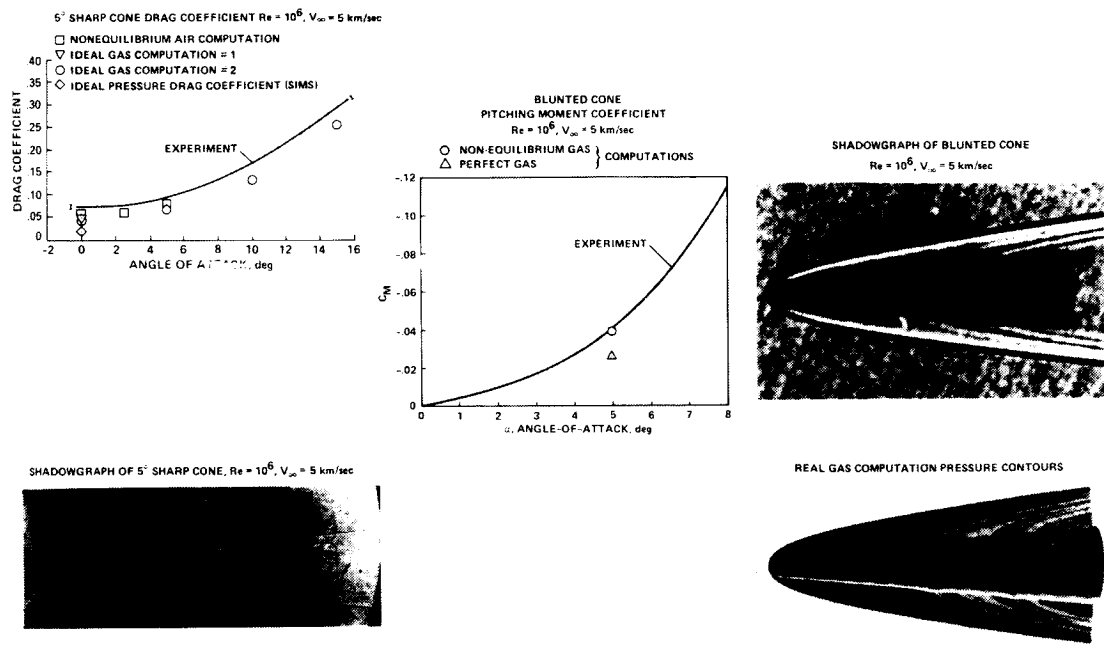


Figure 9.34. Real-Gas Data from Ballistic Range and CFD Validation

9.35 REAL-GAS DATA FROM BALLISTIC RANGES AND CFD CALIBRATION

9.35.1 Objective

To obtain experimental data which exhibit the effects of chemically-reacting flows (real-gas flows) to aid in the understanding of fluid physics in such environments and to calibrate CFD codes for their suitability for predicting flows about full scale vehicles such as the National Aero-Space Plane.

9.35.2 Approach

The approach involved devising and conducting ballistic range tests which provide the basis for understanding real-gas effects and experimental data which can be compared against the results from state-of-the-art CFD computations. These calibrations, when complimented by those from other ground facilities and flight experiments, will provide the database needed to validate that the CFD codes are reliable for the use in the design of full scale vehicles.

9.35.3 Accomplishments

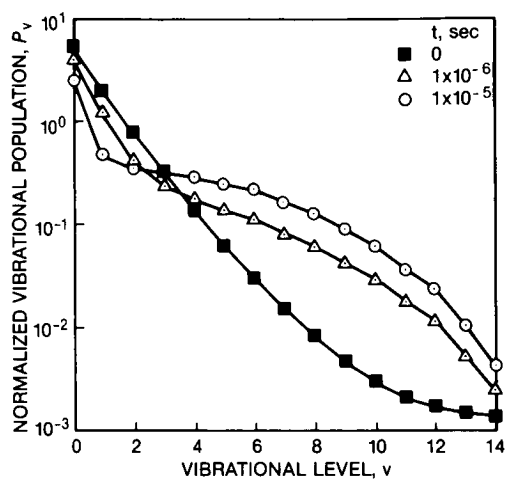
Aerodynamic coefficients for sharp, five degree, half-angle cones were measured at velocities of five and six km/sec and for Reynolds numbers from 0.1 to 1 million where up to 50 percent of the total drag arises from skin friction. Figure 9.34 shows a shadowgraph of the sharp cone in free-flight and a comparison of the measured drag coefficient as a function of angle of attack with PNS codes using nonequilibrium and ideal-gas models. These results indicate that nonequilibrium chemistry is important in computing skin friction and that the codes calibrate well for this parameter. Additional tests have been made with a blunted cone fitted with two shock generators. The figure also shows a shadowgraph from the ballistic range test and pressure contours computed with a combined Navier-Stokes and PNS code which accounts for nonequilibrium chemistry. The pitching moment combined coefficient curve for the blunt cone is compared against that computed at an angle-of-attack of five degrees for cases with nonequilibrium chemistry and ideal gas models. The comparison between computation and experiment indicate that the nonequilibrium code can predict the pitching moment at this angle with good precision and that nonequilibrium effects are important.

9.35.4 Status/Plans

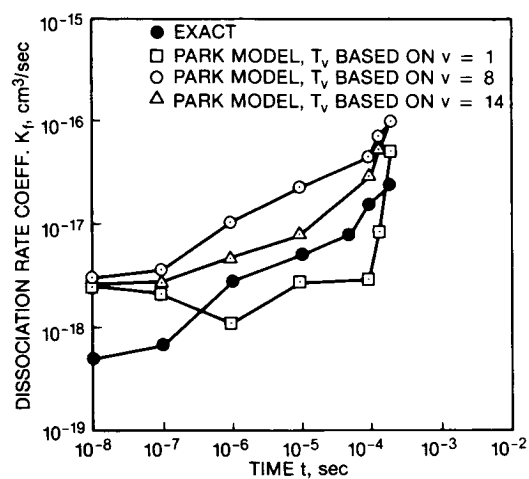
Additional tests will be conducted with flare-cones in air and He-Argon mixtures and the results will be compared with computations to verify the codes ability to predict real gas effects in an environment.

A. W. Strawa
Aerothermodynamics Branch
Ames Research Center
(415)604-3437

S. L. Lawrence
Applied Computational Fluids Branch
Ames Research Center
(415)604-4050



NORMALIZED VIBRATIONAL
POPULATION AT SELECTED TIMES
IN HEATING ENVIRONMENT
 $T_0 = 2000\text{K} \rightarrow T = 3000\text{K}$



DISSOCIATION RATES AS A
FUNCTION OF TIME IN A HEATING
ENVIRONMENT
 $T_0 = 2000\text{K} \rightarrow T = 3000\text{K}$

Figure 9.35. Rates for a Coupled Rotation-Vibration-Dissociation
Phenomenon in Diatomic Molecules

9.36 RATES FOR COUPLED ROTATION-VIBRATION-DISSOCIATION PHENOMENON IN DIATOMIC MOLECULES

9.36.1 Objective

To study the behavior of the dissociation and recombination rates for the coupled rotation-vibration-dissociation phenomena in diatomic molecules undergoing nonequilibrium relaxation in hypersonic flows.

9.36.2 Approach

State-to-state, bound-bound and bound-free transition rates are computed using a quasi-classical trajectory method. These rates are used to obtain numerical solutions to the master equation for rotational and vibrational population densities as well as the bulk thermodynamic properties such as (1) the atomic number density; (2) average energy loss due to dissociation; (3) average vibrational, rotational and combined rotational-vibrational densities and (4) dissociation and recombination rates coefficients (See Figure 9.35).

9.36.3 Accomplishments

Solutions for Hydrogen in constant volume and isothermal cooling and heating environments were obtained. The results indicate that the lower, mid and upper vibrational levels relax at different rates. During the relaxation process the vibrational energy is temporarily transferred to the rotational energy thereby delaying the dissociation process. Average energy loss due to dissociation is found to be as much as 80 to 90 percent of the dissociation energy. It was concluded that the single temperature rate formulation can be used to approximate the exact rates, if a two-temperature geometric average is used and the incubation period is taken into account.

9.36.4 Status/Plans

The computation will be repeated for a series of temperatures to create a database for more accurate formulation of the dissociation and recombination rate coefficients for use in CFD computations. The analysis will be repeated for other molecules, i.e., nitrogen and oxygen.

Surendra P. Sharma
Aerothermodynamics Branch
Ames Research Center
(415)604-3432

David W. Schwenke
Computational Chemistry Branch
Ames Research Center
(415)604-6634

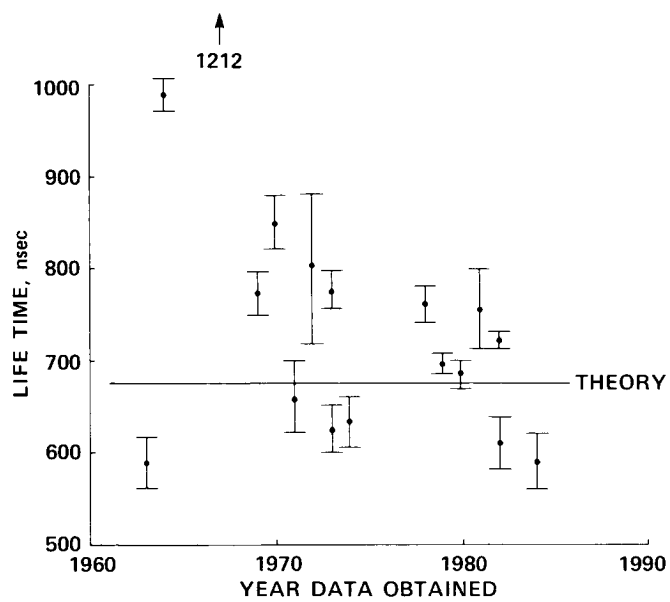


Figure 9.36. OH A² Σ⁺ Life Time

9.37 RADIATIVE PROPERTIES OF THE OH MOLECULE

9.37.1 Objective

To accurately determine via state-of-the-art computational chemistry methods, the radiative and spectroscopic properties of the OH molecule.

9.37.2 Accomplishments

The massive memory of the NAS CRAY 2 was used to calculate "exact" values of the electronic transition moment, dipole moment and radiative lifetimes of the hydroxyl (OH) molecule. These theoretically determined values are typically accurate to two percent which is considerably less than the uncertainty in the existing experimental data. Figure 9.36 is a comparison of the experimental lifetimes (in nanosec.) for the $A^2\Sigma^+$ state of OH with the theoretical value. The theoretical value is represented by the solid line performed in October 1988.

9.37.3 Significance

The OH radical is an important constituent of hydrogen air mixtures that occur, i.e., in the hydrogen burning supersonic combustion scramjets currently being proposed for the NASP. The OH radical also is an important component of the terrestrial atmosphere and of both cometary and interstellar gases. The prevalent occurrence of the OH molecule in these sources makes it an ideal candidate for diagnostic purposes and consequently it is used in all combustion facilities for this purpose. It is used to determine temperature profiles and the OH concentrations deduced from the various sources serve as validation for theoretical models.

9.37.4 Status/Plans

Radiative intensity factors for air and air plus hydrogen will be determined to enable the CFD/Aerothermodynamics simulation of real gas hypersonic flows. In addition, radiative intensity factors for planetary and ablation product species will be determined.

David M. Cooper
Computational Chemistry Branch
Ames Research Center
(415)604-6213

N_2 1 POS. SYS. $A^3\Sigma_u^+ - B^3\Pi_g$

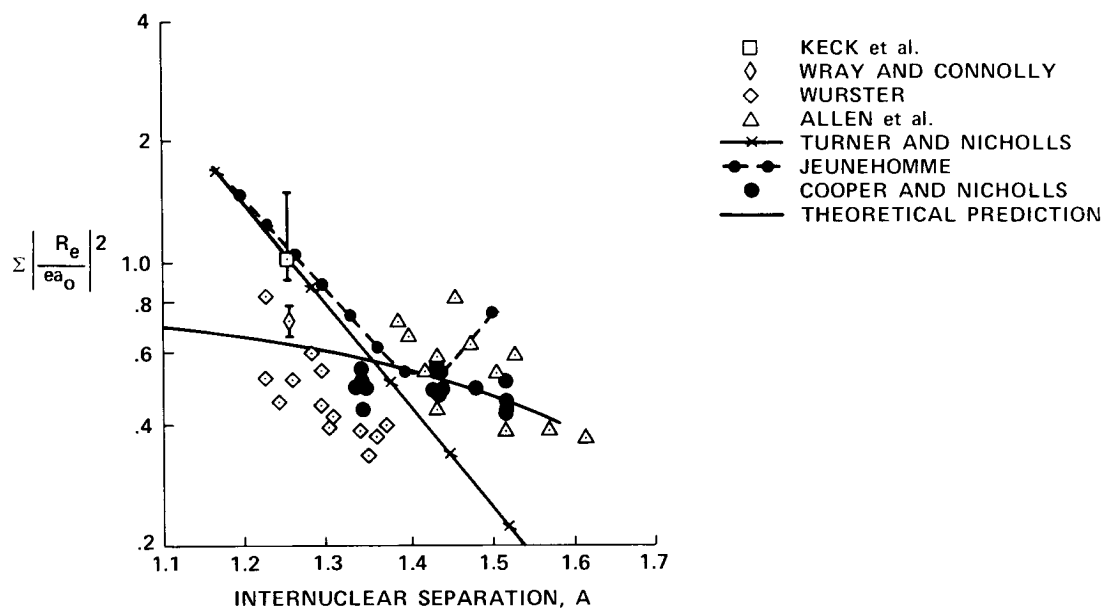


Figure 9.37. Electronic Transition Moments

9.38 RADIATIVE INTENSITY FACTORS FOR AIR SPECIES

9.38.1 Objective

To accurately determine the radiative intensity factors (transition moments, lifetimes, Einstein A-coefficients) for all strongly radiating systems in air. These factors were calculated using state-of-the art computational chemistry methods.

9.38.2 Accomplishment:s

The radiative intensity factors (electron transition probabilities which control the absolute strength of radiation from transitions in molecules) for all strongly radiating transitions in N₂, O₂, NO, N₂⁺ and O₂⁺ were determined. State-of-the-art computational chemistry methods were used to obtain these results. Figure 9.37 is a comparison of the theoretical value (represented by the solid line) of the electronic transition moment for the N₂ First Positive System (transition: A ³Σ_g⁻ - B ³Π_g) with experimental data. As illustrated, there is considerable scatter in the experimental data. The theoretical data are accurate to plus or minus two percent.

9.38.3 Significance

In order to accurately predict the radiative heating of a vehicle as it enters a planetary atmosphere or one which travels at high speeds in a dense atmosphere, the radiative intensity factors for atoms, molecules and ions must be known. The present results will allow the CFD/Aerothermodynamic codes (assuming they realistically model the Flowfield chemistry and physics) to accurately determine the radiative heating rates encountered by vehicles traveling in air.

9.38.4 Status/Plans

Radiative intensity factors will be determined for planetary and ablation product species.

David M. Cooper
Computational Chemistry Branch
Ames Research Center
(415)604-6213

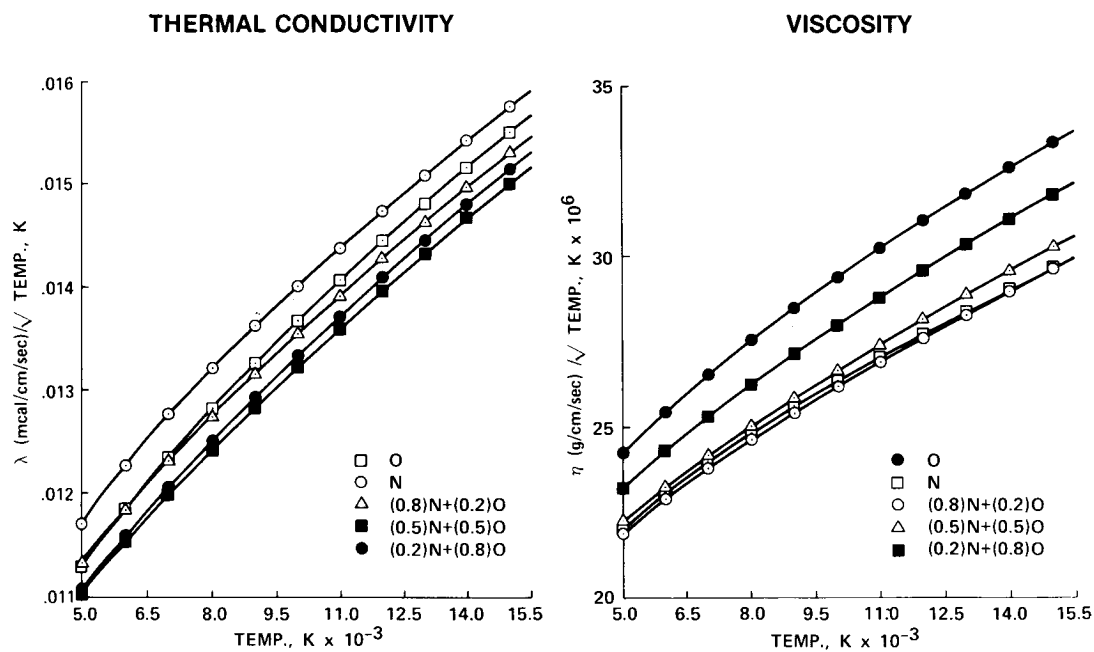


Figure 9.38. Transport Properties for Air Species

9.39 TRANSPORT PROPERTIES FOR AIR SPECIES

9.39.1 Objective

To provide accurate, high-temperature transport properties (viscosity, thermal conductivity and diffusion coefficients) for air species.

9.39.2 Approach

A general computer code was developed and used to accurately predict high-temperature transport properties of air species. This work incorporated three major improvements, (1) accurate representation of the potential interaction curves for a large number of interacting atomic, ionic and molecular species; (2) use of spline curves to fit the potential data with no apriori constraints as to the functional form and (3) incorporation of quantum effects such as tunneling, resonance charge exchange and nuclear symmetry effects. State-of-the-art computational chemistry calculations were performed to obtain the potential energy curves.

9.39.3 Accomplishments

Potential energy curves and collision integrals were determined for ground state interactions of N-N, O-O, N-O, N-O⁺, N-N⁺ and O-O⁺. All states for which the molecule dissociates into ground state atoms were included in the calculations. The results include accurate potential energy curves for the higher-lying states which were previously unknown. The results demonstrate that for some species, i.e., NO, the major contribution to the collision integrals comes from the higher-lying states. The nine collision integrals needed to determine transport properties to second order were calculated and are tabulated for translational temperatures from 250 K to 100,000 K. Figure 9.38 shows plots summarizing selected transport properties.

9.39.4 Significance

Transport properties involving high-temperature air species are required for a real gas analysis of both the equilibrium and non-equilibrium shock-layer flows about Aeroassisted Space transfer vehicles (ASTVs) during their aerobraking maneuvers in the earth's atmosphere and for design studies of both generic and specific hypersonic vehicles. These results, when completed and coupled with electron and molecular interaction data,, will allow the complete modeling of the transport properties of high-temperature air.

9.39.5 Status/Plans

The energies and collision integrals for N⁺-O interactions will be completed. Atom-molecule interactions and transport properties similar to those described also will be calculated. Transport properties for high-temperature air accounting for all contributions from atoms, ions, molecules and electrons will be determined.

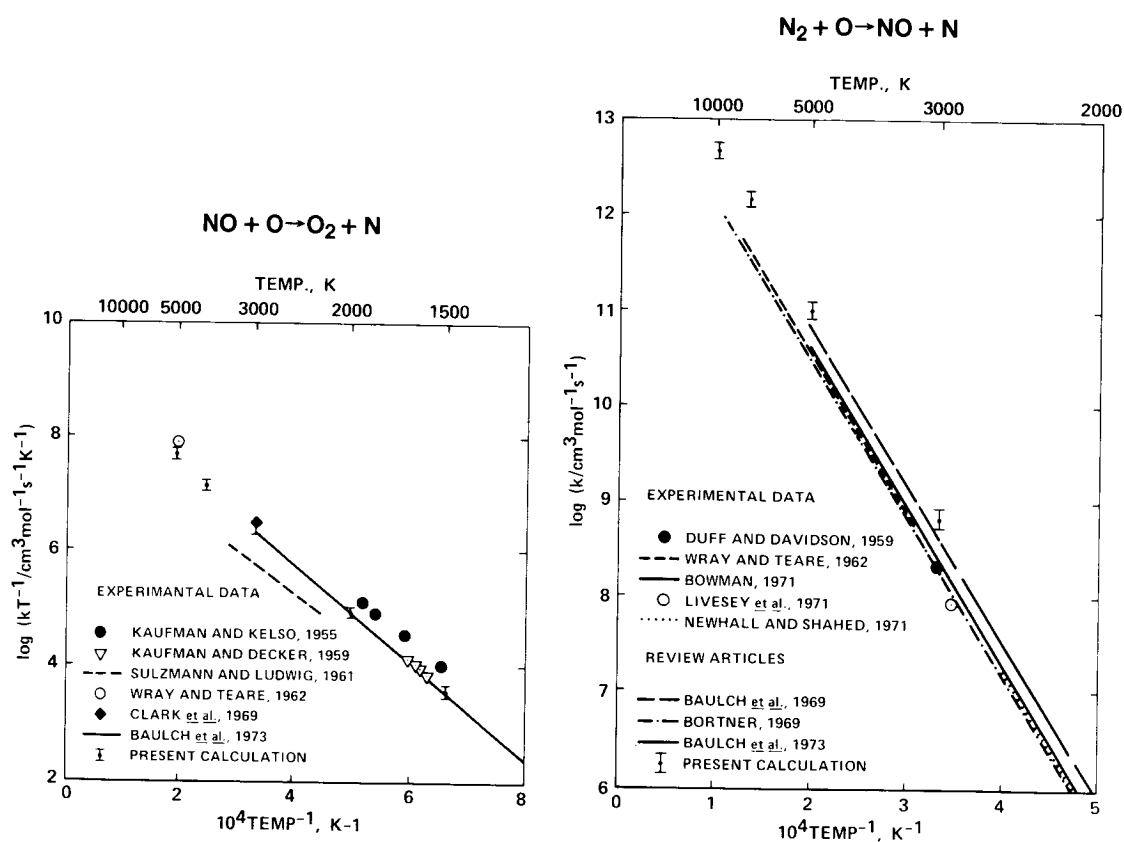


Figure 9.39. Reaction Rate Constants

9.40 REACTION RATE CONSTANTS

9.40.1 Objective

To calculate high temperature reaction rate constants for air and air plus hydrogen species.

9.40.2 Approach

Theoretical studies to calculate the rate constants of selected reactions for air ($T=500$ - $5,000$ K) and hydrogen-air mixtures ($T<5,000$ K) are in progress. The theoretical determination of these rates is a three-step process. The first step is the calculation of the accurate ab initio potential energy surface (PES) which represents the interaction energy between the reacting species at any geometrical arrangement of the atoms. The PES is related to a map of the forces between the species during a collision leading to the reaction. The second step is the analytical fitting of the PES data points generated under step one to a mathematical expression that can be used to calculate the interaction energy of the system for any geometrical arrangement of the atoms. This represents both interpolation and extrapolation of the set of PES data points. The resulting expression must duplicate the ab initio PES data and not exhibit any extra local maxima or minima. The final step is the classical mechanical simulation of individual collisions between the reactants generated from the PES expression derived in step two. A large ensemble of such simulations (each one is called a trajectory) is used to determine cross sections and rate constants.

9.40.3 Accomplishments

Reaction rate constants were determined for several reactions. Figure 9.39 shows plots comparing the calculated results with experimental data. The experimental data included in the figure is not intended to be complete, but is only representative of that available in the literature. The calculated rate constants have an uncertainty of ± 20 percent. As illustrated in the figure, the theoretical rate constants complement low temperature data and provide data at higher temperatures where little or no experimental data exists; furthermore, the calculated reaction rates, i.e., $H+H+H_2 \rightarrow H_2+H_2$, often provide clarity to a confusing maze of experimental data.

9.40.4 Significance

Accurate calculations of the flow-fields around hypersonic vehicles such as the NASP and ASTV must account for real-gas effects. Rate constants for chemical reactions of air species at high temperatures are crucial to these calculations. Experimental rate constants are seldom available and almost impossible to obtain at high temperatures. Consequently, computational chemistry methods represent the only alternative to obtaining these critical rates.

9.40.5 Status/Plans

The calculation of reaction rate constants will continue for both air and air plus hydrogen species. In particular, the rate constants for selected three body recombination reactions will be determined. These reactions have the largest experimental uncertainties and are among the most difficult to measure.

David M. Cooper
Computational Chemistry Branch
Ames Research Center
(415)604-6213

CHAPTER TEN

HYPERSONIC AERODYNAMICS

10.1 INTRODUCTION

NASA currently is pursuing hypersonics in two programs, (1) the relatively shorter-term National Aero-Space Program (NASP), which is the dominant hypersonics program and (2) the longer-term Generic Hypersonics Program which is scheduled to replace the NASP Technology Maturation Program (TMP) efforts. The current NASP program, including the TMP, constitutes "source material" which highlights areas that are technological imperatives for air-breathing hypersonic vehicles. The generic program addresses related fundamental aspects of these issues without commitment to any particular mission. NASP activities address the development, test, analysis and design methods for the aerodynamic, aerothermodynamics and CFD codes for application to hypersonic cruise and transatmospheric vehicles. The work includes analytical and empirical evaluation of performance as well as trade-off benefits/penalties resulting from integration of speed range. In addition, this activity is directed to the development of advanced computational flow methods that were fully tested, verified and converted to design tools for use by industry. This work in external aero/aerothermodynamic CFD methods is to develop and extend both generic and specific code techniques to specific vehicle configurations of interest. These codes will be verified and tested for accuracy through benchmark experimental testing and comparison with reference cases.

The Hypersonic Aerodynamics Program is a long range endeavor directed toward a fundamental understanding of the physics and chemistry of gas dynamic behavior as it pertains to slender, air-breathing hypersonic vehicles that use highly integrated airframe/propulsion systems. It focuses on key and enabling technologies in hypersonics with the aim of establishing a robust hypersonic database to satisfy the very demanding aerospace vehicle requirements for future NASA/DoD missions. Key problems exist in the areas of hypersonic boundary layers (esp. turbulent), mixing and combustion at supersonic speed, real gas effects at high temperature and rarefied flows at high altitude. Research is being conducted in four main areas.

10.1.1 Configuration Aerodynamics

This activity involves developing a database and establishing methods for the full integration of air breathing propulsion systems into super/hypersonic vehicles. The state-of-the-art in high Mach number vehicle integration was attempted six times and is contained in the 25-year-old, SR-71 design. This program will conduct aerothermodynamics research in the definition of the forebody flowfield and boundary layer development; inlet location and angle-of-attack effects, nozzle exhaust flowfield, afterburning, thrust vector changes and nonaxisymmetric nozzle effects on the vehicle afterbody. The relationship between airframe/propulsion integration effects and the stability and control and performance of such vehicles is a primary product of this research. Wind tunnel simulation techniques, powered and unpowered cold gas test techniques and CFD results will be used in developing ground-to-flight scaling procedures.

A fundamental research activity is underway to assess the aerodynamic behavior of a class of high L/D shock-exploiting planforms known as waveriders. These configurations are believed to be optimum for hypersonic cruise. Advances are being made in using inverse techniques based on given arbitrary shock shapes and of the evaluation of the tip-to-tail performance of a propulsion-integrated cone-derived waverider cruise vehicle. Future waverider studies will emphasize off-design performance and higher order effects (viscous interaction and chemically reacting flows).

10.1.2 Hypersonic Flight Physics

Research focuses on Boundary Layer Transition Physics and modeling, turbulence physics and modeling, real-gas effects and rarefied flows. Boundary layer transition strongly dominates the design of a scramjet engine inlet, affects the overall drag from vehicle components, influences the choice and selection of materials, controls the heat loads a vehicle must sustain and may determine overall mission success or failure. The calculation and prediction of this condition at hypersonic speeds is currently based on empirical data and the wide safety excessive vehicle weight and performance compromises. The NASP program has initiated an interim program to provide a near term set of design criteria that will be utilized for the X-30 research vehicle. The Generic Hypersonics program provides a sustained NASA in-house effort, with major support from industry and academia, utilizing the unique NASA facility and computational assets, to develop a general design code formulation for boundary layer transition and high-speed mixing phenomena. This program requires the "quiet tunnels" capabilities, major efforts in theoretical studies, significant advances in non-intrusive diagnostic instrumentation and the conduct of several carefully constructed flight research experiments, such as HYFIRE or SWERVE, to assure that "real" flow effects were understood and incorporated in the design code formulation.

10.1.3 Flight Experiments Research

A small continuing research program directed at several specific deficiency areas is required, including the development of a national capability for the conduct of dedicated and piggyback research flight experiments, airborne inflight instrumentation and vehicle stability and control concepts and simulation. Reactivation of flight research capability at Wallops Flight Facility with the proposed HYFIRE Program and consideration of a SWERVE vehicle will be studied. Dedicated remote sensing and airborne measurement instrumentation systems are required and flight definition research activities will be initiated. Generic baseline concepts for an accelerator and cruise vehicle will serve as the basis for research activities in stability and control, engine airframe control integration and advance control concepts. Selected simulation concepts will be developed for specific research activities. A current low-cost flight experiment is on-board PEGASUS. NASA will conduct an aerothermal survey of the winged first stage to Mach 8.7.

10.1.4 Hypersonic Facilities Research

The demand for ground-based testing, the physical limitations of scale size, inadequate test duration and lack of availability of sufficiently high enthalpy to simulate

hypersonic flight conditions, require that advanced facility concepts be explored. These include very large megawatt arc-heating concepts, larger pulse facilities using advanced driver concepts, Ram accelerators, electromagnetic launchers, etc. Research is also underway to address the "new" issue of flow quality (free stream contamination, chemical and flow dynamics-sound, dynamic vorticity) through investigation of concepts for low-disturbance operation.

10.1.5 Summary

The overall Hypersonic Aerodynamics Program complements the ongoing NASP Technology Maturation program and provides an expanded technology base for future vehicles and NASP improvements through long-term activities in fundamental and applied research in hypersonics. In particular, it advances the high pay-off technologies identified in the NASP program but without reference to specific applications.

Program Manager: Dr. Isaiah M. Blankson
OAST/RF/RN
Washington, DC 20546
(202)453-5420

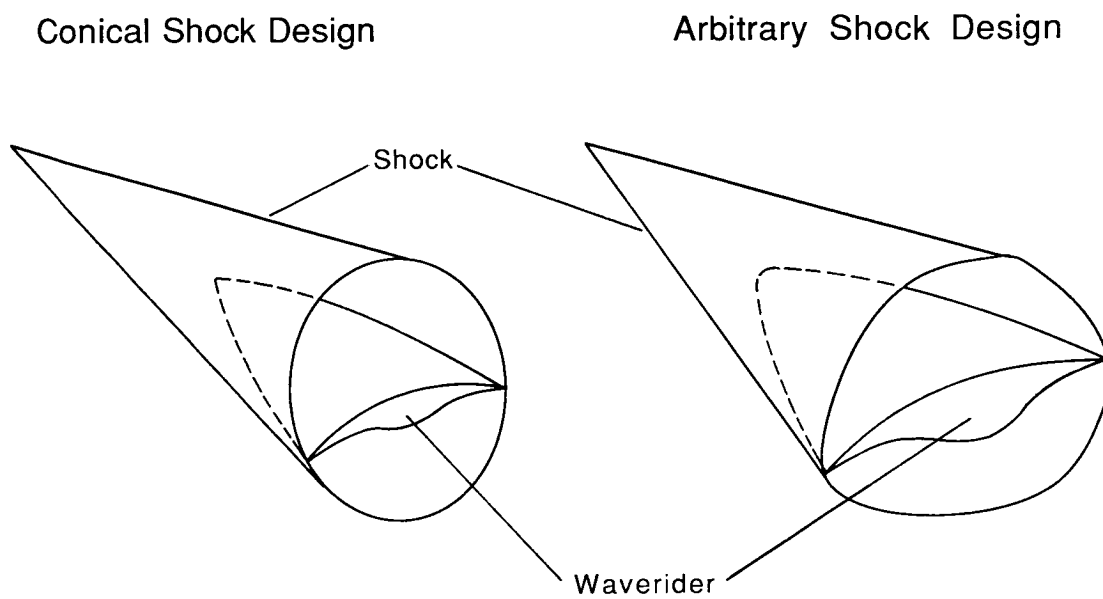


Figure 10.1. Inverse Waverider Design

10.2 INVERSE WAVERIDER DESIGN

10.2.1 Objective

To develop an approach utilizing the three-dimensional Euler equations for the inverse design of hypersonic waveriders based on arbitrary shock shapes.

10.2.2 Approach

Previous investigators developed methods for the inverse design of hypersonic waveriders based on conical shock shapes. The approach utilized the three-dimensional Euler equations for the inverse design of waverider shapes based on shock shapes (See Figure 10.1). A series of waverider geometries is being designed using this method and is being evaluated with higher order methods such as Euler and Navier-Stokes codes. Performance benefits of the arbitrary shock generated waveriders are being determined through comparison with the conical shock generated waveriders. The study is being conducted under a grant to the University of Colorado.

10.2.3 Accomplishments

The inverse solution marching algorithm was developed and applied to a computer code. Using this code, waverider geometries were generated for conical shapes to validate the code.

10.2.4 Significance

These methods will provide for optimization of hypersonic waveriders which will not be limited to configurations based on conical shock shapes.

10.2.5 Status/Plans

The generation of waverider geometries from arbitrary shock shapes is being evaluated using a thin-layer Navier-Stokes solver. If significant performance benefits are predicted from this study, wind-tunnel models will be built and tested to validate the code results.

Steven X. S. Bauer
Supersonic/Hypersonic Aerodynamics Branch
Langley Research Center
(804)864-5946

ORIGINAL PAGE
BLACK AND WHITE PHOTOGRAPH

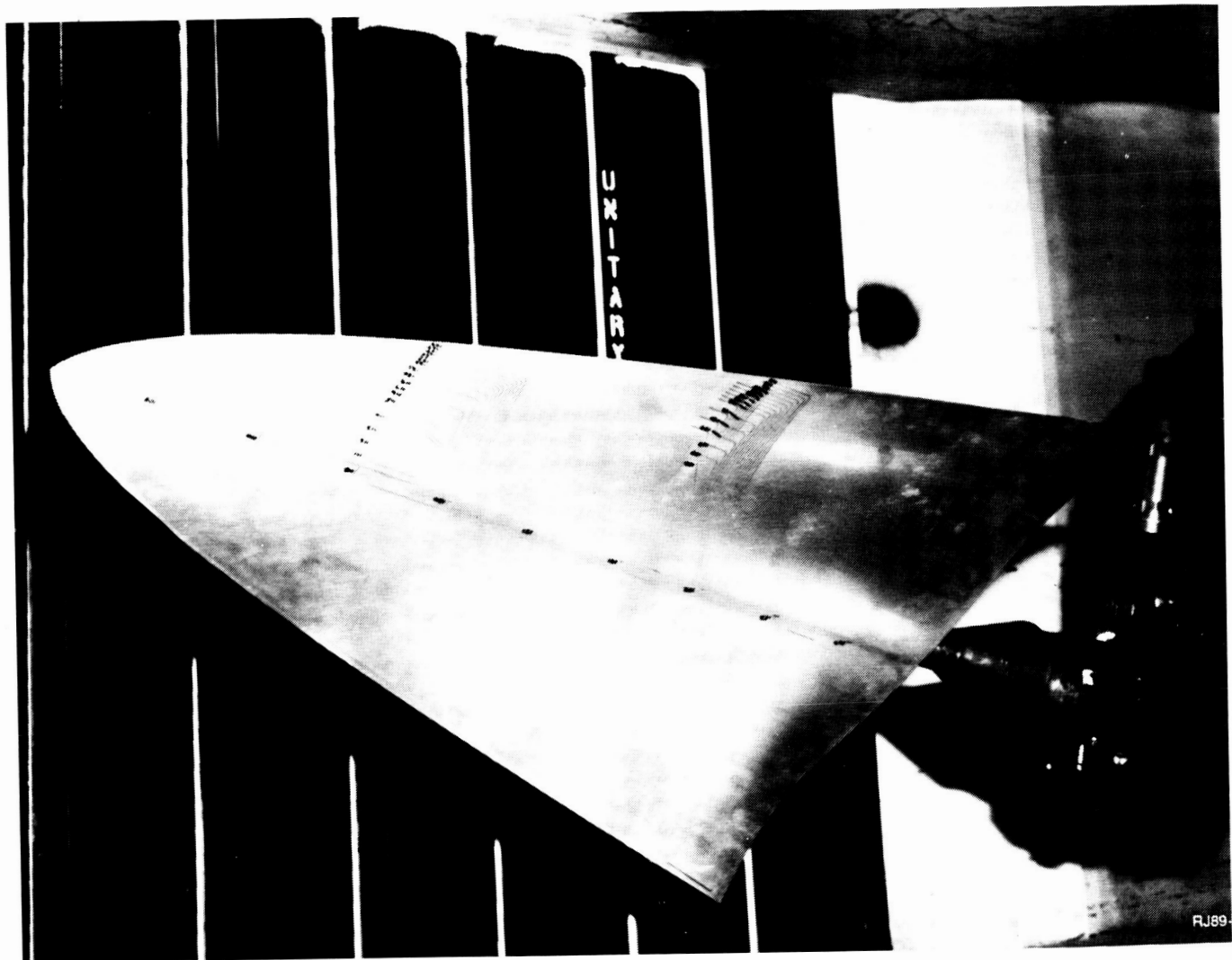


Figure 10.2. Mach 4 Turbulent Waverider

10.3 EVALUATION OF OPTIMIZED WAVERIDERS

10.3.1 Objective

To (1) evaluate a hypersonic cone-derived waverider optimization code and (2) determine the aerodynamic performance benefits of waverider configurations.

10.3.2 Approach

A hypersonic, cone-derived waverider optimization developed under a grant at the University of Maryland was used as the design tool for the waverider geometries. Validation of this code was accomplished through comparison with wind tunnel data obtained on several test geometries. In addition, the aerodynamic benefits of the waverider shapes were assessed by comparison with flat wing shapes of the same planform and volume (See Figure 10.2). Finally, the capability of full-potential, Euler and Navier-Stokes codes to predict waverider aerodynamic characteristics was assessed.

10.3.3 Accomplishments

The optimization code was exercised over a wide Mach number range to assess any limitations in the code. Turbulent Mach 4 and Mach 6 configurations were designed. Two flat reference configurations also were designed in which the same cross-sectional area distribution was preserved. The Mach 4 design was tested in the Unitary Plan Wind Tunnel over a Mach range of 1.5 to 4.5.

10.3.4 Significance

The optimization code was verified experimentally at Mach 4, thus proving that high levels of aerodynamic performance are possible with waverider configurations.

10.3.5 Status/Plans

Wind tunnel testing of the other models is scheduled for late 1989 and early 1990. Euler and Navier-Stokes analyses of all the configurations also are planned.

Steven X. S. Bauer
Hypersonic Aerodynamics Branch
Langley Research Center
(804)864-5946

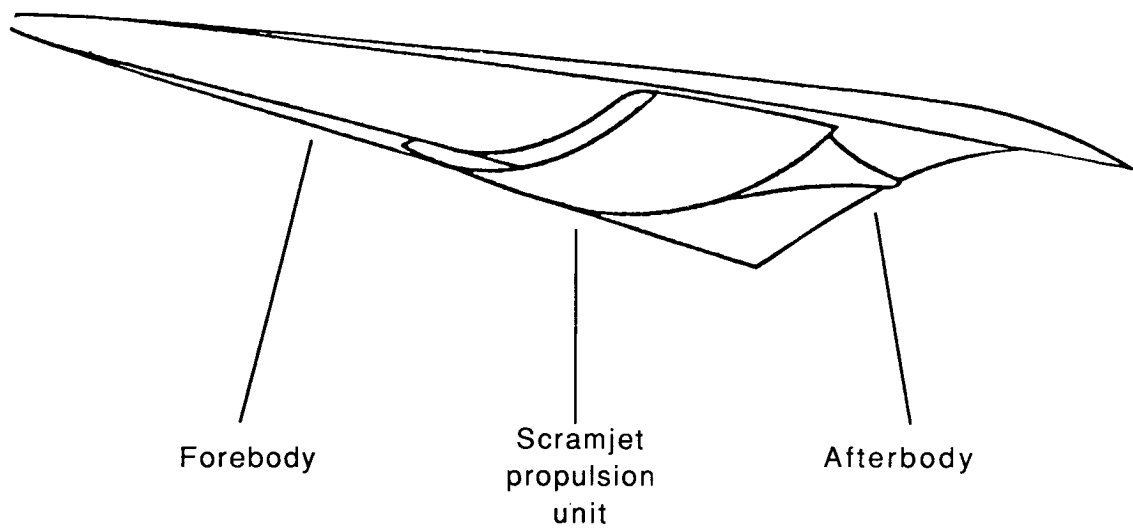


Figure 10.3. Conceptual Design and Optimization of Waverider Configurations

10.4 CONCEPTUAL DESIGN AND OPTIMIZATION OF WAVERIDER CONFIGURATIONS

10.4.1 Objective

To develop an approach to integrate a forebody (waverider), an engine package (scramjet) and an afterbody (nozzle) into a hypersonic vehicle.

10.4.2 Approach

Initially, codes to design waverider forebody shapes and to size the nozzle given the combustor characteristics will be developed. Parametric studies are being conducted to develop optimized geometries for analysis using higher-order codes supplied by NASA (See Figure 10.3). The forebody, combustor and nozzle design codes are being combined into a single design package upon verification of each code. The study is being conducted under a grant to the University of Oklahoma.

10.4.3 Accomplishments

The individual components of a waverider design code were developed. A simple method for estimating combustor size was implemented and a nozzle geometry can be produced by means of the theory of minimum length nozzles.

10.4.4 Significance

The unified method developed in this study will facilitate the design of hypersonic waverider configurations.

10.4.5 Status/Plans

Analysis of several optimized configurations is planned with the higher order methods.

Steven X. S. Bauer
Supersonic/Hypersonic Aerodynamics Branch
Langley Research Center
(804)864-5946

ORIGINAL PAGE
BLACK AND WHITE PHOTOGRAPH

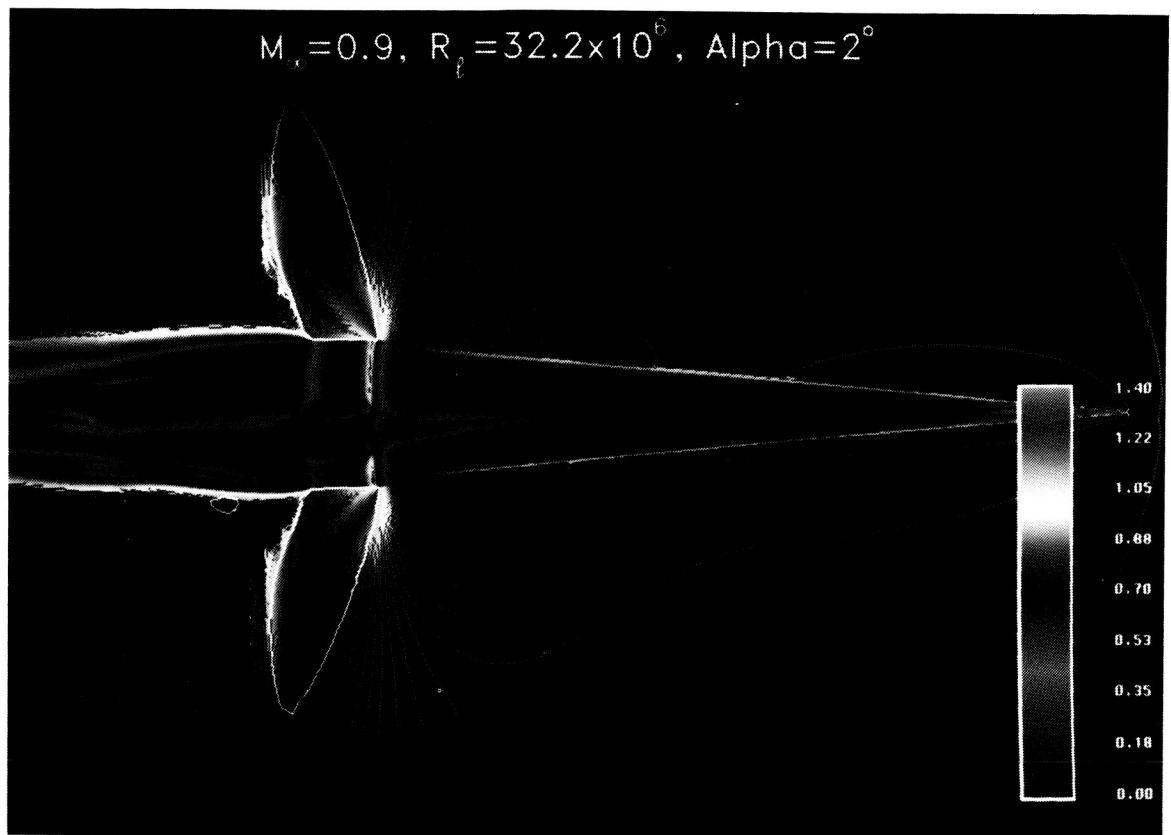


Figure 10.4. Navier-Stokes Mach Contours

10.5 TRANSONIC NAVIER-STOKES SOLUTIONS ABOUT A COMPLEX, HIGH-SPEED CONFIGURATION

10.5.1 Objective

To develop transonic aerodynamic predictions for a National Aero-Space Plane (NASP) class of configurations, using advanced Navier-Stokes methodology.

10.5.2 Approach

An accelerator configuration recently tested in the Langley 16-foot Transonic Tunnel was selected for the study. This model was comprised of a cone-cylinder-frustum body, a wrap-around engine nacelle, forebody and afterbody engine fillets and a 70 degree delta wing at incidence. The configuration surface was represented analytically; a blocked flowfield domain of approximately 373,000 points was then constructed with hybrid topologies using established transfinite interpolation methodology. Steady-state solutions to the compressible thin-layer, Navier-Stokes equations were obtained with an implicit finite volume algorithm developed at Langley (CFL3D). These solutions were achieved using Van Leer's upwind-biased, flux-vector-splitting technique and an extended version of the Baldwin-Lomax algebraic turbulence model.

10.5.3 Accomplishments

Turbulent results were obtained at $\alpha=2$ degrees, $R_j=32.2 \times 10^6$ (j =body length) and $M_\infty=0.9$ which correspond to flow conditions included in the recent wind-tunnel tests mentioned above. Mach contours on the surface and in the plane of symmetry demonstrated a smooth solution. Figure 10.4 is a blocked representation of this configuration. After a subsonic and mainly attached forebody flow, the flow accelerated supersonically at the cowl-lip of the faired-over engine inlet and subsequently shocked down at the exhaust cowl-lip. (The sonic line is represented with a contour line in the plane of symmetry to highlight the supersonic flow region.) The shock produced an adverse pressure gradient which caused the flow to separate massively and envelop the boattail region. Predicted forebody pressures agreed with experimental data reasonably well; a qualitative prediction of the separated boattail flow also was achieved.

10.5.4 Significance

Navier-Stokes predictions about NASP-like configurations can be achieved for transonic flows which include regions of massive separation.

10.5.5 Status/Plans

Computations for other wind tunnel flow conditions are underway. Computations which include a propulsion simulation are planned, pending scheduled extensions of CFL3D.

James M. Luckring, Farhad Ghaffari and Brent L. Bates
Transonic Aerodynamics Branch
Langley Research Center
(804)864-2869

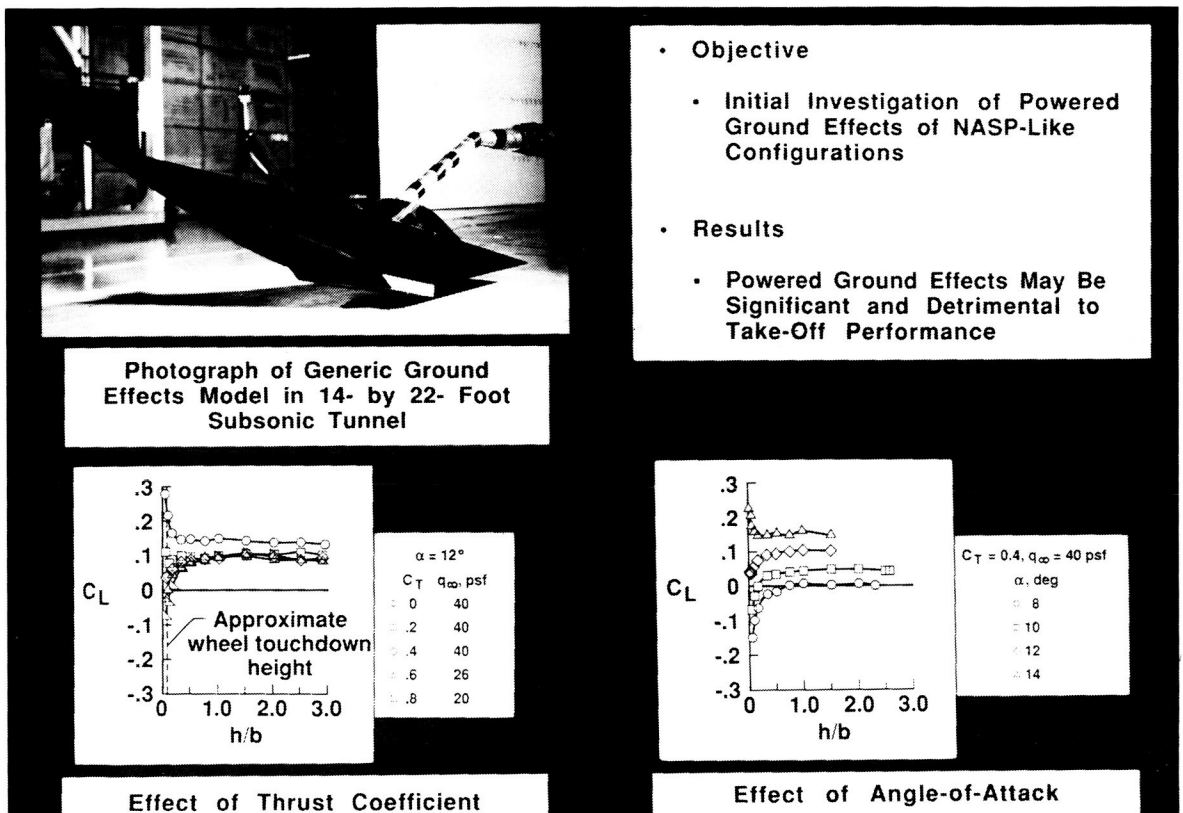


Figure 10.5. Powered Ground Effects for Generic NASP-Like Configurations

10.6 LOW SPEED PROPULSION/AIRFRAME INTEGRATION

10.6.1 Objective

To establish and demonstrate test techniques for assessing low-speed performance, stability and control and ground effects of NASP-like configurations (See Figure 10.5).

10.6.2 Approach

NASA is conducting experimental investigations on the 14-foot by 22-foot subsonic tunnel using generic powered NASP-like configurations. Force and moment data, surface pressures and off surface flow visualization will be obtained and used to analyze configuration characteristics both in and out of ground effect. This analysis also will be used to verify testing techniques employing power simulation to give installed performance.

10.6.3 Accomplishments

Using the Generic Ground Effects Model (GEM), NASA conducted a wind tunnel test of a powered NASP-like model in ground effect to provide the first extensive set of data showing interaction of exhaust flow, airframe and ground plane. Results show significant ground effects which are detrimental to take-off performance. While there are certainly configuration effects to be included in a final analysis, it appears that powered NASP-like configurations will suffer lift losses in ground effect. On the Test Techniques Demonstrator Model (TTD), a low-speed powered model was designed and fabrication is underway.

10.6.4 Significance

The GEM model provided the first significant data set indicating the potential detrimental ground effects that may severely limit NASP take-off performance.

10.6.5 Status/Plans

The GEM model is being modified for further testing scheduled for Fall 1989. TTD fabrication is scheduled for completion in August 1989 with initial testing in late Fall 1989 or early Winter 1990.

John W. Paulson, Jr.
Subsonic Aerodynamics Branch
Langley Research Center
(804)864-5071

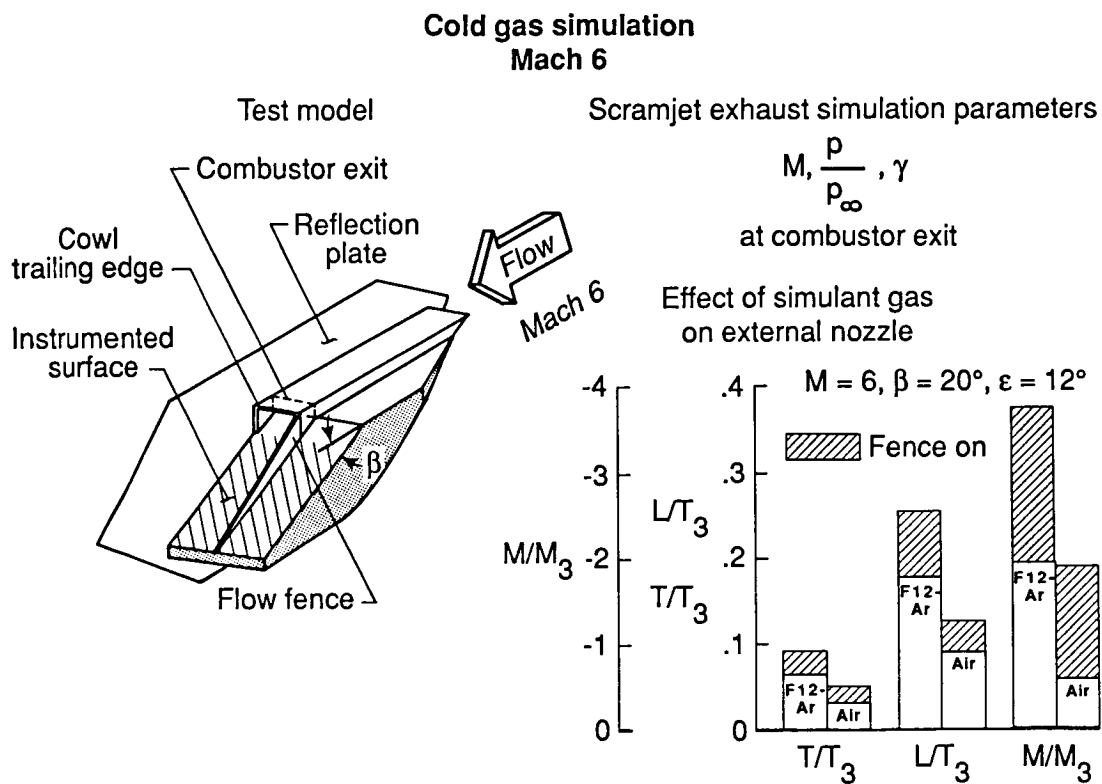


Figure 10.6. Scramjet Exhaust Simulation Model

10.7 SCRAMJET EXHAUST SIMULATION STUDIES AT MACH 6

10.7.1 Objective

To develop an experimental cold gas technique which correctly simulates the effects of a hot scramjet exhaust on the external forces and moments of a hypersonic vehicle in support of the National Aero-Space Plane (NASP) Program (See Figure 10.6).

10.7.2 Approach

Suitable cold gases were defined for scramjet exhaust simulation. They were validated by comparisons with hydrogen-air combustion products at flight enthalpy in a shock tunnel. The selected cold gas was used for wind-tunnel studies of internal and external nozzle geometries. CFD codes were modified for validation studies.

10.7.3 Accomplishments

The inviscid simulation parameters are the Mach number, the static pressure ratio and the ratio of specific heats (γ) at the combustor exit. A Freon-Argon mixture (F12-Ar) was found to match all three parameters and to simulate the surface-pressure characteristics of a hydrogen-air combustion mixture at flight enthalpy at Mach 6 and 8. These validation tests were performed in the Grumman Shock Tunnel under NASA contract. A wind tunnel model that represents the nozzle/afterbody of a hypersonic, airbreathing vehicle was then constructed to internal and external nozzle geometries in the Langley 20-inch Mach 6 Tunnel. The cross-hatched area of the external nozzle was instrumented with static pressure taps to provide pressure data for integration to obtain forces and moments on the external nozzle. The nondimensionalized lift (L/T_3), thrust (T/T_3) and pitching moment (M/M_3) are shown for four cases; two cases are for a F12-Ar scramjet exhaust simulation, flow fence off and on and the other two cases are for an air scramjet exhaust simulation, flow fence off and on. These experimental results show that air cannot be used to simulate the underexpanded scramjet exhaust and the addition of flow fences provides significant increases in external nozzle thrust and lift. A two dimensional Navier-Stokes solver was modified to address the simulant gas and external gas stream simultaneously and the results compared favorably with surface pressure data.

10.7.4 Significance

The use of a safe, non-combustible gas mixture for suitable scramjet exhaust simulation was demonstrated experimentally at Mach 6. A simple geometric device, the flow fence, was shown to provide a nearly 50 percent increase in external nozzle thrust.

10.7.5 Status/Plans

In support of the NASP Technology Maturation Program, the cold gas scramjet exhaust simulation technique will be used in several Langley supersonic and hypersonic facilities to measure the effect of the scramjet exhaust on the Langley Test Technique Demonstrator configuration. The wind tunnel data will also provide the basis for developing a flight scaling methodology and for validating three dimensional Navier-Stokes solvers.

James L. Pittman, William J. Monta and James M. Cabbage
Supersonic/Hypersonic Aerodynamics Branch
Langley Research Center
(804)864-5585

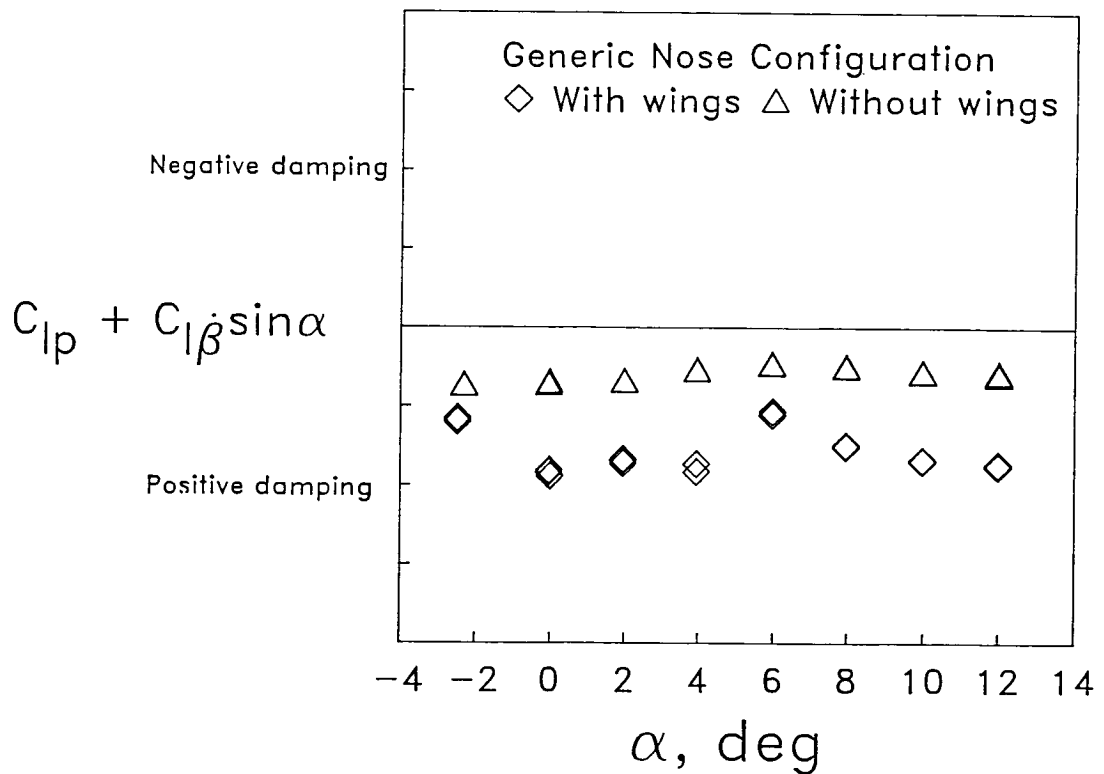


Figure 10.7. Roll Damping at Mach 4.6

10.8 NASP HIGH-SPEED DYNAMIC STABILITY TESTS

10.8.1 Objective

To (1) develop dynamic stability test techniques for slender hypersonic configurations; (2) measure experimentally the dynamic stability derivatives in pitch, yaw and roll of slender hypersonic configurations at subsonic, transonic and supersonic speeds and (3) provide dynamic stability derivatives as part of a database for use in the validation of engineering codes and for use in stability and control evaluations and simulations.

10.8.2 Approach

The existing force-oscillation dynamic stability equipment which had not been used for about eight years, was refurbished. The online data acquisition and reduction hardware and software were updated because the old hardware was obsolete. NASA used an existing Space Shuttle Orbiter model for system verification because of the large amount of dynamic stability data available on that configuration. Design and construction was started on a Test Techniques Demonstrator (TTD) model which was compatible with the existing dynamic stability balances. In addition, an agreement was made with the McDonnell Douglas Corporation to test both proprietary and non-proprietary configurations of its NASP design.

10.8.3 Accomplishments

The Orbiter model was used to check out the operation of the dynamic stability hardware and software. Supersonic dynamic stability tests of the McDonnell Douglas model were made in the Unitary Plan Wind Tunnel. Figure 10.7 shows an example of the roll damping results for the NASP model with a generic nose.

10.8.4 Significance

Pitch, yaw and roll damping data at supersonic speeds were obtained on a slender hypersonic configuration. The successful operation of the high-speed dynamic stability equipment after a long period of inactivity restores an experimental test capability which had been dormant.

10.8.5 Status/Plans

Offline data reduction and analysis of the supersonic results are in progress. Subsonic and transonic tests of the McDonnell Douglas model were planned for July 1989 in the 8-foot Transonic Pressure Tunnel. Tests with the TTD model over the speed range are scheduled for late 1989 and early 1990.

Richmond P. Boyden and David A. Press
High-Reynolds-Number Aerodynamics Branch
Langley Research Center
(804)864-5160

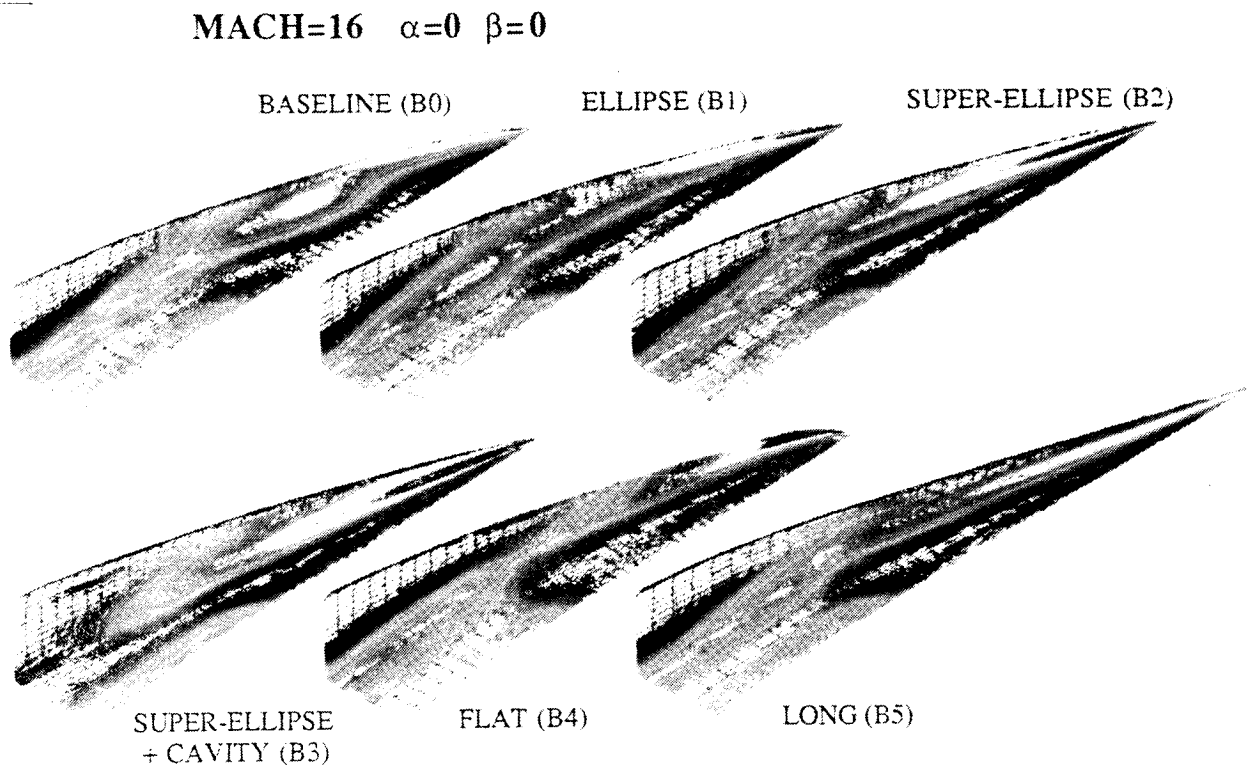


Figure 10.8. Load Heat Transfer Rates (\dot{q})

10.9 HYPERSONIC FOREBODY DESIGN STUDY

10.9.1 Objective

To determine the effects of forebody shaping on vehicle aerodynamic performance and the quality of flow generated at the inlet face of bottom-mounted scramjets in support of the National Aero-Space Plane (NASP) Program.

10.9.2 Approach

The approach involved using a validated thin-layer Navier-Stokes solver, ARC3D, was used to assess the effects of cross-sectional and planform variations on flow quality at the inlet face, body heating and forebody aerodynamic performance at hypersonic speeds.

10.9.3 Accomplishments

The forebody of the Langley Test Technique Demonstrator configuration was defined as the baseline. Three variations of cross section for a constant area distribution and two variations of planform were analyzed at Mach 16. Figure 10.8 shows an example of the computed surface heat-transfer ratio for all six bodies at Mach 16 is given in the figure. The variation of angle of attack was minus five degrees to five degrees and a sideslip angle of three degrees was examined at zero angle of attack. The cross-sectional variations provided significant changes to the inlet flow without significantly changing the forebody aerodynamic performance. Rounding the planform nose yielded better aerodynamic performance, improved inlet flow and showed a relative insensitivity of inlet-face flow to sideslip. An elongated planform also reduced drag compared to the baseline and relieved the local nose heating problem of the other planforms.

10.9.4 Significance

This systematic computational study provided much needed insight into the parameter sensitivities of hypersonic forebody design for bottom-mounted scramjets.

10.9.5 Status/Plans

The study was extended to Mach 6 and 10. Experimental studies are planned, based on the combined results of this study and a similar study performed by McDonnell-Douglas Corporation as another part of the NASP Technology Maturation Program.

Warren H. Davis
Grumman Aerospace Corporation
(516)575-9979

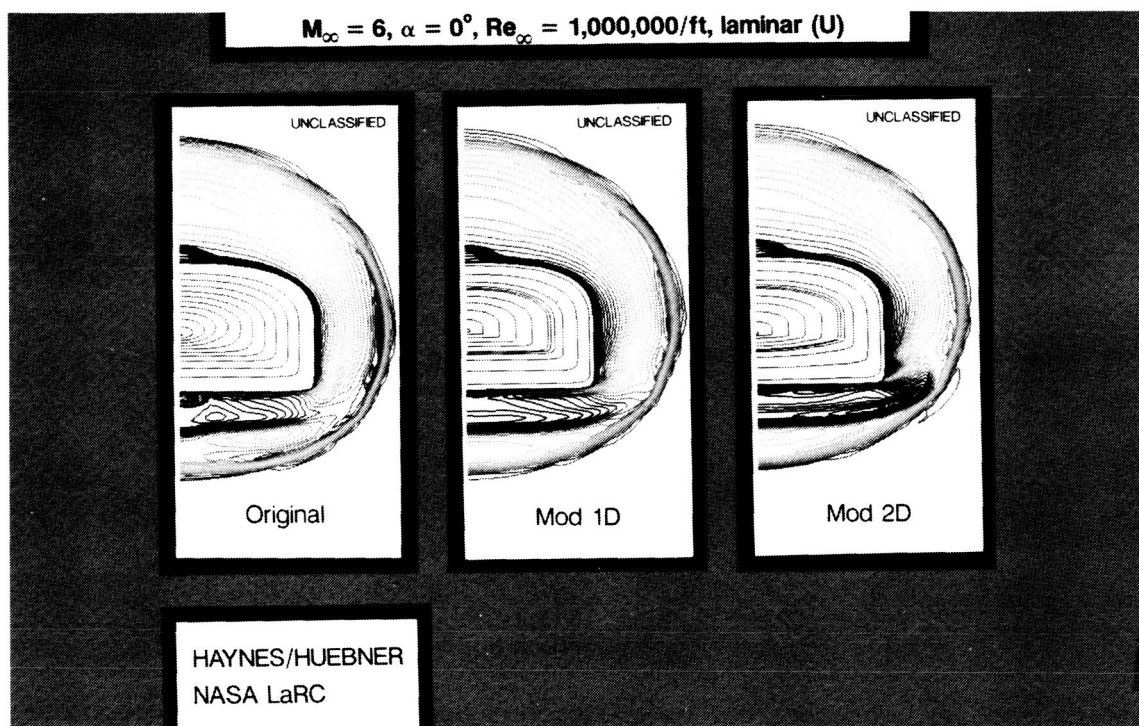


Figure 10.9. Computational Design of the TTD Forebody

10.10 TTD FOREBODY REDESIGN

10.10.1 Objective

To eliminate undesirable forebody flow characteristics observed computationally and experimentally for the original Langley Test Technique Demonstrator (TTD) geometry. These undesirable characteristics included undesirable compressions and shocks, significant lower-surface inflow and centerline boundary layer pileup which are difficult to quantitatively assess experimentally and very difficult to scale to flight conditions. This effort was in support of the National Aero-Space Plane (NASP) Program.

10.10.2 Approach

NASA used the CFL-3DE Parabolized Navier-Stokes (PNS) computational method to systematically evaluate parametric variations of the TTD forebody geometry (See Figure 10.9). NASA held the original TTD planform and profile so that geometry variations were restricted to cross-section shaping only. NASA used the PNS parametric evaluations to select a modified TTD forebody geometry and experimentally validated the redesigned forebody in the 20-inch Mach 6 facility.

10.10.3 Accomplishments

Seven forebody geometry variations were computationally evaluated. Particle trace, x-momentum, mass flow and drag data all were used to examine the parametric effects. Based upon these results, an alternate TTD forebody was selected which would best eliminate or minimize the observed undesirable flow characteristics of the original TTD geometry. Wind tunnel models of the modified TTD were fabricated and tested in the 20-inch Mach 6 facility. These tests confirmed an overall improvement in the TTD forebody flow characteristics. This entire project was performed in a six month time period in support of the NASP TMP.

10.10.4 Significance

NASA demonstrated a hypersonic forebody design methodology using a PNS method. NASA improved the flow quality at the inlet face provided by the TTD forebody making it more representative of NASP goals and more suitable for evaluating scramjet installation and operation effects on overall vehicle performance.

10.10.5 Status/Plans

The project was completed and reported at the Sixth NASP Symposium in Monterey, California. The Langley TTD is the focus for the development of powered test techniques for hypersonic vehicles.

Davy A. Haynes and Lawrence D. Huebner
Supersonic/Hypersonic Aerodynamics Branch
Langley Research Center
(804)864-5584

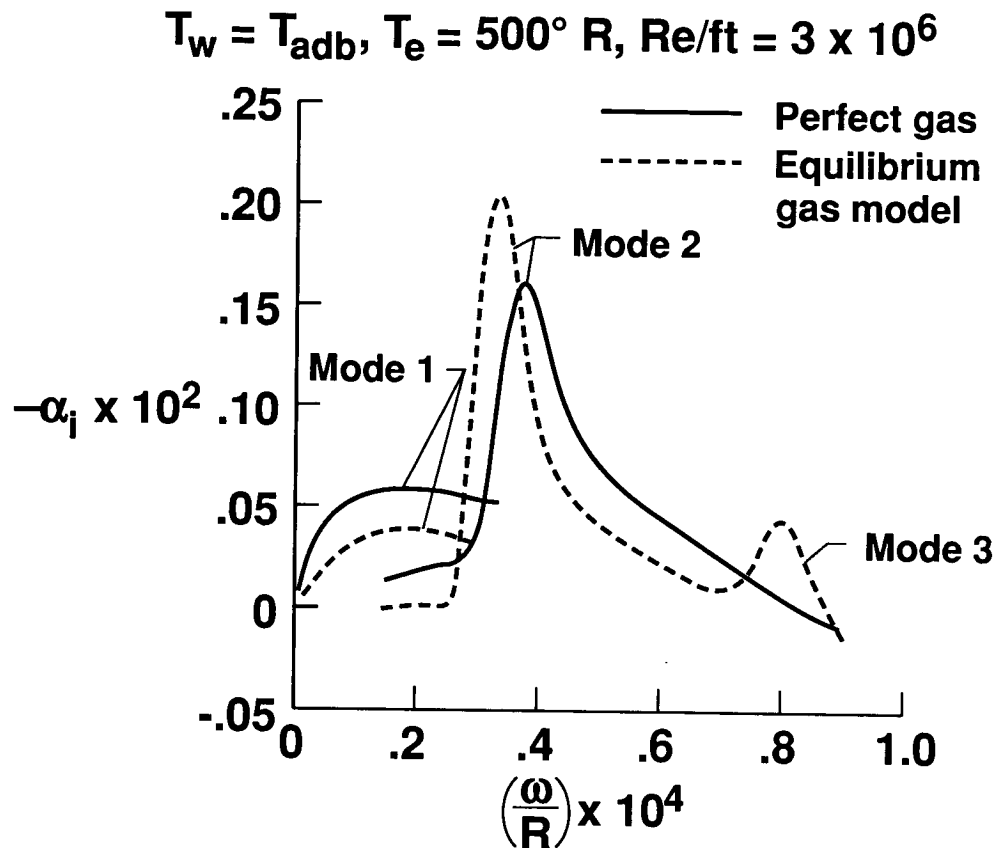


Figure 10.10. Effect of Gas Chemistry on Spatial Growth Rates in a Mach 10 Boundary Layer

10.11 EFFECT OF REAL-GAS ON FIRST AND SECOND MODE INSTABILITY IN HYPERSONIC BOUNDARY LAYERS

10.11.1 Objective

At high temperatures, air departs from the perfect-gas behavior due to vibrational excitation and gas dissociation. Since high Mach number flows at flight conditions are generally associated with high temperatures, the effect of real-gas on boundary layer transition was considered.

10.11.2 Approach

A newly developed spatial stability analysis code (e^{Malik}) was used for transition prediction. This code uses linear stability theory and incorporates an equilibrium real-gas model. The calculations were made for an adiabatic wall boundary layer where the local edge Mach 10 and the edge temperature was 500°R. The adiabatic wall condition was chosen to generate sufficient temperature to observe any effect of real-gas on the mean flow and its stability. For a perfect-gas and an equilibrium real-gas, stability results for a Reynolds number (R) of 2,000 were presented where the spatial growth rate was plotted as a function of nondimensional frequency ωR (See Figure 10.10).

10.11.3 Accomplishments

Three instability modes are identified in the calculations and the curves show that the equilibrium gas growth rates are less (more stable) for Mode 1 and Mode 3 disturbances and enhanced (less stable) for Mode 2 disturbances.

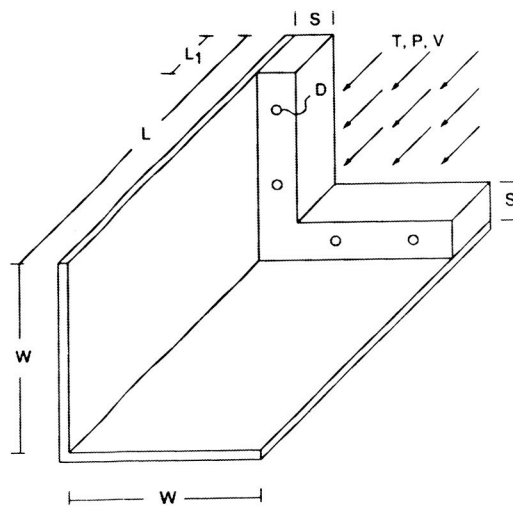
10.11.4 Significance

Even though the effect of chemical reactions is to increase the second mode growth rate, it lowers the growth rate of the first and third modes. The overall effect of a real-gas on the first and second mode growth rate is very similar to the effect of wall cooling, as previously observed both computationally and experimentally for a perfect-gas; that is, in high Mach number flows, second mode disturbances can dominate and real-gas effects can have a significantly destabilizing influence and may lead to early transition.

10.11.5 Status/Plans

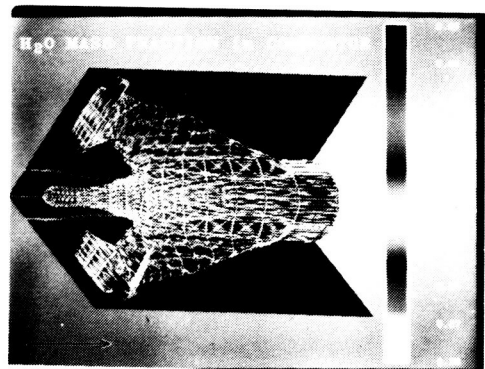
Calculations will be made for high altitude flight transition data on cones to correlate the results of stability theory with the experimental observations.

Mujeeb R. Malik
Viscous Flow Branch
Langley Research Center
(804)864-5564



$L = 20.0 \text{ cm}$, $W = 10.0 \text{ cm}$
 $S = 2.0 \text{ cm}$, $L_1 = 1.5 \text{ cm}$, $D = 3.5 \text{ mm}$
 $T = 1000 \text{ K}$, $P = 0.5 \text{ atm}$, $V = 1500 \text{ m/s}$

Schematic of generic scramjet combustor.



Water mass fraction distribution in combustor.

Figure 10.11. Generic Scramjet Combustor

10.12 MODELING FUEL-AIR MIXING AND REACTION IN A SCRAMJET COMBUSTOR

10.12.1 Objective

To (1) model the flowfield in a scramjet combustor and (2) use the numerical results to improve fuel-air mixing and combustion efficiency in the engine.

10.12.2 Approach

The combustor flowfield was modeled by numerically solving the Navier-Stokes and species continuity equations that describe a high-speed, chemically reacting flow. Chemical reaction was modeled using an eighteen reaction, H_2 -air finite rate, chemistry model. Laminar diffusion was described using kinetic theory based models and turbulent diffusion was modeled with an algebraic or differential turbulence model.

10.12.3 Accomplishments

The flowfield in a three-dimensional generic scramjet combustor was modeled using the SPARK combustion program developed with the described approach (See Figure 10.11). Each of the four bounding walls (only two are shown) contained a step with several H_2 fuel injectors. The fuel mixed with air from the engine inlet as the air flowed over the step. Chemical reaction of the hydrogen and air then occurred, producing water. The analysis showed that the fuel and water are drawn down into the corner of the combustor suppressing further reaction and lowering the overall combustion efficiency and thrust. Fuel mixing enhancers are now being added to the combustor to improve combustion efficiency. Similar analyses are aiding in the design of the enhancers.

10.12.4 Significance

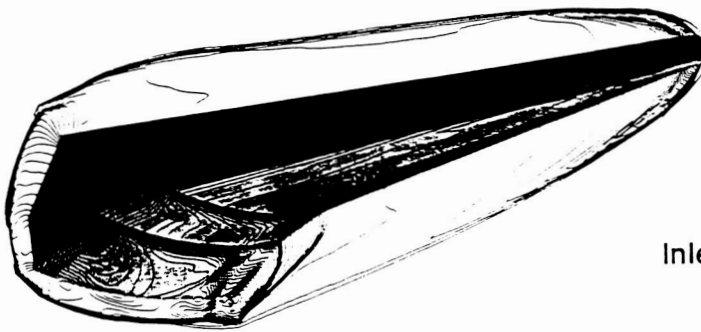
Combustor analyses provided a better understanding of the flowfield in scramjet combustors and are now providing the researcher and designer with a technique for assessing the degree of fuel-air mixing and reaction. The combustor code previously described now provides a means for evaluating an engine design and for optimizing the fuel injector design to achieve maximum combustion efficiency.

10.12.5 Status/Plans

Work is now underway to further develop the combustor code and to use the code to develop advanced mixing enhancers for scramjet combustors.

J. Philip Drummond and Mark H. Carpenter
Computational Methods Branch
Langley Research Center
(804)864-2298

Forebody Pressure Contours



Inlet Mach Number Contours

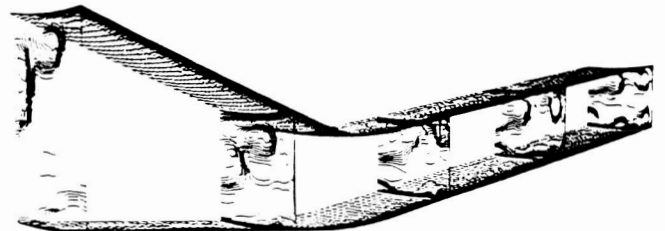


Figure 10.12. Forebody/Inlet Configurations

10.13 A ZONAL METHODOLOGY FOR HIGH SPEED FOREBODY/INLET CONFIGURATIONS

10.13.1 Objective

To develop a zonal analysis technique capable of providing efficient and accurate forebody/inlet solutions for hypersonic air-breathing vehicles.

10.13.2 Approach

A state-of the-art, thin layer Navier-Stokes code was enhanced to include a multi-zone capability. The multi-zone approach permitted the appropriate communication between grid zones by use of patching interpolation or a one-to-one block boundary condition. The use of multiple zones allowed desired grid clustering and orientation with minimal computational effort. Also, an inlet sidewall sweep was modeled with a "jagged" wall/no wall boundary condition allowing grid cross-sections to remain perpendicular to the streamwise direction. This was the desired grid orientation for thin layer calculations.

10.13.3 Accomplishments

The zonal methodology was used to investigate inlet flows with spillage effects. Computational results for a high speed forebody/inlet configuration compared reasonably well with available experimental data. Figure 10.12 shows computed pressure contours in the symmetry plane, the outflow plane and on the bottom surface of the three-dimensional forebody. Mach number contours in several cross sections in the inlet also are shown. The results indicated a finer grid was needed to more accurately resolve the flow in the inlet. The fine grid calculation is in progress. The zonal methodology also was used to analyze National Aero-space Plane contractor forebody/inlet configurations. Results from these calculations were used to evaluate the contractor's designs.

10.13.4 Significance

The analysis of high speed forebody/inlet flow fields requires accurate modelling of inlet spillage effects. The zonal methodology developed during this effort correctly models spillage around the sidewall and beneath the inlet. With accurate flowfield solutions in the inlet, scramjet engine designers can obtain more realistic performance estimates and increase the design confidence of National Aero-Space (NAS) plane-like vehicles.

10.13.5 Status/Plans

The zonal methodology described here is part of a nose-to-tail computational effort. A demonstration nose-to-tail calculation is planned for the coming months.

William M. Eppard, George F. Switzer and Arthur D. Dilley
Computational Methods Branch
Conley Research Center
Langley 64-2288
(804)8

(Stainback, Fischer, & Wagner 1972)

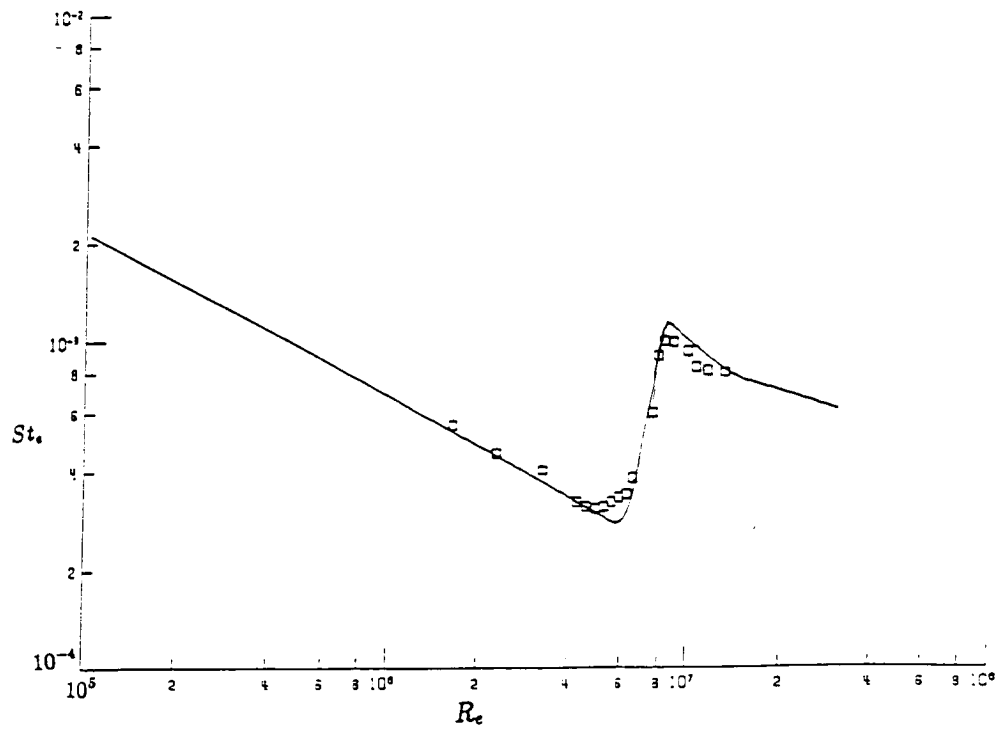


Figure 10.13. Transition Model Versus Mach 6 Cone

10.14 ALGEBRAIC HYPERSONIC TRANSITION MODELING

10.14.1 Objective

To develop and calibrate algebraic Reynolds-averaged models of the transition region for hypersonic boundary layers.

10.14.2 Approach

The location of transition onset was presumed given, for example, by a N-factor method and the length and properties of the transition zone were desired. The models should be readily insertional in conventional CFD codes with algebraic turbulence models (See Figure 10.13).

10.14.3 Accomplishments

The zero-equation transition function model of Arnal was adapted to the Baldwin-Lomax formulation. It was implemented both in a compressible boundary layer code and in a three-dimensional parabolized Navier-Stokes (PNS) code. The model was calibrated against natural transition data for incompressible flow past a flat plate and for Mach 6 flow past a cone. It agreed well with the flat plate mean flow profiles in the transition zone and for the surface properties for the supersonic cone.

10.14.4 Significance

Transition prediction and modeling are crucial items for hypersonic vehicle design. The model described here can be readily inserted in production CFD codes which already contain a Baldwin-Lomax turbulence model. This model was demonstrated to be effective at low hypersonic speeds for two-dimensional and axisymmetric configurations.

10.14.5 Status/Plans

The model will be tested at higher speeds and will be extended to three-dimensional mean flows; moreover, alternative algebraic models, such as those suggested by Renormalization Group methods, will be examined. Two-equation and second-order closure models will be developed.

S. Dinavahi and T. A. Zang
Computational Methods Branch
Langley Research Center
(804)864-2307

ORIGINAL PAGE
BLACK AND WHITE PHOTOGRAPH



Figure 10.14. Pegasus

10.15 PEGASUS AEROTHERMAL FLIGHT MEASURES

10.15.1 Objective

To (1) evaluate tools used in the Pegasus TPS design and (2) develop instrumentation techniques for heat flux measurement in flight structures (See Figure 10.14).

10.15.2 Accomplishments

Flight One experiment definition and sensor fabrication were completed.

10.15.3 Significance

Flight results provide a benchmark for application of current aerothermal design tools. The results provide flight experience with the unique heat flux sensor concept and obtain useful data for refinement of the Pegasus design.

10.15.4 Status/Plans

Following installation of sensors and flight vehicle fabrication, the first flight is expected in January 1990.

Robert Curry
Ames/Dryden Research Centers
(415)604-3715

This page is intentionally left blank.

CHAPTER ELEVEN

GENERAL AVIATION/COMMUTER AERODYNAMICS

11.1 INTRODUCTION

The objective of the General Aviation/Commuter Aerodynamics Program is to provide the technology database to improve the performance efficiencies of general aviation and commuter aircraft. To accomplish these objectives, the program currently is focusing on three primary areas, (1) natural laminar flow certification, (2) airflow boundary layer transition physics and (3) aerodynamic characteristics of crescent wing planforms.

The Natural Laminar Flow (NLF) Certification Program is a joint NASA, Cessna Aircraft Company and FAA program using a Cessna T210 airplane with a NASA-designed NLF airfoil section and a horizontal stabilizer. Flight tests are being conducted to determine the effect of laminar flow loss on airplane characteristics and performance with respect to FAA certification.

In order to understand details about flow instabilities that initiate transition from laminar to turbulent flow, boundary layer transition physics flight experiments are being conducted using a Lear Jet 28/29 airplane having a specially designed, instrumented wing glove. The flight tests are being conducted in flight environments representative of commuter and transport aircraft operations. These tests also will help validate Computational Fluid Dynamics (CFD) codes.

Subsonic wind tunnel experiments showed that wings with crescent planforms have less induced drag than the classical elliptic wing shape (with equal wing loading); therefore, the aerodynamic characteristics of crescent-wing planforms are being investigated computationally and experimentally to determine the induced-drag characteristics of planar wings with crescent planforms and wings with highly-swept sheared tips. These planforms will be investigated from low to high angles of attack and their application to typical wing planforms will be studied with respect to improved airplane performance.

In addition to the previously described primary research areas, advanced personal air transportation systems are being studied to provide technology to increase general aviation's contribution to the national transportation system efficiency. The goal is to develop control and display concepts for novice pilots which will increase utility by making general aviation airplanes safer and easier to fly. An easy to fly automatic decoupled control system was developed and a pictorial display format is currently under investigation.

Program Manager: Dr. Raymond E. Rose
OAST/RF
Washington, DC 20546
(202)453-2818

ORIGINAL PAGE
BLACK AND WHITE PHOTOGRAPH

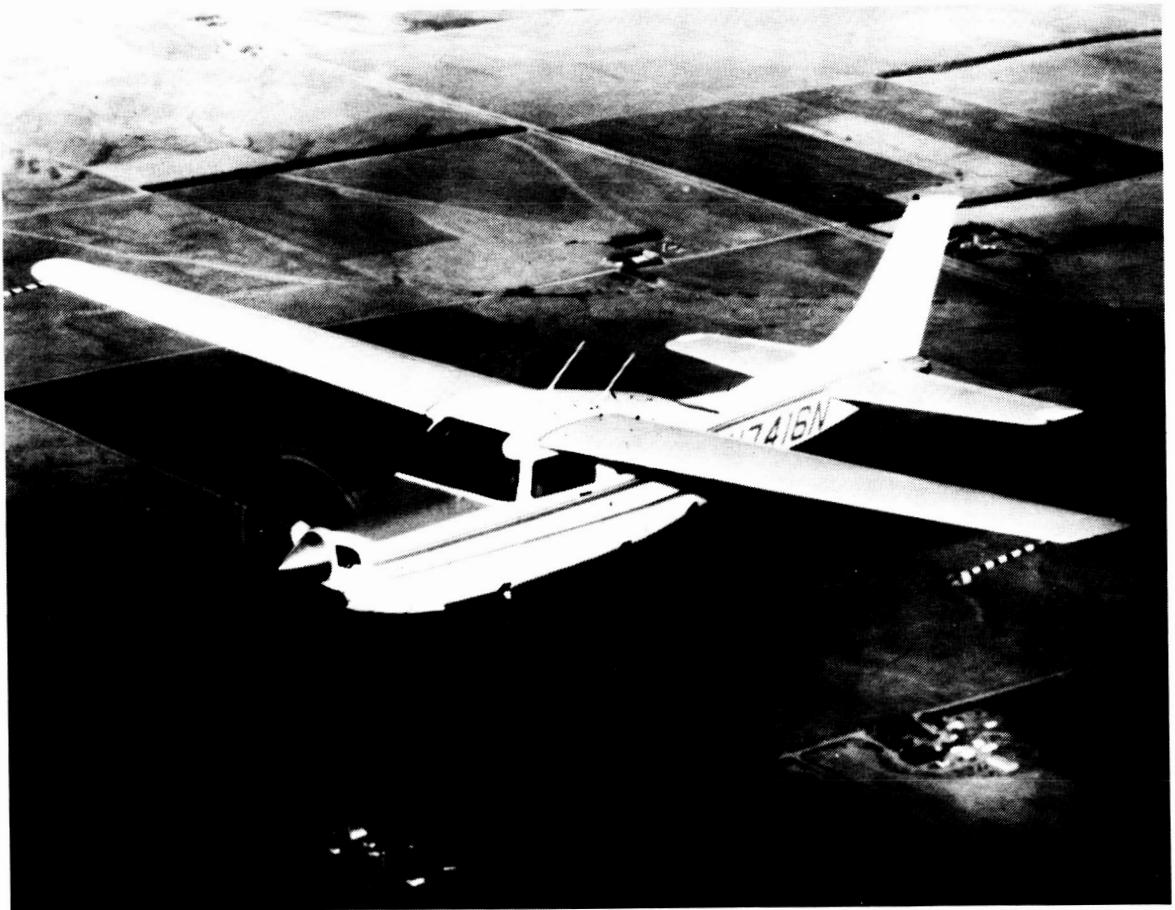


Figure 11.1. Cessna T210

11.2 NATURAL LAMINAR FLOW CERTIFICATION PROGRAM

11.2.1 Objective

To assess the effect of loss of laminar flow on airplane characteristics with respect to certification in accordance with Federal Aviation Regulations (FAR) Part 23.

11.2.2 Approach

In a joint NASA, Cessna Aircraft and FAA program, a Cessna T210 airplane was tested in accordance with FAR Part 23 with a modified wing incorporating a NASA-designed, Natural Laminar Flow (NLF) airfoil section, a NLF horizontal stabilizer and a smoothed vertical stabilizer. Research flights addressed the aircraft's performance, stability, controllability and stall characteristics with combinations of laminar and turbulent boundary layer configurations on the aircraft's wing and tail surfaces (See Figure 11.1).

11.2.3 Accomplishments

Tests to date show that the fully turbulent surface configuration degrades airspeed by 15 knots compared to the fully laminar configuration without degrading handling characteristics.

11.2.4 Significance

The results will assess adequacy of the existing FAR Part 23 for certification of new general-aviation-type aircraft having significant NLF.

11.2.5 Status/Plans

Research flights continued through September 1989.

Gregory S. Manuel
Flight Research Branch
Langley Research Center
(804)864-3864

ORIGINAL PAGE
BLACK AND WHITE PHOTOGRAPH

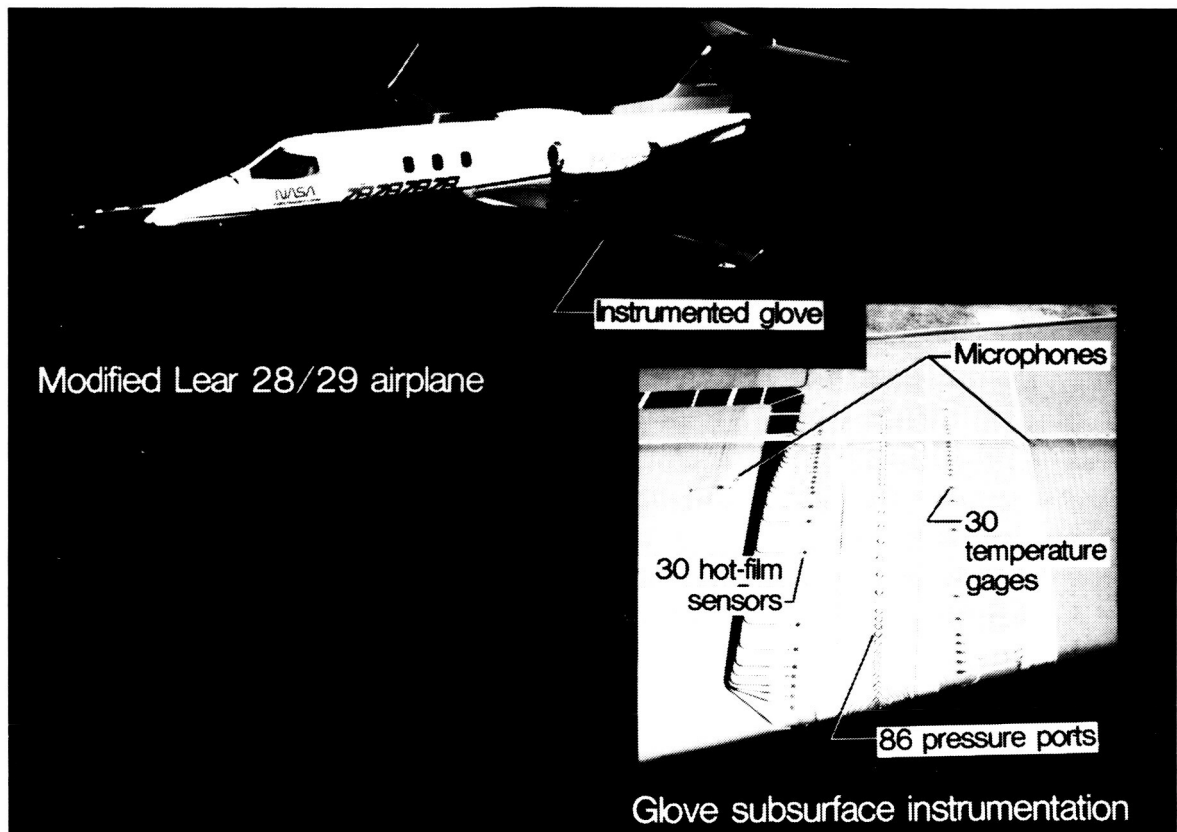


Figure 11.2. Transition Physics Flight Experiments

11.3 TRANSITION PHYSICS FLIGHT EXPERIMENT

11.3.1 Objective

To (1) understand details about flow instabilities responsible for initiating transition from laminar to turbulent flow, with emphasis on the growth of Tollmien-Schlichting (T-S) instabilities and (2) help validate computational fluid dynamics (CFD) compressible linear stability theory.

11.3.2 Approach

A one quarter inch thick, six foot span, fiberglass and foam glove was installed on the left wing of a Lear 28/29 to provide a shape that is conducive to long runs of laminar flow and to incorporate subsurface instrumentation for streamwise measurement of temperature, pressure and growth of T-S instabilities. Measurements were made in the flight environment over a range of altitudes and Mach numbers representative of commuter and transport aircraft operations.

11.3.3 Accomplishments

Theoretical calculations were made to determine appropriate flight conditions for maximum T-S amplification. The wing glove was fabricated and instrumented. Flight tests defined conditions for detailed measurements. Flight tests demonstrated ability to move transition from leading edge to 60 percent chord by varying flight conditions while making nonintrusive streamwise measurements (See Figure 11.2).

11.3.4 Significance

These flight experiments are the first of their kind to measure streamwise growth patterns and are the first flight experiments to offer temperature distribution information as input to compressible CFD codes. This research will provide information on disturbance growth and transition mode which is essential to the development of practical design limits for applications of laminar flow technology.

11.3.5 Status/Plans

NASA planned to complete flight experiments by July 15, 1989.

Cynthia C. Lee
Flight Research Branch
Langley Research Center
(804)864-3865

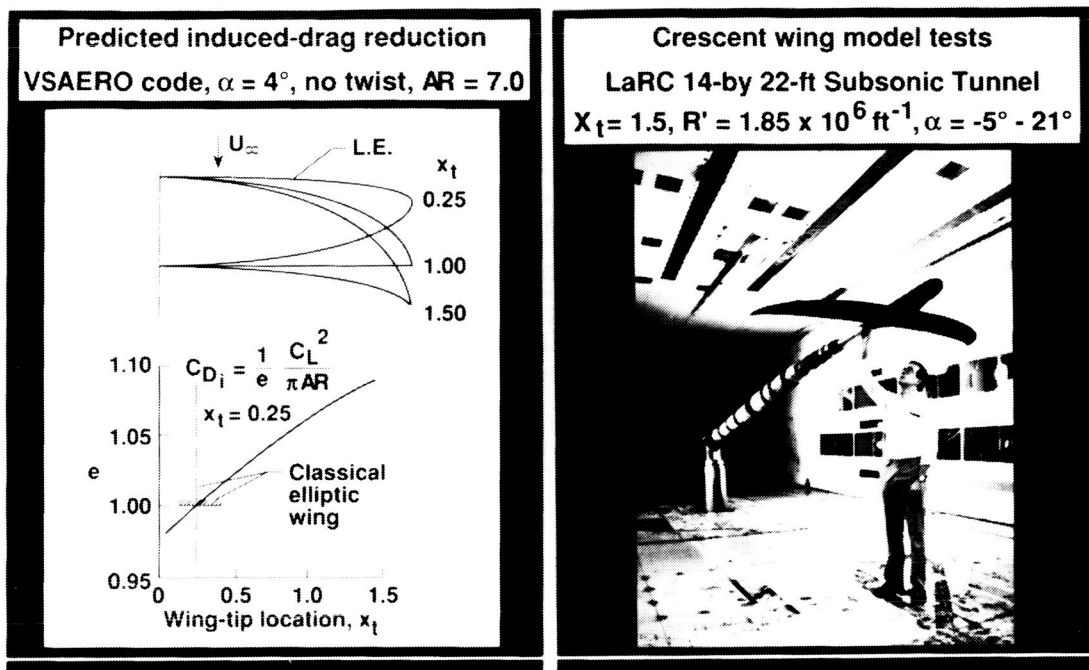


Figure 11.3. Aerodynamic Characteristics of Crescent Wings

11.4 AERODYNAMIC CHARACTERISTICS OF CRESCENT-WING PLANFORMS

11.4.1 Objective

To (1) investigate computationally and experimentally the induced-drag characteristics of planar wings with crescent planforms and wings with highly-swept sheared tips, (2) conduct subsonic wind-tunnel experiments to measure the aerodynamic characteristics of these planforms at low and high angles of attack and (3) investigate the application of sheared and crescent wing tips to typical wing planforms.

11.4.2 Approach

The approach involved measuring a three to four percent reduction in induced drag for the crescent planform in comparison to the classical elliptic wing shape (with equal wing loading). At high angles of attack, the presence of leading edge, separation induced, vortical flow over the highly-swept wing tips resulted in an increase in maximum lift (eight percent) and lateral-directional static stability. Wind-tunnel tests also showed a 3.3-percent reduction in induced drag for a high-aspect-ratio unswept wing with sheared tips, as predicted by the inviscid analysis method (See Figure 11.3). The drag reduction presumably originated from the favorable influence of trailing-wake deformations on the pressure distribution of the highly-swept tips.

11.4.3 Significance

The results suggest that the classical minimum-induced-drag findings (based on linear inviscid aerodynamic theory) may need to be re-examined. In particular, the present results indicate that reduced induced drag can be obtained for planar wings with crescent planforms or with sheared tips. The presence of vortical flow over the highly-swept outboard wing regions at high angles of attack could contribute to the design of planforms with improved stall and spin-entry behavior.

11.4.4 Status/Plans

Wind-tunnel force measurements of crescent planforms are nearly completed. The design of models for wind-tunnel measurement of surface pressures and wake development has been started. The feasibility of flight experiments for measurement of induced drag is being studied. Navier-Stokes methods will be used to study the induced-drag estimation of planar wing planforms.

P. Vijgen, C. P. Van Dam and B.J. Holmes
Flight Research Branch
Langley Research Center
(804)864-3942

This page is intentionally left blank.

CHAPTER TWELVE

FIGHTER/ATTACK AIRCRAFT

12.1 INTRODUCTION

The objective of the Fighter/Attack Aircraft Program is to provide enabling technologies for fighter/attack aircraft to achieve efficient, sustained supersonic cruise and maneuver performance, efficient store carriage and deployment at supersonic speeds, increased agility at subsonic speeds, acceptable handling qualities at extreme angles of attack and short takeoff and vertical landing (STOVL) operation.

Improved prediction methods and/or experimental techniques are now available for high-lift aerodynamics, propulsion integration, weapon carriage, supersonic store cavity and separation aeroacoustics, integrated flight controls and systems design for fighter/attack aircraft. Wind-tunnel and piloted simulation studies have demonstrated the potential effectiveness of multi-axis thrust vectoring for propulsive control at extreme angles of attack. In addition, powered lift systems consistent with the operation of advanced STOVL aircraft have been identified and configuration studies have been conducted to assess the impact of integrating these systems with supersonic airframe designs.

The Fighter/Attack Aircraft Program is focused on (1) CFD modeling and validation of cavity effects and near-field trajectory simulation for weapons launch during maneuver and modeling of 3-D flow fields for vehicles at high angles of attack with separated flow; (2) development of innovative propulsive and aerodynamic control systems concepts to provide increased vehicle control at angles of attack near and beyond maximum lift; (3) improved understanding of control requirements for control concepts throughout the relevant flight envelope; (4) large-scale, ground-based testing of a STOVL fighter concept using ejector lift/vectored thrust to define critical transition aerodynamics; (5) studies of STOVL ground effects including inlet reingestion and ground erosion and (6) integration studies to quantify the impact of emerging technologies and define the critical research areas for supersonic STOVL.

Program Manager: Dr. Lawrence E. Olson
OAST/RF
Washington, DC 20546
(202)453-8606

ORIGINAL PAGE
BLACK AND WHITE PHOTOGRAPH

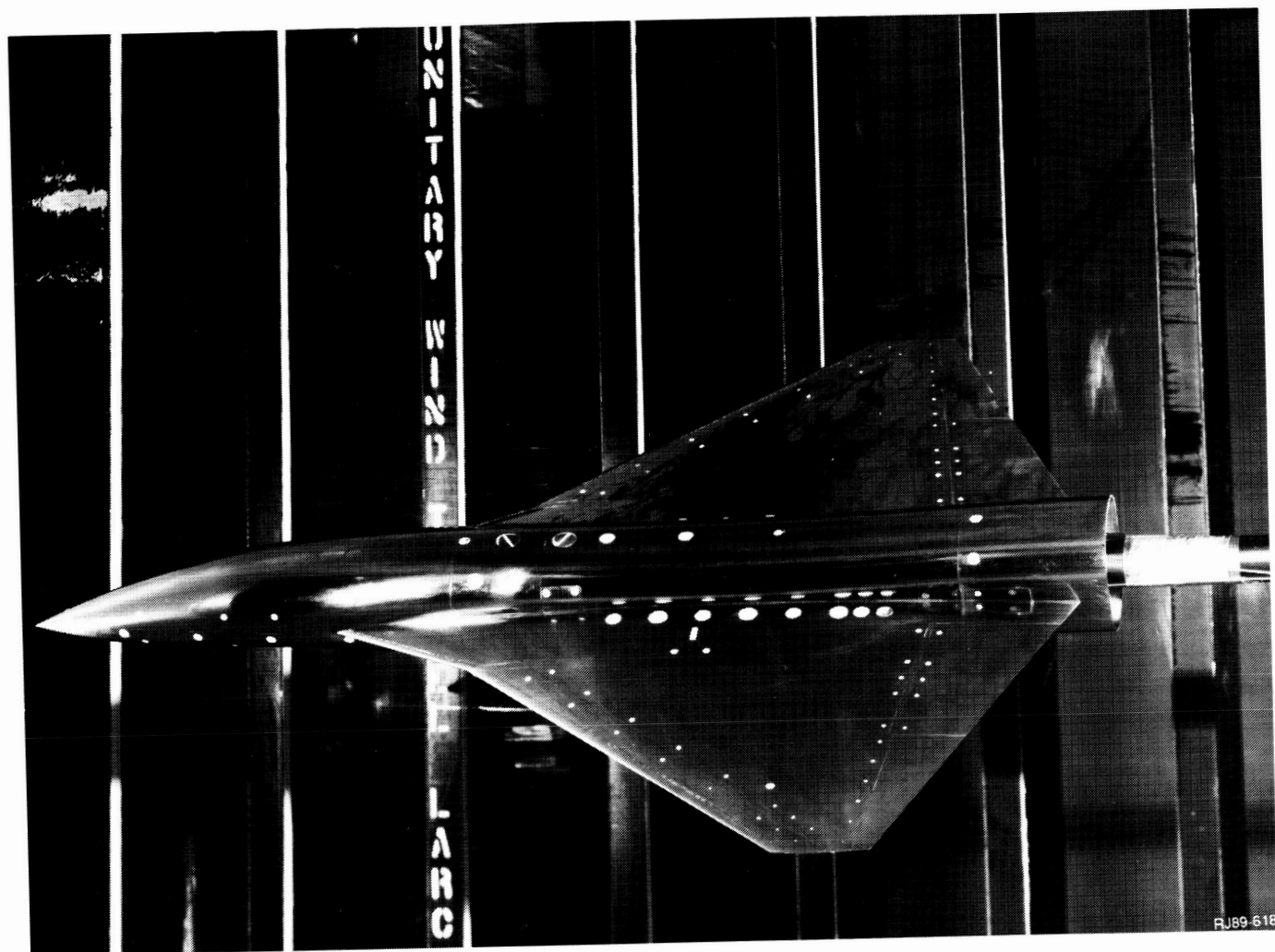


Figure 12.1. Flat and Cambered Delta Wing

12.2 EVALUATION OF LEADING- AND TRAILING- EDGE FLAPS ON A FLAT AND CAMBERED DELTA WING AT SUPERSONIC SPEEDS

12.2.1 Objective

To evaluate the supersonic aerodynamic performance benefits associated with leading- and trailing-edge flaps on a flat and cambered wing.

12.2.2 Approach

A cooperative program was established between NASA and General Dynamics to perform the research. The criteria used in designing an optimized cambered wing with leading- and trailing-edge flaps included high acceleration requirements. The effects of camber on the flap performance then could be assessed through comparison with a flat, uncambered wing of the same planform and flap geometry (See Figure 12.1).

12.2.3 Accomplishments

Based on the design criteria, a clipped delta planform of moderate leading-edge sweep (50 degrees) was chosen for the wind tunnel investigation. The tests were conducted in the Langley Unitary Plan Wind Tunnel at Mach 1.60 to 2.16. Leading-edge flap deflections up to 15 degrees and trailing-edge flap deflections up to -30 degrees were tested on both wings. The results show that the flap effectiveness varies between a cambered and flat wing, with the largest differences occurring with leading-edge flaps; however, Mach number effects on flap effectiveness are similar for both flat and cambered wings.

12.2.4 Significance

The results of this research show that the performance benefits associated with leading- and trailing-edge flaps are camber surface dependent.

12.2.5 Status/Plans

The study was completed. The results will be documented in a formal NASA publication.

Gloria Hernandez, Richard Wood and Bob Collins
Supersonic/Hypersonic Aerodynamics Branch
Langley Research Center
(804)864-5572

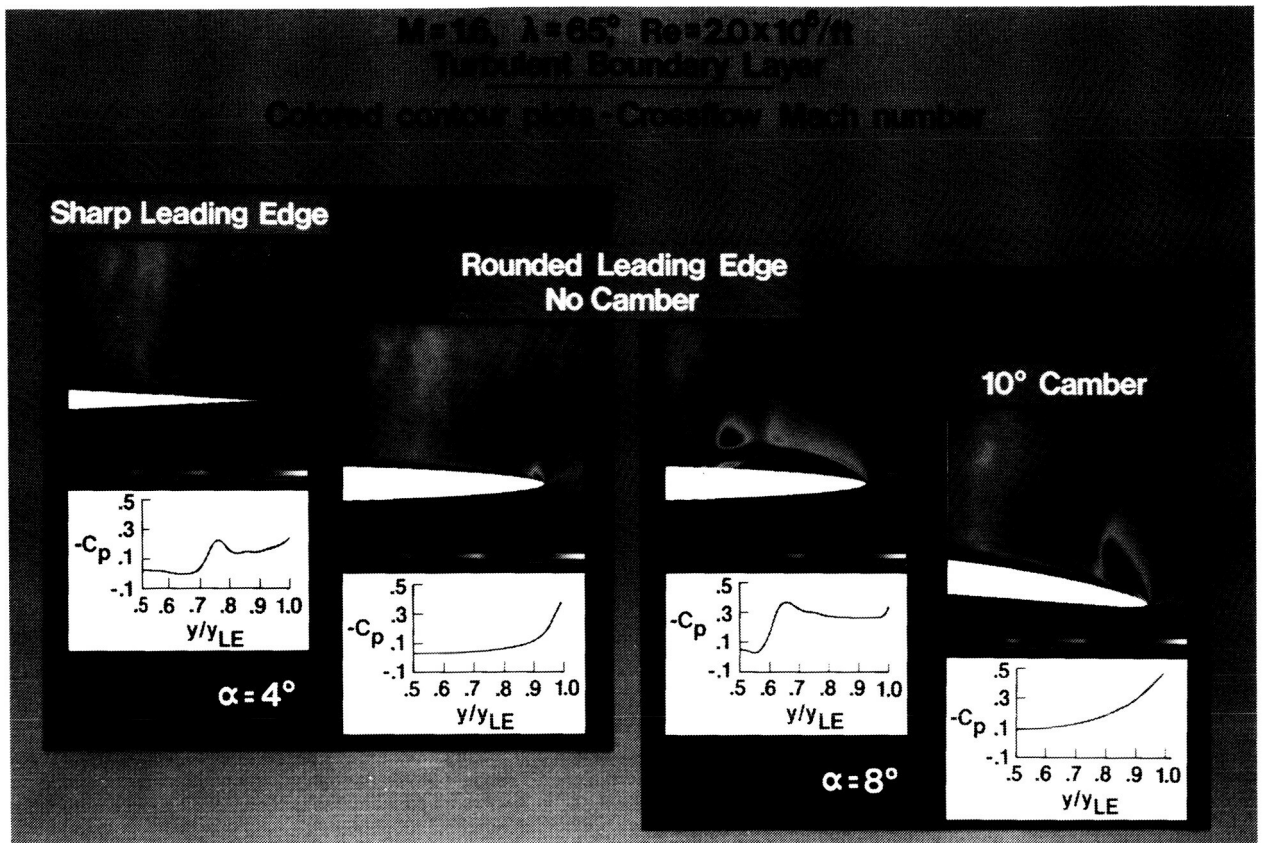


Figure 12.2. Incipient Separation Computational Study

12.3 A PARAMETRIC CFD STUDY OF INCIPIENT LEADING-EDGE SEPARATION

12.3.1 Objective

To systematically study the effectiveness of leading-edge radius and camber for controlling leading-edge separation over the leeside of delta wings at supersonic speeds.

12.3.2 Approach

The approach involved making a computational parametric study on a 65 degrees swept, conical delta wing at Mach 1.6 using CFL3D--a Navier-Stokes computational code. The computational results will be used to guide the development of an experimental confirmation study of key findings.

12.3.3 Accomplishments

For this initial study, all geometries examined were conical. The influence of leading-edge radius was investigated on an uncambered 65 degrees swept delta wing and the influences of spanwise camber were investigated on swept rounded leading-edge delta wings. Conical Navier-Stokes solutions were obtained at Mach 1.6 and $Re=2.0 \times 10^6$ feet for a turbulent boundary layer (See Figure 12.2). The results are presented as colored contour plots of crossflow Mach number distribution in the flowfield and spanwise surface-pressure distributions. The first solution is for the sharp leading-edge geometry at $\alpha=4^\circ$. For these conditions, the code predicted a leading-edge separation bubble. In contrast, for the rounded, leading-edge geometry, the code predicted attached flow with an isentropic compression occurring inboard of the leading edge. This difference in flow structure due to a change in leading edge radius also is clearly evident in the surface-pressure distributions. A similar change in flow structure can be affected by the use of spanwise camber. The addition of 10 degrees of spanwise, circular arc camber was sufficient to alter the separated, leading-edge flow to an attached flow.

12.3.4 Significance

The Navier-Stokes computational code showed that leading-edge radius and spanwise camber can be effective tools for controlling incipient leading-edge separation over delta wings.

12.3.5 Status/Plans

NASA plans to test wind-tunnel models equipped with extensive pressure instrumentation to verify the previously described results experimentally.

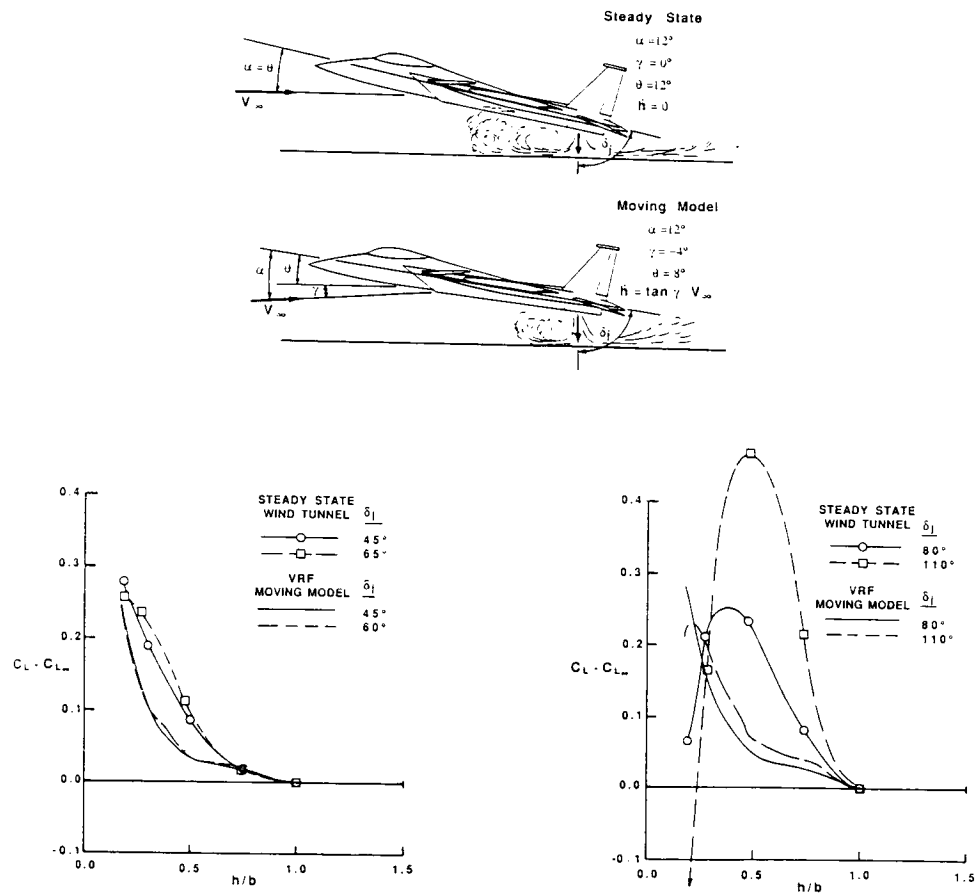


Figure 1 Comparison of static and dynamic ground effects on the lift coefficient of the F-15 S/MTD configuration.

Figure 12.3. Comparison of Static and Dynamic Ground Effects

12.4 STOL/STOVL CONCEPTS FOR HIGH PERFORMANCE AIRCRAFT

12.4.1 Objective

To provide advanced aerodynamic technology and advanced concepts applicable to STOL/STOVL operations of current and future high performance aircraft.

12.4.2 Approach

The approach involved conducting experimental (wind tunnel) and analytical studies using powered models in the Langley 14-foot by 22-foot subsonic tunnel to (1) examine key problems, (2) identify promising solution concepts providing advanced aircraft with STOL/STOVL capabilities and (3) define and develop new test/analysis methods where essential. The 14-foot by 22-foot subsonic tunnel is uniquely equipped for the study of take-off and landing aerodynamics in and out of ground effects (See Figure 12.3).

12.4.3 Accomplishments

An initial investigation of advanced high lift and control concepts on a high sweep fighter model indicates that pneumatic spoilers can produce roll control. Full span leading and trailing edge flaps will be needed for high lift. For dynamic ground effects, analysis of data from the Vortex Research Facility on the F-15 S/MTD, shows significant differences between static and dynamic testing results. NASA developed plans for an improved ground effects testing technique and research program using dynamic hardware and a data system for the 14-foot by 22-foot subsonic tunnel.

12.4.4 Significance

Advanced pneumatic controls could provide control of high performance aircraft without conventional control surfaces. Ground effects testing must include the rate of descent to yield correct answers during ground based testing.

12.4.5 Status/Plans

NASA plans to expand advanced control studies using a high sweep fighter model. NASA also plans to implement dynamic testing will begin in the 14-foot by 22-foot subsonic tunnel in FY 1990-1991 as well as continuing CFD development of ground effect analysis with Ames Research Center.

John W. Paulson, Jr.
 Subsonic Aerodynamics Branch
 Langley Research Center
 (804)864-5071

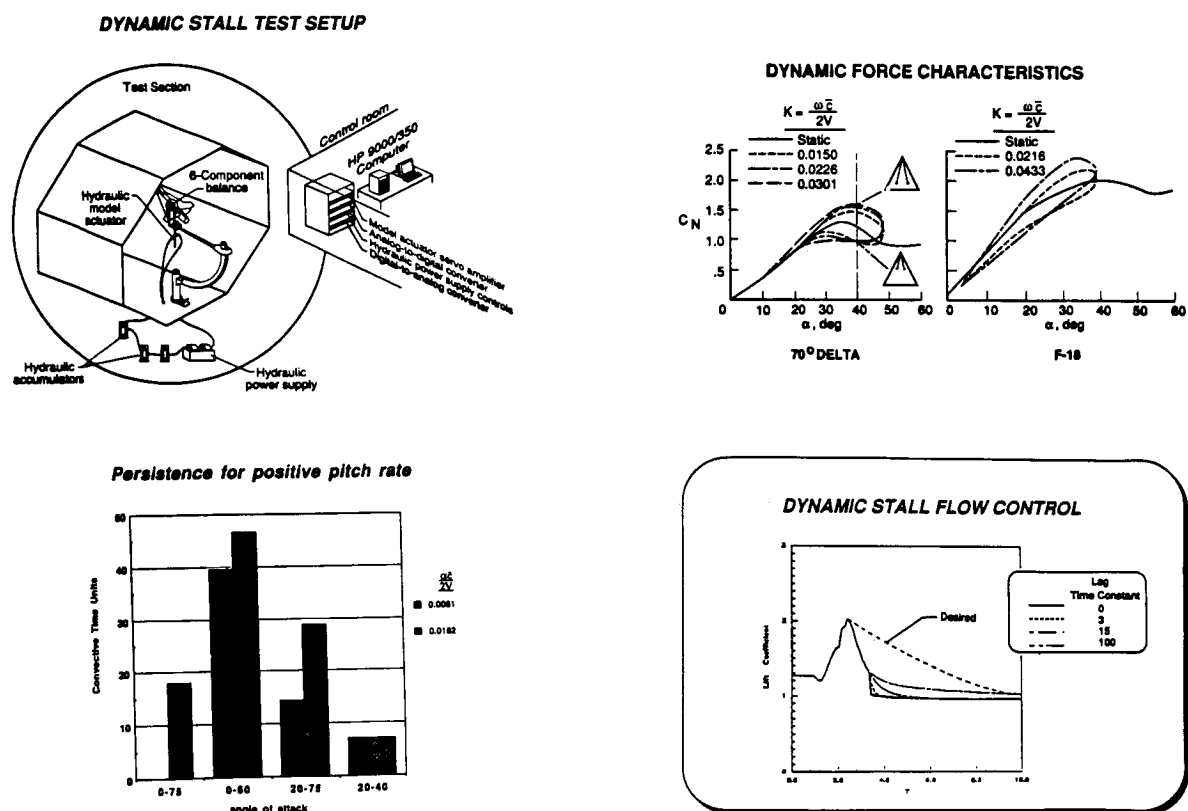


Figure 12.4. Dynamic Stall Research

12.5 DYNAMIC STALL RESEARCH

12.5.1 Objective

To study these phenomena on 3-D aircraft configurations and to assess the impact on maneuvering capability. Wind tunnel tests have shown significant lift overshoots on 2-D airfoils undergoing large amplitude pitching motions. These overshoots are a strong function of angle of attack, α and pitch rate.

12.5.2 Approach

Wind tunnel tests were made on models undergoing large amplitude pitching motions in the Langley 12-foot Low-Speed Wind Tunnel. Figure 12.4 shows a schematic of the test set-up. Dynamic force data were obtained with a series of flat, plate delta wings and on an F-18 model to study the behavior of the unsteady aerodynamic loads during large amplitude oscillatory and ramp motions at high- α . Simulation studies are being made on the Langley Differential Maneuvering Simulator (DMS) using the F-18 simulation database to obtain insight into the effects of dynamic stall on maneuvering capability.

12.5.3 Accomplishments

The ongoing study is focusing on simple harmonic motions with varying frequency and amplitude and ramp motions at various rates starting and ending at different angles of attack. The results show large effects of pitch rate on aerodynamic coefficients. The qualitative effects of pitch rate, which include significant lift and drag overshoot, were found to decrease as the wing sweep increased. The normal force overshoot is increased. Figure 12.4 also shows a comparison of normal force data between the 70 degree flat plate delta wing and the F-18 configuration. Due to flow lags, as pitch rate is increased, the normal force overshoot is increased. The figure shows the persistence of the dynamic effects. These data were obtained by pitching the F-18 model with a ramp motion at different rates and between various initial and final α s. The figure shows that the persistence of dynamic effects is a strong function of the final α and pitch rate. To evaluate the significance of these effects, a simple mathematical model was evaluated on an existing F-18 real-time simulation. The figure shows the simulated lift coefficient during a pitch-up maneuver. The persistence of the simulated effects were varied by using a lag time constant as indicated. Preliminary results show only modest increases in turn performance even with very long persistence values. Testing is continuing to develop methods to control and exploit high- α unsteady aerodynamic effects for maneuvering enhancements.

12.5.4 Significance

Future fighter aircraft will likely use technologies such as thrust vectoring controls that will provide a very high degree of agility and maneuverability. This capability will allow aggressive maneuvering in the high-alpha flight regime which is typically dominated by unsteady vortex flows. A broader understanding of the mechanisms involved in such flows is of great importance in developing methods of improving the high-alpha, stall/post-stall combat maneuverability of modern fighter aircraft.

12.5.5 Status/Plans

Follow-on studies, including studies of arbitrary motions, scale effects and dynamic vortex control techniques are planned. Mathematical models will be developed for a simulation study using the DMS. The study will be used to assess the impact of unsteady flow on aircraft flight dynamics and combat effectiveness. Validation of maneuvering capability, flow behavior and vortex control techniques will then be made through flight testing with NASA's F-18 High-alpha Research Vehicle.

Jay M. Brandon and Gautam H. Shah
Flight Dynamics Branch
Langley Research Center
(804)864-1142

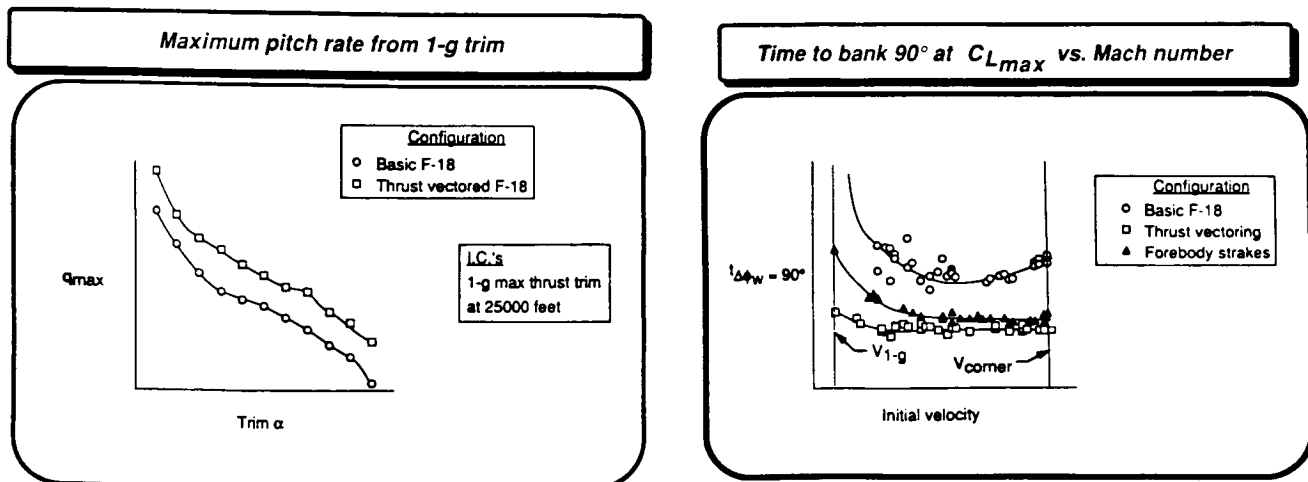


Figure 12.5. Simulation Studies of Enhanced Combat Maneuvering

12.6 SIMULATION STUDIES OF ENHANCED COMBAT MANEUVERING FOR F-18 USING ADVANCED CONTROLS

12.6.1 Objective

To evaluate the enhancements in maneuverability provided by advanced control concepts under realistic combat conditions and to define control law requirements to maximize these benefits. Air combat studies show the importance of providing future fighter aircraft with extreme levels of agility and maneuverability.

12.6.2 Approach

The Differential Maneuvering Simulator (DMS) was used to develop the design methodologies required to implement these concepts on future aircraft. The simulations focused on two classes of concepts (1) multi-axis propulsive control (thrust vectoring) and (2) unconventional aerodynamic control devices such as deflectable forebody strakes. Representations of a propulsive control system for vectoring the thrust in pitch and yaw and forebody strakes for additional aerodynamic yaw control were developed and added to a full-envelope simulation of the F-18. Control law requirements to maximize the maneuvering benefits were developed for each concept and these benefits were quantified by performing air combat maneuvers. The DMS studies have included evaluation of the pilot/cockpit environment (See Figure 12.5).

12.6.3 Accomplishments

The control laws developed to take advantage of the additional control power to maximize the maneuver enhancements incorporated two fundamental requirements, (1) blending of the aerodynamic and propulsive controls and (2) provision of high angular rate capability while maintaining acceptable levels of controllability. The results from simple maneuvering tasks showed significant improvements in combat performance across an expanded angle-of-attack envelope for the airplane equipped with propulsive control or with forebody strakes. Improvements in maximum attained pitch rates were obtained by using pitch thrust vectoring in addition to the aerodynamic pitch controls. Roll performance also was greatly improved by the use of yaw thrust vectoring or the forebody strakes which provided the additional yaw control required for coordinated rolling maneuvers over the entire critical speed range for subsonic maneuvering.

12.6.4 Significance

The use of advanced aerodynamic and propulsive controls greatly enhanced the combat maneuvering capability of a simulated F-18 airplane. The results have been used to define the fundamental control effectiveness and control law requirements for implementation on the F-18 HARV research testbed for flight evaluation. Concepts for pilot information systems and control which were developed as part of the simulation effort also are being considered for the HARV.

12.6.5 Status/Plans

Maneuvering tasks and simulated one-on-one air combat revealed the benefits offered by advanced controls. These benefits will continue to be evaluated using simulated two-on-one air combat as well. Additional work in several related areas is planned, particularly (1) the effect of more detailed modeling of the high angle-of-attack aerodynamics, (2) advanced control effector hardware design, (3) multi-effector control law design optimization to meet critical flying qualities requirements and (4) cockpit information systems for improved pilot awareness and maneuver guidance.

Marilyn E. Ogburn and Keith D. Hoffler
Flight Dynamics Branch
Langley Research Center
(804)864-1175

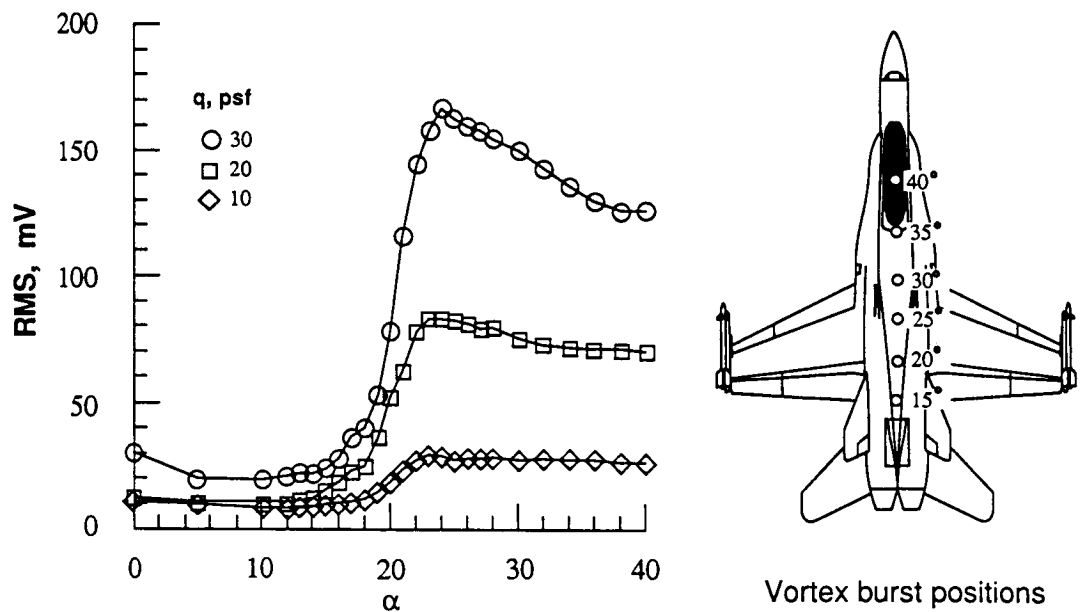


Figure 12.6. F/A-18 Fin Root Bending Moment

12.7 VORTEX INTERACTION RESEARCH

12.7.1 Objective

To provide fundamental insight into the interaction of both burst and unburst vortices with tail surfaces.

12.7.2 Approach

The approach involved studying the surface and off-body flowfield on both simple delta wings with tails and complex fighter configurations in the Basic Aerodynamics Research Tunnel. Instrumentation being used in these studies includes three-component laser Doppler velocimeter, hot-film surface sensors, strain-gage sensors and high frequency response pressure transducers.

12.7.3 Accomplishments

In November 1988, NASA studied the effect of an F-18 LEX vortex on the vertical tail throughout the angle-of-attack range. The root bending moment was measured on the right-hand vertical tail using a strain gage and surface velocity fluctuations were measured at one point using a surface hot-film gage. The location of the vortex burst at high angles-of-attack also was determined.

12.7.4 Significance

The root bending moment results indicate a sharp rise in the tail root bending moment at an angle-of-attack of approximately 20 degrees (See Figure 12.6). The vortex burst location is just forward of the vertical tails at this angle-of-attack. The root bending moment data compares well with previous wind tunnel and flight tests. The surface hot film data shows high-turbulence flow at angles-of-attack greater than 20 degrees. Although the trend of highly turbulent flow at high angles-of-attack agrees with previous water tunnel tests by Wentz, the discrete frequencies shown by Wentz were not found in the spectral analysis of this data.

12.7.5 Status/Plans

Detailed flowfield measurements will be made over a 76 degree delta wing with and without vertical tails. The tails include a rigid tail instrumented with Kulite pressure transducers and a flexible tail instrumented with accelerometers and strain gages. This test is part of a cooperative program with McDonnell Aircraft Company to study the interaction of a single vortex with vertical tail surfaces.

William L. Sellers, III
Analytical Methods Branch
Langley Research Center
(804)864-1287

ORIGINAL PAGE
BLACK AND WHITE PHOTOGRAPH



Figure 12.7. Supersonic STOVL Technology

12.8 SUPERSONIC STOVL TECHNOLOGY

12.8.1 Objective

To provide the necessary powered-lift research and technology development for an improved validated database of new aerodynamics and flight dynamics technology for application to future generations of supersonic short takeoff and vertical landing (STOVL) fighter attack aircraft (See Figure 12.7).

12.8.2 Approach

This objective was accomplished by conducting analytical, ground-based and flight research investigations. As part of the joint US/UK Advanced STOVL (ASTOVL) technology development program, four airframe and three engine contractor design studies of candidate ASTOVL concepts were completed and all designs were evaluated and "normalized" using in-house design synthesis and independent systems analyses. A joint assessment and ranking of the US and parallel UK, candidate concepts was completed to determine a focus for future technology development.

12.8.3 Accomplishments

The resulting US/UK ASTOVL Technology Program Plan was written and coordinated between the two countries. In addition, DoD and NASA developed a US National STOVL Plan which includes the possibility of a research/ demonstrator aircraft.

12.8.4 Significance

The US/UK ASTOVL Technology Development Program reached a major milestone when the decision was made after a thorough assessment and ranking activity to pursue, in the future, only those concepts which utilize remote lift for jet-borne flight and conventional mixed-flow propulsive systems for wing-borne flight. In addition, the seven most critical technologies for supersonic STOVL were identified and these are addressed by the jointly formulated US/UK ASTOVL Technology Development Program Plan.

12.8.5 Status/Plans

Detailed plans are being formulated for developing the critical supersonic STOVL technologies. Technology research investigations will continue in FY 1990 as baseline funding permits. A major augmentation in funding has been advocated to support increased research in FY 1991 and beyond. Efforts will continue to define the roles of the various participants in the US National STOVL Plan. A R&D task order contract will be awarded to several US airframe companies for supersonic STOVL technology development in support of the US National STOVL Plan and the US/UK ASTOVL Program in FY 1990.

K. Clark White
STOVL/Powered-Lift Technology Branch
Ames Research Center
(415)604-5653

**ORIGINAL PAGE
BLACK AND WHITE PHOTOGRAPH**

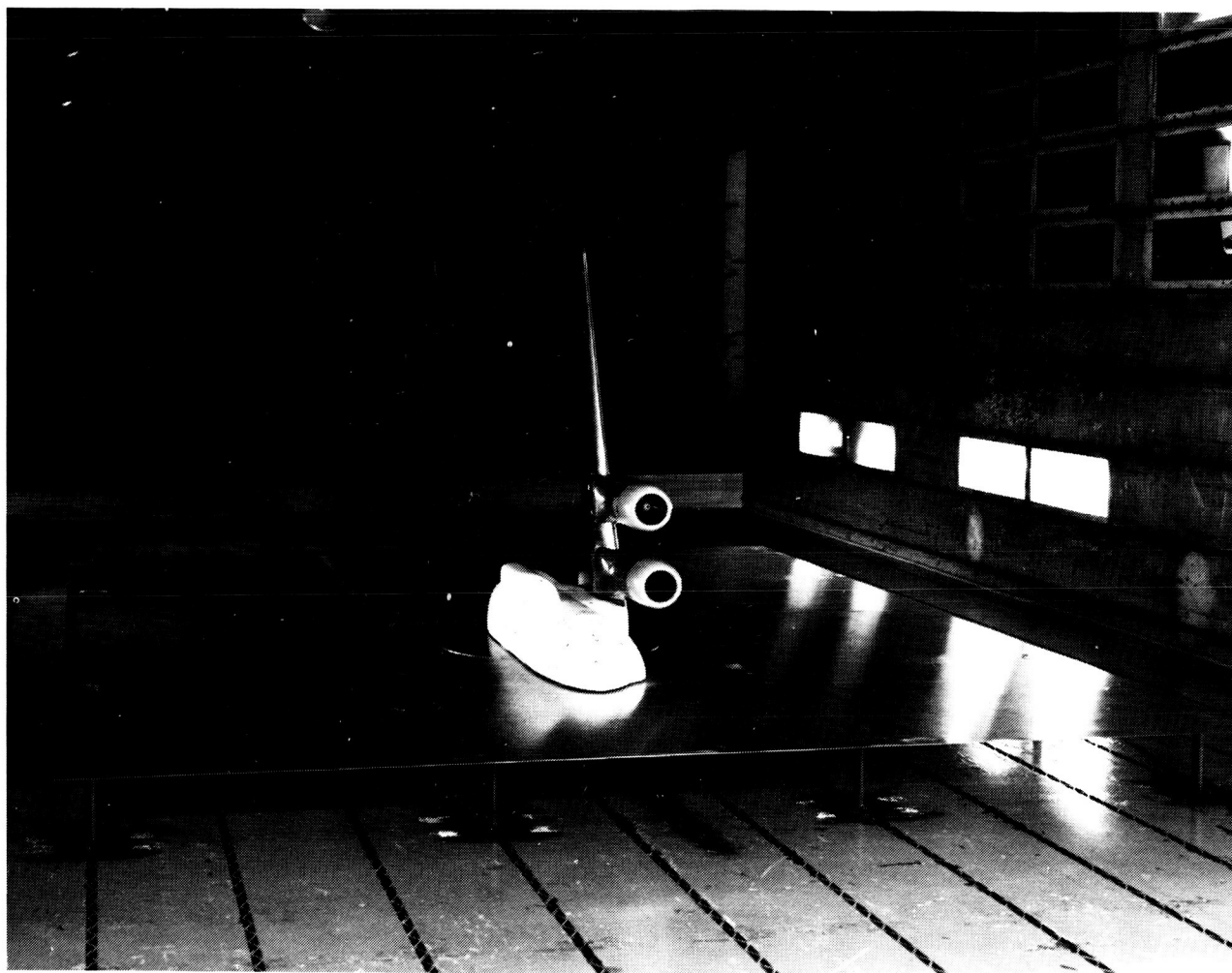


Figure 12.8. STOL Transport Technology

12.9 STOL TRANSPORT TECHNOLOGY

12.9.1 Objective

To provide the necessary powered-lift research and technology development for a validated database of new aerodynamics and flight dynamics technology for application to future generations of civil and military subsonic STOL transport aircraft.

12.9.2 Approach

This objective was accomplished by conducting in-house and contracted analytical, ground-based and flight research investigations of powered-lift STOL configurations applicable to transport aircraft.

12.9.3 Accomplishments

Flight and wind tunnel tests of the Japanese National Aerospace Laboratory (NAL) "ASKA" USB transport research aircraft were conducted as part of the NASA/NAL cooperative pilot and technology interchange agreement. NASA QSRA test pilots and engineers went to Japan in October 1988 to conduct flight evaluations of the handling and performance characteristics of the ASKA aircraft. Tests of the NAL ASKA seven percent scale, semispan cruise-configuration powered model in the Ames 14-foot Transonic Wind Tunnel were completed in May 1989 (See Figure 12.8). Balance force data, wing pressure data and nacelle inlet and internal and exhaust pressure data were obtained over a range of power settings, angles of attack and Mach numbers up to 0.775. A contract was awarded for the design and fabrication of a nose gear "jump strut" to be flight tested on the QSRA under a joint program funded by the Air Force.

12.9.4 Significance

The ASKA flight evaluation greatly expands the available information on the handling and performance capabilities of USB STOL aircraft, adding to the powered-lift transport design and certification database that NASA built through programs such as the Augmentor Wing STOL Research Aircraft and the Quiet Short-Haul Research Aircraft (QSRA). The NASA/NAL wind tunnel data provides an assessment of the USB exhaust scrubbing drag cruise penalty and the interference effects associated with spanwise nacelle placement. The detailed exhaust jet flowfield data are essential for validating advanced in-house CFD code development and configuration optimization studies.

12.9.5 Status/Plans

NASA plans to continue to support Air Force Advanced Tactical Transport and Special Operations Forces activities through in house studies and technology transfer. NASA will publish the results of the ASKA flight evaluations as a joint NASA/NAL report this year and the ASKA wind tunnel test data in FY 1990. The application and validation of advanced CFD methods for powered-lift USB configurations is underway with preliminary Navier-Stokes solutions expected this fall. NASA will design, fabricate and ground test the QSRA nose-gear "jump strut" in FY 1990.

K. Clark White
STOVL/Powered-Lift Technology Branch
Ames Research Center
(415)604-5653



Figure 12.9. STOVL Flying Qualities Evaluation

12.10 STOVL FLYING QUALITIES EVALUATION

12.10.1 Objective

To (1) evaluate the STOVL aircraft transition envelope, (2) determine takeoff performance and procedures, (3) determine control power during powered-lift operations and (4) evaluate the integration of the aircraft's flight and propulsion controls.

12.10.2 Approach

The approach involved (1) developing a simulation model for the STOVL concept, (2) predicting transition and takeoff characteristics, (3) defining integrated flight/propulsion control and (4) conducting piloted evaluations in the Interchangeable Cab Facility (See Figure 12.9).

12.10.3 Accomplishments

A powered-lift aerodynamics/propulsion model was developed based entirely on analytical predictions. Transition and takeoff performances were defined, including the effects of thrust vectoring efficiency and excess thrust. Thrust margins were defined for vertical landing as a function of ground effect and hot gas ingestion. Control power utilization, including reaction control bleed, was established for powered-lift operations. The influence on transition and vertical landing flying qualities of integrated flight/propulsion control modes was determined.

12.10.4 Significance

Design and performance of STOVL aircraft during powered-lift operations are critically dependent on aerodynamics/propulsion interactions and requirements for excess thrust, thrust deflection, reaction control and integrated flight/propulsion controls. This simulation provided the first step in defining these interactions and requirements; furthermore, the potential for achieving Level I flying qualities throughout the powered-lift envelope was established for this STOVL concept.

12.10.5 Status/Plans

Moving-base simulations and flight experiments are required to achieve highly credible assessments of control of the transition and vertical landing, particularly for definition of thrust margins, minimum acceptable acceleration and integrated control modes. These experiments will be conducted on the Vertical Motion Simulator for two mixed-flow remote-lift STOVL concepts and on the VSRA for control mode evaluation.

ORIGINAL PAGE
BLACK AND WHITE PHOTOGRAPH

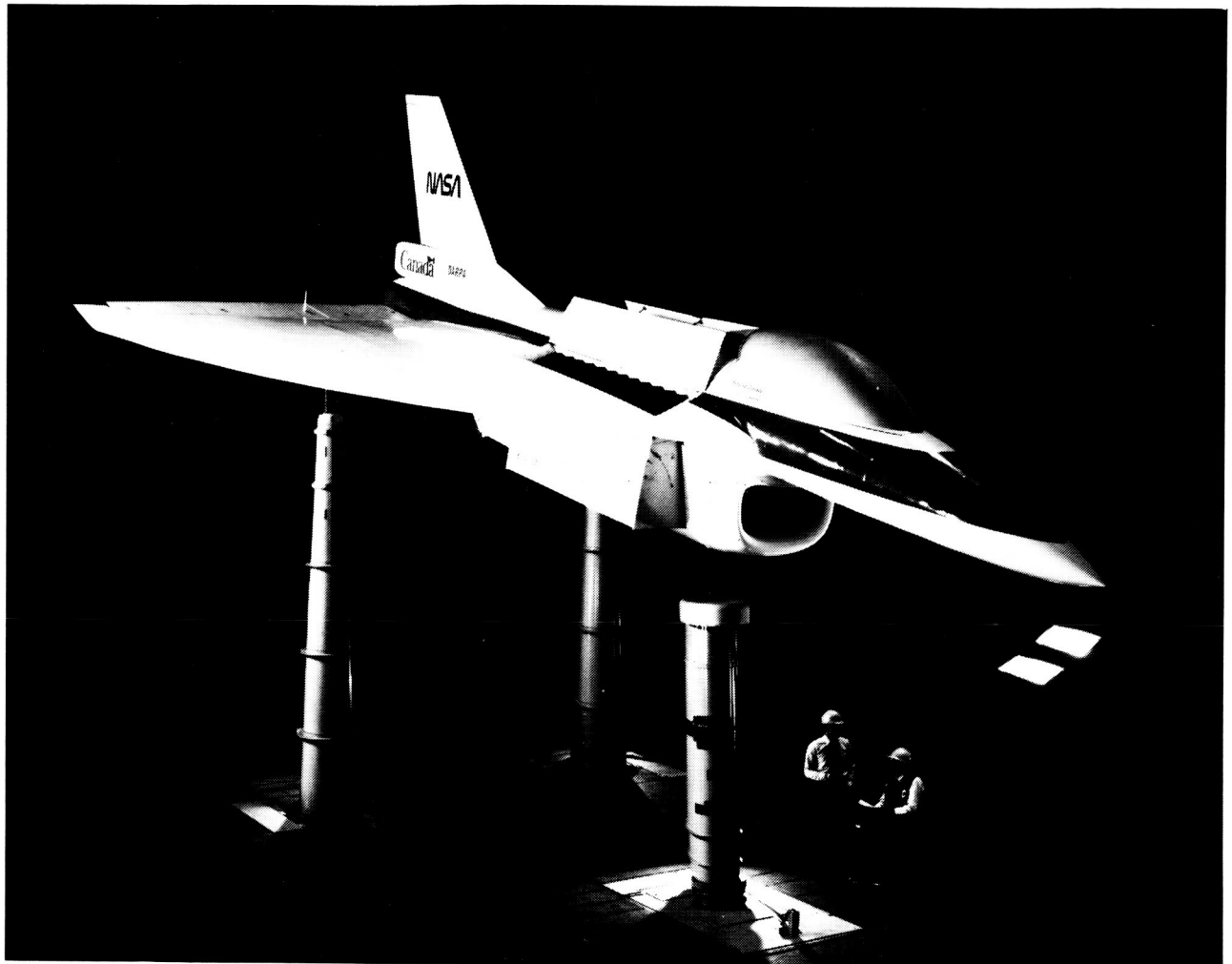


Figure 12.10. STOVL E-7A Tests in the 40-Foot by 80-Foot Wind Tunnel

12.11 STOVL E-7A TESTS IN THE 40-FOOT BY 80-FOOT WIND TUNNEL

12.11.1 Objective

To measure and validate large scale E-7 ejector performance for hover and low speed flight with a primary emphasis on augmentation ratios and accelerating and decelerating performance margins.

12.11.2 Approach

A full-scale powered model of the E-7 aircraft was tested in the 40-foot by 80-foot test section of the National Full-Scale Aerodynamics Complex (NFAC). Tunnel balance, ejector rake and wing pressure instrumentation documented the low speed performance of the vehicle (See Figure 12.10).

12.11.3 Accomplishments

Ejector performance on the full-scale E-7 aircraft was very encouraging. It was the highest, full-scale aircraft augmentations ratios to date (augmentation ratio=1.4 to 1.8). The E-7 aircraft has an adequate acceleration and deceleration corridor enabling it to transition from hover to forward flight and back to hover in level flight. Elevon effectiveness was shown to be independent of model configuration changes and forward speed.

12.11.4 Significance

The E-7 STOVL concept is one of those favored in the U.S./Great Britain cooperative research STOVL technology program. The data gathered in this test confirmed the viability of the concept by demonstrating good hover and low speed performance.

12.11.5 Status/Plans

Testing of the E-7 model in the 80-foot by 120-foot test section of the NFAC currently is underway. The larger tunnel test section yields low speed transition performance data with less tunnel recirculation effects. A pure hover test of this aircraft on an outdoor static test rig is planned for Spring 1990.

Brian Smith
Fixed Wing Aerodynamics Branch (FFF)
Ames Research Center
(415)604-6669

ORIGINAL PAGE
BLACK AND WHITE PHOTOGRAPH

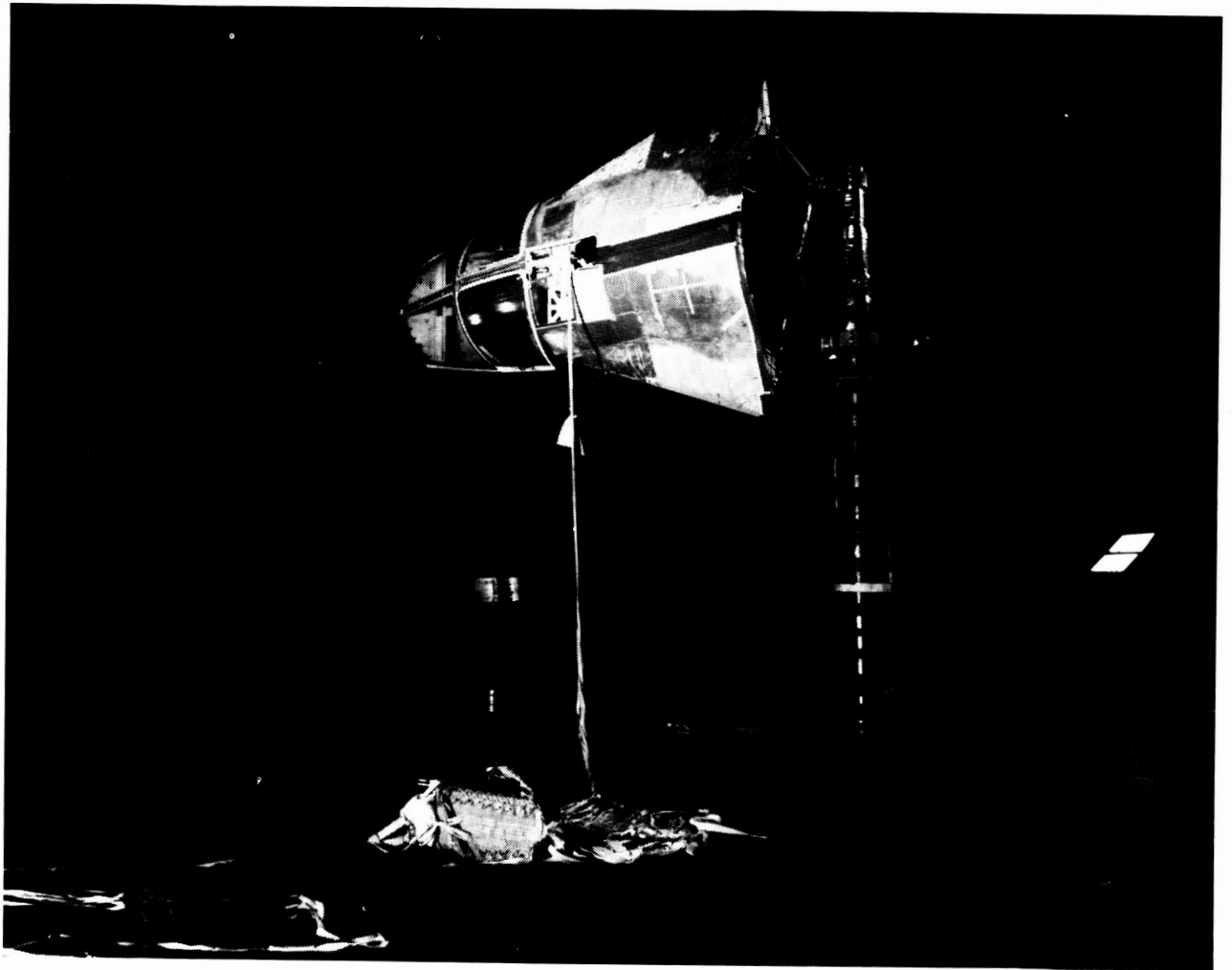


Figure 12.11. F-111 Crew Escape Module

12.12 F-111 CREW ESCAPE MODULE 40-FOOT BY 80-FOOT WIND TUNNEL TEST

12.12.1 Objective

To (1) define the aerodynamic drag behavior of newly proposed pilot parachutes for a redesigned F-111 Crew Escape Module and (2) validate the design of the deployment phase of the recovery system over a full range of escape module attitudes.

12.12.2 Approach

The F-111 Crew Escape Module was mounted in the 40-foot by 80-foot wind tunnel at a range of angles of attack simulating separation attitudes of the module. The drag of the pilot chutes were measured and compared with design predictions. The pilot chutes were fired from the escape module and the deployment phase of the recovery system was observed and recorded (See Figure 12.11).

12.12.3 Accomplishments

This highly successful test program acquired critical pilot parachute design data that were not achievable in drop testing. Module angle of attack ranges of from +30 degrees to -90 degrees were tested at flow velocities up to 170 knots. As a result of these tests, the design was modified by strengthening the packing line-ties of the deployment mechanism.

12.12.4 Status/Plans

No future testing requirements were identified.

Rob Faye
Research Operations Branch (FFN)
Ames Research Center
(415)604-3545

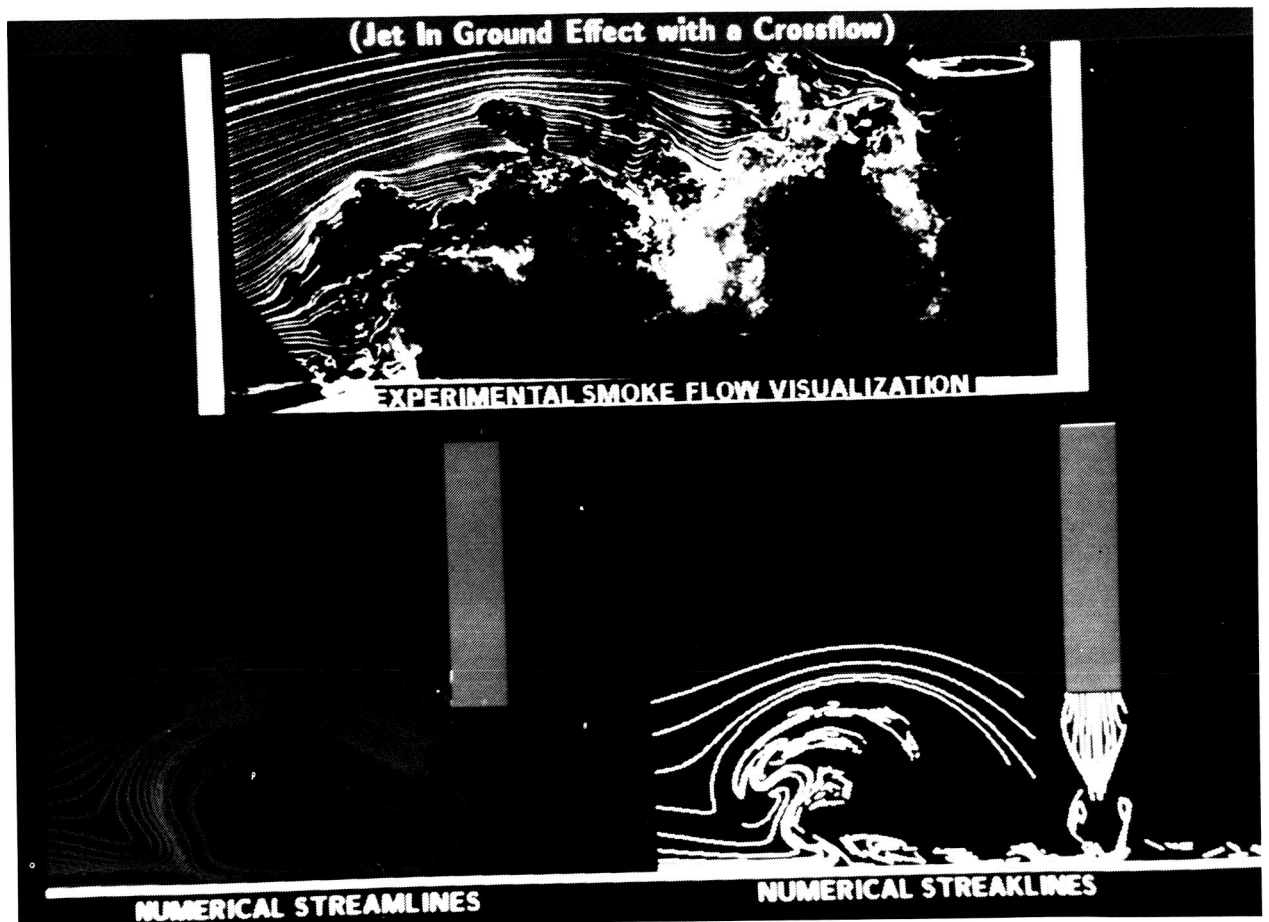


Figure 12.12. Experimental Versus Numerical Flow Visualization

12.13 NUMERICAL SIMULATION OF STOVL AIRCRAFT AERODYNAMICS

12.13.1 Objective

To predict STOVL aircraft performance from take-off through transition and to cruise conditions, including aero-thermal, -acoustic, -propulsion, -control and -structural interactions.

12.13.2 Approach

The approach involved coupling Navier-Stokes code with a thermal conduction solver for an aero-thermal interaction (See Figure 12.12).

12.13.3 Accomplishments

Detailed Harrier YAV-8B surface definition was completed. Navier-Stokes flow and thermal conduction solvers were combined and are currently undergoing time and spatial accuracy validation tests.

12.13.4 Significance

Supersonic STOVL and other powered-lift programs require validated interdisciplinary numerical simulation capability.

12.13.5 Status/Plans

NASA will continue grid development, utilizing overlapped/patched and adaptive strategies to reduce grid generation time and solution cost. Results of the calculations will be compared to experimental data to validate the accuracy of the calculations.

W. R. Van Dalsem
Applied Computational Fluids Branch
Ames Research Center
(415)604-4469

This page is intentionally left blank.

CHAPTER THIRTEEN

ROTORCRAFT

13.1 INTRODUCTION

The objective of the Rotorcraft Program is to provide the enabling technologies for helicopters and other rotor-borne aircraft to achieve quiet, low vibration operation with increased performance, agility, maneuverability and stability, all with acceptable handling qualities. Much of the work is done in conjunction with the U.S. Army and the FAA and in cooperative programs with industry.

Improved analysis can now handle many local aerodynamic phenomena but the transonic, unsteady, complex wake interaction flow requires another generation of codes; therefore, much of the rotorcraft program still is empirically based, with validation of analysis as a goal. This approach requires new test techniques, upgraded test facilities, carefully instrumented models, sophisticated simulation and increased use of the latest generation of computers. New ideas also are part of the program, since the complexity of rotorcraft makes it a fertile area for innovative approaches.

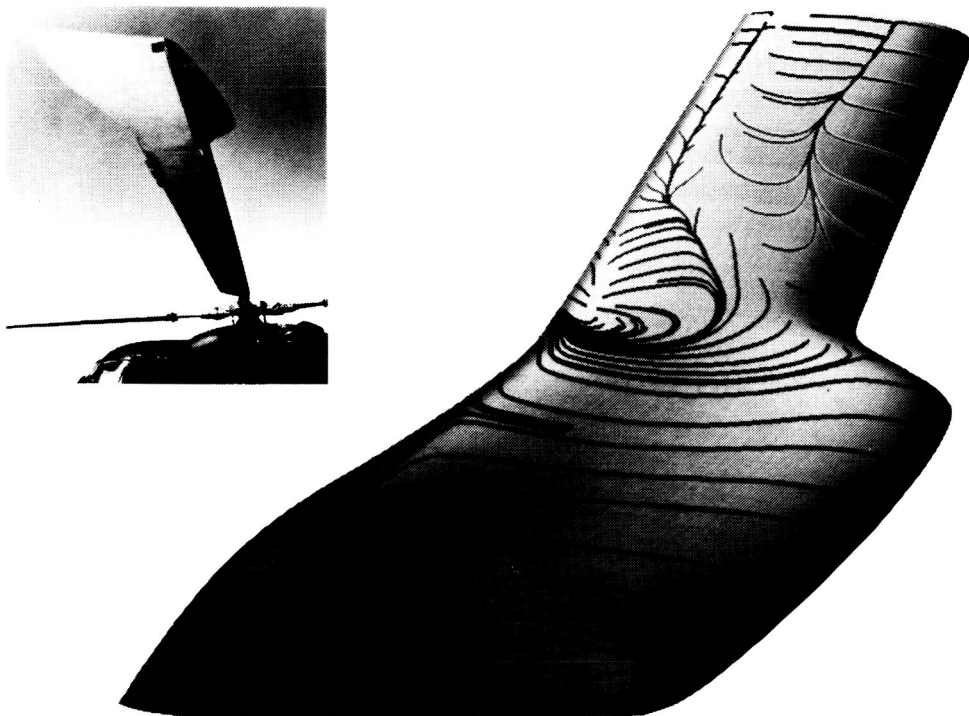
The heart of the aerodynamic portion of the program is airloads research. Small scale, pressure-tapped blade data are becoming available with the full-scale results due in 1990. Complimentary efforts are underway in component, interference and wake testing and prediction. These databases are used in acoustic and vibration research, which constitutes more than half of the program resources. The airload models also will be used for rotor state control and higher-harmonic control to suppress noise or vibration or to enhance maneuverability.

Handling qualities research in the Aerodynamics Division is based on vehicle flight dynamics, with emphasis on simulation and flight test using the variable stability CH-47. New flight test capability is planned, with research challenges in integrated control, automation and higher-frequency control a focus.

Higher speed rotorcraft will continue to be dominated by tiltrotor efforts. Certification issues are being addressed on the simulator and in noise testing and prediction. Also underway are improvements in performance, interior noise, vibration and stability. The importance of these research opportunities for civil applications will be evaluated under contract to Boeing Commercial Airplane Company.

Program Manager: George Unger
OAST/RF
Washington, DC 20546
(202)453-2815

$\alpha = 20^\circ$, $Re = 1.5 \times 10^6$, $M = 0.2$



E.P.N. DUQUE, U.S. ARMY AEROFLIGHTDYNAMICS DIRECTORATE, AVSCOM

Figure 13.1. BERP Rotor

13.2 NUMERICAL SIMULATION OF ROTORCRAFT AERODYNAMICS

13.2.1 Objective

To develop and validate code for a three-dimensional, viscous flow about arbitrary rotorcraft configurations.

13.2.2 Accomplishments

The accomplishments were the (1) numerical, simulated, computed, detailed calculations of tip vortex formation; (2) analysis of highly nonlinear flow past complex tip shapes and (3) calculation of acoustic wave formation and propagation (See Figure 13.1).

13.2.3 Significance

This program is pioneering the application of computational fluid dynamics to important national defense problems. It has reduced risk for new configurations with increased performance, efficiency and maneuverability as well as reducing vibrations, noise and detectability.

13.2.4 Status/Plans

The program is developing code to analyze retreating blade stall. NASA is studying rotor-body interactions with rotating and fixed-block zonal grid topology and solution-adaptive grids for vortex wakes.

W. J. Mc Croskey
Applied Computational Fluids Branch
Ames Research Center
(415)604-6428

TWO BLADES, RECTANGULAR NACA 0012 BLADE,
RADIUS = 3.428 FT, AR = 13.71

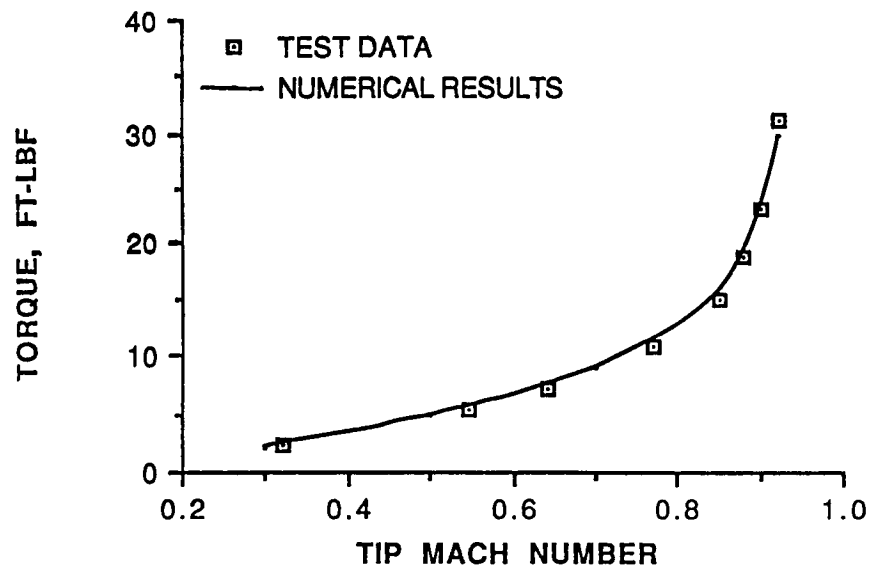


Figure 13.2. Comparison of Predicted and Measured Torque
for a Nonlifting, Hovering Aircraft

13.3 THREE DIMENSIONAL DRAG PREDICTION FOR ROTOR BLADES

13.3.1 Objective

To provide an efficient analytical tool for rotor blade drag prediction and to enable accurate design of new, advanced rotor systems with improved performance in both hover and forward flight.

13.3.2 Approach

A viscous-inviscid interaction approach was used. Very near the blade surface, the flow was assumed viscous and was governed by the three-dimensional, boundary layer equations. Outside the boundary layer, the flow was assumed inviscid and was governed by the full-potential equations. These two sets of equations were solved on a rotating reference frame separately, but were coupled together through pressure and displacement thickness (See Figure 13.2).

13.3.3 Accomplishments

The analysis was first used to predict drag force on a two dimensional, NACA 0012 airfoil. The analysis slightly underpredicts the drag coefficient for high Reynolds number flow. For lower Reynolds number flow, the prediction is very good. The analysis was then used to predict the drag force of a nonlifting, two-bladed, hovering rotor. The predicted torques are in excellent agreement with test data.

13.3.4 Significance

The state-of-the-art in rotor drag prediction uses two dimensional airfoil tables to extrapolate the viscous drag. This approach cannot be used in airfoils not yet tested. It also does not include the effects of Reynolds number or the rotational motion of the blade. The current approach can solve the two shortcomings and the initial results also show good accuracy.

13.3.5 Status/Plans

The analysis now predicts nonlifting hovering rotor performance. It is planned to use the analysis to (1) simulate nonlifting and lifting rotor flows and advanced blade performance, airfoils and twist distribution to further evaluate the accuracy and applicability of the analysis and (2) investigate the effect of rotational motion of the blade on the development of the boundary layer to understand the basic aerodynamic phenomena of the boundary layer.

Ching S. Chen
Rotorcraft Aeromechanics Branch (FFR)
Ames Research Center
(415)604-5043

ORIGINAL PAGE
BLACK AND WHITE PHOTOGRAPH

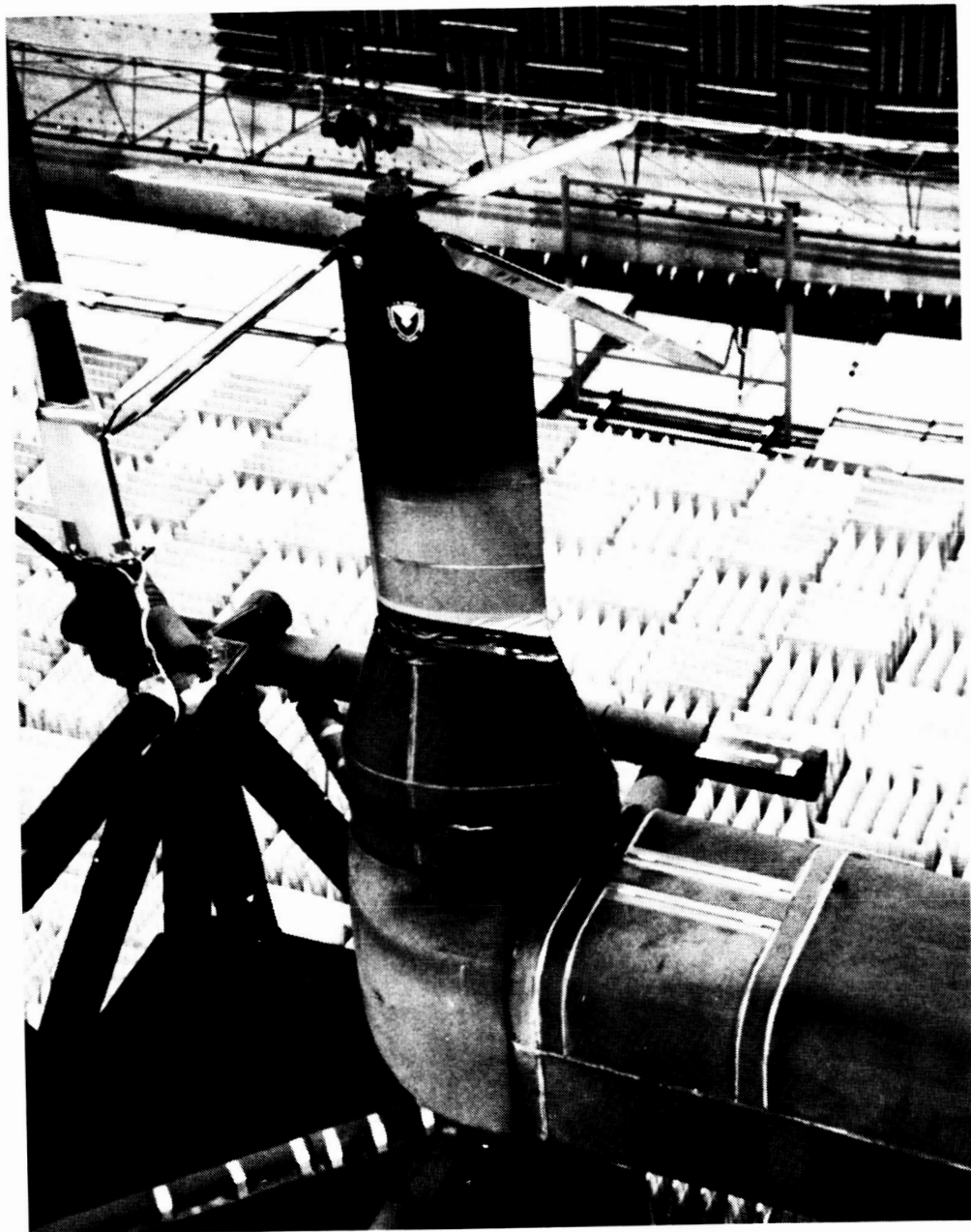


Figure 13.3. UTRC Model Rotor System

13.4 PRESSURE-INSTRUMENTED MODEL ROTOR NOISE TEST

13.4.1 Objective

To acquire model rotor impulsive noise due to Blade Vortex Interactions (BVI) and the concurrent surface pressure data for use with cross correlation and coherence calculations. These analyses will increase the understanding of the physical process by which BVI noise propagates to the farfield.

13.4.2 Approach

An experiment was performed jointly by the staff of the Army Aeroflight Dynamics Directorate, United Technologies Research Center, Sikorsky Aircraft Company and NASA Ames and Langley Research Centers during Spring 1989 in the Duits-Nederlandse Wind Tunnel (DNW). The project tested the UTRC, highly instrumented, model rotor system, a model equipped with 176 subsurface pressure transducers. High quality dynamic surface pressure data were acquired simultaneously with blade-vortex interaction acoustic data for a wide range of vehicle flight speeds.

13.4.3 Accomplishments

Online examination of the measured noise and surface pressure data showed strong impulsive blade loading in the downwind half of the rotor disk, where the radiated BVI noise originates. Figure 13.3 shows an example of a strong BVI noise measured and a leading edge transducer signal, both indicating considerable impulsive content.

13.4.4 Significance

This experiment provided an extensive high-quality database for furthering present understanding of the BVI process.

13.4.5 Status/Plans

NASA initiated efforts in (1) performance of mathematical cross correlation and coherence calculations of the acoustic and blade pressure data, (2) pinpointing the source of the BVI noise in the dynamic surface pressure and (3) defining the process by which the impulsive surface loading radiates to the farfield.

R. M. Martin and M. A. Marcolini
Aeroacoustics Branch
Langley Research Center
(804)864-3631

ORIGINAL PAGE
BLACK AND WHITE PHOTOGRAPH



Figure 13.4. UH-60 with Instrumented Blade Set

13.5 UH-60 LOADS AND PERFORMANCE FLIGHT INVESTIGATIONS

13.5.1 Objective

To (1) investigate high speed rotor aerodynamics and structural dynamic limits in maneuvering and non-maneuvering flight and (2) correlate flight data with wind tunnel results and comprehensive prediction codes to validate aircraft modeling and prediction capabilities. A secondary objective was to evaluate the viability of a gust suppression technique using Individual Blade Feedback. This effort was a precursor to the more extensive UH-60 airloads program.

13.5.2 Approach

A cooperative program with the U.S. Army Aviation Engineering Flight Activity (AEFA) was conducted utilizing a UH-60 helicopter with an instrumented blade set from the U.S. Air Force Night Hawk program (See Figure 13.4). The Army provided the test aircraft and the tests were conducted at AEFA, Edwards AFB, with Army operations personnel. Ames provided program specific instrumentation, final data processing and a research engineering team. The Ames engineering team provided onsite data quality checks, flight test support and testing guidance.

13.5.3 Accomplishments

The flight test program has been completed. The flight data were entered in a TRENDS database and errors were corrected or removed. A hands-on workshop was conducted to train the Government/industry/academic researchers in the use of the database. A preliminary correlation study using CAMRAD was completed and the results compiled as a NASA report (currently in review). A draft data summary report was prepared for publication as a NASA report. A blade shake test was conducted with a final report in publication. A NASTRAN model of the UH-60 was completed and its predictions were compared to an airframe shake test. A grant was awarded to UCSD to improve the NASTRAN model with the inclusion of secondary airframe structures.

13.5.4 Significance

The database which contains high speed conditions unavailable from other sources, is available to the rotorcraft user community. Initial reaction was very favorable. The NASTRAN model and blade shake test are key elements of providing complete documentation on the UH-60 aircraft. The CAMRAD correlation results are one of the first flight validation studies of this industry-wide, comprehensive prediction code.

13.5.5 Status/Plans

NASA will complete all reports and eventually combine these data with the UH-60 airloads database. Correlation studies with other modeling codes as well as full scale and model scale wind tunnel tests will be conducted. The reports currently in the publication cycle will be released as soon as it is practical.

Edward I. Seto and Jeffrey Cross
Flight Experiments Branch/Rotorcraft Technology Branch
Ames Research Center
(415)604-5664/6570

ORIGINAL PAGE
BLACK AND WHITE PHOTOGRAPH



Figure 13.5. The UH-60

13.6 UH-60 ROTOR AIRLOADS PROGRAM

13.6.1 Objective

To (1) provide a comprehensive research database for a state-of-the-art rotor, using the latest measurement technology; (2) investigate rotor blade pressure airloads and dynamics and (3) conduct investigations of specific rotor phenomena in flight, including aerodynamics, acoustics and dynamics, with correlation/validation using predictive codes, small and full scale wind tunnel test results and CFD.

13.6.2 Approach

A UH-60 will be flight tested with very highly instrumented rotor blades including, pressure taps and strain gages and accelerometers, extensive airframe sensors and both ground and airframe acoustic microphones, concentrating on unique flight conditions such as high and low speed, transition, partial and full powered descents and steady and dynamic maneuvers (See Figure 13.5). To maintain the highest quality, data evaluation will be completed prior to the next flight. The database will reside on a large interactive storage device for ready access by the user community.

13.6.3 Accomplishments

The instrumented blade set was fabricated, balanced, calibrated and delivered to Ames. The test aircraft was instrumented and calibrated and currently is flying for pilot check-out with standard blades and the Phase I instrumentation system. The ground station real-time telemetry and data processing system is being checked out. Two contracts were awarded for the investigation of rotor hub impedance. A UH-60 newsletter is being published periodically with the aim of keeping the user community apprised of the program status. The pressure-instrumented model scale UH-60 blades were tested in the DNW wind tunnel by a joint Army/NASA/UTC team.

13.6.4 Significance

The flight data currently available for correlation and validation of prediction and design codes is old (1950s technology rotors), incomplete and of poor quality due to outmoded measurement capability. This UH-60 database will provide a quantum increase in high quality, useable data on state-of-the-art rotor technology. It will include high frequency pressure data correlated with airframe vibration and vehicle acoustics for the first time. This will allow researchers to finally validate theories developed over the last 10 years of increased emphasis on noise and vibration.

13.6.5 Status/Plans

NASA plans to commence research flights during the fourth quarter of FY 1989. Proposals involving experiments are anticipated from the user community which will involve active participation during the acquisition of data.



ORIGINAL PAGE
BLACK AND WHITE PHOTOGRAPH

Figure 13.6. The AH-1G Rotor

13.7 COMPLEMENTARY ROTOR AIRLOADS AND ACOUSTIC PROGRAMS

13.7.1 Objective

To provide a rotor airloads research database, complementary to the UH-60 database for unique rotor configurations and flight conditions unobtainable with the UH-60. These unique configurations will provide data for correlation and validation of codes and methodologies required for the special characteristics of these rotor configurations and flight conditions.

13.7.2 Approach

Three special rotor types were included in this program of small and large scale wind tunnel testing and flight testing. The high speed advanced BV-360 was designed for airspeeds in excess of 200 knots. The bearingless HARP rotor has unique dynamic characteristics due to high effective hinge offset. The AH-1G rotor, for which the flight tests were completed, is two-bladed. Tests of these rotors will be more limited in scope than those for the UH-60 (See Figure 13.6).

13.7.3 Accomplishments

Publication of a major reference publication (RP) on the AH-1G "TAAT" program was completed. AH-1G data currently is being correlated with the FPR (Full Potential Rotor) code coupled with CAMRAD/JA. Vibration reduction flight experiments with the baseline BV-360 rotor and aircraft are continuing in an effort to fine tune the aircraft for high speed performance testing. The final whirl tower test report on the baseline BV-360 rotor was published and a preliminary correlation of the new hover acoustic code with the whirl tower data showed promising results. Design of the pressure instrumented BV-360 blade was completed and pressure transducer calibration at Ames is in progress. Flight testing at Ames of a MDHC pressure instrumented HARP blade is at the preliminary discussion stage.

13.7.4 Significance

The "TAAT" RP represents the first major NASA publication on rotor airloads since the mid-sixties and provides industry and government researchers with an early database for code validation. The BV-360 is the only US helicopter capable of sustained speeds of 200 plus knots. Dynamic characteristics of the bearingless HARP rotor will provide unique data on the effects of blade and hub dynamics on airloads.

13.7.5 Status/Plans

NASA will continue "TAAT" data correlation with coupled FPR/CAMRAD, resolution of BV-360 wind tunnel issues and go-ahead on pressure instrumented blade/fabrication. NASA also will initiate agreement with MDHC for HARP testing if funding will permit.

William Snyder, Martin Maisel, Michael Watts and Jeffrey Cross
Rotorcraft Technology Branch
Ames Research Center
(415)604-6311

ORIGINAL PAGE
BLACK AND WHITE PHOTOGRAPH



Figure 13.7. Bell 412 Rotor/Model 576 Test Stand in a 40-Foot
by 80-Foot Wind Tunnel

13.8 ROTOR/FUSELAGE AERODYNAMIC INTERACTIONS

13.8.1 Objective

The flowfield around any single helicopter component, such as the main rotor or the fuselage, is extremely complex. When isolated aerodynamically, each component has its own unique flowfield and resultant aerodynamic characteristics; however, when in close proximity to one another, as in a helicopter, each component encounters an unsteady, non-uniform flow induced by all the other components; hence, the total flowfield is influenced not only by the flow around each component, but also by the mutual interactions between the components.

13.8.2 Approach

Several, small-scale, experimental and theoretical investigations were conducted to provide quantitative information on the aerodynamic and acoustic interactions that occur between various helicopter components. A major, full-scale test program only recently was completed, investigated the rotor/fuselage interactions for a Bell 412 helicopter rotor and modified NACA 0035 body of revolution. The body was independently mounted on the test stand with load cells. Combined rotor/body loads were measured with the tunnel balance system. A series of body-hub runs allowed for evaluating the individual interactions between the rotor and the body (See Figure 13.7).

13.8.3 Accomplishments

Data were acquired in the 40-foot by 80-foot wind tunnel in hover and up to an advance ratio of 0.3. Shaft angle was varied between minus four degrees and minus twelve degrees. The Mach number ranged from 0.62 to 0.68. A large number of test conditions were run to get various rotor wake/fuselage interactions. Baseline acoustics data were acquired for a future main rotor/tail rotor aerodynamics and acoustics test program. This safe and successful test program was the first wind-on helicopter rotor test in the NFAC since 1980.

13.8.4 Significance

This data set is the first full-scale data acquired to specifically evaluate rotor/fuselage aerodynamic interactions. No corrections are necessary to performance due to Reynolds number or to acoustics due to tip Mach number effects. The body forces and moments are significantly altered by the presence of the rotor hub. An isolated body at negative angle of attack which experiences a negative thrust in isolation sees a significant positive thrust due to the presence of the hub. The acoustics data set is also the first for a full-scale helicopter rotor in the acoustically treated 40-foot by 80-foot wind tunnel.

13.8.5 Status/Plans

Data reduction and analysis will be performed together with correlation and theory. Additional phases of the test program include main rotor/tail rotor testing with a Lynx tail rotor and a Bell 412 tail rotor.

Gloria Yamauchi (FFR)
Rotorcraft Aeromechanics Branch
Ames Research Center
(415)604-6719

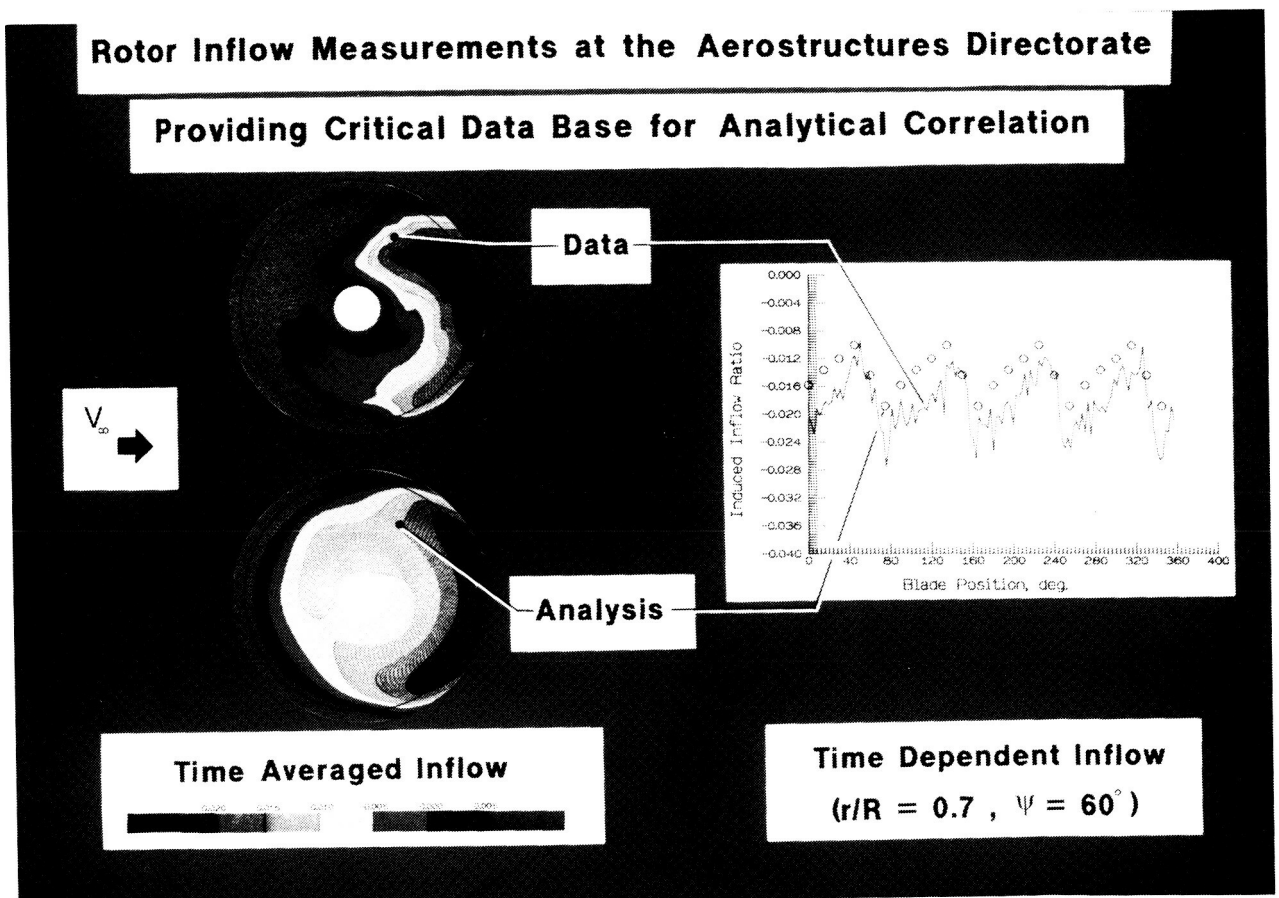


Figure 13.8. Rotor Inflow Measurements

13.9 ROTOR INFLOW/WAKE RESEARCH (USING THE LASER VELOCIMETER)

13.9.1 Objective

To develop a carefully selected database of the detailed flowfield environment in and around a generic helicopter rotor system to be used for rotor inflow/wake prediction code validation.

13.9.2 Approach

The Two Meter Rotor Test System (2MRTS) was installed in the Langley 14-foot by 22-foot subsonic tunnel along with the dedicated laser velocimeter. The rotor system and the tunnel were jointly operated to provide the desired helicopter operating condition and the laser velocimeter was used to acquire the local velocity information required to expand the inflow database. These tests are typically time and labor intensive and require multiple wind tunnel entries to complete the desired database. In this case, it was a full inflow map above the rotor system at one thrust coefficient and five distinct advance ratios: 0.15, 0.23, 0.30, 0.35 and 0.40. Advance ratio, m , is the ratio of forward flight speed to rotor tip speed (See Figure 13.8).

13.9.3 Accomplishments

Four test programs were conducted with the latest accomplished in November 1988. A complete data set ($m=0.15, 0.23, 0.30, 0.35$ and 0.40) was acquired for a generic, four bladed, rectangular-planform rotor. These measurements were acquired at a thrust coefficient of 0.0064 and zero propulsive force. The results of these tests, as well as comparison with some existing computational methods, were included in a collection of publications, two American Helicopter Society conference papers, one AIAA conference paper, seven NASA technical memorandums and one NASA technical paper.

13.9.4 Significance

In the process of predicting the performance of a new helicopter configuration, the computational methods utilized currently either assume an inflow distribution to the rotor system or calculate this distribution from wake methods of various complexity. Validation of current wake methods has never addressed accuracies in calculating the induced velocities that are an integral part of the local angle-of-attack calculation and thus the aerodynamic conditions of the local rotor blade section.

13.9.5 Status/Plans

With the completion of one data set above the rotor, the next step is to begin the acquisition of another complete set at $C_T=0.0064$ and $C_x=0.0$, but the measurement plane will be a representative distance below the rotor.

Daniel R. Hoad, Joe W. Elliott and Susan L. Althoff
Rotorcraft Aerodynamics Office, SAB, AAD
Langley Research Center
(804)864-5055

13.10 ROTOR WAKE GEOMETRY IN FORWARD FLIGHT USING WIDE-FIELD SHADOWGRAPHY

13.10.1 Objective

The performance, acoustics and dynamic behavior of a helicopter rotor or tiltrotor is very dependent on its interaction with its own wake. Additionally, the rotor wake interacts with the fuselage at low and moderate speeds to induce periodic loads on the fuselage and alter the aerodynamic loading on the fuselage. To understand the behavior of the rotor system for both performance and dynamics, the generation of the rotor wake and its subsequent interaction with other rotor blades, as well as the fuselage, must be understood to improve rotor performance, reduce radiated acoustics under blade vortex interaction conditions and minimize periodic fuselage loadings.

13.10.2 Approach

Using the wide-field shadowgraph technique developed at Ames and applied to rotor flow fields, NASA documented the geometry of the trailed tip vortices for a helicopter rotor in forward flight. By varying rotor and wind tunnel operating conditions, we determined the wake geometry of the trailed vortices for verifying analytical rotor wake models. NASA investigated blade vortex interaction (BVI) conditions to identify specific azimuth and radial locations for BVI encounters. NASA quantified the wake/fuselage interactions and the distortion of the rotor wake due to its flow over and around the fuselage.

13.10.3 Accomplishments

The first ever forward flight wide-field shadowgraphs were obtained using a 5.42-foot diameter rotor. The wind tunnel test included a large number of low and moderate speed conditions. Very clear and definite wake filaments were visualized for up to three or four blade passages.

13.10.4 Significance

In a non-intrusive manner, a complete snapshot of the rotor wake geometry was captured in forward flight. Periodic wake interactions with the fuselage were documented and specific blade vortex interactions were visualized at several radial and azimuth allocations. These data will provide a badly needed capability for verifying rotor performance, loads and acoustics codes as well as providing the best understanding to date of rotor/fuselage aerodynamic interactions.

13.10.5 Status/Plans

Initial cataloging and data reduction were initiated. Because of the large amounts of data obtained, a major effort will be necessary to fully analyze the photo and VCR data. Future test programs will be conducted both in small- and full-scale wind tunnel tests. Correlation with analytical models using prescribed and free-wake rotor models will be conducted and shortcomings of current analyses will be identified.

Jeffrey Light, Alex Frerking and Tom Norman
Rotorcraft Aeromechanics Branch
Ames Research Center
(415)604-4881

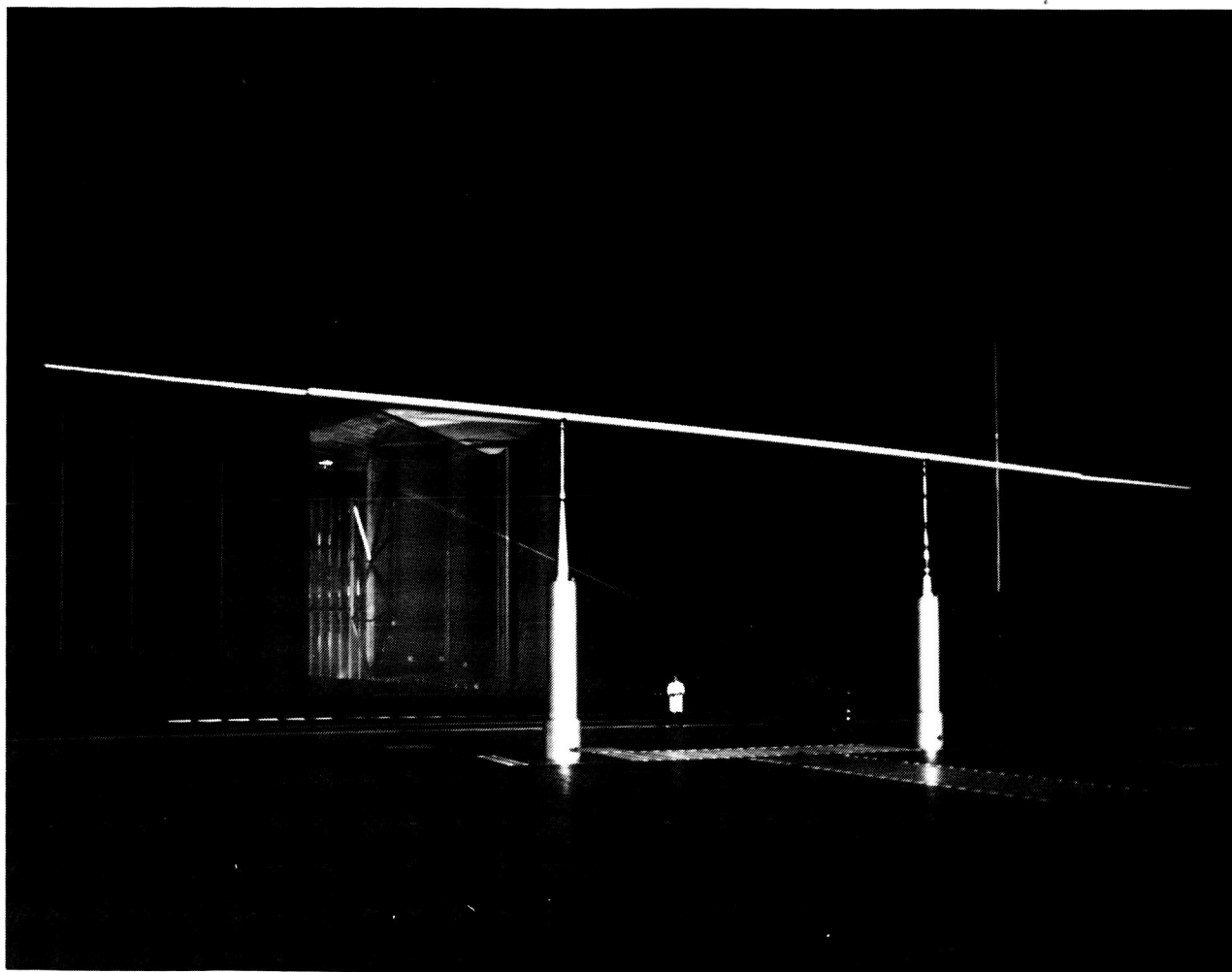


Figure 13.9. Long-Range Laser Velocimeter Test

13.11 LONG-RANGE LASER VELOCIMETER PERFORMANCE TEST

13.11.1 Objective

To measure the boundary layer in the aft part of the test section using the Long-Range Laser Velocimeter (LRLV) and evaluate the performance of the instrument when exposed to the 80-foot by 120-foot wind tunnel environment, as part of the 80-foot by 120-foot wind tunnel flow calibration and the 80-foot by 120-foot base drag test. Another objective of the base drag test was to conduct velocity surveys and laser flow visualization to compare the results with CFD predictions. Finally, the feasibility and requirements for seeding of the 80-foot by 120-foot flow were investigated..

13.11.2 Approach

The approach involved testing the performance of the LRLV by measuring the boundary layer with both the standard and extended focus zoom optics using the natural seeding present in the flow. NASA experimented with localized artificial seeding of the flow at a location upstream of the 80-foot by 120-foot inlet and evaluated the improvement in LRLV performance. NASA used the LRLV as a planar light source for flow visualization studies (See Figure 13.9).

13.11.3 Accomplishments

Velocity surveys in the boundary layer were made during the 80-foot by 120-foot flow calibration at speeds up to 100 knots while artificially seeding the flowfield. Vortex patterns were successfully visualized in the separated regions of the Base Drag Test.

13.11.4 Significance

Requirements for operating in the 80-foot by 120-foot wind tunnel are now better understood and problem areas were identified. Improvements to the LRLV system will be made based on this experience. Qualitative correlations between measurements of separated flow on bluff bodies and CFD predictions were made.

13.11.5 Status/Plans

NASA plans to further investigate the feasibility of artificially seeding the 80-foot by 120-foot wind tunnel on a larger scale and to use the improved LRLV system to conduct the ground environment velocity survey during the STOVLE7 outdoor hover test in Spring 1990.

Michael Reinath
Fixed Wing Aerodynamics Branch (FFF)
Ames Research Center
(415)604-6680

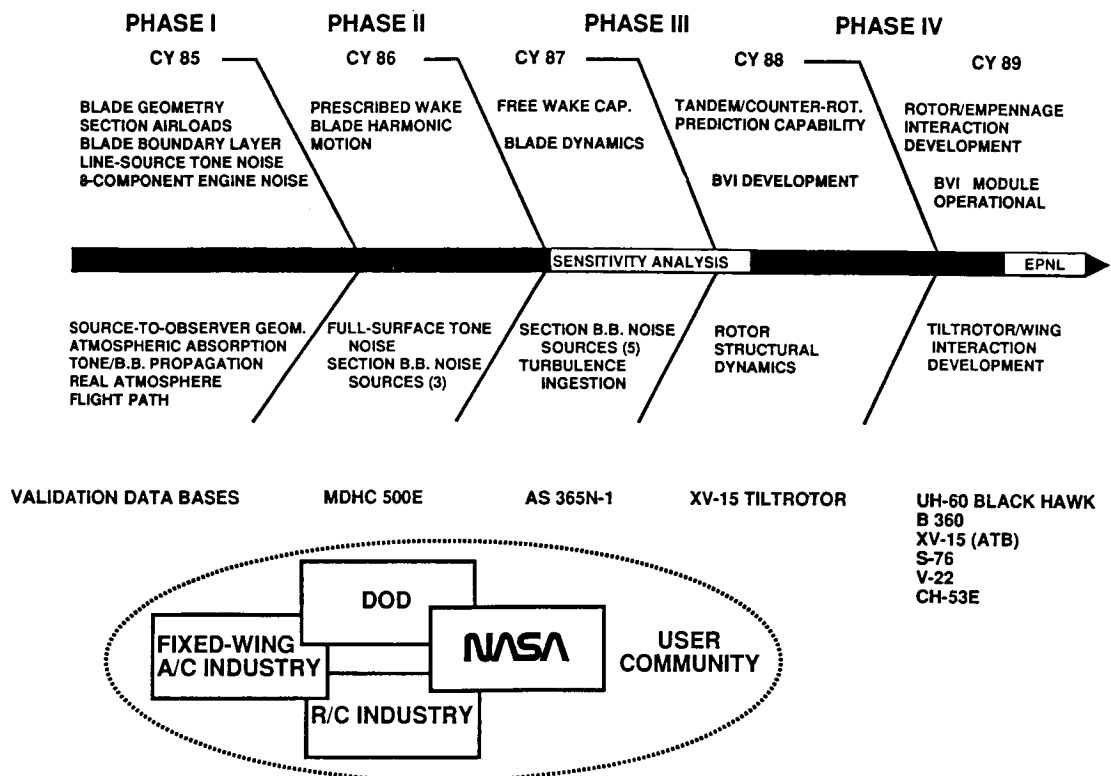


Figure 13.10. ROTONET Development

13.12 ROTONET DEVELOPMENT

13.12.1 Objective

To develop a comprehensive computer program for the prediction of the total noise signature of helicopters which can be used to optimize the helicopter acoustics characteristics during the initial design phase.

13.12.2 Approach

ROTONET was planned to have a modular code architecture, be well documented and be incrementally developed in phases. The methodology included analytical and empirical techniques. The basic code structure was divided into four parts, (1) main-rotor and tail-rotor geometry, (2) rotor performance calculations, (3) source noise calculations and (4) source-to-observer propagation (See Figure 13.10).

13.12.3 Accomplishments

A Phase I System (1985), a Phase II System (1986) and a Phase III System (1988) were distributed to the helicopter industry. The Phase I System is simplistic and intended to give quick results. It can handle any rotor planform geometry but uses only a simplistic uniform rotor inflow model and lifting line source model for the rotor tone noise calculation. The Phase II and III Systems are increasingly more complex in modeling the rotor in-flow and for the calculations of rotor performance and source noise. Additional noise sources such as broadband noise, engine noise and turbulence ingestion noise were also added. The Phase II and III codes require increasing greater computer execution time but yield increasingly greater accuracy in the prediction results.

To improve the prediction capability of ROTONET, acoustic flight experiments are being performed to yield the comprehensive, accurate databases required to validate the prediction methods. The first three tests were completed. The aircraft tested are a MDHC 500E helicopter, an Aerospatiale 365N-1 Dauphin 2 helicopter and a XV-15 Tiltrotor aircraft.

13.12.4 Significance

The success of the ROTONET noise prediction code effort is best demonstrated by its acceptance and active use by the major helicopter companies, portions of the fixed-wing aircraft industry, the U.S. Army, the U.S. Air Force and NASA.

13.12.5 Status/Plans

It was planned that the Phase IV ROTONET System would be operational by October 1989. It would introduce a Blade Vortex Interaction acoustics prediction capability and a Rotor Structural Dynamics acoustics prediction capability.

ORIGINAL PAGE
BLACK AND WHITE PHOTOGRAPH

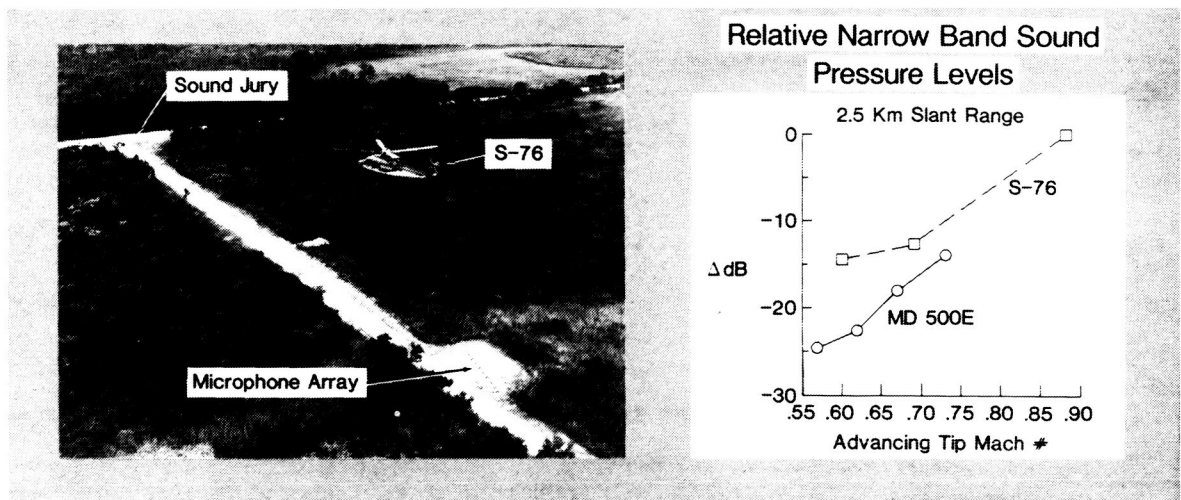


Figure 13.11. Acoustic Results of the Sikorsky S-76 Variable Rotor-Speed Tests

13.13 ACOUSTIC RESULTS OF THE SIKORSKY S-76 VARIABLE ROTOR-SPEED TESTS

13.13.1 Objective

To study the sound reduction which occurs as a helicopter's main-rotor speed is reduced during flight. It is known that as the main-rotor speed of a helicopter is reduced, its advancing tip Mach number is reduced along with the associated sound.

13.13.2 Approach

The approach involved designing a field experiment using the Sikorsky S-76 helicopter, which is the only commercially available helicopter capable of varying its main-rotor speed over a wide range of values during flight. The experiment consisted of operating the helicopter at six different advancing tip Mach numbers and measuring the reduced sound levels with microphones and a jury of persons signaling when they first heard the helicopter.

13.13.3 Accomplishments

Narrowband sound pressure levels were determined for the main-rotor tones of each helicopter at a range of 2.5 km. and an angle of approximately four degrees above the horizon. The highest level of the S-76 was selected as the "zero" reference value and other levels were made relative to that value. The data showed the S-76, weighing 9,800 pounds, had levels higher than the MD 500E, weighing 2,700 pounds, over the range of advancing tip Mach numbers. The data also showed that as the main-rotor speeds (advancing tip Mach number) are reduced, the trend of reduced sound levels for the S-76 is similar to that established for the experimental helicopter. Figure 13.11 shows the S-76 helicopter in the test area and some preliminary data results compared to results obtained for an experimental version of a McDonnell Douglas 500E helicopter. The first part of the figure is an aerial view of the S-76 helicopter, microphone array and sound jury. The second part of the figure presents the relationship of the S-76 sound levels to those of the MD 500E.

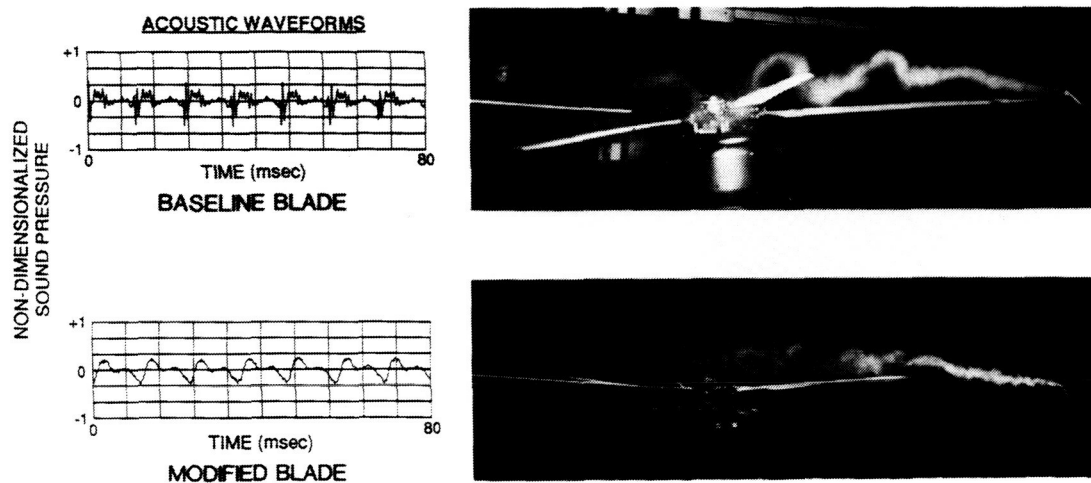
13.13.4 Significance

Previous to the S-76 test, data available to study the sound levels generated by reducing the rotor speed of a helicopter were limited to recorded sound for an experimental version of the McDonnell Douglas 500E. Data obtained from the S-76 test significantly enlarged the database for noise reduction research on helicopters by reducing their main-rotor speeds.

13.13.5 Status/Plans

The data will be used to study the predicted results of computer codes (ICHIN, ARCAS and ROTONET) as they relate to measured field results.

HELICOPTER DESCENT NOISE REDUCTION



ORIGINAL PAGE
BLACK AND WHITE PHOTOGRAPH

Figure 13.12. Helicopter Blade-Vortex Interaction Noise Reductions

13.14 HELICOPTER BLADE-VORTEX NOISE INTERACTION REDUCTION

13.14.1 Objective

To reduce the noise generated by the interaction between helicopter rotor blades and the tip vortices shed by the individual blades in the rotor system.

13.14.2 Approach

A previous, non-rotating, rotor blade test program had been run to study the formation of the tip vortex and to define blade parameters and modifications that would affect the vortex formation, growth and dissipation. Using this data, a study defined rotor blade modification(s) that had the potential for reducing the BVI noise.

13.14.3 Accomplishments

The ten foot diameter model of the Boeing 360 model rotor system was modified and tested (rotating) in the Boeing Helicopter Company wind tunnel. The first tests run, incorporating several different modifications, were not successful. Analysis showed that attempts to modify the vortices did not produce the desired results in the rotating system because the modifications to the vortex did not take effect until after the intersection with a following blade had occurred. It was decided to try a blade modification that would significantly reduce the total energy within the vortex. This approach was successful and the BVI noise was significantly reduced (See Figure 13.12).

13.14.4 Significance

A method for substantially reducing the BVI noise of helicopter rotors was demonstrated using a model rotor in a wind tunnel. With additional studies, this approach could result in rotor designs with significantly reduced BVI noise. The BVI (bang) noise is the major source of objectionable approach noise.

13.14.5 Status/Plans

While the principle was demonstrated, additional analysis is required to understand the results and to make the design practical from a performance stand point.

Otis S. Childress, Jr.
Applied Acoustics Branch
Langley Research Center
(804)864-5278

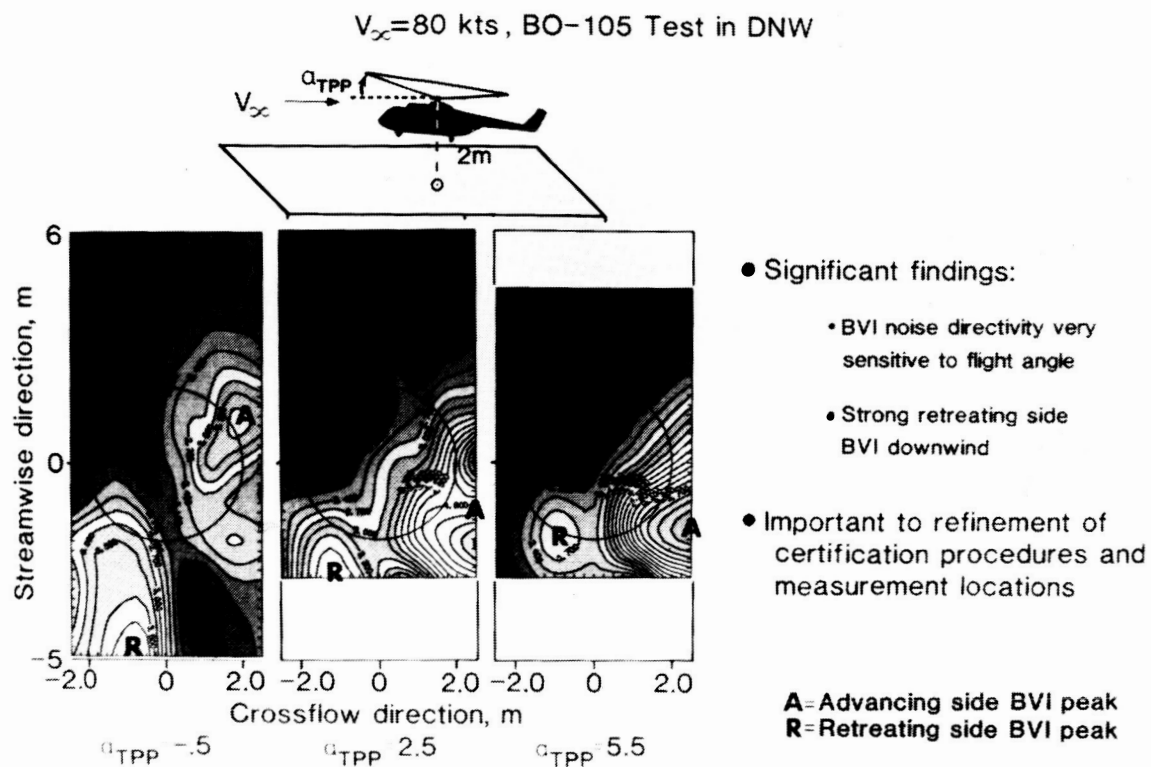


Figure 13.13. Variation of BVI Noise Directivity with Flight Angle Discovered

13.15 ROTOR BLADE-VORTEX INTERACTION NOISE DIRECTIVITY

13.15.1 Objective

To define high resolution directivity patterns of main rotor impulsive noise due to blade-vortex interaction (BVI) as a function of flight conditions. This research is part of an overall program aimed to improve the fundamental understanding of helicopter noise sources.

13.15.2 Approach

NASA participated in a recent model rotor acoustics experiment performed by the German aerospace research establishment (DLR) in the German-Dutch acoustic wind tunnel (DNW). A large database of main rotor noise data were acquired for a 40 percent scale model of the MBB BO-105 helicopter. Directivity patterns in a large plane under the rotor flight path were acquired using a nine-microphone traversing array. Earlier BVI noise tests had shown the strongly directional nature of BVI noise and its dramatic dependence on flight conditions (forward speed and tip-path-plane angle α_{TPP}). The present test investigated the cause of these directivity changes in closer detail (See Figure 13.13).

13.15.3 Accomplishments

To quantify the BVI content, the dominant BVI radiation in the mid-frequency spectral band was calculated and normalized for spherical spreading with respect to BVI sources located on the advancing and retreating side. The normalized BVI metric results were then plotted as directivity contours for a forward speed of 80 knots for three tip-path-plane angles α_{TPP} . The changing noise levels as well as the changing direction of strongest noise radiation clearly can be seen. The primary radiation direction of the advancing side BVI noise moves to the right and downwind of the flight path and increases in level as tip-path-plane angle increases. The location of the retreating side peak moves toward the center line and becomes more focused as rotor angle increases.

13.15.4 Significance

Whereas early work found that BVI radiates strongly upstream along the flight path, these more extensive data show that BVI noise can radiate strongly both toward the advancing-side sidelines and downwind of the retreating side. The changing radiation patterns can be generally correlated with the changing wake geometry with tip-path-plane angle. This unique result has considerable practical importance to refinement of noise certification procedures and noise measurement locations.

13.15.5 Status/Plans

Rotor wake and loads predictions of the interaction geometry will be compared with the acoustic source locations to further the understanding of BVI noise directivity change with flight conditions.

TIP MACH NO. = 0.67
ADVANCE RATIO = 0.15
TIP PATH PLANE ANGLE =
1.5 DEGREES AFT.
PRESSURE AT:
3% CHORD FROM
LEADING EDGE
RADIAL STATION (r/R) =
0.867

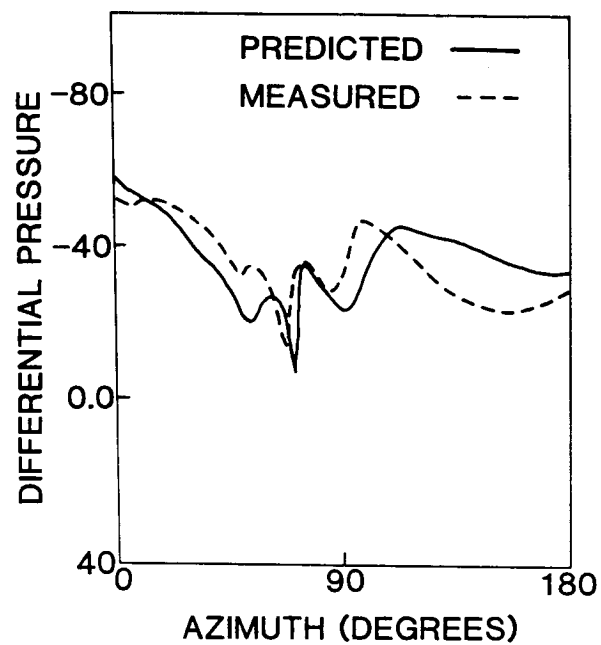


Figure 13.14. Predicted and Measured Surface Differential Pressure for Self-Generated BVI

13.16 SIMULATION OF REALISTIC BLADE-VORTEX INTERACTIONS

13.16.1 Objective

In efforts to understand and, hence, alleviate BVI problems, scientists have relied primarily on wind tunnel data, simple linear mathematical models or nonlinear models which only mimic idealized conditions for these interactions. This research, accomplished by McDonnell Douglas Helicopter Company, complements and extends these efforts through the simulation of the more complex or "realistic," three-dimensional, self-generated BVI.

13.16.2 Approach

To predict the rapid variations in the sectional blade loads during BVI, a finite-difference solution procedure of the simple, yet nonlinear, transonic full potential equation was employed. The interaction velocity field was obtained through a nonlinear superposition of the rotor flowfield (computed using a unsteady 3-D full potential rotor flow solver) and the rotational vortex field. In the potential flow model, vortex effects were simulated using the velocity "transpiration" approach. To satisfy the tangency boundary condition, a modified surface condition was prescribed and enforced at each time step of the computations. Potential blade-vortex encounters were identified using CAMRAD. This information then was utilized in an interpolation routine to compute the instantaneous position of the interaction vortex elements with respect to the blade.

13.16.3 Accomplishments

The approach described was used to simulate a number of wind tunnel BVI experiments where a lifting one-seventh scale AH1-OLS model rotor was allowed to interact with elements of its own generated wake. Figure 13.14 shows a comparison between the predicted and measured differential pressures at a point near the blade's leading edge. As seen, the interactions are characterized by the rise and drop of the leading edge pressures as the BVI vortex elements pass by the blade's leading edge. The second BVI near the 78 degree azimuth is clearly the most dominant among the three being modeled. The simulations were performed on the CRAY X/MP computer and required six CPU minutes.

13.16.4 Significance

It was demonstrated that 3-D rotor BVI can be economically and accurately predicted using the velocity "transpiration" technique in a full potential model. When using the present aerodynamic load prediction methodology in conjunction with an appropriate acoustics analysis model, the design engineer can quickly obtain trends relating to airfoil thickness distribution and 3-D blade tip effects on the rotor-generated, acoustic signal.

13.16.5 Status/Plans

The task was completed.

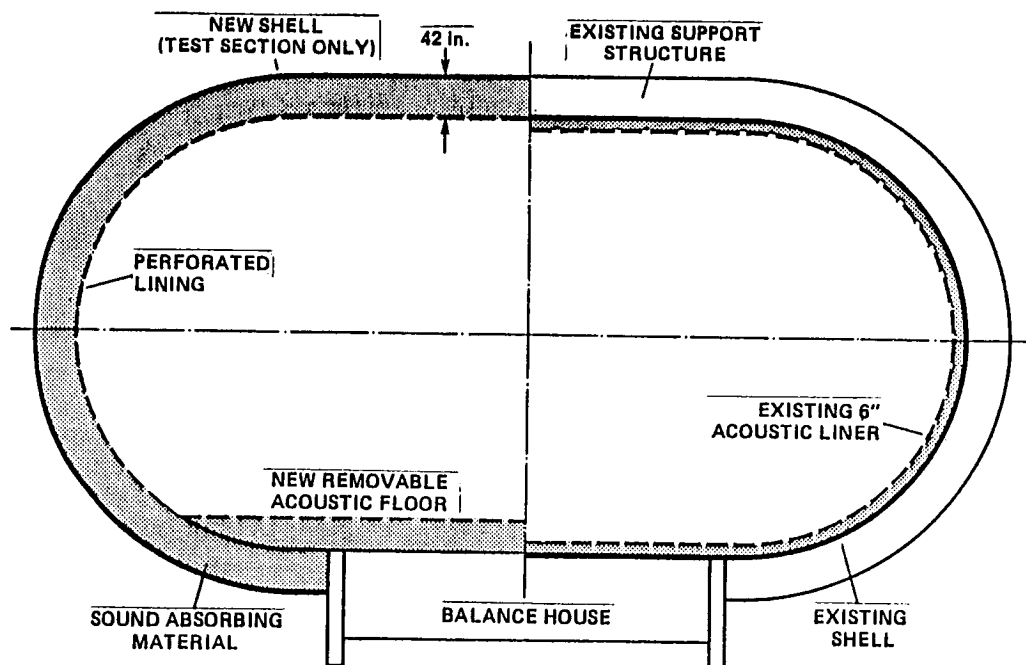


Figure 13.15. New Aeroacoustic Lining Concept for 40-Foot by 80-Foot Test Section

13.17 AEROACOUSTIC MODIFICATION OF THE 40- BY 80- FOOT WIND TUNNEL

13.17.1 Objective

To enhance the acoustic treatment of the 40-foot by 80-foot wind tunnel to become the largest near-anechoic wind tunnel in the world. The modification will make it possible to aeroacoustically test large and full-scale models of rotorcraft, prop-fan and other advanced aircraft up to Mach numbers of .45.

13.17.2 Approach

A thick, 40-foot by 80-foot test section lining (three feet) was proposed to replace the half foot lining now in place. The pressure surface of the test section was moved from inside of the main structural members to the outside to maintain the same 40-foot by 80-foot test section size while providing a near-anechoic environment at low frequency (100). Acoustic treatment of two of the interior end walls was proposed as well as an enhancement of the lower RPM capability of the fan drive to lower fan drive background noise (See Figure 13.15).

13.17.3 Accomplishments

Pre-PER work completed to date validated the concept. Excellent absorption of a sample of the deep acoustic lining was demonstrated. An in-house study looking at the design alternatives for low RPM operation was completed.

13.17.4 Status/Plans

Additional pre-PER studies are underway to look at low RPM operation, the effect of flow over the proposed lining and optimization and additional validation of the proposed acoustic treatment. An architectural model of the proposed test section treatment is being made. The project is endorsed by center management and is being proposed as a 1992 Code RF project.

Fred Schmitz (FF) and Paul Soderman (FFF)
Full-Scale Aerodynamics Research Division
Ames Research Center
(415)604-4166

ORIGINAL PAGE
BLACK AND WHITE PHOTOGRAPH

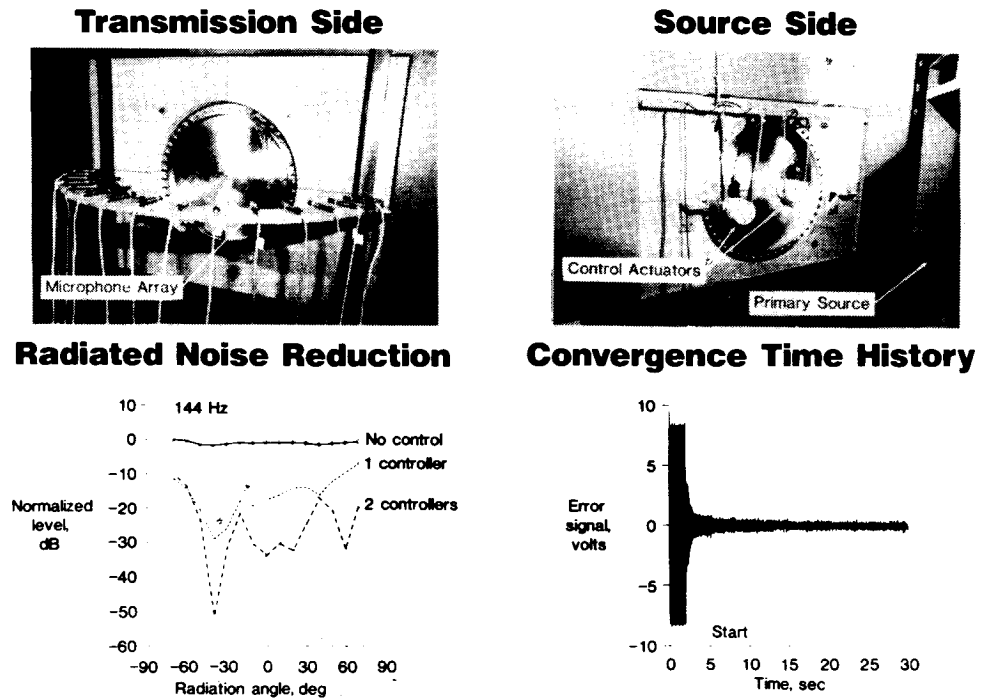


Figure 13.16. Active Control of Panel Radiated Noise

13.18 ACTIVE CONTROL OF PANEL RADIATED NOISE

13.18.1 Objective

To experimentally evaluate the feasibility of controlling sound transmission through a panel using force inputs.

13.18.2 Approach

An 18 inch diameter, 0.05 inch thick, aluminum plate was installed in an opening between two rooms. A loudspeaker (primary source) set at an oblique angle on the source side radiated noise which vibrated the plate. This resulted in an acoustic field on the transmission side of the plate, which was measured by an array of 15 microphones. Using either one or two shakers attached to the plate, the vibration input was adjusted in such a way to control the transmitted acoustic field sensed by two of the microphones located at -40 degrees and +50 degrees (See Figure 13.16).

13.18.3 Accomplishments

The performance of the control system at 144 Hz shows a reduction in the radiated noise for two configurations. Compared to the no control case, the single shaker control provided a 10 to 15 dB reduction with the largest reduction occurring at one of the error microphones (-40 degrees). A theoretical model predicted that a second shaker would provide additional control of the radiated sound. This is validated by the experimental results where two control shakers provided significantly enhanced reduction with more than 20 dB over most of the radiated field. Finally, the time history of one of the error microphone signals demonstrates the rapid convergence of the adaptive control algorithm.

13.18.4 Significance

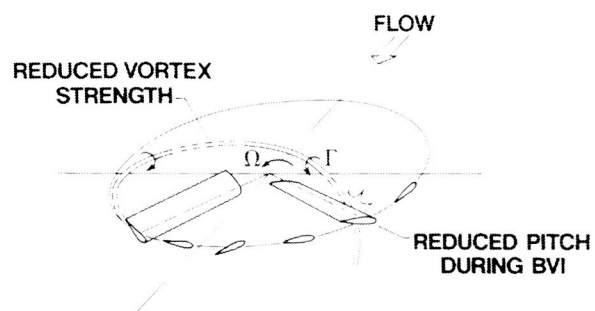
The experimental program provided validation for a previously derived theory and demonstrated the feasibility of implementing such a system.

13.18.5 Status/Plans

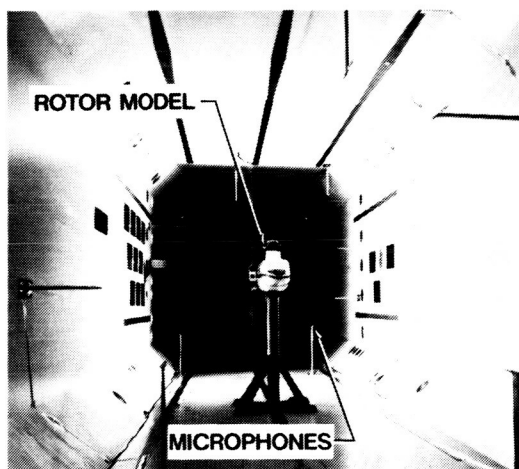
Work to integrate piezoelectric actuators onto the plate surface is underway as well as techniques to allow the radiated sound to be minimized using sensors integrated on the plate.

R. J. Silcox and V. L. Metcalf
Structural Acoustics Branch
Langley Research Center
(804)864-3590

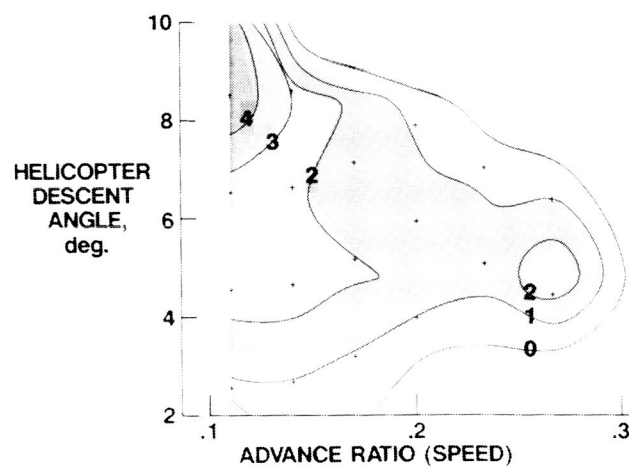
RECEIVED
JAN 10 1988
STRUCTURAL ACOUSTICS BRANCH



ARES NOISE TEST IN TDT



REDUCTION IN BVI NOISE LEVEL (dB)



ORIGINAL PAGE
BLACK AND WHITE PHOTOGRAPH

Figure 13.17. BVI Noise Reduction by Higher Harmonic Pitch

13.19 REDUCTION OF ROTOR BLADE-VORTEX INTERACTION NOISE USING HIGHER HARMONIC PITCH CONTROL

13.19.1 Objective

To evaluate the use of higher-harmonic pitch (HHP) control of rotor blades to reduce BVI noise. Blade-vortex interaction (BVI) is one of the most objectionable types of impulsive helicopter noise.

13.19.2 Approach

Impulsive BVI noise, due to the interaction of shed vortices of preceding blades with the following rotor blades, was a major topic of rotorcraft acoustics research for several years. One noise reduction concept is to decrease the blade lift and vortex strength during the vortex encounters, to reduce the intensity of the interactions and, thus, noise. To evaluate the concept, an experimental study was conducted of rotor acoustics and vibration. Figure 13.17 shows the Aeroelastic Rotor Experimental System (ARES) in the freon gas Transonic Dynamics Tunnel (TDT). Specially calibrated microphones are shown positioned upstream and downstream of the model. A sound power measurement technique was applied to the measured data because of the TDT reverberant environment.

13.19.3 Accomplishments

Using a specially developed, open-loop control system, prescribed HHP control modes were superimposed on the basic cyclic trim pitch for a broad range of rotor operating conditions. Rotor operation included (1) normal one-per-rev cyclic control; (2) four-p collective pitch control; and (3) special pitch control to simulate individual blade control, all for zero flapping trim. HHP significantly increased or decreased the noise depending on the amplitude and azimuth of the pitch control. For normal flight conditions without HHP, descent angles between 40 degrees to 100 degrees produce high BVI noise levels, especially at low speeds. Using HHP, noise levels for matched flight conditions are significantly altered, with the highest BVI noise levels being reduced 4.7 dB.

13.19.4 Significance

The results demonstrate HHP to be an effective noise reduction technique for descending flight where BVI noise dominates. Selective use of HHP, such as during landing approach, should prove practical.

13.19.5 Status/Plans

Detailed data processing was initiated. It will produce a complete parametric mapping of the effect of HHP on BVI noise and the practicality of particular pitch controls for noise reduction. The results will be compared to rotor performance predictions and a HHP/BVI noise prediction program currently under development.

T.F. Brooks, E.R.Booth, Jr. and Ralph Jolly, Jr.
Aeroacoustics Branch
Langley Research Center
(804)864-3634

W.T. Yeager, Jr. and M.L Wilber
Configuration Aeroelasticity Branch
Langley Research Center
(804)864-1271

ORIGINAL PAGE
BLACK AND WHITE PHOTOGRAPH

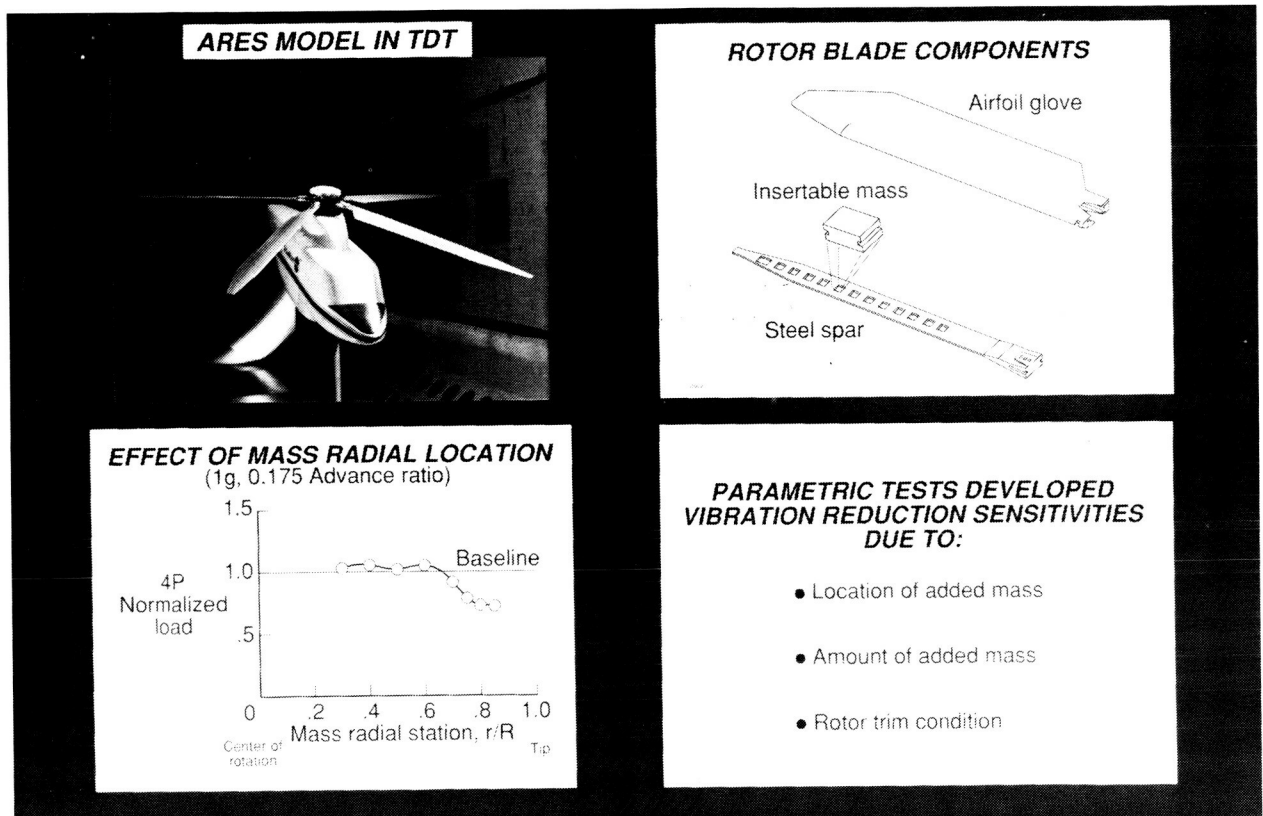


Figure 13.18. Use of Blade Non-Structural Mass Reduces Rotorcraft Vibrations

13.20 USE OF BLADE NON-STRUCTURAL MASS REDUCES ROTORCRAFT VIBRATIONS

13.20.1 Objective

To systematically investigate helicopter vibration reduction through the use of non-structural blade masses and obtain an experimental database for correlation, validation and development of analytical prediction methods. Historically, rotorcraft have experienced substantial vibration problems. One means of reducing these vibrations is through the addition of non-structural mass to the rotor blades (See Figure 13.18). These masses are intended to "tune" the blades so that the vibrations are reduced to an acceptable level. Generally, these problems were addressed in the post-design phase. Many of the early attempts to design low vibration rotors were unsuccessful due to the inadequacy of the prediction methods.

13.20.2 Approach

Aeroelastically scaled, model rotor blade hardware was fabricated for testing on the Aeroelastic Rotor Experimental System (ARES) in the Transonic Dynamics Tunnel (TDT). These blades were comprised of two major components, an airfoil glove, which had an internal channel centered about its quarter chord and a steel spar which could be inserted in the channel. A tungsten or steel mass could be mounted in any of the cutouts on the steel spar which was then mated with the airfoil glove for the complete blade assembly. Testing was conducted in the TDT to provide a parametric study of the effects of mass radial placement on rotorcraft vibrations throughout a representative forward flight speed range.

13.20.3 Accomplishments

In the wind tunnel test, four per revolution vertical fixed-system loads were obtained for a single tungsten mass located at several different radial locations. Reductions of up to 30 percent may be achieved by the appropriate selection and placement of a non-structural mass. Results were obtained for three different thrust conditions at representative propulsion forces throughout the forward flight speed range. Parameters varied including the amount and location of the added mass and the rotor trim condition.

13.20.4 Significance

This research provided a parametric study of the effects of non-structural blade masses on rotorcraft vibration reduction. The database developed will be significantly useful in the verification of existing rotorcraft analytical design methods and in the development of new, low vibration, rotor design techniques.

13.20.5 Status/Plans

A report will be released documenting the results of the wind tunnel test. The results will also be used in a correlation effort with CAMRAD, a government owned and developed rotorcraft analysis.

Matthew L. Wilbur, William T. Yeager, Jr.,
Paul H. Mirick, Jeffrey D. Singleton and W. Keats Wilkie
Configuration Aeroelasticity Branch
Langley Research Center
(804)864-1971

ORIGINAL PAGE
BLACK AND WHITE PHOTOGRAPH

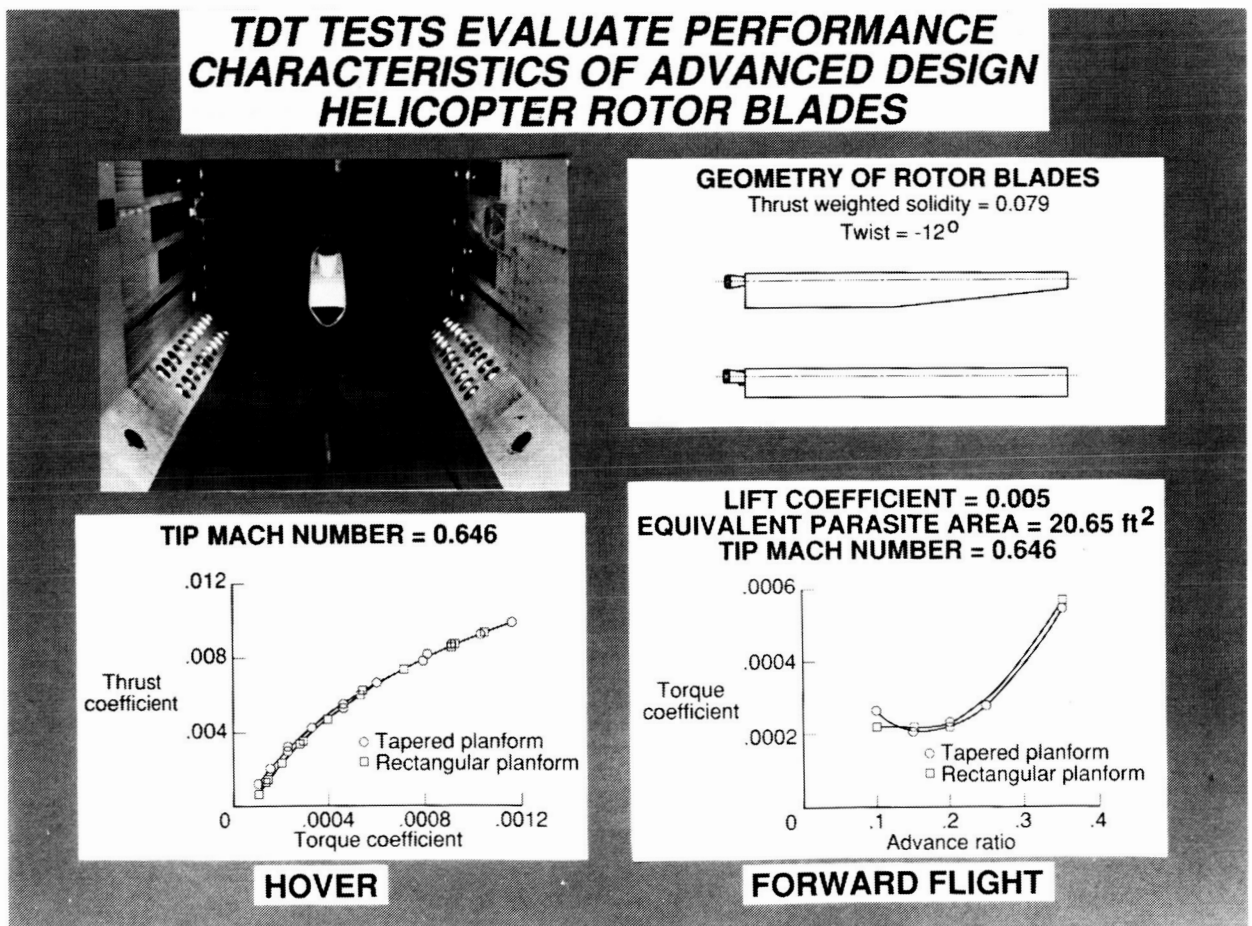


Figure 13.19. TDT Tests

13.21 TDT TESTS EVALUATE PERFORMANCE CHARACTERISTICS OF ADVANCED DESIGN HELICOPTER ROTOR BLADES

13.21.1 Objective

To evaluate the effects the effects of rotor planform shape on aerodynamic performance. A cooperative program with Bell Helicopter Textron to couple advanced aerodynamic blade shapes with a blade structure designed for minimum hub vibratory loads is in progress.

13.21.2 Approach

Two sets of rotor blades were designed for specified aerodynamic performance requirements, a rectangular planform blade designed by Bell and a tapered planform blade designed by the Army Aerostructures Directorate personnel. Each blade set was designed structurally to result in minimum hub shears and moments. The thrust-weighted solidity, twist distribution and inboard airfoil section were the same for both blade sets. Tests were conducted in the Langley Transonic Dynamics Tunnel (TDT) because of its unique ability to use Freon-12 as a test medium. Both rotors were 1/5-size aeroelastically scaled models and were tested at conditions simulating various rotor tasks defined by aircraft gross weight and propulsive force requirements up to an advance ratio of 0.425. At each test condition, measurements of main-rotor torque were made to evaluate differences in performance between the two configurations (See Figure 13.19).

13.21.3 Accomplishments

These results were obtained for a hover tip Mach number of 0.646, which represents sea level standard conditions. The hover data indicates that the tapered planform provides a performance improvement for thrust coefficients both above and below the design value of 0.0051. The forward flight data also indicates a performance advantage for the tapered blades at advance ratios above 0.15. The hover performance trend is consistent with pretest predictions while the forward flight trend is not entirely consistent with analytical results.

13.21.4 Significance

The use of a highly tapered rotor blade can result in hover improvements without degradation of forward flight performance relative to a rectangular blade. The inability of the design analysis to correctly predict forward flight performance trends may lead to modification or abandonment of this analysis in the future.

13.21.5 Status/Plans

These test results will be documented in a formal NASA publication. A correlation of these measured performance trends with analytical results from an analysis not used in the design process also will be conducted.

Kevin W. Noonan
U. S. Army Aerostructures Directorate
William T. Yeager, Jr., Matthew L. Wilbur and Paul H. Mirick
Configuration Aeroelasticity Branch
Langley Research Center
(804)864-3967

ORIGINAL PAGE

BLACK AND WHITE PHOTOGRAPH

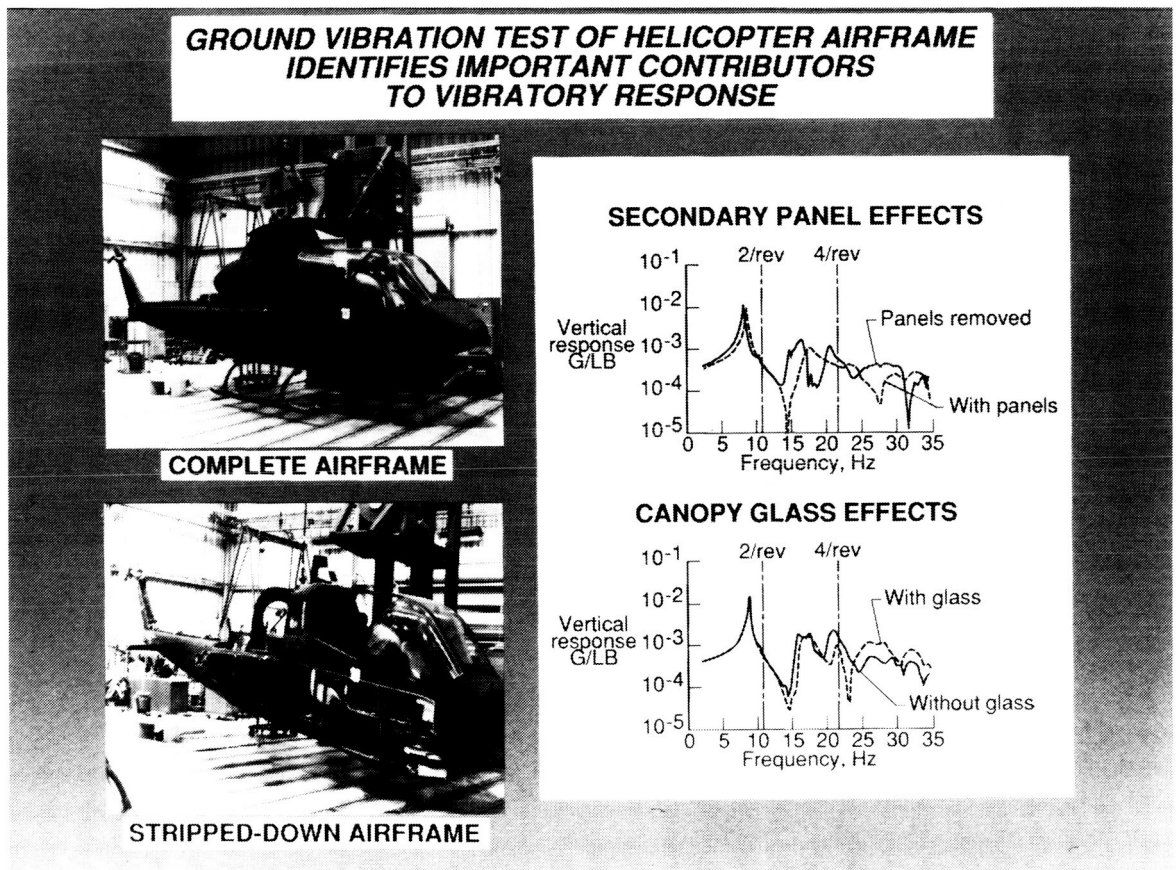


Figure 13.20. Ground Vibration Test of Helicopter Airframe

13.22 GROUND VIBRATION TEST OF HELICOPTER AIRFRAME IDENTIFIES IMPORTANT CONTRIBUTIONS TO VIBRATION RESPONSE

13.22.1 Objective

To establish the foundations for developing a superior design analysis capability for vibrations. Excessive vibration is the most common technical problem to arise as a "show stopper" in the development of a new rotorcraft. With only a few exceptions, vibration problems have not been identified until flight test. Vibration predictions have not been relied on by the industry during design because of deficiencies in current vibration analysis methods. With a view toward establishing a capability in the industry to fully utilize vibration analysis during design, the NASA Langley Research Center has underway a program, designated DAMVIBS (Design Analysis Methods for Vibrations). Among the many activities under the DAMVIBS program is one aimed at identifying those "difficult components" which are the important contributors to airframe vibratory response and which require more detailed finite element representation (See Figure 13.20).

13.22.2 Approach

Typically, only the primary structure is represented fully (stiffness and mass) when forming the finite element model (FEM) of an airframe. There are many components, i.e., transmission, engines and stores and secondary structures, i.e., fairings, doors and access panels, which are represented only as lumped masses. To isolate the effects of each component on overall vibratory response, multiple ground vibration tests were conducted with each test representing a progressive removal of the suspect component until only the primary airframe structure remains. At each stage, analyses were performed using an existing FEM of the airframe modified as necessary to reflect the specific configuration tested. Both full-scale airframes and their components and small-scale generic models of both metal and composite construction were studied.

13.22.3 Accomplishments

The initial effort in this area was conducted by Bell Helicopter Textron utilizing an AH-1G helicopter airframe. To isolate the effects of each component on vibratory response, ground vibration tests were conducted on a total of eight aircraft configurations.

13.22.4 Significance

The difficult components studies on the AH-1G helicopter represent the first such studies conducted on an airframe structure. The results obtained have identified several components which are important contributors to airframe vibratory response at the higher frequencies of interest and which require improved representation in the FEM.

13.22.5 Status/Plans

The difficult components studies are to continue through a combination of tests and analyses utilizing both full-scale composite airframes and their components as well as small-scale generic models of both metal and composite construction.

Raymond G. Kvaternik
Configuration Aeroelasticity Branch
Langley Research Center
(804)864-1228

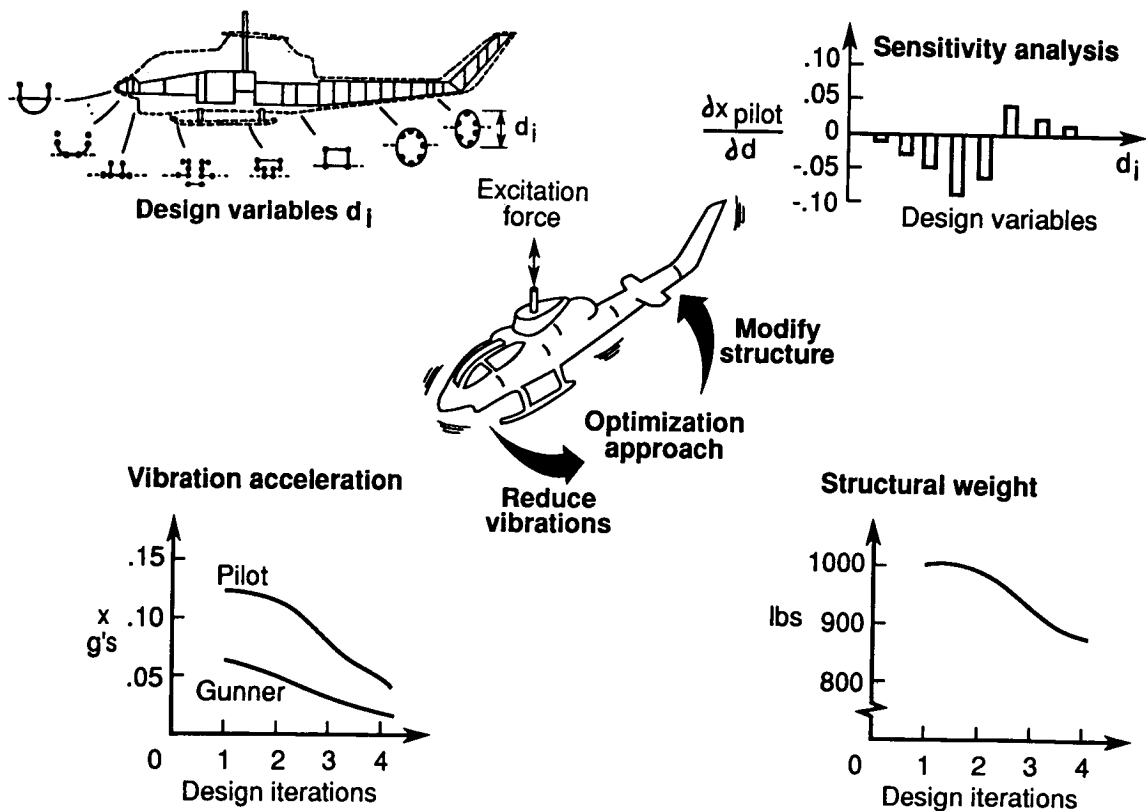


Figure 13.21. Optimization Approach for Helicopter Vibration Reduction Demonstrated

13.23 OPTIMIZATION APPROACH FOR HELICOPTER VIBRATION REDUCTION DEMONSTRATED

13.23.1 Objective

To investigate and develop analytical and computational tools for optimization of helicopter structures for vibration reduction. Considerable emphasis to achieve significantly lower vibrations in the advanced helicopters under development has brought about an increased need to establish better analytical methods to be used during design for vibration reduction. A vibration reduction method which has gained attention recently is based on the idea of designing the helicopter airframe structure so as to minimize the vibration responses in the airframe under the action of rotor-induced loads. The design of airframe structure for vibration reduction involves extensive study of the airframe dynamic characteristics to guide the modification of vibration related design parameters. The design study requires multi-degree of freedom structural analysis, multi-dimensional search of design variables and multi-disciplinary considerations.

13.23.2 Approach

The nonlinear mathematical programming approach is being pursued for optimization of helicopter airframe structures. Some of the areas addressed in the study are (1) mathematical formulation of the airframe optimization problem, including establishment of a relevant set of design variables, constraints and objective function; (2) analytical methods of sensitivity analysis which are unique to helicopter airframe structures; (3) computer implementation of optimization procedures and (4) demonstration of the approach to real helicopters.

13.23.3 Accomplishments

The DYNOPT, code for DYNAmics OPTimization of airframe structures for vibration reduction, features a unique operational combination of the MSC/NASTRAN finite element structural analysis code, extended to include calculation of steady-state dynamic response sensitivities, with the the CONMIN optimizer. Initial application of the DYNOPT program to a Bell AH-1G helicopter airframe structure was completed. Figure 13.21 indicates one design model (referred to as a preliminary design model) which considers the distribution of the depth of the primary structure as design variables. Typical numerical results obtained for the model using the program are also shown in the figure. The sensitivity analysis results indicate that a reduction in forced response displacement at the pilot seat can be brought about by reducing the depth of the tail structure and increasing the depth of the forward fuselage structure. The design iteration histories indicate a reduction in the vibration acceleration at the pilot and gunner locations and also a reduction in the structural weight as a result of the airframe optimization.

13.23.4 Significance

The demonstration of the airframe optimization approach for vibration reduction proves feasibility of the approach and provides a basis for the helicopter industry to pursue the design of low vibration airframes.

13.23.5 Status/Plans

NASA plans to extend the overall research study to include structural damping, computational methods for large-scale, structural optimization and multi-disciplinary airframe design considerations.

T. Sreekanta Murthy
Configuration Aeroelasticity Branch
Langley Research Center
(804)864-1929

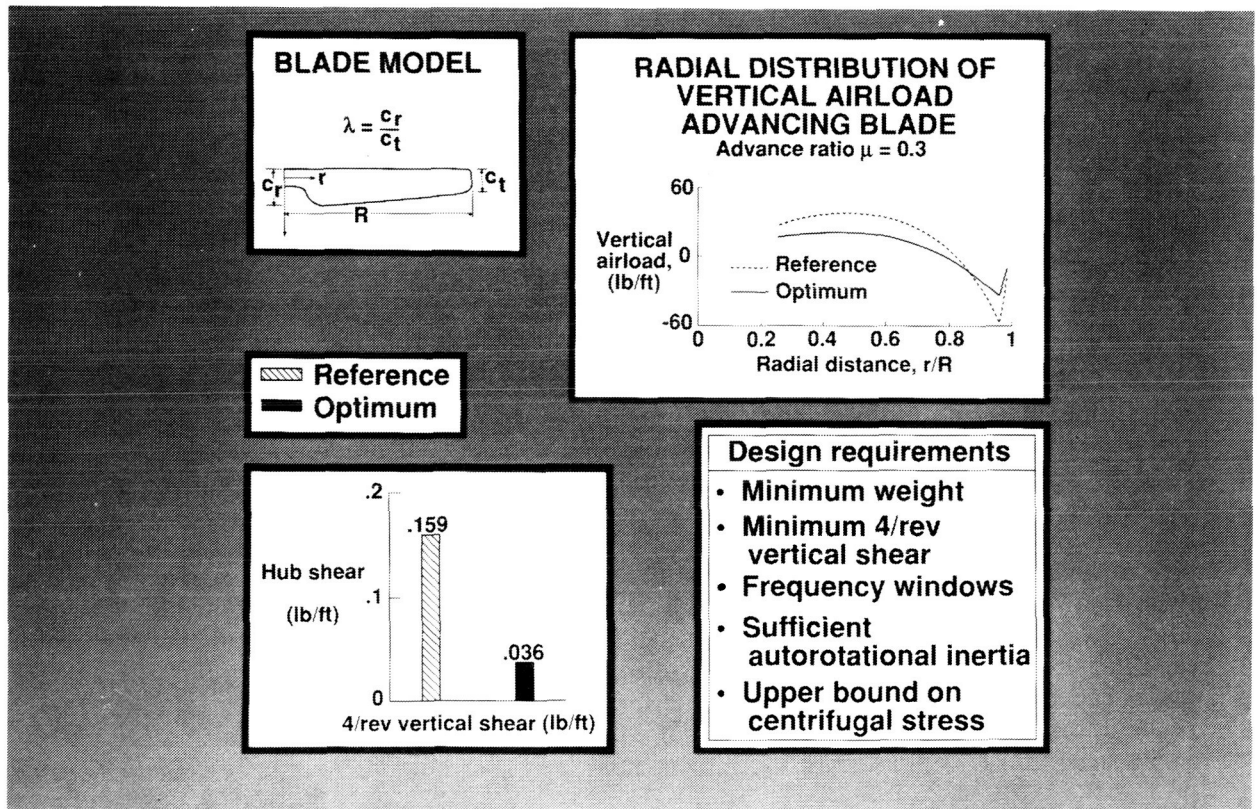


Figure 13.22. Integrated Aerodynamic Load/Dynamic Optimization of Helicopter Rotor Blades

13.24 INTEGRATED AERODYNAMIC LOAD/DYNAMIC OPTIMIZATION OF HELICOPTER ROTOR BLADES

13.24.1 Objective

To develop an integrated aerodynamic load/dynamic design optimization procedure for helicopter rotor blades in forward flight. This work is part of a centerwide activity at Langley to improve helicopter rotor blade design procedures by accounting for discipline interactions in the design process.

13.24.2 Approach

Blade aerodynamic and dynamic analyses were integrated with an optimization program. The helicopter comprehensive analysis code CAMRAD was used for the analyses and the program CONMIN was used for optimization. The optimization problem was formulated to minimize blade weight and 4/rev (per rev) vertical hub shear. Constraints were imposed on natural frequencies, autorotational inertia and centrifugal stress. The twelve design variables included blade stiffness at the root, root chord, taper ratio, radius of gyration at the root and magnitudes of nonstructural masses located spanwise. A sensitivity analysis was part of the procedure and produced analytical gradients of the weight, autorotational inertia and centrifugal stress and forward difference gradients of the vertical shear and frequencies (See Figure 13.22).

13.24.3 Accomplishments

The coupling of CAMRAD and CONMIN was accomplished. The procedure was applied to a reference blade and optimum designs were obtained in 7-10 cycles, i.e., 92 to 131 CAMRAD analyses. A cycle consists of a CAMRAD analysis for the nominal design variable values and for each perturbed design variable for the finite difference derivatives and a call to the optimizer. The integrated procedure yielded a blade design with a 10.6 percent reduction in weight and a 77.6 percent reduction in hub shear from that of the reference blade. Significant reductions in amplitudes of spanwise and azimuthal vertical airload distributions also occurred.

13.24.4 Significance

This is a unique optimization procedure which integrates aerodynamic and dynamic analyses through accounting for variations in airloads due to changes in the design variables. This is also unique in that it combines CAMRAD and a formal optimization program. It is a significant step toward integrating all appropriate disciplines in analytical rotor blade design optimization.

13.24.4 Status/Plans

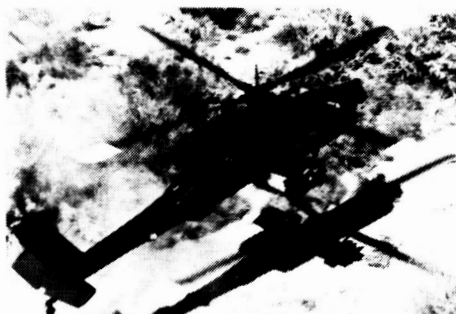
NASA will include additional constraints such as 4/rev inplane shear and rolling and pitching moments and additional design variables such as pretwist. NASA also will develop a helicopter performance optimization procedure and merge with this procedure to produce a fully integrated aerodynamic/dynamic optimization procedure.

Adfti Chattopadhyay, Joanne L. Walsh and Michael F. Riley
Interdisciplinary Research Office
Langley Research Center
(804)864-2801

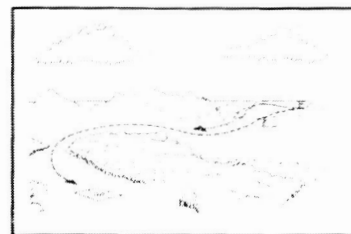
ORIGINAL PAGE BLACK AND WHITE PHOTOGRAPH



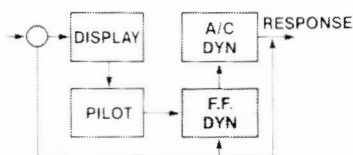
DISPLAY LAW
METHODOLOGY



APACHE DISPLAY



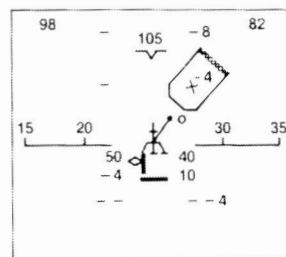
NOE



FORCE FEEL SYSTEM



SIDE STICK TRIMMING



VSRA DISPLAY

Figure 13.23. CH-47 Flight Research--1989

13.25 CH-47 FLIGHT RESEARCH--1989

13.25.1 Objective

To utilize the unique capability of the variable-stability of the CH-47 to conduct handling qualities research.

13.25.2 Approach

Five experiments and one data gathering exercise were performed concurrently. Specifically, experiments with the following objectives were conducted to (1) determine effectiveness of gain versus integrator characteristics for the command element in rotorcraft displays; (2) simulate the AH-64 flight and display characteristics to demonstrate required improvements; (3) simulate the VSRA Harrier dynamics and displays to prepare for flight of that aircraft in 1990; (4) define for the first time in a rotorcraft context, the influence of force-feel dynamic characteristics on handling qualities; (5) investigate in conjunction with a concurrent, VMS, ground-based simulation experiment, the influence of auto-trim requirements on sidesticks and (6) obtain actual visual flowfield data from flight for verification of image processing algorithms being developed for automated NOE flight (See Figure 13.23).

13.25.3 Accomplishments

All of these experiments have been completed. The display philosophy experiment and the VSRA display experiment are nearly complete and have resulted in fundamental changes to the methodology to be used for the VSRA. The force-feel dynamics experiment is underway in a ground simulation mode, with results corroborating previous laboratory work. The AH-64 in-flight simulation was scheduled for the end of July 1989. The sidestick trim experiment was conducted at the same time.

13.25.4 Significance

The display design philosophy work is an extension of work performed at Ames. It promises significant improvements in the capability of rotorcraft to operate in limited visibility conditions; this hypothesis will be demonstrated in the in-flight simulation of the Apache and its display design. The sidestick trim requirements are a major hole in the revised military specification for handling qualities being prepared by the Army and the flight work directly supports the development of such a requirement. The force-feel dynamics experiment is expected to demonstrate for the first time for helicopters the fashion in which the pilot modifies his control strategies to accommodate them. This type of work has been initiated only recently for fixed-wing aircraft and has never been done for rotorcraft.

13.25.5 Status/Plans

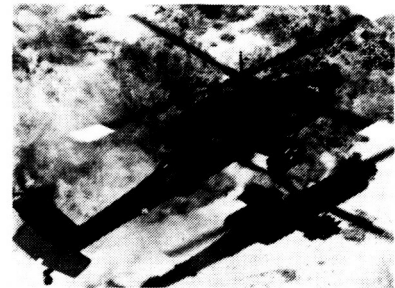
The flight research is underway and should have been completed by mid-August 1989. NASA plans to have the research equipment removed from the aircraft and the aircraft trucked to Boeing Helicopter for conversion to a CH-47D.

W.S. Hindson, M.M. Eshow, J.A. Schroeder and D.C. Watson
Flight Dynamics and Controls Branch
Ames Research Center
(415)604-5008

ORIGINAL PAGE BLACK AND WHITE PHOTOGRAPH



GEN HEL UH-60A



GBER/AH-64

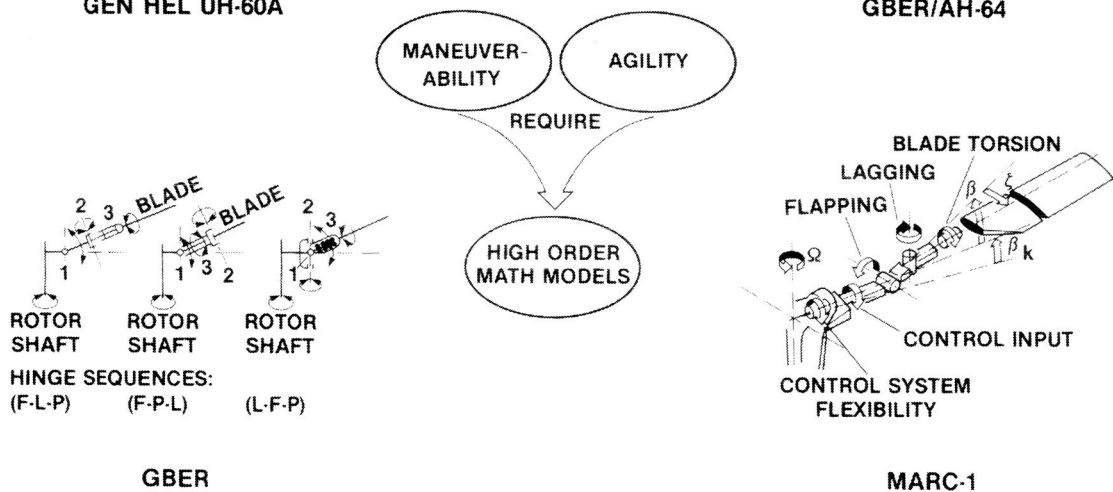


Figure 13.24. Rotorcraft Flight Dynamics Math Model Development

13.26 ROTORCRAFT FLIGHT DYNAMICS MATH MODEL DEVELOPMENT

13.26.1 Objective

To develop rotorcraft mathematical models of sufficiently high order and fidelity to capture the dynamics of interest for design of high-order, high-gain control systems aimed at enhancing agility and maneuverability. A particular requirement is the development of such models that can operate real-time and thereby serve as the basis for ground simulation investigation of the developed technologies.

13.26.2 Approach

For the real time model, the approach was to develop in-house, a new, real-time rotor module (GBER) which correctly represents for the first time arbitrary hinge sequences. This module was then configured to represent the UH-60 rotor for inclusion into GENHEL, which is a contractor-developed, UH-60 math model or the AH-64 rotor for inclusion into FLYRT, which is a contractor developed, AH-64 model. Several parallel efforts under University grants and through Army MOUs are being used to augment this in-house work (See Figure 13.24).

13.26.3 Accomplishments

The GBER rotor module was derived using both conventional techniques and new symbolic programming techniques (MACSYMA), with perfect agreement between the two approaches. It was configured to represent the UH-60 and implemented into GENHEL. Additional contractor work to update and improve GENHEL was accomplished and these improvements are currently being evaluated in a simulation validation experiment on the VMS. A new fuselage module appropriate to the AH-64 was developed under one of the MOUs and is available for incorporation into FLYRT. A non-real-time UH-60 model, MARC-1, was developed to complement these real-time models and was validated against UH-60 flight and GENHEL data. This model incorporates blade twist degrees of freedom and additional air-mass degrees of freedom and can be used to examine the effects of torsional flexibility on the stability and control of hingeless and bearingless rotor helicopters such as the LHX or the HIMARCS rotor.

13.26.4 Significance

Current real-time rotorcraft models (GENHEL and ARMCOP) are notable to accurately represent the high-order dynamics for modern rotors; the GBER formulation permits this representation for any articulated rotor with arbitrary hinge sequences. The development of these models is a prerequisite to the examination of strategies for enhancing maneuverability and agility for rotorcraft, since the fundamental limitations arise from the rotor dynamics and resulting loads.

13.26.5 Status/Plans

The improved GENHEL, without GBER, is currently operating in a simulation validation experiment. GBER was checked and is ready for incorporation into GENHEL as a new rotor module. MARC-1 was verified against UH-60 data and is in the final clean-up process. Plans are to develop agility and maneuverability design requirements in Fall 1989 using a "perfect" helicopter and then to use the models developed to evaluate requirements.

R.T.N. Chen, M.D. Takahashi, M.G. Ballin and M.H. Mansur
Flight Dynamics and Controls Branch
Ames Research Center
(415)604-5008

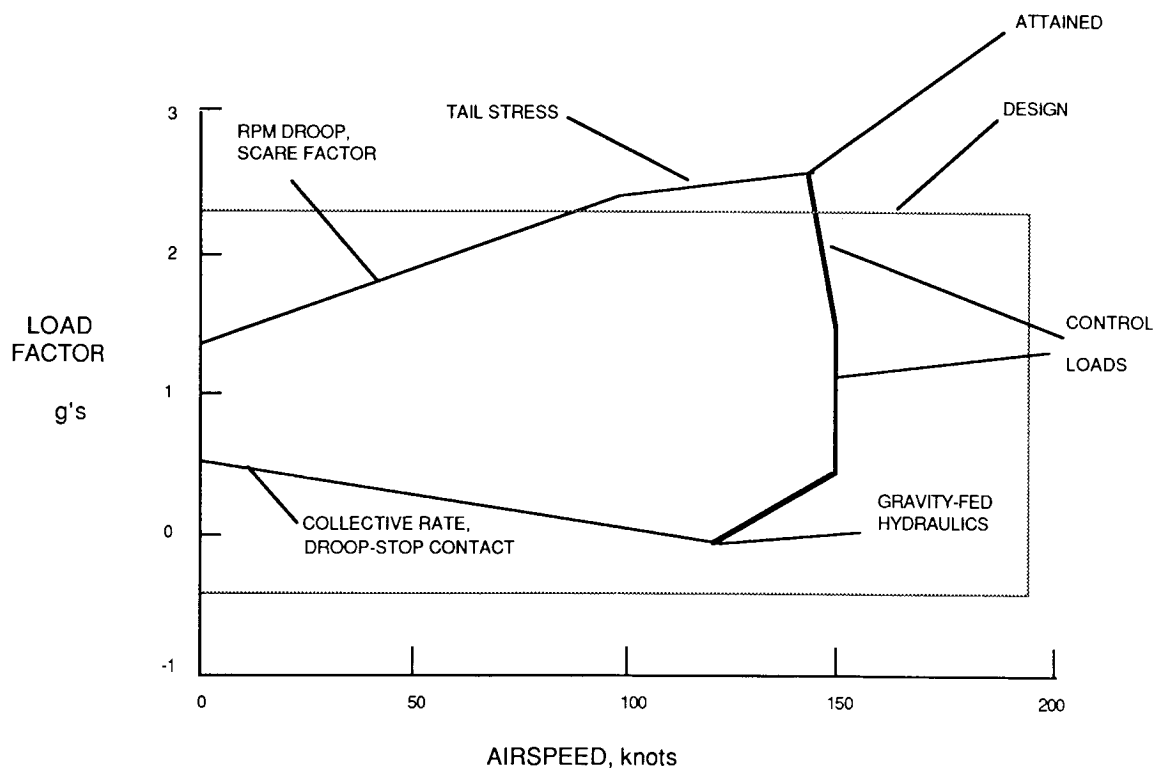


Figure 13.25. Typical Helicopter Limits

13.27 HELICOPTER MANEUVER ENVELOPE ENHANCEMENT (HeIMEE)

13.27.1 Objective

To define the limits on helicopter performance and develop methodologies that enable safe utilization of the flight envelope by the pilot out to these limits. This work was motivated by the fact that many of the actual limits on today's operational helicopters are unknown to the users and that little or no cueing is available to monitor the approach to the limits; accordingly, the flight demonstration of new helicopters typically is conducted only to the specification and the full available envelope is not utilized. A particular objective then was to define the limits and develop and demonstrate methods to utilize fully the helicopter's performance capabilities, which is sometimes called carefree maneuvering.

13.27.2 Approach

The approach involved conducting a contracted study using the UH-60 Blackhawk as the example helicopter. Key structural and aerodynamic maneuver limiting phenomena were identified and then the contractor's fixed base simulation was extended with an in-house simulation conducted on the Vertical Motion Simulator at Ames (See Figure 13.25).

13.27.3 Accomplishments

The study determined that there are three principal limiting factors in the helicopter's flight envelope, (1) main rotor control loads, (2) tail rotor movement and (3) main rotor moment. Because the most important of these, control loads, was not available in the simulation model, measures which approximate the same envelope were developed. They were an approximate measure of retreating blade drag and an approximate measure of average blade angle of attack. For the simulations, these two measures plus main rotor moment, were used to drive a variety of cues for the pilot, including lights, tones, additional symbols on a head-up display, or stick shaking. These concepts were incorporated into a UH-60 simulation for both the contracted and in-house simulations and representative tasks to push the flight envelope usage were examined in manned simulation. This simulation showed through both pilot ratings and comments that the cueings tested did not allow a pilot to use more of the available envelope without an increase in workload. The pilots were able to develop strategies after much practice to minimize limit exceedances for the canned tasks considered.

13.27.4 Significance

Rotorcraft pilots are unable to exploit fully the full flight envelope of their aircraft. It is clear from the results of this study that these limits are dynamic in nature and avoiding their exceedance in a "carefree maneuvering" sense requires more than displaying some of the information to the pilot. Accordingly, automated limit exceedance and envelope enhancement must be considered as the next step.

13.27.5 Status/Plans

The need for carefree maneuvering is being addressed in the HIMARCS and SCAMP programs. In HIMARCS, the envelope required is being developed for paradigm maneuvers and SCAMP is addressing the incorporation of the automated limiting and enhancement as part of the integrated controls work.

J. A. Schroeder and M.S. Whalley
Flight Dynamics and Controls Branch
Ames Research Center
(415)604-4037

ORIGINAL PAGE
BLACK AND WHITE PHOTOGRAPH



Figure 13.26. Tiltrotor Technology

3.28 TILTROTOR TECHNOLOGY

13.28.1 Objective

To (1) explore advanced tiltrotor technology and economic, environmental and technology factors critical to the success of a civil or military tiltrotor aircraft and (2) transfer NASA research results to industry and other government agencies for application to tiltrotor development programs such as V-22 or planning efforts to introduce a civil tiltrotor into the National Transportation System.

13.28.2 Approach

The approach included the following tasks: (1) plan, advocate and support analytical and experimental programs including CFD, piloted simulations, small and large scale wind tunnel tests; (2) conduct flight research using the XV-15 and a prototype V-22; (3) conduct in-house and contracted studies and internal assessments and (4) work cooperatively with industry, other federal agencies such as DOT, DOC and FAA and state, regional and local transportation and aviation authorities (See Figure 13.26).

13.28.3 Accomplishments

NASA (1) completed XV-15 flight tests to validate and improve the existing tiltrotor simulation math model; (2) evaluated the acceleration coupling found in the initial ground tests of the V-22 airframe and control system, (3) participated in V-22 digital control system CDR, (4) established a NASA position on the V-22 Multi-Service Test Team and (5) provided funding to increase the tiltrotor CFD effort at Ames Research Center by hiring a new contract researcher. NASA also prepared a civil tiltrotor data package for state and regional tiltrotor and vertiport feasibility studies. NASA initiated a follow-on to the FAA/NASA Tiltrotor Applications Study with (1) a market reassessment, (2) a high payoff civil technology cost/benefits assessment, (3) an operational analysis utilizing simulators for TERPS criteria and (4) a flight validation program plan. Contributions also were made to national transportation studies and the National Civil Tiltrotor Implementation Plan.

13.28.4 Significance

The United States holds a commanding lead in tiltrotor technology and NASA has the opportunity to further this national objective by vigorously pursuing the problems associated with both civil and military applications. The expansion and enhancement of the tiltrotor technology database will reduce the technical risk to industry.

13.28.5 Status/Plans

NASA plans to (1) continue the XV-15 flight research program; (2) support the V-22 and other tiltrotor development programs; (3) award the FAA/NASA Tiltrotor augmented contract in FY 1989 and (4) continue close working relationships with all government agencies studying civil tiltrotors.

William Snyder and John Zuk
Rotorcraft Technology Branch
Ames Research Center
(415)604-6570/6568

ORIGINAL PAGE
BLACK AND WHITE PHOTOGRAPH



Figure 13.27. V-22 Rotor/Wing Performance Test

13.29 V-22 ROTOR/WING PERFORMANCE TEST

13.29.1 Objective

To (1) measure V-22 rotor performance at high speeds, including rotor/wing interactions; (2) measure mean and oscillatory rotor system and hub loads; (3) evaluate isolated rotor performance at high speeds and (4) determine effect of wing flap angle, nacelle angle and rotor rotation direction on wing downloads.

13.29.2 Approach

The approach involved (1) testing a two thirds scale, V-22 rotor on the Prop Test Ring in the 40-foot by 80-foot wind tunnel up to 300 knots, both isolated and in the presence of a 2/3-scale pressure instrumented semispan V-22 wing; (2) performing hover tests in the 40-foot by 80-foot test section with and without the wing, using an image plane to simulate the plane of symmetry and (3) evaluating the effect of rotor rotation direction by testing with both a left-hand and right-hand wing (See Figure 13.27).

13.29.3 Accomplishments

The first phase of the test program was completed, including both hover and forward flight. The hover download results showed that reversing the direction of rotation of the rotors does not reduce download over that measured with the present rotation direction. The forward flight portion of the test was limited by rotor control system loads to a speed range of 220 knots. The rotor performance data validated analyses for the range of operating conditions covered to date. The Navy's concern about large, adverse, interference effects on the rotor performance due to the wing appears to be unfounded.

13.29.4 Significance

These results support the Navy's V-22 Osprey development program. The rotor performance results serve to validate the Bell/Boeing analysis. Also, the rotor performance results will support the V-22 flight test program by allowing airframe drag to be deduced from flight test results. This will allow any development work aimed at improving the aircraft's cruise performance and range to be currently focused. Also, rotor hub oscillatory loads caused by the interaction with the wing were directly measured. These data will be used to validate aircraft vibration analyses, leading to an improved capability to predict and reduce tiltrotor vibration in cruise flight.

13.29.5 Status/Plans

The rotor control system hardware is being upgraded to allow testing up to the full 300 knot capability of the V-22 aircraft. In addition, the spinner is being instrumented to directly measure the spinner drag during high speed flight. Current plans call for the second phase of the test program to begin in November 1989 in the National Full-Scale Aerodynamics Complex. The data from this test and the previous entry will be analyzed, compared with analyses and documented. These data will document tiltrotor download, rotor performance, rotor/wing aerodynamic interactions in forward flight and oscillatory hub loads and vibration.

Fort Felker
Rotorcraft Aeromechanics Branch (FFR)
Ames Research Center
(415)604-6096

ORIGINAL PAGE
BLACK AND WHITE PHOTOGRAPH



Figure 13.28. XV-15 Tiltrotor Research Aircraft

13.30 XV-15/ATB FLIGHT INVESTIGATIONS

13.30.1 Objective

To design, build and flight test Advanced Technology Blades (ATB) on the XV-15 Tiltrotor Research Aircraft to expand the validated tiltrotor database beyond the standard XV-15 rotor designed in the early 1970s. Flight research goals included investigations of performance, acoustics, dynamics, aeroelastic stability and the acquisition of airloads data. Flight and ground tests will provide data to validate advanced codes such as CAMRAD.

13.30.2 Approach

The ATB incorporated advanced aerodynamic and structural dynamic features made possible with composite materials. The blades were highly twisted with a compound planform and a thin tip for greater lift capability in hover without degrading performance at high speeds in the airplane mode. The ability to change tip and cuff section geometry, as well as blade sweep also were incorporated. Pressure transducers were installed in one blade to acquire airloads data (See Figure 13.28).

13.30.3 Accomplishments

Initial ATB flight tests revealed high rotor control loads in the helicopter mode. Extensive analyses and experiments determined that the high feathering inertia of the ATB introduces a resonance in the operating RPM range. In addition, the XV-15 rotor control system "softness" resulted in a cyclic/collective coupling that reduces stability margins. CAMRAD/JA was modified to predict these control characteristics and analyses of parametric variations were completed. Based on hangar demonstrations of the ability to shift the resonant frequency, a modification to stiffen the controls and reduce the cyclic/collective coupling was incorporated and pre-flight ground test validation is in progress.

13.30.4 Significance

Investigation of the XV-15/ATB rotor/control dynamics resulted in greatly increased understanding of the phenomena involved and accelerated the development of improved methodology for analyzing these dynamics. The validation of this methodology through correlation with flight data will significantly enhance industry's capability to predict and design for dynamic and aeroelastic phenomena.

13.30.5 Status/Plans

XV-15 tests to evaluate the loads reduction obtained with a stiffened control system, blade chord balance and blade sweep modifications were initiated. Initial flight tests to expand a flight envelope will be followed by a planned aircraft inspection/overhaul; then, the full spectrum of tiltrotor flight investigations will be continued. Design of a pressure instrumented blade was completed, but fabrication is on hold pending outcome of ATB envelope flight testing.

Martin Maisel and L. Schroers
Rotorcraft Technology Branch/Flight Experiments Branch
Ames Research Center
(415)604-6372/5456

ORIGINAL PAGE
BLACK AND WHITE PHOTOGRAPH

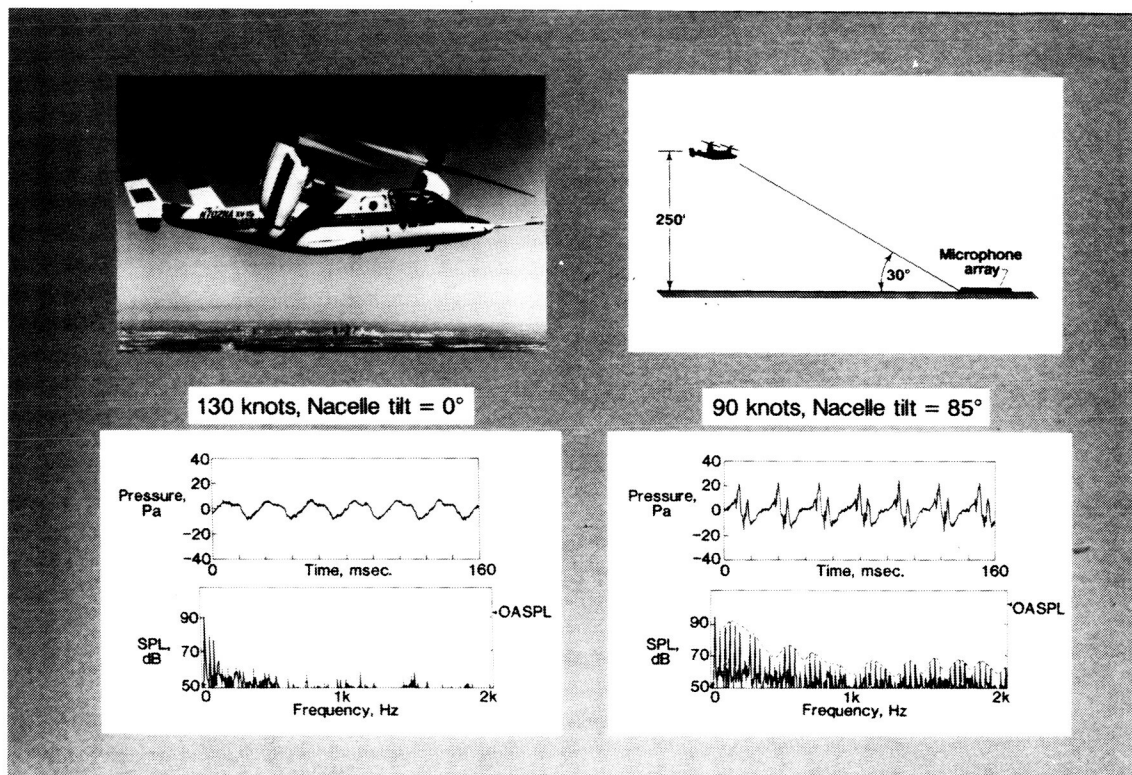


Figure 13.29. XV-15 Tiltrotor Noise Test

13.31 XV-15 TILTROTOR NOISE TEST

13.31.1 Objective

To determine the acoustic impact of a current tiltrotor aircraft used as an inter-city commuter and to establish a high confidence level (90 percent), accurate (± 1.5 dB) far-field acoustics database.

13.31.2 Approach

Langley Research Center jointly with Bell Helicopter conducted noise tests on the XV-15 aircraft as part of the NASA/AHS Program. Ames Research Center made the aircraft available for these tests. The tests consisted of level flyovers, ascents, descents, hover and noise abatement approaches (See Figure 13.29).

13.31.3 Accomplishments

The aircraft was repeatedly flown over a 20 element microphone array to provide ensemble-averaged overhead and sideline acoustic measurements. The data are preliminary results based on single microphone measurements. For these data, the aircraft was at an altitude of 250 feet and approximately 30 degrees above the horizon with respect to the microphone position. The time history and narrowband analysis are for the aircraft flying at 130 knots in the airplane mode (nacelle tilt=0 degrees). The data are typical of a quiet turboprop aircraft with a sound pressure level of 92 dB. The corresponding data are for the aircraft flying at 90 knots in the helicopter (approach) mode (nacelle tilt=85 degrees). The double peak seen in the time history indicates an impulsive content in the acoustic signal. The scalloped shape of the harmonics in the frequency plot is typical of helicopter blade-vortex interaction noise. The sound pressure level for the approach configuration is 101 dB.

13.31.4 Significance

The tiltrotor aircraft is relatively quiet when operating in the airplane mode; however, when operating in the helicopter or approach mode, the noise level increases significantly due to the impulsive content of the acoustic signal. Since the approach mode is most critical to community acceptance, the high noise levels could present problems at inter-city heliports.

13.31.5 Status/Plans

The data are being analyzed using the ensemble-averaging technique. These results will be incorporated into the ROTONET (helicopter noise prediction program) database and used to validate predictions. Also, approach and noise abatement data are being analyzed to define low noise operating techniques.

David A. Conner and Otis S. Childress, Jr.
Applied Acoustics Branch
Langley Research Center
(804)864-5278

13.32 MV-22 TILTROTOR SIMULATION

13.32.1 Objective

As part of the recent NASA/Navy MOU on tiltrotor technology, a joint project was initiated among the Marines, the Navy and NASA to investigate maneuver and control requirements for a tiltrotor aircraft engaged in one versus one air combat with a fixed wing aircraft or helicopter.

13.32.2 Approach

A ground-based simulation was conducted which included transport or agile armed escort tiltrotor opposed by a fixed wing aircraft or helicopter, simple missile and gun models and maneuver within terrain environment.

13.32.3 Accomplishments

The tiltrotor was mechanized in one, fixed-base cab with the opponent mechanized in a second fixed-base cab. Two tiltrotor configurations were simulated, (1) a transport aircraft similar to the V-22 and (2) a conceptual design for an agile armed escort aircraft. Over 800 evaluation runs were flown by pilots from the Marines, Navy and Bell Helicopter with support by the Ames research pilots. Results demonstrated the usefulness of quick conversion to outfly an opponent, either a helicopter or a fixed wing airplane.

13.32.4 Significance

The ground-based simulation provided the Marines with an early look at operational issues and provided data needed to develop a draft V-22 operations manual. In addition, the operational focus of the simulation experiment provided the NASA/Navy/Industry team with an understanding of tiltrotor air combat maneuver and flight controls issues requiring further development.

13.32.5 Status/Plans

The development of flight control design guidance and requirements for tilt rotors will continue as will further DoD/NASA efforts to develop design requirements for high speed, rotorcraft air combat.

William A. Decker
Flight Dynamics and Controls Branch
Ames Research Center
(415)604-5362

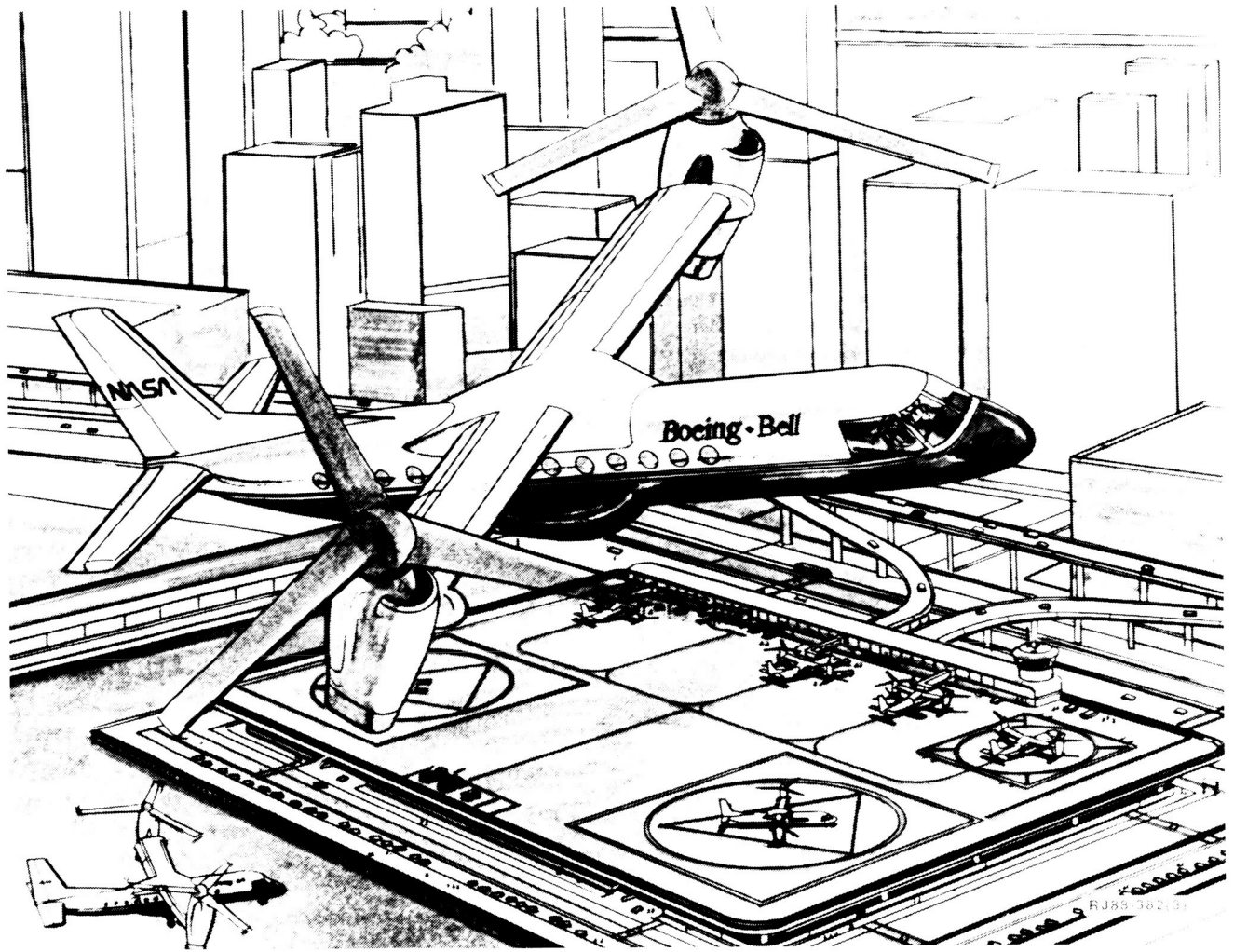


Figure 13.30. Civil Tiltrotor Airworthiness Criteria

13.33 CIVIL TILTROTOR AIRWORTHINESS CRITERIA

13.33.1 Objective

To examine airworthiness aspects of certification that are unique to tiltrotor aircraft. The motivation was that provisional certification of a civil version of the MV-22 may be accomplished in order that the ramifications of introducing tiltrotor aircraft into the national airspace system can be assessed.

13.33.2 Approach

There was renewed interest in the definition of suitable airworthiness criteria for this class of aircraft including a new FAA set of interim criteria published in July 1988. These criteria, however, are based largely on attempts to blend criteria for conventional aircraft and rotorcraft and are based on data for configurations substantially different from tiltrotors. Accordingly, experiments on the Ames Vertical Motion Simulator were initiated to address these operational and airworthiness issues for tiltrotor class aircraft (See Figure 13.30).

13.33.3 Accomplishments

The initial experiments were conducted in 1983 and were based on the 13,000 pound XV-15 aircraft in order to attempt some flight correlation. These experiments examined the manner in which conversion from airborne to thrust-borne flight is effected, the coupling between conversion and aircraft pitch and heave control and the allowable range of airspeeds at given thrust inclination angles. This simulation model was revived in October 1988 and a ground-based simulation was conducted of similar variations for a new set of FAA and Civil Aviation Authority experts. This simulation confirmed the influences found earlier and initiated an examination of one-engine-inoperative situations, which is a key driver for operational acceptance of the tiltrotor.

13.33.4 Significance

Airworthiness and operational issues are tightly coupled for tiltrotor class vehicles and these studies define technology advances that are required to meet the safety objectives of civil operations; for example, the requirement for one-engine-out operations can be a major design driver for the next generation of tiltrotor.

13.33.5 Status/Plans

The concepts that were examined for the XV-15 class of tiltrotor are being carried over to a new model of a 40,000 pound tiltrotor very similar to the V-22, at least in performance. A Vertical Motion Simulator experiment with this model will begin early in FY 1990.

J. V. Lebacqz and W.A. Decker
Flight Dynamics and Controls Branch
Ames Research Center
(415)604-5009

1. Report No. NASA TM-4175		2. Government Accession No.		3. Recipient's Catalog No.	
4. Title and Subtitle NASA Aerodynamics Program Annual Report 1989				5. Report Date February 1990	
				6. Performing Organization Code RF	
7. Author(s) Bruce Holmes, Edward Schairer, Gary Hicks, Stephen Wander, Isiaiah Blankson, Raymond Rose, Lawrence Olson, and George Unger				8. Performing Organization Report No.	
				10. Work Unit No.	
9. Performing Organization Name and Address NASA Office of Aeronautics and Space Technology Aerodynamics Division (OAST/RF)				11. Contract or Grant No. NASW 4430	
				13. Type of Report and Period Covered Technical Memorandum	
12. Sponsoring Agency Name and Address National Aeronautics and Space Administration Washington, DC 20546				14. Sponsoring Agency Code	
15. Supplementary Notes This report is an annual accomplishments review for the Aerodynamics Division (Code RF). The information contained herein covers FY 1989.					
16. Abstract This report is the annual accomplishments review for the Aerodynamics Division (Code RF) during FY 1989. The Aerodynamics Division sponsors research in fluid and thermal physics and applied aerodynamics. This report contains a comprehensive review of the following aerodynamics elements: computational methods and applications, CFD validation, transition and turbulence physics, numerical aerodynamic simulation, drag reduction, test techniques and instrumentation, configuration aerodynamics, aeroacoustics, aerothermodynamics, hypersonics, subsonic transport/commuter aviation, fighter/attack aircraft and rotorcraft.					
17. Key Words (Suggested by Author(s)) aerodynamics subsonic waverider aeroacoustics supersonic flowfield aerothermodynamics NAS crossflow hypersonics' NASP rotorcraft Navier-Stokes				18. Distribution Statement Unclassified - Unlimited Subject Category 47	
19. Security Classif. (of this report) Unclassified		20. Security Classif. (of this page) Unclassified		21. No. of pages 466	
				22. Price A20	